THE UNIVERSITY OF CHICAGO

TETRAPOD EVOLUTION AND COMMUNITY ECOLOGY IN THE POST-DEVONIAN WORLD

A DISSERTATION SUBMITTED TO

THE FACULTY OF THE DIVISION OF THE BIOLOGICAL SCIENCES

AND THE PRITZKER SCHOOL OF MEDICINE

IN CANDIDACY FOR THE DEGREE OF

DOCTOR OF PHILOSOPHY

COMMITTEE ON EVOLUTIONARY BIOLOGY

BY

BENJAMIN KOBINA ASUANTSI OTOO

CHICAGO, ILLINOIS

MARCH 2023

=:

Figure 0.1. Restoration of two *Whatcheeria deltae* individuals fighting over an unfortunate fish, middle Mississippian of Iowa. © Adrienne Stroup, Field Museum. 2022.

In loving memory of my grandmother Donna Roselle Ward (nee McCullough). May you enjoy many more 39th 39th birthdays.

TABLE OF CONTENTS

LIST OF FIGURES

LIST OF TABLES

ACKNOWLEDGEMENTS

And so we come to the end! It's been an incredible adventure, and I have so many people to thank. To my co-advisors Mike and Ken, thanks for believing in my ideas and my ability to see things through to the end. Especially as various parts of my dissertation shifted and took new forms along the way (which happened a lot!) and I sometimes struggled to fully get a handle on things. To the rest of my committee, Dave and Graham, for always cultivating a rich environment for ideas and discussion. You've all been extremely supportive during my time here.

Thanks to the others who put me on to this whole realm of paleontology. To Jenny, who was the one to induct me into the fascinating world of early tetrapods. To John Bolt and Eric Lombard, who very kindly opened their office and brought me onboard to work on *Whatcheeria*. Additional thanks to Tim Smithson, Marcello Ruta, Christian Kammerer, Stig Walsh, and Elsa Panciroli for welcoming me into the field and helping me find my path.

Thanks to all the staff at UChicago and the Field Museum: Carolyn Johnson, Audrey Aronowsky, Marcy Hochberg, Bill Simpson, Adrienne Stroup, Akiko Shinya, and all the preparators who worked on specimens I used. Without you I wouldn't be in Chicago and none of this research would be possible. And thank you to all the curators, collections managers, and other museum staff who opened their doors to me. To Colleen at the Dissertation Office, you've been supremely patient and understanding through this final process of formatting and uploading

this document. I salute a fellow fighter in the war against the perverse incentives of the word processing software industry.

Thank you so much for the psych professionals I've worked with while in Chicago: Dr. Marie Nicholas, Dr. Erin Hurst, and, most of all, Marcellus Rose. You've helped me change my life for the better, and you have my perpetual gratitude.

To the members of the Coates and Angielczyk labs, thank you for bringing my workdays to life over this last six-and-a-bit-more-than-a-bit years. Thanks to Kate, Dave, Dallas, Jackie, and Tom for sharing the benefits of their wisdom and experience when I pitched up here all new, and over the years since then. Special mention to Tim- not a labmate but an invaluable teacher. I've been holding onto that bottle of tequila you gave me- and now the special occasion is finally here. To Tristan, Caroline, Isaac, Danny, Sarah, Brandon, Pia, Steph, and Spencer- thanks for so many energizing conversations and expanding my horizons. Jason, Yara- I wish we had more time together here: to the promise of many future conversations. To Stephanie, Abby, Vish, Kristen, and Tetsuto (the last two late of this parish, as Mike would say) and Aliss the lungfish, some of the most interesting and chaotic odd ducks I've ever known. Dear friends, all of you. You've carried me through the many ups and downs to get here and taught me so much. Our whirling chaos has its own particular charm. I'm not changing my mind on cyclostomes, though.

To my other friends in CEB and throughout Chicago, past and present, especially Brooke, Peter, Mariah, Taylor, and Jordan: thanks for reminding me to hold on to that human part of me. I hope we get to dance again. Special mention to those I've had the bittersweet pleasure of befriending

so close to the end of my time here: Brandon, Ben, Tati, Melvin, and Emily. Emily, you've been incredibly gracious this past quarter as I've been wrapping up- TA MVP for sure.

To my friends from elsewhere. The Unfriendly Alternative Kids- Matt, Daniel, Jake, Defne- and the Cambridge crowd, especially Nelson, Nick, Becca, and The Powerpuff Girls- Rick, Sarah, and Jas. Though we're far apart, I'm so grateful you're a part of my life.

Finally, to my family. You've been behind me all the way. I love you all very much.

ABSTRACT

Tetrapods currently comprise over 30,000 species distributed globally and occupying a stunning diversity of bodyplans and ecologies. After many years of fruitful work, the early evolutionary history of the group can be considered well-understood. We have a detailed sequence of anatomical change across the fish-tetrapod transition in the Devonian period and a rich fossil record from the late Early Carboniferous (Mississippian) and Late Carboniferous (Pennsylvanian). These two datasets reveal the initial assembly of the tetrapod bodyplan at one end and the proliferation of early members of crown group lineages at the other. However, there remains an unbridged divide between the apparently low-diversity, obligately aquatic, fishlike Devonian tetrapod assemblage and the speciose, ecologically diverse post-Devonian assemblage. This divide is inflected by the end-Devonian mass extinction (EDME), which is itself followed by a ~15 million year hiatus in the tetrapod fossil record (Romer's Gap) that is just now beginning to be populated.

In this dissertation I attempt to understand the evolution of early tetrapods through the end-Devonian mass extinction and its aftermath by integrating data from comparative morphology, phylogenetics, and community ecology. In Chapter 2, I redescribe the postcranial skeleton of the middle Mississippian stem tetrapod *Whatcheeria deltae* to generate new anatomical and character information and better understand its relationships. In Chapter 3, I analyze a new early tetrapod phylogenetic dataset to more evaluate the effect of new *Whatcheeria* data on the structure of the apical tetrapod stem group, hypotheses of tetrapod crown group membership, and inferred patterns and timing of branching events during the Late Devonian and Mississippian. Finally, in Chapter 4 I use comparative ecological methods to

evaluate effect of the end-Devonian mass extinction on richness of guilds (=functional groups) and community-level resistance to perturbation across environments, with special attention paid to the middle Devonian-middle Mississippian origin of terrestrial communities.

In Chapter 2 I redescribe the postcranial anatomy of *Whatcheeria* on the basis of hundreds of previously unstudied specimens. *Whatcheeria* is revealed to be an unusual large-bodied form with an elongate neck, robust appendicular skeleton, and regionalized trunk ribs. Limb proportions resemble those of terrestrial crown tetrapods from the Permian such as *Eryops*, but the presence of a well-developed cranial sensory canal system indicate that *Whatcheeria* was an aquatic animal, albeit one adapted for walking rather than swimming in the water column. Using a diagnosis improved by new character data, the family Whatcheeriidae can be restricted to the earliest Mississippian *Pederpes* and middle Mississippian *Whatcheeria*. Whatcheeriid autapomorphies can now be recognized in several Mississippian specimens as well. *Whatcheeria* indicates that Mississippian stem tetrapods were capable of much more morphological, physiological, and likely functional complexity than previously appreciated. Moreover, such complexity was not necessarily tied to terrestrialization.

In Chapter 3 I analyze a new phylogenetic dataset incorporating new postcranial character data from *Whatcheeria* as well as recent discoveries from Romer's Gap. The dataset combines new characters with those of multiple dataset 'lineages'. Parsimony analysis finds a well-supported, monophyletic Whatcheeriidae composed of *Whatcheeria* and *Pederpes* located deep on the tetrapod stem. Contra recent hypotheses, large aquatic embolomeres and the limbless aistopods and adelospondyls are found within the amniote total group. The colosteids have an

ambiguous relationship to the tetrapod crown node, alternating between the sister group of crown tetrapods to the sister group of the temnospondyls within the lissamphibian total group. Analysis of anatomical partitions of characters indicates similar levels of signal in cranial and postcranial data but divergent patterns of evolution across partitions, particularly between the anterior and posterior appendicular skeletons. Estimation of node ages supports a Devonian origin for most stem tetrapod lineages but not terrestriality. Node age estimation and anatomical partition analyses both support at minimum one independent origin of terrestriality in each of the crown tetrapod lineages.

In Chapter 4 I analyze a dataset of 16 paleocommunities from the middle Devonian (Givetian) through the end of the Mississippian (Serpukhovian). Non-metric multidimensional scaling (NMDS) analysis finds a strong time-environment separation between axes when the diversity of high-level taxonomic groups is used, but this distinction breaks down substantially when diversity of ecological guilds is used. These results suggest substantially greater functional continuity than taxonomic continuity through the EDME. Simulation of paleocommunity response to perturbation using the Cascading Extinction on Graphs (CEG) model finds no clear difference in response between communities before and after the Frasnian-Famennian invertebrate extinction or the EDME. The response of paleocommunities is bimodal with low variance, shifting extremely rapidly from low to high levels of secondary extinction at approximately 50% perturbation. Curiously, variance in secondary extinction is low throughout. I propose that this response pattern is due to a combination of low guild richness, high guild evenness, broad prey profiles among predators, and top-down pressure from high-trophic-level predators. At low levels of perturbation, the generalist nature of predators results in low per-

species predation pressure. However, at high levels of perturbation, increasing secondary extinction, in combination with low guild richness, begins to rapidly eliminate entire guilds. Top-down predation pressure is still being widely applied, and the entire food web collapses. Gilboa, a middle Devonian terrestrial paleocommunity, and East Kirkton, the oldest terrestrial tetrapod paleocommunity (a diverse arthropod assemblage is also present), both share this response pattern with the aquatic localities, though variance in secondary extinction values is greatly increased by the lower species diversity. Terrestrial communities appear to have developed through the diversification and proliferation of plants and arthropods; tetrapods later fit into guilds which had been previously defined and occupied solely by arthropods. I propose the origin of more fully terrestrial vertebrate communities may lie somewhere in the Mississippian, and previous hypotheses that late Pennsylvanian/early Permian assemblages represent the initial organizational structure of the first terrestrial tetrapod communities are not supported.

Datafiles for the Chapter 4 paleocommunity food web analyses are contained in the "Supplementary Files" ZIP file online. This ZIP file contains faunal lists, guild assignments, and model parameter information in Excel (.xlsx) format

CHAPTER 1: INTRODUCTION

1.1 CONTEXT FOR RESEARCH

Over the last 30 years, early tetrapod research (Coates et al., 2008; Clack, 2012; Pardo et al., 2020) has benefitted tremendously from an influx of new data. We now have a detailed picture of evolutionary and environmental events during the origin and initial radiations of tetrapods (Figure 1). In the 1990s, the Famennian tetrapods *Acanthostega* (Coates, 1996; Ahlberg and Clack, 1998; Clack, 1998, 2002a, 2002b), *Ichthyostega* (Jarvik, 1996), and *Tulerpeton* (Lebedev and Clack, 1993; Lebedev and Coates, 1995) were (re)described. These taxa confirmed presence of gills and polydactyly in the earliest limbed tetrapods (Coates and Clack, 1990, 1991). Character investigations and phylogenetic analyses used these anatomical data to resolve longstanding questions of the extant tetrapod sister group and tetrapod monophyly (Panchen and Smithson, 1987, 1988; Cloutier and Ahlberg, 1996). Increasing information on the panderichthyids *Panderichhthys* (Vorobyeva, 1995; Ahlberg et al., 1996) and *Elpistostege* (Schultze and Arsenault, 1985) more firmly established these taxa as the immediate outgroups to limbed tetrapods. The discovery of the more complete panderichthyid *Tiktaalik* in the mid-2000s (Daeschler et al., 2006) provided new data and reframed research on the origin of limbed tetrapods. *Tiktaalik* retained fins but possessed a neck, elbow, and enlarged pelvis (Shubin et al., 2006, 2014; Downs et al., 2008; Stewart et al., 2019) The result of this work is that we now have a set of taxa with which to trace trait evolution through the fish-tetrapod transition in the Devonian.

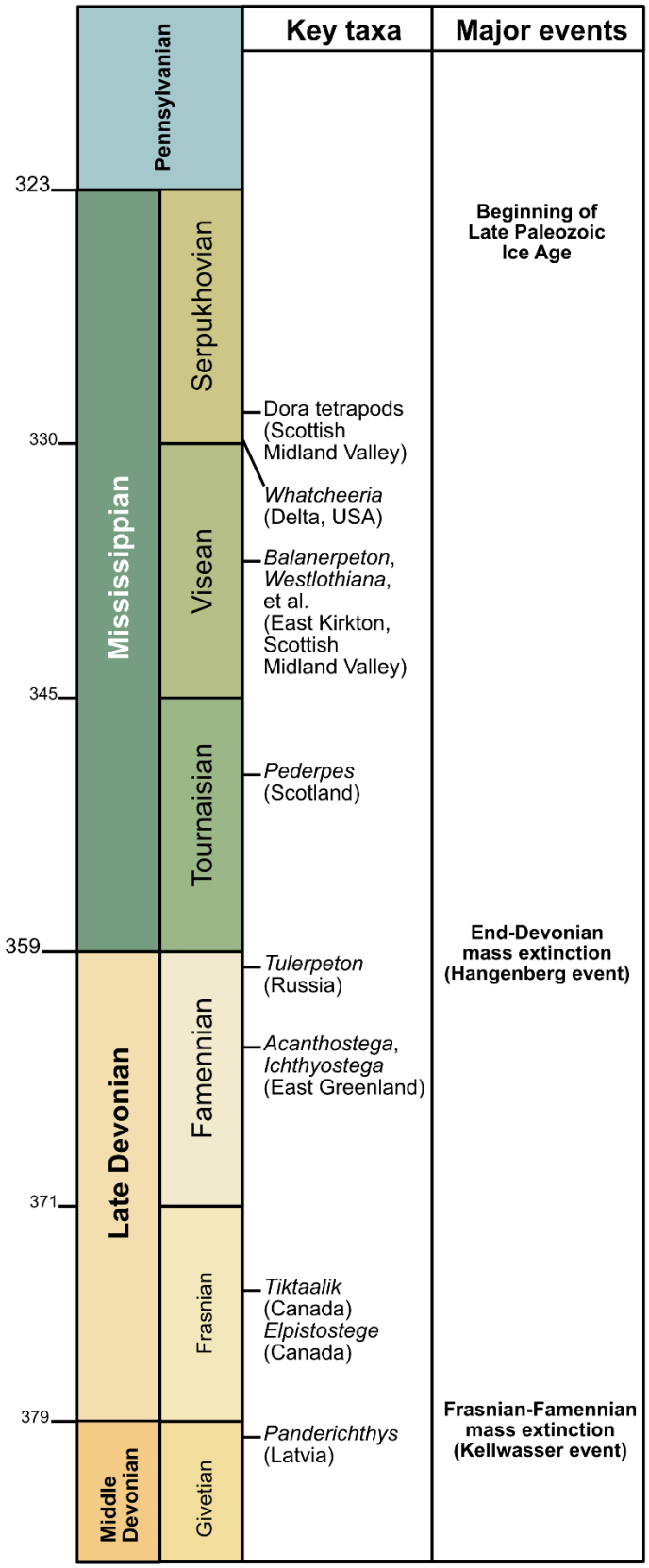

Figure 1.1. Devonian-Carboniferous timescale with key taxa and major events.

During the same period, new Early Carboniferous (Mississippian) data were generated by excavations of the Dora (Smithson, 1980) and East Kirkton localities (Wood et al., 1985) in the Scottish Midland Valley. Numerous historical collections from the Scottish Midland Valley and northern England have been made (Panchen, 1964, 1966, 1972; Milner, 1980a; Panchen, 1981; Smithson, 1985a; Clack, 1987a) but the Dora and East Kirkton excavations were much more systematic. Both localities produced diverse assemblages. The diverse and disparate East Kirkton biota, the older of the two, includes temnospondyl *Balanerpeton* (Milner and Sequeira, 1993) and stem amniote *Westlothiana* (Smithson et al., 1993), which are often (Ruta, 2011; Clack et al., 2016; Pardo et al., 2017b, 2020) used as first appearances of total group Lissamphibia and Amniota, respectively.

As research on the Late Devonian and new Mississippian tetrapods proceeded, attention returned to Romer's Gap. Historically, studies of early tetrapods struggled to bridge the conceptual and data gaps between the beginning and end of the fish-tetrapod and water-land transitions. The Frasnian tristichopterid *Eusthenopteron* and Permian temnospondyl *Eryops* were used to represent the morphological endpoints, with *Ichthyostega* as a challenging aberration (reviewed by Jarvik (1996)). Romer struggled with the paleobiological gap between the aquatic earliest tetrapods- represented by *Ichthyostega*- and the latest Pennsylvanian/early Permian terrestrial tetrapods such as *Diadectes*, *Eryops*, and *Dimetrodon* (Romer, 1956). By the end of the 20th century, the fish-tetrapod morphological gap had been narrowed substantially and the minimum age for tetrapod terrestrialization had moved from the terminal Pennsylvanian to the middle Visean. However, full reconstruction of the water-land transition- and indeed, connection between the Devonian and post-Devonian tetrapod radiations- was still frustrated by a lack of

earliest Mississippian (Tournaisian and early Visean stages) tetrapod fossils (Coates and Clack, 1995). This hiatus was named 'Romer's Gap' by Coates and Clack (1995). This opaque interval presumably contained the transition between the aquatic, fishlike Late Devonian tetrapods (*Acanthostega*, *Ichthyostega*) and the terrestrial crown tetrapods from East Kirkton (*Balanerpeton*, *Westlothiana*).

Romer's Gap took on new significance after a large-scale faunal study by Sallan and Coates (2010). They found that vertebrate turnover across the Devonian-Carboniferous boundary was not gradual but rapid and severe. The 'Late Devonian mass extinction' (Droser et al., 2000; McGhee et al., 2004, 2013) was decomposed into the invertebrate Frasnian-Famennian mass extinction (Kellwasser event) and the vertebrate end-Devonian mass extinction (EDME, Hangenberg event). The multi-institution TW:eed (Tetrapod World: Early Evolution and Diversification) project was put together in the 2010s to discover Romer's Gap tetrapods in the Tournaisian of northern England and southern Scotland. Hypotheses explaining Romer's Gap included low oxygen levels suppressing diversity (Ward et al., 2006), a post-extinction diversity lull (Sallan and Coates, 2010), and sampling failure (Clack, 2009; Smithson et al., 2012). Persistent environmental disruptions during the Mississippian (Yao et al., 2015) may also have played a role.

The prospect of Tournaisian tetrapods had been raised over 15 years prior by work in North America. In the 1980s Bolt, Lombard, and colleagues conducted extensive fieldwork at Delta, a new latest Visean/earliest Serpukhovian tetrapod locality (Bolt et al., 1988). This was the first discovery of a new tetrapod locality from the Mississippian of North America in decades. Until

the discovery of the Famennian Red Hill tetrapods (Daeschler et al., 1994; Daeschler, 2000), the Delta tetrapods were the oldest from North America. Chief among the Delta discoveries was *Whatcheeria* (Lombard and Bolt, 1995). *Whatcheeria* was clearly more derived than *Acanthostega* and *Ichthyostega* but did not easily fit into contemporary hypotheses of tetrapod relationships (Figure 2). Shortly thereafter, *Pederpes* was discovered from the Tournaisian of Scotland (Clack, 2002c). Recognized as a similar kind of tetrapod to *Whatcheeria*, Clack erected the family Whatcheeriidae to contain *Whatcheeria* and *Pederpes* (Clack, 2002c; Clack and Finney, 2005). The Australian Visean tetrapod *Ossinodus* was soon added to the family as well (Warren and Turner, 2004; Warren, 2007). The whatcheeriids represented a unique tetrapod lineage within Romer's Gap.

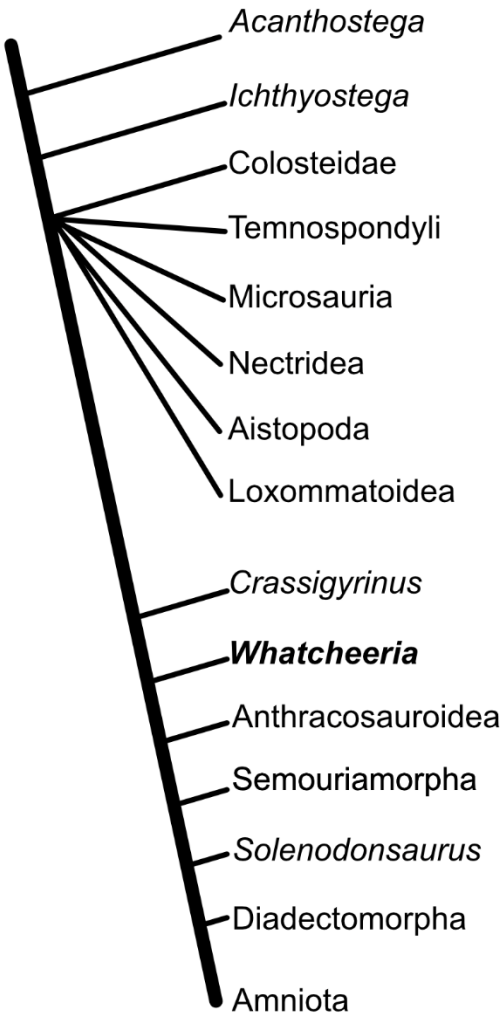

Figure 1.2. Initial hypothesis of relationships between Whatcheeria and other early tetrapod taxa. Modified from Lombard and Bolt (1995). Terminology follows the original figure.

The lower (Devonian) portion of the tetrapod stem has been thoroughly investigated as part of the origin of stem tetrapods (Ahlberg, 1995, 2018; Ahlberg et al., 1996, 2008; Coates, 1996; Ahlberg and Johanson, 1998; Callier et al., 2009; Beznosov et al., 2019; Stewart et al., 2022). Much attention has been paid to the origins of the lissamphibian and amniote total groups (Laurin and Reesz, 1995; Lebedev and Coates, 1995; Laurin and Reisz, 1997; Reisz, 1997; Marjanović and Laurin, 2007, 2008, 2013; Ruta and Coates, 2007; Maddin et al., 2012; Pardo et al., 2017, 2020; Atkins et al., 2019), but the upper (post-Devonian) portion of the tetrapod stem

has not received the same amount of scrutiny. Since the erection of the family Whatcheeriidae, the term ‘whatcheeriid’ has been applied to an increasingly broad set of specimens from both the Devonian (Daeschler et al., 2009; Olive et al., 2016; Broussard et al., 2018) and Mississippian (Anderson et al., 2015; Greb et al., 2016). Many of these are fragmentary and the basis for these attributions is unclear. The result is spurious phylogenetic precision: numerous whatcheeriids but no clear idea of what a ‘whatcheeriid’ is. The potential of the whatcheeriids to contribute to understandings of lineage diversity and timing of branching events within Romer’s Gap is thus greatly limited.

Fortunately, significant new data are available. *Whatcheeria* is now represented by hundreds of specimens, most of which are unstudied. These include three-dimensionally preserved bones, complete skulls, and multiple articulated individuals. Such a collection is extremely rare and provides a golden opportunity to build a complete anatomy of an early tetrapod. These new *Whatcheeria* data may provide the basis for an improved character diagnosis for Whatcheeriidae and resolution of the ‘whatcheeriid question’. Mobilization of these new data requires the creation of new characters and a new data matrix to test phylogenetic hypotheses. What is the structure of the tetrapod stem group? How is the crown group diagnosed and defined? What is the reconstructed pattern of character evolution along the tetrapod stem into the tetrapod crown?

Previous hypotheses (summarized by Romer (1958) and Clack and Coates (1995)) of early tetrapod paleoecology focused on the origin of limbs. These hypotheses differed on the environmental conditions and functional drivers of limb evolution; Romer’s midcentury

synthesis proposed that that tetrapod limbs evolved in order to haul tetrapods from drying pools to healthier water bodies (Romer, 1958). This is the origin of the popular images of the lobe-finned fish hauling itself overland and the 'half-in and half-out' early 'amphibian'. The consensus was that Devonian tetrapods were primarily aquatic. Importantly, Romer noted that in addition to the lack of apparent terrestrial adaptations in the limbs of *Ichthyostega*, there did not appear to be much extrinsic motivation for tetrapod terrestriality in the Devonian (Romer 1958, p.367):

> Like their crossopterygian ancestors, the early tetrapods appear to have been, universally, eaters of animal food […] And the potential food supply on land appears to have been meager […] Scorpions do not, however, appear to be too nourishing a base upon which to found a flourishing terrestrial vertebrate fauna.

Assemblage descriptions (Milner, 1980b; Smithson, 1980; Boyd, 1984; Clarkson, 1985) and larger biogeographic studies were compiled (Milner et al., 1986; Milner, 1987), but these were all restricted to the coal swamp localities of the Late Carboniferous (Pennsylvanian). While the non-tetrapod organisms of the East Kirkton tetrapods were described in detail (Clarkson et al., 1993; Jeram, 1993; Shear, 1993), the three primary Devonian tetrapods are not so well-contextualized. There have yet not been any comparative ecological syntheses spanning the Late Devonian and Mississippian. Taxonomic loss and functional loss have been known to vary separately in other mass extinctions (McGhee et al., 2004; Foster and Twitchett, 2014; Foster et al., 2022). Paleoecological modeling of paleocommunities bracketing the end-Permian mass extinction has found changes in community-level properties such as stability and resistance to perturbation following the extinction event (Roopnarine, 2009; Roopnarine et al., 2018, 2019; Huang et al., 2021). What does the taxonomic change through the EDME mean for the structure

and properties of post-EDME communities? What evolutionary and ecological processes created the post-Devonian world?

1.2 SUMMARY OF RESEARCH

The aim of this dissertation is to investigate the anatomical and functional transitions between the tetrapod stem and crown groups, the timing of the tetrapod crown group origin during the early Mississippian, and ecological response to the end-Devonian mass extinction. In the first chapter, I redescribe the postcranial anatomy of the Mississippian tetrapod *Whatcheeria*. *Whatcheeria* has been part of early tetrapod phylogenetic datasets since its description in 1995 and is the namesake and type genus of the family Whatcheeriidae. Originally restricted to the Tournaisian-Visean (Clack, 2002c), taxa and specimens from the Frasnian-Serpukhovian have been either explicitly included within the family (*Ossinodus*) or provisionally referred to as 'whatcheeriid' or 'whatcheeriid-like' (Clement et al., 2004; Anderson et al., 2015; Greb et al., 2016; Olive et al., 2016; Broussard et al., 2018; Otoo et al., 2018; Ahlberg and Clack, 2020). Preparation has revealed hundreds of *Whatcheeria* specimens, which represent a rich new body of data with which to refine the definition of Whatcheeriidae and resolve the status of associated problematica. In the second chapter, I conduct a phylogenetic analysis of early tetrapods using a new dataset. This dataset includes new data from *Whatcheeria* as well as recently discovered tetrapods from Romer's Gap. The character list includes characters drawn from multiple existing matrices as well as new creations for a more independent test of relationships. This is done to test the impact of new *Whatcheeria* data on tree topology and patterns of character change along the tetrapod stem into the crown group. Analyses of anatomical partitions attempt to assess patterns of phylogenetic signal across the early tetrapod skeleton and their possible paleobiological

implications. Age estimates for the tetrapod crown group are considered within the context of the origin of Mississippian tetrapods broadly, and the extent to which this diversity is the product of Devonian or Mississippian divergence events. In the third chapter, I use a new dataset of Givetian-Serpukhovian vertebrate communities and ecological modeling methods to analyze community structure and perturbation response through the end-Devonian mass extinction. This is done to test the hypothesis that the taxonomic turnover at the Devonian/Carboniferous boundary was accompanied by changes in the diversity and richness of functional groups and that stability of ecological communities decreased in the aftermath of the extinction (Tournaisian) followed by recovery and increase in stability (Visean and later).

CHAPTER 2: THE POSTCRANIAL ANATOMY OF *WHATCHEERIA DELTAE*

Published in modified form as: Otoo, B.K.A., Bolt, J.R., Lombard, R.E., Angielczyk, K.D., and Coates, M.I., 2021, The postcranial anatomy of *Whatcheeria deltae* and its implications for the family Whatcheeriidae: Zoological Journal of the Linnean Society, v. 193, p. 700–745.

2.1 ABSTRACT

Here we describe the postcranial skeleton and present the first full-body reconstruction of the early tetrapod *Whatcheeria deltae* from the Viséan of Iowa. The skeletal proportions, including an elongate neck and large limbs, are unlike those of other Devonian and Mississippian tetrapods. The robust limbs of *Whatcheeria* appear adapted for a walking gait, but the lateral lines of the cranium are fundamentally unsuited for sustained subaerial ex*posure.* Thus, although *Whatcheeria* bears a general resemblance to certain terrestrially-adapted Permian and Triassic members of crown tetrapod lineages, its unusual form signals a broader range of early amphibious morphologies and habits than previously considered. From the exceptionally rich collection it is evident that most *Whatcheeria* specimens represent immature individuals. Rare specimens suggest an adult body size of at least 2m, over twice that of the holotype. Further comparison suggests that the *Pederpes* holotype might also be a juvenile and reveals a combination of hindlimb characters unique to *Whatcheeria* and *Pederpes*. These new data contribute to a revised diagnosis of the family Whatcheeriidae and a reevaluation of fragmentary Devonian-Carboniferous fossils reported as ‘whatcheeriid’ but sharing no synapomorphies with the more precisely defined clade.

2.2 INTRODUCTION

Whatcheeria deltae was first described by (Lombard and Bolt, 1995). Dating to the middle/late Viséan, it was then the second-oldest tetrapod from North America. Characterized as "gratifyingly primitive"(Lombard and Bolt, 1995), it combined a plesiomorphic lower jaw and lateral line system with 'anthracosaur'-like tabular horns, minimal dermal ornament, and lack of an ossified gill skeleton. Since the original description, the study of early tetrapods has been transformed by new discoveries (Clack, 2002c; Warren and Turner, 2004; Clack and Finney, 2005; Warren, 2007; Clack et al., 2016; Ahlberg and Clack, 2020), new descriptions (Coates, 1996; Jarvik, 1996; Clack, 1997; Ruta et al., 2002, 2020), new phylogenies (Ruta et al., 2003a; Ruta and Coates, 2007; Clack et al., 2016; Pardo et al., 2017b; Marjanović and Laurin, 2019) and applications of new methods (Ruta et al., 2006, 2018; Wagner et al., 2006; Ruta and Wills, 2016; MacIver et al., 2017). Imaging technology advances have enabled the extraction of previously unavailable anatomical data (Porro et al., 2015; Clack et al., 2016; Pardo et al., 2017b; Herbst and Hutchinson, 2018; Lennie et al., 2020). The net result has been a sea-change in terms of knowledge, perspectives, and the sophistication of questions asked. More and more, the field has moved from reconstructing patterns of character acquisition to explorations of the diversity and paleobiology of the early tetrapod radiations (Sallan and Coates, 2010; Bennett et al., 2016; Clack et al., 2016; Bennett et al., 2017; Otoo et al., 2018; Pardo et al., 2019b; Byrne et al., 2020). In particular, the broad shift in phylogenetic hypotheses around the turn of the millennium (Ruta and Coates, 2007) transferred many taxa- including *Whatcheeria*- from the tetrapod crown to the tetrapod stem (Coates, 1996; Paton et al., 1999). This has raised two key questions: which, and how many, taxa populate the tetrapod stem?

After the discovery of *Pederpes* from the Tournaisian of Scotlaclack 2002nd, the family Whatcheeriidae was erected to contain it and *Whatcheeria* (Clack, 2002c). The family was not defined by autapomorphies but on the basis of a combination of seemingly primitive and derived characters. *Ossinodus,* from the Viséan of Australia (Warren, 2007) was initially referred to the family on the basis of shared characters and a phylogenetic analysis that placed it as the immediate sister taxon to *Whatcheeria*/*Pederpes*. However, subsequent discoveries and analyses challenged this hypothesis (Warren, 2007) and moved *Ossinodus* to branch from a more basal node on the tetrapod stem. Discoveries of additional Devonian-Carboniferous tetrapod fragments with putative anatomical similarities to *Pederpes* or *Ossinodus* or close relationships to them in phylogenetic analyses (Clack and Ahlberg, 2004; Daeschler et al., 2009; Anderson et al., 2015; Olive et al., 2016; Broussard et al., 2018; Ahlberg and Clack, 2020) further weakened the definition of Whatcheeriidae. In many cases, the cited characters are not unique to *Whatcheeria*/*Pederpes*/*Ossinodus* or shared by all three genera. This has, in turn, led to the hypothesis that whatcheeriids are not a clade but are instead a grade. Furthermore, *Pederpes* and *Ossinodus,* not *Whatcheeria*, have been used as comparisons in classifying fragmentary 'whatcheeriid' material, which currently encompasses ~50Ma spanning the Devonian/Carboniferous boundary. Despite these uncertainties, whatcheeriids are an important but ill-defined part of our understanding of tetrapod evolution in the period spanning the Hangenberg event and its aftermath (Becker et al., 2016; Kaiser et al., 2016; Zhang et al., 2020).

Here we describe the postcranial skeleton of *Whatcheeria deltae*. Since the original description of *Whatcheeria* (Lombard and Bolt, 1995), a series of publications have discussed its general morphology and inferred ecology (Bolt and Lombard, 2000), described the lower jaw

(Lombard and Bolt, 2006), and palate and braincase (Bolt and Lombard, 2018). Over this period, preparation of specimens increased the quantity of informative *Whatcheeria* material and so the amount of available anatomical data. These data will be presented in a comparative context and used to reevaluate the taxonomic status of whatcheeriids.

2.3 MATERIALS AND METHODS

All *Whatcheeria* specimens come from the now-defunct Jasper Hiemstra Quarry (Bolt et al., 1988; Lombard and Bolt, 1995; Bolt and Lombard, 2018). For details of geology and sedimentology see Snyder (2006); for details of specimen preparation see (Lombard and Bolt, 1995; Bolt and Lombard, 2018). All *Whatcheeria* specimens studied are stored at the Field Museum of Natural History. Additional comparative material was examined at the Field Museum, Museum of Comparative Zoology, Queensland Museum, and Cleveland Museum of Natural History. Further comparative data were obtained from the literature. Specimen photos were taken using a Nikon D50 camera with Nicor 18-55mm lens, Canon EOS7D camera with a Canon 17-55mm lens, and a Canon EOS70D camera with Canon 17-55mm, Canon 100mm, and Sigma 18-50mm lenses. Figures were created in Photoshop CC 2018 (Adobe, San Jose, CA).

To quantitatively compare *Whatcheeria*'s body proportions to other early tetrapods, linear measurements were gathered from published figures using Photoshop and used to calculate dimensionless ratios. Taxa were selected primarily on the basis of data availability, as well as ecomorphological disparity. Although the sample is focused on Famennian and Mississippian tetrapods, select Permian (White, 1939; Berman et al., 2000; Pawley and Warren, 2006; Bazzana et al., 2020) and Triassic (Schoch, 1999; Schoch and Rubidge, 2005) taxa were also included.

Principal components analysis (PCA) was conducted to compare taxa and visualize the data. PCAs were conducted in RStudio (RStudio Team, 2019) for R (R Core Team, 2019) using the following packages: stats (R Core Team, 2019), graphics (R Core Team, 2019), factoextra (Kassambara and Mundt, 2020), ggplot2 (Wickham, 2016), ggfortify (Tang *et al*., 2016), and ggrepel (Slowikowski, 2020).

2.3.1 Institutional abbreviations

FMNH, Field Museum of Natural History, Chicago, Illinois, USA; SUI, University of Iowa, Iowa City, Iowa, USA; QMF, Queensland Museum, Brisbane, Queensland, Australia; NSM, Nova Scotia Museum, Halifax, Nova Scotia, Canada; YPM PU, Yale Peabody Museum, New Haven, Connecticut, USA; CMNH, Cleveland Museum of Natural History, Cleveland, Ohio, USA; CMC, Cincinnati Museum Center, Cincinnati, Ohio, USA; MCZ, Museum of Comparative Zoology, Harvard University, Cambridge, Massachusetts, USA; IRSNB, Institut royal des Sciences naturelles de Belgique, Brussels, Belgium; NMMNH, New Mexico Museum of Natural History and Science, Albuquerque, New Mexico, USA.

2.3.2 Anatomical abbreviations

4TR, fourth trochanter; AB, adductor blade; ACT, acetabulum; AFPC, anterior facet of pleurocentrum; ATL, atlas; ATR, anterior trunk rib; ATRN, notch in anterior trunk rib; AX, axis; AZYG, anterior zygapophysis; BIN, brachialis inferior; BSO, basioccipital; CAR, caudal rib; CER, cervical rib; CLE, cleithrum; CLELO, cleithrum lateral overlap with scapulocoracoid; CLEMO, cleithrum medial overlap with scapulocoracoid; CLV, clavicle; CLVDP, dorsal process of the clavicle; CLVG, groove on the dorsal process of the clavicle; CLVP, clavicle plate; CPL,

carpal; CRV, cervical vertebra; DLT, deltoideus; DP, deltoid process; DPC, deltopectoral crest; DR, dorsal ridge; DTR, distal tarsal; FC, fibular condyle; FEM, femur; FIB, fibula; HFC, humerus foramen ‘C’; HP2, humerus process 2; HP3, humerus process 3; HP4, humerus process 4; HS, hemal spine; HUM, humerus; IC, intercentrum; ICLV, interclavicle; ICLVO, interclavicle facet for clavicle overlap IL, ilium; ITR, internal trochanter; LDO, latissimus dorsi; LDP, latissimus dorsi process; LSC, levator scapuli; FLA, flexor radialis; FLU, flexor ulnaris; NS, neural spine; OFA, obturator foramen; OMO, omohyoideus; PBL, postbranchial lamina; PC, pleurocentrum; PEC, pectoralis; PFPC, posterior facet of pleurocentrum; PHLG (MAN), manual phalanges; PHLG (PED), pedal phalanges; PHLG, phalanges; PLC, pleurocentrum; PLS, popliteal space; PLV, pelvis; PNF, pineal foramen; PP, pectoral process; PR, pectoral rib; PSP, parasphenoid; PTR, posterior trunk rib; PZYG, posterior zygapophysis; RA, radius; SCH, scapulohumeralis; SCR, scapulocoracoid; SLO, supinator longus; SUC, supracoracoideus; SUS, subscapularis; TC, tibial condyle; TIB, tibia; TR, trunk rib; TRC, triceps; TRP, trapezius; TV, trunk vertebrae; TVP, transverse process of neural arch; UL, ulna; VRH, ventral ridge of the humerus; XRA, extensor radialis; XUL, extensor ulnaris; ZYG, zygapophysis.

2.4 RESULTS

2.4.1 Systematic paleontology

TETRAPODA (Jaekel, 1909)

WHATCHEERIIDAE (Clack, 2002c)

Revised diagnosis: Tetrapods characterized by: narrow, steep-sided skull; orbit subrectangular, deeper than wide; steeply angled suspensorium with deep temporal notch; tooth rows on vomers, palatines and ectopterygoids; maxillary caniniform teeth; nearly continuous row of coronoid teeth; lateral lines manifest as grooves and canals in cranial dermal bone; tabular with small ornamented 'button' termination; intertemporal/squamosal contact; mandibular lateral line (=oral lateral line) runs from splenials onto surangular; dermal ornament minimal; grooved, denticulated parasphenoid; parasphenoid very short behind basipterygoid processes with U-shaped posterior margin; uncinate processes on ribs; opening or notch proximal to uncinate process on at least some trunk ribs; spike-like latissimus dorsi process on humerus; ilium with short, broad dorsal and posterior processes; striations or grooves on posterior iliac process; femoral internal trochanter absent; femoral adductor blade bears fourth trochanter; fourth trochanter broad, flat-topped, and rugose.

GENUS *Whatcheeria deltae* (Lombard and Bolt, 1995)

Type and only species: *Whatcheeria deltae* (Lombard and Bolt, 1995)

Holotype: FMNH PR 1700, skull associated with presacral vertebral column, partial shoulder girdle, ribs, and partial right hindlimb.

Type horizon and locality: Fills within two adjacent collapse structures formed in the Waugh and Verdi Members of the Iowa 'St Louis' Limestone, exposed at the Jasper Hiemstra Quarry (SW1/4, S11/4, section 15, T75N, R13W) near Delta, Keokuk County, Iowa, USA (Figure 2.1).

See (Bolt et al., 1988; Lombard and Bolt, 1995) for additional details. The Hiemstra Quarry has been dated to the latest Viséan-earliest Serpukhovian, 333-326Ma (Snyder, 2006).
Referred specimens: 26 specimens; approximately 375 additional specimens are referable with varying degrees of confidence. See Supplementary Information for details.

Revised diagnosis: Whatcheeriid with the following apomorphies: cleithrum dorsal apex subrectangular with posterior notch; pleurocentra fused dorsally and open ventrally; posterior iliac process broad, rounded, with marked fluting; entepicondyle massive, approximately 50% of total humerus volume. Characters with broader distribution: large parietal foramen surrounded by raised rim; prefrontal forms thick ridge at anterodorsal orbit margin with mesial projections; stapes with short shaft; large maxillary fangs at positions 6 and 7; premaxilla with substantial palatal shelf; pectoral ribs morphologically distinct; anterior trunk ribs approximately 80% of scapular length in lateral view; interclavicle fan-shaped; forelimb and hindlimb lengths equal; olecranon process large; manus with digital formula 3-4-5-5-4 (2-3-4-4-3 excluding 'metacarpals'); pes with digital formula 3-4-5-5-5 (2-3-4-4-4 excluding 'metatarsals'); phalanges as broad or broader than long; adult body size ~2m or greater.

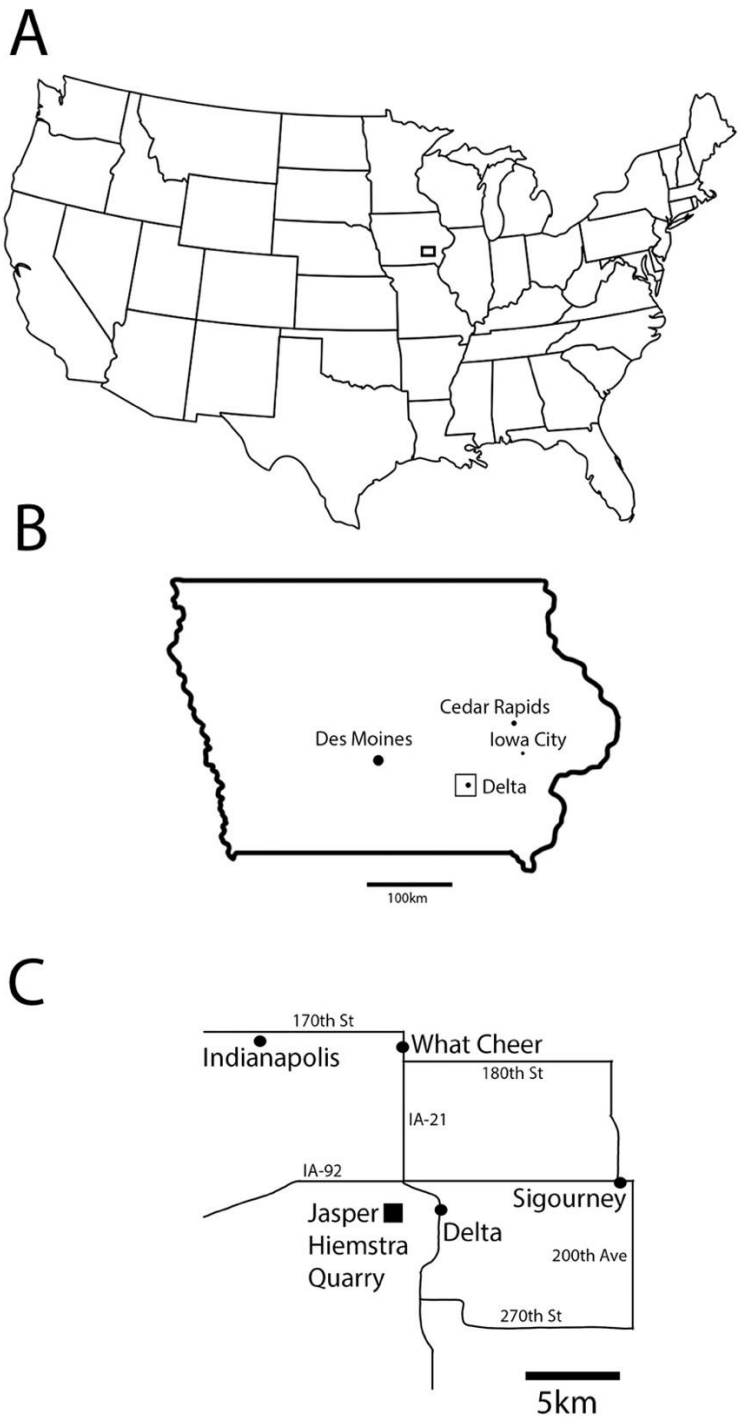

Figure 2.1. Location of the Jasper Hiemstra Quarry. A) map of the contiguous United States with a rectangle highlighting the relevant area; B) simplified map of Iowa showing major cities and Delta, rectangle highlighting Keokuk County; C) partial map of Keokuk County, Iowa showing the Jasper Hiemstra Quarry in relation to Delta and other nearby towns. Keokuk County map modified from (Snyder, 2006)

2.4.2 Comparative description

2.4.2.1 Axial skeleton

The full-body reconstruction (Figure 2.2, Figure 2.3) has been restored with an axial column comprised of 54 vertebrae. There are 26 presacral vertebrae, including the atlas-axis complex (counted as two vertebrae). This is slightly more than the estimate of 24 for *Pederpes* (Clack and Finney, 2005). The cervical series (Figure 2.3, Figure 2.6) includes five vertebrae posterior to the atlas-axis, contributing to a total count of seven. The following two vertebrae are associated with the pectoral region, and the remaining 17 presacral vertebrae form the trunk. The single sacral vertebra precedes a caudal series restored with 27 vertebrae, estimated from multiple specimens (see description of vertebrae and Supplementary Information). Specimens with the most complete axial skeletons forming the basis of the restored vertebral column include the holotype FMNH PR 1700 (Figure 2.4), FMNH PR 1816 (Figure 2.5, Figure 2.6), and FMNH PR 1875 (Figure 2.7).

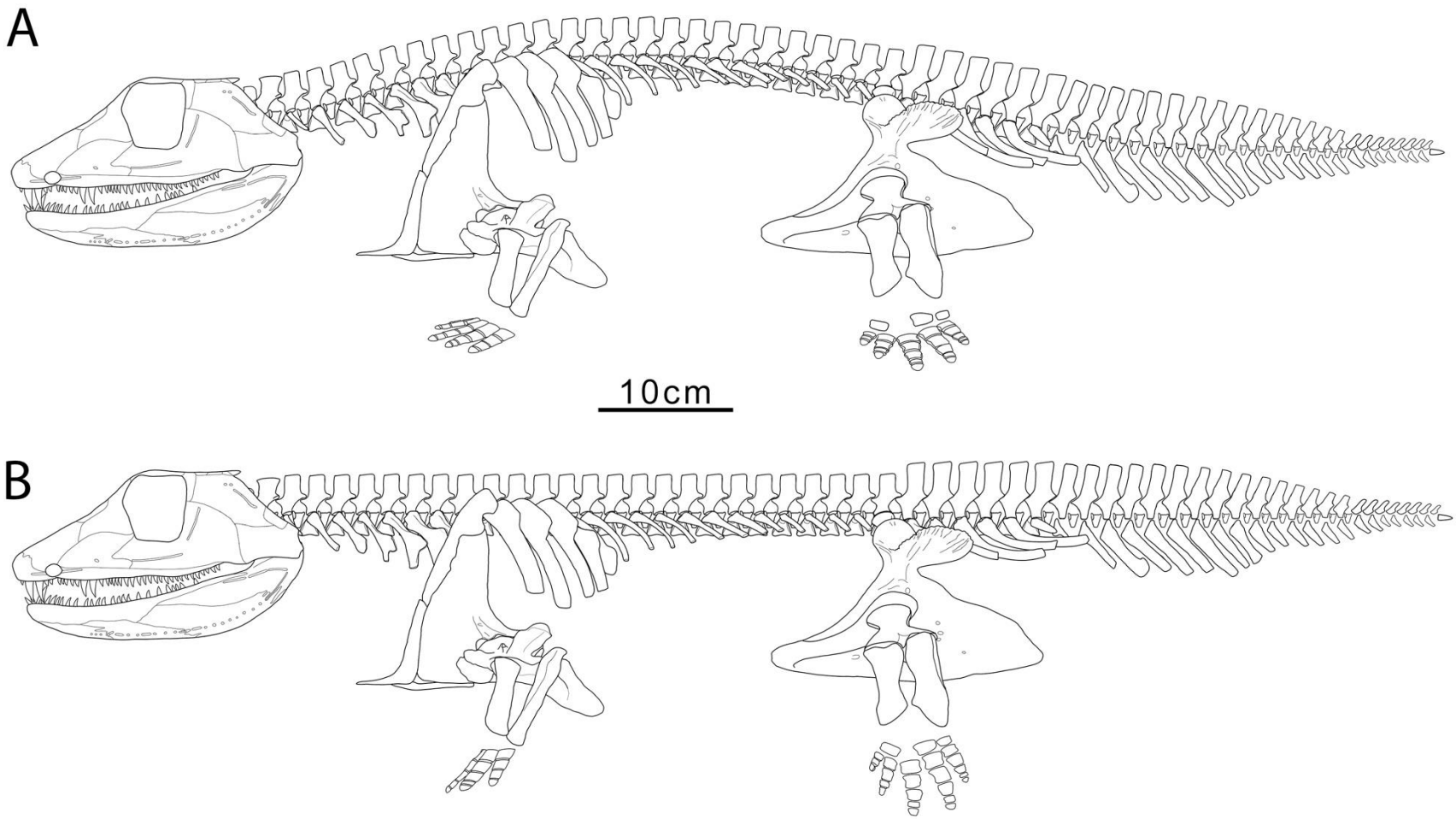

Figure 2.2. *Whatcheeria deltae* full-body reconstruction in left lateral view. A, standing posture; B, floating posture. The reconstruction is meant to depict an anatomically mature individual of approximately 1m body length.

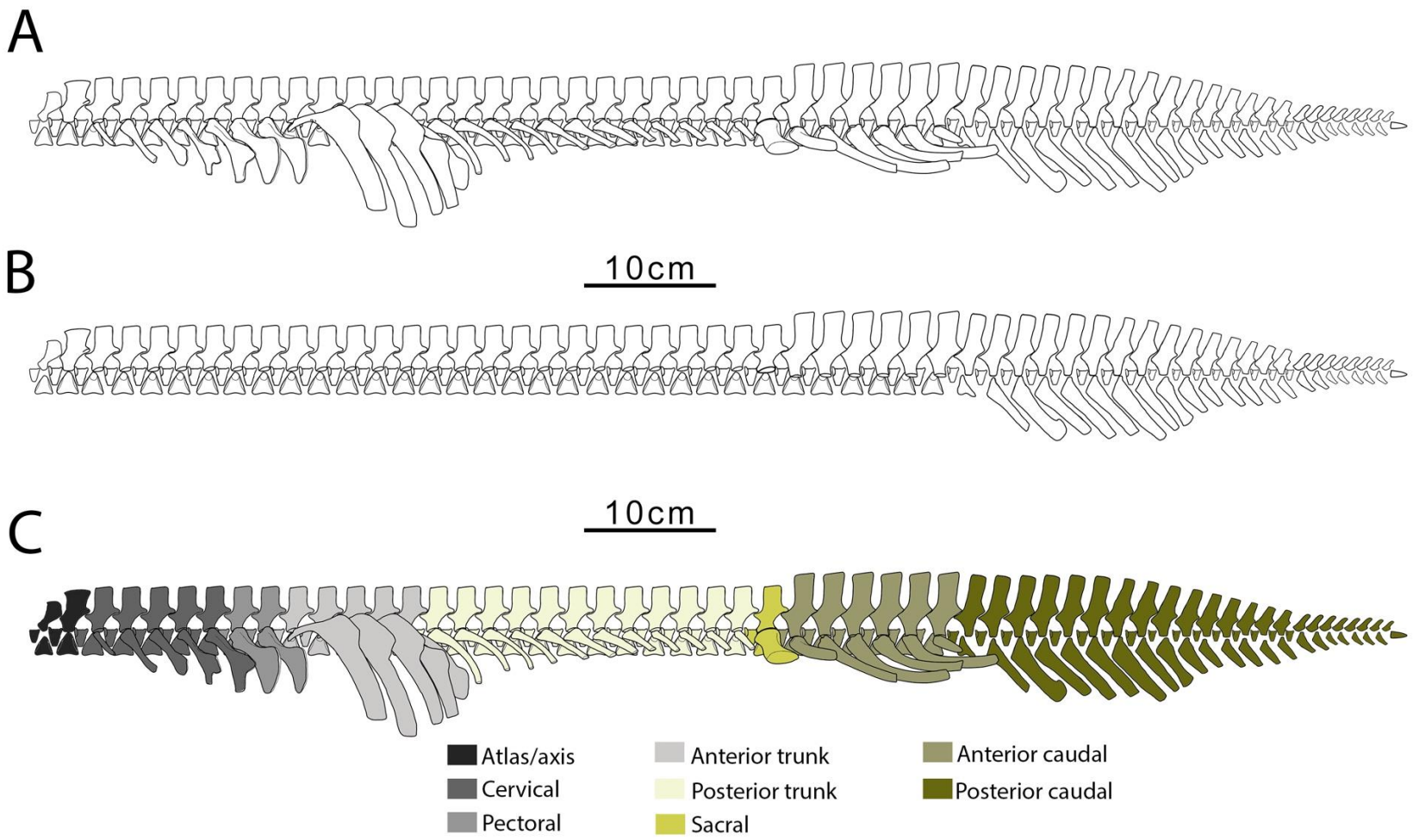

Figure 2.3. *Whatcheeria deltae*, reconstruction of axial skeleton with ribs (A), without ribs (B), ribs, colour-coded by region (C).

Figure 2.4. FMNH PR 1700, articulated holotype of *Whatcheeria* (skull removed for study). A, specimen photo; B, interpretive drawing with labels. Arrows point anteriorly.

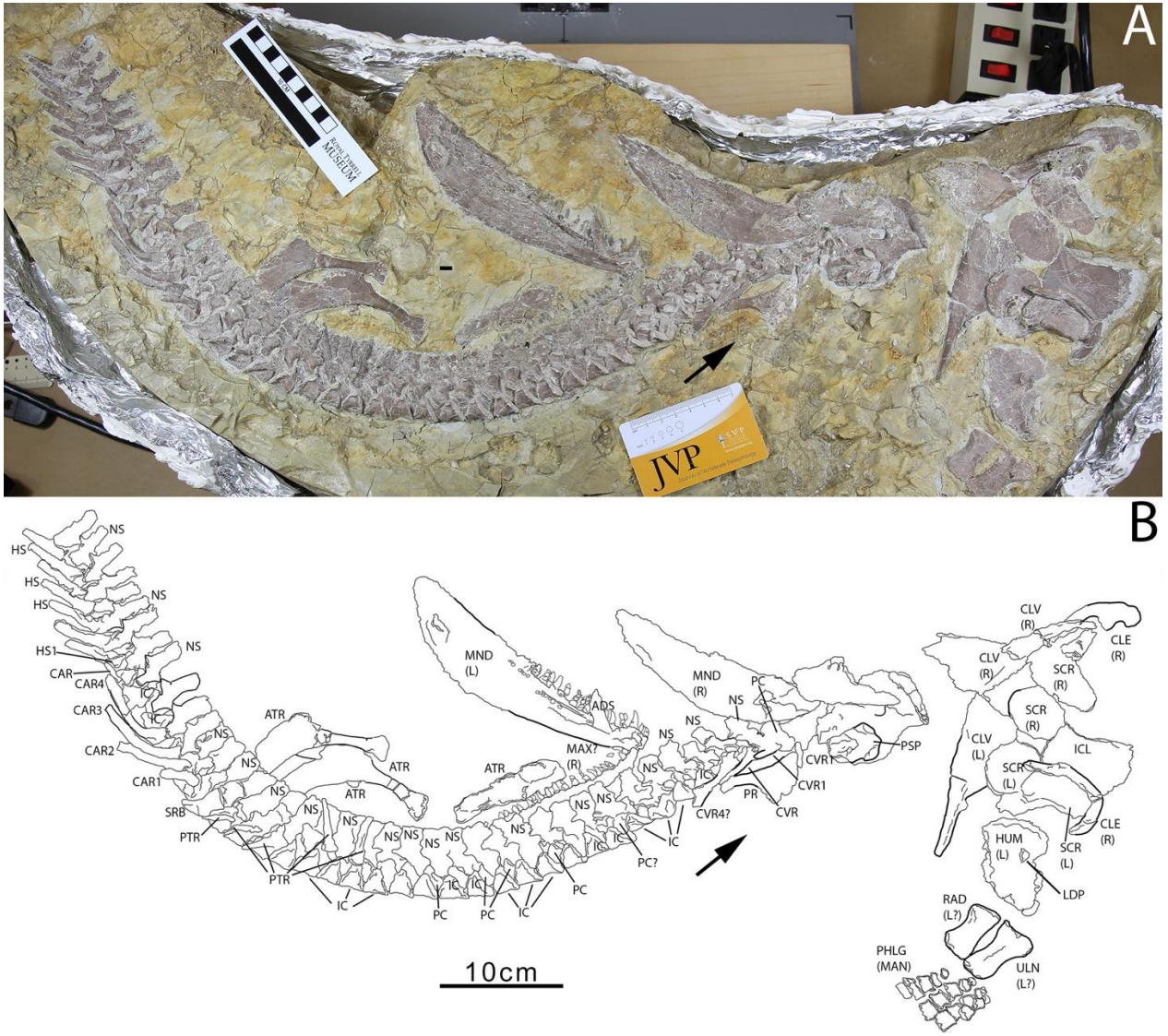

Figure 2.5. FMNH PR 1816, articulated specimen of *Whatcheeria*. A, specimen photo; B, interpretive drawing with labels. Arrows point anteriorly.

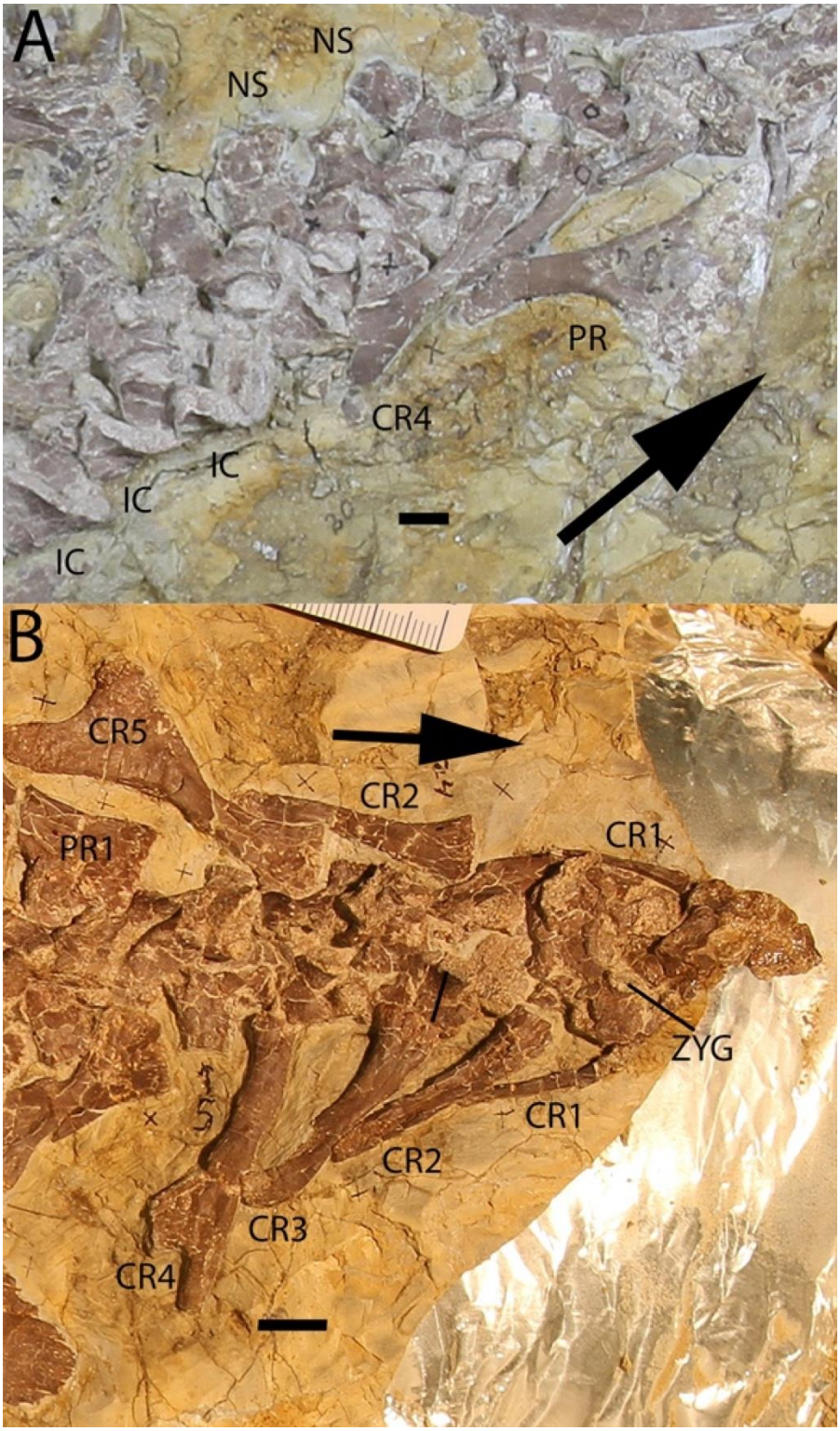

Figure 2.6. Articulated cervical vertebrae and ribs of *Whatcheeria*. A, cervical region of FMNH PR 1816 in ventrolateral view; B, cervical region of FMNH PR 1700 in dorsal view. Arrows point anteriorly. Scale bar in here and in following figures equals 1 cm unless otherwise noted.

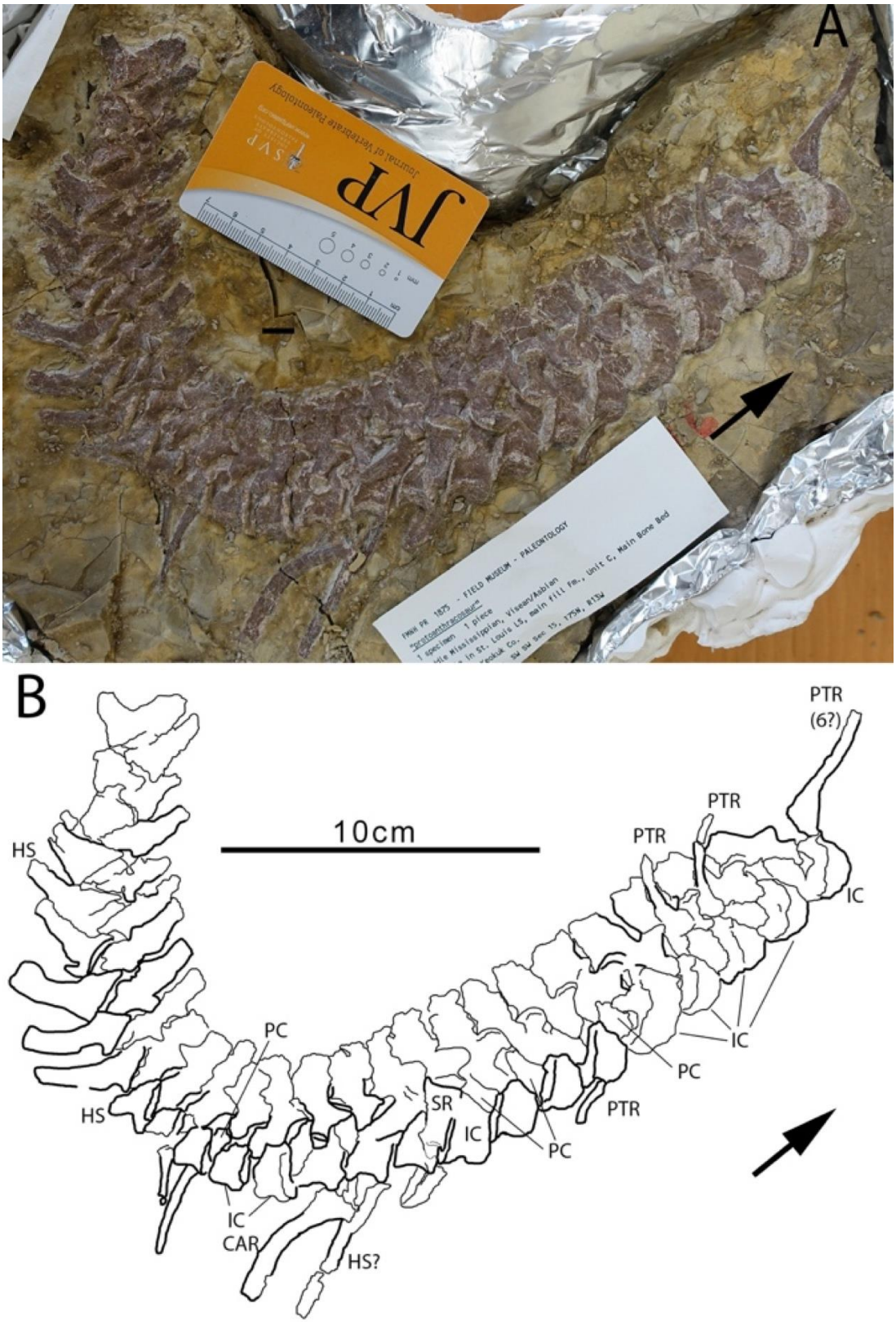

Figure 2.7. FMNH PR 1875, articulated specimen of *Whatcheeria*. A, specimen photo; B, interpretive drawing with labels. Arrows point anteriorly.

The precaudal vertebrae of *Whatcheeria* are rhachitomous, each composed of an anterior pleurocentrum (open ventrally), intercentrum (open dorsally) and neural spine (Figure 2.8). Each individual intercentrum or pleurocentrum is a single fused structure with no trace of a midline suture. The dorsal fusion of the pleurocentra and their opening ventrally is highly unusual, and thus far unique among Mississippian tetrapods. Each pleurocentrum has two large anterior facets for the preceding neural arch, and two much smaller posterior facets for the succeeding neural arch. Each intercentrum has a small lateral facet at each apex for articulation with the rib. The intercentra are about half again as large as the pleurocentra. Determining the degree of notochordal constriction is difficult, but was probably greater than that in *Greererpeton* (Godfrey, 1989) and comparable to *Ossinodus* (Warren, 2007). The neural spines are fused at the midline without trace of suture. The zygapophyses of the neural spines are well-developed throughout the presacral column. The anterior and posterior zygapophyses are roughly equal in length, in common with *Archeria* (Holmes, 1989b) and *Proterogyrinus* (Holmes, 1984), but unlike *Acanthostega* (Coates, 1996), *Greererpeton* (Godfrey, 1989), and *Pederpes* (Clack and Finney, 2005; Pierce et al., 2013b), where the enlarged anterior zygapophysis has a slanted appearance. The proportional lateral width of the anterior zygapophyses is similar to that in *Proterogyrinus*, *Greererpeton* and (probably) *Pederpes* (Pierce et al., 2013b) and greater than in *Acanthostega.*

As preserved, the dorsal margins of the neural arches often appear ragged (Figure 2.4-Figure 2.9). A similar phenomenon has been reported in *Caerorhachis*, where it has been interpreted as evidence of a cartilage cap in life (Ruta et al., 2002). However, this raggedness is

less prominent or absent in the best-preserved *Whatcheeria* specimens and might instead be partly a taphonomic artifact.

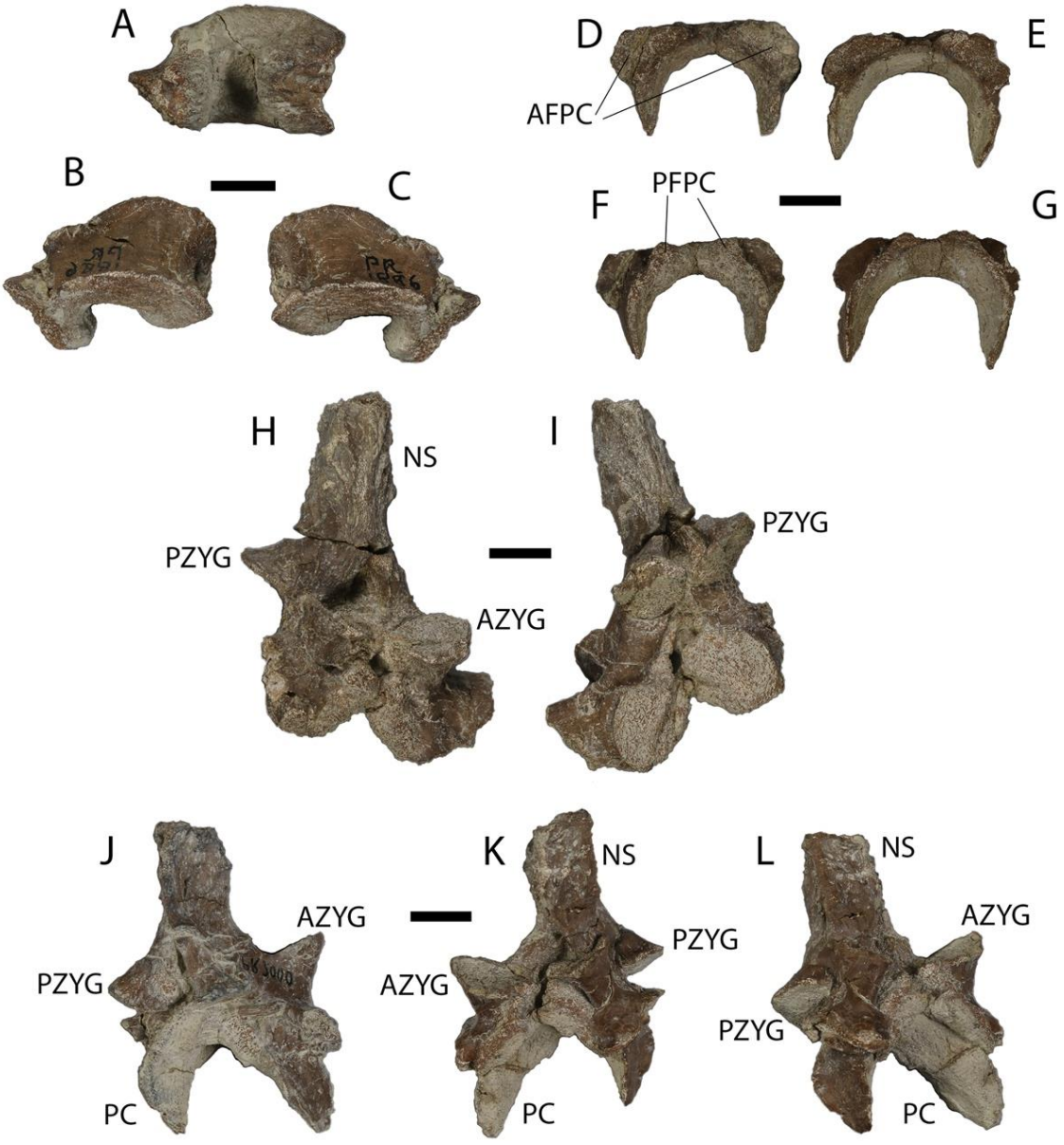

Figure 2.8. Vertebral components of *Whatcheeria*. FMNH PR 1886 intercentrum in dorsal (A) and ventrolateral (B, C) views; FMNH PR 1712 pleurocentra in anterior (D, E) and posterior (F, G) views; FMNH PR 4989 neural spine in anterior (H) and posterior (I) views; FMNH PR 2000 neural spine and pleurocentrum in right-posterior (J), anterior (K), and left-posterior (L) views.

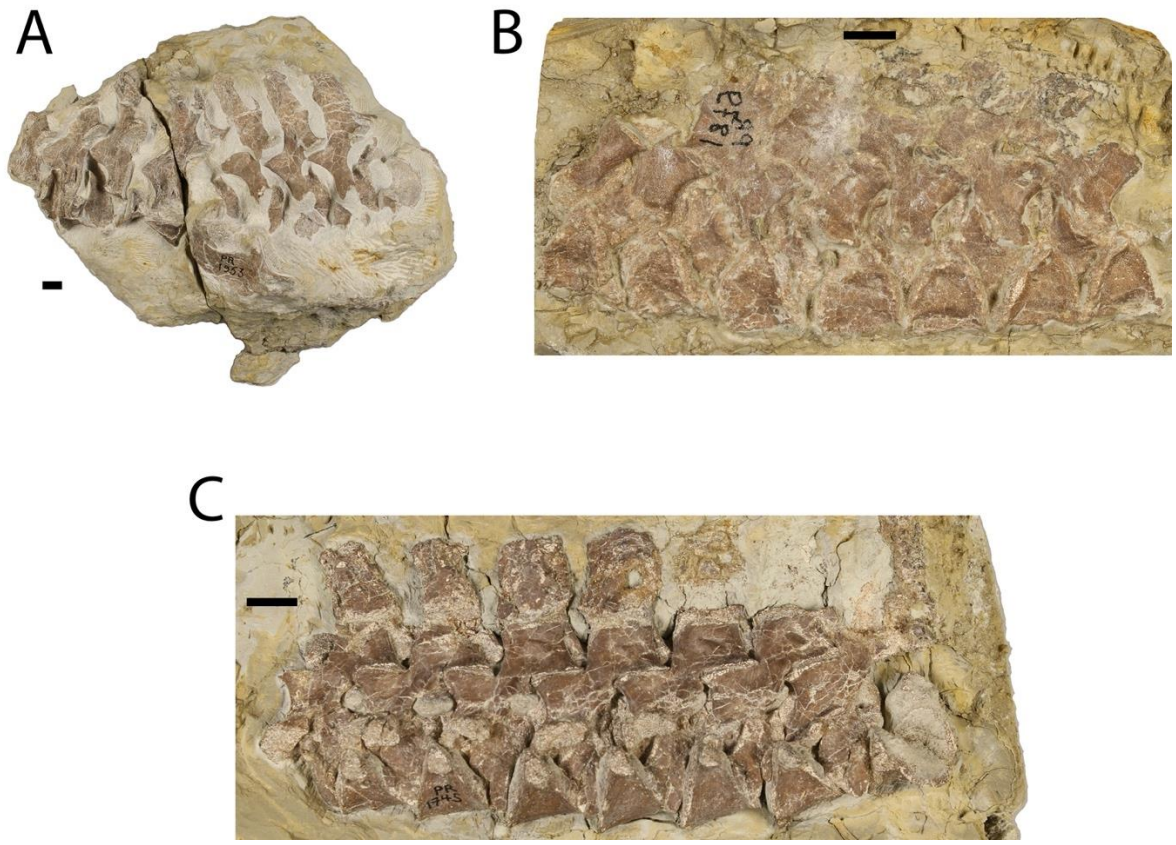

Figure 2.9. Articulated vertebrae of *Whatcheeria*. FMNH PR 1953 articulated caudal vertebrae in left lateral view (A); FMNH PR 1879 articulated vertebrae in left lateral view (B); FMNH PR 1745 articulated vertebrae in left lateral view (C). In all specimens, anterior is on the left and posterior is on the right.

Parts of the atlas/axis complex are present in FMNH PR 1701 and probably in FMNH PR 1634, FMNH PR 1635, and FMNH PR 1700 (Fig.10). In FMNH PR 1701, three centra are exposed in ventral view immediately posterior to the braincase (Figure 2.10C). Though all three are flattened, the anteriormost centrum is laterally broader than the other two and appears to have a median break or discontinuity. It is unclear whether or not this is taphonomic damage or if the two halves of the centrum were unfused. These centra likely belong to the atlas/axis complex, although their identities are uncertain. Atlantal/axial neural spines appear to be present in FMNH PR 1634 immediately posterior to the occiput, but the more anterior of these spines is very small

and covered by the more posterior, resembling a diminutive copy of other spines in the presacral series. The axial arch lacks an obvious facet for articulation with a rib, in contrast with *Pederpes* (Clack and Finney, 2005). At least some of the same bones preserved in FMNH PR 1634 seem to be present in FMNH PR 1700, but they are small and their state of preservation makes them hard to identify. We assume that none of the cervical material associated with the skull of FMNH PR 1700 is assignable to the cervical vertebrae that remain with the rest of the FMNH PR 1700 postcranial skeleton.

The reconstructed atlas/axis complex is shown in Figure 2.10J, mostly based on FMNH PR 1634 with significant guidance from *Acanthostega* (Figure 2.10H) and *Pederpes (*Figure 2.10I). As in those genera, the atlantal neural spine is restored without an anterior zygapophysis. The intercentra are restored without articulations for ribs but otherwise following the morphology of the other presacral intercentra. Atlas/axis centra size, relative to each other and to other presacral counterparts, cannot be assessed directly without a more complete presacral column in FMNH PR 1701 or better-preserved atlas/axis centra in FMNH PR 1534 and FMNH PR 1700. In the restored atlas/axis, the atlantal centra are smaller than those of the axis, following *Greererpeton* (Godfrey, 1989) and *Pederpes* (Clack and Finney, 2005).

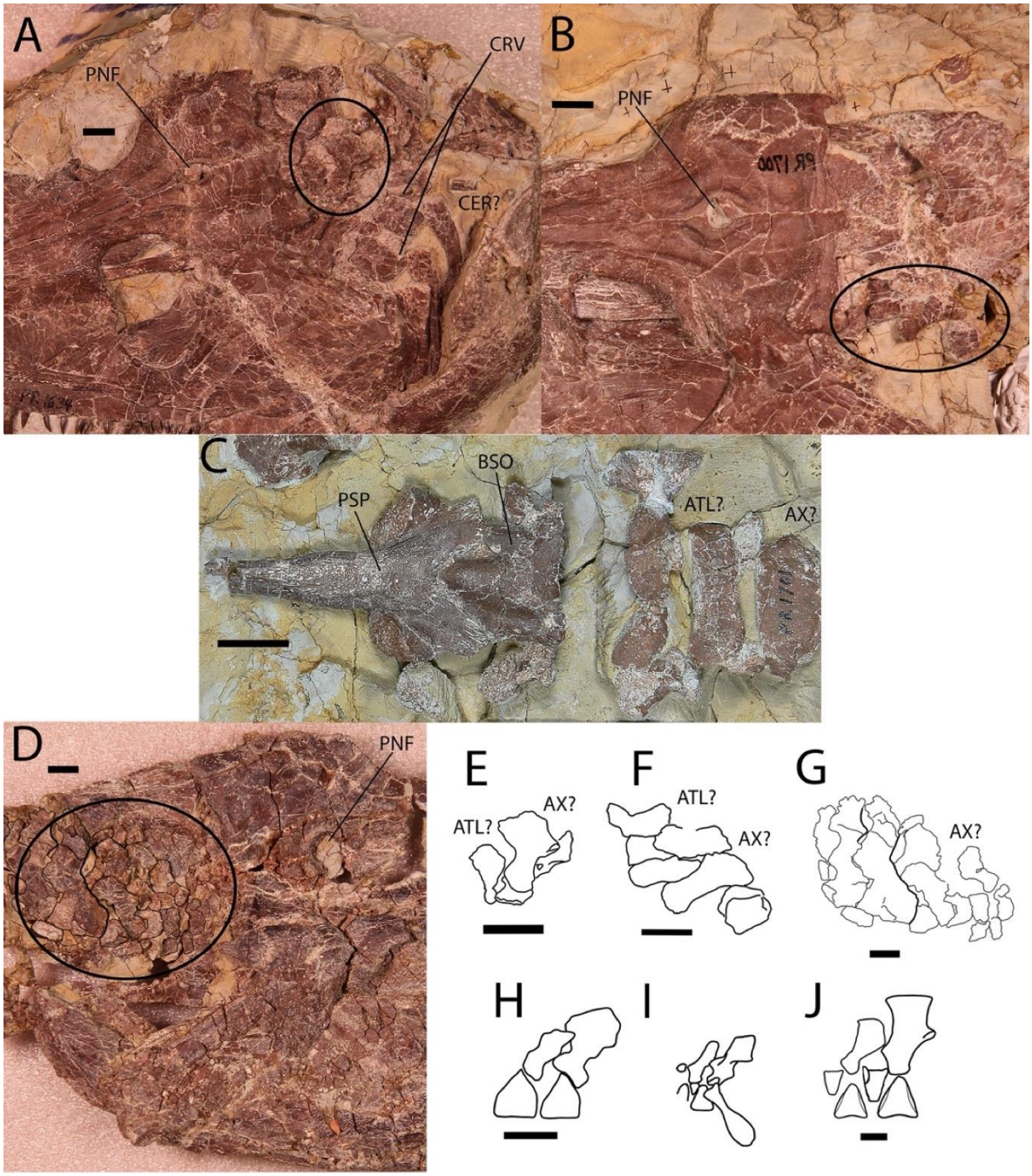

Figure 2.10. The atlas/axis of *Whatcheeria*. A, FMNH PR 1634, skull with jaws, cervical vertebrae, and partial shoulder girdle; B, FMNH PR 1700, skull with jaws; C, FMNH PR 1701, parasphenoid, basioccipital and partial atlas/axis complex; D, FMNH PR 1635, skull with jaws and cervical material. Areas where atlas/axis material is likely preserved are circled in A, B and D. E, interpretive drawing of possible atlas/axis material in FMNH PR 1634; F, interpretive drawing of possible atlas/ axis material in FMNH PR 1700; G, interpretive drawing of possible atlas/axis material in FMNH PR 1635; H, atlas/axis of *Acanthostega* modified from (Coates, 1996: fig. 7); I, atlas/axis of *Pederpes* modified from (Clack and Finney: fig. 18A); J, reconstructed atlas/axis of *Whatcheeria* in left-lateral view.

Vertebral morphology changes throughout the *Whatcheeria* axial skeleton. Neural spine height slightly increases posteriorly along the cervical series. Thereafter, the spines remain mostly uniform until the sacral neural spine, which has a much larger diapophysis for articulation with the sacral rib. The caudal neural spines are initially taller than the presacrals, and the first six caudal vertebrae have longer zygapophyses than the presacrals (Figure 2.2, Figure 2.3, Figure 2.5). After the caudal ribs (vertebra 34 onwards) the pleurocentra decrease in size and the neural spines become progressively shorter and have smaller zygopophyses. From vertebra 42 (caudal vertebra 16 onwards) the tail is poorly preserved. Vertebrae 42-54 have been restored taking into account the available specimens- FMNH PR 4998, FMNH PR 1816, and FMNH PR 1875- and guided by caudal series known from *Acanthostega* (Coates, 1996) and *Ichthyostega* (Jarvik, 1996; Pierce et al., 2012). No articulation facets for radials have been observed on any neural spines, and no radials have been found.

Ribs are present on all presacral vertebrae except for the atlas/axis (see above), as well as the sacral vertebra and the first six caudal vertebrae. In the following description, the numbering of ribs follows that of their respective centra.

The ribs are bicipital (Figure 2.11), though as in most early tetrapods the facets are incompletely separated. This poor definition is usually exacerbated by taphonomic flattening. The presacral ribs are morphologically differentiated into the following regions: cervical, pectoral, anterior trunk, and posterior trunk (Figure 2.3). Ribs 3-7 belong to the cervical series. The cervical ribs increase in size along the series, rib 3 being about 40% the length of rib 6. Ribs 5-7 bear uncinate processes near the distal end. The uncinate process of rib 5 is weakly

developed and contiguous with the rest of the rib, giving the distal tip a spoon-shaped appearance. Rib 6 is approximately 30% longer than rib 5, and is narrowed distal to the trapezoidal uncinate process. Rib 7 is thicker than rib 6 and about 20% longer. Its uncinate process is larger than that of rib 6 and more triangular in shape.

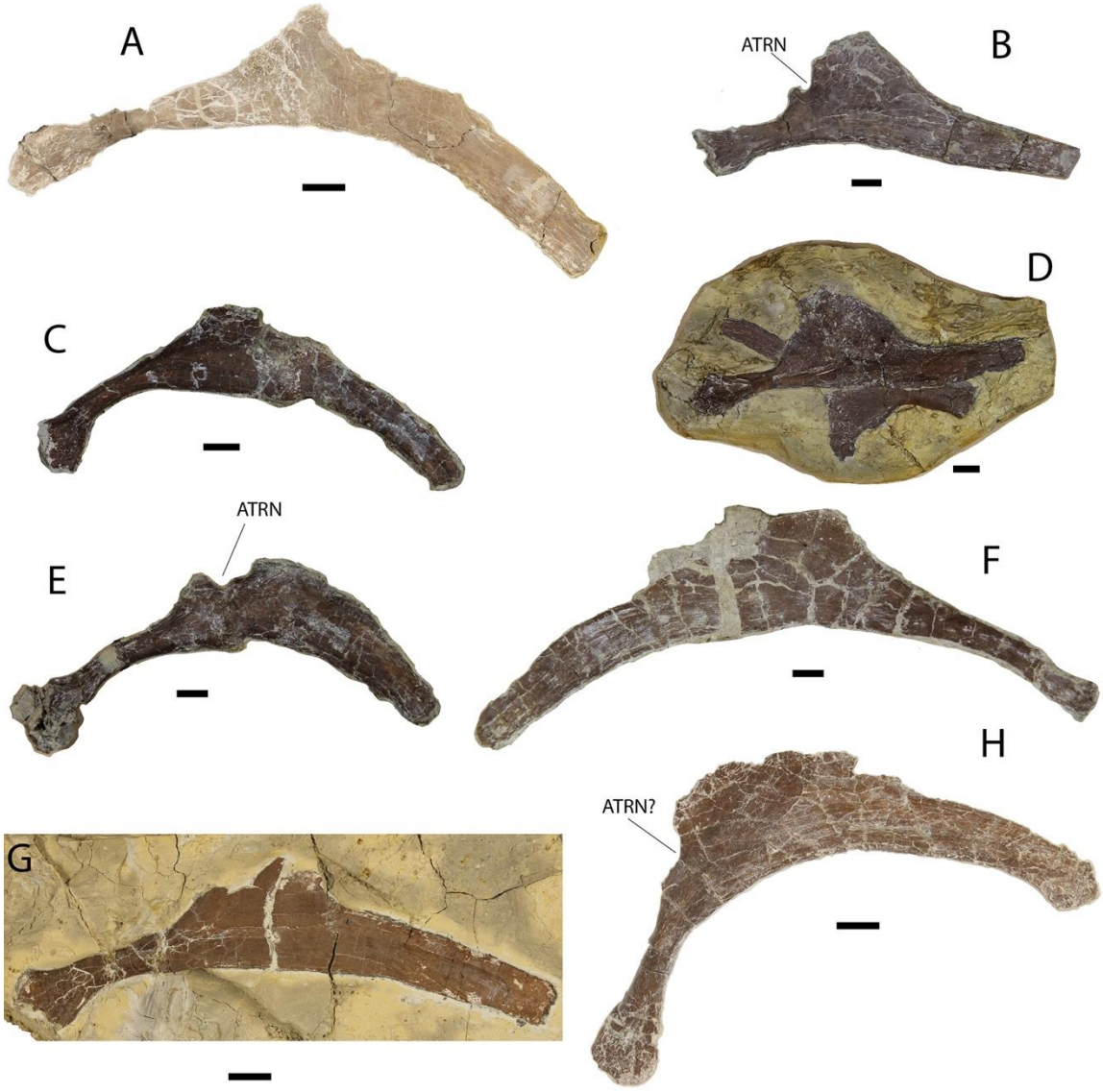

Figure 2.11. Isolated anterior trunk ribs of *Whatcheeria*. A, SUI 52036; B, FMNH PR 4991; C, FMNH PR 4992; D, FMNH PR 4993; E, FMNH PR 4990; F, FMNH PR 4994; G, FMNH PR 4995; H, FMNH PR 4996. Note the proximal notch in FMNH PR 4991 and FMNH PR 4990. In all specimens, proximal is on the left and distal is on the right.

The pectoral ribs, ribs 8 and 9, can be distinguished from the preceding cervical ribs and the following trunk ribs by their size and shape. Both are similar in length to rib 7 but much thicker. Although only about half as long as the anterior trunk ribs, these ribs are much stouter proximally, with larger articulations. Their uncinate processes are large and triangular, giving them a distinctive, bladed outline. The pectoral ribs are very similar in shape to similarly placed ribs in *Proterogyrinus* (Holmes, 1984) and *Archeria* (Holmes, 1989b) that are associated with the pectoral girdle. This assists with their identification in *Whatcheeria* as well as with pectoral girdle placement (see pectoral girdle description).

As noted in the original description, the anterior trunk ribs (ribs 10-14) are among the most distinctive features of *Whatcheeria* (Lombard and Bolt, 1995). The first three are long and curved, with trapezoidal or rectangular uncinate processes. The processes are smaller and more angular than those in *Ichthyostega* (Jarvik, 1996; Pierce et al., 2012) or *Eryops* (Moulton, 1974), though as in those taxa they most likely overlapped the following rib in life. Some isolated anterior trunk ribs (Figure 2.11) show a notch immediately proximal to the uncinate process (Figure 2.11, D, E). Clack and Finney (2005) described similar notches on ribs from the same region in *Pederpes*. Jarvik (1996) also noted similar features in isolated ribs of *Ichthyostega* and concluded that they received cutaneous blood vessels. However, this feature is not preserved well enough or consistently enough to determine its distribution in the rib series of *Whatcheeria*, so it has been omitted from the reconstruction. Rib 11 is the longest trunk rib overall and is about as long as the scapular blade of the scapulocoracoid; when projected in the reconstruction its apparent length in lateral view is reduced (Figure 2.2, Figure 2.3). This is similar to ribs in the same region in *Proterogyrinus*, *Archeria*, and *Ichthyostega*, as well as possibly *Eryops* (Moulton,

1974) and *Seymouria* (White, 1939; Berman et al., 2000). Rib 13 resembles its anterior neighbors but has a longer shaft and smaller uncinate process. The distal part of rib 14 is similar to that of rib 5, the uncinate process being contiguous with the rest of the rib and forming a spoon-shaped tip. A similar sequential change in anterior trunk rib size and uncinate process morphology is seen in *Mastodonsaurus* (Schoch, 1999).

The posterior trunk ribs (ribs 15-26) progressively decrease in length and curvature until about rib 20, at which point the rib shaft is straight and approximately the length of a neural spine. From rib 21 posteriorly they decrease in length until they are about the height of an intercentrum immediately anterior to the sacrum. They lack uncinate processes and are circular or ovoid in cross-section.

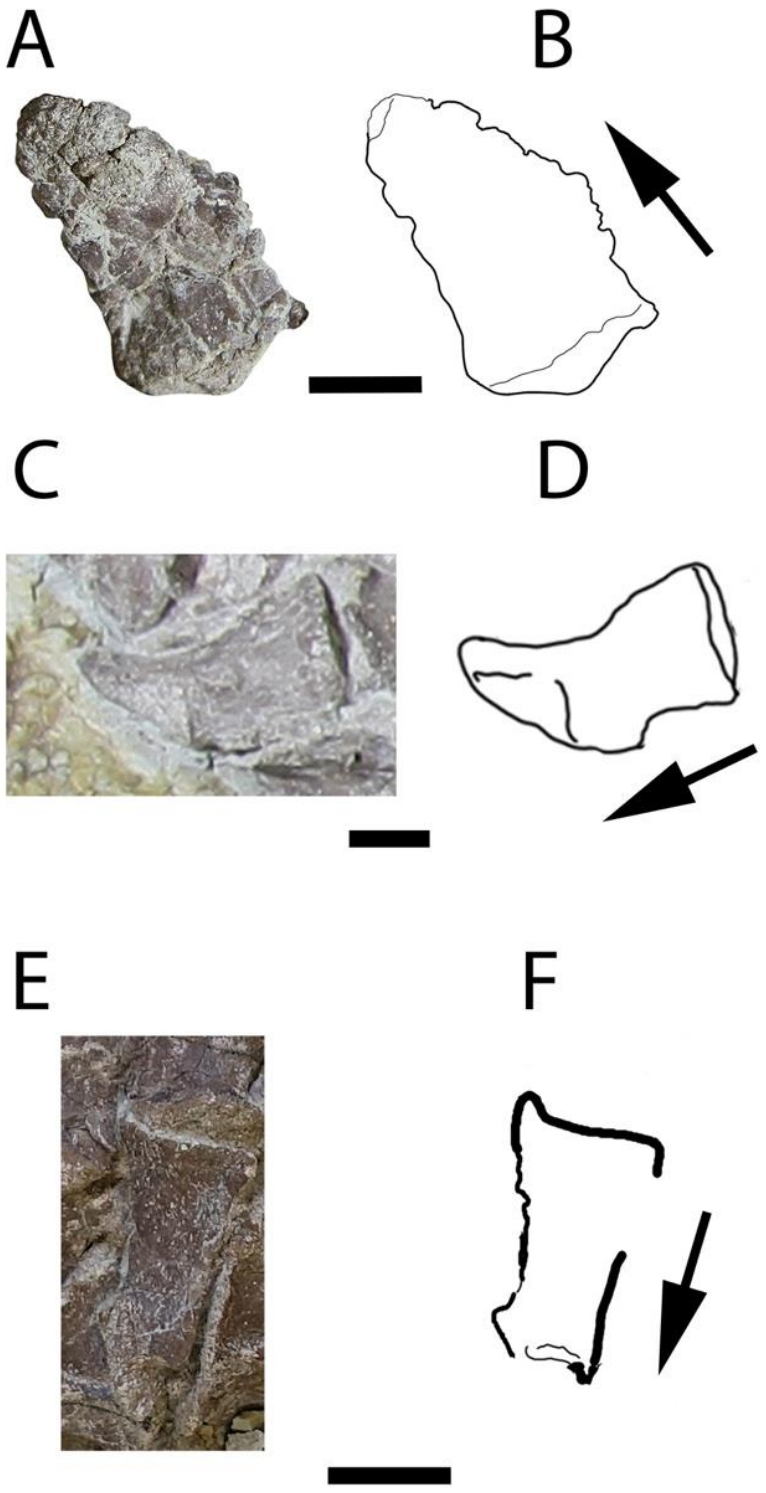

Figure 2.12. Sacral ribs of *Whatcheeria*. FMNH PR 4997 sacral rib specimen photo (A) and interpretive drawing (B); FMNH PR 1816 sacral rib specimen photo (C) and interpretive drawing (D); FMNH PR 1875 sacral rib specimen photo (E) and interpretive drawing (F). Arrows point distally (in the direction of the articulation with the ilium).

The sacral rib (Figure 2.12) is robust. The distal end is 30-50% broader than the proximal end and there is slight waisting at the midshaft. It superficially resembles a much more compact version of a pectoral rib and is roughly as long as the sacral neural spine is tall.

The six caudal ribs (Figure 2.3, Figure 2.5, Figure 2.6) are thicker and more robust than the trunk ribs and are rounded in cross-section. They lack flanges or uncinate processes. The first and last are short and mostly straight, whereas the rest are much larger and curved caudally. The degree of curvature increases in successive posterior ribs. The penultimate caudal rib (rib 32) has a kink immediately distal to the head and a semi-straight shaft. This morphology is useful in correlating caudal series across specimens.

The hemal spines (Figure 2.5, Figure 2.6, Figure 2.13) are fused to their intercentra without trace of suture. In common with *Acanthostega* (Coates, 1996), the first hemal spine is very small, a morphology that seems otherwise to be unique among early tetrapods. The remaining hemal spines are squared off and fairly broad anteroposteriorly, with straight margins and minor tapering from the proximal to distal end. The second hemal spine is the broadest and has an expanded distal end with a slight hook that is visible in multiple specimens (Figure 2.8, Figure 2.9). Height is mostly consistent for the second through the eighth hemal spine, which are slightly longer than the height of their corresponding neural spines. After this (vertebra 41 onwards), hemal spines decrease in length and become more pointed, triangular, and posteriorly inclined. In the reconstruction this transition is pronounced and rapid, producing the unusual tail profile. No specimen preserves a complete and articulated tail, but the specimens that do preserve caudal segments suggest that this depth transition is genuine. The distal end of the tail is

not discernible in any specimen, and has been restored with a terminal axial segment after *Acanthostega* (Coates, 1996) and *Ichthyostega* (Jarvik, 1996; Pierce et al., 2012).

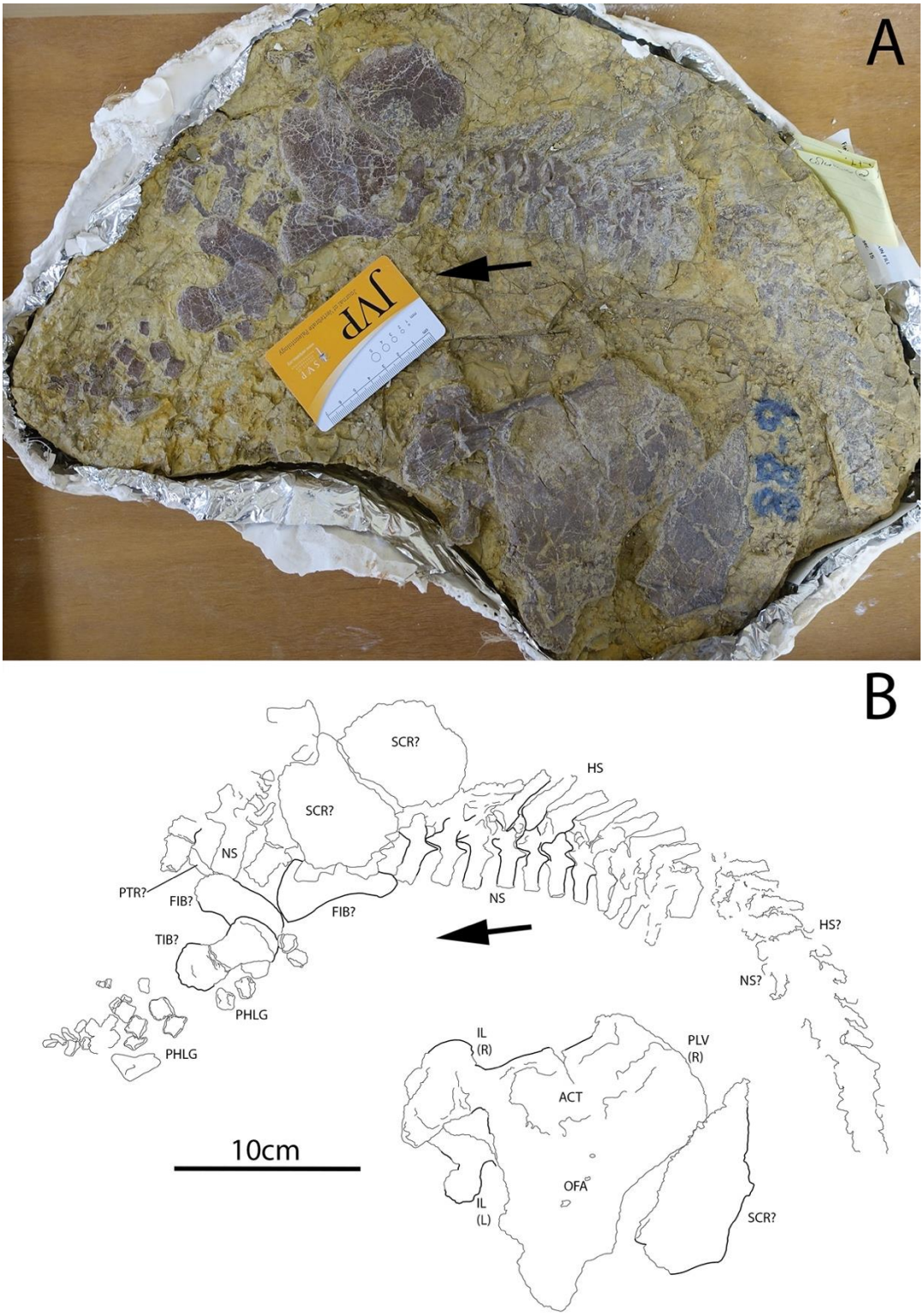

Figure 2.13. FMNH PR 4998, articulated and associated *Whatcheeria* material. A) specimen photo; B) interpretive drawing with labels. Arrows point anteriorly.

2.4.2.2 Pectoral girdle

The pectoral girdle consists of a median interclavicle (Figure 2.14), paired clavicles (Figure 2.15), scapulocoracoids (Figure 2.16), and cleithra (Figure 2.17). In the full-body reconstruction the girdle is placed so that the scapular blade overlaps the two pectoral ribs. This position is selected for several reasons. In FMNH PR 1700, the pectoral girdle remains are in close proximity to the pectoral ribs, and specimen preservation suggests that they have not drifted far from their position in life. In *Proterogyrinus* (Holmes, 1984) and *Archeria* (Holmes, 1989b), the two ribs immediately posterior to the cervicals have a distinctive morphology and are distally overlapped by the scapular blade. *Whatcheeria* pectoral ribs are identified as such because they share the same morphology and placement as their counterparts in *Proterogyrinus* and *Archeria*, and likely had the same relationship with the girdle. A reconstruction with the pectoral girdle moved anteriorly to immediately behind the skull reveals discontinuity in the rib series (see Supplementary Information), supporting the placement in our preferred reconstruction (Figure 2.2).

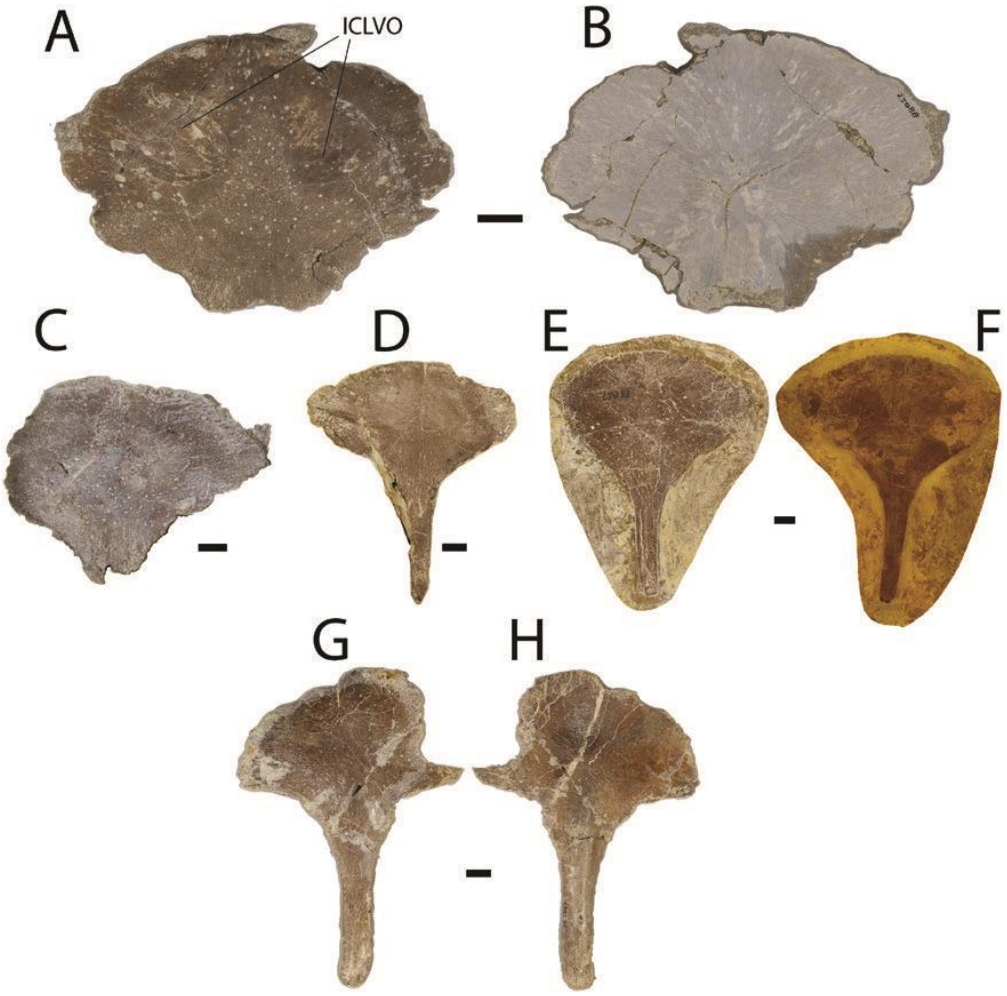

Figure 2.14. Interclavicles of *Whatcheeria*. SUI 52088 interclavicle plate in external (A) and internal (B) views; C, FMNH PR 4999 in external view; D, FMNH PR 1740 interclavicle in external view; FMNH PR 1957 interclavicle mounted in resin in external (E) and internal (F) views; FMNH PR 1743 interclavicle in external (G) and internal (H) views. In allspecimens, anterior is at the top and posterior is at the bottom.

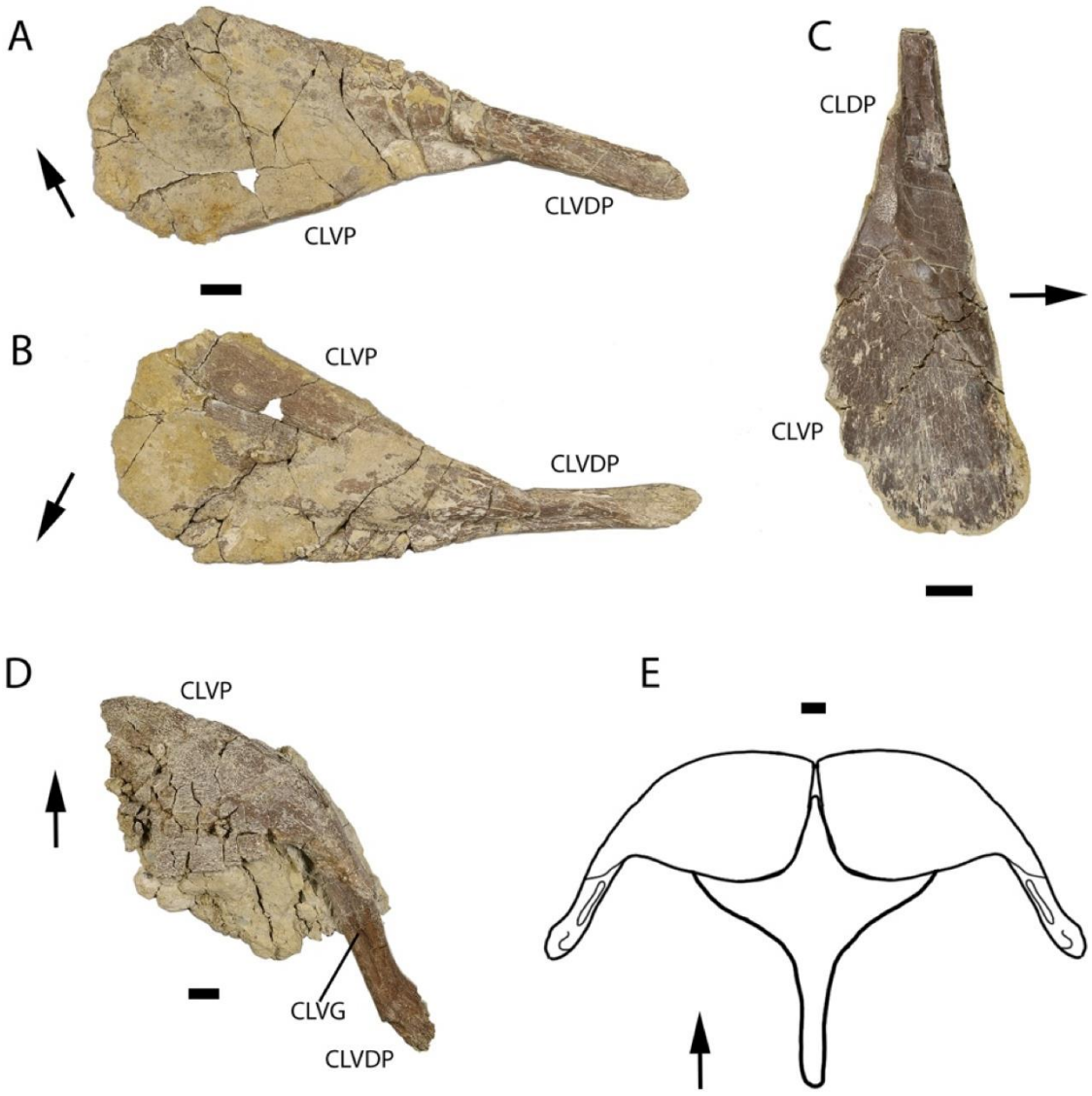

Figure 2.15. Clavicles of *Whatcheeria*. FMNH PR 5018 right clavicle in internal (A) and external (B) views; C, FMNH PR 5000 left clavicle plate in internal view; D, FMNH PR 5001 partial clavicle in posteroventral view; E, reconstruction of clavicles and interclavicle in articulation. Arrows point anteriorly.

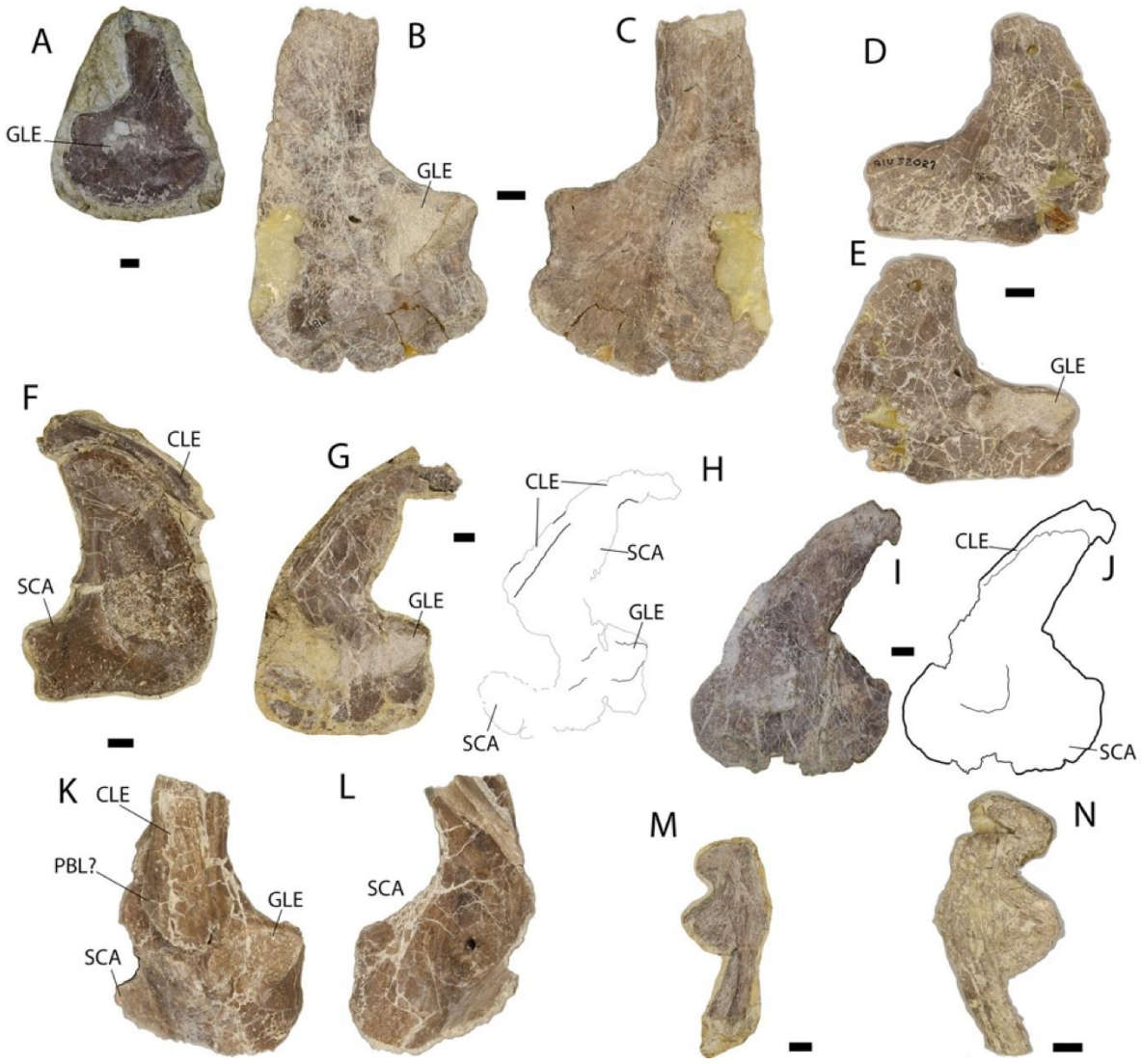

Figure 2.16. Cleithra and scapulocoracoids of *Whatcheeria*. A, FMNH PR 5005 left scapulocoracoid in external view; FMNH PR 1789 left scapulocoracoid in external (B) and internal (C) views; SUI 52027 left scapulocoracoid in internal (D) and external (E) views; F, FMNH PR 1703 left scapulocoracoid and cleithrum in internal view; FMNH PR 5004 right scapulocoracoid and cleithrum in external view, specimen photo (G) and interpretive drawing (H); FMNH PR 5006 right scapulocoracoid and cleithrum in internal view, specimen photo (I) and interpretive drawing (J); FMNH PR 1766 partial right scapulocoracoid and cleithrum in external (K) and internal (L) views; FMNH PR 5003 partial left cleithrum in internal view (M); FMNH PR 5002 partial left cleithrum in external view (N).

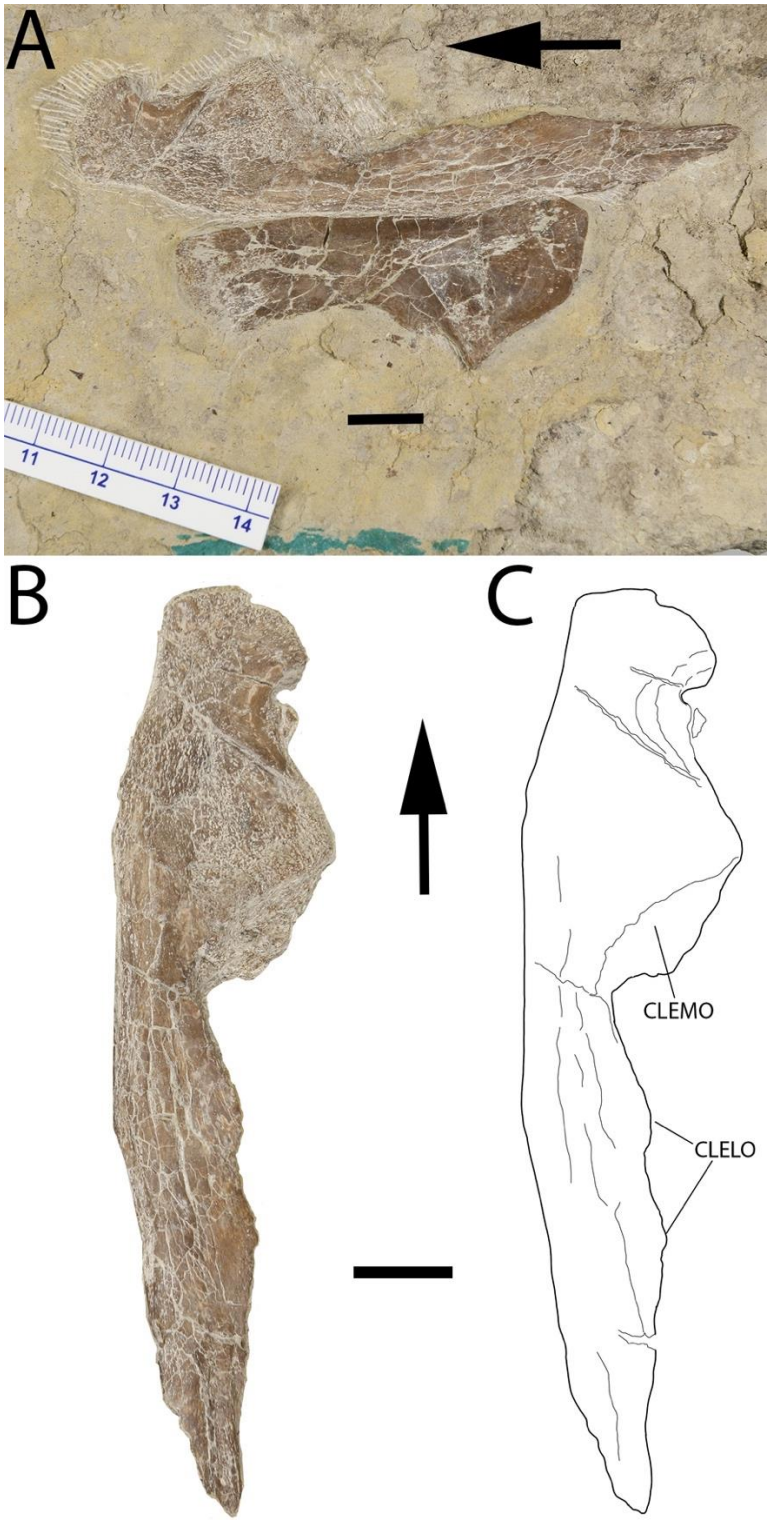

Figure 2.17. Cleithrum of *Whatcheeria*. A, FMNH PR 5007, left cleithrum in lateral view (above) and unknown bone (below); B, left cleithrum; C, interpretive drawing of cleithrum. Arrows point dorsally for the cleithrum.

The interclavicle (Figure 2.14) is fan shaped and concave on its interior surface. The parasternal process is narrow and longer than the length of the interclavicle body but shorter than its width and would have extended posterior to the clavicles. The interclavicle is noticeably thicker in larger specimens. Depressions on the external surface indicate that the clavicles contacted each other anteriorly in life (Fig.14, Fig.15E). The interclavicle resembles that of *Ichthyostega* (Jarvik, 1996) but has a smaller parasternal process. Similar interclavicle morphologies are also found in *Seymouria* and *Discosauriscus* (White, 1939; Klembara and Bartík, 1999). The *Ossinodus* interclavicle (Warren and Turner, 2004) shares the long parasternal process, but the body is diamond-shaped. The *Pederpes* interclavicle is incomplete; the shape resembles that of *Ossinodus* but the parasternal process was probably shorter.

The clavicle (Figure 2.15) has a subtriangular plate and a narrow, grooved dorsal process. The plate is broad and rounded at the midline margin. The clavicle is very similar to those of *Ichthyostega* (Jarvik, 1996; Pierce et al., 2012) and *Seymouria* (White, 1939), and, to a lesser extent, *Eryops* (Pawley and Warren, 2006). It is unclear whether a posterior lamina was present.

Cleithrum shape (Figure 2.16, Figure 2.17) is difficult to determine because of complete or near-fusion with the scapulocoracoid in most specimens. Thus, the single, free specimen of a cleithrum (FMNH PR 5007) provides unique information (Figure 2.17). The cleithrum dorsal apex is blunt and the posterior margin includes a distinct, rounded notch; this feature is autapomorphic for *Whatcheeria* (Lombard and Bolt, 1995). Immediately ventral to the notch the mesial surface is depressed to receive the scapulocoracoid, but the suture between these two bones is difficult to trace in articulated (fused). The external lamina of the cleithrum reaches its

greatest breadth at its dorsoventral midpoint before narrowing ventrally. There is no postbranchial lamina. Lombard and Bolt (1995) cited a small medial flange at the ventral tip of the cleithrum in FMNH PR 1766 ('PBL?' in Fig.15K) and compared it to that in *Acanthostega*. However, the flange in PR 1766 is smaller and placed more ventrally than the postbranchial lamina in *Acanthostega* or *Greererpeton*, and there is no indication of a similar flange in any other *Whatcheeria* specimens, including FMNH PR 5007 (Figure 2.17). There is no evidence of an anocleithrum.

The scapulocoracoid (Figure 2.16) has substantial ossified coracoid and scapular portions, like that of *Tulerpeton* (Lebedev and Coates, 1995), and, to a lesser extent, examples from *Archeria* and *Proterogyrinus*. The scapular blade is broad, unlike *Ichthyostega*, *Acanthostega*, *Pederpes*, and *Ossinodus*. Dorsally the blade tapers gently to a rounded point overlain laterally by the cleithrum. In some immature individuals, such as FMNH PR 1816 (Figure 2.5), there are two coracoid ossifications and a scapular ossification, but in most specimens the scapulocoracoid is fused into a single unit without trace of suture. Unlike in *Archeria*, *Greererpeton*, and *Acanthostega*, the glenoid is not subterminal. The glenoid has the rounded subrectangular shape seen in *Tulerpeton* and *Proterogyrinus*. The anterior half of the glenoid faces more posteriorly whereas the posterior half faces more laterally. There does seem to have been some twist to the articular surface, producing the 'screw-shaped' glenoid seen in other early tetrapods. The supraglenoid foramen is well-defined. There are probably at least two supracoracoid foramina, but no specimens are well-preserved enough to determine the morphology of that part of the coracoid with complete confidence.

2.4.2.3 Forelimb

The forelimb consists of the humerus (Figure 2.18), radius and ulna (Figure 2.19, Figure 2.20), and manus (Figure 2.20, Figure 2.21, Figure 2.22).

The humerus (Figure 2.18) has the basic L-shape common to early tetrapods. It is massive, well-ossified, and distinguished by its large muscle attachments. The entepicondyle is as large as the rest of the humerus combined, and the ectepicondyle and deltopectoral crest are both prominent. Relative to the rest of the humerus, the entepicondyle of *Whatcheeria* is the largest among early tetrapods by area. In dorsal view, when combined the deltopectoral crest and supinator process are about as long as the humeral shaft. The proximal margin of the entepicondyle projects at an approximate right angle relative to the long axis of the shaft, but the distal margin extends beyond the level of the ulnar facet at an angle of approximately 120 degrees. Thus, the posterior rim of the entepicondyle is longer than the anterior boundary where it meets the humeral shaft.

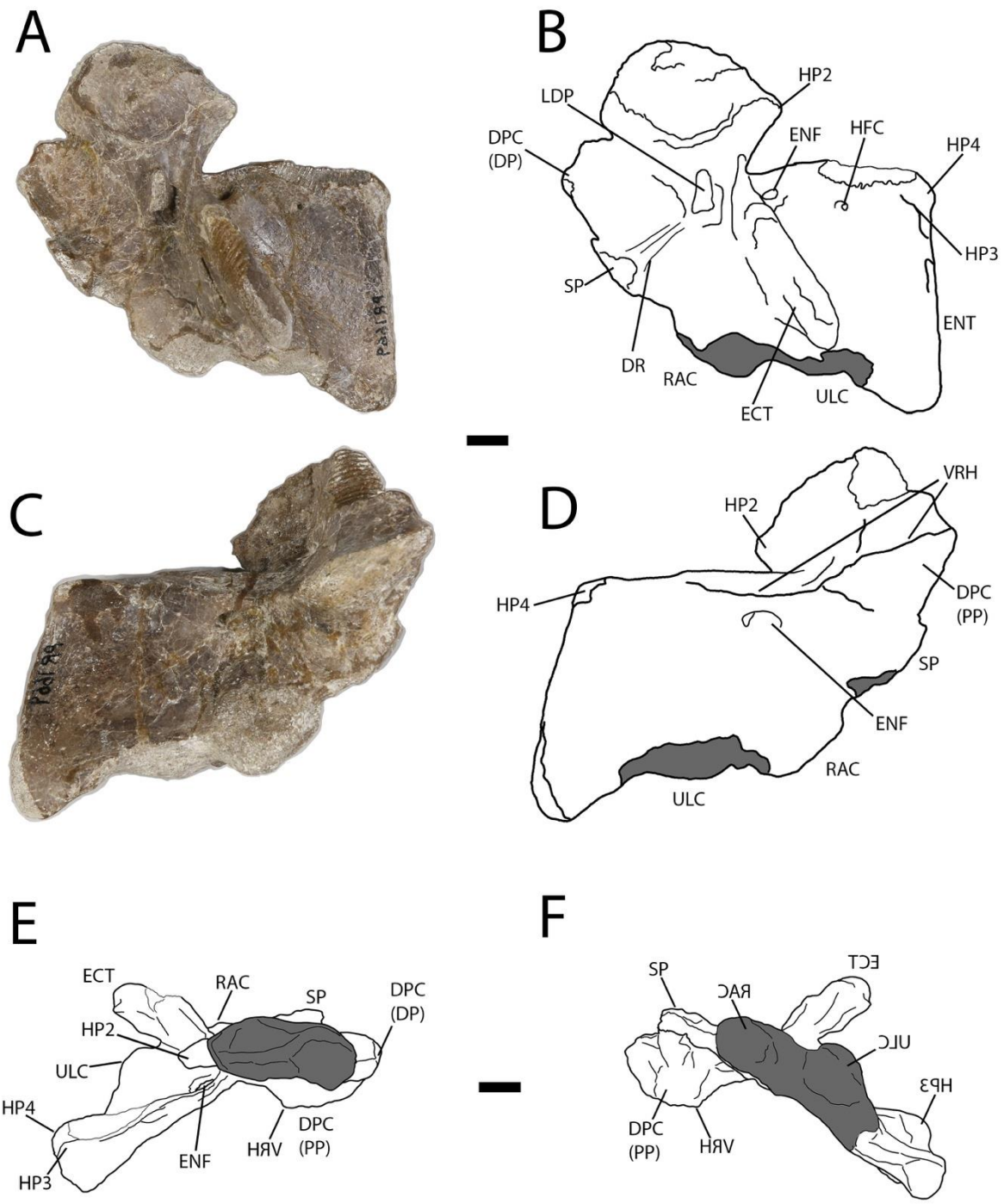

Figure 2.18. FMNH PR 1669 left humerus of *Whatcheeria*. Dorsal view, specimen photo (A) and interpretive drawing (B); anteroventral view, specimen photo (C) and interpretive drawing (D); proximal view, interpretive drawing (E); distal view, interpretive drawing (F). In A–D, proximal is at the top and distal is at the bottom. Both E and F are oriented such that the longest axis of the proximal end of the humerus is at horizontal.

Figure 2.19. Radii and ulnae of *Whatcheeria*. A, FMNH PR 1705 associated forelimb and manus; FMNH PR 1993 radius in probable internal/ventral (B) and probable external/dorsal (C) views; D, FMNH PR 5008 radius; E, FMNH PR 5009 ulna and phalanges; FMNH PR 1765? right ulna in external (F) and internal (G) views; FMNH PR 1998? right ulna in internal (H) and internal (I) views; FMNH PR 2006 olecranon process in dorsolateral (J) lateral (K, L), and articular (M) views. In B–I, proximal is at the top and distal is at the bottom.

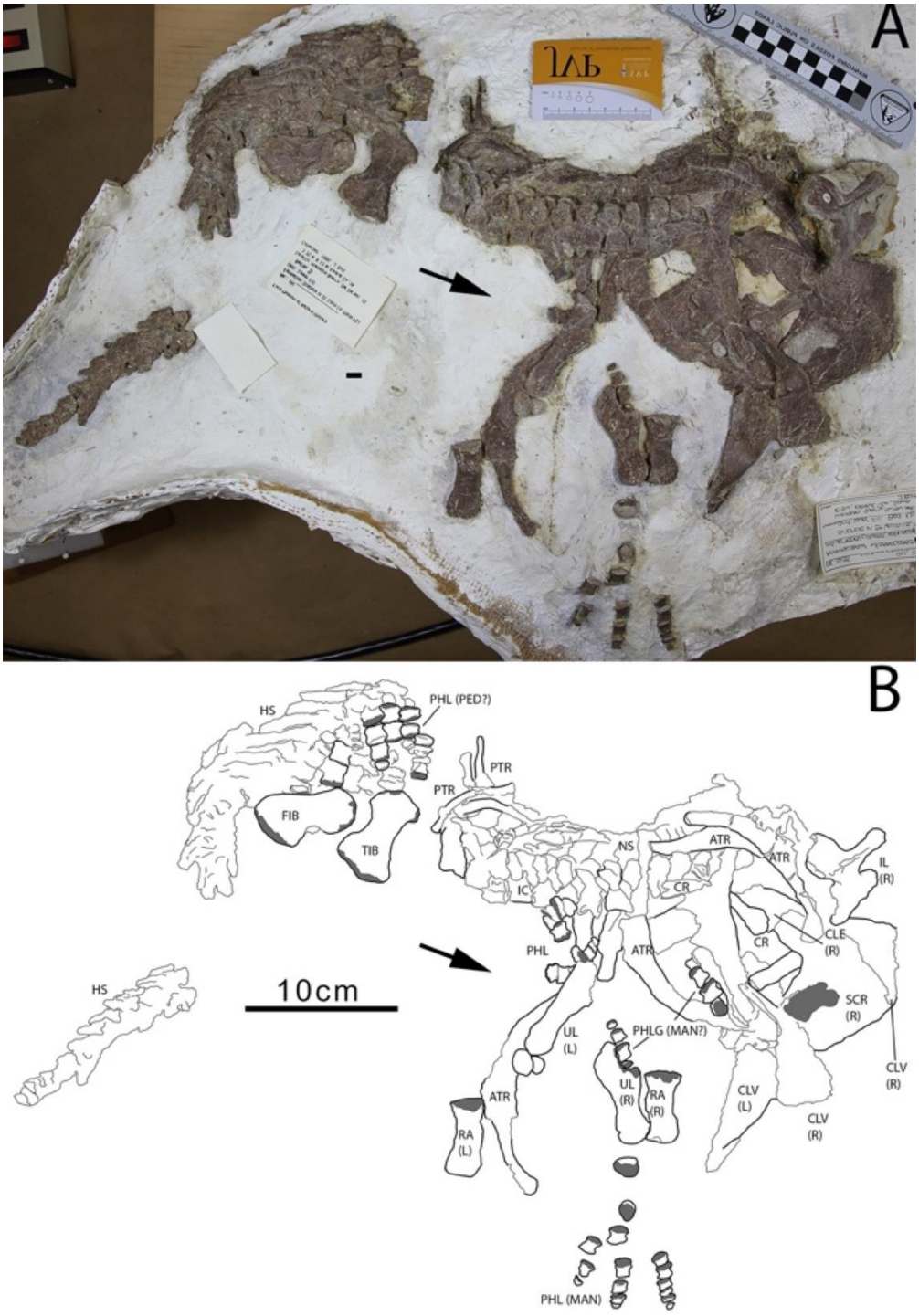

Figure 2.20. FMNH PR 1635, articulated material from at least one *Whatcheeria* individual. A, specimen photo; B, interpretive drawing with labels. Articular surfaces have been coloured in grey. Arrows point anteriorly.

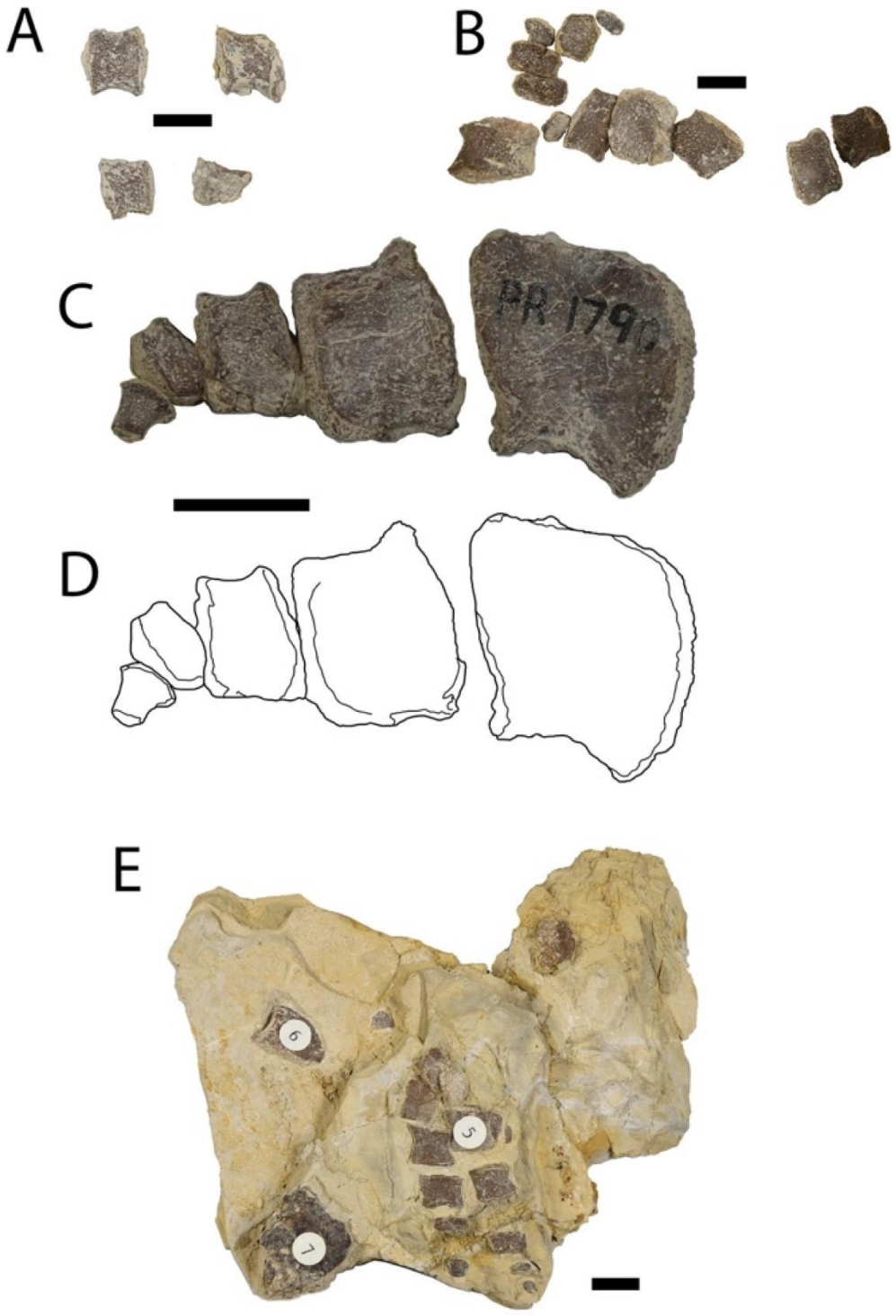

Figure 2.21. Phalangeal material of *Whatcheeria*. FMNH PR 5010 isolated phalanges (A, B); FMNH PR 1790 articulated digit (possibly pedal digit IV) specimen photo (C) and interpretive drawing (D); phalanges from FMNH PR 1635, including two articulated digits, probably IV and V (E).

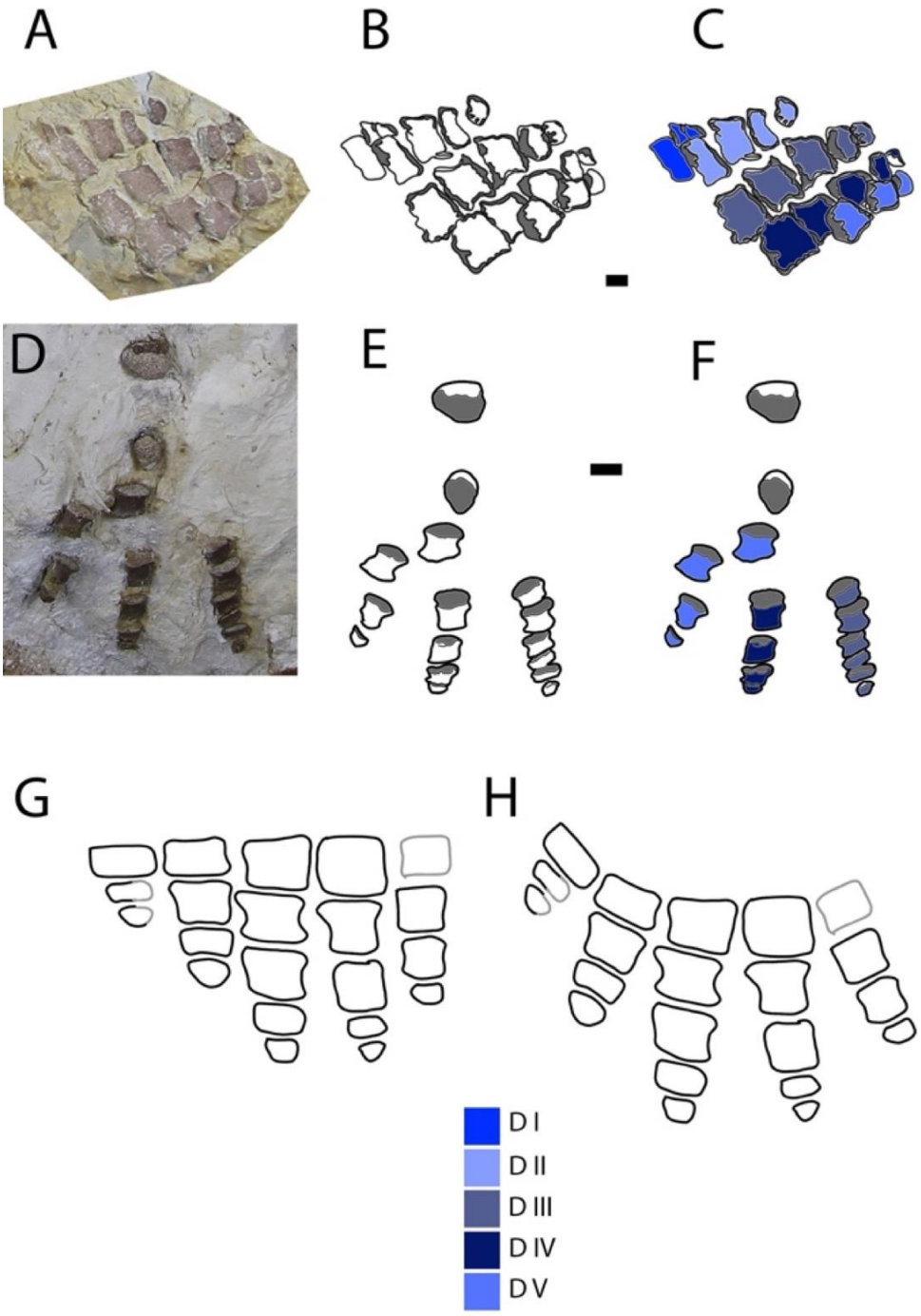

Figure 2.22. Manus of *Whatcheeria*. A, FMNH PR 1816, specimen photo of articulated digits; B, interpretive drawing of FMNH PR 1816 digits; C, interpretive drawing colour-coded by digit; D, FMNH PR 1635 specimen photo of associated digits; E, interpretive drawing of FMNH PR 1635 digits; F, interpretive drawing colour-coded by digit; G, restoration of *Whatcheeria* manus; H, restoration of *Whatcheeria* manus with digits in life posture. In G and H grey lines represent restored portions not present or exposed in specimens.

The proximal articular surface of the humerus is screw-shaped, matching that of the glenoid. Process 2 *sensus* (Coates, 1996) is broad and angular, projecting posteriorly distal to the humeral head. The deltopectoral crest extends anteriorly from the leading edge of the humeral shaft. The crest is broad, deep, and triangular, with distinct deltoid and pectoral processes, the latter of which is much larger than the former. The latissimus dorsi process is a distinctive feature anterior to the ectepicondyle. It is broken near the base in all specimens, so its true height remains uncertain, but the remnant implies a spike-like shape similar to *Pederpes* and *Baphetes* (Milner and Lindsay, 1998). Process 2 (‘pr2’) of FMNH PR 1635 in the original description (Lombard and Bolt, 1995) is in fact the damaged supinator process. The supinator process is a medium-sized triangular swelling on the dorsal surface of the leading edge of the humerus. A dorsal ridge extends from the latissimus dorsi process to the supinator process, as in *Acanthostega* (Coates, 1996).

The ectepicondyle is large, at least as tall as the deltopectoral crest is deep in anterior view. It is a parallelogram in anterior/distal view and is shorter at its proximal corner than its distal. It extends between the radial and ulnar condyles and stops at about the transition from finished bone to the articular surface. However, if the maximum width of the humeral head is referenced as horizontal, then the ectepicondyle inclines posteriorly and the distal extremity projects above the ulnar condyle. There is no ectepicondylar canal.

The entepicondyle, extends along the humeral shaft for ~60% of the total proximodistal length. Distally it is thickened at the margins. The posterior proximal extremity is expanded further, and processes 3 (dorsal) and 4 (ventral) can be identified, separated by a groove as in

Acanthostega (Coates, 1996). The posterior distal extremity extends further laterally than the radial and ulnar condyles. The entepicondylar foramen is large. There is a smaller circular foramen on the dorsal face of the entepicondyle near the proximal margin, halfway between the anterior origin and the posteromesial corner. It does not extend through to the ventral surface of the humerus and probably corresponds to foramen c in *Acanthostega* (Coates, 1996).

The ventral ridge of the humerus is very prominent, originating on the deltopectoral crest, extending over the entepicondylar foramen, and joining with process 4 at the distal end of the entepicondyle. A similarly extensive ventral ridge is found in ANSP 21476 (Shubin et al., 2004; Daeschler et al., 2009) and *Ichthyostega* (Jarvik, 1996, Fig.45F as 'cr. 4-6').

The radial and ulnar condyles are two distinct swellings, but they are not separated by finished bone. Both are approximately oval in shape and have substantial exposure in dorsal view. The face of the radial condyle is slightly inclined dorsally relative to the plane of the humeral shaft. The ulnar condyle is larger than the radial condyle.

The angle of torsion between the proximal and distal ends of the humerus in *Whatcheeria* is 20 degrees when measured through the radial and ulnar condyles, and approximately 36 degrees when measured through the radial condyle and distal edge of the entepicondyle in distal view. The first of these measurements is probably the one that is most comparable to those obtained from other early tetrapods for biomechanical inference. The measurement of 20 degrees in *Whatcheeria* matches that of *Acanthostega*, and is less than the other early tetrapods which can be measured: 25-30 degrees in *Ossinodus*, 35 degrees in *Pederpes*, and 45 degrees in

Eoherpeton (Smithson and Clack, 2018). Angles of 60 degrees are known from *Tulerpeton* and one of the humerus morphotypes from Blue Beach (Smithson and Clack, 2018).

The humerus of *Whatcheeria* is unusual. Its proximodistal/anteroposterior length ratio is greater than that of *Acanthostega*, on par with *Ichthyostega* (Callier et al., 2009; Pierce et al., 2013a) and *Proterogyrinus* (Holmes, 1984). The large size of the anterior muscle attachments means that the head is contiguous with the rest of the humerus. The small base of the latissimus dorsi process resembles *Pederpes* (Clack and Finney, 2005). The ectepicondyle is intermediate in size between examples known in embolomeres (Romer, 1957; Holmes, 1984) that of *Tulerpeton* (Lebedev and Coates, 1995) but resembles *Tulerpeton* more closely in shape.

Both the radius and ulna (Figure 2.19) are elongate and flattened. Although this is in part a taphonomic artifact in some specimens (Figure 2.19B-D), the flattened morphology seems to be largely genuine (Figure 2.19A, F-I, Figure 2.20). The radius is shorter than the ulna; when preserved together the radius:ulna length ratio is 2:3 including the olecranon process (Figure 2.19, Figure 2.20). The margins of the radius are straight along its length, and its shape resembles an elongated version of the radius of *Baphetes* (Milner & Lindsay, 1998). The proximal end is expanded into a large concave facet. There is some striation or fluting at the distal end. There is no indication of ridges on the flexor surface as seen in *Pederpes* (Clack and Finney, 2005).

As in *Archeria* and *Tulerpeton* (Lebedev & Coates, 1995), the margins of the ulna are roughly equal in curvature, unlike in *Proterogyrinus* (Holmes, 1984) and *Eryops* (Pawley and

Warren, 2006), in which the mesial/flexor margin is more curved than the lateral/extensor margin. The proximal articular surface is slightly narrower than the distal articular surface. The olecranon process is large, proportionally comparable to that of *Eryops* (Pawley and Warren, 2006). It curves medially toward the proximal articular surface, as in *Archeria* (Romer, 1957). However, this process is only weakly developed or absent in smaller *Whatcheeria* specimens (see Ontogenetic Considerations). There is a fossa immediately beneath the articular surface of the olecranon that extends to the distal end of the ulna on the extensor and flexor surfaces. The fossa is deepest proximally, near the olecranon, and shallows distally. A similar but much more limited fossa is found on the ulnae of *Ichthyostega*, *Proterogyrinus*, and *Eryops*, where it is located only on the posterior side of the ulna and is usually only present near the proximal articular surface. The distal end is rounded, and the articular surface is fairly broad, somewhat similar to *Tulerpeton* (Lebedev and Coates, 1995).

2.4.2.4 Manus

Here all bones distal to the wrist and ankle are described as ‘phalanges’. Conventional descriptions identify the cylindrical bones just distal to the wrist or ankle as ‘metacarpals’ or ‘metatarsals’, but a broader working definition is used in the present description to avoid spurious precision when characterizing disturbed material. In early tetrapods morphological disparity between metatarsals or metacarpals and bones extending into the digits is usually minimal. Moreover, we have little idea of the extent of ‘free’ portions of such digits in life. Therefore, employing a single term to include all digit-associated bones is sufficient for this study. For the sake of comparison, we report digit formulae using both conventional counts and our more inclusive estimate.

There are no remains of ossified carpals. Their presence may have been ontogenetically variable, but unossified wrists are common in early tetrapods, even in (presumed) adults. The intermedium in *Acanthostega* and the fully ossified wrist in *Tulerpeton* are exceptions (particularly the latter), with the caveat that well-preserved wrists and manus are rare. The phalanges of *Whatcheeria* (Figure 2.19A, E, Figure 2.20-Figure 2.22) are rectangular in dorsal view and usually broader than long. When preserved in three dimensions, the proximal phalanges are oval in cross-section whereas the more distal phalanges are increasingly flattened dorsoventrally and have an almost rectangular cross-section. In the proximal phalanges, the concavity of the dorsal and ventral surfaces is approximately equal. There are no indications of pronounced attachments for ligaments. The terminal phalanges (unguals) are broad and blunt. As noted for *Pederpes* and possibly other taxa (Clack and Finney, 2005) some of the phalanges are bilaterally asymmetrical. This asymmetry occurs mainly in the most proximal phalanges of digits III, IV, and, to a lesser extent, digit V of both the manus and pes. An attempt has been made to retain some of this phenomenon in the reconstructions, but it might be underestimated.

A complete, articulated manus does not exist for *Whatcheeria*, but FMNH PR 1816 (Figure 2.22A-C) preserves five nearly complete digits and provides the primary basis for the reconstructed manus (Figure 2.22G, H). Additional information was taken from FMNH PR 1635 (Figure 2.20, Figure 2.22D-F), which is more disrupted but is not as flattened. The digit formula for the reconstructed manus is 3-4-5-5-4. This includes all bones distal to the wrist. If the bones regarded by other authors as ‘metacarpals’ are excluded, the digit formula is 2-3-4-4-3.

2.4.2.5 PELVIS

The pelvis of *Whatcheeria* (Figure 2.23) is triangular and composed of the ilium, ischium, and pubis. These are fused without visible sutures. The anterior half of the pelvis is dorsoventrally shorter than the posterior half, with the change in proportions occurring near the anteroposterior midpoint. The acetabulum is long with a prominent anterior extension, and is open anteriorly as in *Acanthostega*, *Ichthyostega*, and *Caerorhachis* (Ruta et al., 2002). As noted in the original description (Lombard and Bolt, 1995), there is a small tongue of unfinished bone that interrupts the margin of the acetabulum posterodorsally. The supraacetabular buttress is much stronger than the ventral buttress. There are three obturator foramina: two stacked dorsally ventral to the highest portion of the acetabulum, and a third anterior to those. Additional foramina are present above the acetabulum and posteriorly on the ischium.

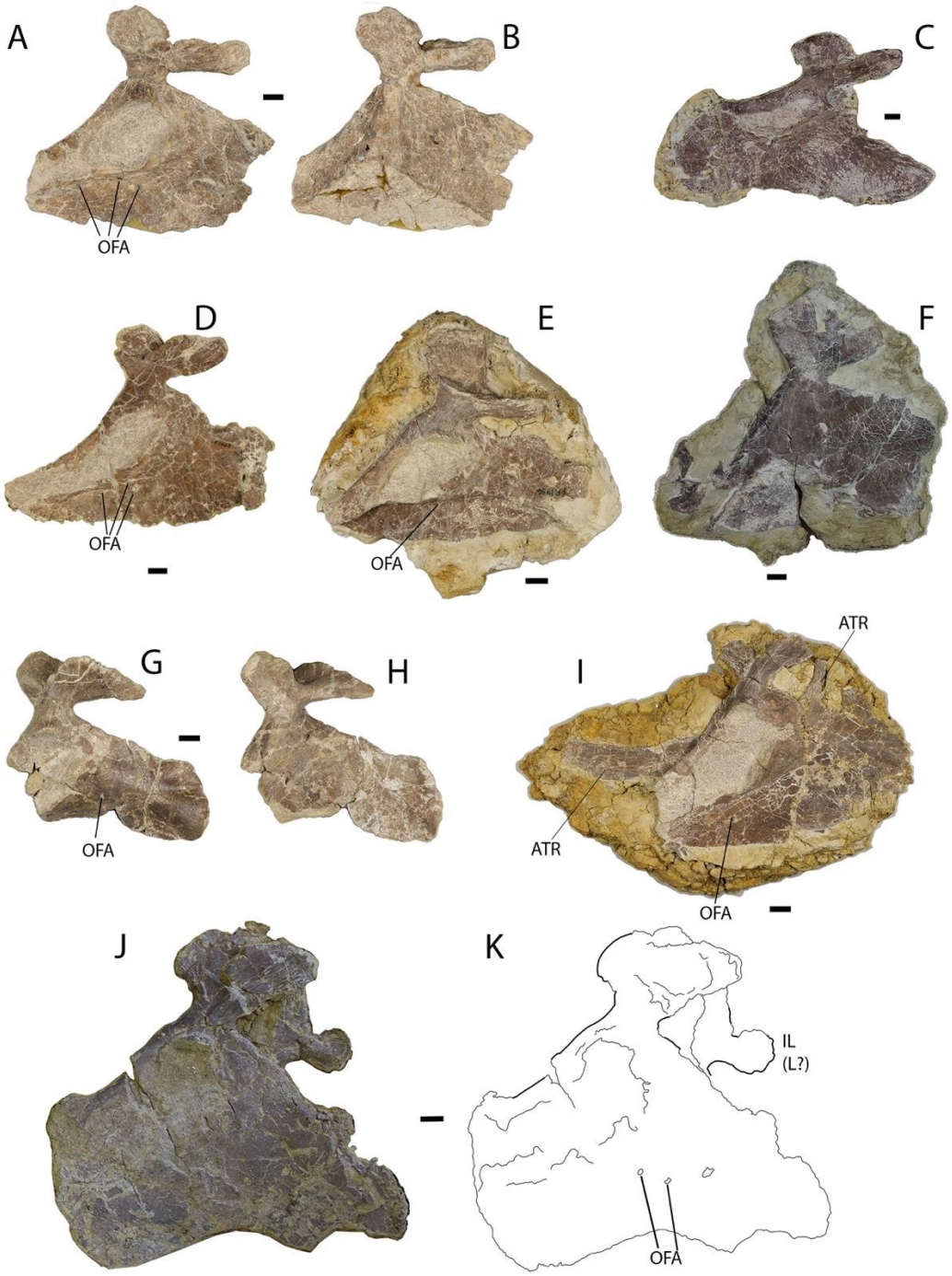

Figure 2.23. Pelvic girdle material of Whatcheeria. SUI 52087 right pelvis in external (A) and internal (B) views; C, FMNH PR 5019 left pelvis in external view; D, FMNH PR 1740 right pelvis in external view; E, FMNH PR 1736 left pelvis in external view; F, FMNH PR 5011 left pelvis in internal view; FMNH PR 1733 partial left pelvis in external (G) and internal (H) views; I, FMNH PR 5003, left pelvis in external view and anterior trunk rib; FMNH PR 4998 left pelvis in external view, specimen photo (J) and interpretive drawing (K). In all specimens, anterior is on the left and posterior is on the right. To maintain consistent orientation, B and H have been flipped horizontally.

The ilium is short and robust, with two processes of equal size. For clarity, we refer to these as the ‘dorsal iliac process’ and ‘posterior iliac process’. The posterior iliac process is deflected laterally and ventrally relative to the dorsal iliac process, such that there is a deep groove separating them. Both are rounded and have strong fluting/striations on their dorsal and posterolateral margins, respectively. The dorsal iliac process is more circular and the posterior iliac process is more ovoid. The shape of the posterior iliac process is somewhat variable, sometimes appearing rectangular or subtriangular. Taphonomy is probably a factor as most pelvis specimens are flattened and/or otherwise damaged, but genuine intraspecific variation may be present. The ilium of *Pederpes* is very similar to that of *Whatcheeria* in the orientations of the processes and their shape. However, the processes do not overlap in lateral view, and the posterior iliac process in *Pederpes* is more triangular than the morphology (or morphologies) observed in *Whatcheeria*. The dorsal iliac process of *Ossinodus* is unknown. The posterior iliac process of *Ossinodus* is smaller than that of *Pederpes* and more rectangular.

The fusion between the bones of the pelvis prevents precise assessment of the shape of the ischium, as its anterior border cannot be discerned. Overall, it seems D-shaped as in other early tetrapods. Its posterior elongation is comparable to *Greererpeton*, and intermediate between *Ichthyostega* and *Proterogyrinus*. It is more robust than the delicate ischium of *Pederpes*. The pubis is elongate, and its dorsal margin is gently concave. The pubis is present in all specimens for which the anterior portion of the pelvis is preserved, suggesting that its degree and timing of ossification were similar to those of the ilium and ischium, unlike in *Proterogyrinus* (Holmes, 1984) and *Greererpeton* (Godfrey, 1989).

The mesial surface of the pelvis is visible in some specimens (Figure 2.23B, F, H). There is a large, rugose triangular symphysial area. The dorsal apex of the symphysial area is approximately half the dorsoventral height of the pelvis without the ilium (Figure 2.23B, H), and there is a strong ridge extending from the apex to the base of the ilium. The ridge appears to be similarly pronounced in *Proterogyrinus* (Holmes, 1984) and *Archeria* (Romer, 1957), but it is weaker in *Acanthostega* (Coates, 1996), *Greererpeton* (Godfrey, 1989), and *Eoherpeton* (Smithson, 1985b). The symphysial area is larger than in all of these taxa, suggesting an unusually well-buttressed pelvis.

2.4.2.6 Hindlimb

The hindlimb consists of the femur (Figure 2.24), tibia and fibula (Figure 2.25, Figure 2.26), and pes (Figure 2.27).

The femur (Figure 2.24) has a short but distinct shaft and expanded proximal and distal ends. In this it contrasts with *Acanthostega* (Coates, 1996) and *Tulerpeton* (Lebedev and Coates, 1995) and to a lesser extent *Ichthyostega* (Jarvik, 1996) and *Pederpes* (Clack and Finney, 2005) and aligns with post-Carboniferous forms. It particularly resembles the femora of *Proterogyrinus* (Holmes, 1984) and *Archeria* (Romer, 1957). The proximal end is about 75% the width of the distal end. The articular surface is comma-shaped, thickest anteriorly and tapering posteriorly while curving distally. The intertrochanteric fossa is only gently depressed. There is no evidence of an internal trochanter; we consider it absent, in common with *Pederpes* and in contrast to other early tetrapods. The fourth trochanter is underlain by the short but robust adductor blade *sensu* (Lebedev and Coates, 1995; Coates, 1996) and together they occupy the entire length of

the shaft on the ventral/flexor surface. The adductor blade is thick and the fourth trochanter is broad with a squared off, rugose top. This combination of characters is also seen in *Pederpes*. The adductor blade of *Ichthyostega* (conflated with the adductor crest as 'oblique ridge' in (Lombard and Bolt, 1995; Jarvik, 1996) is similar but proportionally larger. The adductor crest is narrow and well-defined. It is as long as the adductor blade and extends distally onto the fibular condyle, subsiding just proximal to the distal articular surface. The tibial and fibular condyles are distinct protrusions but are not separated by finished bone. They are very similar in morphology to their counterparts in *Proterogyrinus* and *Archeria*. The tibial condyle has a flattened 'D' shape in distal view and the fibular condyle is a broader, rounded rectangle. They intersect at a roughly 120-degree angle. The depth of the intercondylar fossa is about half the breadth of the tibial condyle.

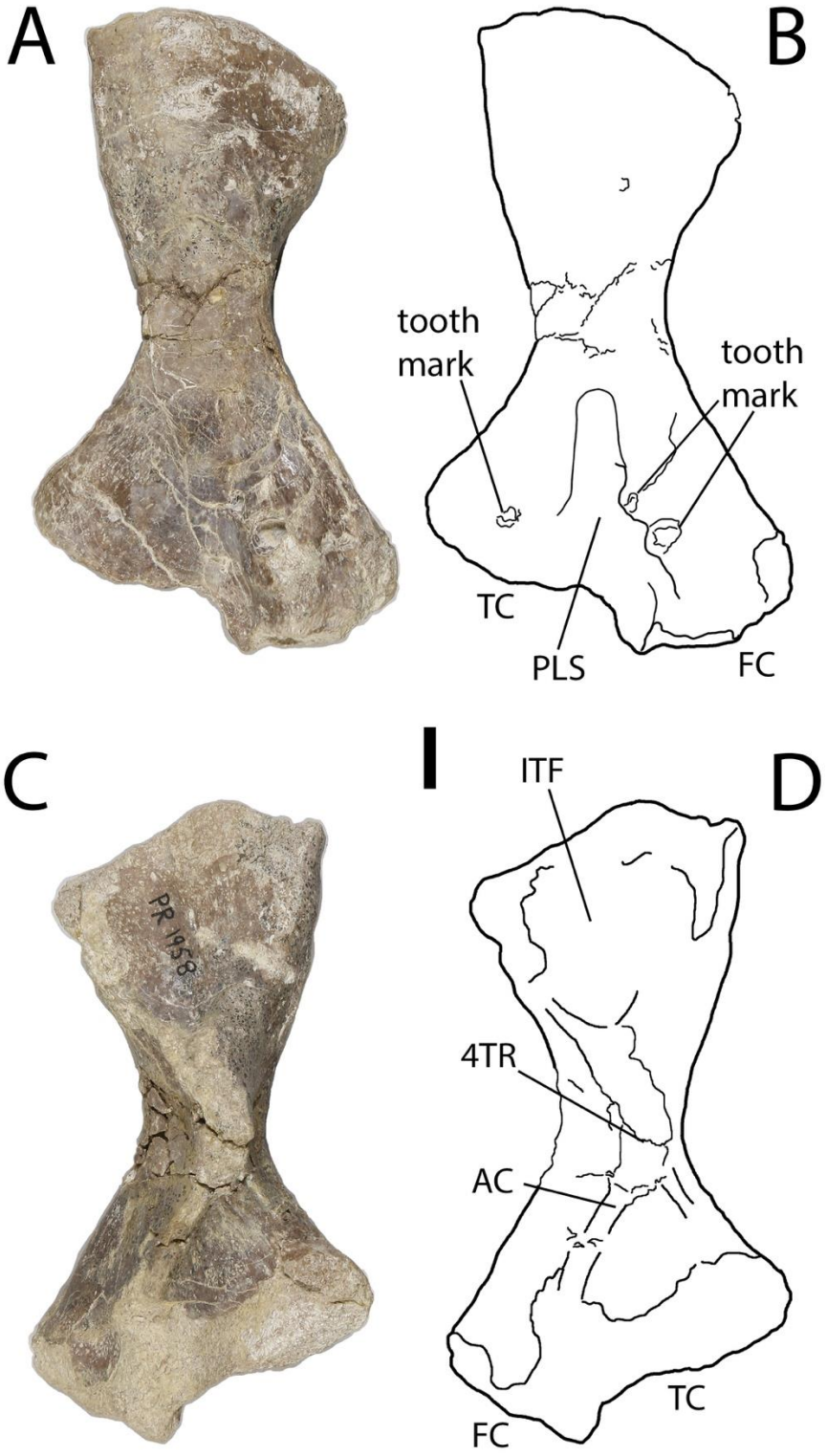

Figure 2.24. FMNH PR 1958 left femur of *Whatcheeria*. Dorsal view, specimen photo (A) and interpretive drawing (B); ventral view, specimen photo (C) and interpretive drawing (D). In all specimens, proximal is at the top and distal is at the bottom.

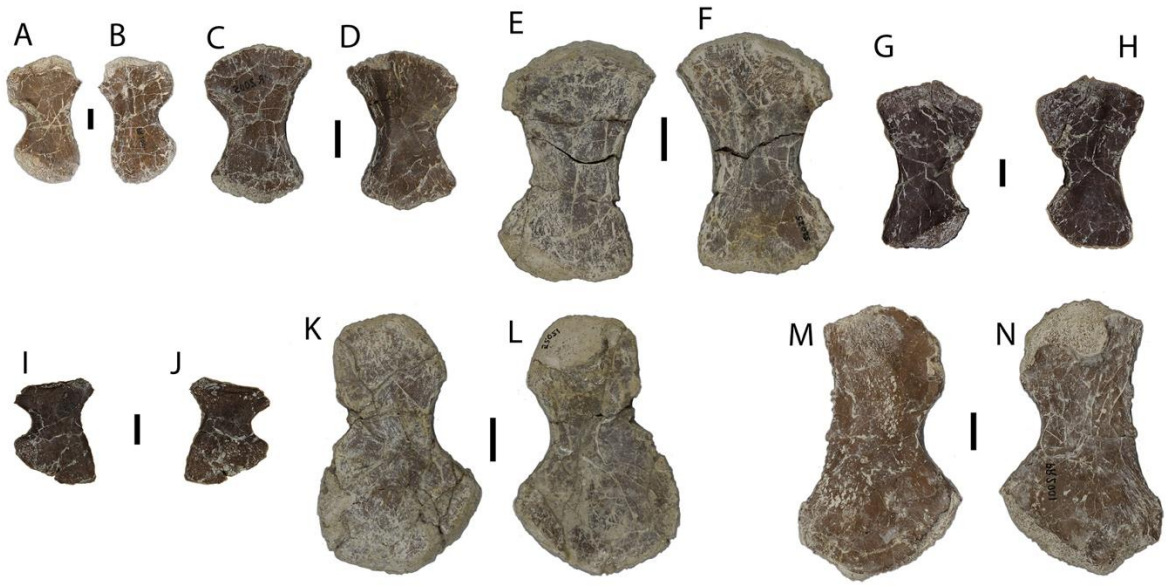

Figure 2.25. Tibiae and fibulae of *Whatcheeria*. FMNH PR 2004 right tibia in external (A) and internal (B) views; FMNH PR 2005 left tibia in external (C) and internal (D) views; SUI 52025 right tibia in external (E) and internal (F) views; FMNH PR 5016 left tibia in external (G) and internal (H) views; FMNH PR 5017 fibula in external (I) and internal (J) views; SUI 52021 right fibula in external (K) and internal. (L) views; FMNH PR 2001 ?right fibula in external (M) and internal (N) views. In all specimens, proximal is at the top and distal is at the bottom.

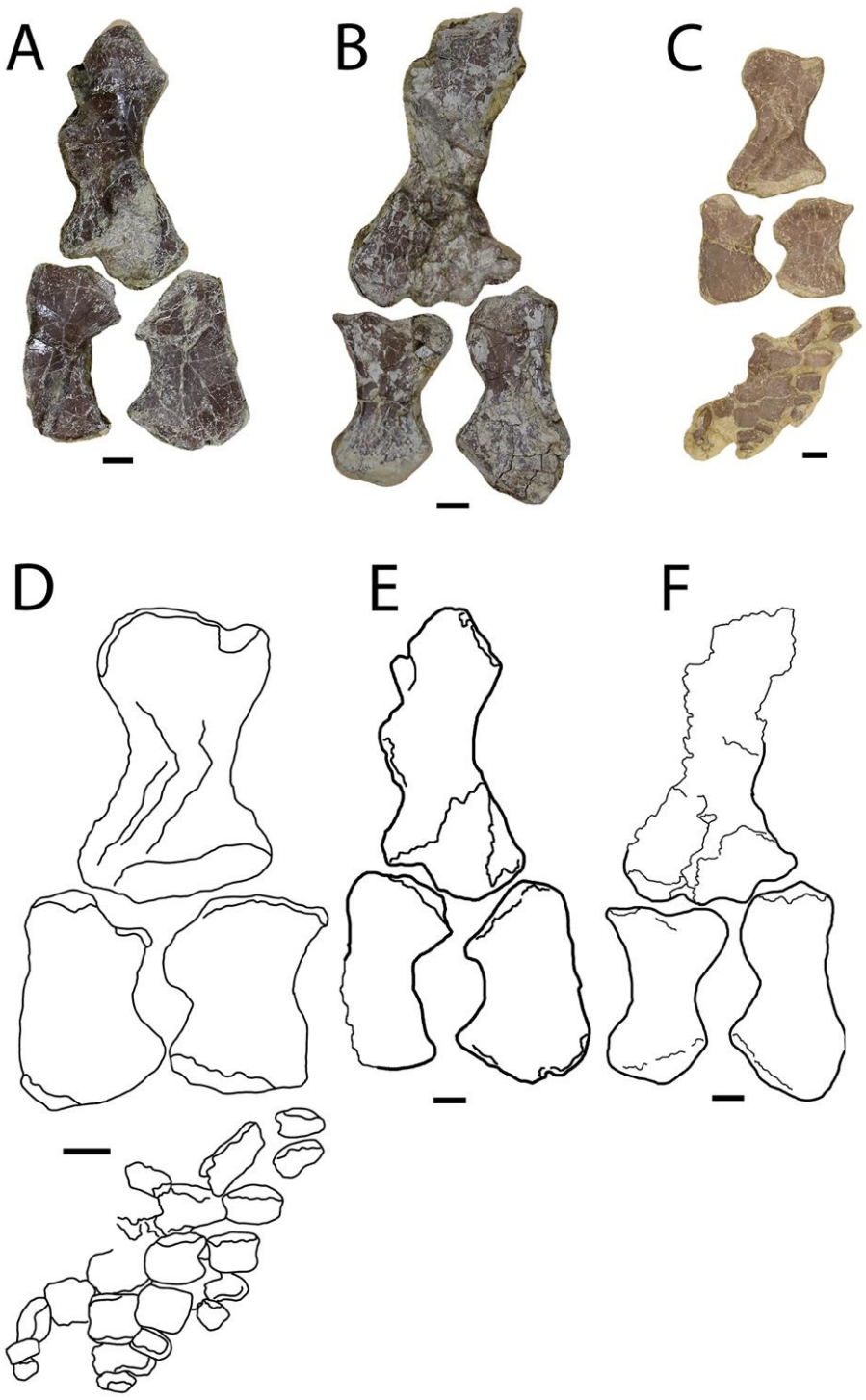

Figure 2.26. Articulated hindlimbs of *Whatcheeria*. A, FMNH PR 5012 probable right hindlimb; B, FMNH PR 5013 probable left hindlimb; B, FMNH PR 5013? left hindlimb; C, FMNH PR 1700 left hindlimb and foot in mesial view; D, interpretive drawing of FMNH PR 1700; E, interpretive drawing of FMNH PR 5012; F, interpretive drawing of FMNH PR 5013. In D and E, drawings have been scaled against F so that all drawings have the same femur length, in order to illustrate differences in proportions between specimens.

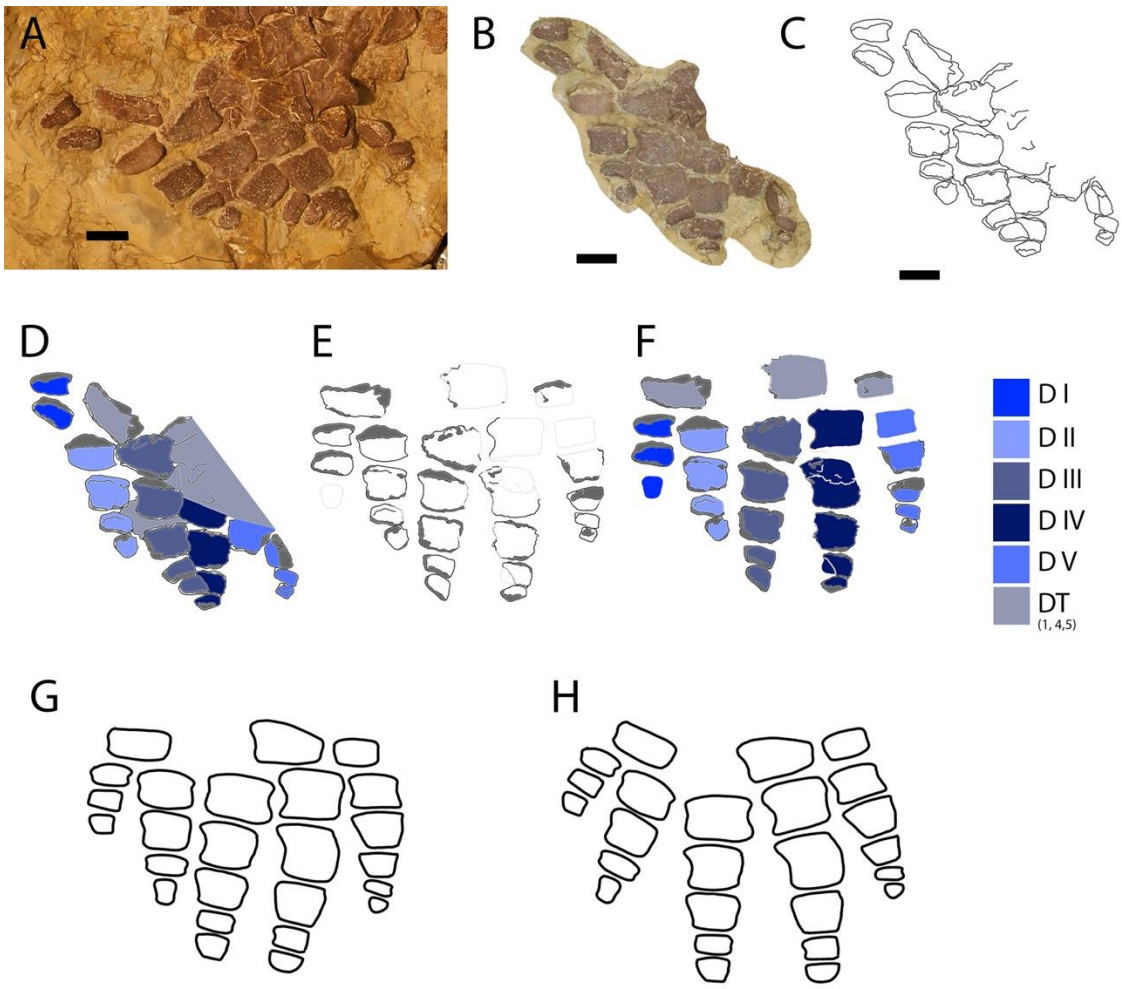

Figure 2.27. Pes of *Whatcheeria*. FMNH PR 1700 foot and ankle, specimen photo (A), cropped view (B) and interpretive drawing (C); interpretive drawing colour-coded; F, rough restoration, with grey representing restored portions not present or exposed in specimens; G, restoration of pes of *Whatcheeria* in single plane; H, restoration of pes with digits and ankle in life posture.

The tibia and fibula (Figure 2.25) are both broad compared to examples in other early tetrapods. This is most pronounced in smaller specimens, in which these epipodials resemble those of *Ichthyostega* or *Acanthostega*, except that they exhibit a distinctive waist, the curvatures of which enclose the interepipodial space. In contrast, larger *Whatcheeria* specimens are more conventionally columnar; the key difference between smaller and larger epipodials is the relative increase in shaft length. When the tibia and fibula are preserved together they are of similar length. They are large relative to the femur, about 60%-80% femur length depending on the specimen (Figure 2.26), with the variation likely stemming from ontogeny (see Ontogenetic Considerations). Among early tetrapods, only *Ichthyostega* approaches these proportions (approximately 70% femur length); 40-60% femur length is more usual, with *Pederpes* being at the higher end of this range.

The anterior margin of the tibia is straight or very gently concave, whereas the posterior margin is strongly concave. The proximal end is more expanded than the distal. A cnemial crest is present and most pronounced proximally as a sharp crest; distally, it becomes a low ridge that parallels the anterior margin of the tibia for about 90% of its length. The distal end of the tibia is slightly deflected posteriorly, as in other early tetrapods. The tibia of *Ossinodus* is very similar to that of *Whatcheeria*, whereas that of *Pederpes* is more expanded proximally and less waisted, resembling smaller/immature specimens of *Whatcheeria*.

The fibula has a concave anterior surface and straight posterior surface. Although the distal end is larger than the proximal, as in other early tetrapods, the difference is relatively small, most similar to *Baphetes*. There are no ridges as in *Tulerpeton*. As mentioned by (Coates,

1996) there is a tubercle on the proximal head that extends over/onto the shaft. Similar tubercles have been described in the fibulae of *Tulerpeton* and *Baphetes*.

When the tibia and fibula were in articulation, they most likely would not have overlapped as in *Acanthostega*, but instead deflected inwards towards each other. The interepipodial space then would have been continuous with the intercondylar fossa of the femur. The shape of this space would have varied depending on the size of the individual. In smaller individuals it would have been circular and closed at either end by the epipodials; in larger individuals it would have been more lenticular and possibly open distally (Figure 2.2, Figure 2.26).

2.4.2.7 Pes

FMNH PR 1700, the holotype, preserves a complete or nearly complete but disrupted foot and ankle (Fig.4), which provided the basis for the reconstruction (Figure 2.2, Figure 2.27). Articulated pedal specimens cannot otherwise be clearly identified, though PR 1635 includes a minimum of three partial toes and may have remains of one or two more. Manual unguals may be more rounded and less triangular than pedal unguals, but otherwise pedal phalanges are very similar in morphology to manual phalanges.

The reconstructed digital formula for the foot (Figure 2.27) is 3-4-5-5-5 (2-3-4-4-4 excluding the 'metatarsals'). As in the manus, several of the larger proximal segments are asymmetrical. This is best seen in FMNH PR 1700 (Figure 2.4, Figure 2.27). There are three ankle ossifications, associated with digits I, IV, and V, respectively. They are tentatively

identified as distal tarsals I, IV, and V, with the caveat that no other ossified tarsals or other ankle ossifications appear to have been present, at least in FMNH PR 1700. Distal tarsal V is the smallest, and distal tarsal IV is the largest. All are subrectangular; distal tarsal IV is larger at its anterior end than its posterior end. This incompletely ossified ankle is similar to those inferred for the poorly represented ankles of *Pederpes* and *Ossinodus*, but contrasts with *Greererpeton* (Godfrey, 1989), *Acanthostega* (Coates, 1996), *Ichthyostega* (Jarvik, 1996), *Archeria* (Romer, 1957) *Proterogyrinus* (Holmes, 1984), all of which have a fully ossified ankle.

2.4.2.8 Gastralia

Bony scales are common in early tetrapods, but none are preserved with *Whatcheeria* material. In tetrapods that have gastralia, they are usually common and preserved in association with other skeletal material. The absence of gastralia in the multiple articulated *Whatcheeria* specimens available suggests that, unusually for an early tetrapod, *Whatcheeria* lacked bony scales.

However, there are numerous isolated tetrapod scales from the Hiemstra Quarry (Figure 2.28). They are elongate and elliptical with pointed tips, and one margin is usually more convex than the other. In at least some examples there is a flattened portion for overlap with the articulating scale. Though these resemble the gastralia of *Pederpes*, very similarly shaped belly scales are found in *Proterogyrinus* (Holmes, 1984) and other embolomeres (Holmes and Carroll, 2010). Of the other Delta tetrapods- the colosteid *Deltaherpeton* (Bolt and Lombard, 2010), the enigmatic *Sigournea* (Bolt and Lombard, 2006), an undescribed embolomere, and a possible

‘microsaur’ (D Snyder pers. comm. October 2018)- only the last can be discounted (on the basis of size) as a possible source for the gastralia.

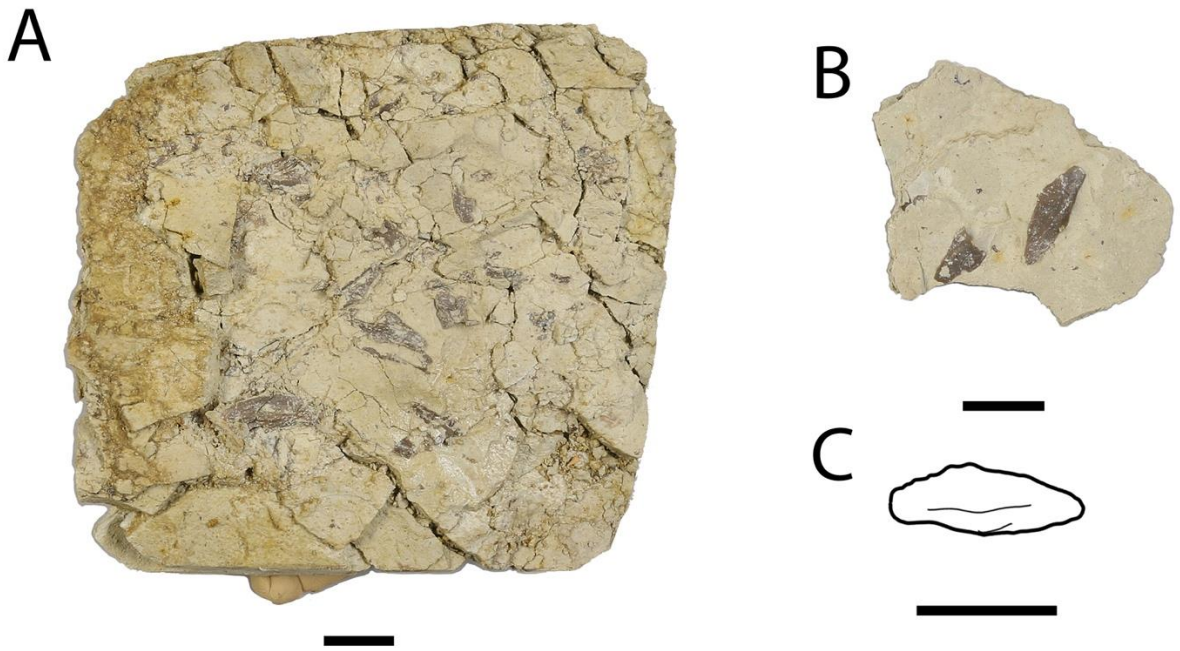

Figure 2.28. Tetrapod scales from the Hiemstra Quarry. A, FMNH PR 5014, tetrapod gastralia; B, FMNH PR 1705, tetrapod gastralia; C, interpretive drawing of scale from FMNH PR 1700.

2.5 DISCUSSION

2.5.1 Ontogenetic variation in the postcranial skeleton of *Whatcheeria*

The *Whatcheeria* collection includes numerous specimens from individuals of quite different sizes. Thus, differences in morphology likely derive from ontogenetic, rather than taxonomic, variation. There is also no clear stratigraphic sorting between smaller and larger specimens, making it unlikely that different sizes represent discrete populations.

The differently sized humeri (Figure 2.29) display considerable variation in shape relative to other parts of the skeleton. Unfortunately, flattening prevents measurements of humeral torsion in humeri other than FMNH PR 1669. The smallest humeri, including the humerus from FMNH PR 1816, are less robust than the characteristic ‘adult’ humerus morphology of *Whatcheeria* (Figure 2.18), with smaller processes and a lower overall degree of ossification. In these features, the humerus of FMNH PR 1816 resembles that of *Pederpes*. However, the entepicondyle is already large, and the spike-shaped latissimus dorsi process is present (Figure 2.29A). In ulnae associated with these smaller humeri (Figure 2.29A, B) the distinctive olecranon process is either absent (another similarity with *Pederpes*) or only weakly developed, contrasting with its presence in slightly larger individuals such as FMNH PR 1635 (Figure 2.29C).

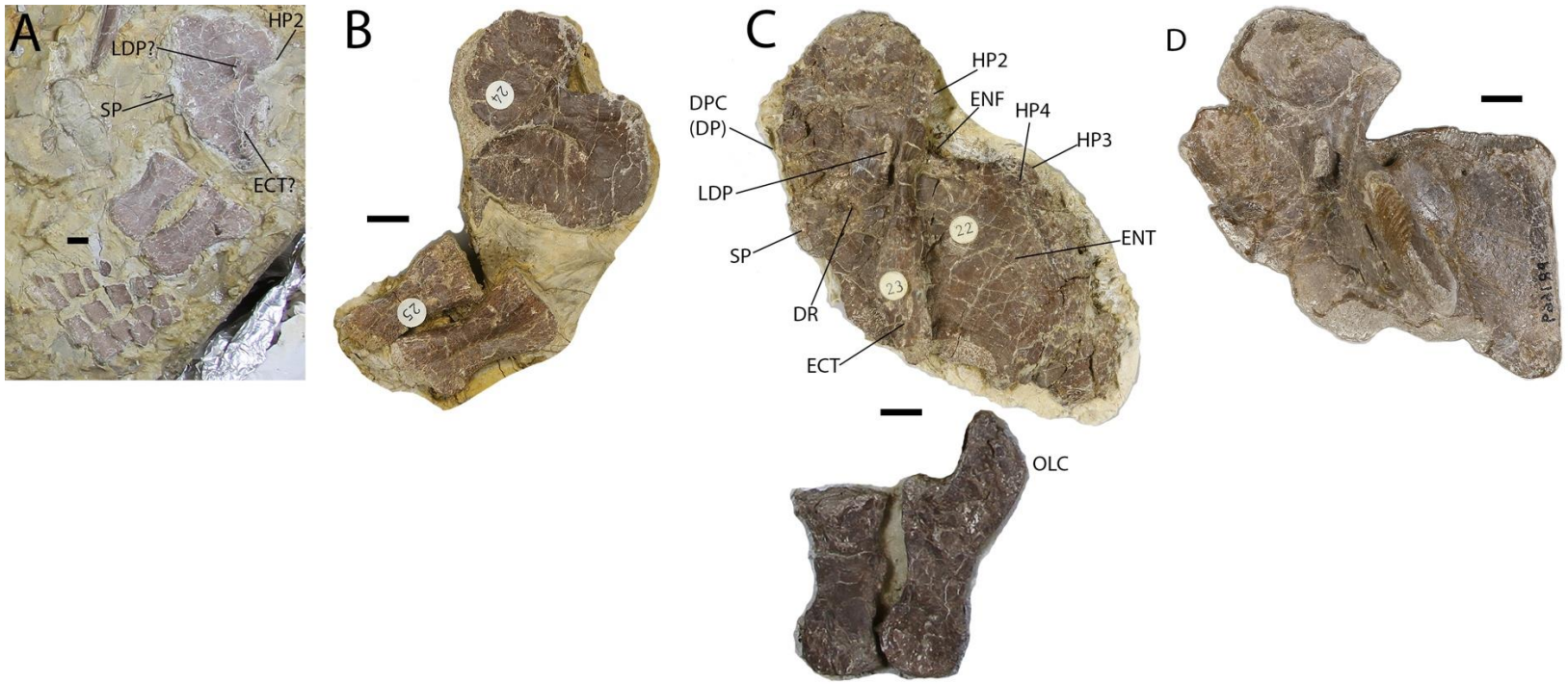

Figure 2.29. Forelimb material of *Whatcheeria* showing variation in morphology at different presumed ontogenetic stages. A, FMNH PR 1816 left forelimb with humerus, radius, ulna, and manus; B, FMNH PR 1635 (smaller individual) left forelimb with humerus, radius, and ulna; C, FMNH PR 1635 (larger individual) left forelimb with humerus, radius, and ulna; D, FMNH PR 1669 left humerus.

Pelvic girdles (Figure 2.23) and femora (Figure 2.24, Figure 2.26, Figure 2.30) are also represented by multiple specimens spanning a range of sizes. In both cases, morphology is consistent between the smallest and largest specimens. Indeed, the greatest source of variation between pelvic specimens is completeness; there is also some variation in the shape of the posterior iliac process (see pelvic girdle description). The smallest and largest stages of the femur are represented by FMNH PR 1700 (Figure 2.4, Figure 2.26) and FMNH PR 1958 (Figure 2.24), respectively. As with the pelvis, femoral morphology is consistent across sizes. Qualitative observations of the femora of *Archeria*, *Greererpeton* (Godfrey, 1989), and *Trimerorhachis* (Pawley, 2007) suggest there may be broad patterns of ontogenetic change of the femur in early tetrapods (BKAO pers. obsv.)

Whatcheeria specimens are sorted into tentative size-age classes in Table 2.1. FMNH PR 1700 and FMNH PR 1816 represent the smallest size class, Class I. Individuals of this class were probably slightly smaller than a meter in length. The shoulder girdle is incompletely ossified, with the scapulocoracoid ossifications separate in at least one specimen (Figure 2.8). The pelvic girdle seems to be mostly the same as in larger specimens. The limbs are similar in length to each other, and the forelimb is less ossified and has smaller processes. The hindlimb is ossified as in larger specimens, but the tibia and fibula are broader and larger relative to the femur (80% femur length).

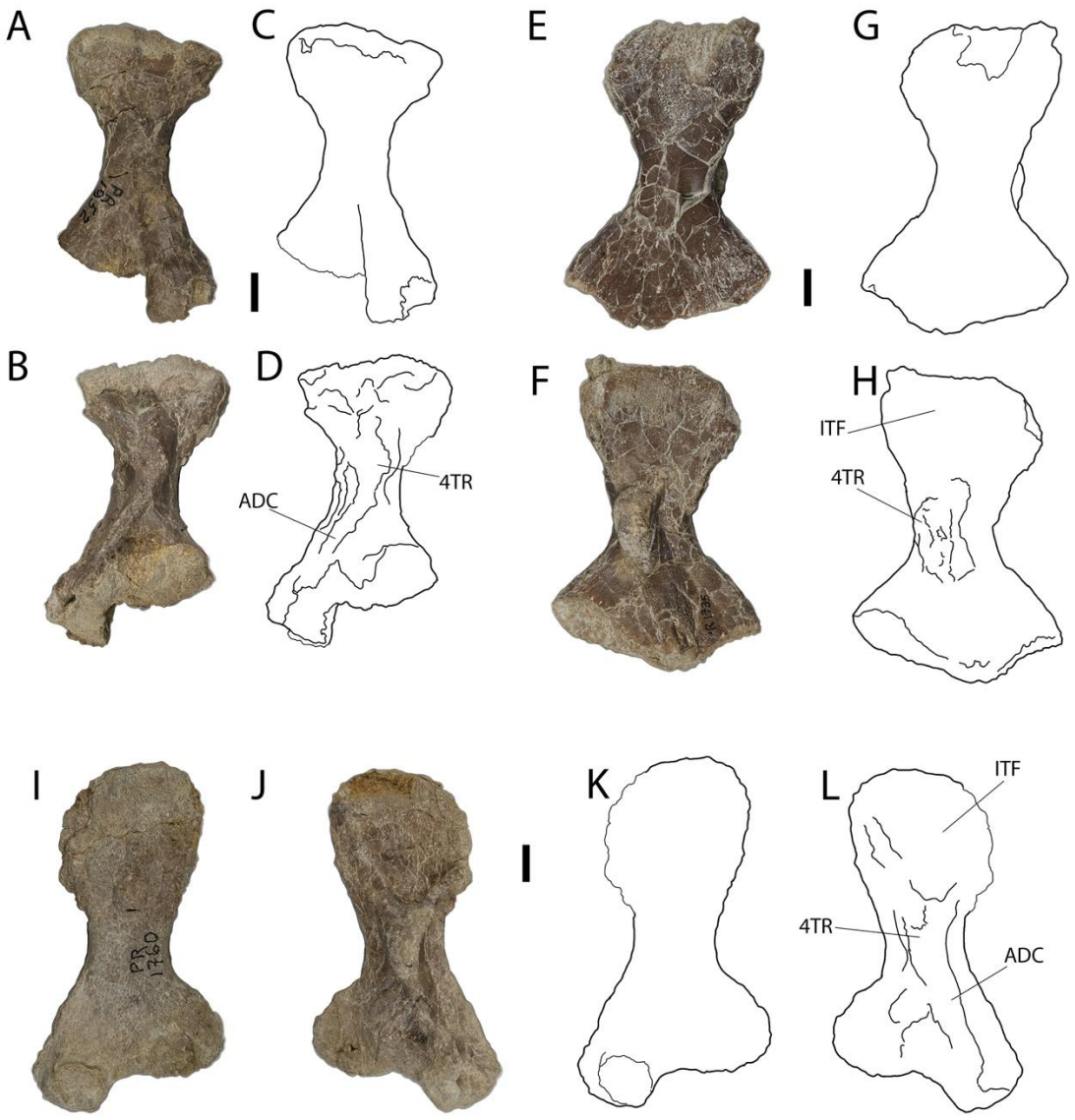

Figure 2.30. Femora of *Whatcheeria* showing size variation. FMNH PR 1952 left femur in dorsal (A) and ventral (B) views, interpretive drawing in dorsal (C) and ventral (D) views; FMNH PR 1735 right femur in dorsal (E) and ventral (F) views, interpretive drawing in dorsal (G) and ventral (H) views; FMNH PR 1760 right femur in dorsal (I) and ventral (J) views, interpretive drawing in dorsal (K) and ventral (L) views. In all specimens, proximal is at the top and distal is at the bottom.

Table 2.1. Size/age classes of *Whatcheeria* identified in this study.

Class	Exemplar specimens	Additional figured specimens	Distinguishing features
I	FMNH PR 1700, FMNH PR 1816	FMNH PR 1635 (smaller individual), FMNH PR 5009, FMNH PR 5016, FMNH PR 5017	Scapulocroacoid ossifications separate; tibia and fibula 80-90% femur length; olecranon process absent or very weakly developed; processes of humerus smaller or indistinct
II	FMNH PR 1635 (larger individual)	FMNH PR 1735, FMNH PR 1952, FMNH PR 2004	Olecranon process well-developed; tibia and fibula approx. 70% femur length; coracoid single ossification
III	FMNH PR 1760	FMNH PR 5012?	Articular surfaces more distinct; fossa on ulna present
IV	FMNH PR 1958, FMNH PR 1669	FMNH PR 4998, FMNH PR 1993, FMNH PR 2006, FMNH PR 5013, SUI-52025, SUI 52021, PR 2001	Olecranon process, processes of humerus maximum observed size; fossa on ulna strongly developed; tibia and fibula approx. 60% femur length

FMNH PR 1635 (Figure 2.18) represents an intermediate size class- Class II- that includes a large portion of the *Whatcheeria* collection. FMNH PR 1635 represents an individual probably only slightly larger than Class I. However, the scapulocoracoid is fully ossified and the ulna has a well-developed olecranon process. The humerus is more completely ossified and the muscle attachments are larger, though they have not reached the sizes seen in presumed adults. The femur is similar to that of Class I but correspondingly larger in size.

Class III is not represented by any articulated specimens and is based primarily on femora that are larger and more mature than Class II but not fully mature. It thus represents a broader and looser range of sizes and presumed ages than Classes I and II. Most isolated specimens probably fall into this class. The tibia and fibula are approximately 70% femur length.

Class IV includes the largest postcranial specimens and (presumably) fully developed adult morphologies. The full-body reconstruction (Figure 2.2, Figure 2.3) is meant to represent

an individual of this size class. Fully adult morphology and maximum size in the humeri and femora has been achieved. There are no articulated specimens to illustrate body/girdle/limb proportions but based on the size and morphology of isolated limb elements, the forelimb and hindlimb are probably still of similar length. The tibia and fibula are approximately 60% femur length, similar to *Seymouria* (White, 1939).

The ontogenetic pattern that emerges is one of increasing development of the appendicular skeleton, as shown by the increase in size, ossification, and elaboration of the girdles and especially the limbs. That said, the size classes described here only represent a portion of the ontogenetic trajectory of *Whatcheeria*, possibly corresponding with the onset of reproductive maturity. The paucity of very small specimens indicates that very young individuals were generally not preserved at the site, though there are rare exceptions (e.g. Figure 2.19E, Figure 2.25I, J) that are morphologically consistent with Class I. The largest *Whatcheeria* individuals are represented only by fragmentary cranial material; whether their postcranial anatomy differed from Class IV individuals is unknown. FMNH PR 1809 is a distal jaw fragment representing one of the largest mandibles available (Lombard & Bolt, 2006, Fig.2.2), which would have been approximately 45cm long when complete. Using the proportions of the full-body reconstruction, the whole FMNH PR 1809 animal would have been approximately 2.1m long.

Recent skeletochronological investigation of *Whatcheeria* (Whitney et al., 2022) supports the size-age hypothesis outlined above. Moreover, it found that in contrast to *Hyneria* (Kamska et al., 2018), *Eusthenopteron* (Sanchez et al., 2014), *Acanthostega* (Sanchez et al., 2016),

Whatcheeria grew rapidly between size classes I and IV. This growth pattern is similar to that found in the seymouriamorphs *Seymouria* and *Discosauriscus* (Estefa et al., 2020). *Whatcheeria* also presents the phylogenetically and chronologically earliest instance of fibrolamellar bone. Such a growth pattern was previously hypothesized to be limited to total group amniotes, linked to increased metabolisms, terrestriality, and the transition to amniotic reproduction (Estefa et al., 2020). The implied elevated growth rates and metabolism in *Whatcheeria* reinforce other indications from this taxon that early tetrapods had a much greater diversity of functions and life history strategies than previously appreciated.

2.5.2 Comparison with other early tetrapods

Comparative data on body proportions drawn from a small set of early tetrapods provide context to the anatomical observations presented here, and the full-body reconstruction of *Whatcheeria* depicted in Figure 2.31. These data show that *Whatcheeria* and *Pederpes* join the Permian diadectid *Orobates* and the Triassic amphibamid *Micropholis* in possessing the largest limbs relative to trunk length. Furthermore, these data confirm that the unusually long neck of *Whatcheeria* is outstanding; relative to trunk length it is twice as long as the necks of *Proterogyrinus* and *Acanthostega*, which have the next-highest neck length/presacral length ratios.

More generally, these data reveal that forelimb/hindlimb length disparity decreases as limb size increases relative to trunk length. However, these changes are not linear or uniform. *Pederpes* has much larger limbs relative to its body than *Proterogyrinus*, but both have similar forelimb/hindlimb length ratios. In terms of limb lengths relative to the body, there are three sets

of taxa: *Acanthostega*/*Trimerorhachis*/*Greererpeton* (‘small’), *Balanerpeton*/*Proterogyrinus*/*Eucritta* (‘medium’), and *Whatcheeria*/*Pederpes*/*Micropholis*/*Orobates* (‘large’). Importantly, from these groups (albeit from a small sample size) there is no clear correlation between proportional limb size and inferences of terrestriality.

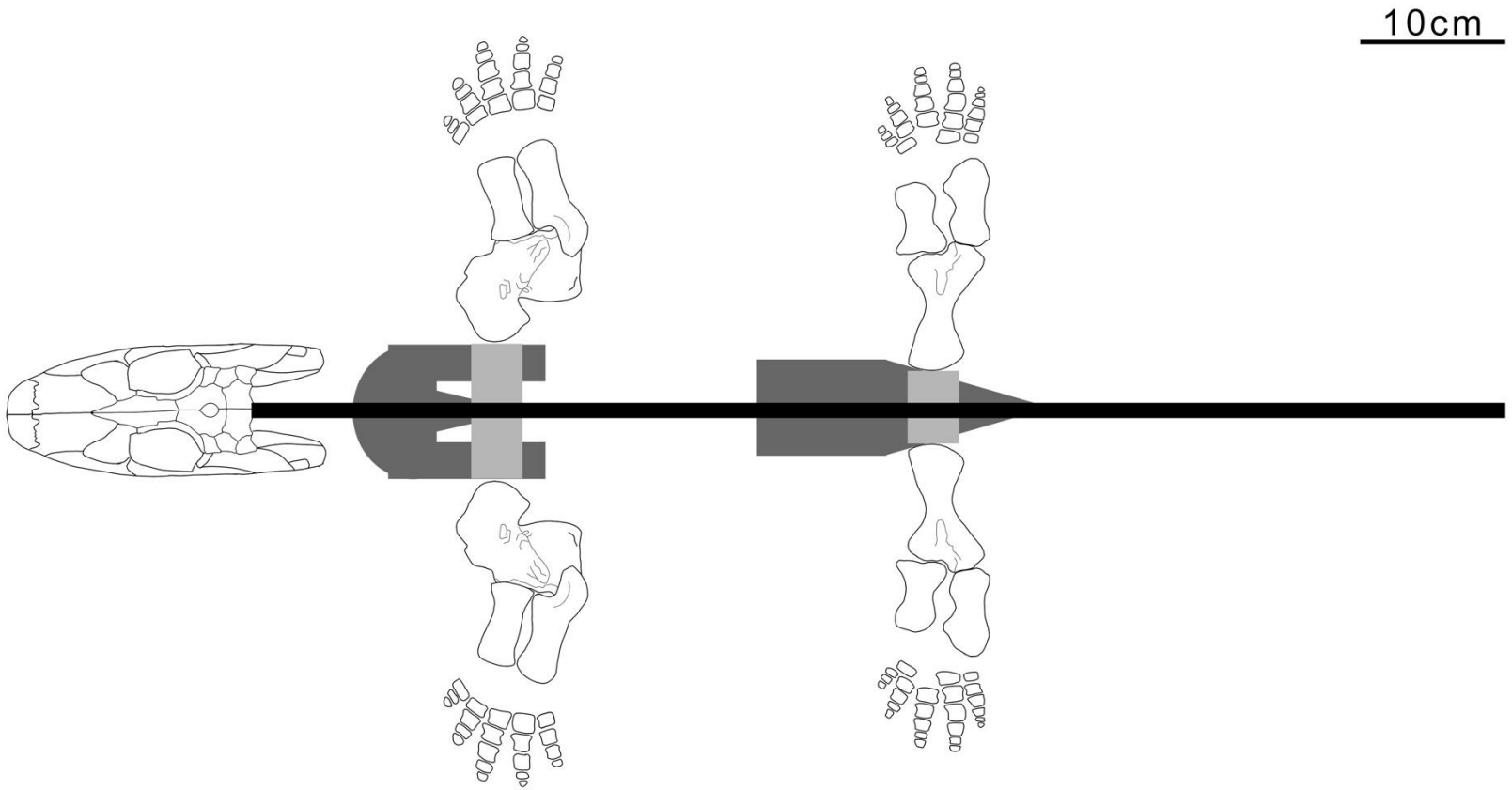

Figure 2.31. Full-body reconstruction of *Whatcheeria* in dorsal view, emphasizing the relatively large limbs. The limb bones are projected flat in a single plane. The axial skeleton and limb girdles are represented by simple geometric shapes.

These numerical results are visualized in the most taxonomically inclusive permutation of the PC analysis (Figure 2.32). Due to difficulty in obtaining reliable limb measurements for *Seymouria*, it was excluded from this permutation. Three morphotypes are discernible: those with large, equal-length limbs (*Whatcheeria, Pederpes*, *Orobates*, *Micropholis*); those with medium-length, medium-disparity limbs (*Ichthyostega*, *Balanerpeton*, *Eucritta*, *Proterogyrinus*); and those with small, medium-to-high-disparity limbs (*Trimerorhachis, Greererpeton*, and *Acanthostega*). There is no discernible phylogenetic clustering. All three morphotypes are represented by both stem tetrapods and crown tetrapods. Notably, *Whatcheeria* and *Pederpes* are the stem tetrapods that converge most closely with the terrestrially-adapted crown tetrapods in terms of limb proportions. Although these results signal that multiple tetrapod lineages converged on similar limb proportions, extrapolations to convergent function are less clear.

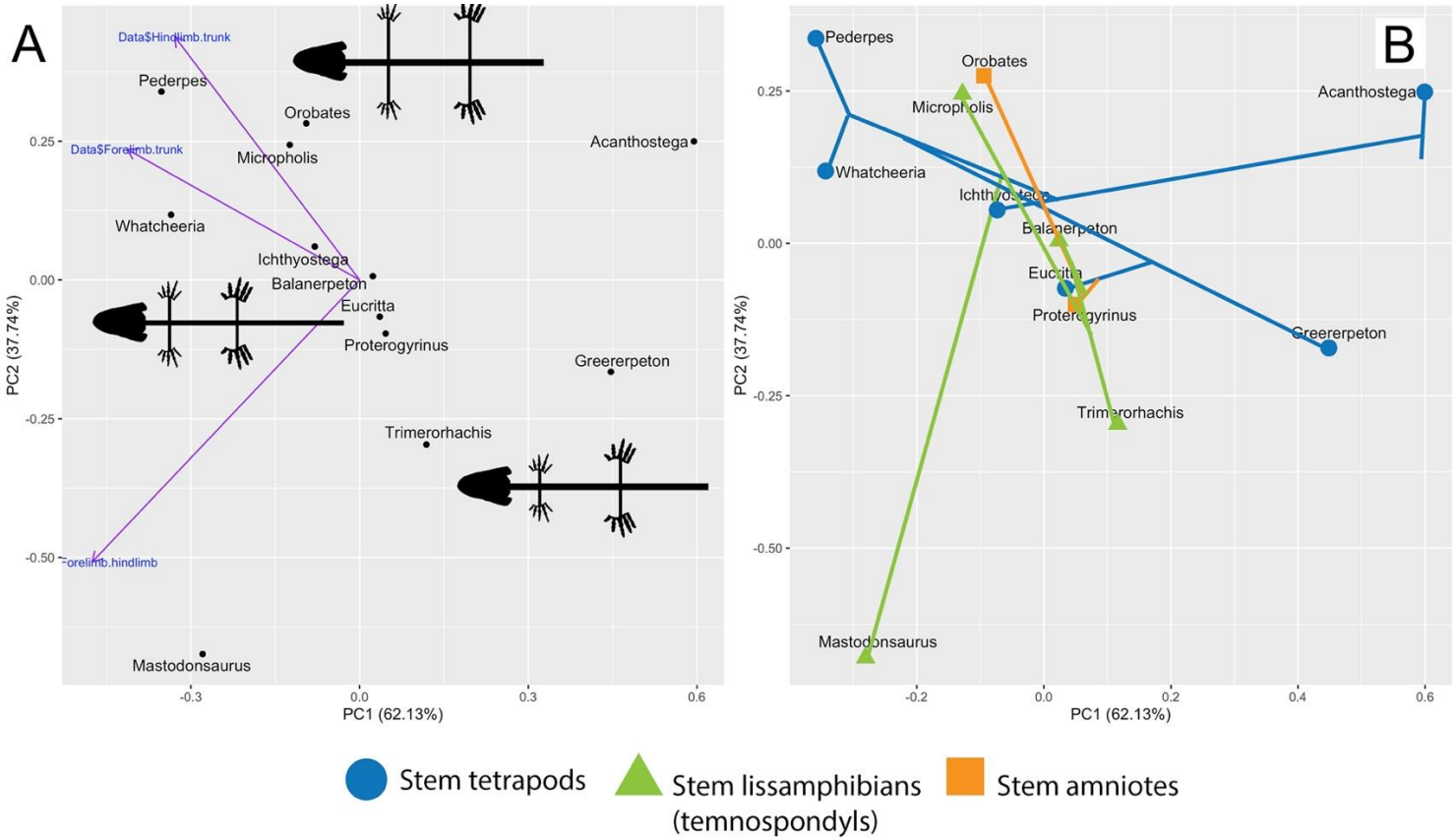

Figure 2.32. Principal components analysis visualizing comparisons of forelimb/hindlimb length, forelimb/trunk length, and hindlimb/trunk length ratios. A, PCA results with schematic representations of the three principal morphotypes and their corresponding areas of morphospace; B, phylomorphospace based on A with colours and symbols representing stem tetrapods, stem lissamphibians (temnospondyls) and stem amniotes. The phylogenetic scheme in B is based on (Ruta and Coates, 2007), assuming a temnospondyl origin of lissamphibians, a monophyletic Whatcheeriidae containing *Whatcheeria* and *Pederpes*, and a stem amniote identity for embolomeres. Skulls for silhouettes in A are based on the skull of *Acanthostega* in (Porro et al., 2015). See Supporting Information, Additional results from Principal Components Analysis.

2.5.3 Standing in the shallows: the functional anatomy of *Whatcheeria*

The *Whatcheeria* postcranium is more of a unique collection of plesiomorphies than a suite of novel characteristics. The uncinate processes of the ribs are particularly large, but uncinate processes are widely distributed across early tetrapods (Coates, 1996; Clack and Finney, 2005). The humerus, with plesiomorphic L-shape and set of processes, is distinguished by size and proportions- including a massive entepicondyle- rather than its derived organization. The wrist and ankle are barely ossified, in common with most other early tetrapods. Indeed, the ankle is less ossified than in *Acanthostega* or *Greererpeton*, which were firmly aquatic and are traditionally recovered as stemward and crownward of *Whatcheeria*, respectively. Furthermore, the phalanges are short and broad, resembling those of the thoroughly ossified pes in the hindlimb paddle of *Ichthyostega*. In summary, rather than ongoing innovation, these morphologies seem more consistent with the phenomenon of constrained character space or character exhaustion (Ruta et al., 2006; Wagner et al., 2006; Bernardi et al., 2016), earlier than might be expected in the initial evolutionary radiation of limbed tetrapods.

Whatcheeria, like *Eryops* and *Ichthyostega*, has a strongly regionalized ribcage with large uncinate processes on the elongate anterior trunk ribs. In all three taxa this arrangement was likely associated with substantial shoulder musculature. The shorter posterior trunk ribs of *Whatcheeria* are most likely plesiomorphic (c.f. *Acanthostega*, Coates 1996). Notably, these ribs are not reduced as in the East Kirkton 'anthracosauroid' *Eldeceeon* which has long anterior trunk ribs but lacks posterior trunk rubs altogether (Smithson, 1993; Ruta *et al.*, 2020).
Increased shoulder musculature accords well with the extensive forelimb musculature implied by the morphology of the humerus and ulna. The limb would have been most powerful in retraction,

with protraction being the recovery stroke. The shape of the humeral head and glenoid would have limited pronation and supination. Similarly, the olecranon process and ectepicondyle might have reduced the ability of the forelimb to extend at the elbow (Holmes, 1984). The forelimb would have provided stable, pectoral-level support, but with limited forelimb extension or rotation, walking would have required retraction to lift the forelimb and lateral flexion of the axial column to swing it forwards. This was likely assisted by the short posterior trunk ribs. Kinematic study of terrestrial locomotion in *Pleurodeles* (Karakasiliotis *et al.*, 2013) found large amounts of lateral flexion occurred in the posterior trunk and the distal half of the tail. Similarly, robotic biomechanical simulations of *Orobates* (Nyakatura *et al.*, 2019) based on trackways and skeletal evidence estimate that greatest lateral bending occurred approximately halfway along the trunk, with additional lateral bending at the base and midpoint of the tail. *Whatcheeria* lacks the morphological adaptations to the posterior trunk ('lumbar') vertebrae hypothesized to limit lateral (and dorsoventral) flexion in *Ichthyostega* (Ahlberg et al., 2005). Therefore, despite their similarities, *Ichthyostega* likely had a very different locomotor strategy than *Whatcheeria*, possibly one unique among early tetrapods (Ahlberg et al., 2005; Pierce et al., 2012).

The squat phalanges of *Whatcheeria* are dissimilar to those of (putatively) terrestrial taxa, which tend to be waisted with ventral grooves to accommodate ligaments to assist grasping (Clack & Finney, 2005). However, like *Pederpes* the asymmetric pedal phalanges imply an anteriorly-oriented foot (Figure 2.4, Figure 2.25, Figure 2.31), which, in turn, is a morphology associated with a walking gait (whether underwater or on land) (Clack & Finney, 2005). The significance of the breadth of the phalanges is unclear. These might have enhanced support (in or

out of the water), or served as paddle-skeleton, acknowledging that broad phalanges occur in the paddles of extinct and extant tetrapods.

Limb length relative to body length (Figure 2.2, Figure 2.31, Figure 2.32) and limb robustness in *Whatcheeria* suggest an increased emphasis on appendicular locomotion and support compared to other early tetrapods (Table 2, Fig.32). The tail lacks the radials and large neural and hemal spines of aquatic early tetrapods, suggesting it was less important for locomotion (although the extent of any soft-tissue fin is completely unknown). The limbs themselves are robust with large muscle attachments (Figure 40), and the girdles and highly consolidated. The lack of bony gastralia in *Whatcheeria* may be related to its limb morphology. Gastralia belly armor is widespread among early tetrapods (Holmes, 1984; Panchen, 1985; Clack, 1987a; Godfrey, 1989; Andrews and Carroll, 1991; Milner and Sequeira, 1993; Lebedev and Coates, 1995; Coates, 1996; Ruta and Clack, 2006; Herbst and Hutchinson, 2018) and would have acted to protect the underbelly of the animal from abrasion by the substrate. The conspicuous absence of belly armor in *Whatcheeria* suggests that the unberbelly of the animal was kept out of contact with the substrate. The elevation of the anterior trunk would also have created more room to facilitate breathing (by expansion of the chest cavity) and movement of the neck.

The elongate neck of *Whatcheeria* is the most striking feature revealed by the present reconstruction (Figure 2.2, Figure 2.3, Figure 40, Figure 41). Neck length must have increased head mobility, relative to the primitive condition wherein the pectoral girdle is close behind the cheek (e.g. *Pederpes*, *Ichthyostega*). Such mobility would have reduced the need to move the

entire body to track, grasp, and manipulate prey. The increased space between the skull and pectoral girdle would also have allowed more room for jaw depression, increasing gape and throat volume. However, estimates of capacity are difficult without a preserved ceratohyal.

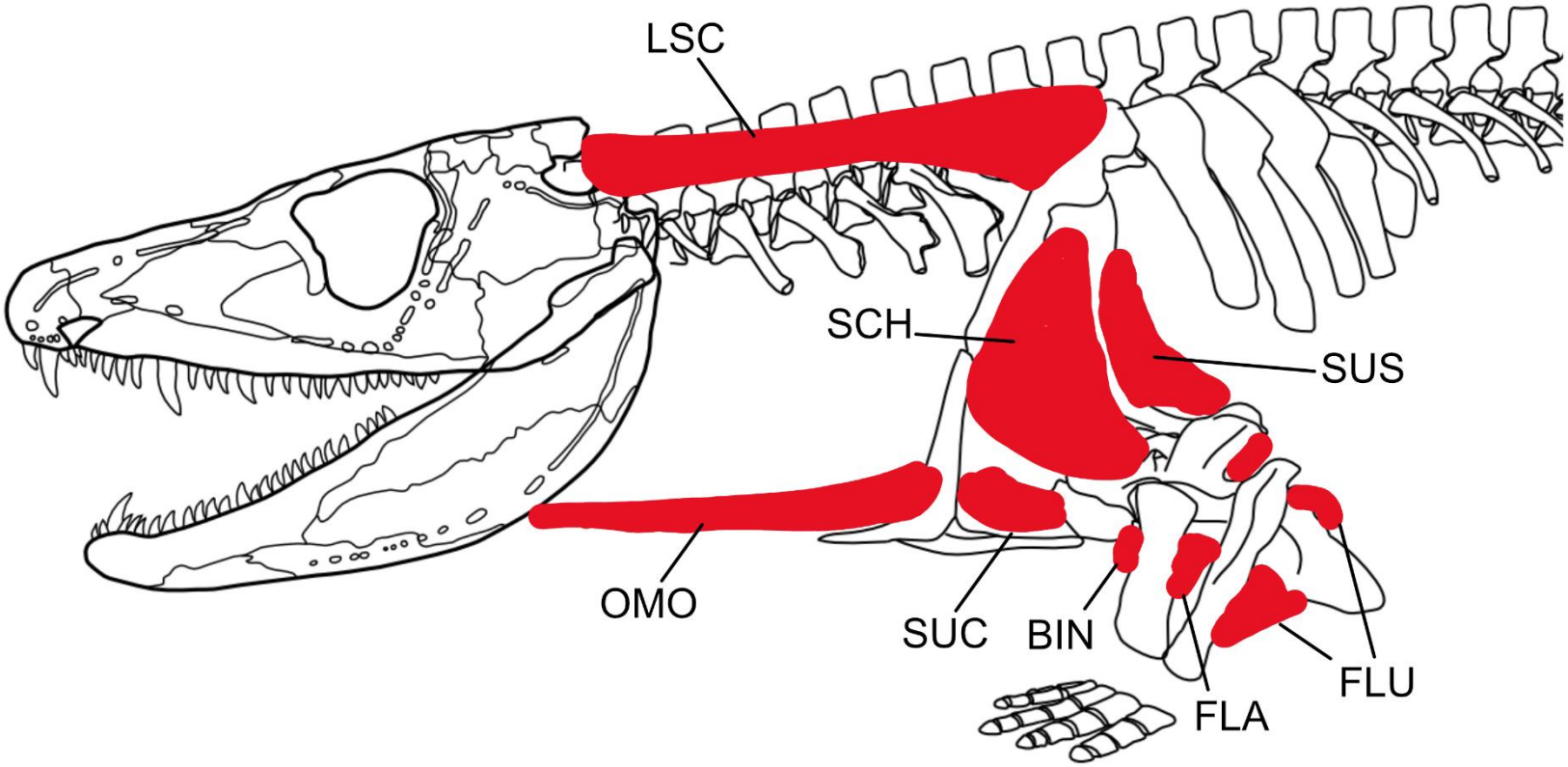

Figure 2.33. Anterior trunk and head of *Whatcheeria* with deep muscles reconstructed after *Ossinodus* by Bishop (2015).

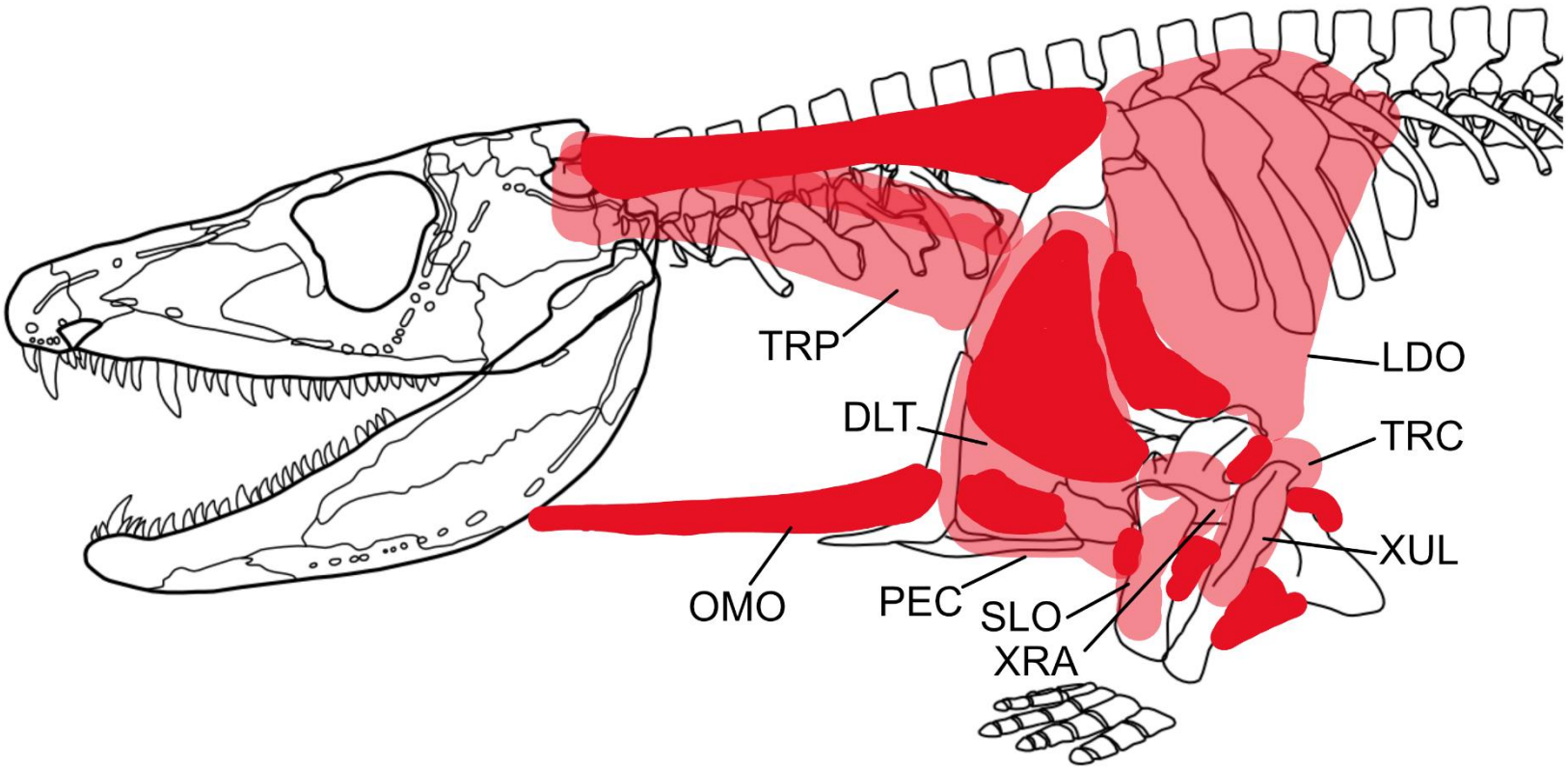

Figure 2.34. Anterior trunk and head of *Whatcheeria* with deep (dark red) and superficial (light muscles) reconstructed after *Ossinodus* by Bishop (2015).

The unusual combination of morphologies present in *Whatcheeria* complicates the inference of its life habits. There is histological evidence that *Greererpeton*, which has small limbs, undertook an overland excursion from their natal water body at the onset of sexual maturity (Whitney and Pierce, 2021). While there is no evidence for a similar life event in *Whatcheeria* (Whitney et al., 2022), it was probably capable of at least a limited amount of terrestrial locomotion if pressed. Such activity, however, would have been minimal; the lack of carpal and tarsal ossifications and (especially) the presence of well-developed cranial sensory canals indicate that *Whatcheeria* was a habitually aquatic animal. An aquatic walking gait, as hypothesized for *Seymouria* (White, 1939) and *Proterogyrinus* (Holmes, 1984), seems plausible in *Whatcheeria*. Indeed, *Whatcheeria* may be a tetrapod specialized for walking in vegetation-choked shallow-water habitats. Aside from the functional anatomy of *Whatcheeria*, its ecological context supports inference of an aquatic habit. The Delta fauna is wholly aquatic with the exception of some terrestrial arthropods (Bolt et al., 1988; Lombard and Bolt, 1995; Bolt and Lombard, 2006, 2010; Snyder, 2006). This is typical of tetrapod localities from the Late Devonian and Mississippian (Smithson, 1985a; Clack et al., 2016; Ross et al., 2018; Clack et al., 2019a).

2.5.4 Reevaluation of whatcheeriid taxa and specimens

2.5.4.1 Reinterpretation of *Pederpes*

Pederpes (Clack 2002) is known from a single, well-preserved and near-articulated specimen. Of relevance to the present discussion, the appendicular skeleton is less ossified than that of adult *Whatcheeria* with smaller or absent processes of the humerus, ulna, and femur.

From the description and figures (Clack, 2002c; Clack and Finney, 2005) it is clear that the limb bone joint surfaces must have been finished with large amounts of cartilage. These observations suggest that *Pederpes* is subadult, and that this is likely the source of many differences between equivalent structures in *Whatcheeria* and *Pederpes*. The degree of ossification in the *Pederpes* appendicular skeleton resembles Class I *Whatcheeria* material, consistent with the size of the *Pederpes* holotype: approximately 50cm presacral length including the skull. However, the limbs of *Pederpes* are already proportionally longer than those of *Whatcheeria* . Class I *Whatcheeria* specimens appear to have already established adult proportions of the pectoral, cervical, and trunk regions. Thus, it appears that a hypothetical adult *Pederpes* (assuming a *Whatcheeria*-like growth trajectory) would have been anatomically distinct from *Whatcheeria*, with somewhat stouter forequarters.

2.5.4.2 The ‘what’ in whatcheeriid: membership of the family Whatcheeriidae

The erection of the Whatcheeriidae (Clack 2002) was noted as the first new family of Mississippian tetrapods to be named in decades (Clack and Milner, 2015). Since *Pederpes*’ publication, *Ossinodus* has also been linked to the group (Warren & Turner, 2004; Warren, 2007), as have isolated cranial and postcranial bones from both Devonian (Daeschler et al., 2009; Olive et al., 2016) and Carboniferous (Anderson *et al.*, 2015) localities. Here we aim to review such material in light of the improved knowledge of the distinctive characteristics of whatcheeriid morphology.

Synapomorphies associating *Ossinodus* with the Whatcheeriidae (Warren and Turner, 2004) include:

- Massive tooth on the maxilla about position 5 or 6
- Very broad interclavicle with acutely angled lateral corners

Whatcheeriid symplesiomorphies also present in *Ossinodus* (Warren and Turner, 2004):

- Supratemporal-postparietal contact
- (Probable) fangs and row of smaller accessory teeth on vomers, palatines, and ectopterygoids
- Nearly continuous row of coronoid teeth
- At least some lateral lines in tubes through bone
- Ilium with postiliac process and dorsal iliac blade

Characters of uncertain polarity shared with whatcheeriids (Warren and Turner, 2004):

- Pronounced angle between skull table and cheek in transverse section
- Trunk ribs with expanded distal flanges

Of the two hypothesized synapomorphies, massive 'caniniform' teeth on the maxilla might indeed be characteristic of *Ossinodus*, *Pederpes*, and *Whatcheeria*. In *Ichthyostega* (Jarvik, 1996), *Acanthostega* (Porro et al., 2015), *Ventastega* (Ahlberg et al., 2008), the colosteids (Panchen, 1975; Smithson, 1982; Hook, 1983; Bolt and Lombard, 2010), the baphetids (Beaumont, 1977), and *Crassigyrinus* (Clack, 1997), maxillary teeth are either uniform in size or decrease gradually in size posteriorly along the maxilla. Embolomeres (Panchen, 1977; Holmes, 1984, 1989a; Klembara, 1985; Clack, 1987b, 1987a) also lack maxillary caniniform teeth.

Conversely, the cited features of interclavicle morphology are neither unique to whatcheeriids nor *Ossinodus*, as the characterization is applicable to colosteids, *Crassigyrinus*, embolomeres (Romer, 1957; Holmes, 1984; Clack, 1987a), and others. Although the interclavicles of *Pederpes* and *Ossinodus* are very similar, they both differ from that of *Whatcheeria*, which resembles *Ichthyostega*. Similarly, distal flanges (uncinate processes) occur

in a scattering of disparate early tetrapods (Coates, 1996). The uncinate processes of *Ossinodus* are similar to those of *Acanthostega*, whereas *Whatcheeria* resembles *Ichthyostega* and *Eryops*. (Warren, 2007) showed that *Ossinodus* differs from *Pederpes* and *Whatcheeria* in skull shape and proportions. We concur and offer no additional support for the hypothesis that *Ossinodus* is a whatcheeriid.

Fragmentary Devonian and Carboniferous material referred to the Whatcheeriidae is listed in Table 2.2. Given that the whatcheeriid status of *Ossinodus* is now doubtful, support for the assignment of many of these specimens is now uncertain or absent, because these, in turn, were based – at least in part – on comparison with *Ossinodus*.

Several 'whatcheeriid' specimens have been collected from the Famennian Catskill Formation Red Hill locality in Pennsylvania (Daeschler et al., 2009; Broussard et al., 2018). ANSP 21873, a postorbital, has been compared to that of *Pederpes* in shape. As figured, the resemblance is suggestive and indicates that the animal likely had non-circular orbits. However, noncircular orbits are not unique to whatcheeriids, and both ANSP 21873 and the only visible postorbital of the *Pederpes* holotype are incomplete. ANSP 21874, a left lacrimal, has similar ornament and probably belongs to the same taxon as ANSP 21873. Neither specimen is sufficiently complete to infer the presence of a Red Hill whatcheeriid.

ANSP 21476, a femur, is unlike those of *Whatcheeria* or *Pederpes*. The shaft is longer and the ends are narrower. It seems to show the short, distally located adductor crest and large adductor blade present in *Acanthostega*, and, to a lesser extent, in *Ichthyostega* and *Tulerpeton*

(cf. Coates 1996) as well as *Ossinodus*. Adductor blade size in ANSP 21476 relative to the rest of the femur resembles *Ossinodus* rather than the Devonian taxa, as does the lack of torsion of the epipodial facets. The distal protrusion of the fibular condyle past the tibial condyle is intermediate between *Tulerpeton* and *Ossinodus*. ANSP 23864, an incomplete femur from the slightly older Trout Run North locality within the Catskill Formation, shows similar overall proportions and positions of the adductor crest and adductor blade. We disagree with the identification of a proximally located internal trochanter in ANSP 23864 (Broussard et al., 2018). Given the apparent abrasion of the specimen, we interpret that feature as being an artifact of wear combined with damage to the proximal end and intertrochanteric fossa, with the internal (and, presumably, fourth) trochanters not preserved. Neither ANSP 21476 nor ANSP 23864 is conclusively whatcheeriid.

Additional Famennian 'whatcheeriid' fragments, a postorbital and a maxilla, have been described from Strud and Becco in Belgium (Clement et al., 2004; Olive et al., 2016). The Strud postorbital, IRSNB A.0006, is much more complete than ANSP 21873, and shares the same ornament pattern as well as (inferred) shape. Once again, there is nothing distinctively whatcheeriid about IRSNB A.0006. The Becco maxilla, IRSNB A.0007, has two large teeth with tooth pits starting at positions three or four. This is the deepest part of the maxilla, with depth and tooth size decreasing posteriorly, unlike the Strud 'ichthyostegid' maxillae which show uniformly sized teeth. As previously discussed, maxillary caniniform teeth might be a characteristic of *Whatcheeria*, *Pederpes*, and *Ossinodus*, but in the absence of further diagnostic features these data are insufficient to refer IRSNB A.0007 to Whatcheeriidae.

Specimens from Tournaisian deposits at Burnmouth in Scotland were recently compared to *Pederpes* and *Whatcheeria* (Otoo et al., 2018). Although more definitive conclusions await further Burnmouth material and a detailed description of the *Whatcheeria* skull, a few remarks can be made here. As previously assigned, the frontal bones, with at least one partial prefrontal, resemble their *Whatcheeria* (Lombard and Bolt, 1995) and *Pederpes* (Clack and Finney, 2005) counterparts. Contra (Otoo et al., 2018) the cleithrum resembles that of *Pederpes* in the slight curvature of the stem, the rounded shape of the dorsal expansion, and the lack of a posterior notch. The radius is slenderer than that of *Pederpes* or *Whatcheeria*, but exhibits no distinctively whatcheeriid features. The phalanges are longer than broad with well-defined flexor attachments (cf. Otoo *et al*. 2018), thus quite unlike *Whatcheeria*. The jaw material with anteroposteriorly compressed teeth is unique. The existence of two disparate size fractions with the collection challenges easy taxonomic assignments, although presence of maxillae with the unique tooth morphology across both size classes suggests that both fractions might represent, in part, the same taxon. Unfortunately, most currently known skeletal material derives from one size class, but at least some of this likely represents a *Pederpes*-like whatcheeriid.

Numerous isolated tetrapod bones have been recovered from the Blue Beach locality at Horton Bluff (both names are used interchangeably to refer to this locality) in Nova Scotia (Anderson et al., 2015). Blue Beach is important because it, and the roughly coeval Ballagan Formation in Britain, provide the entirety of the Tournaisian tetrapods currently known (Clack and Finney, 2005; Smithson et al., 2012; Chen et al., 2018; Smithson and Clack, 2018; Clack et al., 2019a; Lennie et al., 2020, 2021).

Pelvis Type 1 (NSM005GF045.001) has iliac processes similar to those of *Whatcheeria* and *Pederpes:* robust, distally expanded, and probably short, though the complete length of the posterior process is unknown. As in many early tetrapod ilia the processes are offset by a notch, but their limited overlap in lateral view is *Pederpes*-like (Clack and Finney, 2005). The dorsal process is subrectangular, but it is not clear whether the flat dorsal margin is complete or not. Unlike *Pederpes* but in common with *Whatcheeria* and most (adult) early tetrapods, the pubis is ossified and sutured to the ischium. The acetabulum is too poorly preserved to offer diagnostic features, but the ischium displays a distinct concave dorsal margin, quite unlike *Pederpes* or *Whatcheeria*. On the basis of a general resemblance of the ilia but little else, we agree with Anderson *et al*. (2015) that NSM005GF045.001 is similar to whatcheeriid pelves.

Femur Type 2 (NSM004GF045.034A, B), contra its original description as a 'tulerpetonid' (Anderson et al., 2015), bears a strong resemblance to the femur of *Ossinodus* (Figure 2.33). The principal difference between the specimen and *Ossinodus* appears to be the relative sizes of the internal and fourth trochanters: in Femur Type 2 the former is larger, and in *Ossinodus* the latter is larger.

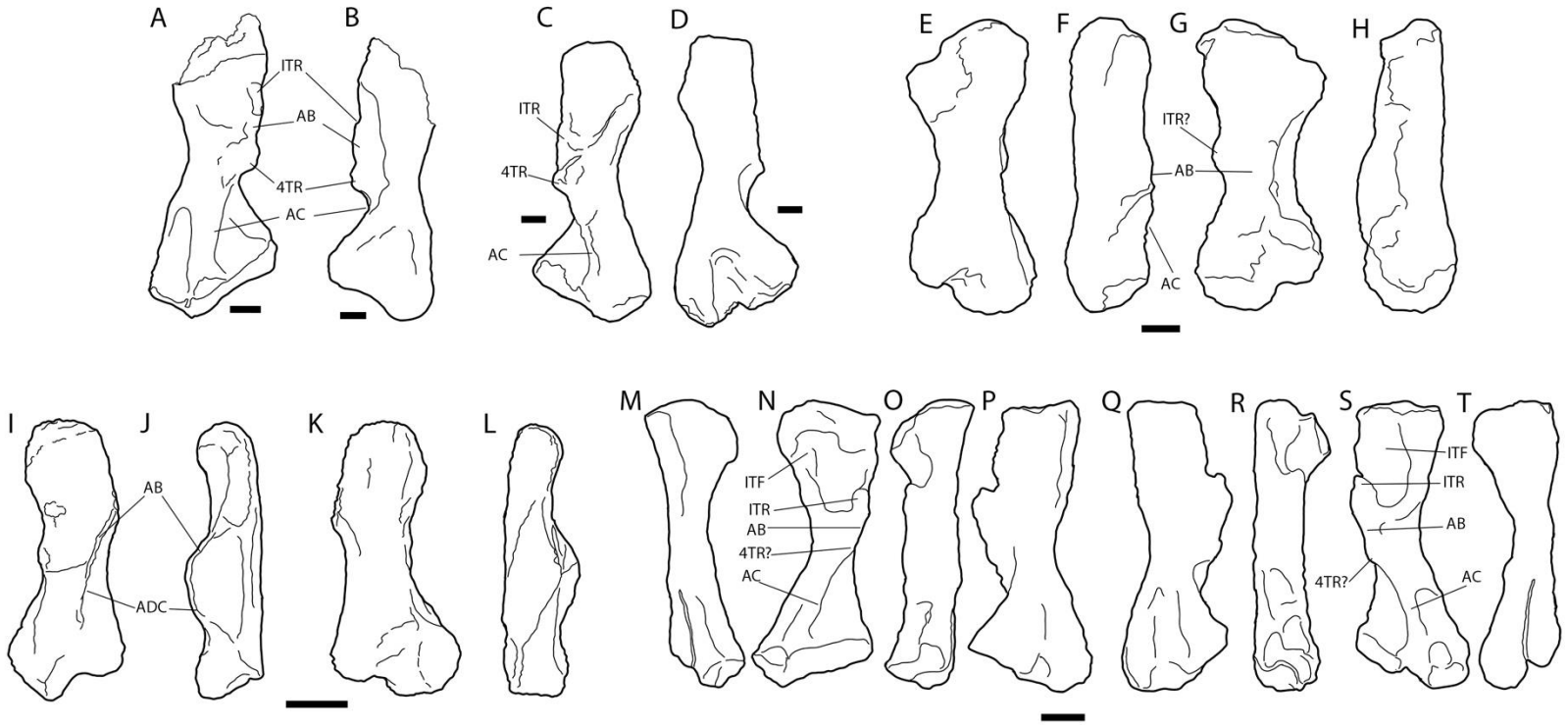

Figure 2.35. Femora of *Ossinodus* and other Devonian–Carboniferous femora. QMF 37432 *Ossinodus* right femur in ventral (A) and dorsal (B) views; QMF 37415 *Ossinodus* left femur in ventral (C) and dorsal (D) views; ANSP 23864 left femur drawn after (Broussard et al., 2018) in dorsal (E), anterior (F), ventral (G) and posterior (H) views; ANSP 21476 left femur drawn after (Daeschler et al., 2009) in ventral (I), posterior (J), dorsal (K) and anterior (L) views; NSM004GF045.034A left femur drawn after Anderson et al. (2015) in posterior (M), ventral (N), anterior (O), and dorsal (P) views; NSM004GF045.034B left femur drawn after (Anderson et al., 2015) in dorsal (Q), anterior (R), ventral (S) and posterior (T) views. In all specimens, proximal is at the top and distal is at the bottom.

Table 2.2. Tentative (re)assignments of fragmentary 'whatcheeriid' material.

Name & specimen number	Material	Location	Age	Identity	References
ANSP 23864	Left femur	Pennsylvania, USA	Frasnian (~376Ma)	Tetrapod indet.	Broussard et al. 2018
ANSP 21476	Left femur	Pennsylvania, USA	Famennian (~362Ma)	Tetrapod indet.	Daeschler et al. 2009
ANSP 21873	Postorbital	Pennsylvania, USA	Famennian (~362Ma)	Tetrapod indet.	Daeschler et al. 2009
IRSNB A.0006	Postorbital	Strud, Belgium	Famennian	Tetrapod indet.	Olive et al. 2016
IRSNB A.0007	Right maxilla	Becco, Belgium	Famennian	Ambiguous	Olive et al. 2016
NSM004GF045.034A	Left femur	Horton Bluff, Nova Scotia	Tournaisian	Tetrapod indet.	Anderson et al. 2015
NSM004GF045.034B	Right femur	Horton Bluff, Nova Scotia	Tournaisian	Tetrapod indet.	Anderson et al. 2015
UMZC 2016.8, UMZC 2017.2.569	Two incomplete frontals (+ nasal?), cleithrum	Burnmouth, Scotland	Tournaisian (~355Ma)	Whatcheeriid (*Pederpes*-like)	Otoo et al. 2018
UMZC 2016.9, UMCZ 2017.2.611, UMZC 2017.2.577, UMZC 2017.3.576	Left maxilla, radius, digit bone, intercentrum	Burnmouth, Scotland	Tournaisian	Tetrapod indet.	Otoo et al. 2018
NSM005GF045.001	Right pelvis	Horton Bluff, Nova Scotia	Tournaisian	Ambiguous	Anderson et al. 2015
NSM014GF036.003	Right tibiae	Horton Bluff, Nova Scotia	Tournaisian	Whatcheeriid (*Pederpes*-like)	Anderson et al. 2015
NSM.014.GF.036.005	Interclavicle	Horton Bluff, Nova Scotia	Tournaisian	Ambiguous	Anderson et al. 2015
NSM005GF045.037, YPM PU 23545	Right humeri	Horton Bluff, Nova Scotia	Tournaisian	Whatcheeriid (*Pederpes*-like)	Anderson et al. 2015
Occidens/GSM 28498	Partial left lower jaw	Northern Ireland	Late Tournaisian or early Visean	Tetrapod indet.	Clack & Ahlberg 2004
CMC VP7328, CMC VP7261, CMC VP 7664	Ilia	Kentucky, USA	Serpukhovian	Whatcheeriid (*Whatcheeria*-like)	Garcia et al. 2006, Greb et al. 2016

Tibia Type 2 (NSM014GF036.003; Anderson *et al*. 2015) was compared to those of *Pederpes* and *Ossinodus*, which differ in their morphology. In fact, it more closely resembles the tibia of *Pederpes*, having greatly expanded ends, virtually no shaft, an almost straight anterior edge (shin) and a small but distinct concavity for the interepipodial space on the posterior rim. Although the diagnostic value of these similarities is uncertain, in view of the strong resemblance to *Pederpes* and the other putative whatcheeriid material from Blue Beach, we refer NSM014GF036.003 to Whatcheeriidae.

Humerus Type 1 (NSM005GF045.037, YPM PU 23545) resembles the humerus of *Pederpes* (Anderson et al., 2015). Both have a similarly-sized deltopectoral process and a spike-shaped latissimus dorsi process, the latter characteristic also evident in *Whatcheeria* and *Baphetes* (Milner & Lindsey 1998). Like *Pederpes* (Clack & Finney 2005) the anterior and distal surfaces are unfinished and the distal articular condyles are undifferentiated. Again, this characteristic occurs in other early humeri, such as those of *Crassigyrinus* (Panchen 1985) and *Ossinodus* (Bishop, 2014), but is quite unlike the far more completely ossified condition of the *Whatcheeria* humerus. The ~90 angle between the shaft and rectangular entepicondyle of Humerus Type 1 closely resembles *Pederpes*, but, once again, this characteristic occurs further afield, in examples such as *Greererpeton* (Godfrey 1989). The humerus torsion angle is very high for an early tetrapod humerus, ~60 degrees- almost twice that of *Pederpes* (Smithson and Clack, 2018) and thrice that of *Whatcheeria.* In summary, Anderson *et al*.'s (2015) comparison with *Pederpes* is supported, but there remains the possibility that the similarities are more general to early tetrapod humeri and that nothing specific to whatcheeriids has been identified.

NSM.014.GF.036.005 is an incomplete interclavicle that was compared with that of *Pederpes* (also incomplete: Clack & Finney 2005) but considered inconclusive as evidence of a whatcheeriid (Anderson *et al*. 2015). We find no evidence to extend beyond this conclusion.

Occidens (Clack and Ahlberg, 2004), known from a partial jaw of suspected late Tournaisian-early Viséan age, has recently been associated with the whatcheeriids in a phylogenetic analysis (Clack et al., 2016). It shares with *Whatcheeria* a single row of teeth on each coronoid and near-absence of dermal ornament. The mandible of *Pederpes* is not known in sufficient detail for comparison. Each of these characters is present in other tetrapods, but their conjunction might be unique to *Occidens* and *Whatcheeria*. However, unlike *Whatcheeria*, the splenial is not sutured to the prearticular posteriorly (Clack and Ahlberg, 2004; Lombard and Bolt, 2006). It seems likely that the various polytomies and sister group combinations of *Occidens* and *Whatcheeria* and *Pederpes* in the analysis of Clack et al. (2016) result from incompleteness rather than genuine similarity. Therefore, its whatcheeriid status is questionable.

Three ilia (CMC VP7261, CMC VP7664, CMC VP7328) from exposures of the Serpukhovian Buffalo Wallow Formation in Hancock County, Kentucky, have been compared to that of *Pederpes* (Garcia *et al.*, 2006; Greb *et al.*, 2016). CMC VP7328 is the largest, the only one figured, and resembles the ilium of *Whatcheeria* (Garcia *et al.*, 2006, Fig.9). The posterior iliac process is more proximally constricted than in *Whatcheeria* and expands posteriorly, producing a spoon-like appearance. The dorsal process is incomplete but CMC VP7328 suggests that it was circular or oval. The two processes are separated by a broad groove and probably would have overlapped in lateral view. There is no indication that either process has the fluting

seen in *Whatcheeria*. Notably, CMC VP7328 is very large, approximately 20cm long (Garcia et al., 2006). This is comparable to the size that would be expected from the largest *Whatcheeri*a individuals. On the basis of the numerous similarities between CMC VP7328, we refer CMC VP7328 (and by extension CMC VP7261 and CMC VP7664) to Whatcheeriidae. It is notable that the Delta and Hancock County localities are geographically close and the latter is probably only slightly older than the former, with the caveat that there is some uncertainty as to their absolute ages. Given this, there is the question of whether or not the Buffalo Wallow whatcheeriid is taxonomically distinct from *Whatcheeria deltae*. Further Buffalo Wallow material is needed to resolve this question. In either case, the Buffalo Wallow whatcheeriid represents the geologically youngest occurrence of the family.

Assignments for the fragmentary material are summarized in Table 2.2. These specimens span the Devonian/Carboniferous boundary and include some of the oldest known fossils of limbed tetrapods. Most material is of uncertain affinity, and only some of it is referrable to Whatcheeriidae. The material that is compared to *Ossinodus* cannot be more precisely identified because it is not yet apparent that the combination of characters seen in the femur of *Ossinodus* is diagnostic for that taxon among early tetrapods.

Significantly, none of the fragmentary specimens permit the identification of whatcheeriids in the Devonian, though IRSNB A.0007 (a Strud maxilla) is suggestive. Thus, the fossil record of whatcheeriids remains limited to the Carboniferous, although a Devonian origin has long been mooted based on the Tournaisian age of *Pederpes*. From the present work, fragment attributions to the family are mostly inconclusive. Given the rarity of morphological

innovation (i.e. apomorphies) among whatcheeriids noted earlier, this seems unlikely to change. It follows that whatcheeriid range extension into the Devonian, in the absence of new specimens, is most likely to depend on implications of phylogenetic results (e.g. Ahlberg & Clack 2020).

2.5.5 Biogeography of the Whatcheeriidae

With the restriction here of Whatcheeriidae to *Pederpes* and *Whatcheeria*, and fragmentary specimens exhibiting shared characteristics, the family has a North American-British Isles distribution. During the Late Devonian and Mississippian, the British Isles and eastern/central North America were part of a common equatorial biome and proximity increased with the final assembly of Gondwana during the Pennsylvanian (Clack and Milner, 2015; Lawver et al., 2015)). Similar biogeographic distributions are known for colosteids, embolomeres, baphetids, rhizodonts, and gyracanths (Clack and Milner, 2015; Ó Gogáin et al., 2016; Otoo et al., 2018).

Whatcheeriids are rare within the general gyracanth-lungfish-rhizodont-tetrapod association that occurs repeatedly in Mississippian continental faunas (Sallan and Coates, 2010; Otoo et al., 2018; Clack et al., 2019a). Both complete and fragmentary they are at most known only from the Burnmouth siltstone, Blue Beach, Delta, and Buffalo Wallow faunas (Bolt *et al.*, 1988; Garcia *et al.*, 2006; Anderson *et al.*, 2015; Greb *et al.*, 2016; Clack *et al.*, 2016; Otoo *et al.*, 2018). The holotype of *Pederpes* is an isolated nodule, but it was probably derived from a fauna at least broadly similar to that described from the Burnmouth siltstone interval (Clack, 2002c; Clack and Finney, 2005; Otoo et al., 2018)- in any case, whatcheeriids are still thin on the ground. The available data do not suggest that we have been sampling the margins of

whatcheeriid biogeographic or ecological distribution, and their minimum temporal range already encompasses much of the Mississippian. This uncertainty is compounded by the scarcity of Carboniferous tetrapod localities outside of equatorial Euramerica, a long-recognized and still unresolved problem (Milner et al., 1986; Pardo et al., 2019b, 2020). Nevertheless, the abundance of *Whatcheeria* specimens indicates that at least in this instance, we have more-or-less-autochthonous preservation alongside other, more widespread tetrapod taxa.

2.6 CONCLUSIONS

The postcranial anatomy of *Whatcheeria deltae* reveals an extremely unusual early tetrapod. Key features include an elongate neck and large, robust limbs and broad manus/pes. Despite the morphology of the appendicular skeleton, the presence of well-developed cranial sensory canals indicates that *Whatcheeria* was an aquatic animal, and any terrestrial activity would have been extremely infrequent and limited. Most known *Whatcheeria* specimens belong to immature individuals and sample a short period of extremely rapid growth that likely corresponds to the onset of sexual maturity. These subadults would have bene approximately 1m in length, but there are very rare fragments that represent much larger (and presumably older) individuals up to 2m long. The new postcranial data contribute to a revised diagnosis for the family Whatcheeriidae. This includes a combination of hindlimb characters unique to *Whatcheeria* and *Pederpes*, and the family is restricted to these two genera. Reevaluation of Devonian-Carboniferous fossils reported as ‘whatcheeriid’ supports the exclusion of *Ossinodus* and the Devonian material, with the caveat that the holotype of the minute Famennian tetrapod *Brittagnathus* is similar to the mandible of *Whatcheeria*. Probable whatcheeriids are present in Nova Scotia (Blue Beach, Tournaisian), the Scottish Midland Valley (upper Ballagan Formation, Tournaisian), and Kentucky (Buffalo Wallow Formation, Serpukhovian). While *Whatcheeria* is

superabundant at Delta and the family Whatcheeriidae spans most of the Mississippian, whatcheeriids generally appear to have been less widespread and abundant than contemporary groups such as the embolomeres and colosteids. The reason for this biogeographic disparity is unclear, but may indicate that whatcheeriids were specialized or ecologically restricted in some way that other early tetrapods were not.

CHAPTER 3: PHYLOGENETIC EVIDENCE FOR AN AQUATIC AND DEVONIAN ORIGIN OF MISSISSIPPIAN TETRAPOD DIVERSITY

3.1 ABSTRACT

Phylogenetic analysis of early tetrapods using a new data matrix finds a diverse tetrapod stem group, much of which diverges in the Devonian. This includes a monophyletic Whatcheeriidae composed of *Whatcheeria* and *Pederpes* and suggests that the lineage and functional diversity of the Devonian tetrapod assemblage extended far beyond the classic Famennian taxa such as *Acanthostega*, *Ichthyostega*, and *Tulerpeton*. Colosteids vary between the sister group of temnospondyls, and thus crown tetrapods, and apical stem tetrapods. Placement of *Caerorhachis* at the base of the amniote total group creates a single unambiguous origin of consolidated (gastrocentrous) vertebrae. In contrast to other recent work, the limbless tetrapods (adelospondyls and aistopods) are recovered deep within the amniote total group, but this may reflect the outsized influence of unreliable vertebral characters. Analysis of character partitions indicates that postcranial data have signal comparable to cranial data. However, the anterior and posterior appendicular skeletons return divergent phylogenetic results. The results of the partition analyses suggest that the homoplasy that frustrates studies of early tetrapod phylogeny may not entirely be the result of poor data and methodological shortcomings. Instead, it may reflect functional diversity and experimentation among the earliest tetrapod radiations.

3.2 INTRODUCTION

3.2.1 Competing tree topologies

Around turn of the 21st century, early tetrapod phylogeny underwent a profound paradigm shift. Through the 1980s and 1990s, most Carboniferous tetrapod diversity was assigned to either the lissamphibian or amniote lineages (Milner et al., 1986; Coates, 1996). The Famennian tetrapod *Tulerpeton* was occasionally included as a stem amniote (Lebedev and Coates, 1995; Coates, 1996) which would require the tetrapod crown group to originate by the Late Devonian. The placements of historically recognized groups such as Colosteidae, Baphetidae, and Lepospondyli were highly uncertain (Fracasso, 1994). A major increase in anatomical data from the Devonian tetrapods *Acanthostega* (Coates, 1996), *Ichthyostega* (Jarvik, 1996), and *Tulerpeton* (Lebedev and Coates, 1995), greatly increased our knowledge of the fin-limb transition. Additional new taxa from the Mississippian, Pennsylvanian, and early Permian helped flesh out the apical portion of the tetrapod stem group and basal portions of the lissamphibian and amniote total groups (Lombard and Sumida, 1992). At the same time, advances in phylogenetic software allowed for the first computational tests (Ahlberg and Milner, 1994; Cloutier and Ahlberg, 1996; Coates, 1996; Clack, 1997; Laurin and Reisz, 1997; Ahlberg and Clack, 1998; Laurin, 1998199; Paton et al., 1999; Laurin et al., 2000) of historical hypotheses.

The analysis of Ruta et al. (2003a) using the parsimony ratchet protocol of Quicke et al. (2001)(Quicke et al., 2001) represented a fundamental shift in early tetrapod phylogenetics, and has framed the landscape of work over the last 20 years. This matrix included 319 characters and 90 taxa. Unlike previous trees, this analysis recovered a substantial tetrapod stem group incorporating Devonian and Mississippian taxa. These included newer discoveries (ex. *Whatcheeria, Pederpes*) and taxa that had previously been considered part of the crown group (ex. *Greererpeton, Crassigyrinus*). The amniote total group was composed of anthracosaurs,

lepospondyls, seymouriamorphs, and diadectomorphs as successive plesions approaching the amniote crown group. The lissamphibian total group is composed of the temnospondyls and crown group lissamphibians, which are placed within the temnospondyls. As used by Ruta et al. (2003a) and other authors (Ruta and Coates, 2007; Ruta et al., 2007; Schoch, 2013; Clack et al., 2016; Pardo et al., 2017b, 2017a), 'Temnospondyli' is a paraphyletic group of stem lissamphibians. For the sake of clarity, in this work 'Temnospondyli' includes both the fossil stem lissamphibians (ex. *Balanerpeton*, *Eryops*, *Trimerorhachis*, etc.) as well as crown group Lissamphibia, making the temnospondyls a monophyletic group.

The minimum age of the tetrapod crown group under the Ruta et al. (2003a) hypothesis was pinned on the Mississippian aistopod 'lepospondyl' *Lethiscus* from Wardie in Scotland (Wellstead, 1982). This was initially reported as Tournaisian (Ruta et al., 2003a) and later changed to Visean following further chronostratigraphic work (Ruta and Coates, 2007). Most subsequent analyses agree with the Visean crown group age based on the more commonly used *Balanerpeton* and *Westlothiana* from Eastt Kirkton, which is slightly younger than Wardie and geographically proximate. However, the tetrapod crown node was only supported by homoplastic characters and had low Bremer support. Analysis of character partitions resulted in substantial topological differences. Cranial-only characters moved many lepospondyls- including the limbless aistopods and adelospondyls onto the tetrapod stem group, but this was reversed when jaw characters are removed. These partition results suggest that patterns of character change differed across the early tetrapod skeleton, which has also been suggested by a small number of subsequent analyses (Ahlberg and Clack, 1998; Coates et al., 2002; Clack et al., 2012a, 2016).

Since the Ruta et al. (2003a,b) analyses, hypotheses of early tetrapod relationships have fallen into one of two camps (Clack and Finney, 2005; Marjanović and Laurin, 2007, 2009, 2013; Ruta and Coates, 2007; Clack et al., 2012b, 2016; Ruta and Wills, 2016; Pardo et al., 2020).; the 'temnospondyl hypothesis' and the 'lepospondyl hypothesis'. The primary difference between these hypotheses is the relationship between lissamphibians and Paleozoic tetrapods: the former places the lissamphibians within the temnospondyls, and the latter places the lissamphibians within the lepospondyls. The temnospondyl hypothesis of lissamphibian origins was articulated across several investigations of the hearing system, dentition, and dermal skull by Milner, Lombard, and Bolt in the 1970s and 1980s (Bolt, 1969; Lombard and Bolt, 1979; Milner, 1982; Milner et al., 1986). Several phylogenetic analyses in the 1990s using cladistics software supported the temnospondyl hypothesis (Panchen and Smithson, 1988; Coates, 1996) before the 'modern' articulation in the Ruta et al. (2003a) analysis. Advocates of the lepospondyl hypothesis dispute numerous character scores from other datasets and favor the use of loss characters (Laurin and Reisz, 1997; Anderson, 2001; Marjanović and Laurin, 2007, 2008, 2013, 2019; Anderson et al., 2008).

Recently, several analyses have presented new variants on the temnospondyl and lepospondyl hypotheses (Figure 3.1). Pardo et al. (2017) affirmed the temnospondyl hypothesis but found lepospondyls to be paraphyletic; most are stem diapsids, but the limbless aistopods are recovered as the earliest-diverging Carboniferous stem tetrapods. Additionally, the embolomeres (the primary clade within the 'anthracosaurs') were moved from the amniote stem group onto a position high on the tetrapod stem group. Their study was motivated by new endocranial data from *Lethiscus*, the earliest aistopod (Wellstead, 1982; Pardo et al., 2017b). A phylogenetic

analysis in the context of new CT scan data from the Mississippian adelospondyl *Acherontiscus* conducted by Clack et al. (2019) found the aistopods and adelospondyls to be part of a single clade, which is itself part of a stem tetrapod clade including the colosteids and urocordylid 'lepospondyls'. This topology would suggest a single origin of limblessness within the stem group.

Marjanović and Laurin reviewed the lepospondyl hypothesis (Marjanović and Laurin, 2013) and recently published a phylogenetic analysis (Marjanović and Laurin, 2019) which is the most recent presentation of the lepospondyl hypothesis. This analysis was conducted on rescored version of the Ruta and Coates (2007) matrix. They found 'anthracosaurs' and temnospondyls to be successive plesions in the apical portion of the tetrapod stem group. Under their hypothesis, Lepospondyli is the lissamphibian total group. The amniote total group is only represented by crown amniotes.

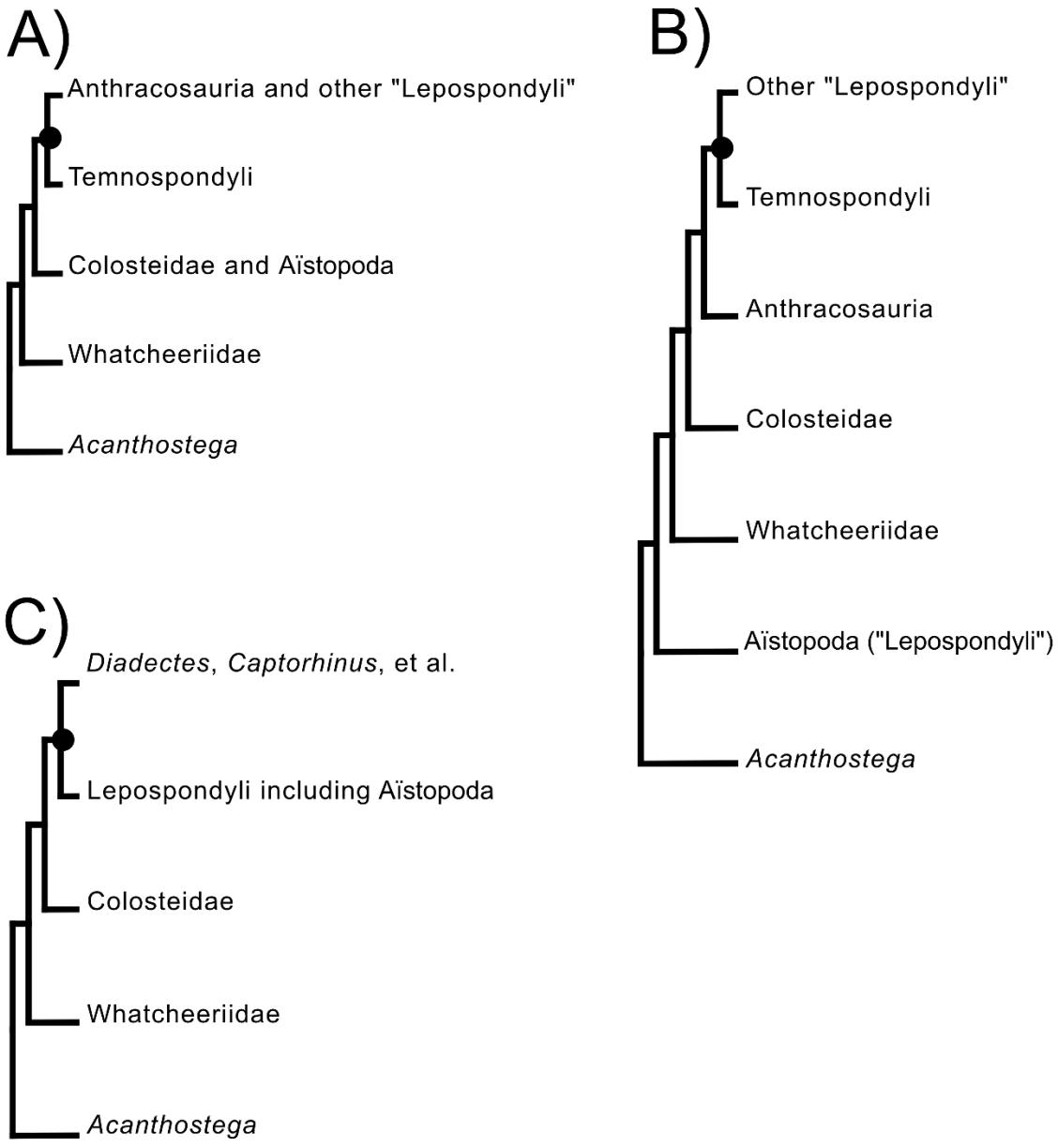

Figure 3.1. Schematic representations of recent phylogenetic hypotheses of early tetrapod relationships particularly relevant to the present work. A: Clack et al. 2019 (shared with Ruta and Coates 2007); B: Pardo et al. 2017; C: Marjanović and Laurin 2019. Circles represent the tetrapod crown node.

There is a potential issue of parent-child relationships between matrices, and the fit of datasets to the questions to be answered. Phylogenetic matrices belong to ‘lineages’, and inherit

their character and taxon sets from previous analyses. Additions of taxa to successive iterations of a dataset are tests of prior hypotheses in the lineage, as each taxon represents a novel combination of characters. The Clack et al. (2019) and Pardo et al. (2017) datasets share common characters from an earlier analysis by Clack et al. (2012). The Clack et al. (2012) dataset is itself part of a genealogy of matrices focused on relationships among stem tetrapods and early members of crown group lineages (Ruta et al., 2003a; Clack and Finney, 2005; Ruta and Coates, 2007; Callier et al., 2009; Ruta, 2011; Clack et al., 2016). The Pardo et al. (2017) derives most of its characters from a previous study on recumbirostran 'lepospondyls' (Huttenlocker et al., 2013), which itself descends from previous 'lepospondyl'-focused matrices (Anderson, 2001; Anderson et al., 2008). The Clack et al. (2016), Clack et al. (2019), Pardo et al. (2017), and Marjanović and Laurin (2019) datasets are all based on characters from the Ruta and Coates (2007) data matrix. However, testing of hypotheses from different 'lineages' requires character and taxon overlap (Ruta et al., 2003b). Until now, the temnospondyl hypothesis and lepospondyl hypothesis have been supported by analyses with limited character/taxon overlap, especially as lepospondyl hypothesis analyses substantially reinterpret characters shared with temnospondyl hypothesis datasets (Marjanović and Laurin, 2013, 2019).

3.2.2 Competing evolutionary scenarios

Both the temnospondyl and lepospondyl hypotheses agree on a Visean minimum age for the crown group, via *Balanerpeton*/*Westlothiana* for the temnospondyl hypothesis, and *Lethiscus* for the lepospondyl hypothesis. The temnospondyl hypothesis requires numerous branching events by the early Mississippian to produce the Late Devonian tetrapod lineages, the post-Devonian tetrapod stem group, and the crown group by the middle/late Visean

(*Balanerpeton*/*Westlothiana*/*Lethiscus*). One benefit of these topologies is a reduced number of range extensions for both the lissamphibian and amniote total groups. By contrast, the lepospondyl hypothesis populates the lissamphibian total group but find no stem amniotes at all (Marjanović and Laurin, 2019). Aside from the enormous amniote ghost lineage that results, this also requires that all the characters that support a position of Lissamphibia within Temnospondyli (*sensu* Ruta et al. (2003a)) be highly homoplastic (Coates et al., 2000; Laurin et al., 2000; Marjanović and Laurin, 2013).

Regardless of the speed of branching events, a Visean origin for the tetrapod crown group implies higher pre-Visean tetrapod diversity than we currently have fossil evidence for. *Parmastega* (if it is assumed to have limbs rather than fins), *Acanthostega, Ventastega*, *Ichthyostega,* and *Tulerpeton* all date to the Famennian and are the only Devonian tetrapods for which there is substantial anatomical data. Additional fragmentary taxa- *Obruchevichthys*, *Webererpeton, Jakubsonia*, *Sinostega*, *Ymeria*, *Rubrognathus*, *Livoniana*, *Metaxygnathus, Elginerpeton*- from the Givetian-Famennian are often excluded from phylogenetic analyses due to incompleteness. Even with this caveat, the Devonian tetrapod radiation appears to be limited and lacks any recognizable representatives of Mississippian lineages. There are then two possibilities: the Devonian radiation was indeed more diverse and will be fully revealed with more fossil discoveries; or post-Devonian tetrapods are all the product of post-Devonian radiations. The former scenario entails high tetrapod survivorship through the EDME, whereas in the latter tetrapods experience a severe bottleneck (Sallan and Coates, 2010).

This is paralleled by different hypotheses about sequences of character change. Devonian tetrapods- e.g. *Acanthostega*- and Mississippian tetrapods- e.g. *Balanerpeton* or *Westlothiana*- are widely considered representatives of the aquatic and terrestrial portions of the water-land transition, respectively. Quantitative analyses of rates of character change using a temnospondyl hypothesis dataset (Ruta et al., 2006; Wagner et al., 2006) found that rates of character change were high in the Late Devonian and Mississippian, but dropped to a lower level from the Pennsylvanian onward. The authors also found that total group lissamphibians (=temnospondyls) had a smaller set of variable characters than basal (=stem [limbed]) tetrapods, and that stem amniotes varied across a larger set of characters than either total group lissamphibians or basal tetrapods. The authors speculate that increasing intrinsic biological constraints reduced rates of character change over time, but expansion into new terrestrial ecospace by stem amniotes yielded more new characters. This scenario joins the origin and diversification of crown tetrapods to terrestrialitzation; the invasion of the land was the watershed event that pressed tetrapods to explore a greater range of morphologies and functions.

The tetrapod fossil record of the early Mississippian- 'Romer's Gap'- is then particularly important. It presumably contains both the origin of the tetrapod crown group and the transition of tetrapods from water to land (Coates and Clack, 1995; Smithson et al., 2012). Historically fossil-poor, the whatcheeriids- via *Pederpes* (Clack, 2002c; Clack and Finney, 2005)- was the post-Devonian group with a record from this interval. Recent discoveries have produced early appearances of *Crassigyrinus* (Clack et al., 2018; Lennie et al., 2020) and the colosteids (Clack et al., 2016), extending their stratigraphic ranges by 25-30 million years. There are also an

increasing diversity of new, albeit fragmentary, tetrapods of uncertain phylogenetic affinity (Clack et al., 2016; Chen et al., 2018; Otoo et al., 2018; Smithson and Clack, 2018).

Even with these new discoveries, the whatcheeriids are the tetrapod group making the single largest contribution of anatomical data filling Romer's Gap. Clack (2002) erected the family to contain the Visean/Serpukhovian *Whatcheeria* and the Tournaisian *Pederpes*. *Pederpes* is represented by a holotype preserving almost the entire precaudal skeleton. *Whatcheeria* is represented by hundreds of specimens and is now one of the most completely known Devonian or Carboniferous tetrapods (Bolt and Lombard, 2018; Otoo et al., 2021; Rawson et al., 2021). While the diagnosis for Whatcheeriidae has recently been revised and the family restricted to *Whatcheeria* and *Pederpes* (Otoo et al., 2021), this has not been tested with a phylogenetic analysis. Resolving the relationships of the whatcheeriids has the potential to increase resolution in the lower portion of the (post-Devonian) tetrapod stem and help polarize characters along the stem into the crown.

Much of the revised Whatcheeriidae diagnosis draws on postcranial data, particularly from the hindlimb, that have not been incorporated in prior phylogenetic analyses (Otoo et al., 2021). This represents an opportunity to construct new characters to use these new data. It is also an opportunity to reassess phylogenetic signal across different anatomical character partitions. In previous analyses, jaw characters have struggled to recover clades (Clack et al., 2012a; Chen et al., 2018). Postcranial data have performed well, but topologies diverge between the anterior and posterior appendicular character sets (Ruta, 2011; Ruta and Wills, 2016). This has been noted elsewhere (Coates et al., 2002); Coates et al. (2002) noted that not only did the anterior

appendicular and posterior appendicular skeletons appear to be evolving out of tandem, but also that character changes in the anterior appendicular skeleton precede changes in the posterior appendicular skeleton. This may reflect functional pressures between the two anatomical partitions. Further investigation of patterns of phylogenetic signal across partitions may help outline the extent and patterns of functional diversity across the earliest tetrapod radiations (Ruta et al., 2006; Wagner et al., 2006; Ruta and Wills, 2016). Stem tetrapods may have reached character exhaustion later than previously hypothesized (Wagner et al., 2006) and achieved greater functional diversity (Dickson et al., 2020).

3.2.3 Aims

The aims of this study are:

- Determine whether the whatcheeriids are monophyletic and elucidate what characters are useful for diagnosing them
- Determine the membership of the tetrapod crown group, character diagnosis of the tetrapod crown group, and relationships in the apical portion of the tetrapod stem
- Determine the timing of branching events with respect to the end-Devonian mass extinction
- Investigate differing levels of signal across anatomical partitions- particularly postcranial partitions- and implications for understanding early tetrapod phylogeny and paleobiology

3.3 MATERIALS

3.3.1 Taxon sampling

The starting taxon list for the analysis is that of Clack et al. (2016) (Table 1), which has broad overlap with numerous other analyses of early tetrapods, particularly in the tetrapod stem group (Ruta et al., 2003a; Clack and Finney, 2005; Ruta and Coates, 2007; Ruta, 2011; Clack et al., 2012b, 2012a; Klembara et al., 2014). This dataset was directly expanded by Clack et al. (2019), which was published while this research was ongoing. The Clack et al. (2016) dataset was then replaced by that of Clack et al. (2019) as the starting taxon list. Additions, and removals

are relative to the Clack et al. (2019) taxon list and enumerated in APPENDIX B. The final list of operational taxonomic units (OTU), full taxonomic notes, and references are presented in APPENDIX B.

Table 3.1. Basic numerical information for primary datasets which supplied preexisting characters for this study.

NTAX	NCHAR	Reference
44	157	Ruta, 2011
46	214	Clack et al., 2016
58	370	Pardo et al., 2017
57	260	Clack et al., 2019

Table 3.2. (Page 118-120) List of OTUs used in this study, with references. NSM refers to Nova Scotia Museum.

OTU	References
Acanthostega	Coates, 1996; Ahlberg and Clack, 1998; Clack, 1998, 2002a, 2002b; Porro et al., 2015
Adamanterpeton	Milner and Sequeira, 1998
Adelogyrinus	Andrews and Carroll, 1991
Adelospondylus	Andrews and Carroll, 1991
Anthracosaurus	Panchen, 1977, 1981; Clack, 1987a
AnthracosaurusPlus	Panchen, 1977, 1981; Clack, 1987a
Archegosaurus	Witzmann, 2005; Witzmann and Schoch, 2006
Archeria	Romer, 1957; Clack and Holmes, 1988; Holmes, 1989, in addition to personal BKAO observations
Aytonerpeton	Otoo, 2015; Clack et al., 2016; Ahlberg and Clack, 2020, pers. obsv. BKAO
*Aytonerpeton*Plus	Otoo, 2015; Clack et al., 2016; Otoo et al., 2018; Ahlberg and Clack, 2020, pers. obsv. BKAO
Balanerpeton	Milner and Sequeira, 1993
Baphetes (*B. kirkbyi*)	Beaumont, 1977; Milner and Lindsay, 1998
Brittagnathus	Ahlberg and Clack, 2020
Caerorhachis	Ruta et al., 2002
Capetus	Sequeira and Milner, 1993

Casineria	Paton et al., 1999; Marjanović and Laurin, 2019
Coloraderpeton	Wellstead, 1982; Anderson, 2003; Anderson et al., 2003; Pardo et al., 2017
Colosteus	Hook, 1983, in addition to personal BKAO observations of specimens
Crassigyrinus	Panchen, 1985; Panchen and Smithson, 1990; Clack, 1997; Herbst and Hutchinson, 2018
Deltaherpeton	Bolt and Lombard, 2010
Dendrerpeton	Carroll, 1967; Godfrey et al., 1987; Holmes et al., 1998; Robinson et al., 2005
Doragnathus	Smithson, 1980
Edops	Romer and Witter, 1942
Eldeceeon	Smithson, 1993; Ruta et al., 2020
Elpistostege	Schultze and Arsenault, 1985; Cloutier et al., 2020
Eogyrinus_attheyi	Panchen, 1964, 1966, 1972; Clack, 1987b
EogyrinusPlus	Panchen, 1964, 1966, 1972; Clack, 1987b
Eoherpeton	Panchen, 1975; Smithson, 1985
Erpetosaurus	Milner and Sequeira, 2011
Eryops	Olson, 1936; Romer and Witter, 1941; Sawin, 1941; Moulton, 1974; Pawley and Warren, 2006 in addition to personal BKAO observations
Eucritta	Clack, 2001
Eusthenopteron	Andrews and Westoll, 1970; Sanchez et al., 2014; Porro et al., 2015
Gephyrostegus	Brough and Brough, 1967b; Carroll, 1970; Ahlberg and Clack, 1998; Klembara et al., 2014
Greererpeton	Smithson, 1982; Godfrey, 1989; Bolt and Lombard, 2001, 2010, in addition to personal BKAO observations
Ichthyostega	Jarvik, 1996; Coates 2001; Ahlberg et al., 2005; Callier et al., 2009; Clack et al., 2012a; Pierce et al., 2012, 2013a, 2013b
Koilops	Clack et al., 2016
Lethiscus	Wellstead, 1982; Anderson, 2003; Anderson et al., 2003; Pardo et al., 2017
Loxomma	Beaumont, 1977; Ahlberg and Clack, 1998
Megalocephalus	Beaumont, 1977; Ahlberg and Clack, 1998
Microbrachis	Brough and Brough, 1967; Carroll and Gaskill, 1978; Vallin and Laurin, 2004; Milner, 2008; Olori, 2015
Neldasaurus	Chase, 1965; Schoch, 2018
Neopteroplax	Romer, 1963 , in addition to personal BKAO observations
NSM_994_GF_1.1	Holmes and Carroll, 2010
Occidens	Clack and Ahlberg, 2004
Ossinodus	Warren and Turner, 2004; Warren, 2007; Bishop, 2014; Bishop et al., 2015, in addition to personal BKAO observations
Palaeoherpeton	Panchen, 1964
Panderichthys	Vorobyeva, 1995; Ahlberg et al., 1996; Boisvert, 2005, 2009; Boisvert et al., 2008
Parmastega	Beznosov et al., 2019
Pederpes	Clack, 2002c; Ahlberg et al., 2005; Pierce et al., 2013b; Otoo et al., 2021
Pholiderpeton_scutigerum	Clack, 1987b

Pholidogaster	Romer, 1964; Panchen, 1975
Platyrhinops	Carroll, 1964; Hook and Baird, 1984, 1986; Clack and Milner, 2009
Proterogyrinus	Romer, 1970; Holmes, 1984 in addition to personal BKAO observations
Seymouria	White, 1939; Berman et al., 2000; Klembara et al., 2006; Bazzana et al., 2020a, 2020b
Sigournea	Clack, 2002c; Ahlberg et al., 2005; Pierce et al., 2013b; Otoo et al., 2021
Silvanerpeton	Clack, 1993; Ruta and Clack, 2006
St_Louis_tetrapod	Clack et al., 2012b, pers. obsv. BKAO
Tiktaalik	Daeschler et al., 2006, 2006; Downs et al., 2008; Shubin et al., 2014; Stewart et al., 2019; Lemberg et al., 2021
Trimerorhachis	Case, 1935; Colbert, 1955; Olson, 1979; Berman and Reisz, 1980; Pawley, 2007; Milner and Schoch, 2013, in addition to personal BKAO observations
Tulerpeton	Lebedev and Clack, 1993; Lebedev and Coates, 1995
*Tulerpeton*Plus	Lebedev and Clack, 1993; Lebedev and Coates, 1995
Ventastega	Ahlberg et al., 1994, 2008
Westlothiana	Smithson et al., 1993
Ymeria	Clack et al., 2012a

3.3.1.1 Alternative OTU compositions

The existing *Tulerpeton* Operational Taxonomic Unit (OTU) from Clack et al. (2016, 2019) included fragmentary cranial material from Andreyevka alongside the *Tulerpeton* holotype, which is exclusively postcranial elements (Lebedev and Coates, 1995). The postcranial skeleton of *Tulerpeton* has long been noted for its derived scapulocoracoid, humerus, and manus/pes morphologies (Lebedev and Coates, 1995; Coates, 1996). In order to determine the effect of the additional Andreyevka material vis a vis the *Tulerpeton* postcrania on the phylogenetic placement of *Tulerpeton*, the existing holotype + fragments OTU was renamed to *Tulerpeton*Plus. This was to distinguish it from a *Tulerpeton* OTU including only the holotype material. *Anthracosaurus* and '*Eogyrinus*' were treated similarly, as the referrals of postcranial material to these taxa are uncertain (Panchen, 1972; Clack, 1987b). *Aytonerpeton* includes only the holotype material (Otoo, 2015; Clack et al., 2016), and *Aytonerpeton*Plus includes a referred

parasphenoid and partial skull table (Otoo et al., 2018). These taxa are collectively the 'maximally-inclusive' versions of their more restrictive counterparts.

3.3.2 Dates

Ages for OTUs are listed in APPENDIX B. These were sourced from the literature. To accommodate uncertainty in absolute ages, stages were used as opposed to numeric dates or ranges. Regional stages were translated to international stages using the latest version of the International Geologic Timescale (Aretz et al., 2020; Becker et al., 2020; Henderson et al., 2020).

3.3.3 New reconstructions

For this study, the opportunity was taken to produce updated skeletal reconstructions of the following taxa:

- *Whatcheeria deltae* (Figure 1.2)
- *Acanthostega gunnari* (Figure 1.3)
- *Ichthyostega* sp. (Figure 1.4)
- *Greererpeton burkemorani* (Figure 1.5)
- *Aytonerpeton microps* (Figure 1.6)

The *Whatcheeria*, *Acanthostega*, and *Greererpeton* reconstructions were done to unite descriptions of 3D crania (Schultze and Bolt, 1996; Porro et al., 2015; Rawson et al., 2021). The *Aytonerpeton* reconstruction is the first to restore the entire skull, integrating both the holotype and referred material. The *Ichthyostega* reconstruction is an attempt to integrate published descriptions and figures of anatomy (Jarvik, 1996; Ahlberg et al., 2005; Blom, 2005; Pierce et al., 2013b, 2013a) with the composite full-body reconstruction based on CT data published by Pierce et al. (2012). Sources and reconstruction notes are presented in APPENDIX B.

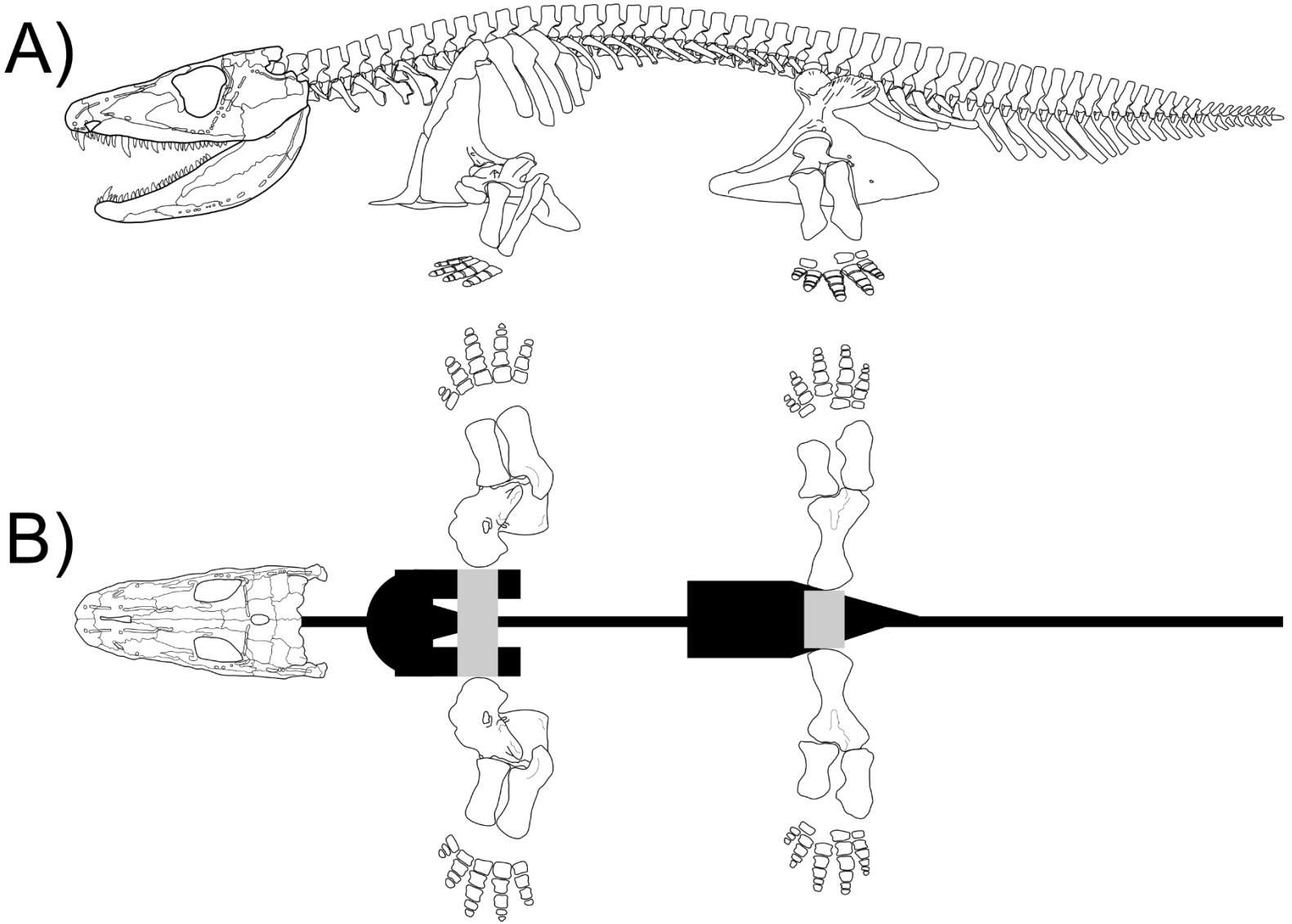

Figure 3.2. Reconstruction of *Whatcheeria* in left lateral view (A) and schematic dorsal view to show body proportions (B).

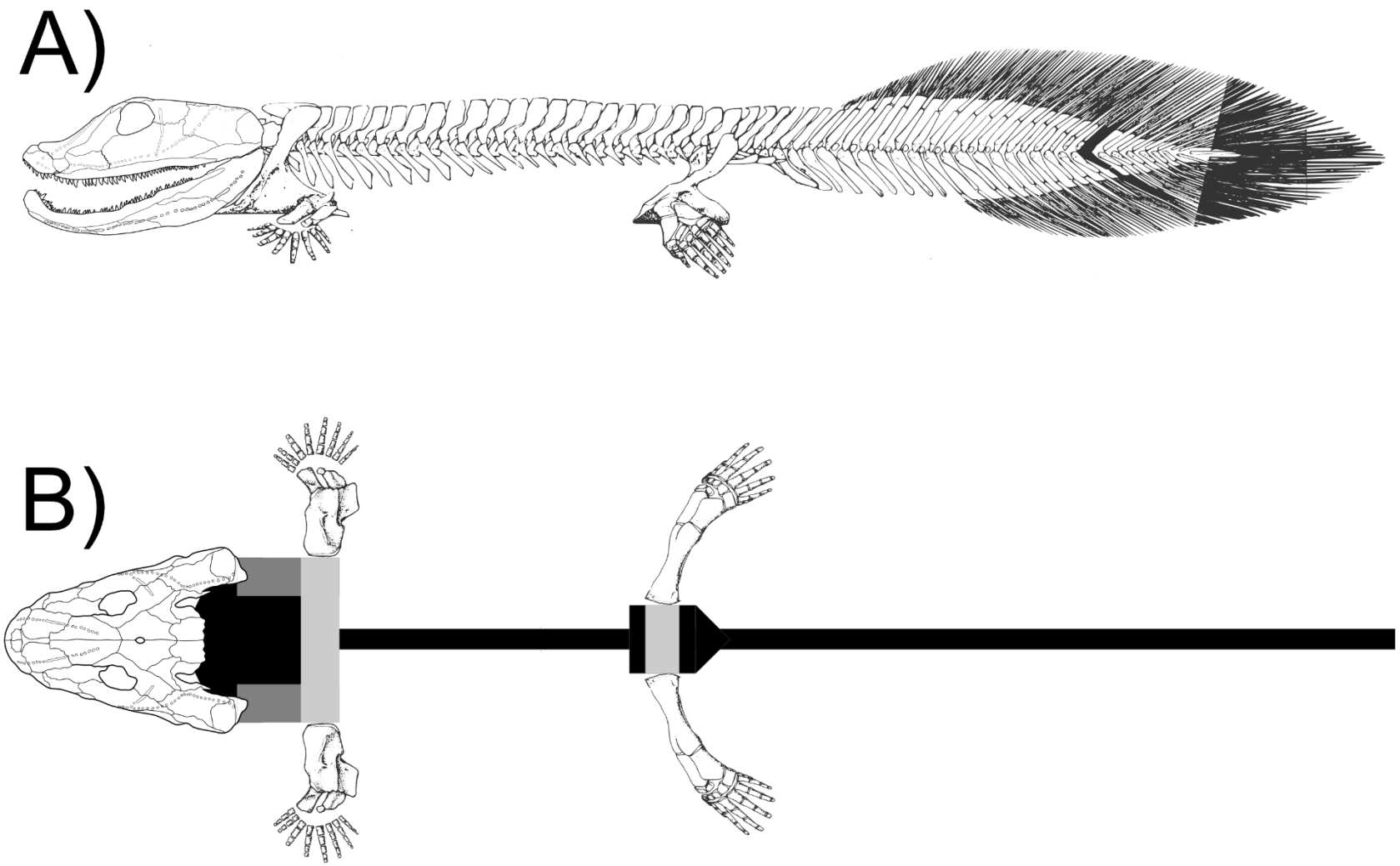

Figure 3.3. New reconstruction of *Acanthostega* in left lateral view (A) and schematic dorsal view to show body proportions (B).

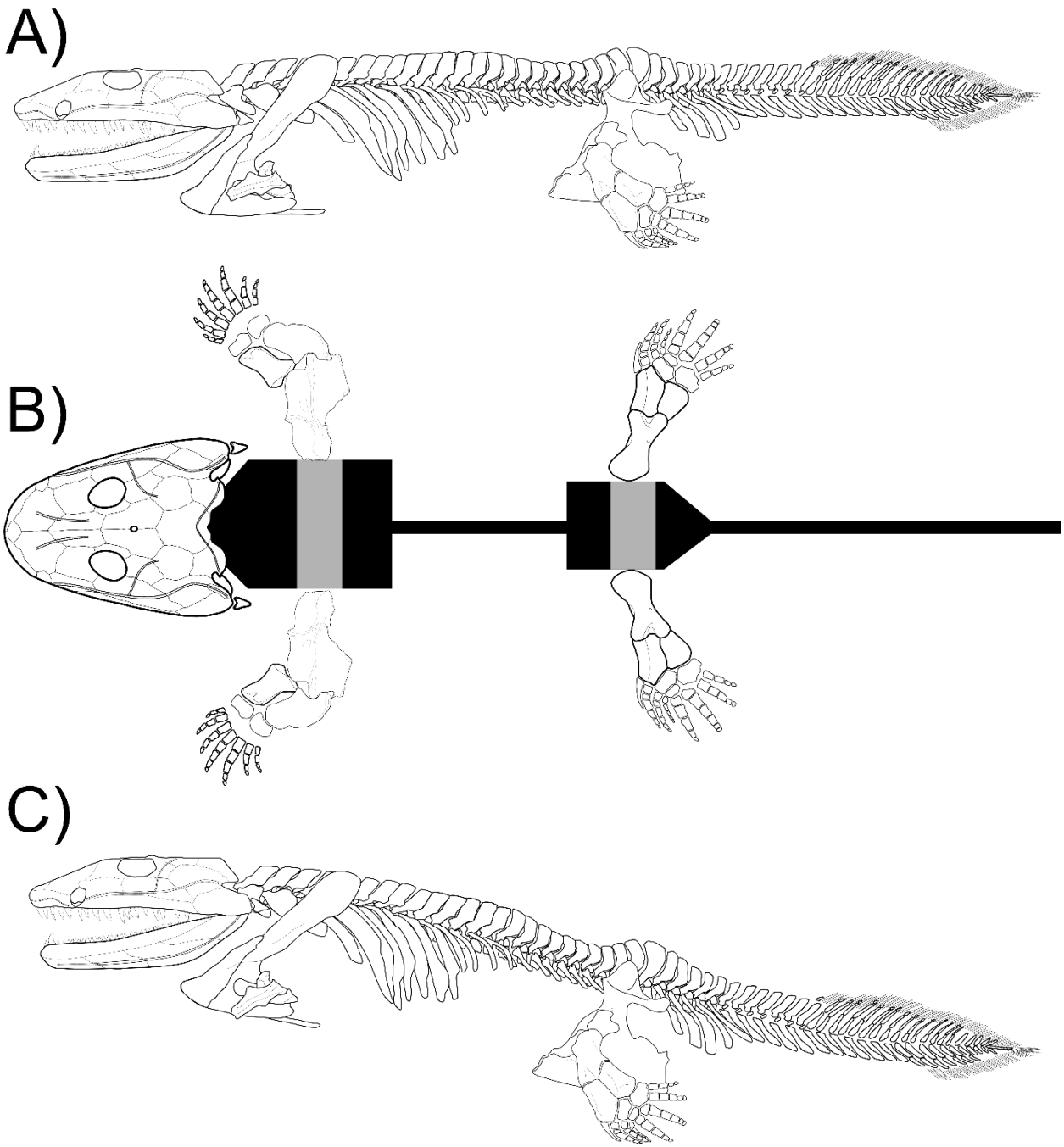

Figure 3.4. New reconstruction of *Ichthyostega* in left lateral view (A) and schematic dorsal view to show body proportions (B). The manus reconstruction is based on a speculative unpublished reconstruction by MI Coates and has not been used to score any characters.

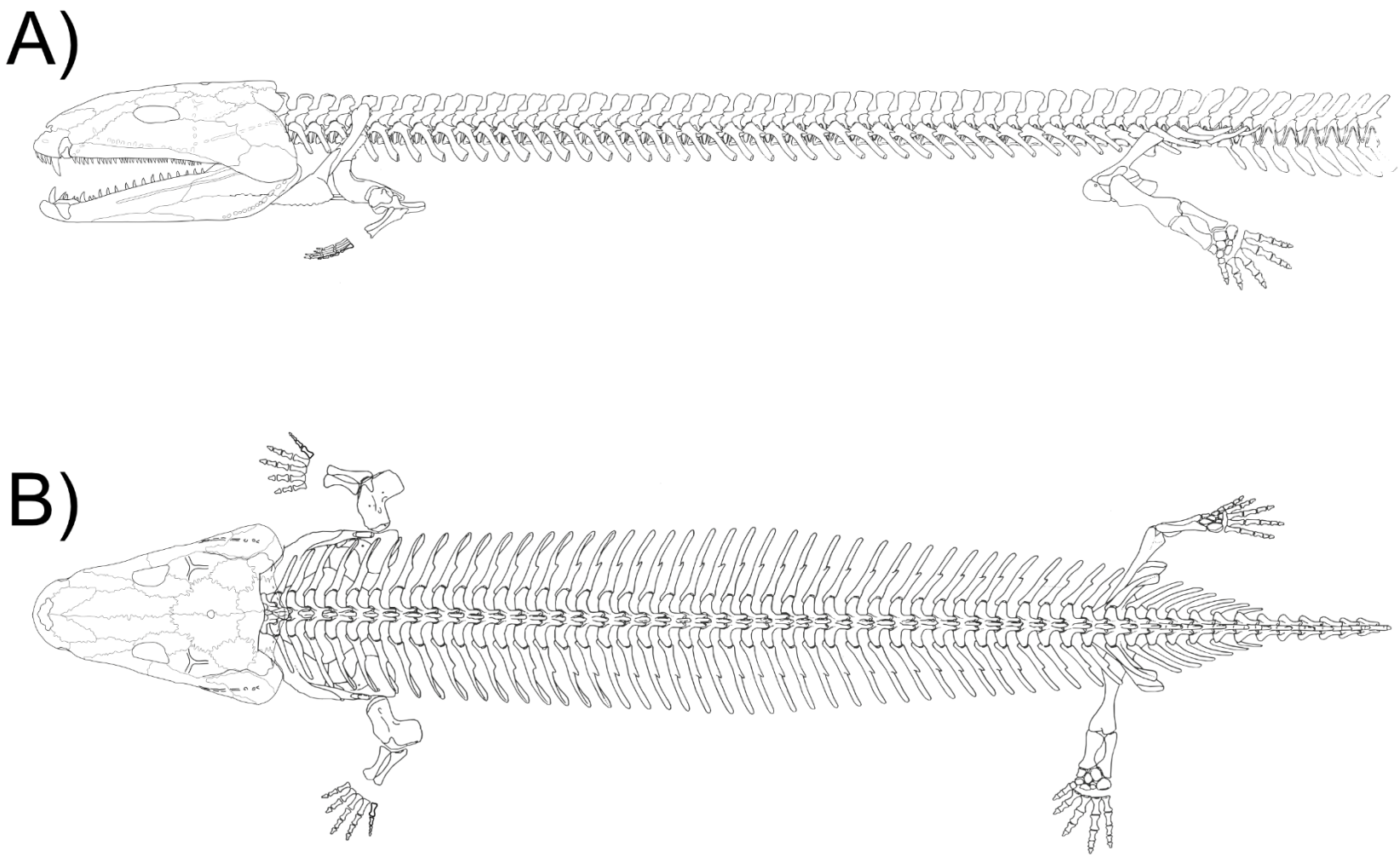

Figure 3.5. New reconstruction of *Greererpeton* in left lateral (A) and dorsal (B) views.

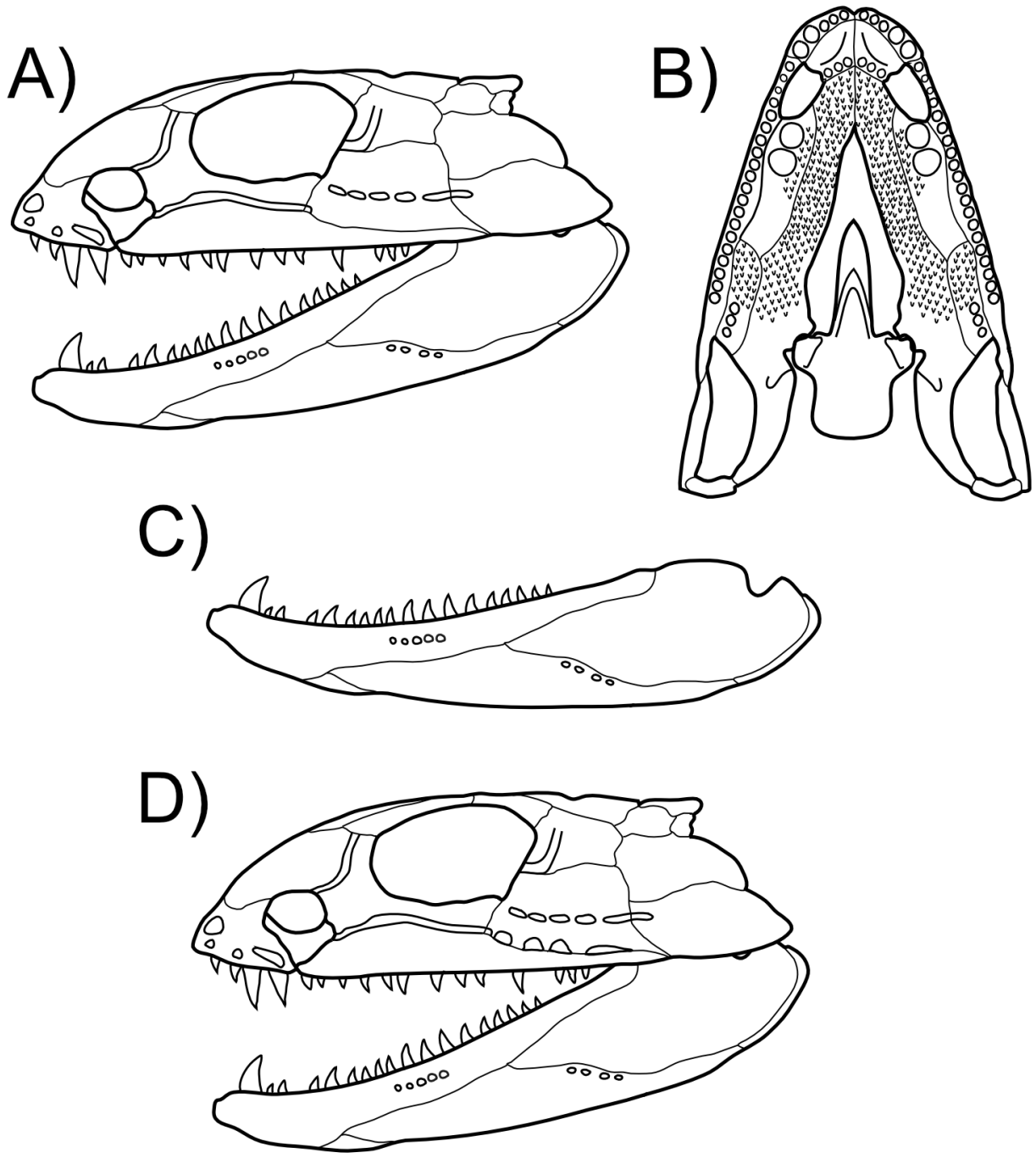

Figure 3.6. New reconstructions of *Aytonerpeton*. Skull in left lateral (A) and palatal (B) views; mandible in left lateral view (C); skull in left lateral view with alternate reconstruction of cranial lateral line (D).

3.3.4 Character list

79 new characters were created for this study. These include contingent characters meant to replace existing characters and *de novo* creations. Character descriptions and explanations of character additions and exclusions are presented in the character list in APPENDIX B.

Table 3-3. Anatomical distribution of new characters created for this study.

Partition name	Number of new characters	Overall partition name
General skull	3	Cranial
Skull roof	7	
Braincase and endocranium	3	
Parasphenoid	8	
Palate	8	
Upper dentition	5	
Lower jaw	3	
Vertebrae	4	Axial
Ribs	2	
Pectoral girdle	10	Anterior appendicular
Humerus	4	
Distal forelimb	0	
Pelvic girdle	5	Posterior appendicular
Femur	8	
Distal hindlimb	3	
Manus and pes	14	Anterior appendicular/Posterior appendicular
Scales	2	
Total	**79**	

Addition of postcranial characters is motivated by the large proportion of postcranial data from *Whatcheeria* (Otoo et al., 2021) and prior hypotheses of divergent signal between the anterior and posterior appendicular skeleton (Coates et al., 2002). Substantial attention has been

paid to the humeri of early tetrapods (Shubin et al., 2004; Boisvert, 2009; Bishop, 2014; Sanchez et al., 2014; Ruta et al., 2018; Smithson and Clack, 2018), but the femur has been much less studied. Of the recent new anatomical characters proposed to contribute to the diagnosis of Whatcheeriidae (Otoo et al., 2021), the most unambiguous of these were identified in the femur (Figure 3.7A,B). There is a strong resemblance in femur anatomy in *Greererpeton* and *Trimerorhachis*. The adult femur morphology shared by these two taxa is very similar to that in *Crassigyrinus* (Panchen, 1985; Panchen and Smithson, 1990). In all three (Figure 3.7C-E), the adductor blade is a robust spike bearing the internal trochanter that is separated from the proximal end of the femur by a deep notch of finished bone. The fourth trochanter is a rugose region on the adductor blade. This may represent phylogenetic affinity or functional convergence; discerning between these two hypotheses is particularly important given recent proposals of a crown tetrapod position for colosteids (Clack et al., 2016), a first-diverging position for the dvinosaurs within the temnospondyls (Pardo et al., 2017a), and the (largely pre-cladistic) history of taxonomic entanglement between the colosteids and dvinosaurs (see Taxon Sampling above). A different femoral pattern (Figure 8) is seen in embolomeres and *Seymouria*, where the adductor blade is absent, the fourth trochanter is an extensive rugose region, the internal trochanter is borne on a ridge contiguous with the proximal end of the femur, and the intertrochanteric fossa is broad.

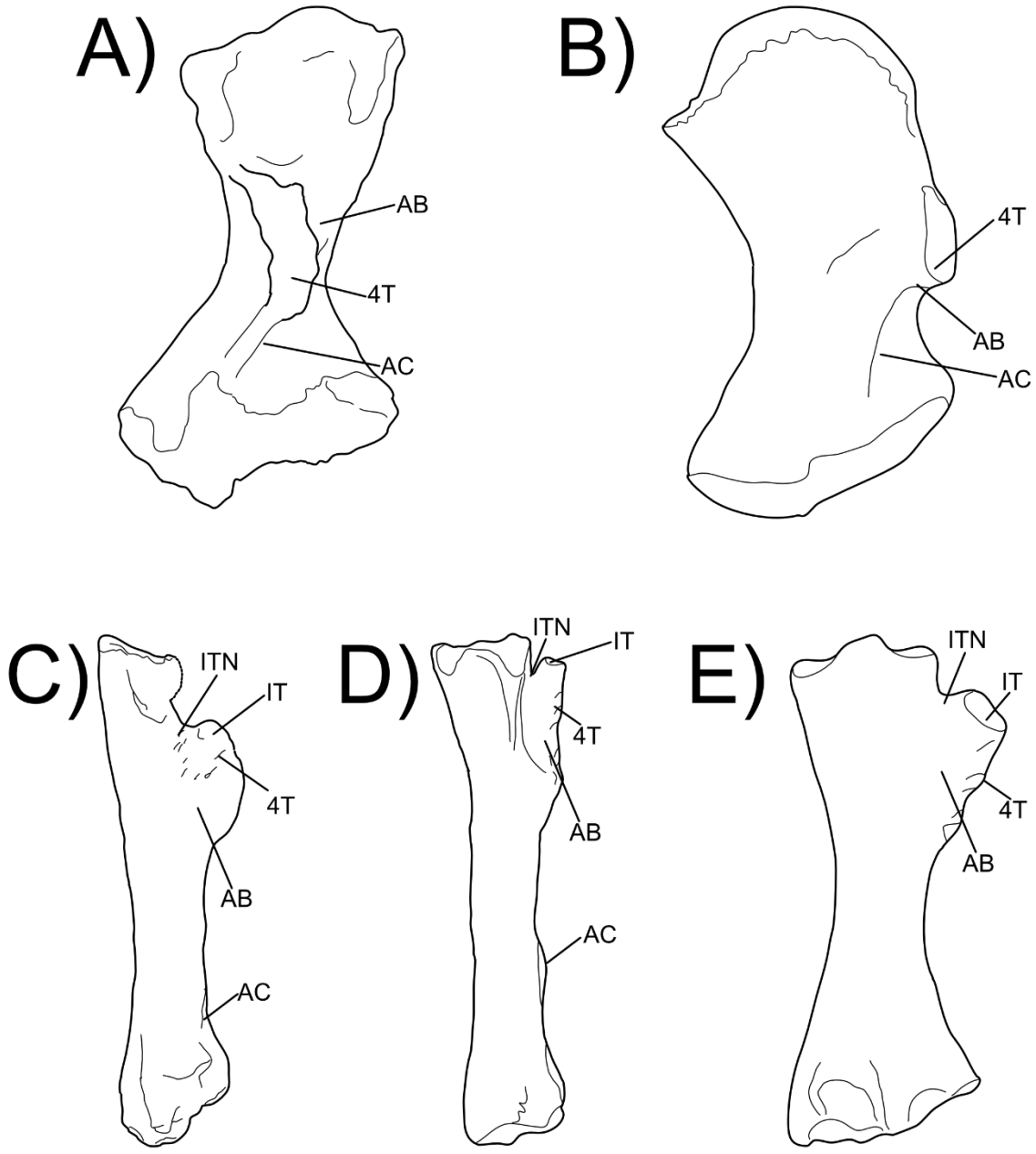

Figure 3.7. Left femora of early tetrapods showing anatomies captured by new characters. All are scaled to the same size. A) *Whatcheeria*, ventral view (Otoo et al., 2021); B) *Pederpes*, ventral view (Clack and Finney, 2005); C) *Greererepton*, dorsal view (Godfrey 1989, supplemented with personal observations of specimens); D) *Trimerorhachis*, posterior view (Pawley 2007, supplemented with personal observations of specimens); E) *Crassigyrinus*, ventral view (Panchen and Smithson 1990). Specimen information is presented in APPENDIX B. Abbreviations: 4T: fourth trochanter; AB: adductor blade; AC: adductor crest; IT: internal trochanter; ITN: intertrochanteric notch

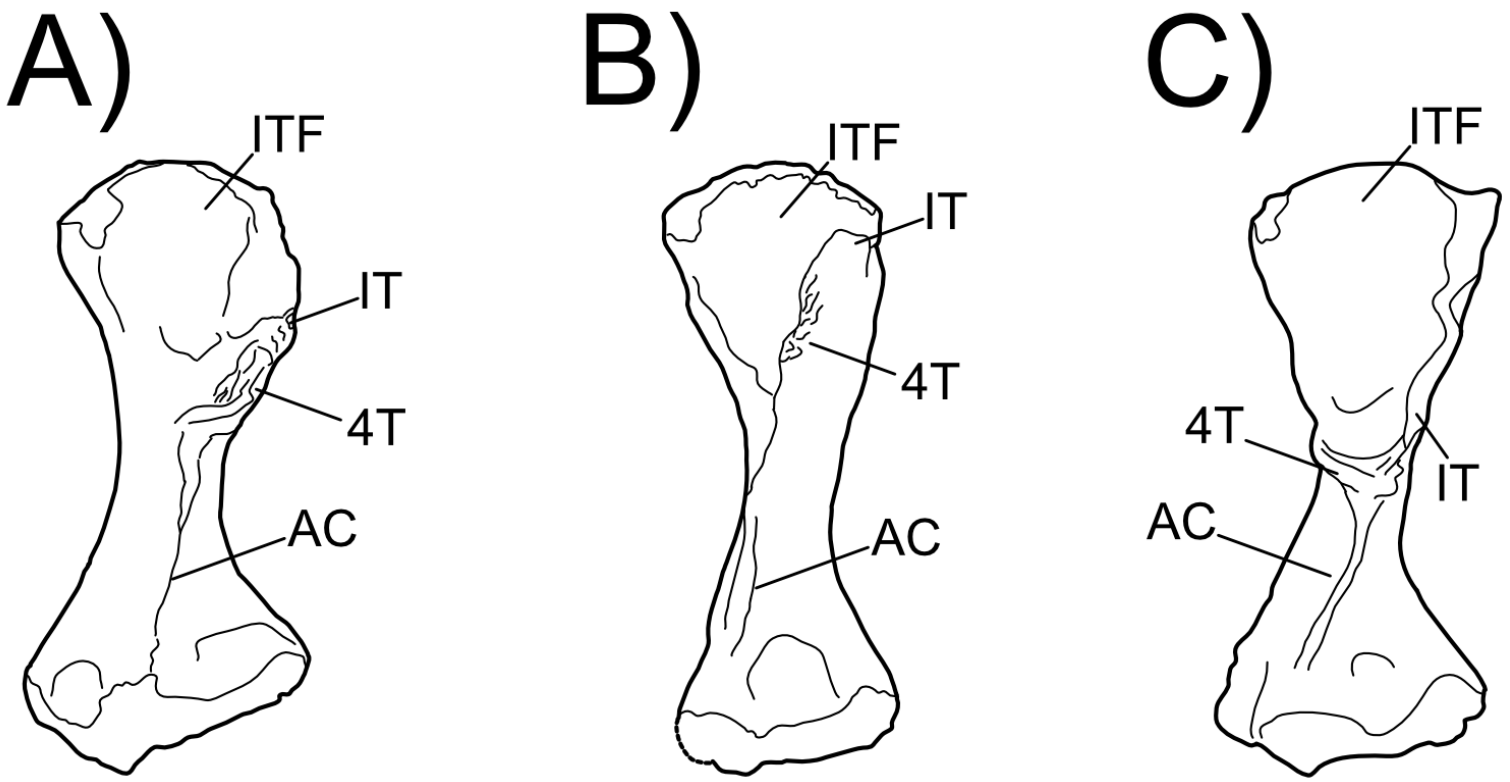

Figure 3.8. Femora of early tetrapods showing anatomies captured by new characters. All femora are right femora in ventral view. A) *Proterogyrinus* (Holmes 1984); B) *Archeria* (personal observations of specimens); C) *Seymouria* (Bazzana et al., 2020). Abbreviations: ITF: intertrochanteric fossa; all other abbreviations as in Figure 3.7.

Interpterygoid vacuities (=medial embayment of pterygoids) are an feature in studies of lissamphibian origins (Anderson, 2001; Schoch, 2002). Various hypotheses have linked the interpterygoid vacuities of lissamphibians to those of temnospondyls (Schoch, 2002, 2012, 2013, 2019) or some 'lepospondyls' (Anderson, 2001; Marjanović and Laurin, 2008200, 2009200, 2013). Interpterygoid vacuities are also present in *Caerorhachis* (Holmes and Carroll, 1977) and colosteids (Smithson, 1982; Hook, 1983) and were previously used to support a temnospondyl affinity. Interpterygoid vacuities are arguably present in various embolomeres (Holmes, 1984, 1989b; Clack, 1987a), which are removed from the question of lissamphibian origins. The morphology of the interpterygoid vacuities vary greatly between these taxa (Kimmel et al., 2009; Lautenschlager et al., 2016; Witzmann and Werneburg, 2017). Previous categorization of interpterygoid vacuities as absent (closed palate), small, or large (Anderson, 2001; Huttenlocker et al., 2013; Clack et al., 2016, 2019b; Pardo et al., 2017b) may obscure phylogenetically useful variation in the structure of the palate. Characters were added to more precisely describe the morphologies of the palatal bones, including: presence/absence and extent of medial contract of the pterygoids (characters 127, 128, 130), morphology of the palatal and quadrate rami of the pterygoids (characters 117, 131), and whether the palatal vacuities intersect the orbit (character 126).

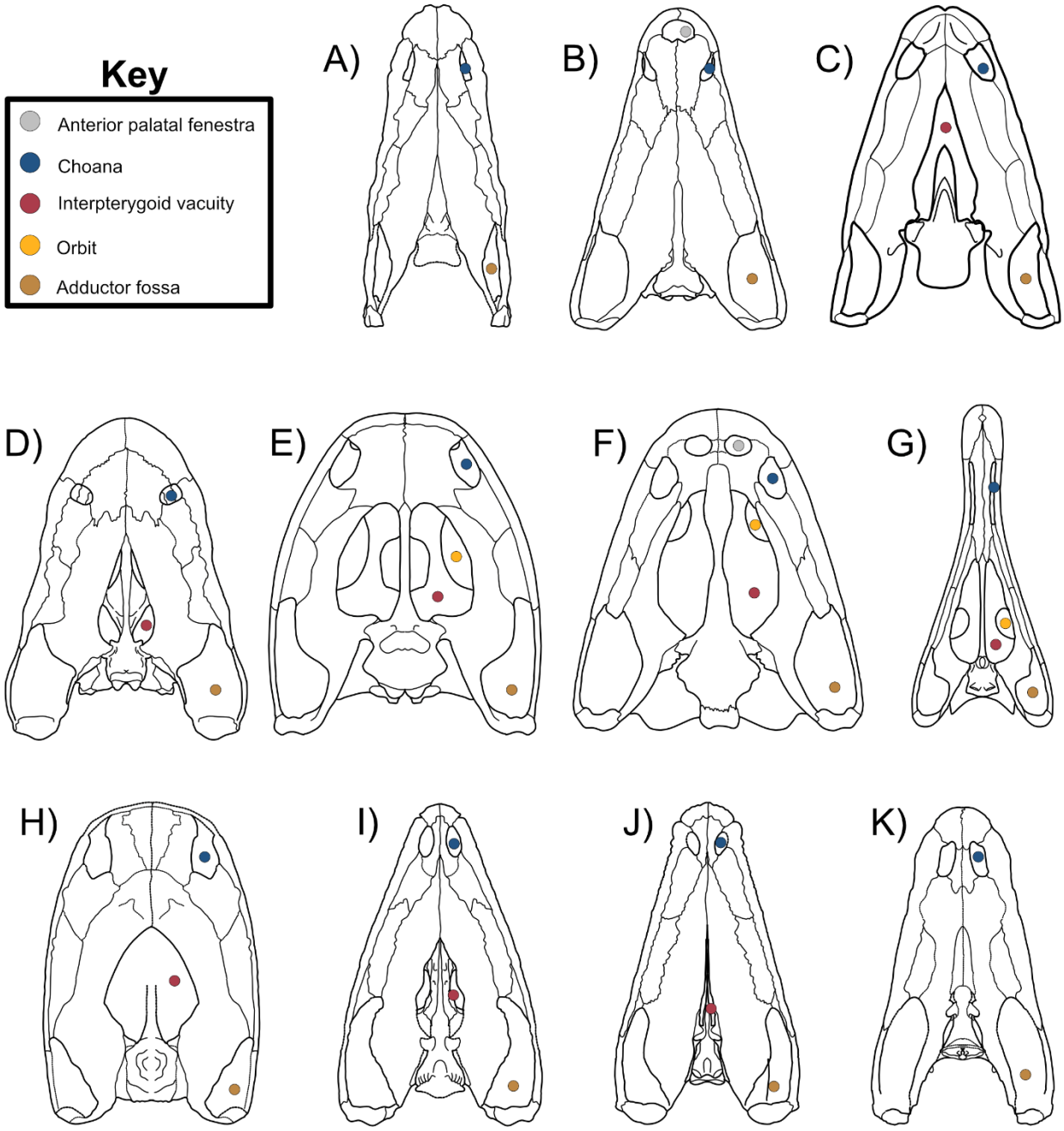

Figure 3.9. Palates of early tetrapods showing conditions across dataset. A) *Whatcheeria* (Rawson et al., 2021); B) *Megalocephalus* (Beaumont, 1977); C) *Aytonerpeton* (Figure 1.6B); D) *Edops* (Romer and Witter, 1942); E) *Balanerpeton* (Milner and Sequeira, 1993); F) *Trimerorhachis* (Milner and Schoch, 2013); G) *Archegosaurus* (Witzmann, 2005); H) *Caerorhachis* (Ruta et al., 2002); I) *Pholiderpeton scutigerum* (Clack, 1987a); J) *Eogyrinus attheyi* (Panchen, 1972); K) *Anthracosaurus* (modified from previous reconstructions by Panchen and Clack (Panchen, 1977; Clack, 1987b). The quadrate distance of the Panchen palate reconstruction was narrowed to match that of the Clack dorsal view reconstruction after both were scaled to the same size).

The full list of 327 characters, with sources, is presented in the APPENDIX B. The starting character list is that of Clack et al. (2019), which replaced that of Clack et al. (2016) as in the case of the taxon list (see Taxon Sampling). This original character set covers the entire skeleton and has a large proportion of jaw and dermal skull characters.

Additional characters were added from other matrices to increase the character set and make this study a more independent test of hypotheses. Characters were added from Rua (2011), which is an entirely postcranial dataset. Additional miscellaneous characters, particularly from the endocranium, were added from the dataset of Pardo et al. (2017). Preexisting characters were slightly reworded for clarity or consistency with other characters. Characters which were inapplicable or invariant for most of the taxon sample and not useful to the questions of this study were removed. Uninformative character states were also removed. These were largely those used to distinguish various tetrapodomorph fish groups from each other and from tetrapods broadly (Ruta, 2011) or pertained to the interrelationships of lepospondyls or (other) derived crown tetrapods (Pardo et al., 2017b).

The final distribution of characters is as follows (see Table 3-3):

- General skull: 1-18
- Skull roof: 19-90
- Braincase and endocranium: 91-99
- Parasphenoid: 100-112
- Palate: 113-131
- Upper dentition 132-157
- Lower jaw: 157-202
- Vertebrae: 203-213
- Ribs: 214-223
- Pectoral girdle: 224-247
- Humerus: 248-266
- Distal forelimb: 267-271

- Pelvic girdle: 272-282
- Femur: 283-298
- Distal hindlimb: 299-310
- Manus and pes: 311-324
- Scales: 325-327

These have been grouped into the following larger anatomical partitions (see Table 3-3):

- Cranial characters: 1-202
- Postcranial characters: 203-327
- Axial characters: 203-223
- Anterior appendicular: 224-271, 311-324
- Posterior appendicular: 272-324

3.4 METHODS

3.4.1 Matrix construction and analysis

The matrix was constructed and edited in Mesquite version 3.6 (build 917) (Maddison and Maddison, 2021). Characters were scored from primary observations and the literature as necessary (see Supplementary Information, Taxon List). Separate symbols were used to represent uncertainty (?) versus inapplicable (-) characters. As per the recommendations of Brazeau (2011), characters were contingent coded (Brazeau, 2011); otherwise characters were multistate. All characters were unordered unweighted.

Parsimony analyses were conducted in PAUP (Swofford, 2003) version 4.0a169. A ratchet procedure was used following (Quicke et al., 2001; Ruta et al., 2003a) to search treespace more efficiently. First, a heuristic search of 50000 replicates was carried out with TBR (tree-branching-reconnection) options (start=stepwise, addseq=random, nreps=50000, swap=tbr). For each replicate, five trees of nonzero length were held at each step and four were discarded, such

that only one tree per replicate was retained (hold=5, nchuck=1, nscore=1). Then a heuristic search of 1000 replicates was run on the trees recovered from the first search (start=current, nreps=1000). The maximum number of trees (maxtrees) was set to increase automatically.

For both parts of the ratchet, all trees were saved. The entire parsimony ratchet procedure was repeated with the characters reweighted once according to their Rescaled Consistency Index (RCI, RC in PAUP code) from the previous search. Re-running analyses with reweighted characters is common practice for datasets for which the consensus trees have low resolution, including early tetrapod datasets (Ruta et al., 2003a, 2020; Ruta and Coates, 2007; Beznosov et al., 2019; Clack et al., 2019b), and our use here was also done in an attempt to increase tree resolution. Sequential iterations of reweighting (Farris, 1989) did not produce different results than reweighting once.

Parsimony ratchet searches were conducted on the full dataset ('standard' dataset). This ratchet was also performed on a version of the dataset with the maximally inclusive *Anthracosaurus*, *Aytonerpeton*, *Eogyrinus*, and *Tulerpeton* OTUs in place of their more conservative counterparts. This analysis was intended to test the effect of the inclusion of the additional data.

The following analyses were conducted to test the amount of signal in anatomical partitions and the potential for contrasting tree topologies:

- Only cranial characters.
- Only jaw characters.
- Only postcranial characters.
- Only appendicular characters.

- Only anterior appendicular (pectoral girdle and forelimb) characters.
- Only posterior appendicular (pelvic girdle and hindlimb) characters.

A bootstrap analysis with 1000 replicates and 100 searches per replicate was conducted in PAUP on the standard dataset. Although bootstrap values for nodes are usually well below the standard 95% threshold for statistical significance, bootstrapping still provides some indication of relative node support. A Bremer analysis (10,000 replicates) was conducted manually as an alternative assessment of node support.

Parsimony and Bayesian analyses of early tetrapod datasets have returned divergent results (Clack et al., 2016, 2019b; Pardo et al., 2017a) and a substantial literature exists on the relative advantages and shortcomings of these methods (Holder and Lewis, 2003; Wright and Hillis, 2014; O'Reilly et al., 2016; Puttick et al., 2017; Goloboff et al., 2018a, 2018b; Sansom et al., 2018; King and Rücklin, 2020; Goloboff and Sereno, 2021). A Bayesian analysis was conducted using all characters and all OTUs in MrBayes (Huelsenbeck and Ronquist, 2001) version 3.2.7a for 10,000,000 generations. This search was done to test the consistency of results under parsimony versus Bayesian treatments. Data were analyzed using the Mkv model, with gamma-distributed rate variation. The analysis was conducted using two runs with four chains each and a burn-in fraction of 0.25 (25%). Trees were sampled every 1000 generations. Analytical convergence was assessed using standard diagnostics in MrBayes (average standard deviation of split frequencies, potential scale reduction factors, and effective sample sizes). Convergence cutoff values were the following: <0.01 (asdsf), 1 (average psrf), >200 (ess). Results were summarized using the mcmc, sump, and sumt commands in MrBayes. In addition to the 50% majority rule consensus tree, the tree with the greatest total likelihood (maximum a posteriori or

MAP tree) was extracted. This was done to produce a single, fully resolved tree for comparison with the parsimony results.

Trees were visualized using FigTree (Rambaut, 2010), Mesquite, and the ape package (Paradis and Schliep, 2019) in RStudio (RStudio Team, 2019) for R (R Core Team, 2019). Log files for all searches are in the Supplementary Information. Timetrees were generated in R using the paleotree (Bapst, 2012), geiger (Alfaro et al., 2009) and strap (Bell and Lloyd, 2015) packages. The "equal" time-scaling method was selected (vartime=1). The "equal" option adds time to the root node so that the additional time on early branches is spread across later branches to bring them up from zero-length. First and last appearances for OTUs were taken as the start of and end of the oldest and youngest stages in which they appear. Within these ranges, tip ages were sampled from a uniform distribution.

The Gap Excess Ratio (GER) is a measure of stratigraphic congruence between the branching pattern of a given tree and the ages of the OTUs at the tips. It represents a quantitative measure of how well a given tree topology reduces ghost lineages (Wills, 1999). It is, then, an alternative criterion to treelength for choosing the 'best' tree topology. GER was calculated in R Studio using the strap package (Bell and Lloyd, 2015).

3.5 RESULTS

3.5.1 Parsimony results

Basic numerical information for all parsimony searches is presented in Table 3-4. Percentage of parsimony-informative characters is high across all analyses (90-95%). Signal, as

measured by the number of trees and proportion of taxa retained in the agreement subtree, is high in the full dataset but much lower in nearly all others.

The unweighted search of the standard dataset yielded 10916 most parsimonious trees (MPTs) of length 1981. The strict consensus tree is presented in Figure 3.10A. *Parmastega* and limbed tetrapods are contained within a large polytomy that is almost completely unresolved. Exceptions are: *Greererpeton*/*Colosteus*, *Neopteroplax*/*Eogyrinus*, (*Lethiscus*/*Coloraderpeton*, *Adelogyrinus*/*Adelospondylus*), and an internally unresolved- except for *Eryops*/*Edops* and *Erpetosaurus*/*Trimerorhachis*- Temnospondyli. The unweighted strict consensus of the more inclusive version of the dataset Figure 3.10B is similar, with the addition of *Microbrachis* and *Westlothiana* to the base of the adelospondyl/aistopod clade, and recovery of the baphetids.

The RCI reweighted search (standard version of the dataset) yielded one tree of length 256.70077 (Figure 3.11.). Reweighting was done to increase signal and attempt to extract a more resolved tree. The topology is broadly congruent with those from previous work by Ruta, Clack, Coates, and others on datasets from which this one descends (Ruta et al., 2003a; Ruta and Coates, 2007; Clack et al., 2016, 2019b). The stem group is diverse, and the crown group is composed of temnospondyls (= lissamphibian total group) and an amniote total group primarily composed of anthracosaurs, 'lepospondyls', and assorted other taxa such as *Westlothiana* and *Gephyrostegus*. Differences in the reweighted tree for the maximally inclusive dataset (Figure 3.12) are minimal.

Table 3-4. Basic numerical information for parsimony searches. Abbreviations: NT: Number of OTUs (=NTAX); NX: Number of characters (=NCHAR); NIC: Number of parsimony-informative characters; PIC: percentage of parsimony-informative characters; R: number of rearrangements; TL: length of most parsimonious tree(s); T: number of most parsimonious trees; ASR: fraction of taxa retained by agreement subtree; NRC: number of reweighted characters; PRC: percentage of reweighted characters; RRCI: number of rearrangements (reweighted); TLRCI: treelength of most parsimonious tree(s) reweighted; TRCI: number of most parsimonious trees (reweighted); ARRCI: fraction of taxa retained in agreement subtree (reweighted).

Analysis	NT	NX	NIC	PIC	R	TL	T	ASR	NRC	PRC	RRCI	TLRCI	TRCI	ASRRCI
Standard	61	327	310	94.80	190089296	1981	10916	25/61	286	87.46	68377	256.70077	1	61/61
Maximally-expanded (ME)	61	327	310	94.80	9783556	1990	556	29/61	288	88.07	16632	251.65802	5	61/61
Cranial	59	202	195	96.53	5587984	1396	314	25/59	183	90.59	54936	153.21395	3	58/59
Jaws	57	48	46	95.83	2262233	238	100	50/55	42	87.5	81693	36.21073	1	57/57
Postcranial	47	125	115	92	144739212	548	9936	28/47	99	79.2	62504	117.84127	5	46/47
Appendicular	45	104	94	90.38	944870072	446	74994	10/45'	80	76.92	917542	107.64927	1	45/45
Appendicular anterior	45	51	46	90.20	5513881949	221	≥500000	35/45	40	78.43	784805	44.58281	1	45/45
Appendicular posterior	40	42	39	92.86	4466990684	166	≥500000	25/40	39	92.86	16925	47.96373	1	40/40

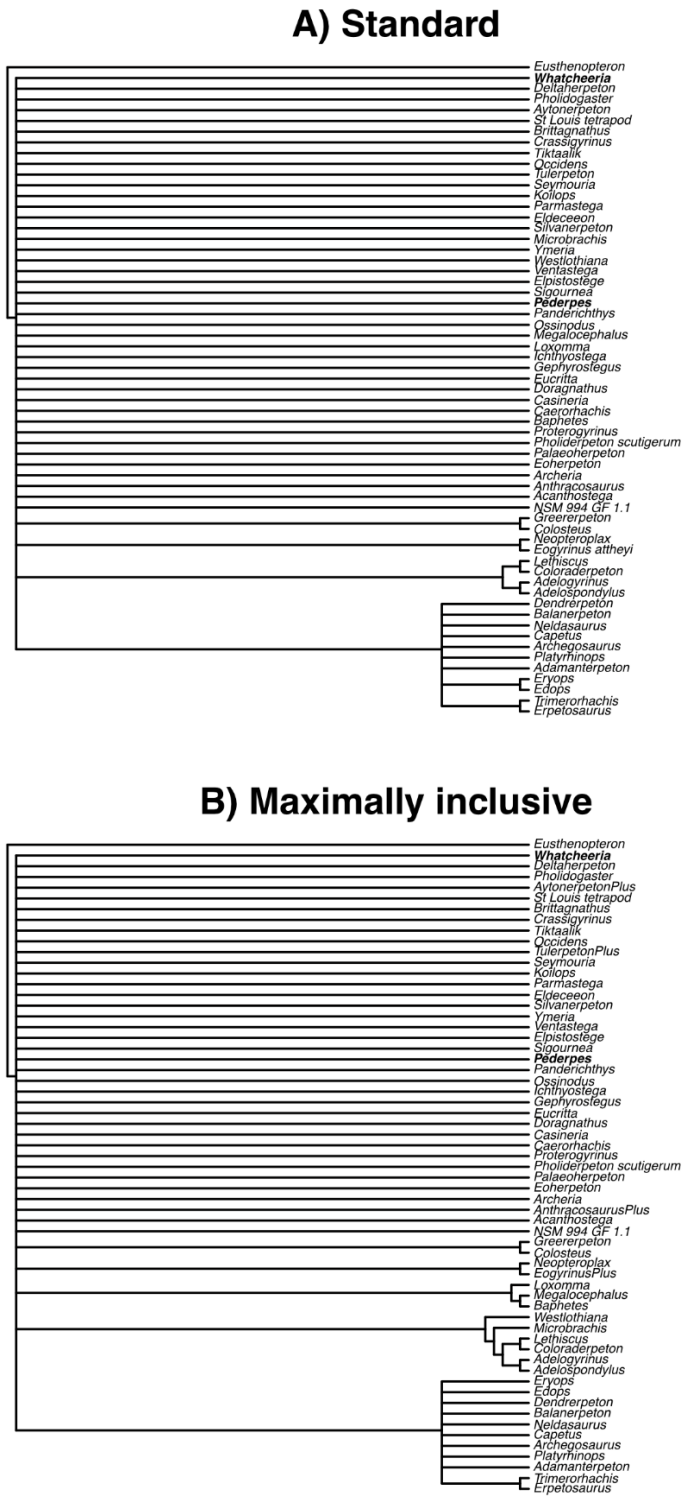

Figure 3.10. Unweighted strict consensus trees from analyses of the standard (A) and maximally inclusive (B) versions of the dataset.

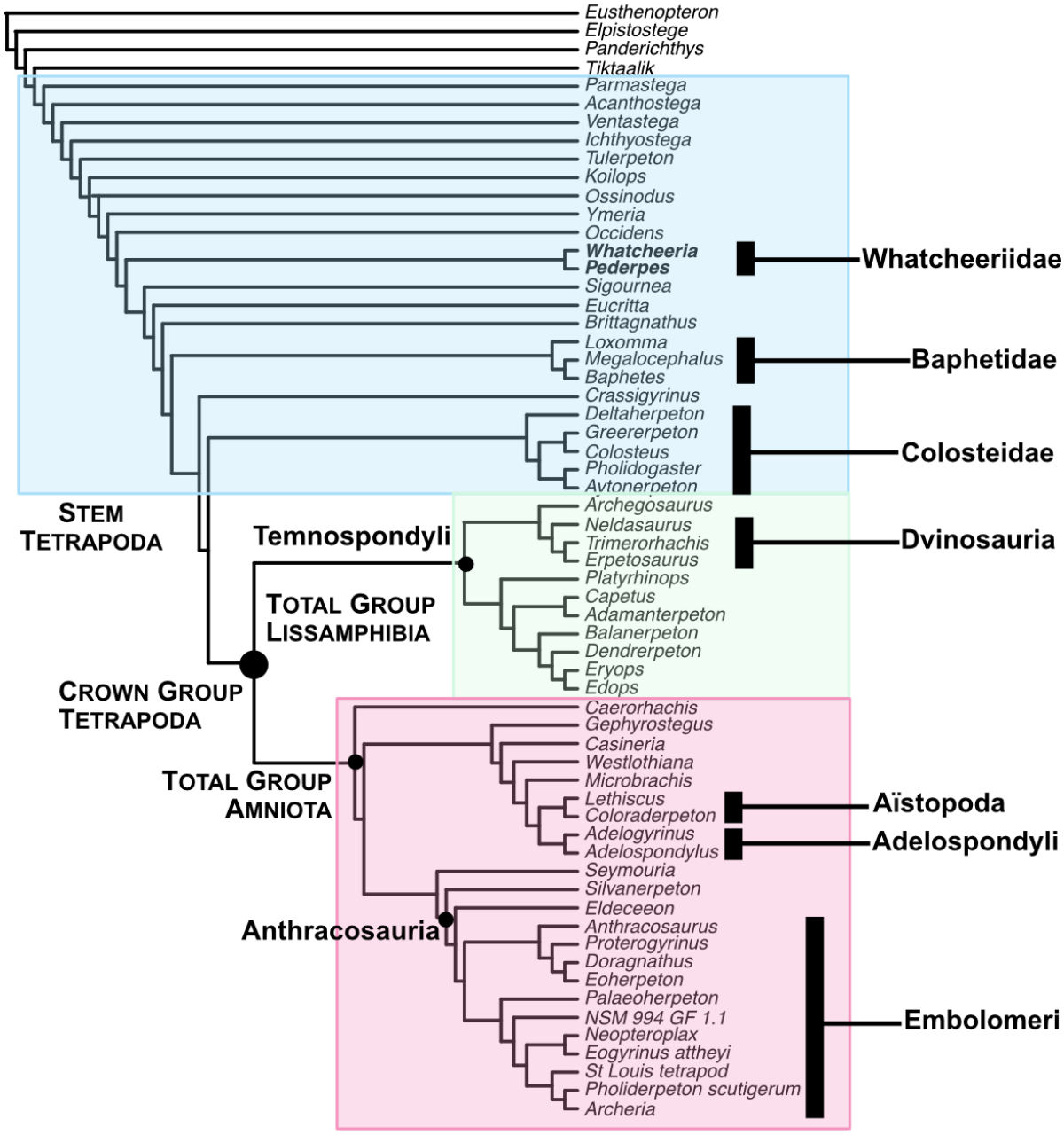

Figure 3.11. Reweighted strict consensus tree from analysis of standard dataset (no alternative OTU treatments, all characters). Colors are used to mark large divisions of phylogeny: *Parmastega* and stem tetrapods (blue), total group Lissamphibia (green), and total group Amniota (pink).

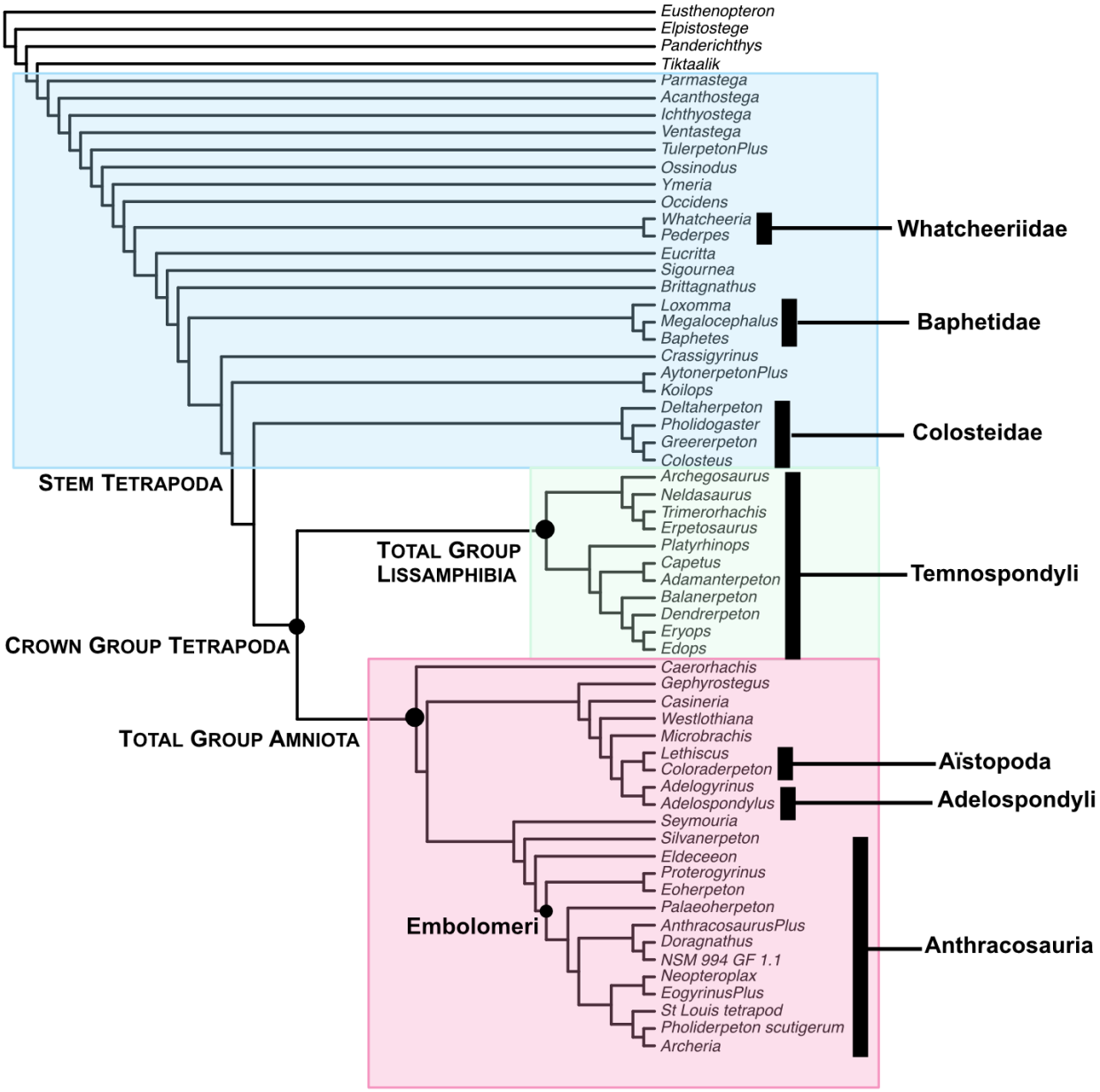

Figure 3.12. Reweighted strict consensus tree from analysis of maximally inclusive dataset (alternative OTU treatments, all characters).

3.5.1.1 Partition analyses

3.5.1.1.1 Unweighted results

The unweighted strict consensus trees from the partition analyses are shown in Figure 3.13, Figure 3.14, and Figure 3.15. Reweighted strict consensus trees from the partition analyses are presented in APPENDIX B. Signal (= number of nodes) is roughly comparable to that of the unweighted full dataset search. Most of the nodes which are recovered are dyads from the unweighted strict consensus from the full character set, suggesting that the signal supporting these groups is distributed across the skeleton. The jaw character set returns a tree with a surprisingly resolved apical portion composed of OTUs found in the crown in other treatments (Figure 3.13). However, larger groups- Whatcheeriidae, Baphetidae, Temnospondyli, etc.- are not recovered. The anterior (Figure 3.15A) and posterior (Figure 3.15B) appendicular character sets are interesting exceptions. The former recovers three unusual but fully resolved clades (notably a (*Eoherpeton*(*Pholidogaster*/*Tulerpeton*)) clade not found elsewhere), and the latter recovers only two dyads: *Crassigyrinus*/*Baphetes* and *Ichthyostega*/*Acanthostega*.

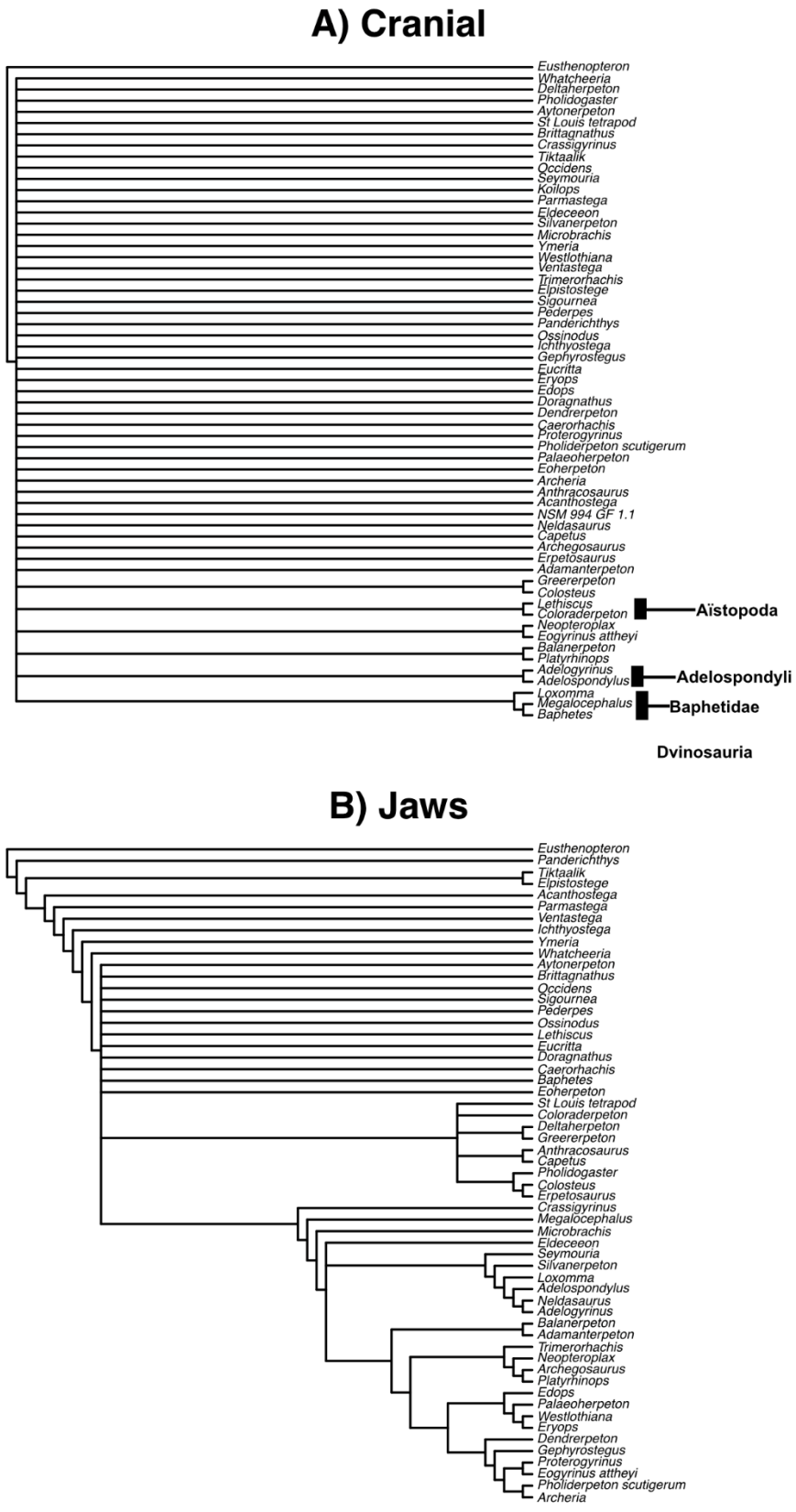

Figure 3.13. Unweighted strict consensus trees from analyses of the cranial (A) and jaw (B) character sets.

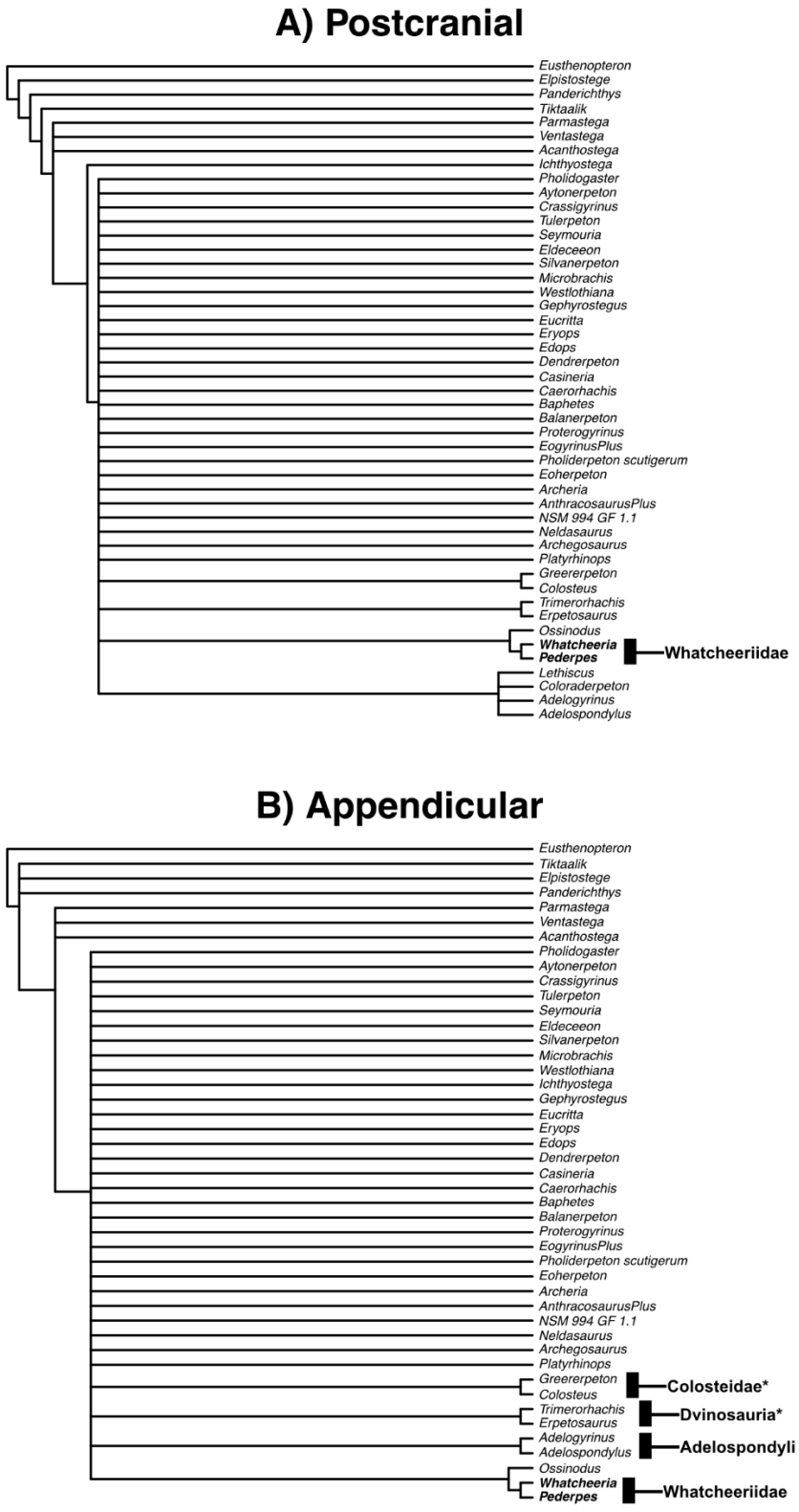

Figure 3.14. Unweighted strict consensus trees from analyses of the postcranial (A) and appendicular (B) character sets.

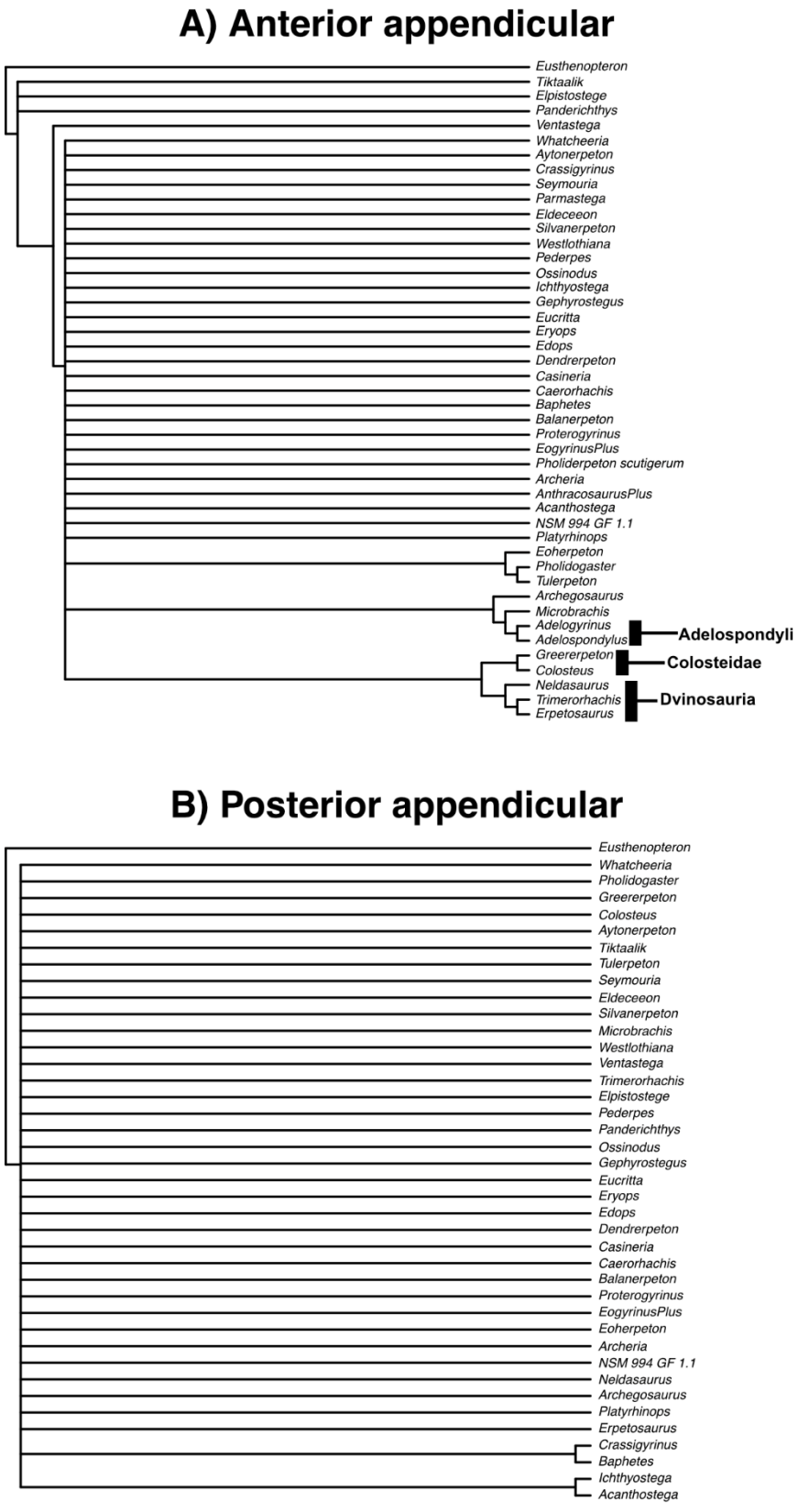

Figure 3.15. Unweighted strict consensus trees from analyses of the anterior appendicular (A) and posterior appendicular(B) character sets.

3.5.1.1.2 Reweighted results

The reweighted strict consensus trees from the partition analyses are shown in Figure 3.15, Figure 3.16, and Figure 3.17. Cranial and postcranial character partitions deliver similar levels of signal, though tree topologies differ. The postcranial character partition (all postcranial characters) produces a tree that is almost entirely consistent with the reweighted tree from the full-dataset analysis (Figure 3.11). By contrast, the cranial character partition produces a substantially different topology. The colosteids move into the lissamphibian total group, and the aistopods and embolomeres are moved onto the tetrapod stem as successive plesions approaching the tetrapod crown. The separation of the aistopods and adelospondyls is notable, as the aistopod/adelospondyl clade has high Bremer support (Figure 3.20). The jaw, anterior appendicular, and posterior appendicular character sets are unable to recover the large clades seen in the full dataset search and other partitions, spreading their component taxa across the tree. In the anterior and posterior appendicular trees, most taxa are contained within two large clades. Both these clades contain a mix of Devonian and Carboniferous taxa.

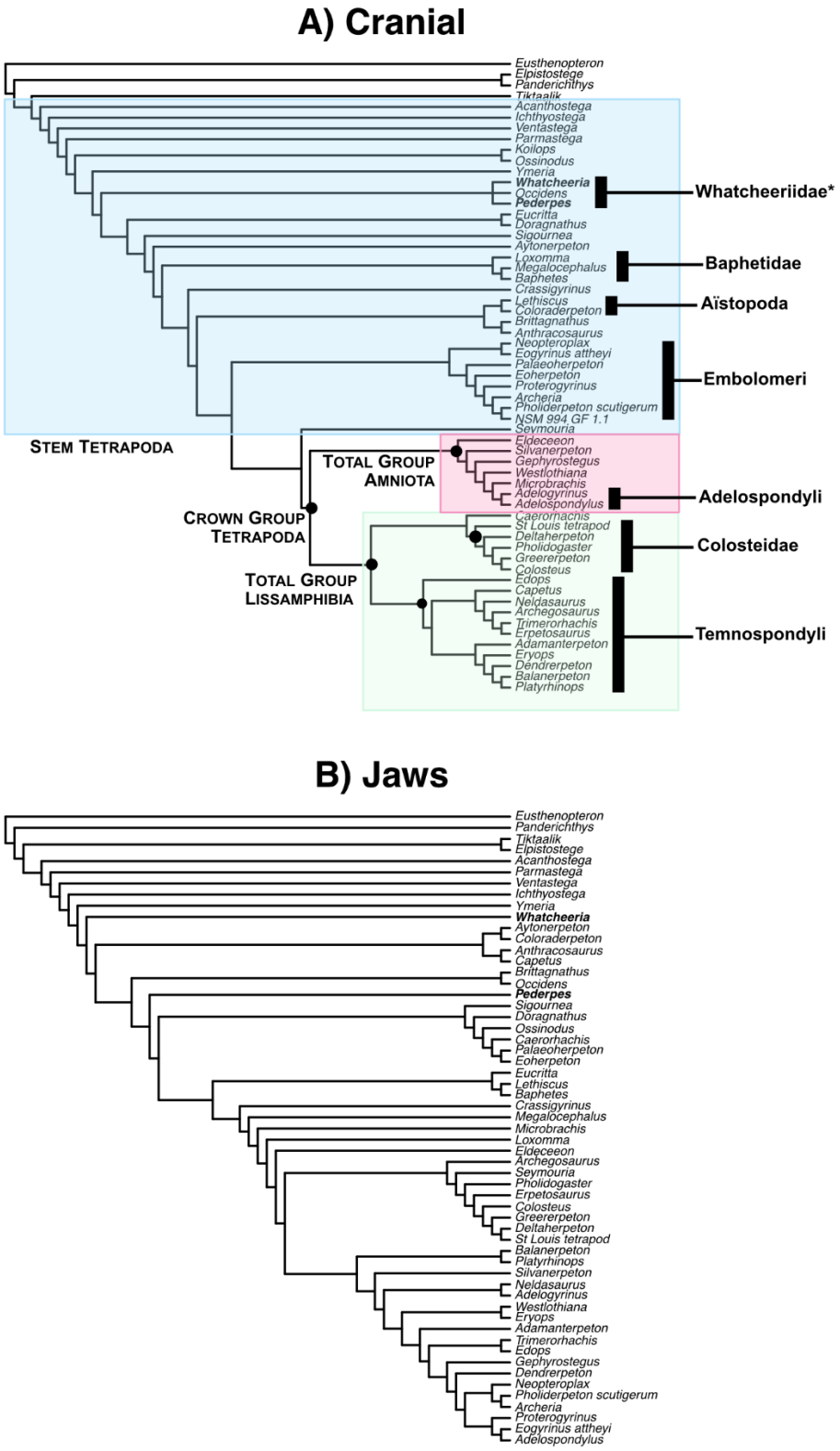

Figure 3.16. Reweighted strict consensus trees from cranial-only (A) and jaw-only (B) analyses.

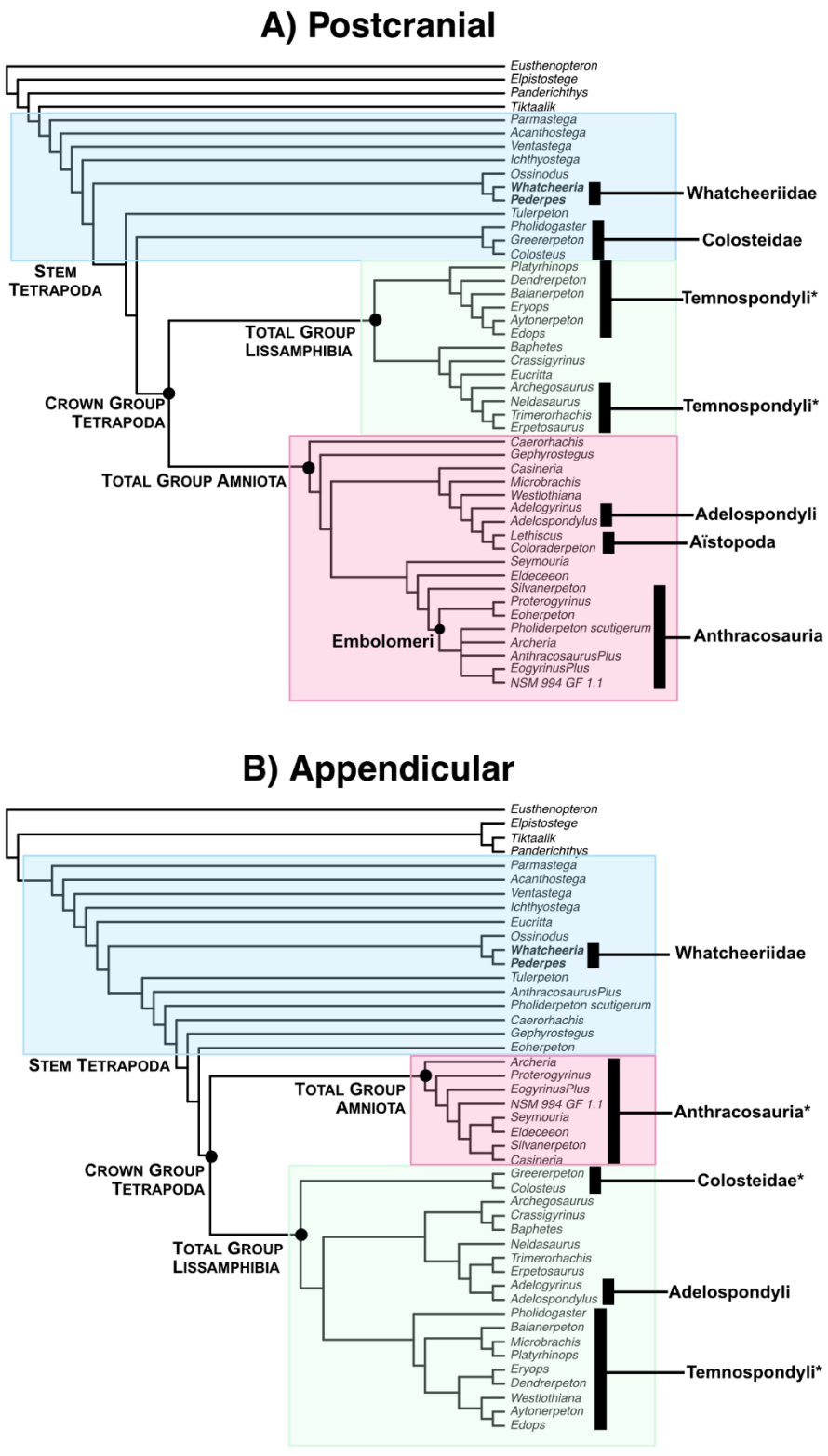

Figure 3.17. Reweighted strict consensus trees from postcranial-only (A) and appendicular-only (B) analyses.

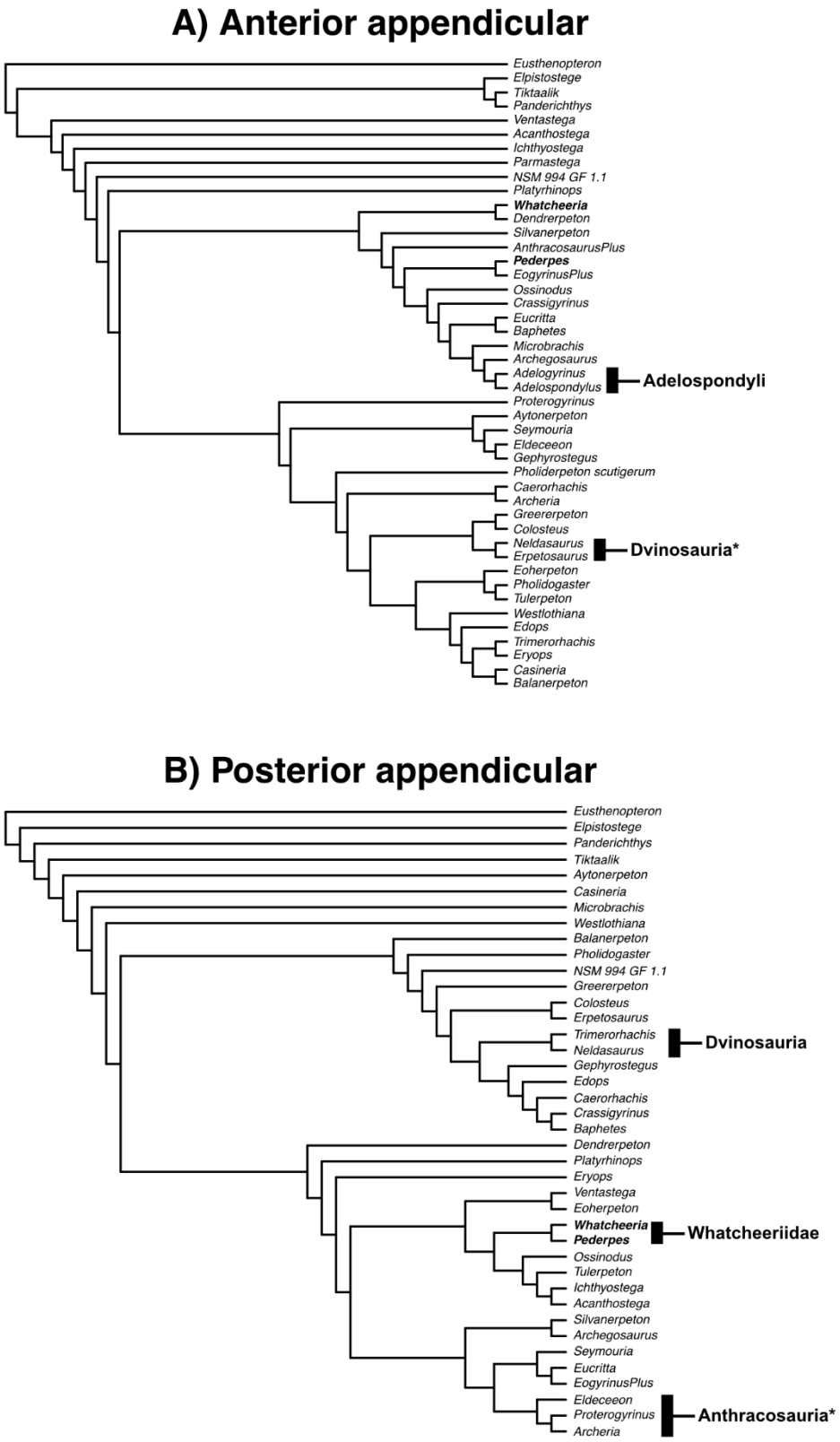

Figure 3.18. Reweighted strict consensus trees from anterior appendicular-only (A) and posterior appendicular-only (B) analyses.

3.5.2 Bootstrap and Bremer support

The bootstrap consensus (50% majority rule) tree is presented in Figure 3.19 and the unweighted strict consensus tree with Bremer support values at nodes is presented in Figure 3.20. *Parmastega* and limbed tetrapods are contained within a large polytomy with high support (81%). The temnospondyls, in contrast to the unweighted strict consensus, have been collapsed into the primary polytomy, but several small clades are recovered that were not present. Bootstrap support values for these nodes is generally low: *Eogyrinus*/*Neopteroplax* (51%), the whatcheeriids (53%), the baphetids (67%) and adelospondyls/aistopods (68%). In the Bremer analysis, most nodes in the strict consensus collapse at a single extra step (Figure 3.20). Notable exceptions are *Trimerorhachis*/*Erpetosaurus* (three extra steps) and the adelospondyls (five extra steps).

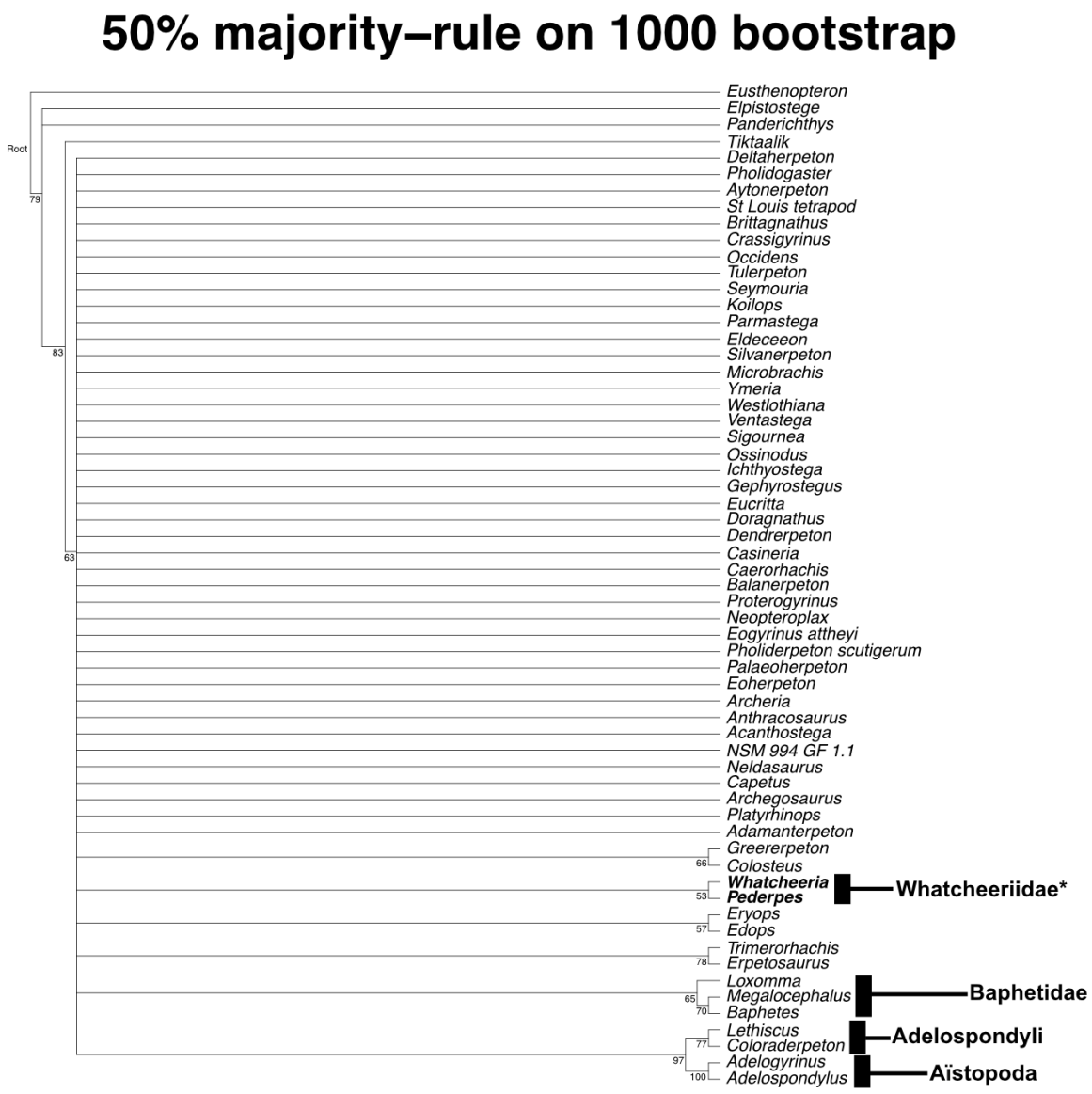

Figure 3.19. Majority rule (50%) for bootstrap analysis of standard version of dataset.

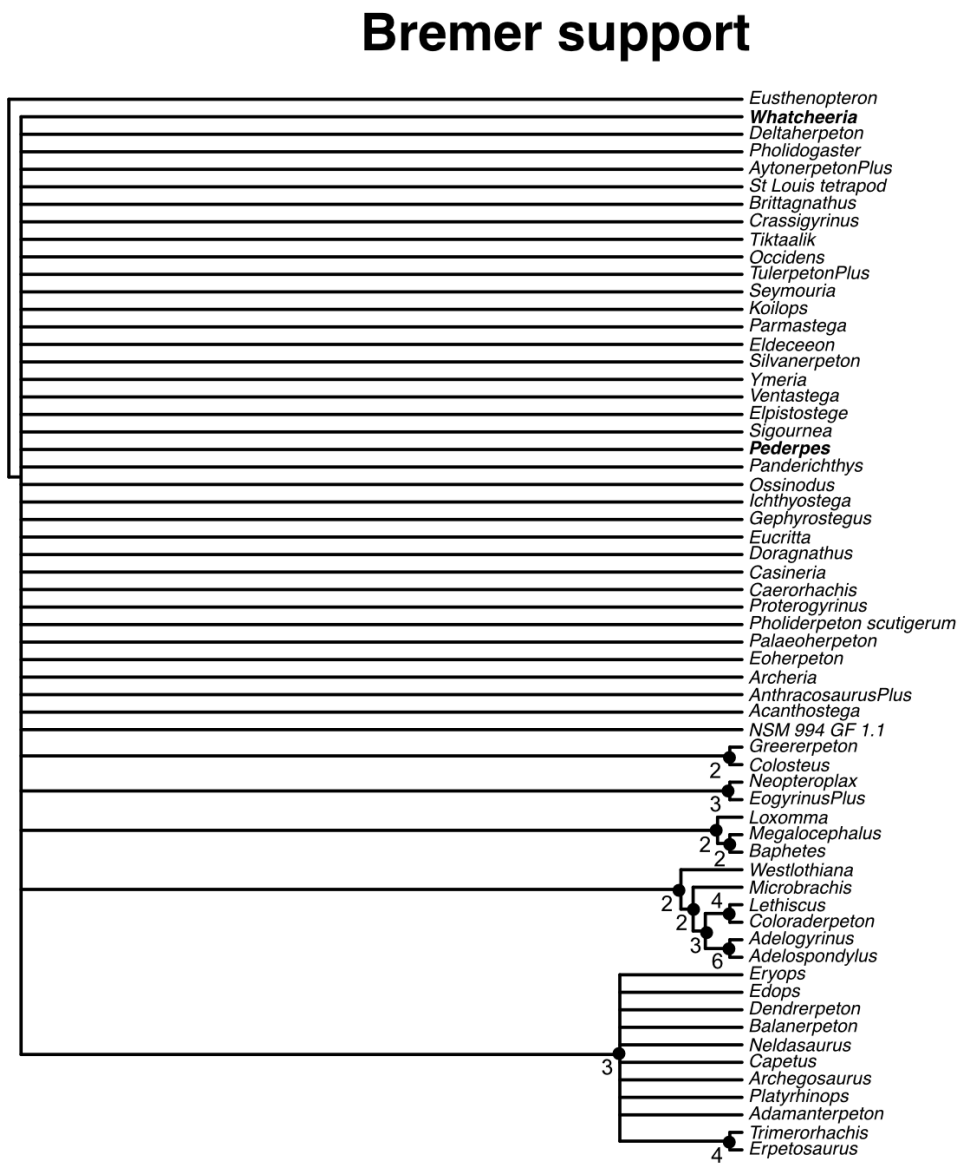

Figure 3.20. Strict consensus tree (unweighted) with number for all nodes with Bremer support values greater than 1.

3.5.3 Bayesian analysis

Convergence diagnostics indicate that both chains converged on the same target distribution (ASDF=0.01, all PRSF<1.01) and that effective sample sizes are adequate for all parameters (min ESS=6164.64). The majority rule (50%) consensus tree is presented in Figure 3.21. Several dyads are the result of standard and more inclusive versions of taxa clustering together (ex. *Aytonerpeton*/*Aytonerpeton*Plus). The topology is very similar to the unweighted strict consensus (Figure 3.10). In the MAP tree (Figure 3.21B), there are two notable differences from the parsimony results: the whatcheeriids are paraphyletic and *Tulerpeton* is at the base of the amniote total group, one node below *Caerorhachis*.

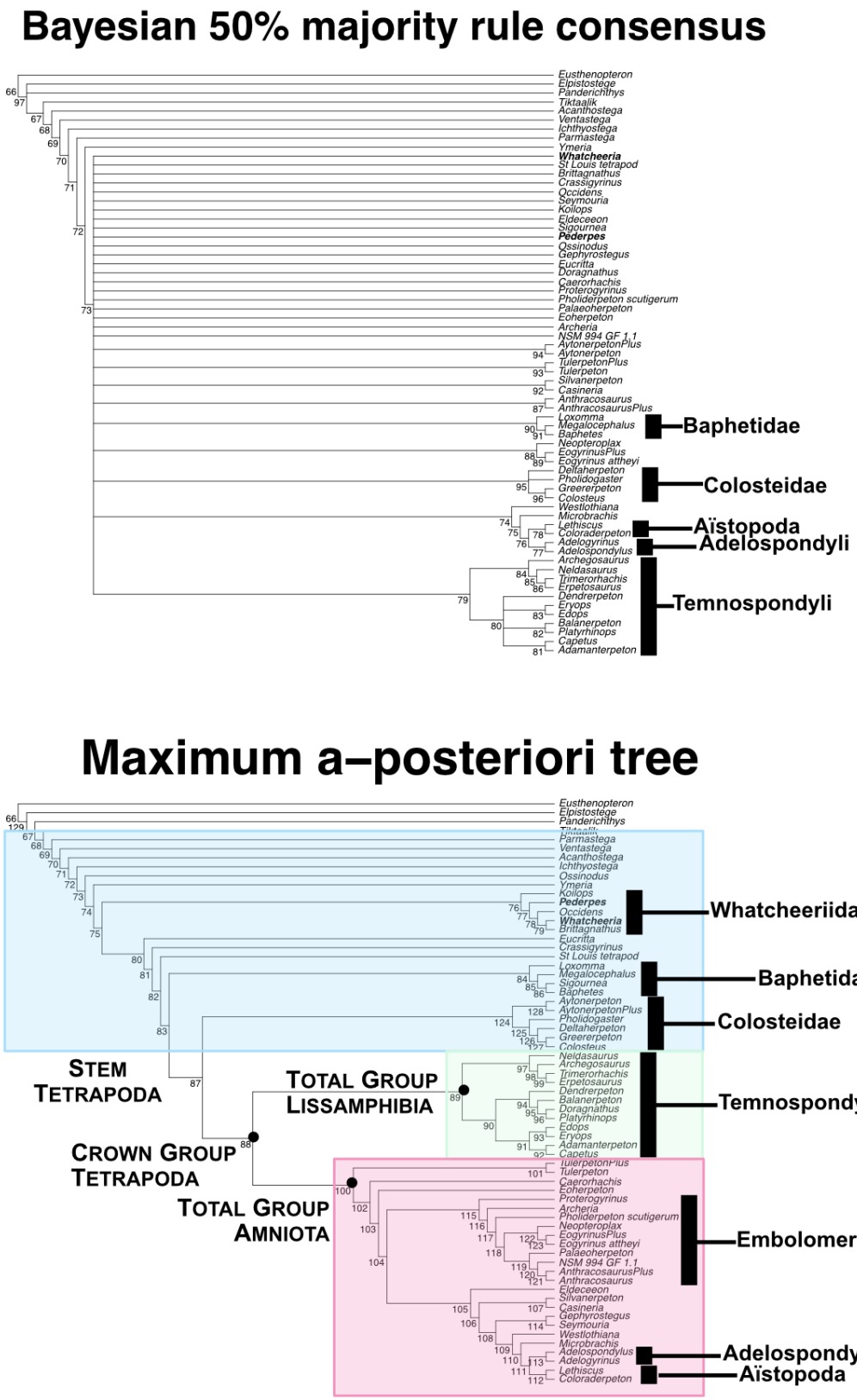

Figure 3.21. Trees from Bayesian analysis. A) 50% majority rule consensus tree; B) maximum a posteriori probability (MAP) tree.

3.5.4 Stratigraphic congruence

The GER for the reweighted tree is relatively high (0.76). The highest value from the unweighted search is 0.80, and the corresponding tree is shown in Figure 3.22. The topology is broadly consistent with that of the reweighted tree, and the implied ages of the whatcheeriids and crown group remain the same. Differences include a (*Pederpes* (*Whatcheeria*/*Occidens*)) clade, *Caerorhachis* as the siter group to crown tetrapods, and the rootward movement of the colosteids + *Sigournea* by one node.

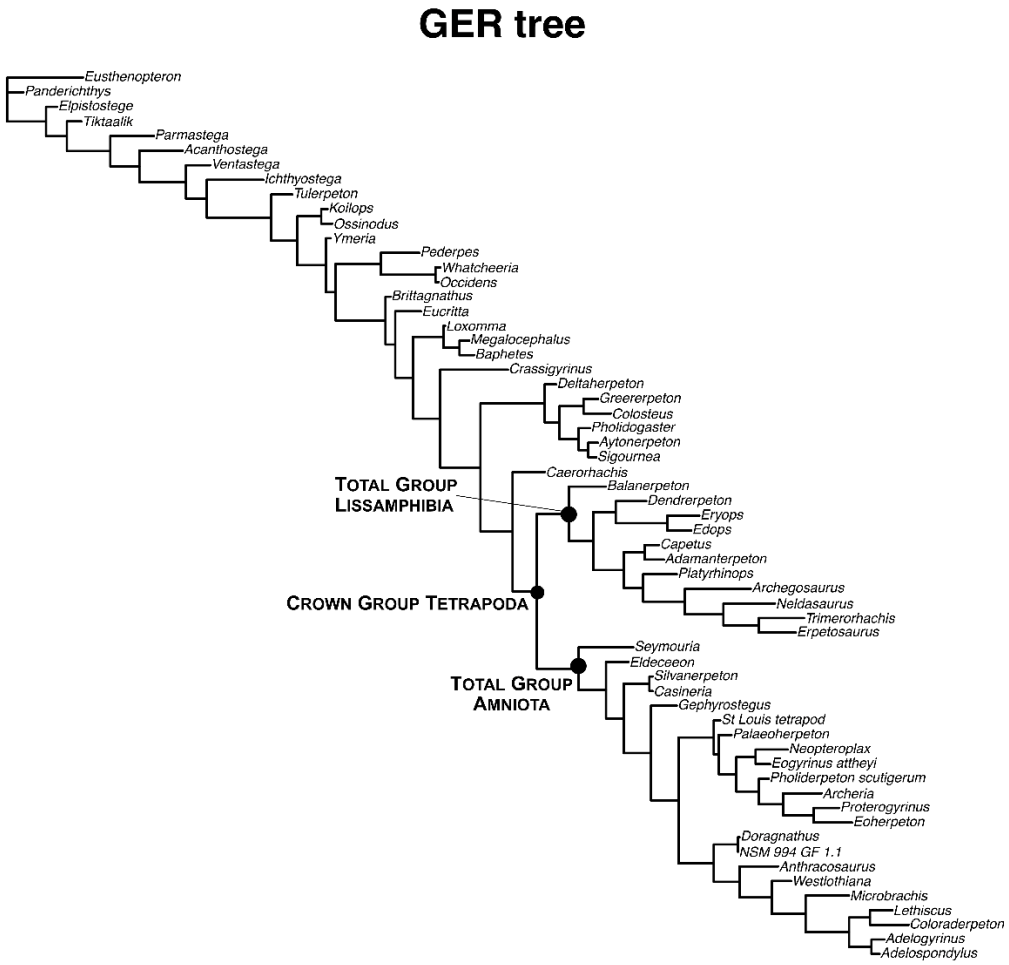

Figure 3.22. Tree from the unweighted analysis of the standard dataset with the highest GER score (0.8024164).

3.5.5 Timetrees

Under the reweighted tree (standard dataset), the hard maximum age of the crown group is Visean as defined by the ages of OTUs at the tips, and its 'soft' age is Tournaisian based on the *Aytonerpeton* dating the colosteids to the Tournaisian (Figure 1.23). Given the presence of *Tulerpeton*, *Ymeria*, and *Brittagnathus* in the Fammenian, the tree topology implies that the following Carboniferous lineages are thus the products of Devonian divergences: *Koilops*, *Ossinodus*, *Occidens*, *Sigournea*, *Eucritta*, Whatcheeriidae (*Whatcheeria*/*Pederpes*). This is the case when the reweighted tree from analysis of the most inclusive dataset (timetree not shown) or the GER tree (Figure 1.24) is used. When the Bayesian MAP tree is used, the inclusion of *Tulerpeton* forces the origin of the crown group into the Late Devonian (Figure 1.25).

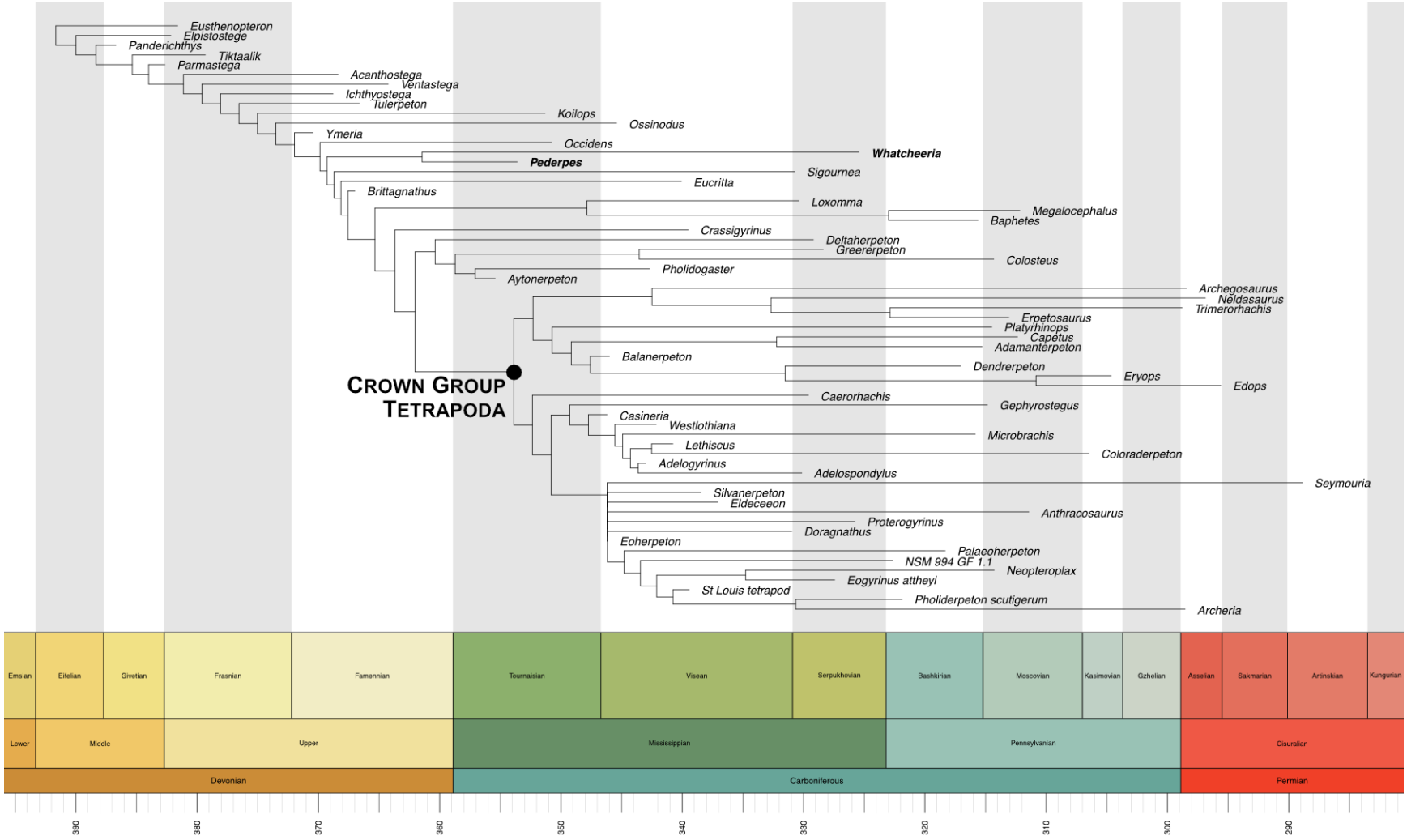

Figure 3.23. Timetree using topology from reweighted tree, standard dataset.

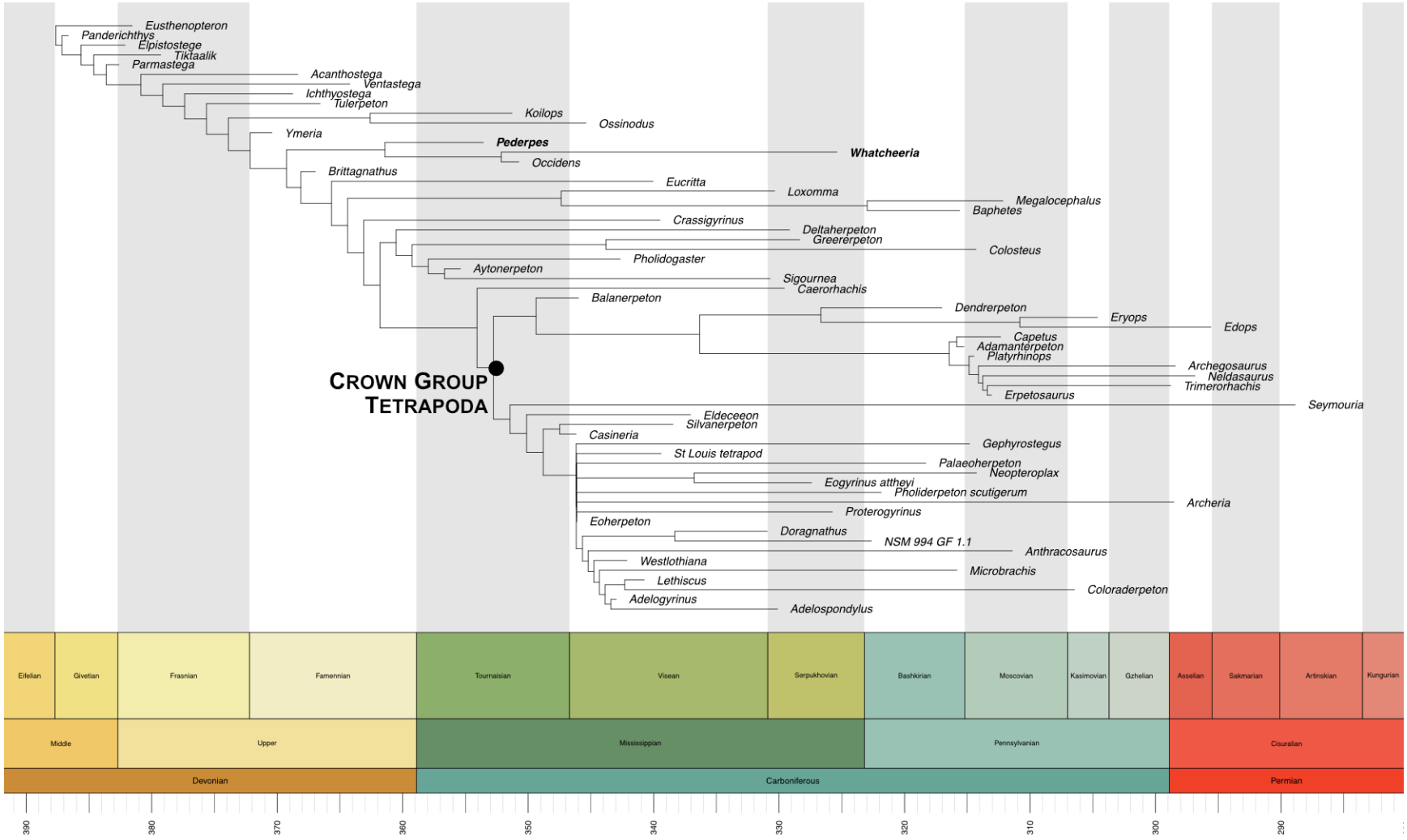

Figure 3.24. Timetree using topology from tree with best GER score (0.80).

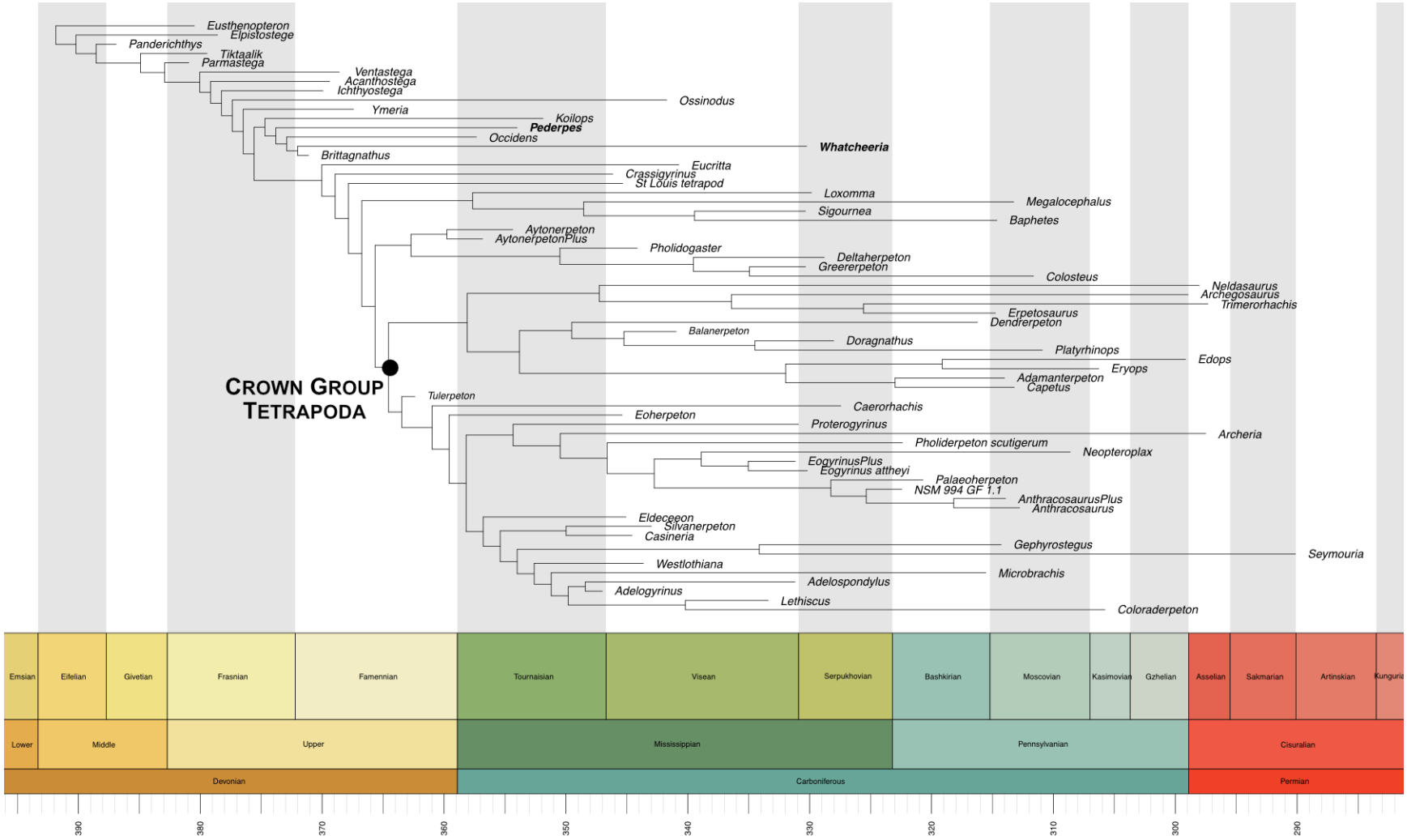

Figure 3.25. Timetree using topology from Bayesian MAP tree.

3.5.6 Selection of the primary hypothesis

The reweighted tree from the full search of the standard dataset (Figure 3.11) is selected as the primary hypothesis for this study. Its GER score (0.76) is only slightly lower than the highest GER (0.8) from the unweighted search, and its character consistency indices are higher. The topology also shares much in common with other that recovered by previous analyses (Ruta et al., 2003a; Ruta and Coates, 2007; Ruta, 2011; Clack et al., 2019b).

3.6 DISCUSSION

3.6.1 The Whatcheeriidae

The whatcheeriids are the most recently created early tetrapod family (Clack, 2002c; Clack and Milner, 2015) and the one with the best Romer's Gap fossil record. *Whatcheeria* and *Pederpes* consistently form a clade, Whatcheeriidae (Figure 3.11, 3.9A, 3.10B, 3.11B). This clade is consistently recovered crownward of Devonian tetrapods- except for *Brttagnathus*- and rootward of all other post-Devonian tetrapods. Most characters supporting this clade are homoplastic (APPENDIX B). However, two characters are unambiguous synapomorphies- femur as long as humerus (288) and manual phalanges as wide as long or wider. Several additional characters pertaining to the ribs, hindlimb, and pes size, while not unique to the whatcheeriids, are rare among the taxon sample and were highlighted for their utility previously (Otoo et al., 2021). The characters diagnosing the whatcheeriid clade reinforce the expanded, revised diagnosis of Otoo et al. (2021).

3.6.2 The tetrapod crown group

Under the primary hypothesis, the tetrapod crown group is diagnosed by seven homoplastic characters (see branch lists in APPENDIX B), all of which are either reversed above and/or convergent with states found in stem tetrapods. The most interesting of these is character 130, which refers to the morphology of the medial margin of the pterygoids. The state at the tetrapod crown node is reconstructed as "greatly concave mesially" (state four). This is due to the presence of such concavity in *Caerorhachis* at the base of the amniote total group and temnospondyls. The interpterygoid vacuities of *Caerorhachis* and *Edops* are distinct from those of (other) temnospondyls in that they intersect the orbit (character 126). The presence of character 130 in the tetrapod crown group diagnosis likely indicates that this character was homoplastic at this node, rather than that the crown tetrapod last common ancestor had large interpterygoid vacuities.

3.6.2.1 The lissamphibian total group

The temnospondyls are here taken as the lissamphibian total group as in other 'temnospondyl hypothesis' analyses (Maddin et al., 2012; Schoch, 2013, 2019; Pardo et al., 2017b, 2017a; Atkins et al., 2019). While the internal relationships of the temnospondyls vary across partitions and treatments used here, the frequency with which the temnospondyls are recovered as a clade suggests that this dataset does well in capturing them.

Part of the uncertainty about the crown group is the relationship between the colosteids and the temnospondyls. The colosteids vary between being the immediate outgroup to crown tetrapods (Figure 3.11, Figure 3.12) and the sister group to temnospondyls within the crown (Figure 3.16). Under the hypothesis of a colosteid + temnospondyl sister group relationship, both

Colosteidae and Temnospondyli would be subclades of total group Lissamphibia; Temnospondyli would be the clade which contains the lissamphibian crown group. For simplicity, the 'Temnospondyli = Lissamphibian' used elsewhere in this study will continue to be used here. Eleven characters support the colosteid + crown tetrapod relationship, but all these are homoplastic and without obvious pattern (APPENDIX B). That the colosteids are occasionally recovered as sister to the temnospondyls but not nested among the dvinosaurs suggests that there may be some support for a derived position for colosteids rather than just convergence. Although the humerus of *Greererpeton* (Godfrey, 1989) is more plesiomorphic than that of *Trimerorhachis* (Pawley, 2007) in lacking an elongate shaft, distinct deltoid and pectoral processes, well-defined latissimus dorsi process, and high level of torsion, their femoral morphologies are near-identical. They share a spike-shaped adductor blade (character 291), deep separated notch of finished bone between the proximal end and internal trochanter (character 282), and fourth trochanter morphology (character 286). These two taxa also share the same pattern of ontogenetic changes to the adductor blade, internal trochanter, and fourth trochanter. *Crassigyrinus* also shares these characters, but the pattern of ontogenetic changes in the femur are unknown in *Crassigyrinus*.

3.6.2.2 The amniote total group

The origin of the amniote total group among Paleozoic tetrapods is highly contentious (Pardo et al., 2017b, 2020; Marjanović and Laurin, 2019; Ruta et al., 2020). Most of this uncertainty centers on the anthracosaurs and 'lepospondyls'. Under the primary hypothesis, these two groups form the main divisions within the amniotes (Figure 3.11). The entire amniote total group is united by three homoplastic characters (APPENDIX B), and one character that is

uniform outside the clade: trunk pleurocentra fused midventrally (character 205, state 1). This represents the gastrocentrous vertebrae of *Caerorhachis* (Ruta et al., 2002). The presence of gastrocentrous vertebrae has been hypothesized as an amniote total group synapomorphy (Ruta et al., 2002) based on the phylogenetic position of *Caerorhachis* recovered here Figure 3.26. There have been historical hypotheses in which, within amniotes, the gastrocentrous condition gives rise to the embolomerous and lepospondylous conditions, possibly independently. While the use of vertebral characters is attractive- and the basis for many traditional tetrapod groups, some of which have survived into the age of modern cladistics- there are some indications that they may be more homoplastic, and thus less useful, than previous appreciated. The presence of embolomerous vertebrae in *Gephyrostegus* (Carroll, 1970; Smithson, 1985b), which primarily has gastrocentrous vertebrae, indicates that multiple vertebral morphologies can coexist within the same animal. The derived Permian temnospondyl *Doleserpeton* (Bolt, 1969; Sigurdsen and Bolt, 2010; Danto et al., 2016, 2017) is not included in this dataset but possesses gastrocentrous vertebrae, indicating at least one derivation of this condition outside amniotes. More concerningly, recent work is increasingly finding the 'lepospondyls' to be paraphyletic, and some may even be stem tetrapods (Pardo et al., 2017b; Clack et al., 2019b). The lepospondylous condition, then, may have been independently derived multiple times across early tetrapod phylogeny.

This is particularly problematic for understanding the relationships of the adelospondyls and aistopods. These 'lepospondyls' form a very robust clade throughout this study (Figure 3.10, Figure 3.11, Figure 3.19, Figure 3.20) that has also been recovered elsewhere (Clack et al., 2019b), suggesting a single origin for limblessness prior to the Visean. Whether this occurred in

the tetrapod stem group (Clack et al., 2019b) or amniote total group (Figure 3.11) is unclear. The placement of this adelospondyl/aistopod clade in the phylogeny and its robustness here may reflect the outsized influence of vertebral characters. These taxa have reduced (adelospondyls) or absent (aistopods) girdles and derived dermal skulls that make homology assessments difficult. Thus, most traditional sources of early tetrapod character data are eliminated, leaving the axial skeleton and (to a lesser extent) jaw. Endocranial data have been proposed as a source of more phylogenetically informative data (Pardo et al., 2017b, 2019a) but the effects of miniaturization and reduction of ossification, likely associated with aquatic habit, are difficult to isolate from genuine phylogenetic signal.

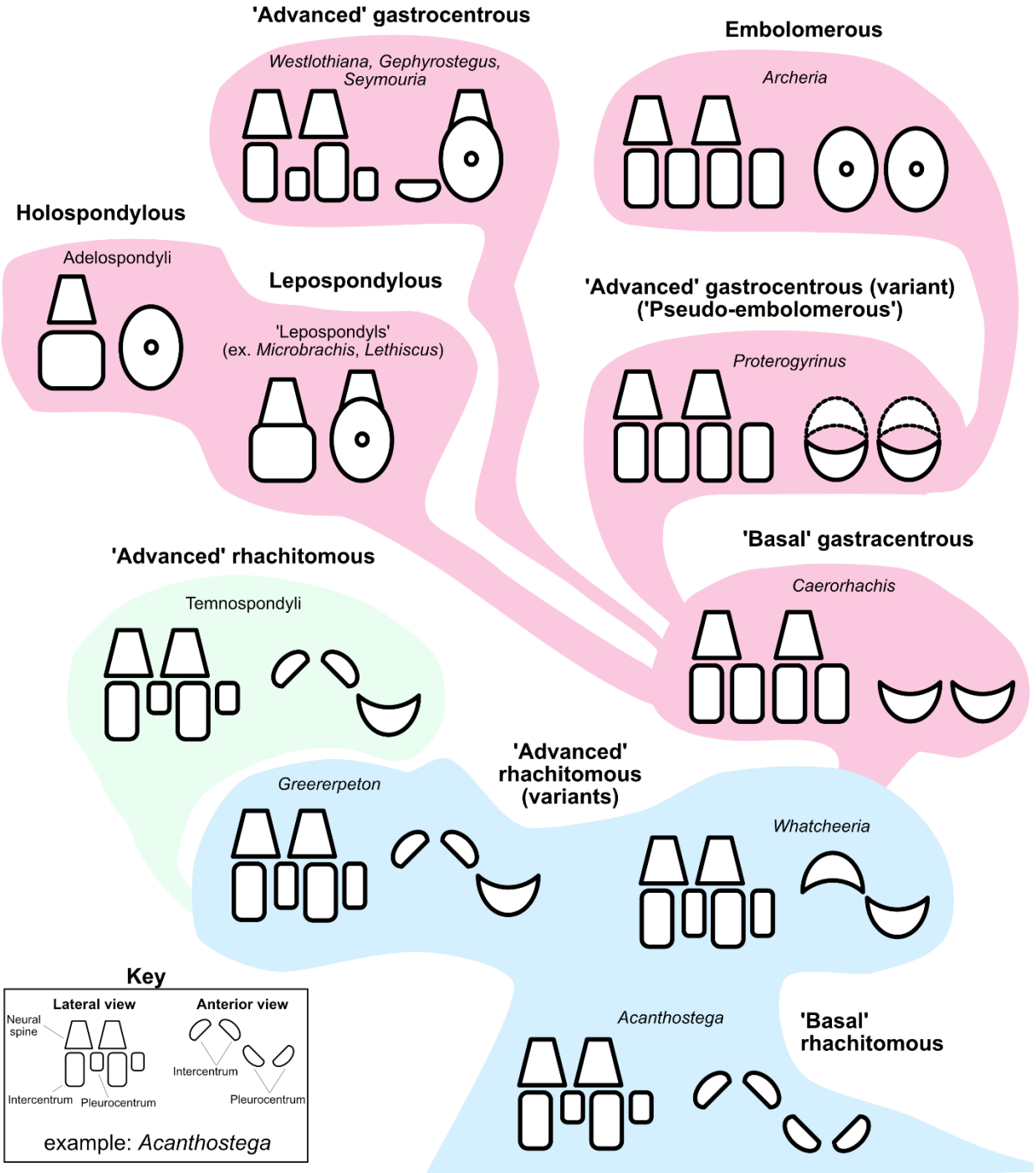

Figure 3.26. Schematic representation of vertebral morphologies across the dataset with representative taxa. Note diversity of consolidated vertebral morphologies within the amniote total group. Colors are as in the previous phylogenies (blue: stem tetrapods; green: total group lissamphibians; pink: total group amniotes). Bubbles represent clusters of vertebral morphologies with implied patterns of derivation; they do not represent clades.

A stem tetrapod position for embolomeres has been part of the 'lepospondyl hypothesis' and has recently been proposed within the context of a variant 'temnospondyl hypothesis' (Pardo et al., 2017b, 2019a). The presence of basal tuberosities (= basal tubera) on the underside of the braincase, possibly supporting bony gill supports, has been cited as a total group tetrapod apomorphy placing them within the stem group (Pardo et al., 2019, p.262):

> Notably, Clack & Holmes (1988) stated that normally rugose terminations of the basal tuberosities were 'ossified' in the embolomere *Archeria crassidisca*. A similar morphology is figured in specimen drawings of *Neopteroplax conemaughensis* (Romer 1963) and *Eogyrinus attheyi* (Panchen 1972). Of particular interest, *N. conemaughensis* in particular preserves an anomalous slender element behind the quadrate ramus of the pterygoid and in articulation with the basal tuberosity in a position essentially equivalent to how we predict the first infrapharyngobrachial might be oriented in *Oestocephalus* (Fig. 5f). Although this element was interpreted by Romer (1963) to be a fragment of the pterygoid ramus, he illustrates a conspicuous proximal facet as well as a postero- medial flange which, if this element is indeed an infrapharyngo- branchial or epibranchial, might serve as the origin for branchial constrictor musculature. If our interpretation here is correct, and if this morphology is more broadly distributed among embolomeres, this would add to growing morphological evidence [including supranueral caudal radials in at least one Pennsylvanian embolomere (Clack, 2011)] for an early divergence for embolomeres within the tetrapod stem-lineage.

Although this matrix does not contain a similar emphasis on endocranial data as that of Pardo et al. (2017), a presence/absence character (character 111) for basal tuberosities was added. Adams (2020) recovered embolomeres within the tetrapod stem group but found that taxon sampling has a stronger influence on tree topology than the presence of braincase characters.

3.6.3 Signal consistency across character partitions

The topologies of the unweighted strict consensus trees for the partition analyses indicate low signal in the partitions, a problem magnified by the reduced numbers of characters. However, the groups recovered, especially the temnospondyls and limbless tetrapods (aistopods+adelospondyls), are consistent. Reweighting creates much more resolved trees, many-

but not all- of which recover larger clades found in the reweighted tree from the full character search. The jaw character set is ostensibly the one with the greatest signal (Figure 3.13, Figure 3.16) but the arrangement of taxa is inconsistent relative to the full dataset search (Figure 3.11), expanded dataset search (Figure 3.12) or other partitions (Figure 3.16, Figure 3.17, Figure 3.18). *Eusthenopteron* and panderichthyids can be discriminated from *Parmastega* and limbed tetrapods, and the number of Meckelian openings (character 182) helps to distinguish between 'lower' tetrapods with three or more openings (ex. *Ichthyostega*, *Ymeria*, *Brittagnathus*, *Whatcheeria*) and 'higher' tetrapods with fewer openings (ex. typically two in embolomeres, one in colosteids). However, jaw characters have limited utility in recovering relationships more precisely than these coarse divisions. This has also been the case in other analyses of jaw characters (Ahlberg and Clack, 1998; Clack et al., 2012a; Chen et al., 2018). These results support previous hypotheses of long-term morphological and functional stasis in the jaw following the origin of limbs (Neenan et al., 2014). This pattern of change and stasis may be related to those in the postcranial skeleton, where changes in the anterior appendicular skeleton precede those in the posterior appendicular skeleton (see below).

That postcranial data perform similarly to cranial data signals their utility in large-scale studies of early tetrapod phylogeny. This follows previous work by Ruta (2011) and Ruta and Wills (2011) using a smaller taxon set that sampled the fish-tetrapod transition more broadly. In common with the results of Ruta and Wills' (2016) work, divergence in the anterior and posterior appendicular skeletons decreases overall signal in the appendicular character set. Coates et al. (2002) found a similar result in their work and commented thusly (p.390):

> In the lower part of the tetrapod stem, character state changes at the pectoral level dominate; comparable pelvic level data are limited. In more crownward taxa, pelvic level

changes dominate and repeatedly precede similar changes at pectoral level. Concerted change at both levels appears to be the exception rather than the rule.

This may be due to functional pressures, as has been hypothesized previously (Ruta and Wills, 2016) and implied by the reweighted trees from the partition searches. The anterior appendicular skeleton provides protection for the anterior viscera- early tetrapods have very large interclavicles compared to panderichthyids (Coates, 1996)- support above the substrate, and direction of movement (via moving the head, neck, and shoulders). The posterior appendicular skeleton provides stabilization and steering assistance (in swimming taxa) or propulsion (in walking taxa). The earlier appearance of anterior appendicular changes among panderichthyids and early-diverging stem tetrapods suggests that greater pressure was initially on the pectoral girdle and appendages for functional modification. Presumably it was only later that the pelvic limb and girdle were more extensively modified for support and propulsion. Significantly, we do not yet know if the anterior and posterior digit sets originated at the same time (or if digits originated multiple times in phylogeny).

The two clades in the anterior appendicular tree (Figure 3.18) reflect a divide between taxa with poorly ossified or reduced versus robust anterior appendicular skeletons. The poorly ossified/reduced category includes such taxa as *Pederpes*, *Ossindous*, *Crassigyrinus*, *Archegosaurus*, *Microbrachis*, and the adelospondyls. Interestingly, *Whatcheeria*, *Dendrerpeton*, and *Silvanerpeton* are placed at the base of the poorly ossified 'clade', implying a scenario in which low-ossification morphologies are derived from a prior robust/well ossified condition. The scapulocoracoids of *Pederpes*, *Archegosaurus*, *Microbrachis*, and *Crassigyrinus* are partly cartilaginous. The humeri of *Ossinodus*, *Crassigyrinus*, and *Archegosaurus* have small or absent muscle attachments, and the adelospondyls lack limbs entirely. There are repeated appearances

of a triangular entepicondyle (character 264, state three) in taxa for which aquatic habit can be inferred from lateral line canal patterns: *Crassigyrinus* (Tournaisian*/Visean-Serpukhovian), *Ossinodus* (Visean), *Baphetes* (Moscovian), *Microbrachis* (Moscovian), *Archegosaurus* (Asselian). This wide distribution suggests that it may indicate a common pattern of low humerus ossification, supported by its presence in the likely-immature *Eucritta*.

The 'robust' category contains a mix of aquatic and terrestrial taxa: *Tulerpeton* (Famennian, ?aquatic), *Balanerpeton* (Visean, terrestrial), *Westlothiana* (Visean, terrestrial), *Greererpeton* (Serpukhovian, aquatic), *Gephyrostegus* (Moscovian, terrestrial), *Eryops* (Kasimovian-Asselian, terrestrial), *Archeria* (Asselian, aquatic). All these taxa, terrestrial and aquatic, have well-developed humeral shafts and rectangular entepicondyles. The extent of ossification of the scapulocoracoid varies; the scapulocoracoid is fully ossified and has a posterior and ventral subglenoid extension in *Tulerpeton*, embolomeres, and *Eryops* (Romer, 1957; Holmes, 1984; Lebedev and Coates, 1995), but the coracoid is unossified in dvinosaurs.

Both categories span a range of body sizes (~10cm to >1m), taxon ages (middle Mississippian- early Permian), and likely functions. Notably, taxa that are found to be closely related in the all-character analyses are spread across the anterior appendicular tree.

In the reweighted posterior appendicular tree, one of the large clades contains taxa which, generally, have a femur with a rugose fourth trochanter, spike-like adductor blade, and notch of finished bone between the internal trochanter and proximal end of the femur (in the adult). Arrangement of muscle attachments likely reflects emphasis of hindlimb muscles related to paddling rather than walking (Panchen, 1985; Panchen and Smithson, 1990; Otoo et al., 2021). This condition is present in *Greererepton*, *Crassigyrinus*, *Trimerorhachis*, and *Caerorhachis*

(Panchen, 1985; Godfrey, 1989; Panchen and Smithson, 1990; Ruta et al., 2002; Pawley, 2007). The adductor blade in *Balanerpeton* is more blade-shaped (Milner and Sequeira, 1993), and the adductor blade, and adductor crest are both greatly enlarged in *Eryops* (Pawley and Warren, 2006) but the relative positions of the adductor blade, adductor crest, internal trochanter, and fourth trochanter appear consistent between them and *Greererpeton*/*Trimerorhachis*.

The underlying support for the other clade is unclear. It includes a mix of Devonian tetrapods, various anthracosaurs, the whatcheeriids, *Ossinodus*, *Eucritta*, and *Archegosaurus*. These can be broken into two sets of femoral morphologies: the embolomere + *Seymouria* set and the Devonian set. These are represented by monophyletic groups with a few exceptions, such as the *Ventastega*/*Eoherpeton* dyad. It is possible that this clade may reflect exclusion from the 'paddling' condition described above rather than any positive resemblance.

Taken together, the (reweighted) partition results suggest that early tetrapods were more mosaic than previously appreciated, and that mosaicism, rather than directional adaptation, was the rule for both stem group and crown group tetrapods. There is no indication that the tetrapod stem group represents increasing functional optimization for terrestriality as hypothesized by Dickseon et al. (2020) based on biomechanical study of humeri. While analyses of individual bones of the skeleton can produce apparent trends, considerations including the rest of the skeleton reveal that these trends are part of a larger pattern of mosaicism. Rather, after the origin of tetrapod limbs, different stem group lineages experimented with character combinations within the aquatic environment. There is no indication that there was convergence on a single character set that was further modified by terrestrial or aquatic tetrapods across both the lissamphibian and amniote lineages. This is supported by the widespread appearance of

appendicular traits in both the stem group and crown group, which is interpreted as rampant homoplasy by character tracing on phylogenetic trees (APPENDIX B).

3.6.4 A greater Devonian tetrapod radiation?

In a recent review, Ahlberg (2018) proposed a scenario of a middle Devonian origin for tetrapods. This is based on the interpretations of trackways from the Eifelian of Poland (Niedźwiedzki et al., 2010; Narkiewicz et al., 2015) and Givetian of Ireland (Stössel, 1995; Stössel et al., 2016) as having been made by tetrapods. Fragmentary fossils from the Givetian and Frasnian (Lebedev, 2004; Clément and Lebedev, 2014; Lebedev and Clément, 2019) are brought up in support, alongside trackways from the ?Frasnian of Scotland (Rogers, 1990; Marshall et al., 1996) and ?Famennian of Australia (Warren and Wakefield, 1972). In Ahlberg's (2018) scenario, tetrapods are plesiomorphically terrestrial, as represented by (the admittedly unusual) *Ichthyostega*. *Acanthostega* is aquatic but represents a return to water higher up phylogeny. Terrestriality, then, would extend to the origin of tetrapods (and possibly to panderichthyids).

This work implies a different evolutionary scenario. Under the hypotheses from the parsimony analyses, the tetrapod crown group is post-Devonian, either Tournaisian (soft) or Visean (hard) (Figure 1.23, Figure 1.24). These results require a Devonian origin for *Koilops*, *Ossinodus*, *Occidens*, Whatcheeriidae, *Sigournea*, *Eucritta*, and the clade containing all crownward tetrapods. The dating of the colosteids to the Tournaisian (*Aytonerpeton*) supports the hypothesis that derived stem group tetrapods- and possibly crown group tetrapods- were radiating by the Late Devonian. Rather than representing the bulk of the Devonian tetrapod

radiation, the Famennian taxa may be reinterpreted as a few early iterations of the tetrapod body plan among many. These may include early specialization (*Ichthyostega*), late occurrences of plesiomorphic conditions (*Acanthostega*), or early appearances of derived conditions (*Brittagnathus*, *Tulerpeton*) within a much more extensive Devonian radiation. While Ahlberg's scenario posits an inland origin for tetrapods in the middle Devonian with a Late Devonian transition to coastal environments following the extinction of the panderichthyids, it is possible that rather than representing a 'cradle' the inland setting of localities such as East Greenland and Red Hill represent a 'grave'. In a review, Gray proposed that since the Paleozoic, inland freshwater environments have been refugia for lineages excluded from nearshore and marine environments (Gray, 1988). This has been hypothesized for post-Devonian lungfish (Lloyd et al., 2012), and Modern restriction of low-diversity non-teleost actinopterygians to select freshwater environments (Wright et al., 2012; Rabosky et al., 2013; Near et al., 2014; Sallan, 2014) suggests a similar process of environmental exclusion. The coastal setting of the latest Devonian *Ventastega* and especially *Tulerpeton* may support the freshwater refugium hypothesis. This hypothesis would be further supported if *Acanthostega* and *Ichthyostega* coexisted with Devonian members of Mississippian lineages. Isotopic evidence of euryhalinity in East Greenland tetrapods (Goedert et al., 2018) is also compatible with the freshwater refugium hypotheses, but does not directly support it.

However, even if Mississippian stem tetrapod lineages are projected back into the Devonian, there is no evidence to support a Devonian origin for tetrapod terrestrialization. Lateral line patterns indicate that baphetids, colosteids, dvinosaurs, and embolomeres were aquatic predators (APPENDIX B). Sustained terrestrial locomotion may still have been a post-

Devonian innovation, resulting from independent origins within the crown group. Under this scenario, the end-Devonian mass extinction may not have created as much of a lineage bottleneck in early tetrapods as previously hypothesized (Sallan and Coates, 2010). What is still uncertain is the extent to which Mississippian stem tetrapod diversity reflects pre- or post-extinction divergences.

3.6.5 Future directions

There is the potential for further analyses of character partitions to produce new knowledge about the relationships and paleobiology of early tetrapods. Different evolutionary rates across anatomical partitions across clades- heterotachy- are implied here and elsewhere (Coates et al., 2002). Simões and Pierce (2021) found different elevated rates of evolution in the crania and postcrania of panderichthyids (elpistostegalians) and Devonian tetrapods using Bayesian inference (Simões and Pierce, 2021). Their dataset focused on broad sampling of dipnomorphs and tetrapodomorphs and included only the Famennian tetrapods *Parmastega*, *Ventastega*, *Acanthostega*, *Tulerpeton*, and *Ichthyostega*. It would be interesting to know if Bayesian methods found similar elevated rates in other anatomical partitions in a more tetrapod-focused dataset. Alternative methods were applied by Lloyd et al. (2012) to a lungfish phylogeny to identify heterogeneity in rates of character evolution. The authors applied a combination of branch randomization (to identify branches with high rates of change) and two likelihood ratio tests- one to determine whether specific branches have rates that are significantly higher or lower than the rest of the dataset and one to determine whether there are clades that have significantly higher or lower rates- to a tree of pre- and post-Devonian fossil lungfish. They found widespread rate heterogeneity but concentrated low rates among post-Devonian lineages. Such rate analyses

would tell us whether evolution across the early tetrapod skeleton varies not only in pattern but also in rate and between clades.

Apart from the 'lepospondyls'- the subject of much current and future active revision- the membership of most other early tetrapod clades is stable across analyses (if the question of lissamphibian origins is momentarily disregarded). The anthracosaurs have historically been considered stem amniotes (Romer, 1966; Carroll, 1970; Holmes, 1984; Smithson, 1985b; Ruta et al., 2003a), but this has been challenged recently (Pardo et al., 2017b; Pardo and Mann, 2018; Adams, 2020). Part of the problem in placing anthracosaurs within early tetrapod phylogeny is the wide morphological gulf between the small, terrestrial 'anthracosauroids' *Eldeceeon* and *Silvanerpeton* and the large, aquatic (*Eoherpeton* and *Anthracosaurus* being possible (partial) exceptions) embolomeres. It is possible that Anthracosauria- *Eldeceeon*/*Silvanerpeton* + Embolomeri- is polyphyletic. This phylogenetic uncertainty is compounded by lack of consensus on embolomere internal relationships (Holmes and Carroll, 2010; Adams, 2020; Ruta et al., 2020). Anthracosaurs benefit from an extensive fossil record and numerous published descriptions (Romer, 1957, 1963; Panchen, 1964, 1966, 1972, 1977, 1981; Boyd, 1980; Holmes, 1984, 1989b; Klembara, 1985; Clack, 1987b, 1987a; Clack and Holmes, 1988; Ruta and Clack, 2006; Holmes and Baird, 2011; Greb et al., 2016; Adams, 2020; Adams et al., 2020; Chen and Liu, 2020; Clack and Smithson, 2020; Ruta et al., 2020). However, much of this work was done decades ago, prior to the 21st century shift in phylogenetic hypotheses driven by cladistics. It would be worthwhile to revisit specimens with modern methods- CT would be particularly helpful- and construct a character set able to clarify anthracosaur interrelationships and the place of the group within early tetrapod phylogeny generally. This would help to clarify character states near the base of total-group Amniota and more conclusively determine whether *Tulerpeton*

belongs within the clade (thus hard-dating the origin of the tetrapod crown group to the Devonian).

There is also the issue of fragmentary fossils. These include some of the oldest tetrapod fossils (Ahlberg, 1995; Lebedev, 2004; Broussard et al., 2018), most of the Devonian tetrapod record (Zhu et al., 2002; Daeschler et al., 2009; Clack et al., 2012a; Clément and Lebedev, 2014; Clack and Milner, 2015; Olive et al., 2016; Gess and Ahlberg, 2018; Ahlberg and Clack, 2020), and almost all tetrapods from Romer's Gap (Anderson et al., 2015; Clack et al., 2016, 2018, 2019a; Chen et al., 2018; Otoo et al., 2018; Smithson and Clack, 2018; Lennie et al., 2021). These fragmentary fossils are in some cases our only records for geographic areas or calibration points for time intervals. While some, such as *Ymeria*, may represent forms similar to well-known taxa such as *Ichthostega*, others, such as *Brittagnathus*, suggest that there is Devonian diversity that remains unexplored. Fragmentary fossils from Romer's Gap have been used to hypothesize post-Devonian survival for 'tulerpetontids' and Tournaisian (or older) origins for whatcheeriids, colosteids, and embolomeres (Anderson et al., 2015). Work is underway (Otoo et al., in prep.) on a phylogenetic analysis of these fragmentary fossils using a purpose-built dataset with the added context of trackway data. This analysis has the potential to synthesize parts of the early tetrapod dataset that are often considered separately and in conflict.

Hypotheses of node ages depend on accurate ages for localities and, therefore, OTUs. Currently, the bulk of the Mississippian tetrapod record- as well as Misssissippian vertebrates generally- consists of specimens from a set of geographically clustered localities in the Scottish Midland Valley. While the chronostratigraphic order of these localities is understood, their

absolute ages are uncertain. This is problematic for dating the tetrapod crown group node, as all the current candidates for earliest crown tetrapod- *Lethiscus* (Wardie), *Balanerpeton*/*Westlothiana* (East Kirkton)- come from this stratigraphic package. Conodont data and ongoing stratigraphic work (Currie, 1954; Wilson, 1989; Marshall et al., 1996; Monaghan et al., 2014; Hill et al., 2018) has constrained the age of Wardie to 333.5-335.5 Ma. This moves the base of the Scottish Midland Valley succession into the late Visean. This would decrease current tetrapod crown group age estimates by a minimum of approximately four to nine million years. Loanhead, which is high in the succession, has previously been dated to the Pendleian regional stage, which corresponds to the earliest Serpukhovian (Aretz et al., 2020). If this age is maintained, the Scottish Midland Valley succession would represent only a few million years of the late Visean and early Serpukhovian. Further work is needed to establish the absolute chronostratigraphy of the Scottish Midland Valley succession.

The 'compression'of these Scottish localities toward the end of the Visean 're-opens' Romer's Gap and emphasizes that data trough that most of the Mississippian represents. This change in locality age estimate does, however, align the succession with Delta and the Buffalo Wallow Formation tetrapod beds, which are most likely earliest Serpukhovian in age. Other similarly aged localities include the Point Edward (middle Serpukhovian), Goreville (mid-late Serpukhovian), and Greer (mid-late Serpukhovian) localities. Wardie and East Kirkton, then, would be more firmly embedded within a broader late Visean-early Serpukhovian burst of tetrapod diversity (preserved) in Euramerica. The recent discovery of a late Visean dvinosaur from Germany (Werneburg et al., 2019) fits with this scenario, especially when dvinosaurs are recovered at the base of Temnospondyli (Pardo et al., 2017a). The apparent lack of tetrapod

fossils between the late/terminal Tournaisian and late Visean in Euramerica remains a mystery, particularly in Scotland.

Methodologically, there are questions of how early tetrapod datasets should be constructed to address various phylogenetic issues (Pardo et al., 2020). Explicit tests of crown tetrapod relationships require the inclusion of unambiguous crown tetrapods, usually from the late Pennsylvanian or early Permian. Comprehensive hypotheses of early tetrapod relationships require broad taxonomic sampling. In both cases, the fit of the character set to the taxon set decreases as the taxon set becomes larger. There is then a tension between dataset size (characters and taxon breadth) and the ability of the dataset to resolve relationships. Large datasets are necessary for understanding broad patterns but are less equipped to deal with the internal relationships of clades. For example, this dataset performs well in capturing the temnospondyls as a clade, but the internal relationships of the group do not fit with hypotheses of temnospondyl interrelationships generated by more focused analyses (Ruta et al., 2007; Schoch, 2013; Pardo et al., 2017a; Atkins et al., 2019). In particular, the *Edops*/*Eryops* dyad, which is also present in previous (2016, 2019) analyses by Clack et al., suggests that these internal relationships may be at least somewhat spurious. This does not mean that the results of this and similar large-scale work should be disregarded, but limitations should be recognized.

3.7 CONCLUSIONS

Creation of new characters and combination of characters from multiple ‘lineages’ of datasets may permit a more independent test of phylogenetic relationships. New postcranial data on *Whatcheeria* provides an opportunity to reassess early tetrapod relationships. The

whatcheeriids (*Whatcheeria* + *Pederpes*) are early-diverging stem tetrapods. Embolomeres and limbless tetrapods (aistopod and adelospondyl 'lepospondyls') are both placed within the amniote total group. Analysis of anatomical partitions of characters finds that postcranial characters perform similarly to cranial data but produce different tree topologies. The colosteids have an ambiguous relationship with the tetrapod crown group, alternating between apical stem tetrapods when all characters are analyzed and total group lissamphibians when only cranial characters are analyzed. Ostensible lack of signal in appendicular data is the result of divergence in patterns of character change between the anterior and posterior appendicular skeletons. Character distributions strongly suggest that appendicular traits historically associated with terrestriality are not limited to terrestrial taxa, and terrestrialization occurred independently in the lissamphibian and amniote total groups. Support is found for a Devonian origin of the whatcheeriids and baphetids. The inclusion of the Tournaisian tetrapod *Aytonerpeton* within Colosteidae suggests that derived stem group tetrapods and early crown group tetrapods may also have been diversifying before the end-Devonian mass extinction. This more extensive Devonian tetrapod radiation very likely did not contain terrestrial forms. Examination of anatomical partitions supports the hypothesis that mosaicism across the early tetrapod skeleton dominated across the stem group and into the crown group throughout the Devonian and Carboniferous.

CHAPTER 4: ECOLOGICAL PERSISTENCE IN VERTEBRATE COMMUNITIES THROUGH THE END-DEVONIAN MASS EXTINCTION

4.1 ABSTRACT

The end-Devonian mass extinction (EDME) significantly impacted vertebrates, removing major groups like placoderms and creating a bottleneck in the evolution of surviving clades. However, the structures of Devonian-Carboniferous ecosystems are not well understood. It is not known if the faunal change through the extinction was accompanied by a change in the identity and richness of functional groups (=guilds), or whether the immediate post-extinction ecosystems show the same instability found after faunal disruption (Richmondian Invasion, Late Oridovician, Campanian-Maastrichtian transition, Late Cretaceous) and mass extinction (end-Permian mass extinction). Quantitative modeling of taxonomic diversity and guild richness reaffirm the sharp taxonomic distinction between pre- and post-EDME ecosystems, but do not find this accompanied by major changes at the guild level. Modeled responses of ecological paleocommunities to perturbation using the Cascading Extinctions on Graphs (CEG) model find an unusual pattern of extinction response, characterized by an abrupt transition from low- to high-secondary extinction regimes. Unexpectedly, variance in secondary extinction is generally low in each regime. This perturbation response can be explained by a combination of broad prey profiles among consumers, low guild richness, and high guild evenness. Post-EDME paleocommunities do not exhibit greater instability than Famennian paleocommunities. Terrestrial paleocommunities before (Gilboa, Givetian) and after (East Kirkton, Visean) the EDME differ starkly from the above pattern. They exhibit uniquely high secondary extinction values and variance for all levels of perturbation. This indicates that while terrestrial

paleocommunities represented a novel form of ecosystem organization, they were highly unstable and marginal to the richer aquatic paleocommunities they existed alongside. It appears that it was only in the Pennsylvanian, likely supported by insect and, later, tetrapod, herbivores, that terrestrial vertebrate paleocommunities began the extended process of separating themselves from the aquatic realm.

4.2 INTRODUCTION

In 1981, JJ Sepkoski described three 'evolutionary faunas' of marine invertebrates: the Cambrian, Paleozoic, and Modern, which successively replace each other (Sepkoski, 1981). Each fauna is more species-rich and ecologically complex than its predecessor(s). In particular, the Modern fauna is distinguished by an increase in durophagy and corresponding anti-predator defenses referred to as the Mesozoic Marine Revolution (Vermeij, 1977; Stanley, 2008; Cueille et al., 2020). Similar results were found by Bambach et al. in their ecocube study (Bambach, 1993; Bambach et al., 2007). They created a theoretical morphospace based on possible combinations of tiering (relationship to sediment/water interface), motility (movement), and feeding conditions. They then classified marine invertebrates from the Ediacaran, Cambrian, Late Ordovician, and Recent into life modes defined by the resulting 'ecospace cube'. They found large increases in ecospace occupation across their study interval. This implies increasing diversity of autecologies and, presumably, varieties of ecological paleocommunities over the Phanerozoic. However, the opposite (Dunne et al., 2008) has been found by direct species-species food webs from the Cambrian and present day modeled by Dunne et al. (2008). Their study found that food web structure across their dataset was largely similar. Studies of benthic invertebrate paleocommunities have found persistence in functional diversity despite faunal

turnover caused by sustained environmental disruption (Strotz and Lieberman, 2020) and biotic crises, up to and including mass extinctions (Erwin et al., 1987; Droser et al., 2000; McGhee et al., 2004, 2012, 2013; Dineen et al., 2014; Foster and Twitchett, 2014; Dunhill et al., 2018; Edie et al., 2018; Song et al., 2018). This suggests that major changes in organismal function may facilitate changes in paleocommunity structure on macroevolutionary timescales.

One such event is the 'invasion of the land', i.e. the origin and proliferation of terrestrial organisms and ecosystems. Terrestrial plants are known from the Ordovician (Salamon et al., 2018; Servais et al., 2019; Bowles et al., 2020; Dahl and Arens, 2020; Gensel et al., 2020), and by the Early Devonian (Pragian, ~410 million years ago) there is evidence for complex diverse terrestrial paleocommunities of plants, fungi, and arthropods (Trewin, 1992; Garwood et al., 2020). Structurally modern forests- multiple heights and morphologies of tree-habit plants- appear soon after in the Givetian; terrestrial arthropod diversity continues to increase (Shear et al., 1984, 1987; Norton et al., 1988, 1988; Shear and Bonamo, 1988; Stein et al., 2012). The Mississippian sees substantial increases in terrestrial arthropod body size, with 1m-long scorpions and multi-meter myriapods becoming numerous for the first time (Rolfe, 1980; Jeram, 1993). Once tetrapods became an established on land during the Mississippian (Clarkson et al., 1993), the fundamental composition of terrestrial ecosystems was set for the following 340 million years.

In the mid-20th century, EC Olson published a series of papers on the origin of terrestrial vertebrate ecosystems (Olson, 1952, 1966, 1975, 1977). Under Olson's model, the earliest terrestrial vertebrate paleocommunity structure was typified by the pelycosaur-temnospondyl-

‘lepospondyl’ ‘Type I’ lowland assemblages of the early Permian redbeds. These paleocommunities had few or no herbivorous tetrapods; aquatic animals and terrestrial insects formed the prey base for the community. As the Permian progressed, the fully terrestrial Type III and Type II arose. Both had terrestrial herbivores- invertebrates in the former, vertebrates in the latter- as the base of the paleocommunities. These were populated by more derived amniotes such as therapsids and arose in upland or dryland environments. Type III and Type II paleocommunities then invaded lowland environments and engaged in competition, such that Type II paleocommunities were the dominant type by the Triassic (Olson, 1966). Under Olson’s model, the key event in the origin of terrestrial tetrapod ecosystems was the origin and diversification of herbivorous tetrapods; the origin of terrestrial tetrapods at large did not meaningfully change paleocommunity structure relative to the more fully aquatic paleocommunities of the preceding Pennsylvanian. Olson’s earliest Permian Type I paleocommunities were representative of whatever earlier terrestrial vertebrate paleocommunities existed in being reliant on aquatic, rather than terrestrial, resources. Olson’s hypotheses have influenced similar work by others, such as Bakker’s megadynasty hypothesis (Bakker, 1986), up to the present time (Pardo et al., 2019b).

Our knowledge of early tetrapod evolution has improved tremendously over the last 30 years (Coates et al., 2008; Clack, 2012; Pardo et al., 2020). While previous hypothesis had assumed that tetrapods had been terrestrial from their origin in the Late Devonian (Briggs and Crowther, 1990; Brenchley and Harper, 1998), we now know that Devonian tetrapods were obligately aquatic (Coates and Clack, 1995), and that walking may have preceded limbs altogether (King et al., 2011). Ecological modeling of middle Devonian estuarine

paleocommunities has found them to have similar predator-prey size relationships to their modern counterparts (Chevrinais et al., 2017). While only three Devonian tetrapods are known in substantial anatomical detail (Lebedev and Coates, 1995; Coates, 1996; Jarvik, 1996), significant lineage diversity is implied by specimens published (Zhu and Ahlberg, 2004; Olive et al., 2016; Gess and Ahlberg, 2018; Beznosov et al., 2019; Ahlberg and Clack, 2020) and under description (Byrne et al., 2022). Multiple Mississippian tetrapod faunas have been described (Smithson, 1985a; Bolt et al., 1988; Schultze and Bolt, 1996; Smithson et al., 2012; Clack et al., 2016, 2019a; Greb et al., 2016; Otoo et al., 2018), including the earliest terrestrial tetrapods at East Kirkton (Clarkson et al., 1993).

This creates a gap of approximately 30 million years between the origin of tetrapods and the origin of terrestrial tetrapods, an interval which is punctuated by the end-Devonian mass extinction (EDME) (Sallan and Coates, 2010). The EDME (Hangenberg event) has recently been recognized as a major vertebrate mass extinction (Becker et al., 2016; Kaiser et al., 2016) distinct from the Frasnian-Famennian invertebrate extinction (Kellwasser event, 'Late Devonian mass extinction' in older parlance (Raup and Sepkoski, 1982)). The Mississippian origin of terrestrial tetrapods may then have been part of a broader extinction recovery that entailed ecological reorganization. However, the driver of tetrapod terrestrialization remains unclear. Historically, feeding on terrestrial arthropods has been hypothesized as motivation for tetrapod transition onto land, dated to the Pennsylvanian (Romer, 1966). However, this hypothesis was built on the assumption that tetrapods were initially terrestrial (and that Mississippian terrestrial arthropod diversity was low). The East Kirkton tetrapods are preserved alongside a diverse arthropod fauna, but it is unclear to what extent this terrestrial tetrapod-arthropod association was novel by

East Kirkton time, and what its taxonomic and structural precursors may have been earlier in the Mississippian. New data from the Tournaisian-aged Ballagan Formation (Smithson et al., 2012; Clack et al., 2016, 2019a; Chen et al., 2018; Ross et al., 2018; Smithson and Clack, 2018) provide an opportunity to investigate this process.

Substantial food web modeling has been done on terrestrial paleocommunities and biogeography in the Permian-Triassic mass extinction (PTME) interval in southern Africa (Roopnarine et al., 2007, 2018, 2019; Sidor et al., 2013; Roopnarine and Angielczyk, 2015, 2016). These studies have found geologically rapid changes in food web structure and resistance to perturbation: paleocommunities from within the extinction interval and immediate aftermath are much more vulnerable to collapse and much more unpredictable in their response. The earliest Triassic paleocommunities from the *Lystrosaurus* Assemblage Zone (LAZ) are also notable for their unusual composition (Roopnarine et al., 2007, 2018). They lack the terrestrial herbivore and carnivores diversity of the pre-extinction Permian paleocommunities. Instead, temnospondyls are dominant, insects are the primary herbivores, and vertebrate consumers are overwhelmingly insectivores (Roopnarine and Angielczyk, 2012). This may represent a recapitulation of an older paleocommunity form similar to Olson's Type I and possibly representative of the earliest terrestrial tetrapod paleocommunities: 'amphibian'-dominated, no tetrapod herbivores, insects significant as both herbivores and prey for vertebrates. If this is the case, increasing paleocommunity stability over time could explain why Type I paleocommunities were replaced.

Does the EDME show the same structural and performance changes seen in the PTME? Are Mississippian faunas generally a functional recapitulation of their Devonian counterparts, or does the faunal turnover at the EDME correspond to a change in ecosystem structure and performance? Is the invasion of land by tetrapods a transformative event for the structure and composition of nonmarine food webs (possibly recapitulated by the Early Triassic disaster fauna), or are these ecosystems still fundamentally aquatic in their structure?

The aims of this study are to investigate these questions as follows:

- Compare the taxonomic and guild composition of food webs across different environmental settings to determine whether taxonomic change corresponds to change in the richness and identity of guilds (=functional groups)
- Model these food webs with CEG to determine whether pre-EDME paleocommunities have greater resistance to perturbation relative to post-EDME paleocommunities and whether these responses vary across environmental setting, particularly if terrestrial paleocommunities differ from aquatic ones

4.3 MATERIALS

4.3.1 Dataset

This paleocommunity dataset was assembled *de novo* for this study. Taxonomic, geographic and stratigraphic occurrence, paleoenvironmental data, and autecological inferences were drawn from the literature and augmented with personal observations of specimens. Organisms were identified to the species level as much as possible. Paleocommunity information and references are presented in APPENDIX C.

Paleopaleocommunities were sampled from the Givetian (late Middle Devonian) through the Serpukhovian (final stage of the Mississippian), across reef, open marine, and continental (=freshwater) environments (Table 4.1). This environmental range was included to detect

possible differences in ecosystem structure and performance across environment. Moreover, Carboniferous continental ecosystems are part of a broader trend of vertebrate movement into estuarine and continental environments beginning in the Devonian (Carpenter et al., 2014; Otoo et al., 2018; Gess and Whitfield, 2020). Geographically (Scotese, 2021), most localities are from Euramerica, and would have been at low paleolatitudes (Figure 4.1, Figure 4.2). This reflects limitations of the fossil record during this interval, which have been longstanding issues (Milner et al., 1986; Pardo et al., 2020).

Table 4.1. Basic information for paleocommunities modeled in this study.

Locality	**Period**	**Stage**	**Environment**	**Geographic locaiton**
Aztec	Devonian	Givetian	Continental	Victoria's Land, Antarctica
Gilboa	Devonian	Givetian	Terrestrial	New York, USA
Gladbach	Devonian	Frasnian	Marine	Germany
Kerman	Devonian	Frasnian	Marine	Kerman, Iran
Gogo	Devonian	Frasnian	Reef	Gogo, Australia
Miguasha	Devonian	Frasnian	Estuarine	Quebec, Canada
Red hill	Devonian	Famennian	Continental	Pennsylvania, USA
Cleveland Shale	Devonian	Famennian	Marine	Ohio, USA
Evieux Formation	Devonian	Famennian	Continental	Namur-Dinant Basin, Belgium
Waterloo Farm	Devonian	Famennian	Estuarine	Eastern Cape, South Africa
Upper Ballagan Formation	Carboniferous	Tournaisian	Continental	Scotland, UK
East Kirkton	Carboniferous	Visean	Terrestrial	Scotland, UK
Glencartholm	Carboniferous	Visean	Marine	Scotland, UK
Bearsden	Carboniferous	Serpukhovian	Marine	Scotland, UK
Bear Gulch	Carboniferous	Serpukhovian	Reef	Montana, USA
Loanhead	Carboniferous	Serpukhovian	Continental	Scotland, UK

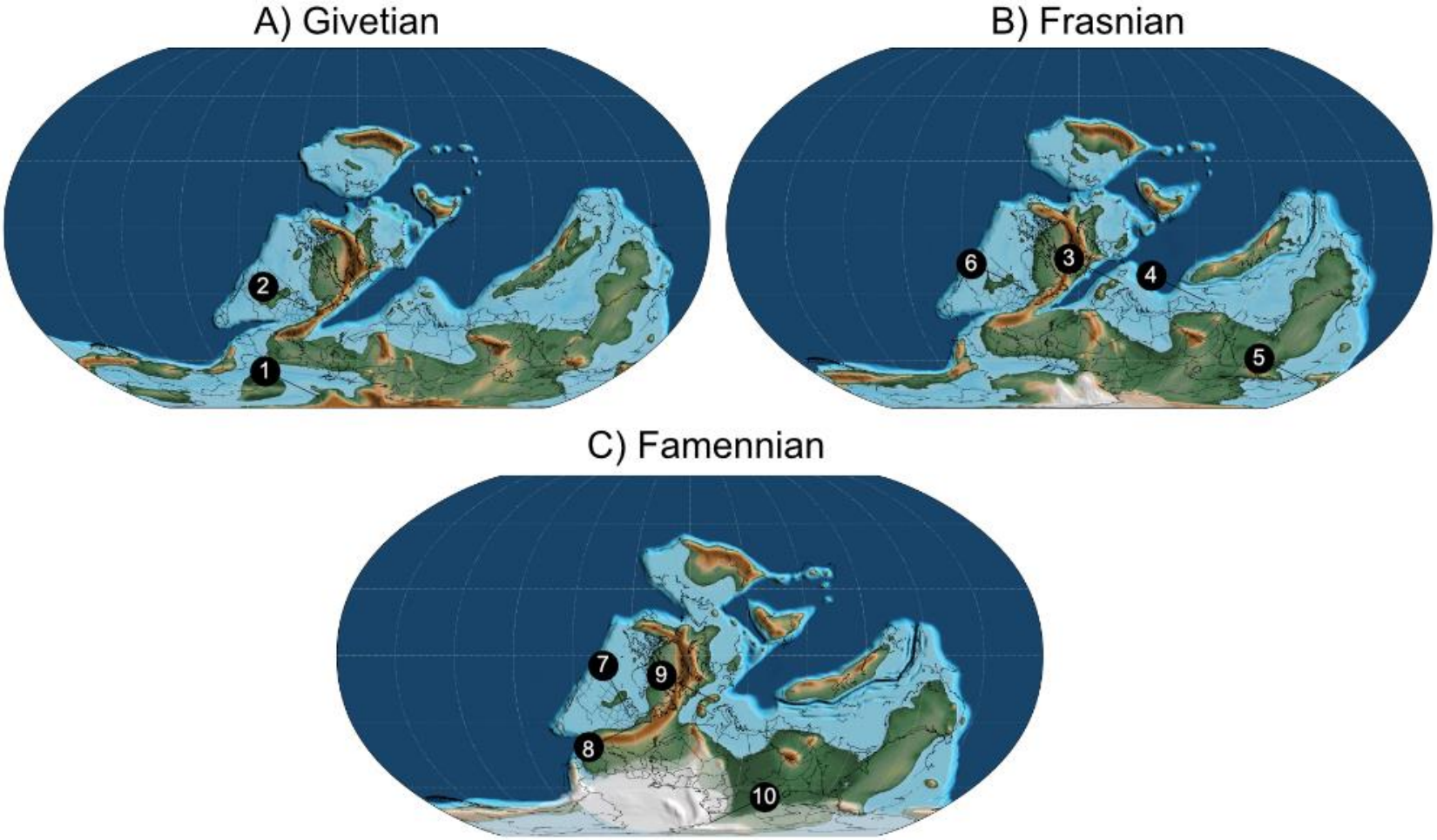

Figure 4.1. Paleomaps showing Devonian localities. 1: Aztec; 2: Gilboa; 3: Gladbach; 4: Kerman; 5: Gogo; 6: Miguasha; 7: Cleveland Shale; 8: Red Hill; 9: Evieux Formation; 10: Waterloo Farm. Paleomaps by Scotese (Scotese, 2021).

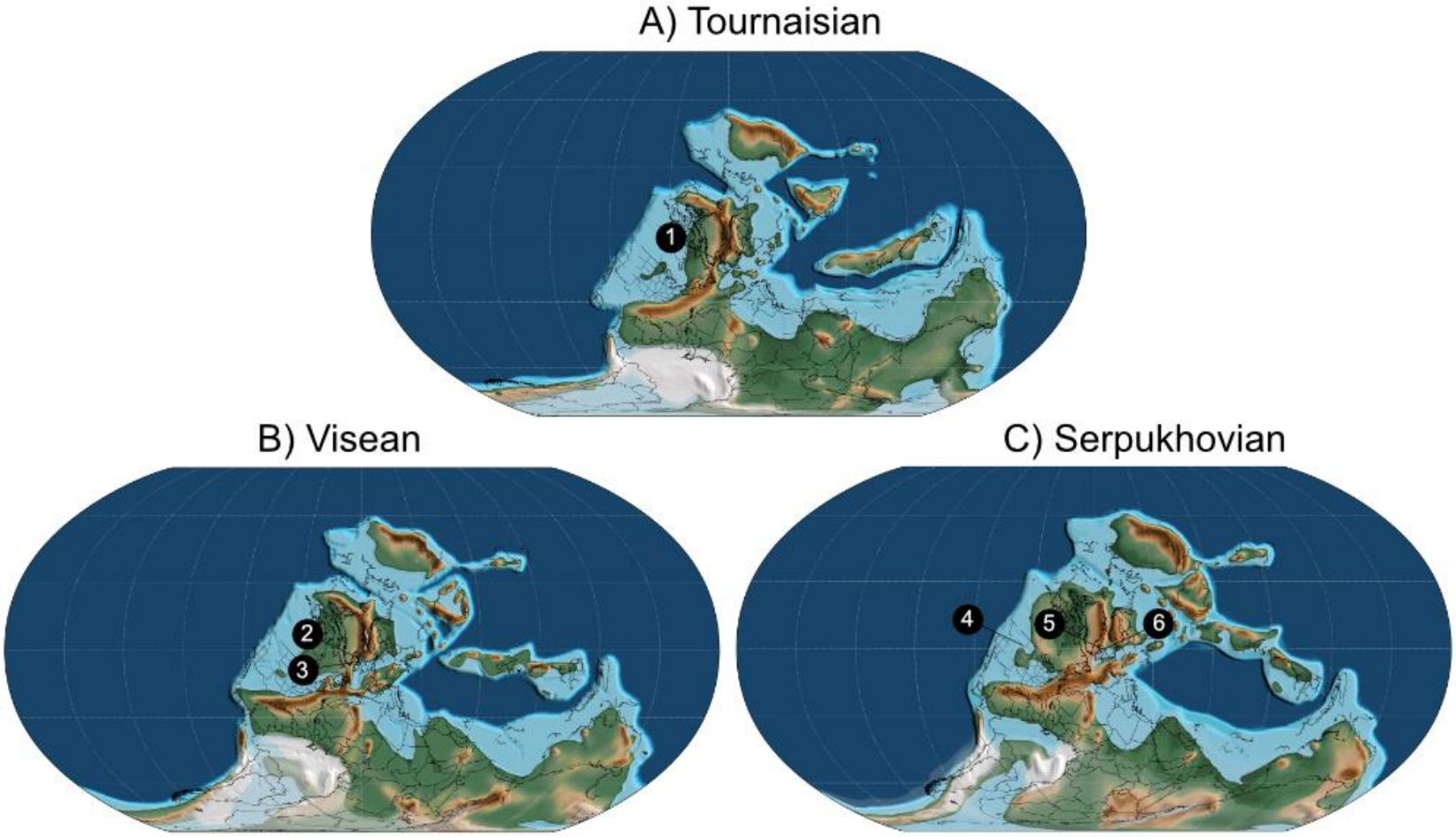

Figure 4.2. Paleomaps of Mississippian localities. 1: Upper Ballagan Formation; 2: East Kirkton; 3: Glencartholm; 4: Bear Gulch; 5: Bearsden; 6: Loanhead. Paleomaps by Scotese (Scotese, 2021).

Givetian and Frasnian paleocommunities were sampled for comparison with Famennian paleocommunities. Other food web studies (Mitchell et al., 2012; Roopnarine and Angielczyk, 2015) have found that food web reorganization can promote species loss during mass extinctions. The Kellwasser Event, also known as the Frasnian-Famennian mass extinction (FFME) or Late Devonian mass extinction (LDME), was a major invertebrate extinction (Buggisch, 1991; Gereke and Schindler, 2012) that included the loss of the massive Devonian coral reef systems and the beginning of a ~40 million year 'coral gap' extending into the Pennsylvanian (Kuznetsov and Zhuravleva, 2018; Jakubowicz et al., 2019; Yao et al., 2020). The effect of this extinction on vertebrates is thought to be minor (Sallan and Coates, 2010). However, ecosystem reorganization increasing vulnerability to perturbation is seen at regional scales in the Late Ordovician Richmondian Invasion (Kempf et al., 2020) and Late Cretaceous Campanian-Maastrichtian transition in western North America (Mitchell et al., 2012). It is possible that while not a mass extinction for vertebrates, the FFME disrupted vertebrate paleocommunities globally such that they were more susceptible collapse ahead of the EDME.

The sampled paleocommunities represent different amounts of temporal averaging- thousands of years across centimeters of stratigraphy (Clarkson et al., 1993) to millions of years across meters (Clarkson, 1985; Clack et al., 2016). Many- ex. East Kirkton, Bear Gulch- represent hundreds or perhaps thousands of years within single lakes (East Kirkton) or restricted bays (Bear Gulch) (Clarkson et al., 1993; Lund et al., 2012, 2015). Others- Cleveland Shale, Gogo- encompass up to a few million years across hundreds of square kilometers (Trinajstic et al., 2022). The Ballagan Formation here refers to a composite of multiple fossiliferous horizons, each likely representing at most thousands of years (Clarkson, 1985; Clack and Finney, 2005;

Bennett et al., 2016; Clack et al., 2016, 2018; Otoo et al., 2018; Ross et al., 2018). Altogether they represent approximately two million years across 40m of vertical section. This composition was done to ensure that diversity was sufficient to allow a Tournaisian locality to be used. Effort was made to sample assemblages with well-studied faunal compositions and a minimum of 15 species to avoid possible artifacts in the CEG model. The Gilboa fauna falls below this 15 species threshold, but was included as it represents a well-studied terrestrial Devonian ecosystem (Shear et al., 1984, 1987; Norton et al., 1988; Shear and Bonamo, 1988; Stein et al., 2012).

Spatial averaging also varies. Most of the Scottish paleocommunities represent single or clustered quarries of over tens of square meters (Schram, 1983; Coates, 1988; Clark, 1989, 1990, 2013; Rolfe et al., 1993; Smith et al., 1994; Wood, 2018). The Ballagan Formation is compiled from four primary localities clustered near the southeast border of Scotland- Willie's Hole, Burnmouth, and Foulden- the greatest distance between which is ~23km. The singleton occurrence of *Pederpes* from Dunbarton is much farther away (~200km) but included because of evidence of a very similar tetrapod at Burnmouth (Smithson et al., 2012; Otoo et al., 2018). Other paleocommunities are based on collections across a much broader area. Gogo fossils are distributed across ~200 square kilometers (Long and Trinajstic, 2018). The long history of research on the Cleveland Shale means that many older collections are not well documented, but the unit is exposed across hundreds of square kilometers in southern and eastern Ohio. At the extreme end the Aztec fish localities are distributed across southern Victoria's Land in a north-south-elongate rectangle approximately 125 x 50km (Young and Long, 2014).

4.3.2 Food web assembly

The assembly of food web models follows the procedure of (Roopnarine, 2009). Full data for each food web is provided in the Supplementary Information. A schematic of an example guild-level food web (=metanetwork) for the Cleveland Shale is displayed in Figure 4.3. Consumers were sorted into guilds, which are here defined as groups of species within a food web with the same trophic relationships- i.e. they have the same set of predator and prey/resource species. The feeding categories, such as. 'durophage,' 'faunivore,' and 'detritivore', are meant to capture functional groups that can be identified straightforwardly across multiple taxa, time intervals, and environmental settings. These broad categories also accommodate the uncertainty inherent in modeling the autecology of fossil organisms.

Size categories were logarithmic (base two) and based on body length measured in centimeters (Table 4.2). Logarithmic size classes were chosen to ensure that the demarcation of size classes followed objective rules across the dataset. Body size data was drawn from the literature, including both compendia (Klasson, 2008; Sallan and Galimberti, 2015; Chevrinais et al., 2017) and descriptions (Coates and Sequeira, 2001; Otoo et al., 2021). In the case of moderately or highly fragmentary fossils, body size was calculated extrapolating based on sister taxon or well-preserved representation taxon of the smallest possible clade. Taxonomic assignments were drawn from the literature using the most recent conclusions or phylogenetic results. Taxa for which sufficient anatomical or taxonomic information could not be obtained or verified- ex. '*Ageleodus*', many of the under- or undescribed Cleveland Shale vertebrates (Carr and Jackson, 2008)- were excluded from the dataset.

Confidence in taxonomic assignments varies. For example, there is strong consensus on the taxonomic identities of the East Kirkton tetrapods, even if there are disagreements on their positions within early tetrapod phylogeny more broadly (Chapter 3). By contrast, while both the Cleveland Shale (Carr and Jackson, 2008) and Bear Gulch (Lund et al., 2012) are represented by many fossil specimens, in each case the diversity of chondrichthyans is likely inflated by reliance on tooth or spine taxa (MI Coates, pers. comm. October 2022). Some Mississippian actinopterygian genera, such as *Elonichthys* and *Rhadinichthys*, are longstanding 'wastebasket' taxa obscuring true diversity (Henderson et al., 2022), some of which are the subject of active revision (Y Mo, AM Caron, MI Coates unpublished data). Where possible, firsthand knowledge of specimens and data have been used to inform taxonomic assignments (ex. the Ballagan Formation tetrapods). However, this work is by its nature dependent on published taxonomic statements, descriptions, and analyses.

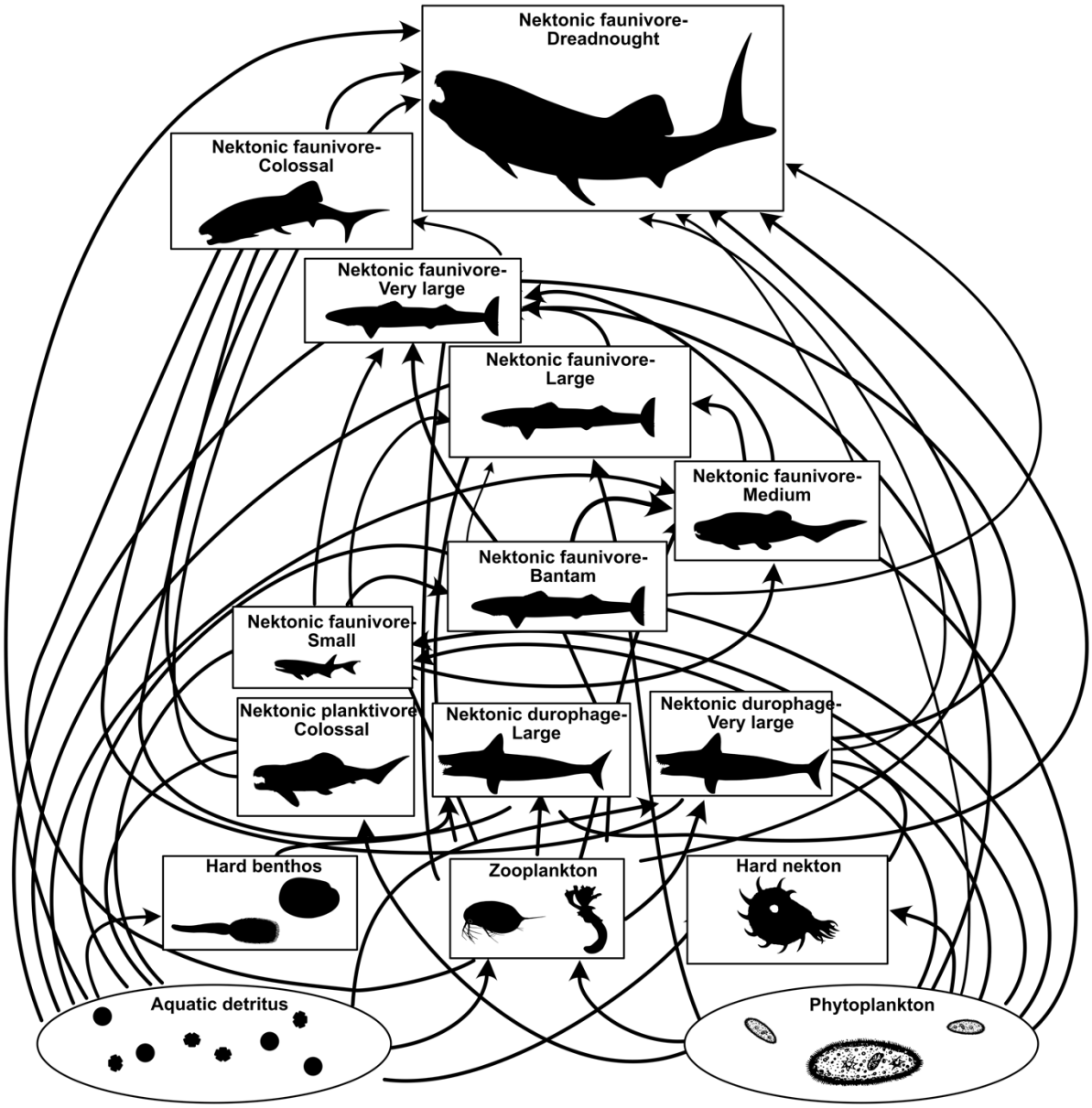

Figure 4.3. Schematic of metanetwork for the Cleveland Shale paleocommunity. Guilds are represented by shapes with silhouettes of representative organisms (these may not necessarily actually be present in the actual paleocommunity). Arrows represent energy flow, pointing from prey guilds to predator guilds. Silhouettes from PhyloPic. Specific sources are listed in APPENDIX C.

Table 4.2. Information on size categories used in this study.

Size category name	Range
Minute	≤1cm
Miniscule	>1-2cm
Tiny	>2-4cm
Very small	>4-8cm
Small	>8-16cm
Bantam	>16-32cm
Medium	>32-64cm
Large	>64-128cm
Very large	>128-256cm
Colossal	>256-512cm
Dreadnought	≥512cm

Habit categories refer to where the organism lives, eg. terrestrial vs semiaquatic, nektonic vs benthic. Each size category is allowed to feed on equal and all smaller size categories (aquatic species and semiaquatic species feeding on aquatic species) or size categories two sizes smaller (terrestrial species and semiaquatic species feeding on terrestrial species). Benthic species can only access benthic resources (this was done for the sake of uniformity in assigning vertebrate and macroinvertebrate consumers to guilds; most if not all benthic invertebrates likely fed on phytoplankton), nektonic species can access benthic, nektonic, and semiaquatic resources, and semiaquatic species can access nektonic and terrestrial resources. Unlike modeling of the PTME (Roopnarine, 2009; Roopnarine and Angielczyk, 2012, 2015; Roopnarine et al., 2019), guilds were not allowed to feed on those larger than themselves. Active feeding by smaller vertebrates on larger ones (as adults) is difficult to assess in the fossil record. There is also a minimum effective prey size for a given size of predator: beyond a certain point, energy expended capturing prey exceeded energy gained from feeding. Acknowledging that this relationship is heavily dependent on the physiology of the organisms involved, a difference of two size classes was chosen as an approximation that could be applied across the dataset. It was decided to use

only adult sizes to avoid compounding ambiguity in reconstructing body size for not only adults but also prior ontogenetic stages. Estimation of body length across ontogeny is particularly problematic in the case of terrestrial tetrapods. Intraspecific and intraguild cannibalism may have been an important part of Paleozoic ecological dynamics (see Discussion) but cannot currently be modeled within the current iteration of CEG.

In addition to these enumerated guilds, 'block' guilds were used for resources or low-level consumers for which presence is known or can be reasonably inferred, but diversity cannot be directly counted. The number of species in these guilds was calculated as ten times the number of species (distributed across the relevant guilds) that feed upon them. Primary productivity guilds were phytoplankton, detritus (aquatic and terrestrial, as applicable), and terrestrial plants. Diversity in these guilds was treated as units of primary productivity. Block consumer guilds include zooplankton, hard benthos (ex. brachiopods, bivalves), and hard nekton (ex. orthocone nautiloids, ammonites, shrimps). Guilds were assigned extinction probabilities based on body size (for consumers) or function/diet (for 'block' guilds) (Table 4.3). Extinction probability was not linked to species abundance because that information is not published for all localities. Relative diversity (number of species in bin/total number of species/units) for taxonomic bins and consumer guilds is presented in APPENDIX C.

Table 4.3. (Pages 192-193). Extinction probabilities assigned in this study.

		Extinction probability (out of 1)
Block guild (calculated diversity)	**Phytoplankton**	**0.01**
	Zooplankton	**0.02**
	Soft nekton	**0.05**
	Hard nekton	**0.05**
	Hard benthos	**0.05**

	Aquatic detritus	**0.01**
	Terrestrial detritus	**0.01**
	Terrestrial plants	**0.01**
Consumer size category (enumerated diversity)	Minute	0.05
	Miniscule	0.1
	Tiny	0.1
	Very small	0.2
	Small	0.2
	Bantam	0.3
	Medium	0.3
	Large	0.4
	Very large	0.4
	Colossal	0.5
	Dreadnought	0.5

4.4 METHODS

4.4.1 Paleocommunity composition comparison

To compare community composition, paleocommunities were ordinated using non-metric multidimensional scaling (NMDS). Bray-Curtis distance was used, as it accounts for both presence-absence of guilds and species richness within them. The ordination was done twice-once using the relative diversity of large taxonomic groups such as placoderms, tetrapods, etc. (see Supplementary Information), and once using the relative diversity of consumer guilds.

4.4.2 CEG model

In order to compare paleocommunity responses to perturbation, paleocommunities were analyzed using the Cascading Extinctions on Graphs (CEG) model, with 100 replicates per food web. The Cascading Extinctions on Graphs (CEG) model was developed by PD Roopnarine to

investigate the response of fossil paleocommunities to perturbations in primary productivity, particularly in the context of mass extinctions (Roopnarine, 2006, 2009). Rather than model direct species-species feeding relationships (Dunne et al., 2008; Chevrinais et al., 2017), CEG incorporates stochasticity in species interactions. Species are sorted into guilds- groups of species sharing the same prey and predators- and then species-species interactions are stochastically reconstructed following the feeding relationships established by the metanetwork (Figure 4.4). A stochastic approach is taken to accommodate uncertainty in inferring the autecology of fossil species, and variation in observed modern food webs across both small and large temporal and spatial scales (Roopnarine, 2009). A species within a predator guild, then, may be reconstructed as feeding on all the species within a prey guild (generalist) or just one (specialist). This is done by drawing from a mixed power-law exponential distribution to assign the species-species feeding links. This distribution is used because, within each guild, it reconstructs more species as specialists than generalists. Once the species-level food web is constructed, units of primary productivity are removed (perturbation). The food web adjusts to the reduced primary productivity input and any resulting species loss (secondary extinction) is recorded. This is repeated until all primary productivity has been removed (perturbation has reached 100%). A new species-level food web is then drawn, and the process begins again.

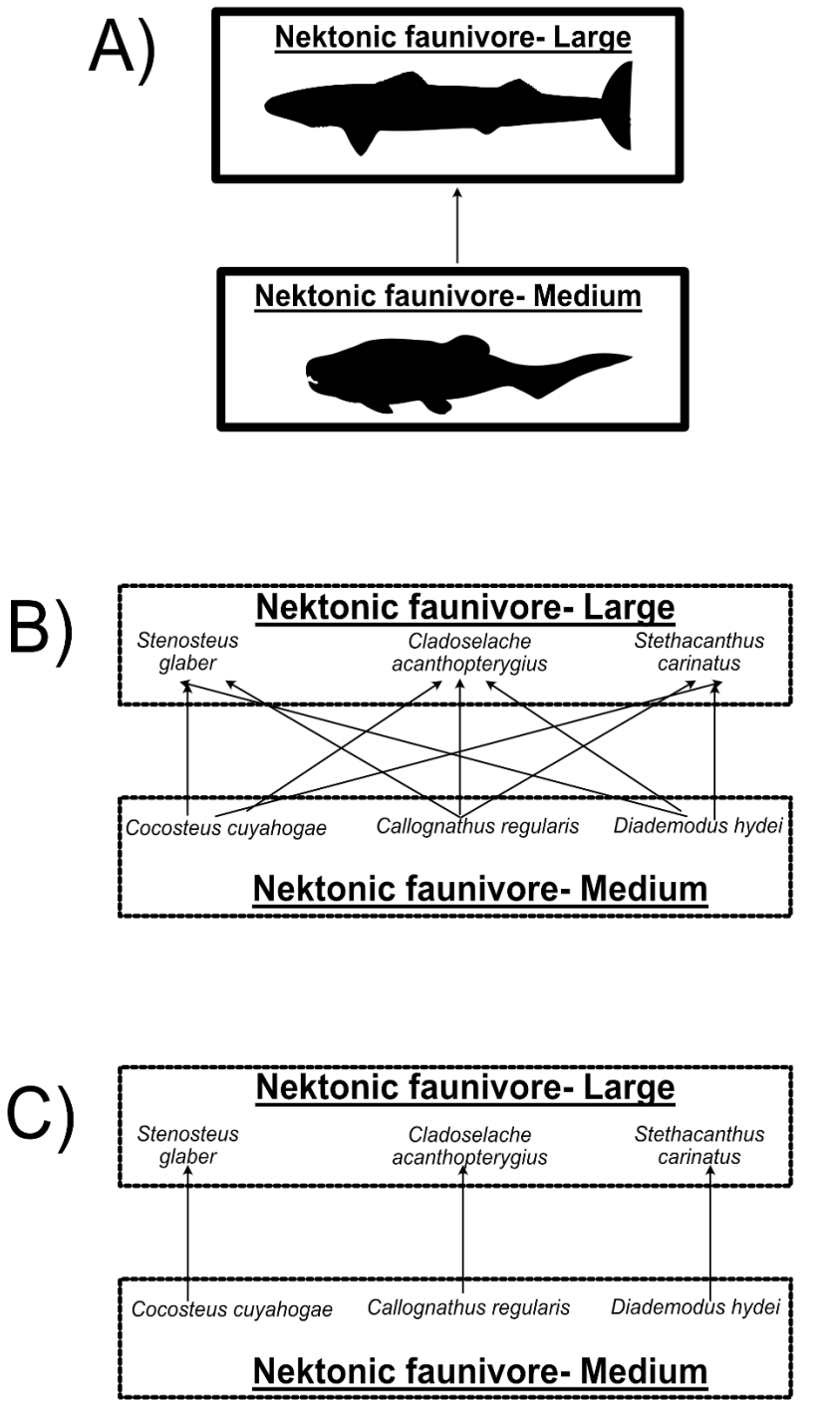

Figure 4.4. Schematic showing the reconstruction of alternate species-level feeding relationships by CEG from the same metanetwork provided by the user. A) initial guild-level relationships provided by user; B) reconstruction of predator species as generalists with broad prey profiles; C) reconstruction of predator species as specialists with narrow prey profiles.

CEG relies on several key assumptions:

- Disruptions of a species can cause the secondary extinction of other species in the food web.
- It is impossible to capture the structure of a fossil paleocommunity with a single food web model.
- The greater number of specialists than generalists can be projected backwards in time and across environments.

CEG has been applied as part of a long-running research program focused on the Permo-Triassic mass extinction as represented by the terrestrial vertebrate record in southern Africa, especially the Karoo Basin in South Africa (Roopnarine, 2006, 2009; Roopnarine and Angielczyk, 2015, 2016; Roopnarine et al., 2018, 2019). It also recently been used in study of a series of Permian-Jurassic biotic crises in China (Huang et al., 2021) and the Late Ordovicia Richmondian Invasion in the Cincinnati Basin (Kempf et al., 2020). This work is the first to apply CEG to Devonian-Carboniferous data. CEG allows for comparison of paleocommunities from various chronological and environmental settings to investigate the possibility of general behavior during extinction intervals and times of possible ecological transition. Moreover, recent work has suggested that stability is a paleocommunity-level property on which selection can operate (Roopnarine and Angielczyk, 2016). CEG allows for testing the hypothesis that paleocommunity structures 'evolve' toward greater stability and that there has been a net increase in tetrapod occupation of ecospace since the Devonian (Sahney et al., 2010).

4.5 RESULTS

4.5.1 NMDS results

In the taxa-based analysis, NMDS1 primarily captures differences in environment and NMDS2 primarily captures differences in time. This is seen most clearly when the sites are

grouped by period (Figure 4.5). By contrast, the Frasnian sites other than Miguasha fall within the space defined by the Famennian ones (Figure 4.6); there are insufficient Tournaisian and Visean paleocommunities to clearly define hulls, but the Serpukhovian hull is a roughly equal distance away from the Tournaisian (Loanhead-Ballagan) and Visean (Bearsden-Glencartholm). When grouped by environmental setting, the hulls- except for the outlier terrestrial paleocommunities - extend along NMDS2: the Devonian paleocommunities have low values, and the Mississippian ones have high values (Figure 4.7). Waterloo Farm (Devonian, estuarine) is solidly within the space defined by the continental paleocommunities, and Red Hill (continental) is the only Devonian paleocommunity- aside from Gilboa- to plot above 0 on NMDS2. The reef-associated paleocommunities are entirely within the space defined by the marine paleocommunities.

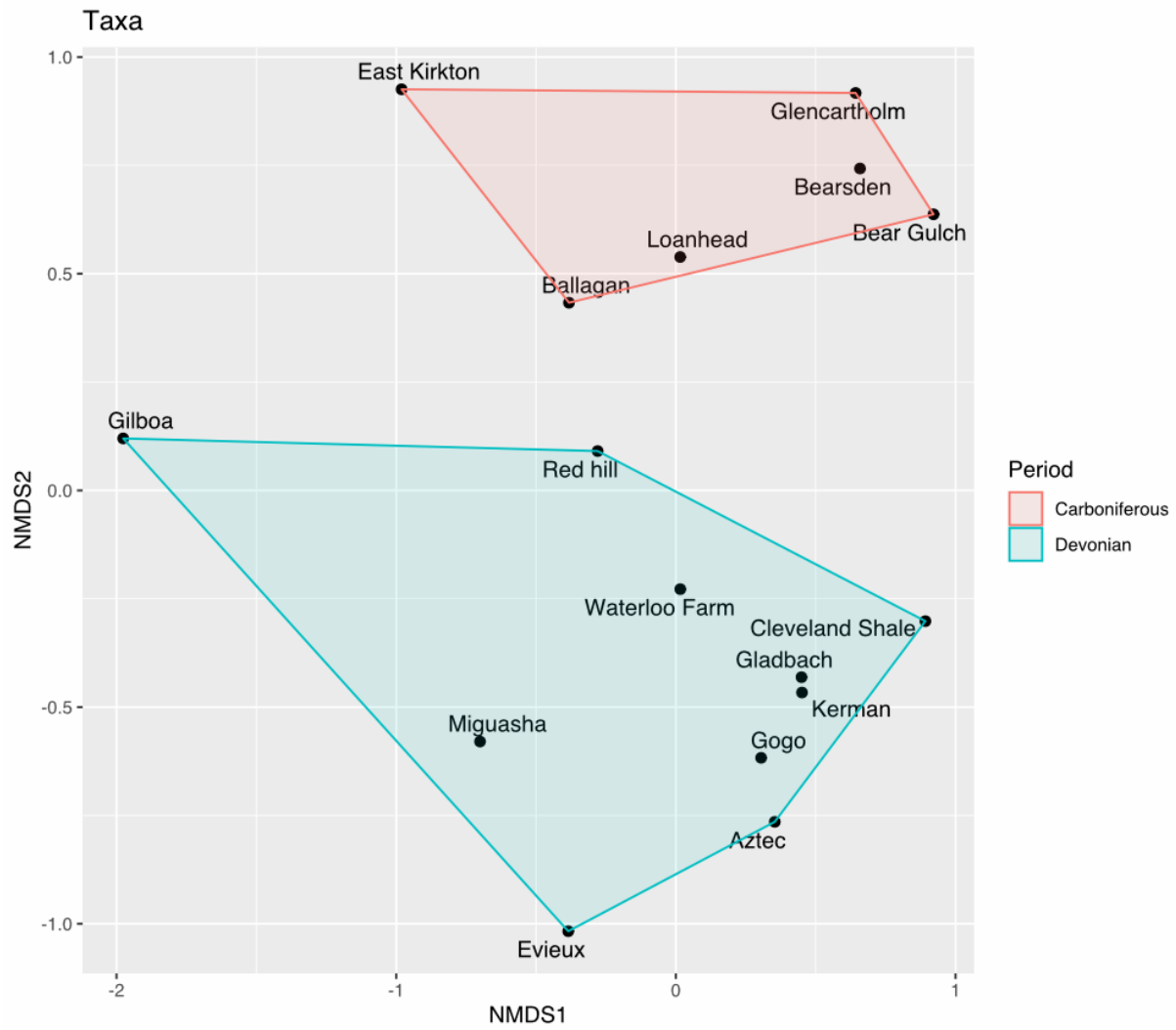

Figure 4.5. Nonmetric multidimensional scaling (NMDS) ordinations of paleocommunity relative taxonomic diversity using Bray-Curtis distance, grouped by period.

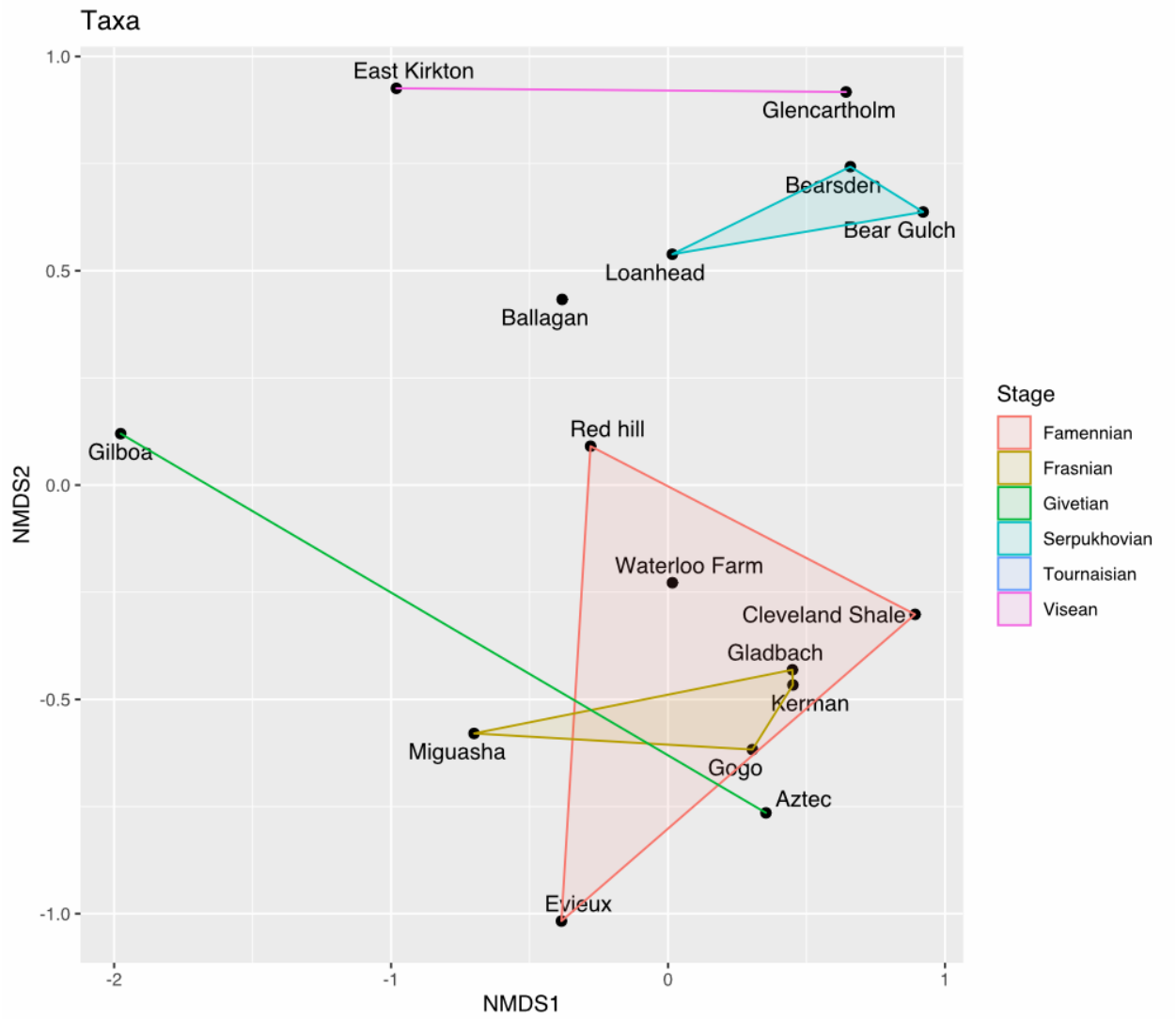

Figure 4.6. Nonmetric multidimensional scaling (NMDS) ordinations of paleocommunity relative taxonomic diversity using Bray-Curtis distance, grouped by stage.

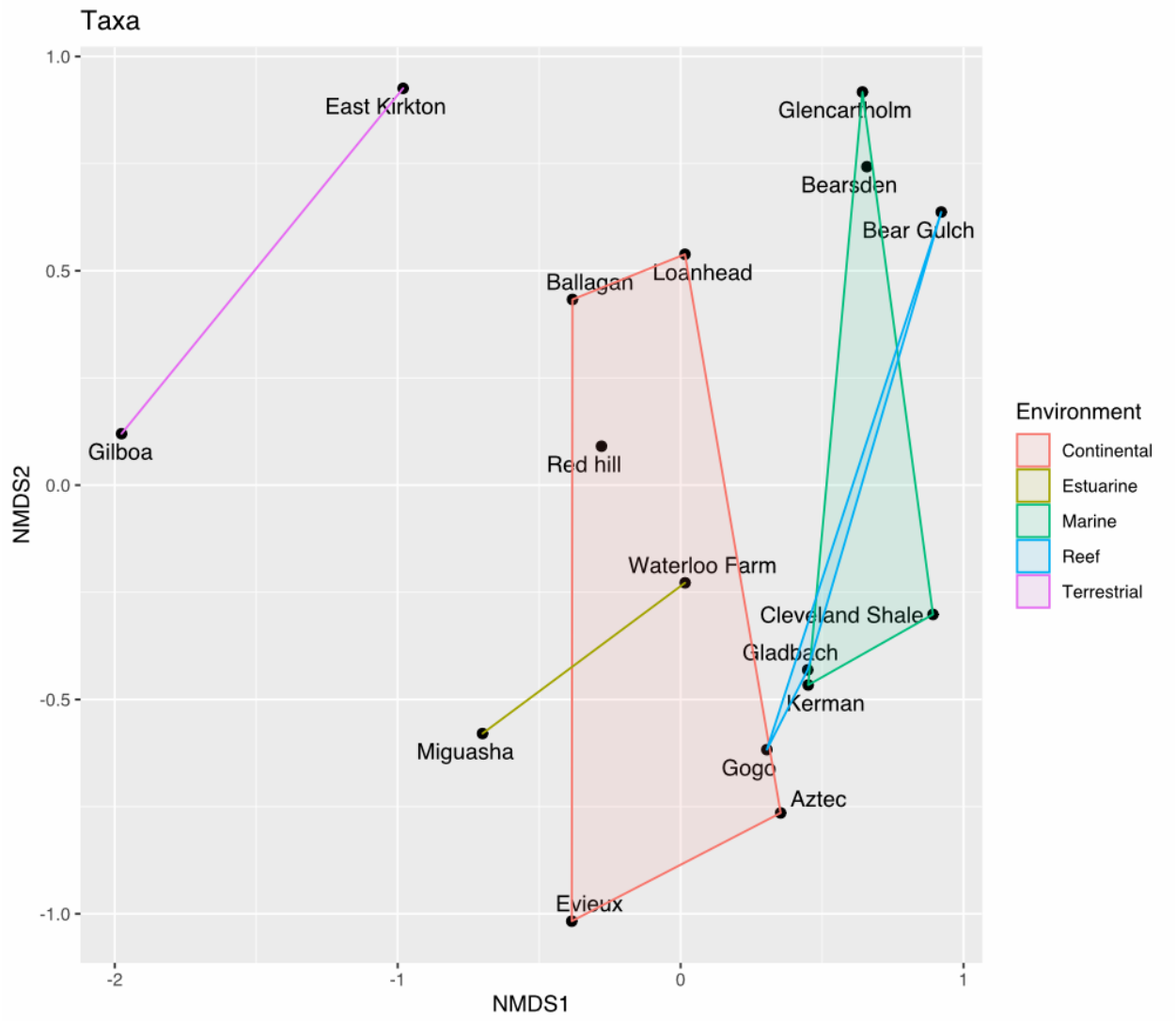

Figure 4.7. Nonmetric multidimensional scaling (NMDS) ordinations of paleocommunity relative taxonomic diversity using Bray-Curtis distance, grouped by environment.

The Devonian-Mississippian separation is likely driven first by the absence of placoderms from the Mississippian (Supplementary Information). The high diversity of panderichthyids/tetrapods in Red Hill brings it closer to the Mississippian paleocommunities of Ballagan and Loanhead, as seen in both the by-stage (Figure 4.6) and by-environment (Figure 4.7) groupings. The high diversity of holocephalans Cleveland Shale and Bear Gulch drives them to similar positions on NMDS1 (Figure 4.5-4.7). Gladbach, Kerman, and Gogo resemble Cleveland Shale in having high placoderm diversity and therefore cluster close but lack the high diversity of non-acanthodian chondrichthyans.

By contrast, once the outliers are removed (Figure 4.8), the clear environment/time separation across NMDS axes from the taxon-based analysis is not seen in the guild-based analysis (Figure 4.9, Figure 4.10). This suggests that despite taxonomic change, persistence of guilds is blurring time- or environment-based differences between paleocommunities. NMDS1 seems to capture higher-level differences in time/environment, and NMDS2 captures lower-level differences in time categories. A Devonian/Carboniferous separation is discernable when the sites are grouped by period (Figure 4.9), though it is not as great as in the taxa-based analysis. The Serpukhovian, Frasnian, and Famennian hulls are distributed along NMDS1 (Figure 4.10). Reef paleocommunities are entirely within the space defined by marine paleocommunities, and estuarine paleocommunities (especially Waterloo Farm) are between the marine and continental spaces (Figure 4.11). The orthogonal variation along axes between the taxa- and guild-based NMDS suggest that different processes govern these two dimensions of ecological paleocommunity composition.

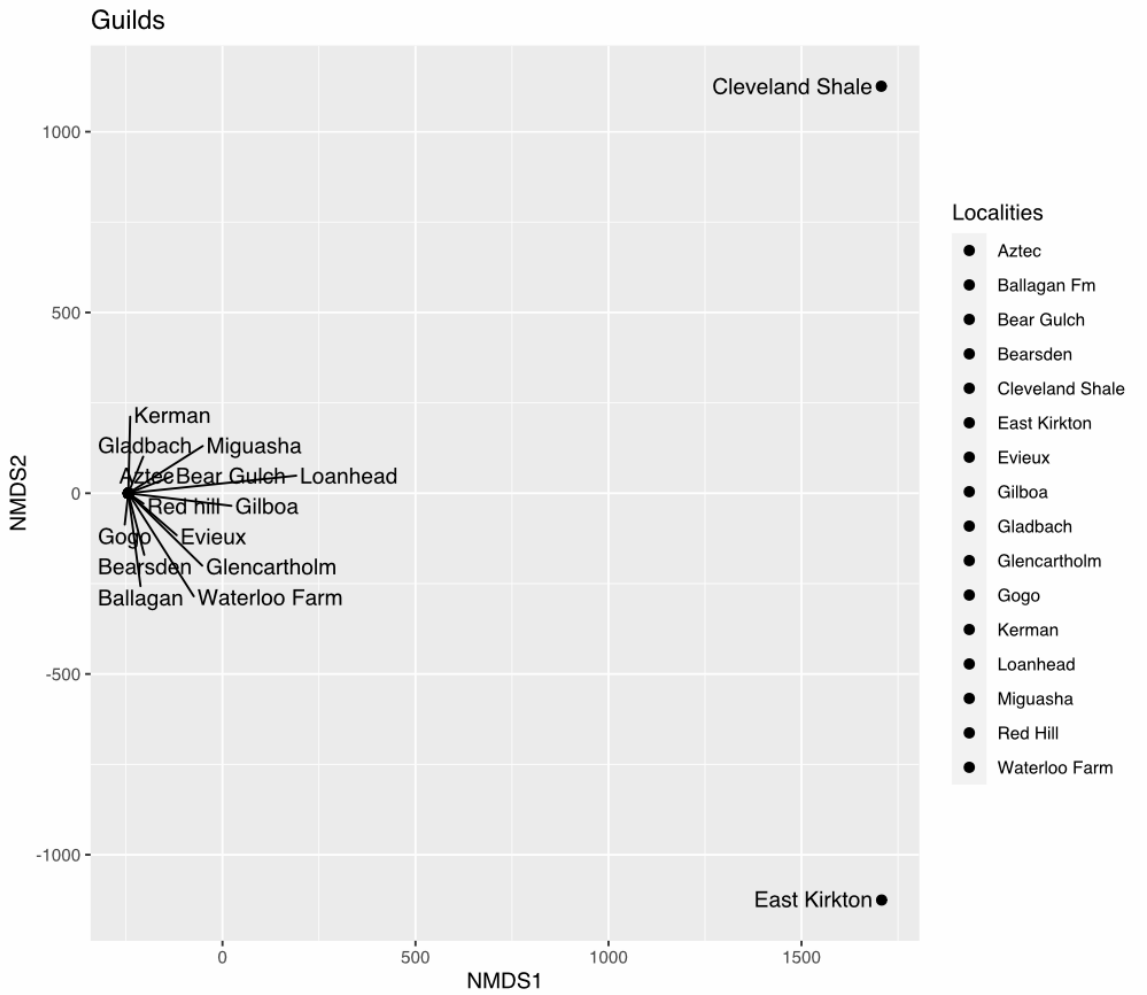

Figure 4.8. Nonmetric multidimensional scaling (NMDS) ordinations of paleocommunity relative guild richness using Bray-Curtis distance. Similar distortion is seen in NMDS analyses of PTME paleocommunities, caused by the aberrant disaster fauna of the *Lystrosaurus* Assemblage Zone (LAZ), with results changing when it is removed (Roopnarine et al., 2018). Cleveland Shale has extremely large placoderm planktivore guilds (ex. *Titanichthys*) that are unique. Similarly, East Kirkton has the greatest number of terrestrial guilds and lacks all but one aquatic guild, and Gilboa only has two terrestrial guilds.

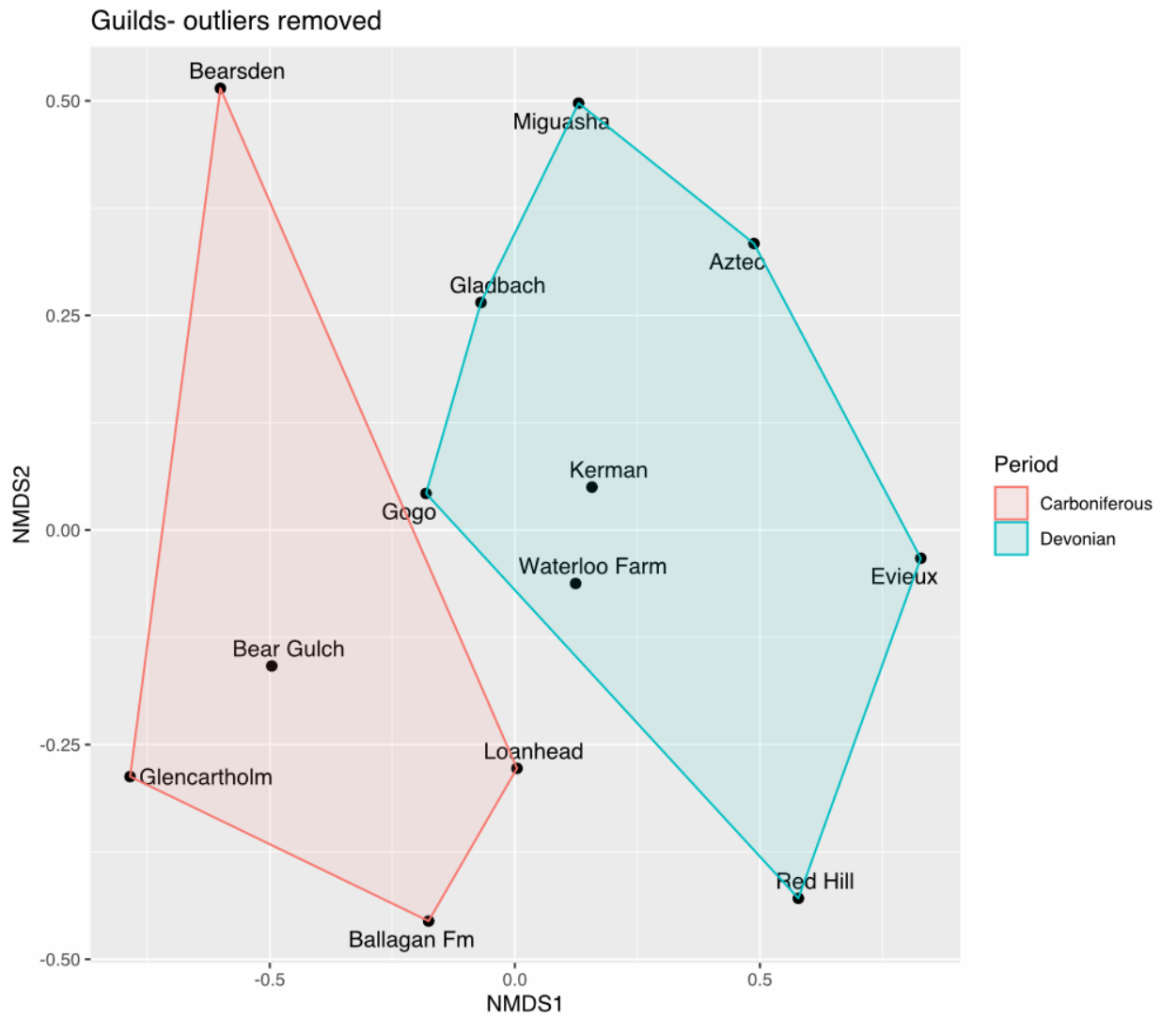

Figure 4.9. Nonmetric multidimensional scaling (NMDS) ordinations of paleocommunity relative guild richness using Bray-Curtis distance (outliers removed), grouped by period.

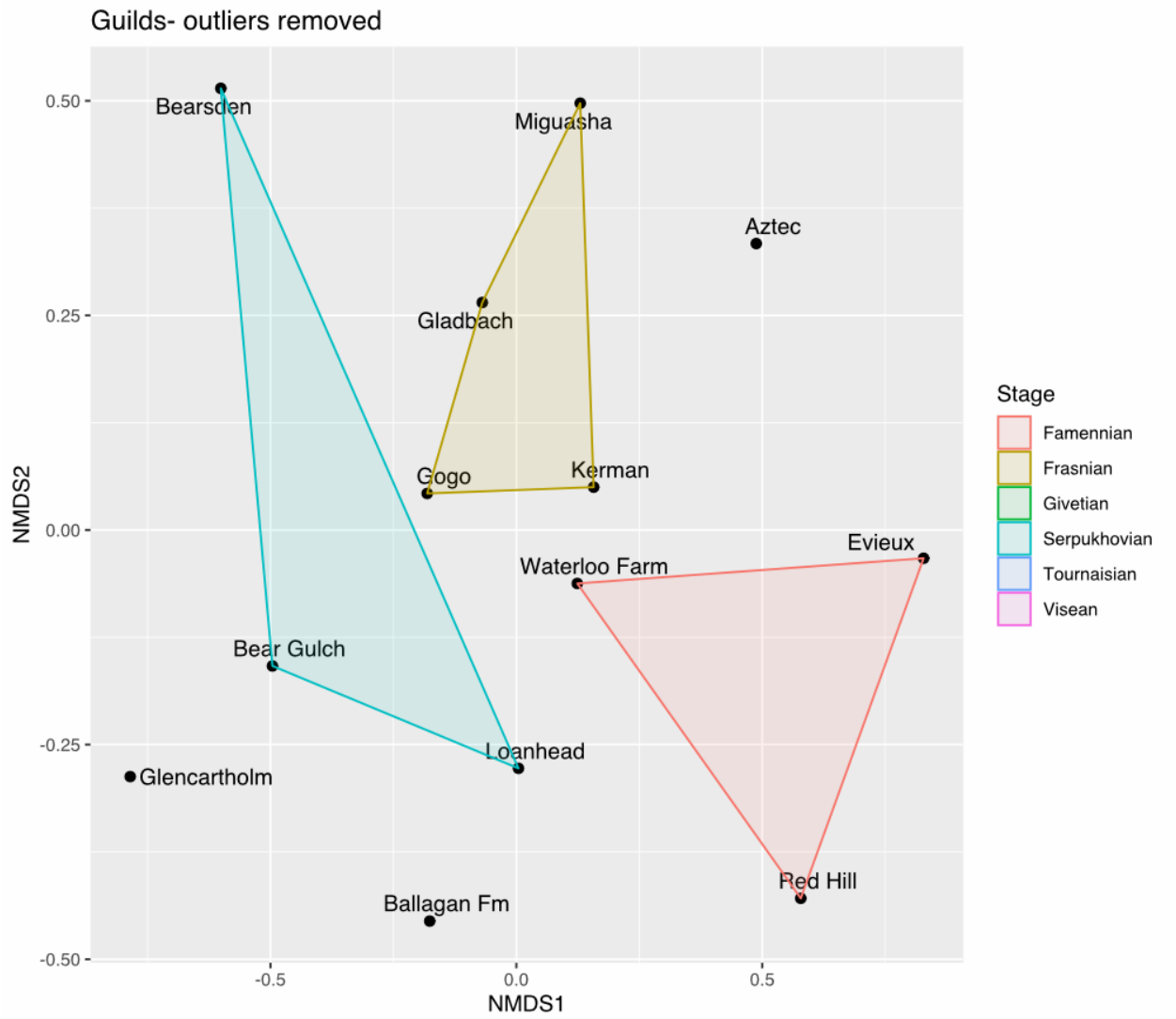

Figure 4.10. Nonmetric multidimensional scaling (NMDS) ordinations of paleocommunity relative guild richness using Bray-Curtis distance (outliers removed), grouped by stage.

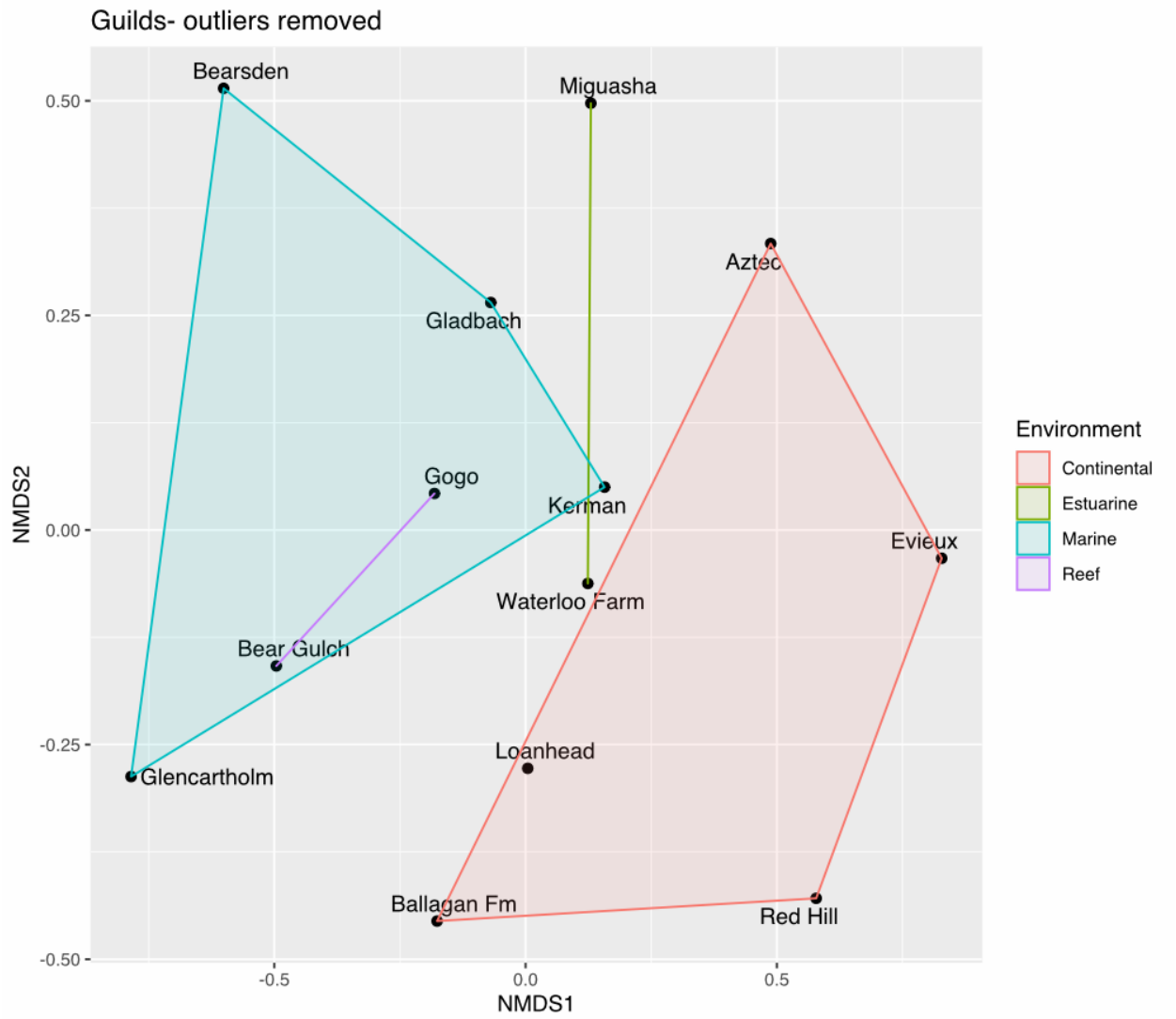

Figure 4.11. Nonmetric multidimensional scaling (NMDS) ordinations of paleocommunity relative guild richness using Bray-Curtis distance (outliers removed), grouped by environment.

Most vertebrate diversity across paleocommunities is concentrated in the nektonic durophage and faunivore guilds, but differences in relative diversity within guilds are low (Supplementary Information). Miguasha and Bearsden have similar proportions of Small and Bantam nektonic planktivores, likely driving their similar values on NMDS2. Loanhead, Red Hill, and Ballagan have similar tetrapodomorph and tetrapod diversity represented by Bantam and Medium nektonic faunivore guilds, possibly pushing all three toward low NMDS2 values.

4.5.2 CEG model results

4.5.2.1 Overall CEG results

CEG results for Devonian and Mississippian food webs (enumerated/consumer guilds) are presented Figure 4.12 and Figure 4.13. Overall CEG results for all guilds are presented in APPENDIX C. The response curve for each paleocommunity can be split into two regimes: low secondary extinction (<25%)/low perturbation (<50%) and high secondary extinction (>80%)/high perturbation (>50%). There is often an abrupt, discontinuous transition between the two. Variance in secondary extinction values is generally low compared to Permo-Triassic food webs (Roopnarine et al., 2018) and lower in the high secondary extinction/perturbation regime than the low secondary extinction/perturbation regime. Notable exceptions are: Gilboa and East Kirkton, where secondary extinction values and secondary extinction variance are high across the whole range of perturbation; Red Hill, where the transition between the low and high regimes is more continuous; and Upper Ballagan Formation, where there is an uptick in secondary extinction at very low perturbation prior to the 50% perturbation threshold.

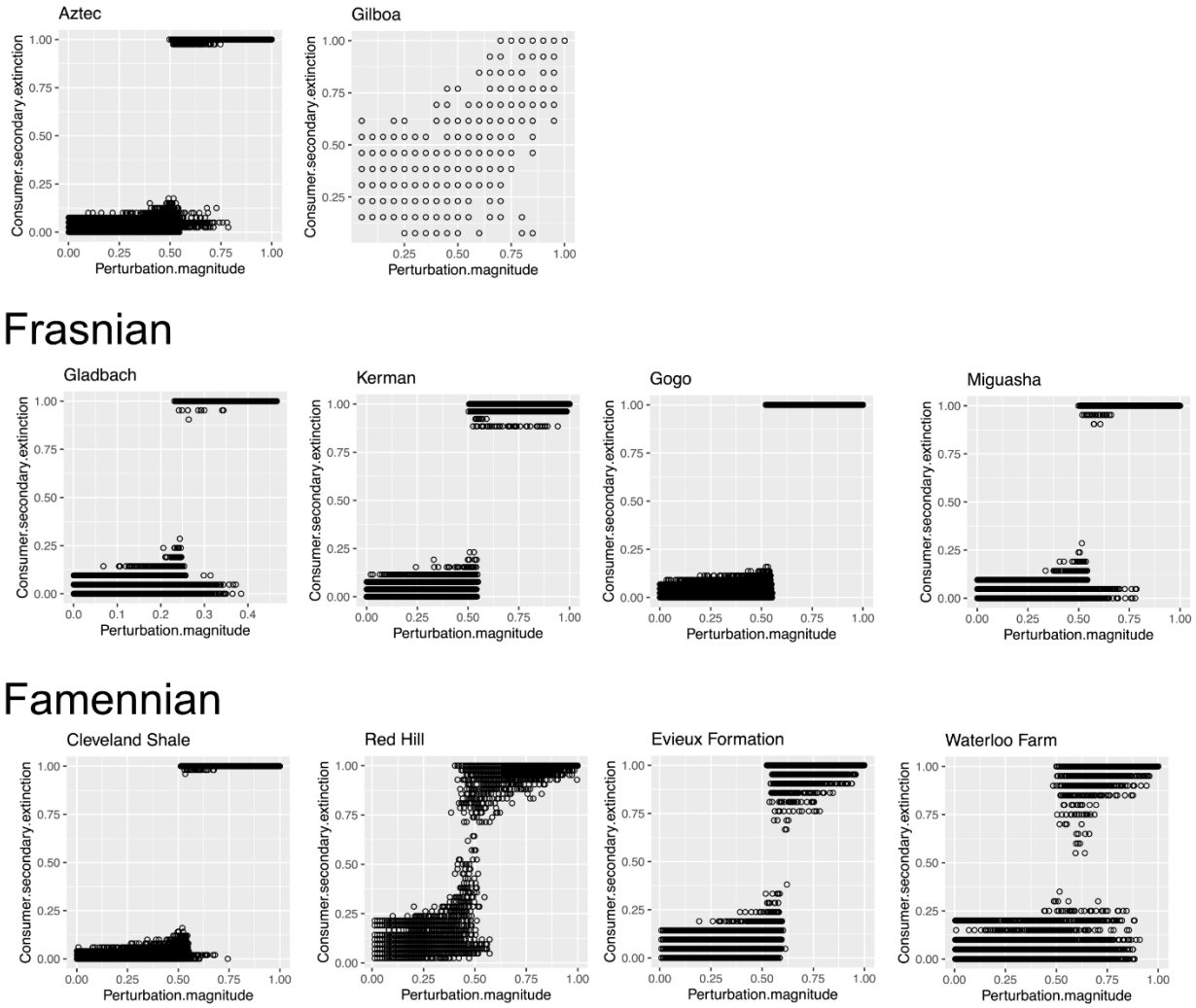

Figure 4.12. CEG response curves plotted for all Devonian paleocommunities (consumers/enumerated guilds only).

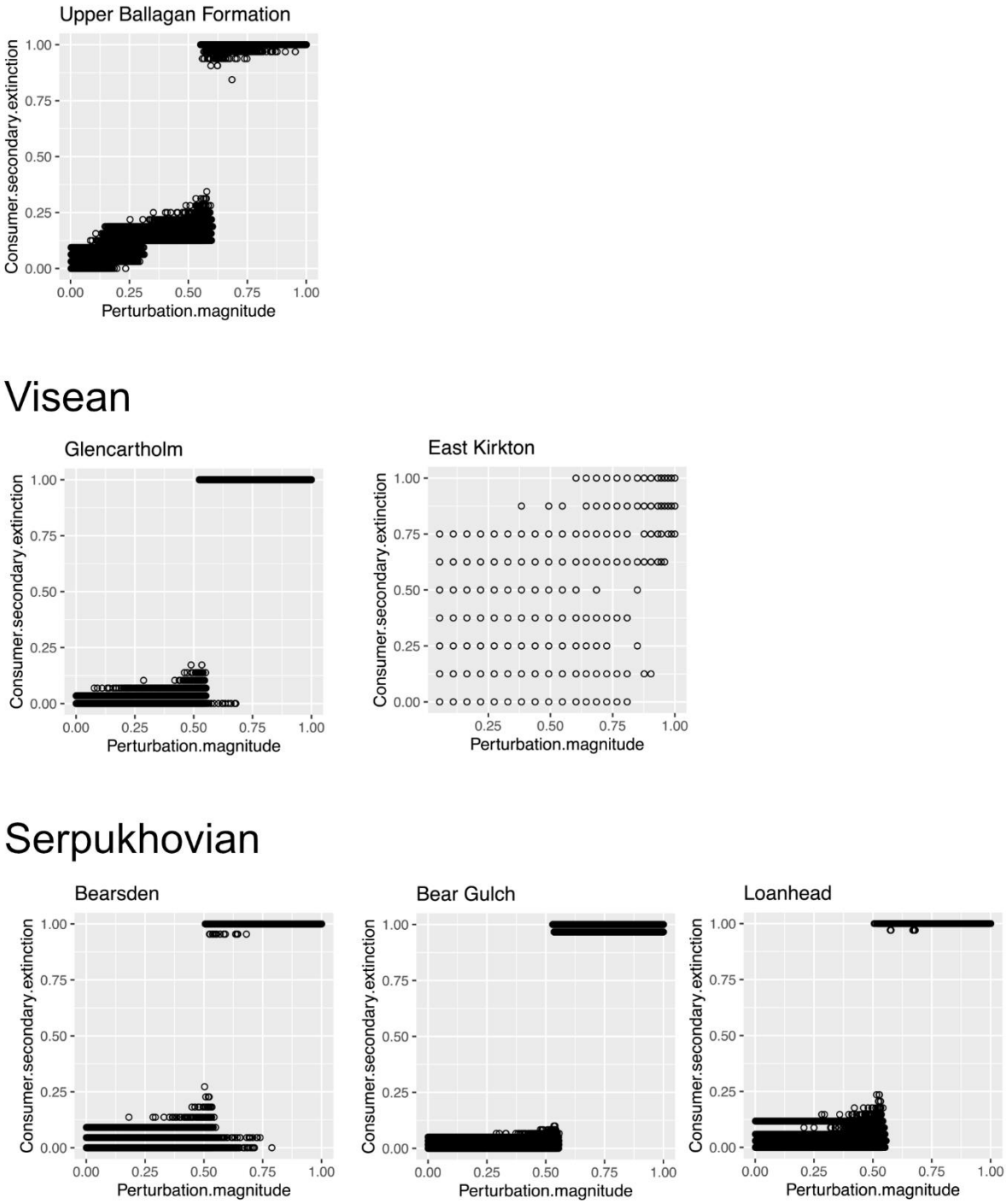

Figure 4.13. CEG response curves plotted for all Mississippian paleocommunities (consumers/enumerated guilds only).

Gilboa and East Kirkton are highly unusual, which is likely due foremost to size effects; these paleocommunities are the smallest in the dataset, and Gilboa does fall below the 15 species threshold (Supplementary Files). They are also structurally unique by virtue of being the only terrestrial paleocommunities. The 'stepped' appearance of the CEG response curves, with discontinuous changes between secondary extinction values, is an exaggeration of that seen in other paleocommunities. The other paleocommunities with the greatest variance, Miguasha (Frasnian, estuarine), Red Hill (Famennian, continental), Evieux Formation (Famennian, continental), and Waterloo Farm (Famennian, estuarine), are all nonmarine and from the Late Devonian. Waterloo Farm has a distinct 'tail' of high perturbation and low secondary extinction extending past the 50% perturbation threshold, indicating unusual persistence in some replicates.

4.5.2.2 By-guild CEG results

Guild-level results (enumerated/consumer guilds) for all paleocommunities are presented in Figure 4.14-Figure 4.28. The guild-level results show that secondary extinction within each guild can rapidly jump to high levels, reflecting low guild richness (=number of species within the guild) across paleocommunities. At low guild richness, complete secondary extinction is possible even at very low perturbation values. Guilds with greater richness show greater persistence, but near or total collapse at 50-75% perturbation is the rule. Neither body size (ex. small-body guilds persisting longer than large-body guilds) nor diet (planktivores and detritivores persisting longer than faunivores) appear to (generally) explain the persistence of some guilds rather than others.

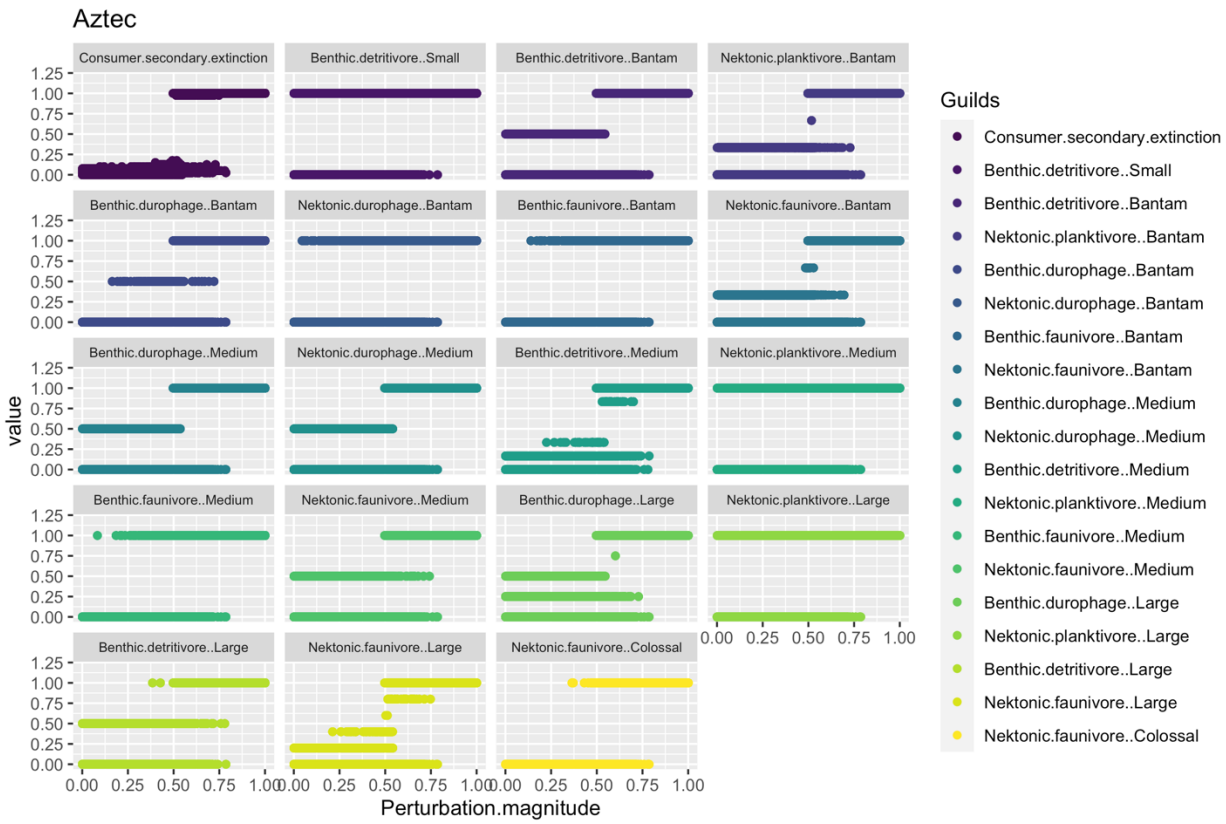

Figure 4.14. Guild-level results of Aztec CEG response (consumers/enumerated guilds only). Perturbation magnitude (x-axis) is plotted against secondary extinction (y-axis) for all guilds combined (first panel) and individual guilds (all other panels).

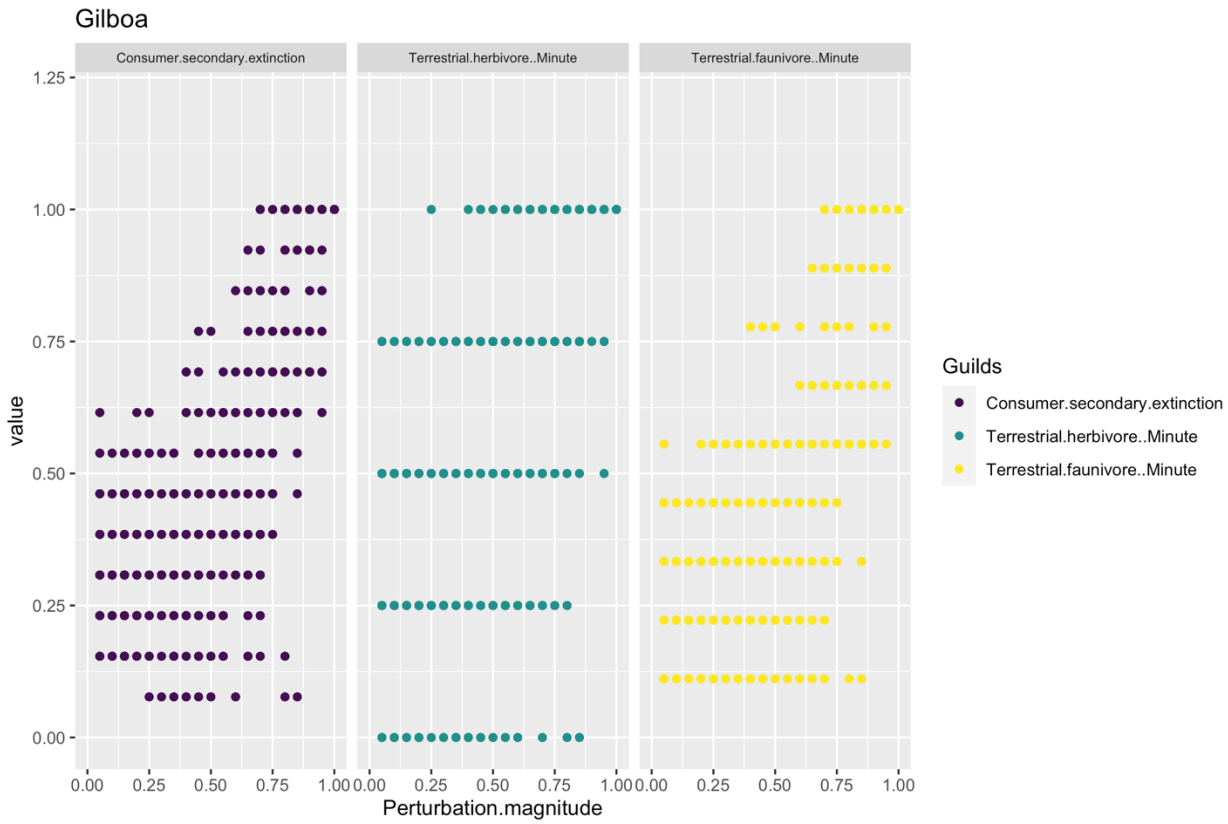

Figure 4.15. Guild-level results of Gilboa CEG response (consumers/enumerated guilds only).

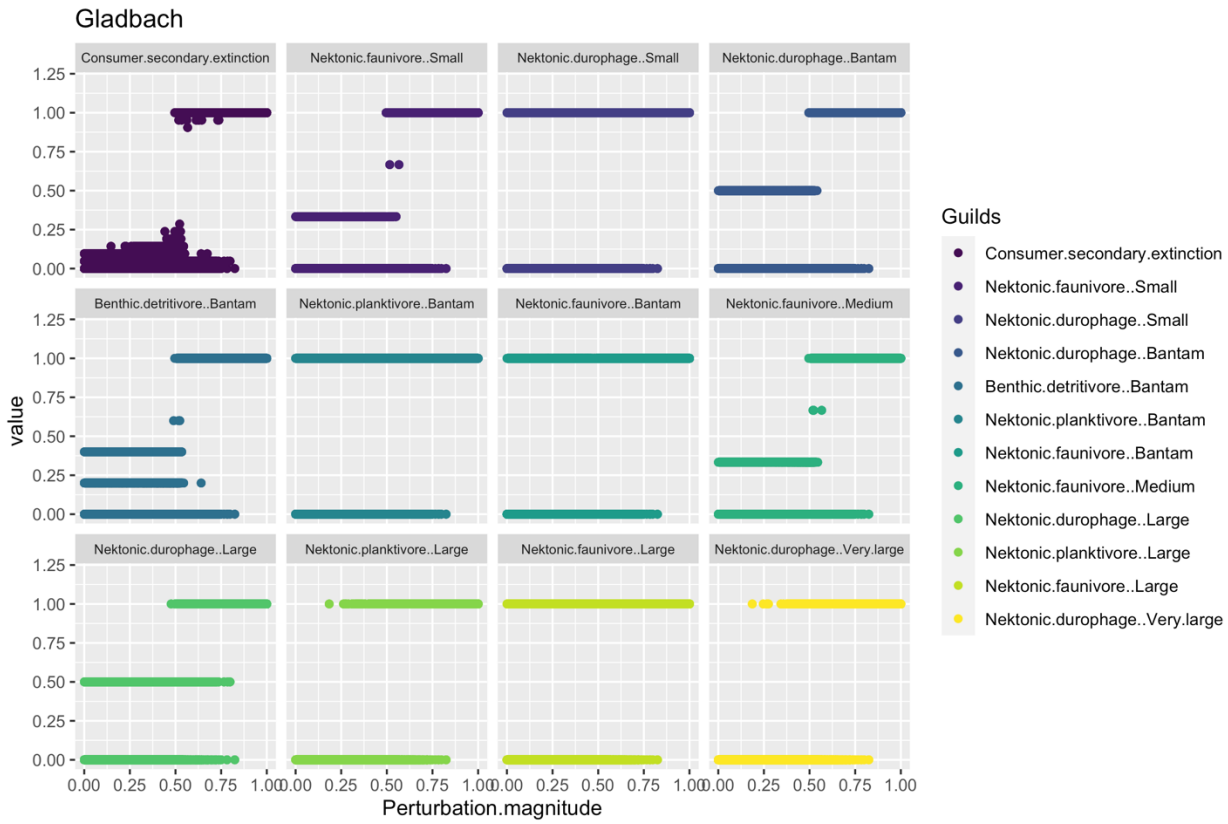

Figure 4.16. Guild-level results of Gladbach CEG response (consumers/enumerated guilds only).

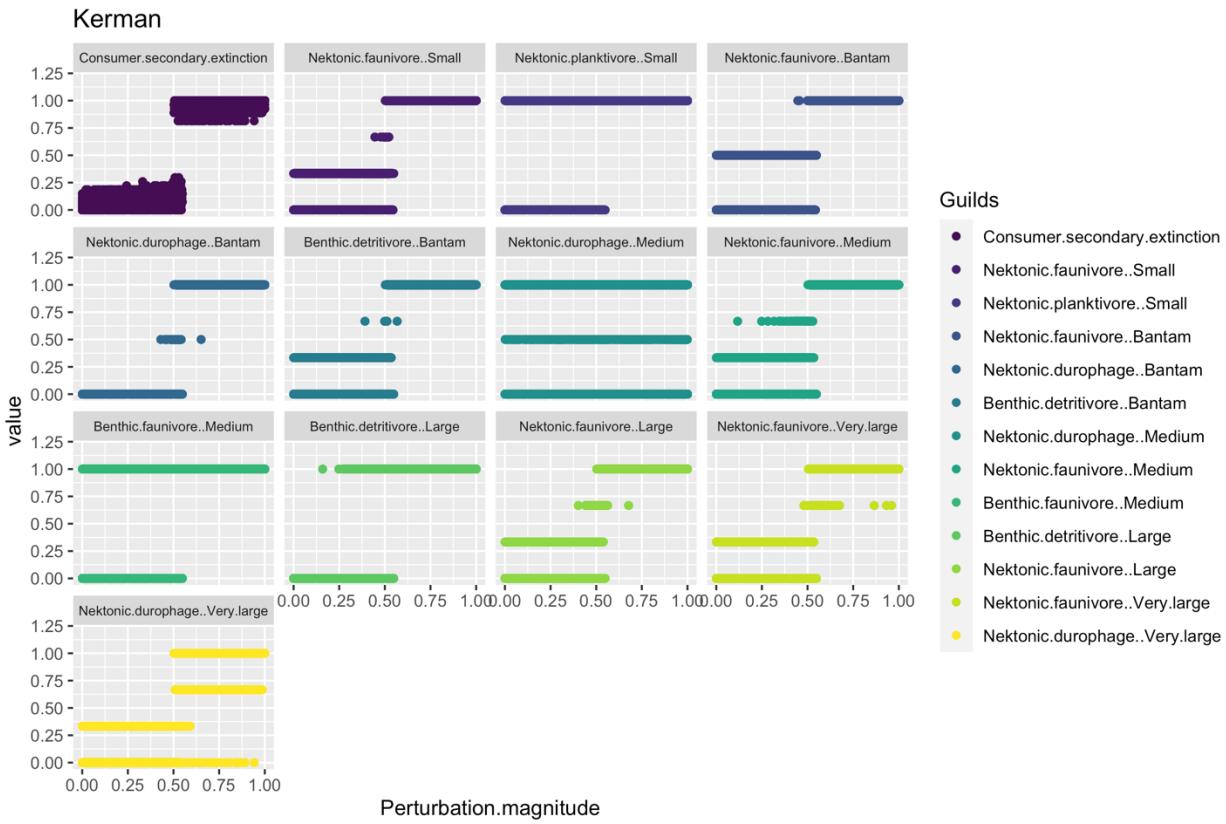

Figure 4.17. Guild-level results of Kerman CEG response (consumers/enumerated guilds only).

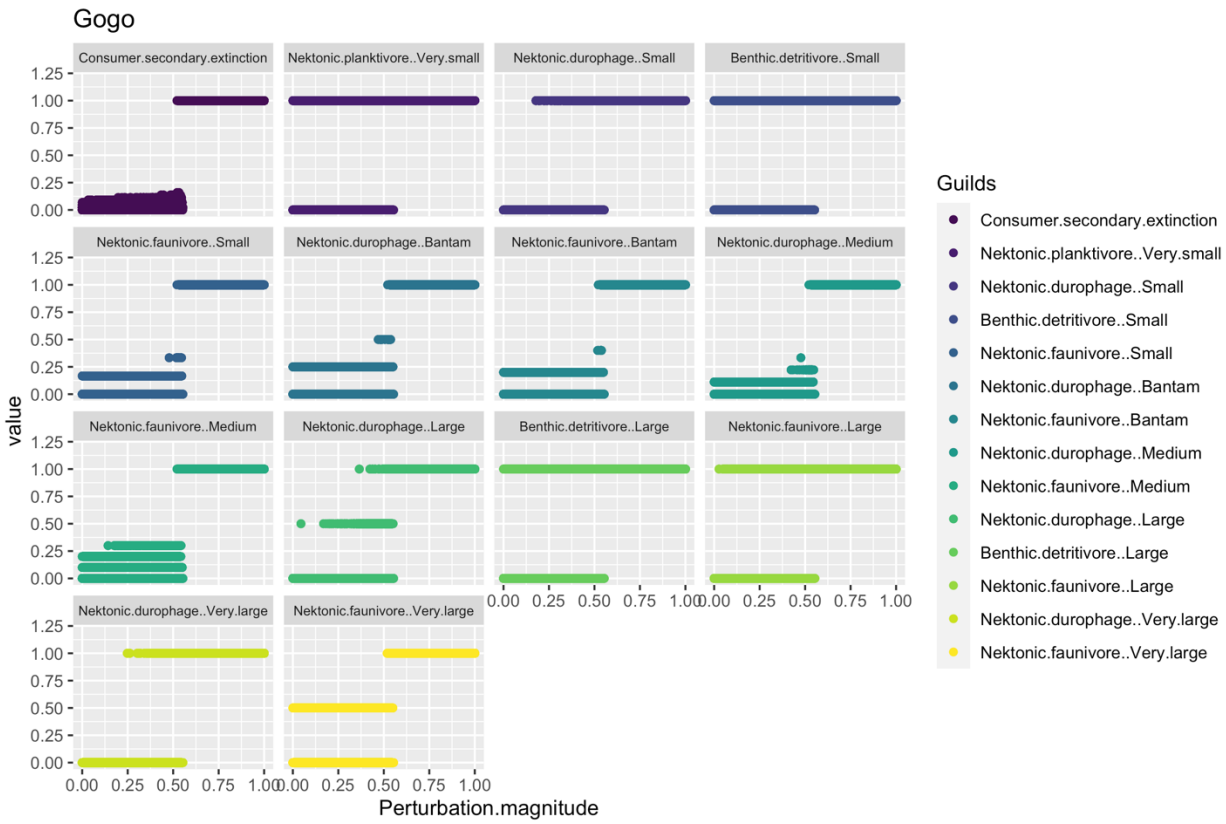

Figure 4.18. Guild-level results of Gogo CEG response (consumers/enumerated guilds only).

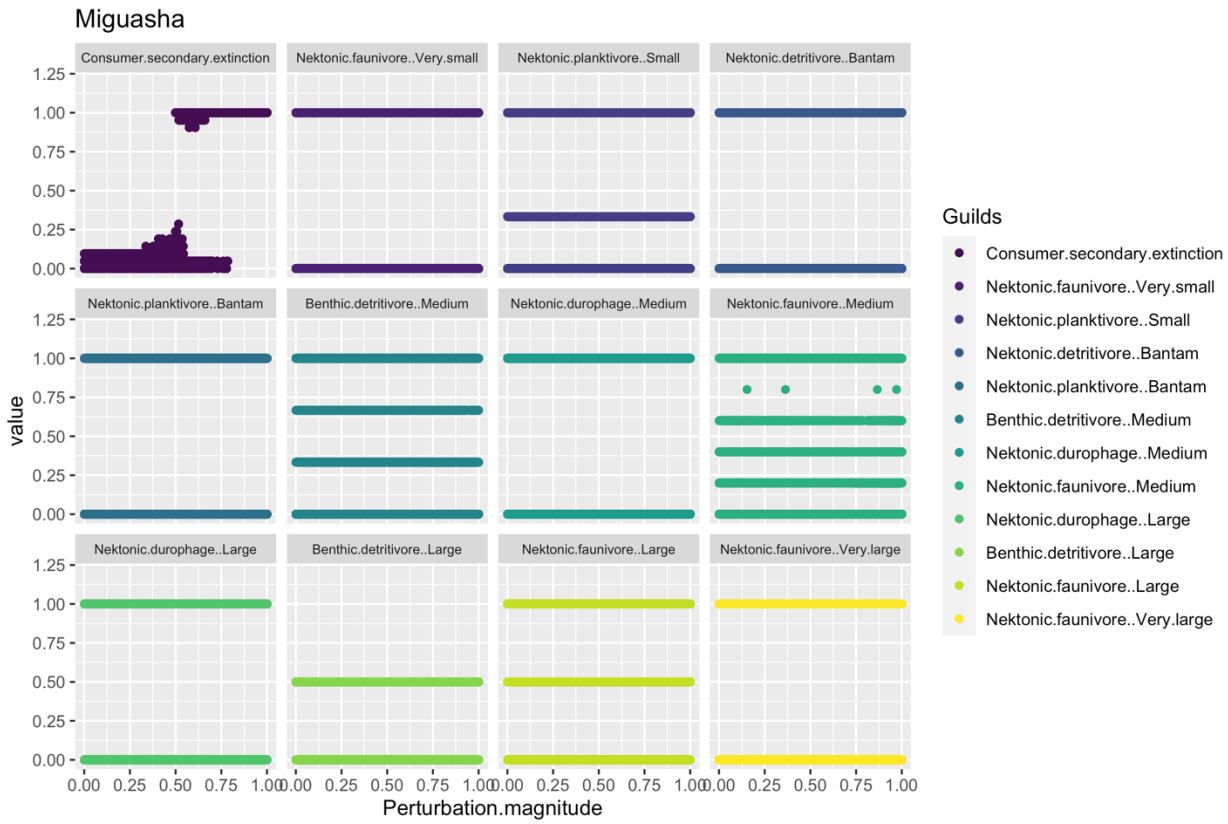

Figure 4.19. Guild-level results of Miguasha CEG response (consumers/enumerated guilds only).

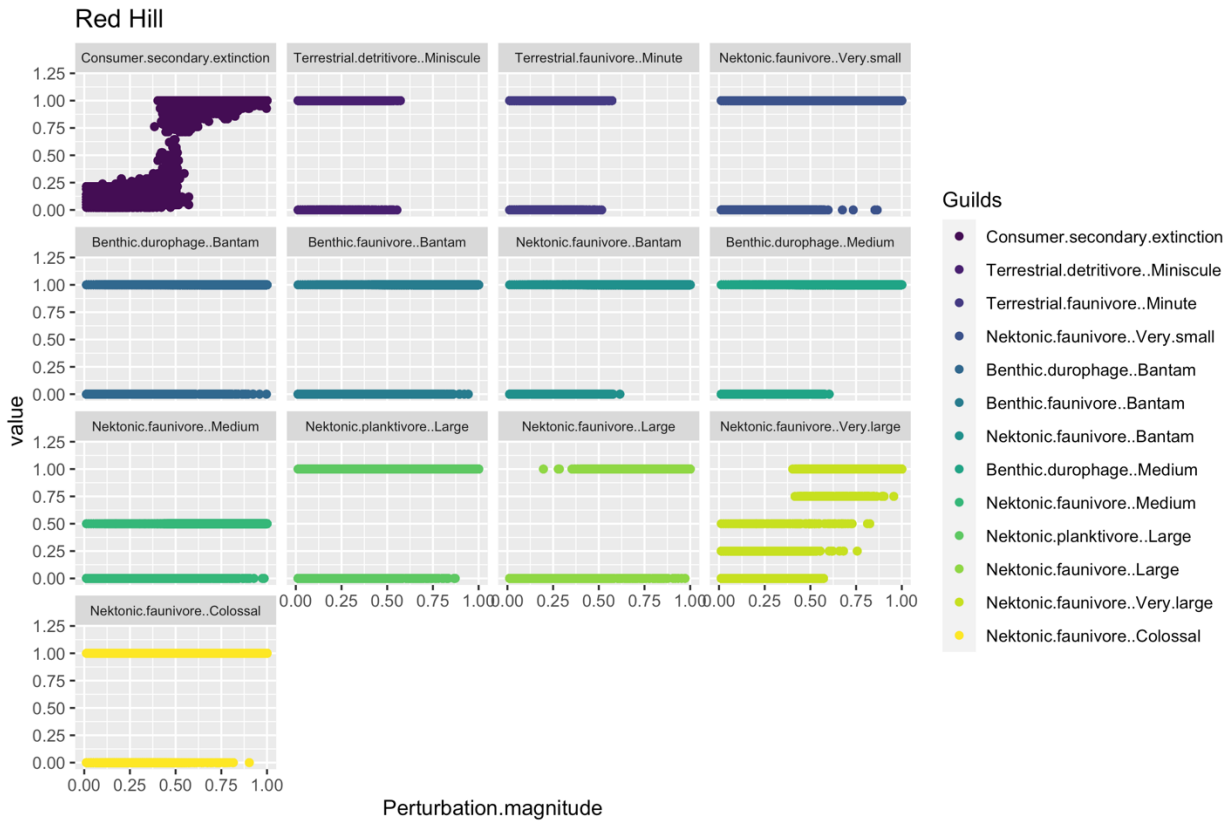

Figure 4.20. Guild-level results of Red Hill CEG response (consumers/enumerated guilds only).

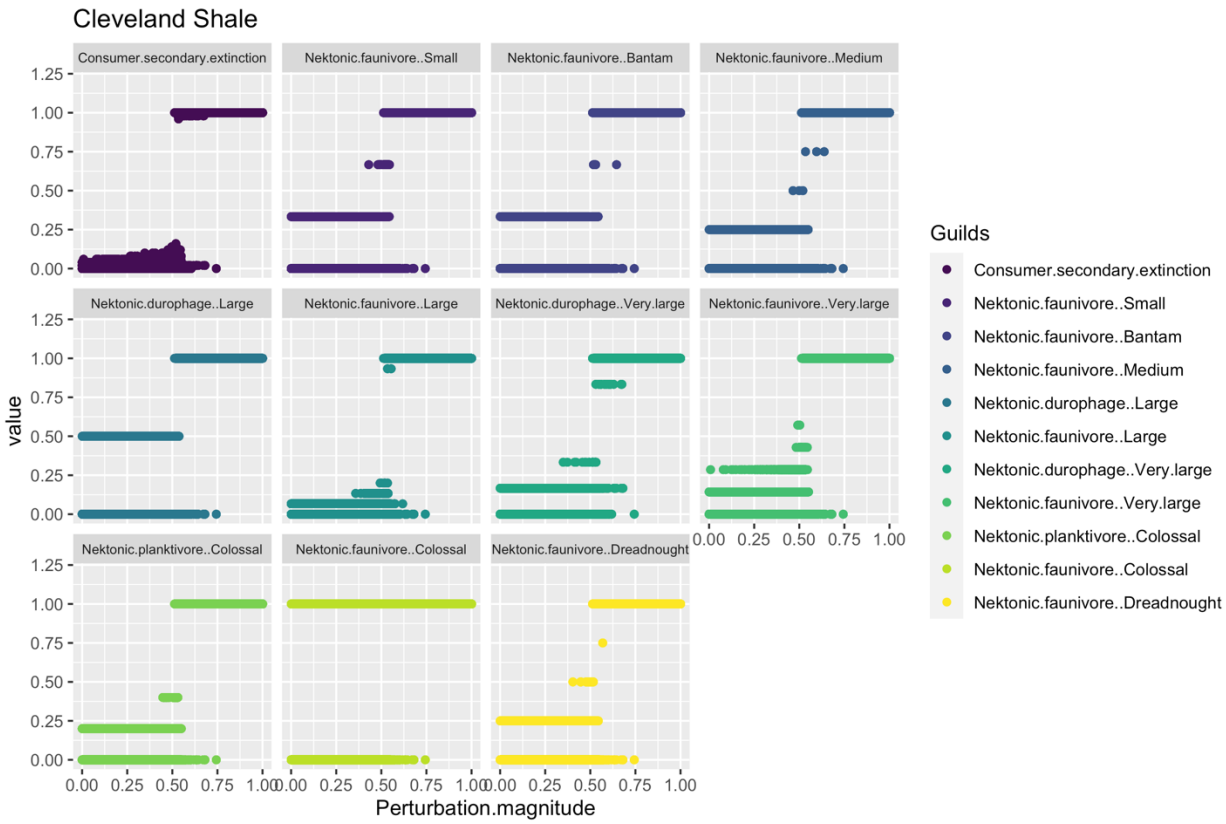

Figure 4.21. Guild-level results of Cleveland Shale CEG response (consumers/enumerated guilds only).

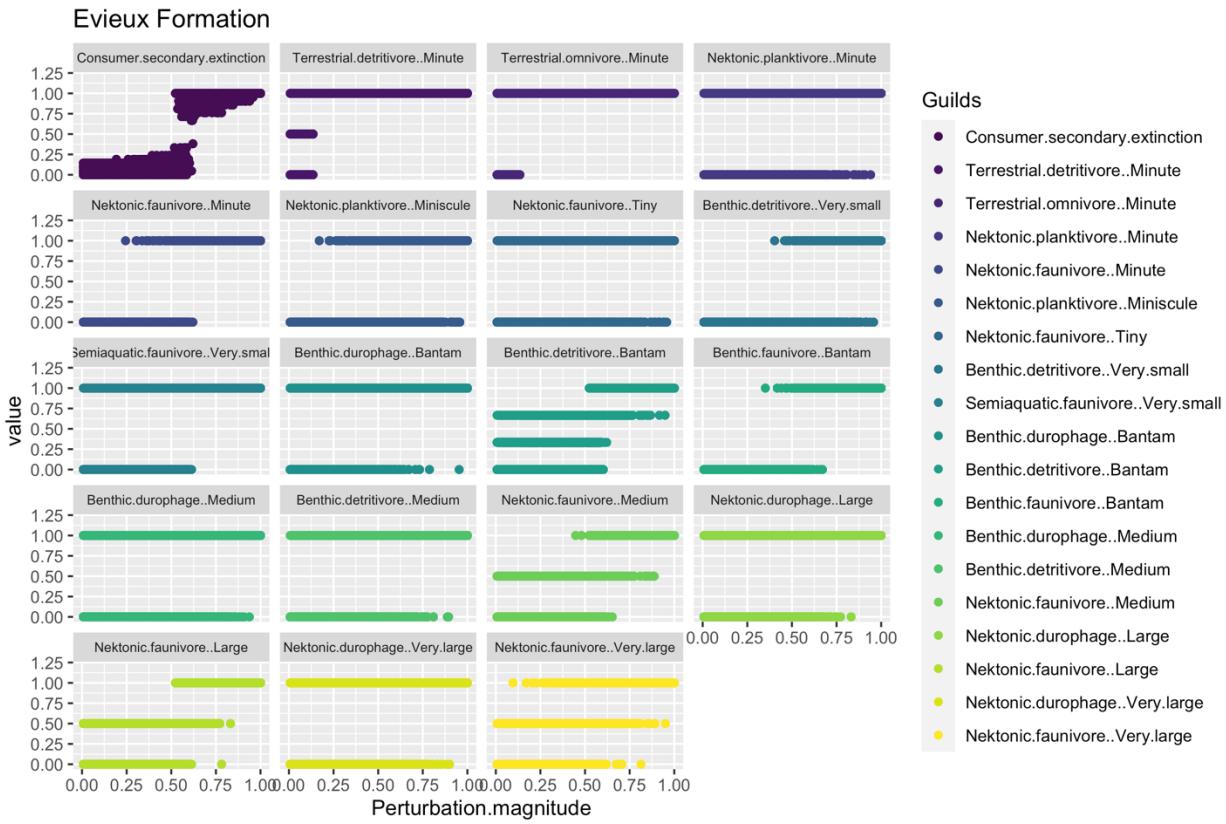

Figure 4-22. Guild-level results of Evieux Formation CEG response (consumers/enumerated guilds only).

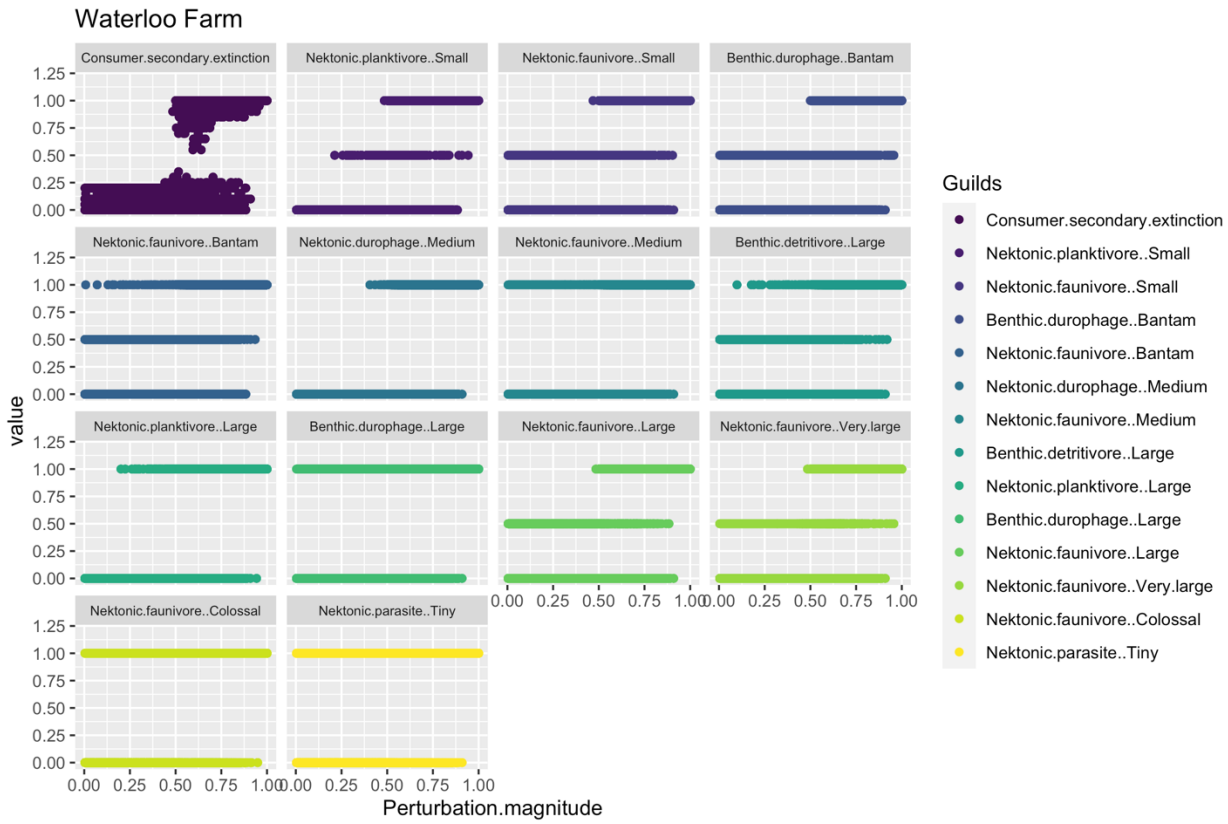

Figure 4.23. Guild-level results of Waterloo Farm CEG response (consumers/enumerated guilds only).

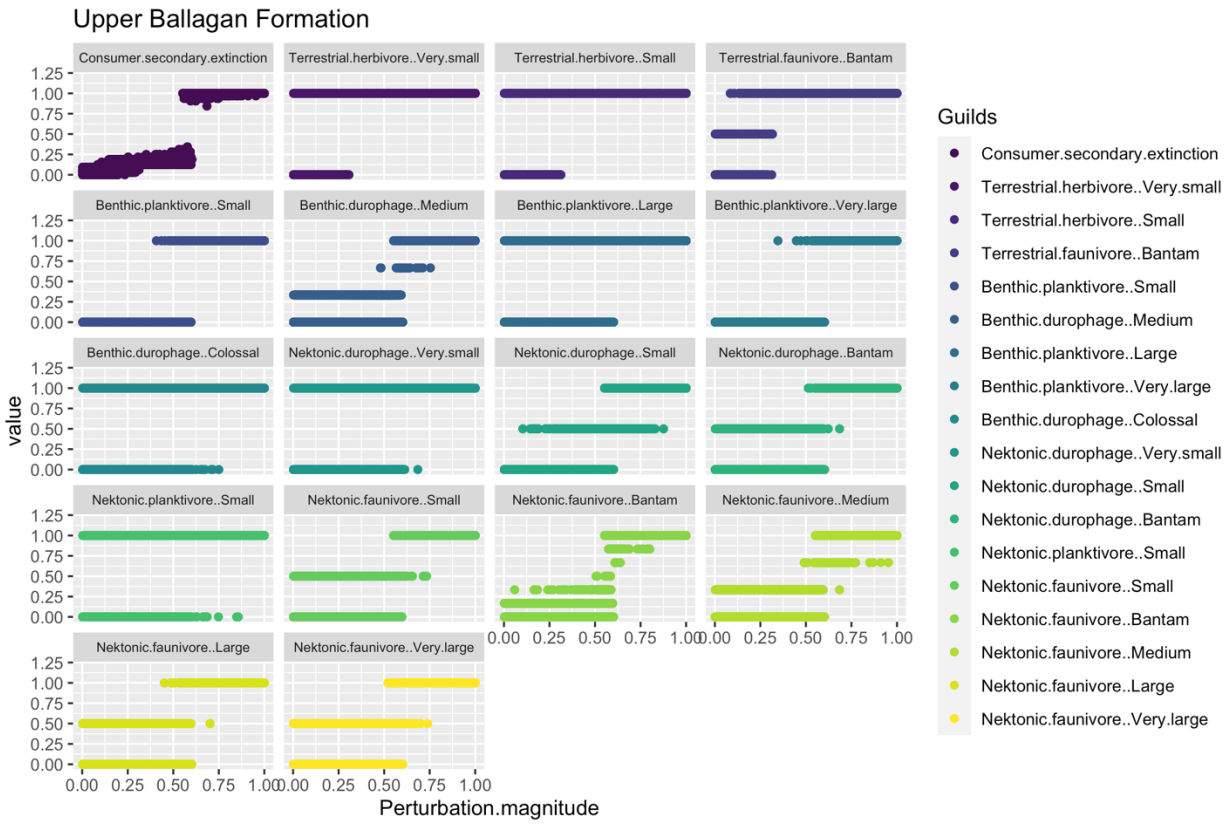

Figure 4.24. Guild-level results of Upper Ballagan Formation CEG response (consumers/enumerated guilds only).

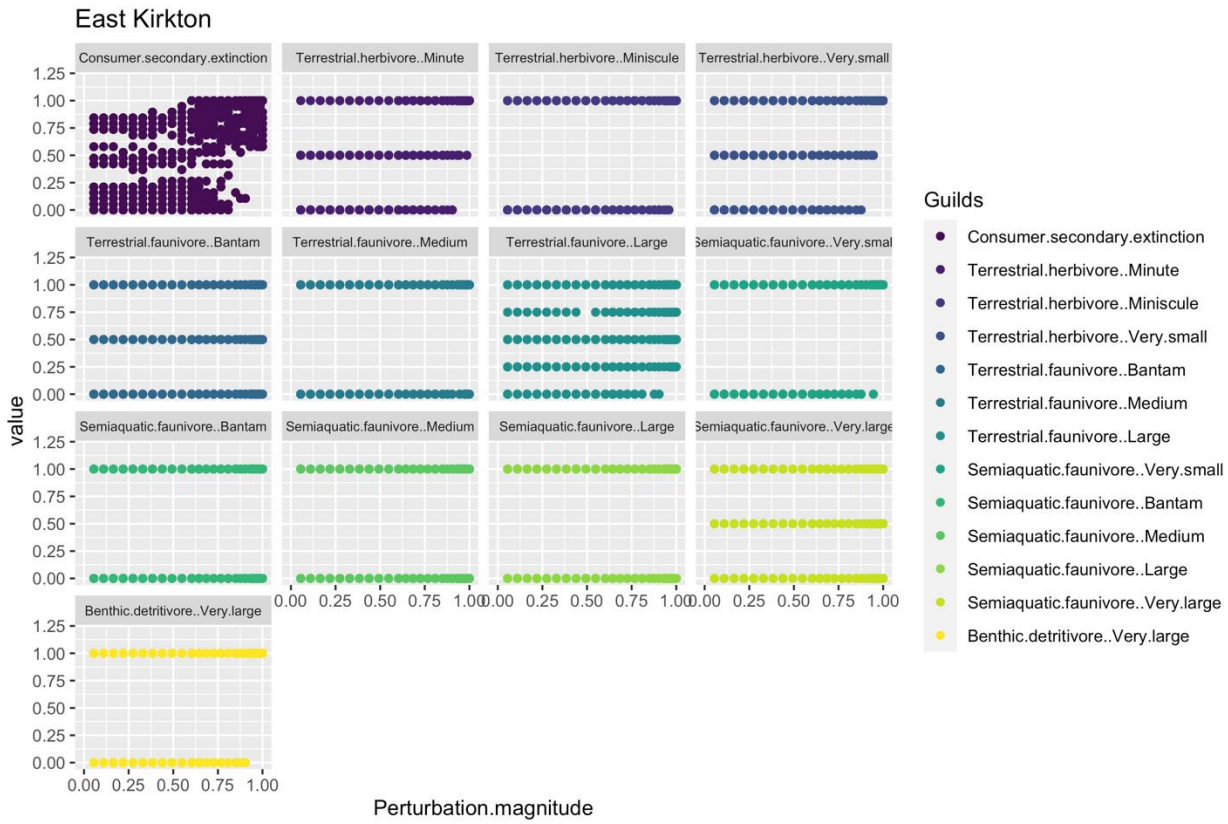

Figure 4.25. Guild-level results of East Kirkton CEG response (consumers/enumerated guilds only).

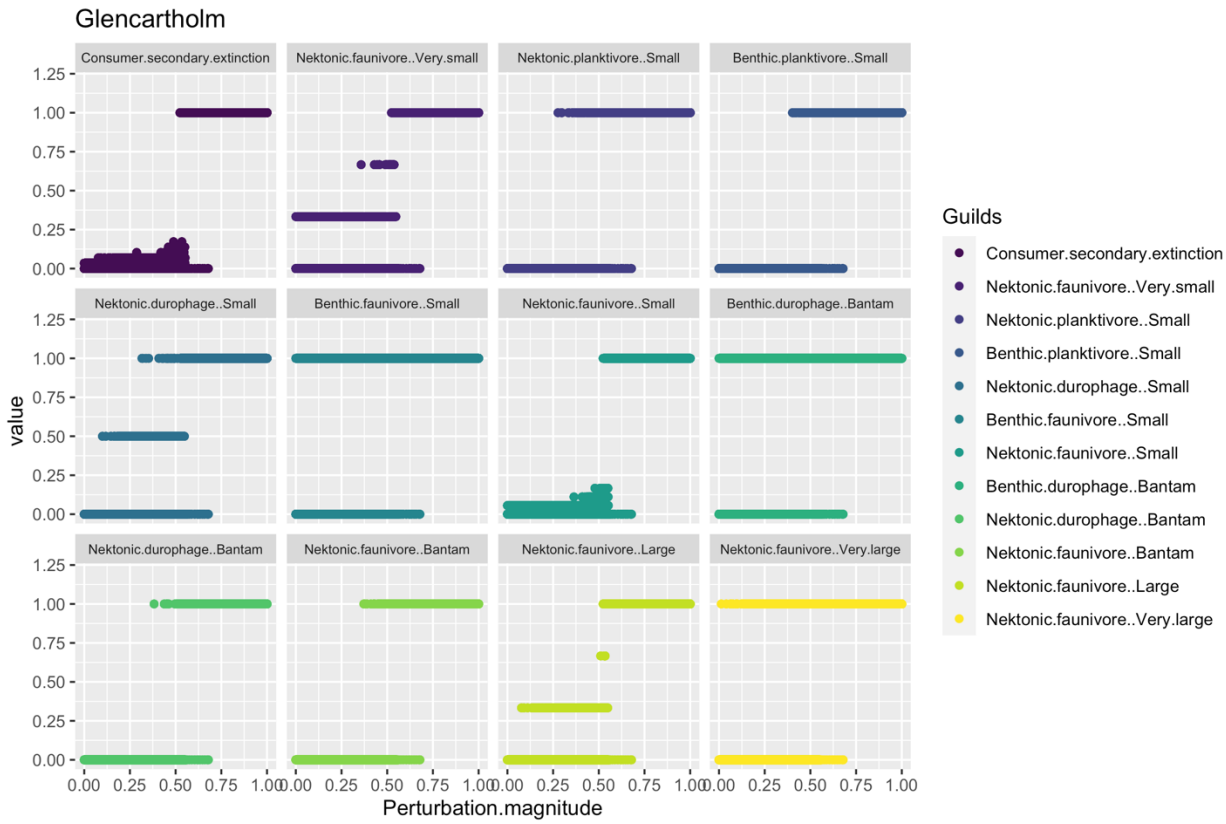

Figure 4.26. Guild-level results of Glencartholm CEG response (consumers/enumerated guilds only).

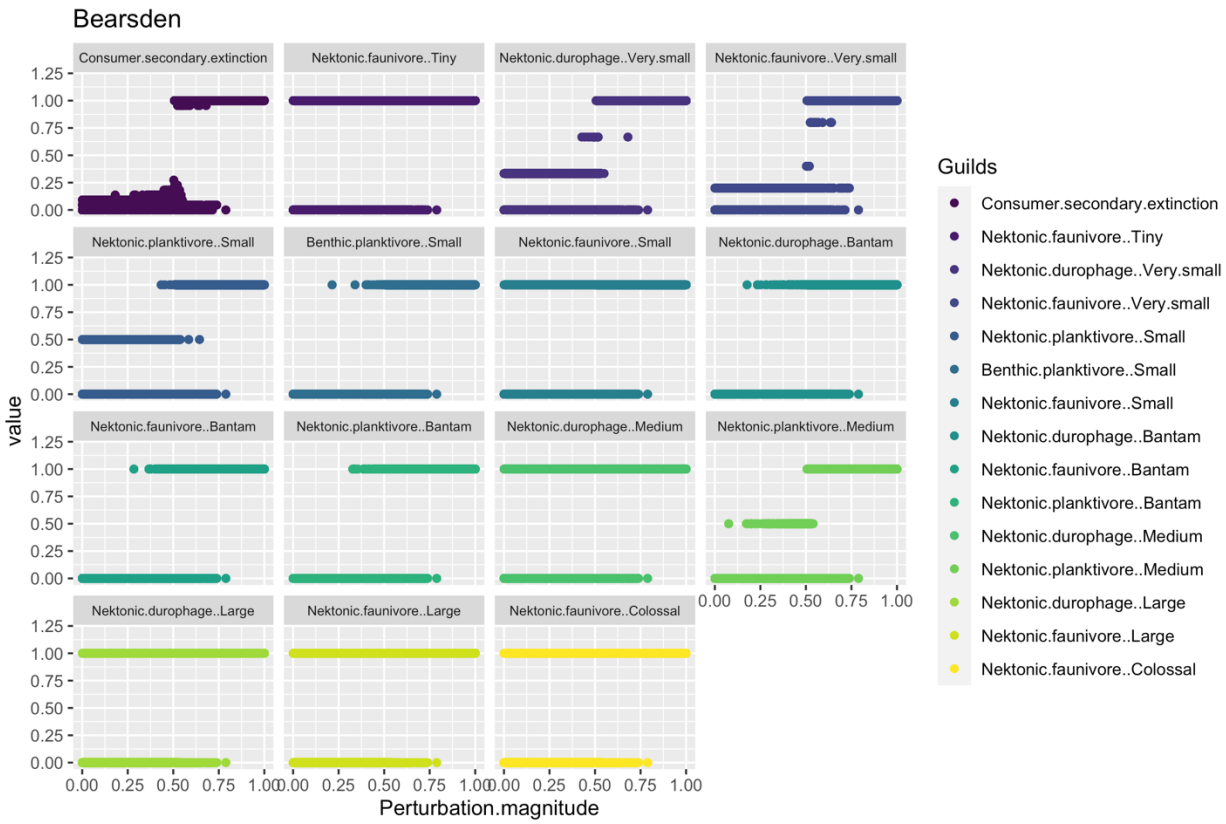

Figure 4.27. Guild-level results of Bearsden CEG response (consumers/enumerated guilds only).

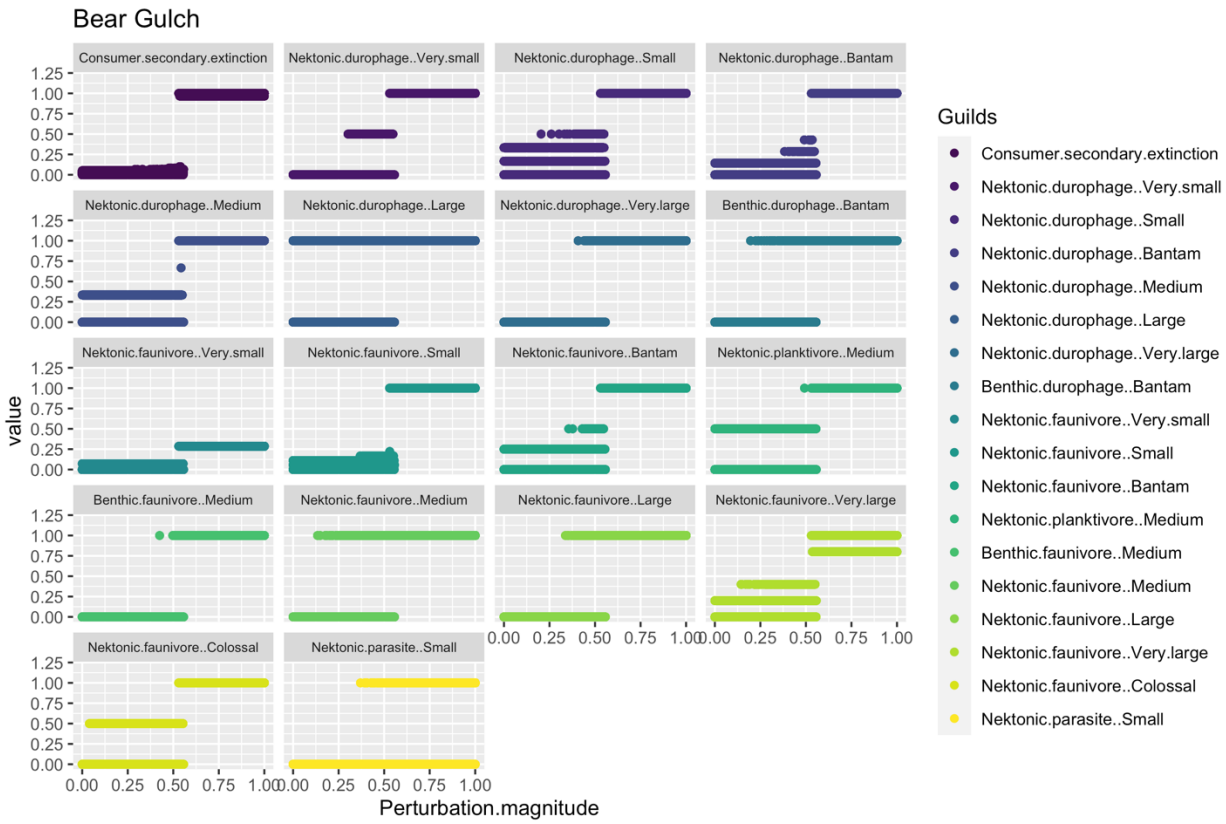

Figure 4.28. Guild-level results of Bear Gulch CEG response (consumers/enumerated guilds only).

4.6 DISCUSSION

4.6.1 Taxonomic and guild composition though the Frasnian-Famennian and end-Devonian mass extinctions

Taxonomically, the primary distinction between Devonian and Carboniferous assemblages is the absence of placoderms from the latter (Sallan and Coates, 2010; Otoo et al., 2018). The absence of the diverse and abundant detritivorous antiarchs from nonmarine paleocommunities is particularly conspicuous. There is some evidence that general (marine) vertebrate diversity declined from the middle to terminal Famennian (Frey et al., 2018), but large macropredators like *Dunkleosteus* and benthic detritivores like *Bothriolepis* persist to the terminal Famennian in Morocco (Frey et al., 2018) and South Africa (Long et al., 1997). Several taxonomic changes explain the dispersal of the Famennian sites relative to the Frasnian ones in NMDS space. Armored jawless fishes were effectively extinct by the start of the Famennian (Sallan and Coates, 2010); if they are removed from Aztec (Givetian, continental) and Miguasha (Frasnian, estuarine) these paleocommunities resemble the sarcopterygian-placoderm-acanthodian assemblages found in similar environments elsewhere in the Devonian (Supplementary Information). Cleveland Shale is famous for its placoderm diversity, but its holocephalan diversity, second only to Bear Gulch (Supplementary Information) sets it apart from Gogo/Kerman/Gladbach (Figure 4.6). *Elpistostege* from Miguasha is the only Frasnian panderichthyid in the data; Waterloo Farm and Red Hill have greatly increased panderichthyid/tetrapod diversity (four species), approaching Mississippian levels. Therefore, there does not appear to be an obvious FFME vertebrate turnover, but rather the further winnowing of declining groups (various armored jawless fishes) and radiation of others (tetrapods and relatives, holocephalans). A caveat is that the lumping all placoderms within a

single taxonomic bin, while circumventing existing challenges in placoderm phylogeny (Carr et al., 2009; Trinajstic and Long, 2009; Brazeau and Friedman, 2014, 2015; King et al., 2016), may obscure lower-level patterns of placoderm loss across the Frasnian-Famennian boundary. However, the more granular analysis of Sallan and Coates did not find evidence of a major placoderm extinction in the FFME (Sallan and Coates, 2010). A guild-based assessment is complicated by the removal of the Cleveland Shale, Gilboa, and East Kirkton which exacerbates existing unevenness in numbers across stages and environmental categories (Figure 4.10, Figure 4.11). But there do not appear to be indications of radical change in guild presence/absence or relative richness through the FFME or EDME. The former appears to still be a relative nonevent for vertebrates These results reinforce the hypothesis that the Frasnian-Famennian extinction was a nonevent for vertebrates. The apparent lack of vertebrate reaction to the FFME reef collapse implies that Devonian reefs represented species congregating together rather than unique biodiversity hotspots as in the modern day (Bellwood and Hughes, 2001; Connolly et al., 2005; Cowman and Bellwood, 2013; Parravicini et al., 2013; Hodge et al., 2014; Bellwood et al., 2019). While the Gogo fauna is a case of exceptional preservation, fragmentary specimens collected from other Devonian reefs may provide other vertebrate assemblages for same-habitat comparisons. By contrast, during the EDME there was large-scale faunal turnover but strong persistence in guild structure. This response is seen in marine invertebrates during the end-Ordovician mass extinction (Droser et al., 1997, 2000; McGhee et al., 2004, 2013) and PTME (Dineen et al., 2014; Foster and Twitchett, 2014).

There is no evidence that EDME extinction response varied systematically at the guild level across environments (reefs having already collapsed in the FFME). This is paralleled by the

taxonomic NMDS results when grouped by environment (Figure 4.7). The results of the guild NMDS (outliers removed) indicate that in terms of guild compositions, continental food webs are effectively 'upriver' transpositions of estuarine food webs. Ecological similarity between continental and estuarine settings was likely maintained by widespread euryhalinity in Devonian-Carboniferous nonmarine vertebrates (Lebedev and Clack, 1993; Lebedev and Coates, 1995; Laurin and Soler-Gijón, 2001; Ó Gogáin et al., 2016; Goedert et al., 2018), though environmental preferences likely varied between taxa (Ó Gogáin et al., 2016). This is what would be expected under a scenario in which the expansion of vertebrates into nonmarine environments was driven (at least initially) by use of nearshore environments for reproduction (Carpenter et al., 2014; Ó Gogáin et al., 2016; Otoo et al., 2018; Gess and Whitfield, 2020). This would create nonmarine (estuarine and continental) faunas that mostly replicated marine ones (as seen here) rather than a taxonomic or functional subset.

The 'true' terrestrial paleocommunities do represent divergences within the dataset, but these deviations may be in part due to how these paleocommunities are categorized and studied, and in part due to the exceptional nature of East Kirkton. Gilboa's arthropods and forest were part of a coastal wetland system, and there is no reason to conclude that proximate water bodies were not populated by aquatic vertebrates, though I have not been able to find published information on these. If the Gilboa terrestrial assemblage and Aztec aquatic assemblage were combined into a single theoretical Givetian paleocommunity, the result would be structurally the same as Red Hill, which has a small fauna of terrestrial arthropods living alongside aquatic vertebrates in a coastal delta system (Cressler et al., 2010). There is no evidence to support modeling feeding relationships across the water-land interface in the case of Gilboa, Aztec, or

Red Hill, but semiaquatic arthropods are seen in the Famennian in the Evieux Formation (Lagebro et al., 2015; Olive et al., 2015; Denayer et al., 2016). Thus, the separation of Gilboa and East Kirkton into a separate category is somewhat artificial in that it creates a hard separation where there would not have been one in life (East Kirkton being a special case). The question of how the earliest 'terrestrial' paleocommunities should be defined or diagnosed as such is explored later in the Discussion.

4.6.2 Top-down pressure and perturbation response in Devonian and Mississippian vertebrate paleocommunities

The CEG results here (Figure 4.12, Figure 4.13, Figure 4-14-Figure 4-29) strongly contrast with previous work on the PTME (Roopnarine et al., 2018). Rather than a smoothly sigmoidal curve with substantial variance throughout (~10% above and below the best-fit), these Devonian-Mississippian curves rapidly transition from a low extinction regime to a high extinction one (with exceptions, see Results). Devonian-Carboniferous and PTME food webs both show increased secondary extinction at approximately 50% perturbation. However, in the Devonian-Mississippian food webs secondary extinction increases to extremely high levels (85-100%). PTME paleocommunities do not consistently reach total secondary extinction until 80% perturbation. The conclusion, then, is somewhat counterintuitive: Devonian-Mississippian food webs were stable but susceptible to total collapse at a relatively low perturbation threshold. This is even true for those paleocommunities- Red Hill, Evieux Formation, Waterloo Farm, and Upper Ballagan Formation- that are closest to the EDME. While the nonmarine Famennian paleocommunities display increased variance in secondary extinction, they are still far more

stable than the earliest Triassic *Lystrosaurus* Assemblage Zone disaster fauna (Roopnarine et al., 2018).

The paleocommunity responses to perturbation may be due to top-down effects. While planktivores, detritivores, and durophages are present, faunivores of various sizes and habits are most common among vertebrates. These have very broad prey profiles, able to feed on any consumer guild of overlapping habit and equal or smaller size. Guild richness is generally low, evenness is high, and patterns of connection in the metanetwork are broad. Predation pressure on individual species is usually low, as each predator species has numerous species it can feed on and will likely not go extinct if a prey species goes extinct. Cascades are thus unlikely. High secondary extinction at low perturbation is likely the result of species-level webs wherein predators are reconstructed as specialists. In these species-level webs, predation pressure on prey species is much higher, predators are much more likely to go extinct, and cascades are much more likely to occur. In both the 'generalist predator' and 'specialist predator' species-level food webs, the severity of secondary extinction cascades is exacerbated by low guild richness. Because in most cases there are few species within each guild, the secondary extinction response of each guild is largely binary: the guild persists or collapses completely. At approximately 50% perturbation, primary productivity loss is sufficient to induce cascades regardless of the topology of the species-level food web. Whereas at lower levels of perturbation the broad patterns of connection in the metanetwork had insulated against cascades, now they allow cascades to propagate to more of the species-level food web. And because of low guild richness, cascades cause near- or total collapse immediately, contrasting with the initial interval of 'intermediate' pre-collapse secondary extinction seen at ~50-75% perturbation levels in other CEG analyses.

In some cases, there are replicates in which the paleocommunity does not collapse and persists at high levels of perturbation (Figure 4.16, Figure 4.19, Figure 4.23). These appear to be the result of particularly resilient species-level food webs (KD Angielczyk pers. comm. October 2022, PD Roopnarine pers. comm. August 2022). Initial inspection of high perturbation/low secondary extinction areas of select CEG curves did not reveal any meaningful patterns, but a more thorough comparative investigation may prove more illuminating. Comparison of Famennian resilient food webs to simulations derived from the same metanetworks (Roopnarine et al., 2019) and models of preserved Mississippian paleocommunities help indicate the likelihood that these resilient food webs could have remained stable and the extent to which they resemble the modeled paleocommunities based on the post-EDME fossil record. Results of these investigations would provide a new way to assess which guild relationships survived the EDME to be part of Mississippian food webs.

The three nonmarine Famennian paleocommunities- Waterloo Farm (estuarine), Evieux (continental), and Red Hill (continental) exhibit increased variance across all perturbation values and a reduced disjunct between the low- and high-extinction regimes (Figure 4.12, Figure 4.20, Figure 4.22, Figure 4.23). All (Red Hill- continental, Evieux Formation- continental, Waterloo Farm- estuarine) are nonmarine, and the appearance of this variance across multiple environmental categories is suggestive. Most straightforwardly, it can be interpreted as further evidence of ecological similarity between continental and estuarine paleocommunities (see above). Similar increased variance was found by Mitchell et al. (2012) in their analyses of Late Cretaceous communities before and after the closing of the Western Interior Seaway and linked to biogeographic changes. However, in the case of these unusual Famennian paleocommunities a

biogeographic driver seems less likely. They vary considerably in taxonomic composition (Figure 4.9, Figure 4.10, Figure 4.11) and are geographically very disparate (Figure 4.1). While this increased variance could be a tantalizing indication of pre-EDME instability, the reason for it is unclear. No common driver is indicated by the guild-level responses (Figure 4.20, Figure 4.22, Figure 4.23) but may be revealed by investigation of food web connectance.

4.6.3 First steps under duress: the first terrestrial vertebrate paleocommunities

The terrestrial paleocommunities, Gilboa (Givetian) and East Kirkton (Visean) are distinct from all other paleocommunities across analyses. In terms of guild structure and arthropod diversity, East Kirkton is a straightforward expansion of Gilboa, adding species and body size diversity. The Late Devonian terrestrial arthropod record supports the hypothesis that the East Kirkton arthropod fauna represents an expansion on pre-EDME diversification trends of lineage diversification and adaptation for terrestrial life, rather than elimination of a Devonian terrestrial arthropod assemblage and wholesale replacement by a taxonomically and functionally distinct one. Tetrapods, then, appear to be late arrivals that fit into faunivore guilds that were already occupied by arthropod faunivores. This must be inferred pending further fossil discoveries, but there is good indirect evidence. The terrestrial guilds at Gilboa and Red Hill are populated by arthropods below ~2cm in length, much smaller than the smallest tetrapod in the dataset (*Kirktonecta*, estimated ~8cm, East Kirkton) and likely below the minimum size threshold for contemporary tetrapods. Tetrapod-sized (~24cm) scorpions appear in the Upper Ballagan Formation but terrestrial tetrapods are absent. At least until East Kirkton time, the expansion of terrestrial guild diversity appears to have been driven by arthropods first, with tetrapods following afterwards.

The high instability of these terrestrial paleocommunities probably reflects the fact that they were spatially and structurally marginal within the broader habitat. The vegetated habitats of the Gilboa arthropods (Stein et al., 2012) and their Late Devonian counterparts (Cressler et al., 2010) were clustered around the same water bodies populated by tetrapods and other vertebrates (while Gilboa is Givetian and no tetrapods are preserved, there is no paleoenvironmental evidence to suggest that the tropical delta system would have been inhospitable to them if given the opportunity). Rather than bold forays into virgin territory and new parts of ecospace, the initial phase of tetrapod terrestrialization appears to have been a hardscrabble existence, competing with arthropod incumbents in a physiologically challenging environment. These paleocommunities have narrower resource bases (no ubiquitous plankton) and a stricter distinction between primary consumers (herbivores and detritivores) and secondary consumers (faunivores). Intraguild cannibalism would have presumably been a particularly important feature of these paleocommunities (not modeled here due to current methodological constraints of CEG). Neither the East Kirkton nor Loanhead (*Caerorhachis* here modeled as being semiaquatic) indicate that the addition of tetrapods to terrestrial paleocommunities conferred greater resilience or stability. Indeed, it is likely that top-down predation pressures only increased as tetrapods made the water/land transition.

Whence, then, tetrapod terrestriality? Feeding on terrestrial arthropods is unlikely, as aquatic resources were both more abundant and more accessible, both at the individual level (ability to feed by suction) and macroevolutionary level (necessity of substantial adaptations of sensory and locomotor systems to move and feed on land to any great extent). If not a pull, then perhaps a push. The terrestrial East Kirkton tetrapods are overwhelmingly small (>60cm;

Ophiderpeton (?semiaquatic) was likely longer (80-100cm), but as a limbless, snakelike form was much less massive than a limbed tetrapod of similar linear body length). Across the CEG results, decreasing body size entails greater top-down predation pressure and reduced prey opportunities. However, small body size, a derived trait for both the lissamphibian and amniote lineages, would have facilitated movement across the water/land interface and overland. The size differential between the smallest tetrapods and potential predators would have been much smaller in the terrestrial (ex. 30cm (*Westlothiana*)/80cm (*Pulmonoscorpius*) than aquatic (~8cm (*Kirktonecta*)/175-200cm (East Kirkton embolomere and temnospondyl) realms. Analogous to the movement of vertebrates into nonmarine environments for reproduction, one-time overland journeys for reproduction, such as indicated by bone histology in the aquatic tetrapod *Greererpeton* (Whitney and Pierce, 2021), may have been a starting point for the evolution of terrestriality. While a comprehensive ecological hypothesis of tetrapod terrestrialization is attractive, phylogenetic and anatomical data (Chapter 3) suggest multiple independent terrestrialization events, possibly via different processes.

It is then possible to designate three phases of terrestrial paleocommunity evolution through the study interval (Figure 4.16). In the first (Givetian), terrestrial plants and invertebrates are few or absent and the terrestrial paleocommunity is extremely simple. In the second (Famennian), vegetation is more extensive, and arthropods are more established. In the third (Visean), arthropod lineage and guild diversities have further increased, and terrestrial and semiaquatic tetrapods are present. The terrestrial tetrapods are relatively small and feed on terrestrial, rather than aquatic, prey.

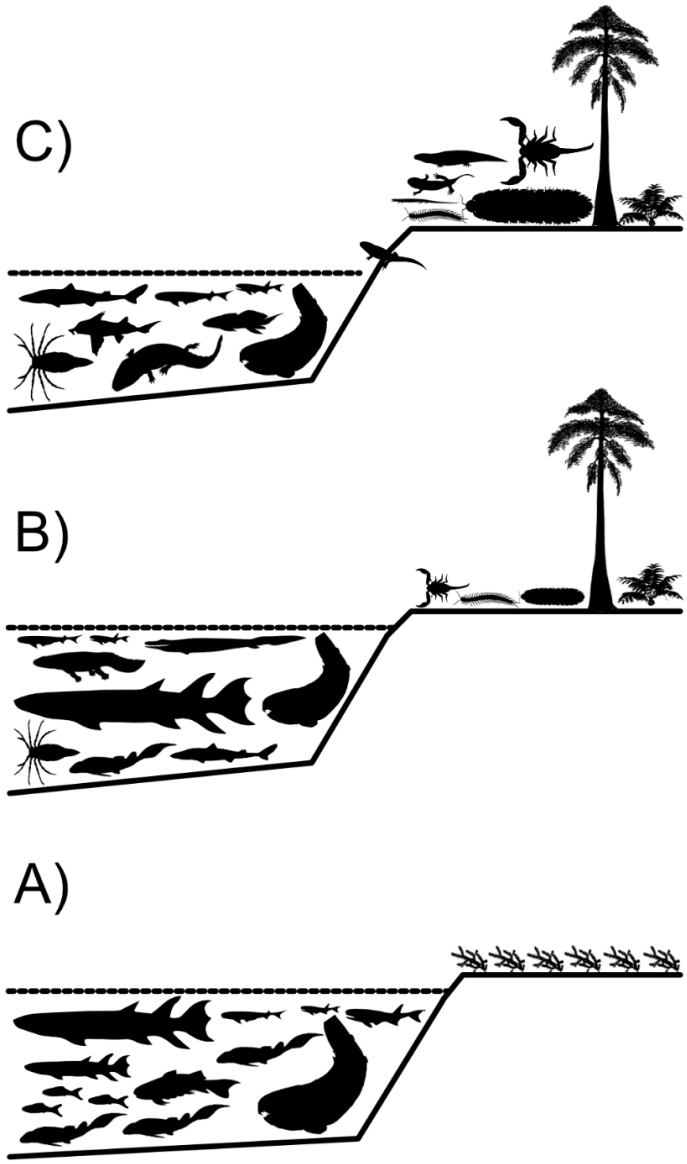

Figure 4.29. Schematic showing progression of continental/'terrestrial' paleocommunity types from the Givetian-Serpukhovian. A) Givetian/Frasnian paleocommunity such as Aztec or Miguasha with minimal or absent terrestrial arthropods, limited terrestrial flora, and high aquatic vertebrate diversity. B) Famennian such as Red Hill or Waterloo Farm, with more complex terrestrial arthropod assemblage, diverse and complex terrestrial flora. Tetrapods are present but aquatic. C) Mississippian paleocommunity such as Loanhead, with increased arthropod diversity. Aquatic, semiaquatic, and terrestrial tetrapods are present. Silhouettes from PhyloPic; individual sources are presented in APPENDIX C.

The uniqueness of East Kirkton as a terrestrial tetrapod assemblage should be emphasized. East Kirkton appears within a dense sequence of tetrapod localities in the Scottish mid-late Visean and Serpukhovian (Smithson, 1985a), none of which resemble East Kirkton. It still lacks clear precursors in the Tournaisian (Smithson et al., 2012; Clack et al., 2016; Otoo et al., 2018) or Late Devonian (Eberle, 2008; Cressler et al., 2010; Broussard et al., 2018, 2020). The next oldest locality to preserve terrestrial tetrapods is the early Pennsylvanian (Moscovian) Joggins fauna (Falcon-Lang et al., 2006; Mann et al., 2020), where 'microsaurs' and crown amniotes are abundant. As at East Kirkton, the lissamphibian lineage is much less diverse by comparison, represented by only *Dendrerpeton* (with the caveat that the taxonomy of the Joggins temnospondyl(s) is an area of active ongoing research (Arbez et al., 2022)). The apparent asymmetry between the lissamphibian and amniote total groups during the origins of terrestrial tetrapods merits further investigation.

In Olson's framework, the distinction between Type I and Type III paleocommunities was that primary productivity base is aquatic plants in Type I and terrestrial plants in Type III (Olson, 1966). In Type III, herbivorous/detritivorous arthropods are the connection between primary productivity and terrestrial predators. From the middle Devonian (Gilboa) onward, terrestrial plants are the primary productivity for terrestrial consumer guilds. East Kirkton, then appears to combine features of Olson's Type I (absence of terrestrial vertebrate herbivores) and Type III (terrestrial plants primary productivity base for terrestrial guilds). East Kirkton could be considered an early iteration of Olson's Type III paleocommunity, his (implicit) assumption that paleocommunities from the Carboniferous-Permian transition represented the initial structure of terrestrial vertebrate ecosystems (Olson, 1966) remains to be tested. The results presented here

suggest that the origin of terrestrial tetrapod paleocommunities may have been less linear than Olson's scenario of succession entails. At the very least, the decoupling of the aquatic and terrestrial realms took place during the Carboniferous instead of during the Permian. Ongoing work (JD Pardo, PA Viglietti, et al., unpublished research) will test whether Olson's community types represent different community stability regimes.

4.7 FUTURE DIRECTIONS

In future iterations of this and related datasets, benthic guilds will be available to access phytoplankton and zooplankton, as observed in benthic invertebrates and inferred in their Paleozoic counterparts (Brower, 2007; Baumiller, 2008; Dynowski et al., 2016; Meyer et al., 2021). Use of empirical invertebrate species counts with very low guild extinction probabilities may produce a model that is not 'swamped' by guilds with thousands of simulated species/units. This method would more precisely capture the significance of the diverse shrimp fauna preserved in the Mississippian Scottish Midland Valley at localities such as Glencartholm (Briggs and Clarkson, 1985, 1989; Cater et al., 1989; Clark, 1990, 2013; Zapalski and Clarkson, 2015; Wood, 2018).

Modeling of additional Late Devonian and Mississippian paleocommunities will help provide a more complete picture of the immediate pre- and post-EDME interval. The Pennsylvanian appears to be when the transition from East Kirkton-type paleocommunities to the beginnings of more modern paleocommunities, with increasing numbers of terrestrial arthropod and tetrapod herbivores, took place. This timing may have been affected by ongoing environmental disturbances in the Mississippian which stabilized early in the Pennsylvanian with

the onset of the Late Paleozoic Ice Age (Yao et al., 2015). Joggins (early Pennsylvanian) preserves numerous species of aquatic and terrestrial vertebrates and invertebrates. These are preserved across a gradient of microhabitats extending from the estuary and shoreline to the alluvial plain (Falcon-Lang et al., 2006). Comparative modeling of the component microhabitat paleocommunities will not only clarify the structure of these diverse ecosystems, but also provide an opportunity to test the impact of spatial averaging on CEG modeling.

The post-EDME 'bloom' of crinoids (Sallan et al., 2011) during the Tournaisian- leading to the formation of characteristic encrinite lithofacies- precedes an increase in the diversity and abundance of vertebrate durophages, particularly actinopterygians and holocephalans, that has garnered increasing attention recently (Schram, 1983; Coates, 1988, 1993; Sallan et al., 2011; Friedman et al., 2018; Richards et al., 2018; Wood, 2018). Further innovations include high-performance suction feeding in chondrichthyans by the Visean, millions of years before the appearance of the feeding mode in actinopterygians (Coates et al., 2019). Work focusing on Devonian and Mississippian marine paleocommunities may find that the broad functional consistency found through the Givetian-Serpukhovian may obscure smaller-scale processes of ecosystem change.

4.8 CONCLUSIONS

The well-attested taxonomic turnover at the Devonian/Carboniferous boundary is not accompanied by a comparable change in guild diversity. In NMDS analyses of taxonomic diversity, temporal and environmental variance separate between the two axes. By contrast, in NMDS analyses of guild richness each axis captures a combination of temporal and

environmental variation at different scales. Simulation of paleocommunity models from the Givetian to Serpukhovian reveals a persistent pattern of response to perturbation across environments. This pattern is defined by a rapid and disjunct transition between a regime of low perturbation/low secondary extinction and a regime of high perturbation/high secondary extinction. This is due to a combination of high guild evenness, broad prey profiles among consumers, and top-down effects. At low levels of perturbation, pressure on individual guilds is low and secondary extinction is unlikely to deprive a consumer of all its potential prey. However, at higher levels of perturbation and secondary extinction, low guild richness means that guilds are unable to accommodate the increasing predation pressure. Moreover, high evenness means that the effects of increasing predation pressure are experienced widely across guilds. The result is a secondary extinction cascade and collapse of the paleocommunity.

These perturbation responses indicate these paleocommunities were highly stable but had lower collapse/cascade thresholds than both Late Ordovician (Kempf et al., 2020) and terrestrial Permo-Triassic (Roopnarine et al., 2018) paleocommunities, indicating that these results do not simply reflect modeling differences between aquatic and terrestrial paleocommunities. From the middle Devonian to the Mississippian, terrestrial paleocommunities developed through increasing diversity of terrestrial arthropods. Tetrapods joined these paleocommunities as competitors to arthropod predators. These earliest terrestrial paleocommunities were highly unstable and both spatially and energetically marginal to the continental aquatic paleocommunities that contained the overwhelming bulk of vertebrate ecological activity (with the caveat that this pattern may be exaggerated by low species diversity of Gilboa and East Kirkton). Future work should leverage the comparatively richer Pennsylvanian tetrapod record to

provide points of comparison to Mississippian and Permian paleocommunities and further elucidate the rise of terrestrial vertebrate ecological paleocommunities.

CHAPTER 5: CONCLUSIONS AND FUTURE DIRECTIONS

5.1 CONCLUSIONS

Information from *Whatcheeria* (Otoo et al., 2021; Rawson et al., 2021) and recent phylogenetic work both here and in the literature (Pardo et al., 2017b; Beznosov et al., 2019) suggests that the earliest tetrapod radiations were more complex than previously appreciated. Rather than being a stepwise acquisition of terrestrial locomotor adaptations suggested by analysis of individual character sets in isolation (Dickson et al., 2020), the tetrapod stem group represents multiple complex character combinations and, possibly, functions. *Whatcheeria* is emblematic of this, combining large, robust limbs and girdles with lateral line canals on the skull (Figure 3.2). Contra previous hypotheses of whatcheeriids or 'whatcheeriids' being a Late Devonian-Mississippian grade of plesiomorphic tetrapods, the whatcheeriids are a clade of stem tetrapods that can be diagnosed by large limbs, regionalized ribs, and a unique femur morphology. The fossil record of the whatcheeriids is limited to the Mississippian (Chapter 2), but phylogenetic analysis supports a Devonian origin for the whatcheeriids, baphetids, and other lineages known from the Mississippian (Chapter 3). The early colosteid *Aytonerpeton* extends the stratigraphic range of Colosteidae into the Tournaisian. The position of colosteids near the tetrapod crown group node (either as the sister group to crown tetrapods or the sister group to temnospondyls within the lissamphibian total group) suggests that crown group tetrapods may also have been part of the Devonian radiation(s). Divergent tree topologies from analyses of anatomical partitions suggest that the homoplasy notorious to early tetrapod datasets stems from diverse character combinations across phylogeny and functions. By contrast, consistency in guild structure and richness is maintained across environments through the end-Devonian mass extinction (Chapter 4). No post-extinction decrease in paleocommunity stability is found;

suggestions of increased instability in nonmarine Famennian ecosystems merits further exploration. The first terrestrial communities developed through increasing diversification of terrestrial arthropods. By the Mississippian, tetrapods joined these communities as competitors to terrestrial predatory arthropods. These terrestrial communities were structurally distinct from aquatic communities but were much more unstable. These terrestrial communities were likely spatially and energetically marginal to aquatic communities into the Pennsylvanian.

5.2 FURTHER DIRECTIONS

New fieldwork and fossil discoveries will always be important. At the same time, advances in CT scanning and surface scanning are allowing us to obtain new data from old specimens. This is particularly exciting for flattened specimens or others for which the internal morphology is obscured (and, in the case of skulls, the original geometry has been distorted). CT data have been used to produce 3D reconstructions of the skulls of *Acanthostega* (Porro et al., 2015), *Whatcheeria* (Rawson et al., 2021), and *Crassigyrinus* (Porro et al., in review), all of which differ substantially from previous reconstructions. Scans of the early temnospodyl *Eugyrinus*, known from a single poorly exposed nodule (Milner, 1980a), have revealed portions of the olfactory system and what may be the oldest clawed tetrapod foot (BKA Otoo, MI Coates, KA Tietjen, J Bevitt, unpublished data). *Eugyrinus* is significant as one of the oldest Pennsylvanian temnospondyls and a possible basal dvinosaur (Milner, 1980a; Schoch, 2013, 2018). A recent hypothesis has proposed the dvinosaurs to be the most basal temnospondyls (Pardo et al., 2017a). Moreover, a fragmentary Visean temnospondyl from Germany (Werneburg et al., 2019) may be a dvinosaur. *Eugyrinus*, then, has great potential to improve our understanding of the early evolution of Temnospondyli.

Recent, ongoing, and future morphological and phylogenetic research has supported the growing field of paleobiology. Very recent skeletochronological work has revealed an unexpected diversity of life history strategies and metabolisms in Mississippian stem tetrapods (Whitney and Pierce, 2021; Whitney et al., 2022). Many functional studies of early tetrapods have focused on locomotion, often using digitized, isolated anatomy (Pierce et al., 2012, 2013a; Dickson et al., 2020). However, as seen in *Whatcheeria*, ostensibly terrestrial limbs can be present in an aquatic animal. The lateral line system is a strong osteological indicator of lifestyle, arguably more conclusive than functional inferences from appendicular anatomy. It will be important to integrate data on the lateral line (V Venkatamaran, unpublished dissertation research) into future hypotheses of early tetrapod function and terrestrialization.

Paleoecological research has great potential to provide insights into early tetrapod evolution that has long been missing. Further modeling of Devonian paleocommunities, such as East Greenland, Lode, and Andreyevka will help us understand the range of food web structures and environmental types across which the earliest tetrapods and their immediate outgroups were distributed. Future work will also benefit from increasing integration of invertebrate (especially arthropod), floral, and paleoenvironmental data (Dunn et al., 2006; Iannuzzi and Labandeira, 2008; Olive et al., 2015; Bennett et al., 2016, 2017, 2021; Kearsey et al., 2016; Opluštil et al., 2016; Millward et al., 2018a, 2018b; Stein et al., 2019; Wang et al., 2019; Alekseeva et al., 2020; Cózar and Somerville, 2021; Strullu-Derrien et al., 2021). The effects of arthropod herbivory on Mississippian and Pennsylvanian food webs will be of particular interest. There is also increasing scope for testing paleoenvironmental hypotheses, such as the dynamism of delta environments

(Bennett et al., 2016, 2017; Kearsey et al., 2016; Otoo et al., 2018) or ‘supertides’ (Ahlberg, 2018; Byrne et al., 2020) in driving tetrapod evolution in the Devonian-Carboniferous. More and more we have the information and tools to study early tetrapods not as ancestors but rather as once-living animals in their delightful, muppetty weirdness.

REFERENCES

Adams, G. R. 2020. Description of Calligenethlon watsoni based on computed tomography and resulting implications for the phylogenetic placement of embolomeres. MS, Carleton University, Ottawa, Ontario, Canada, 155 pp.

Adams, G. R., A. Mann, and H. C. Maddin. 2020. New embolomerous tetrapod material and a faunal overview of the Mississippian-aged Point Edward locality, Nova Scotia, Canada. Canadian Journal of Earth Sciences 57:407–417.

Ahlberg, P. E. 1995. Elginerpeton pancheni and the earliest tetrapod clade. Nature 373:420–425.

Ahlberg, P. E. 2018. Follow the footprints and mind the gaps: a new look at the origin of tetrapods. Earth and Environmental Science Transactions of the Royal Society of Edinburgh 109:115–137.

Ahlberg, P. E., and A. R. Milner. 1994. The origin and early diversification of tetrapods. Nature 368:507–514.

Ahlberg, P. E., and J. A. Clack. 1998. Lower jaws, lower tetrapods-a review based on the Devonian genus Acanthostega. Transactions of the Royal Society of Edinburgh: Earth Sciences 89:11–46.

Ahlberg, P. E., and Z. Johanson. 1998. Osteolepiforms and the ancestry of tetrapods. Nature 395:792–794.

Ahlberg, P. E., and J. A. Clack. 2020. The smallest known Devonian tetrapod shows unexpectedly derived features. Royal Society Open Science 7:192117.

Ahlberg, P. E., J. A. Clack, and E. Luksevics. 1996. Rapid braincase evolution between Panderichthys and the earliest tetrapods. Nature 381:61–64.

Ahlberg, P. E., J. A. Clack, and H. Blom. 2005. The axial skeleton of the Devonian tetrapod Ichthyostega. Nature 437:137–140.

Ahlberg, P. E., J. A. Clack, E. Lukševičs, H. Blom, and I. Zupiņš. 2008. Ventastega curonica and the origin of tetrapod morphology. Nature 453:1199–1204.

Alekseeva, T. V., G. V. Mitenko, and A. O. Alekseev. 2020. The ecology of a late Visean forest at Catcraig (East Lothian, Scotland) based on multiproxy study of paleosol and root-casts. Palaeoworld S1871174X20300433.

Alfaro, M. E., F. Santini, C. Brock, H. Alamillo, A. Dornburg, D. L. Rabosky, G. Carnevale, and L. J. Harmon. 2009. Nine exceptional radiations plus high turnover explain species diversity in jawed vertebrates. Proceedings of the National Academy of Sciences 106:13410–13414.

Anderson, J. S. 2001. The Phylogenetic Trunk: Maximal Inclusion of Taxa with Missing Data in an Analysis of the Lepospondyli (Vertebrata, Tetrapoda). Systematic Biology 50:24.

Anderson, J. S., R. R. Reisz, D. Scott, N. B. Fröbisch, and S. S. Sumida. 2008. A stem batrachian from the Early Permian of Texas and the origin of frogs and salamanders. Nature 453:515–518.

Anderson, J. S., T. Smithson, C. F. Mansky, T. Meyer, and J. Clack. 2015. A Diverse Tetrapod Fauna at the Base of "Romer's Gap." PLOS ONE 10:e0125446.

Andrews, S. M., and R. L. Carroll. 1991. The Order Adelospondyli: Carboniferous lepospondyl amphibians. Transactions of the Royal Society of Edinburgh: Earth Sciences 82:239–275.

Arbez, T., J. B. Atkins, and H. C. Maddin. 2022. Cranial anatomy and systematics of *Dendrerpeton* cf. *helogenes* (Tetrapoda, Temnospondyli) from the Pennsylvanian of Joggins, revisited through micro-CT scanning. Papers in Palaeontology 8.

Aretz, M., H. G. Herbig, X. D. Wang, F. M. Gradstein, F. P. Agterberg, and J. G. Ogg. 2020. The Carboniferous Period; pp. 811–874 in Geologic Time Scale 2020. Elsevier.

Atkins, J. B., R. R. Reisz, and H. C. Maddin. 2019. Braincase simplification and the origin of lissamphibians. PLOS ONE 14:e0213694.

Bakker, R. T. 1986. The Dinosaur Heresies: New Theories Unlocking the Mystery of the Dinosaurs and Their Extinction, 1st ed. Morrow, New York, 481 pp.

Bambach, R. K. 1993. Seafood Through Time: Changes in Biomass, Energetics, and Productivity in the Marine Ecosystem. Paleobiology 19:372–397.

Bambach, R. K., A. M. Bush, and D. H. Erwin. 2007. Autecology and the filling of ecospace: key metazoan radiations. Palaeontology 50:1–22.

Bapst, D. W. 2012. paleotree: Paleontological and Phylogenetic Analyses of Evolution. .

Baumiller, T. K. 2008. Crinoid Ecological Morphology. Annual Review of Earth and Planetary Sciences 36:221–249.

Bazzana, K. D., B. M. Gee, J. J. Bevitt, and R. R. Reisz. 2020. Postcranial anatomy and histology of Seymouria, and the terrestriality of seymouriamorphs. PeerJ 8:e8698.

Beaumont, E. H. 1977. Cranial morphology of the Loxommatidae (Amphibia: Labyrinthodontia). Philosophical Transactions of the Royal Society B: Biological Sciences 280:29–101.

Becker, R. T., S. I. Kaiser, and M. Aretz. 2016. Review of chrono-, litho- and biostratigraphy across the global Hangenberg Crisis and Devonian–Carboniferous Boundary. Geological Society, London, Special Publications 423:355–386.

Becker, R. T., J. E. A. Marshall, A.-C. Da Silva, F. P. Agterberg, F. M. Gradstein, and J. G. Ogg. 2020. The Devonian Period; pp. 733–810 in Geologic Time Scale 2020. Elsevier.

Bell, M. A., and G. T. Lloyd. 2015. strap: an R package for plotting phylogenies against stratigraphy and assessing their stratigraphic congruence. Palaeontology 58:379–389.

Bellwood, D. R., and T. P. Hughes. 2001. Regional-Scale Assembly Rules and Biodiversity of Coral Reefs. Science 292:1532–1535.

Bellwood, D. R., R. P. Streit, S. J. Brandl, and S. B. Tebbett. 2019. The meaning of the term 'function' in ecology: A coral reef perspective. Functional Ecology 33:948–961.

Bennett, C. E., T. I. Kearsey, S. J. Davies, D. Millward, J. A. Clack, T. R. Smithson, and J. E. A. Marshall. 2016. Early Mississippian sandy siltstones preserve rare vertebrate fossils in seasonal flooding episodes. Sedimentology 63:1677–1700.

Bennett, C. E., A. S. Howard, S. J. Davies, T. I. Kearsey, D. Millward, P. J. Brand, M. A. E. Browne, E. J. Reeves, and J. E. A. Marshall. 2017. Ichnofauna record cryptic marine incursions onto a coastal floodplain at a key Lower Mississippian tetrapod site. Palaeogeography, Palaeoclimatology, Palaeoecology 468:287–300.

Bennett, C. E., T. I. Kearsey, S. J. Davies, M. J. Leng, D. Millward, T. R. Smithson, P. J. Brand, M. A. E. Browne, D. K. Carpenter, J. E. A. Marshall, H. Dulson, and L. Curry. 2021. Palaeoecology and palaeoenvironment of Mississippian coastal lakes and marshes during the early terrestrialisation of tetrapods. Palaeogeography, Palaeoclimatology, Palaeoecology 564:110194.

Berman, D. S., A. C. Henrici, S. S. Sumida, and T. Martens. 2000. Redescription of *Seymouria sanjuanensis* (Seymouriamorpha) from the Lower Permian of Germany based on complete, mature specimens with a discussion of paleoecology of the Bromacker locality assemblage. Journal of Vertebrate Paleontology 20:253–268.

Bernardi, M., K. D. Angielczyk, J. S. Mitchell, and M. Ruta. 2016. Phylogenetic Stability, Tree Shape, and Character Compatibility: A Case Study Using Early Tetrapods. Systematic Biology 65:737–758.

Beznosov, P. A., J. A. Clack, E. Lukševičs, M. Ruta, and P. E. Ahlberg. 2019. Morphology of the earliest reconstructable tetrapod Parmastega aelidae. Nature 574:527–533.

Bishop, P. J. 2014. The humerus of *Ossinodus pueri*, a stem tetrapod from the Carboniferous of Gondwana, and the early evolution of the tetrapod forelimb. Alcheringa: An Australasian Journal of Palaeontology 38:209–238.

Blom, H. 2005. Taxonomic revision of the Late Devonian tetrapod Ichthyostega from East Greenland. Palaeontology 48:111–134.

Boisvert, C. A. 2009. The humerus of *Panderichthys* in three dimensions and its significance in the context of the fish-tetrapod transition. Acta Zoologica 90:297–305.

Bolt, J. R. 1969. Lissamphibian Origins: Possible Protolissamphibian from the Lower Permian of Oklahoma. Science 166:888–891.

Bolt, J. R., and R. E. Lombard. 2000. Palaeobiology of Whatcheeria deltae; pp. 1044–1052 in H. Heatwole and R. L. Carroll (eds.), Amphibian Biology. Surrey Beatty & Sons, Chipping Norton, New South Wales, Australia.

Bolt, J. R., and R. E. Lombard. 2006. Sigournea multidentata, a new stem tetrapod from the Upper Mississippian of Iowa, USA. Journal of Paleontology 80:717–725.

Bolt, J. R., and R. E. Lombard. 2010. Deltaherpeton hiemstrae, a new colosteid tetrapod from the Mississippian of Iowa. Journal of Paleontology 84:1135–1151.

Bolt, J. R., and R. E. Lombard. 2018. Palate and braincase of *Whatcheeria deltae* Lombard & Bolt, 1995. Earth and Environmental Science Transactions of the Royal Society of Edinburgh 1–24.

Bolt, J. R., R. M. McKay, B. J. Witzke, and M. P. McAdams. 1988. A new Lower Carboniferous tetrapod locality in Iowa. Nature 333:768–770.

Bowles, A. M. C., U. Bechtold, and J. Paps. 2020. The Origin of Land Plants Is Rooted in Two Bursts of Genomic Novelty. Current Biology S0960982219315957.

Boyd, M. J. 1980. The axial skeleton of the Carboniferous amphibian Pteroplax cornotus. Palaeontology 23:273–285.

Boyd, M. J. 1984. The Upper Carboniferous tetrapod assemblage from Newsham, Northumberland. Palaeontology 27:367–392.

Brazeau, M. D. 2011. Problematic character coding methods in morphology and their effects. Biological Journal of the Linnean Society 104:489–498.

Brazeau, M. D., and M. Friedman. 2014. The characters of Palaeozoic jawed vertebrates: Early Gnathostome Characters. Zoological Journal of the Linnean Society 170:779–821.

Brazeau, M. D., and M. Friedman. 2015. The origin and early phylogenetic history of jawed vertebrates. Nature 520:490–497.

Brenchley, P. J., and D. A. T. Harper. 1998. Palaeoecology: Ecosystems, Environments, and Evolution, 1st ed. Chapman & Hall, London ; New York, 402 pp.

Briggs, D. E. G., and E. N. K. Clarkson. 1985. The Lower Carboniferous shrimp *Tealliocaris* from Gullane, East Lothian, Scotland. Earth and Environmental Science Transactions of the Royal Society of Edinburgh 76:173–201.

Briggs, D. E. G., and E. N. K. Clarkson. 1989. Environmental controls on the taphonomy and distribution of Carboniferous malacostracan crustaceans. Transactions of the Royal Society of Edinburgh: Earth Sciences 80:9.

Broussard, D. R., J. M. Trop, J. A. Benowitz, E. B. Daeschler, J. A. Chamberlain, and R. B. Chamberlain. 2018. Depositional setting, taphonomy and geochronology of new fossil sites in the Catskill Formation (Upper Devonian) of north-central Pennsylvania, USA, including a new early tetrapod fossil. Palaeogeography, Palaeoclimatology, Palaeoecology 511:168–187.

Broussard, D. R., C. J. Treaster, J. M. Trop, E. B. Daeschler, P. A. Zippi, M. B. Vrazo, and M. C. Rygel. 2020. VERTEBRATE TAPHONOMY, PALEONTOLOGY, SEDIMENTOLOGY, AND PALYNOLOGY OF A FOSSILIFEROUS LATE DEVONIAN FLUVIAL SUCCESSION,

CATSKILL FORMATION, NORTH-CENTRAL PENNSYLVANIA, USA. PALAIOS 35:470–494.

Brower, J. C. 2007. The application of filtration theory to food gathering in Ordovician crinoids. Journal of Paleontology 81:1284–1300.

Buggisch, W. 1991. The global Frasnian-Famennian »Kellwasser Event«. Geologische Rundschau 80:49–72.

Byrne, H. M., J. A. M. Green, S. A. Balbus, and P. E. Ahlberg. 2020. A key environmental driver of osteichthyan evolution and the fish-tetrapod transition? Proceedings of the Royal Society A: Mathematical, Physical and Engineering Sciences 476:20200355.

Byrne, H. M., G. Niedźwiedzki, H. Blom, B. P. Kear, and P. E. Ahlberg. 2022. A new tetrapod from the terminal Famennian of East Greenland. .

Callier, V., J. A. Clack, and P. E. Ahlberg. 2009. Contrasting Developmental Trajectories in the Earliest Known Tetrapod Forelimbs. Science 324:364–367.

Carpenter, D. K., H. J. Falcon-Lang, M. J. Benton, and E. Henderson. 2014. Carboniferous (Tournaisian) fish assemblages from the Isle of Bute, Scotland: systematics and palaeoecology. Palaeontology 57:1215–1240.

Carr, R. K., and G. L. Jackson. 2008. The Vertebrate Fauna of the Cleveland Member (Famennian) of the Ohio Shale. 20.

Carr, R. K., Z. Johanson, and A. Ritchie. 2009. The phyllolepid placoderm *Cowralepis mclachlani* : Insights into the evolution of feeding mechanisms in jawed vertebrates. Journal of Morphology 270:775–804.

Carroll, R. L. 1970. The Ancestry of Reptiles. Philosophical Transactions of the Royal Society B: Biological Sciences 257:267–308.

Cater, J. M. L., D. E. G. Briggs, and E. N. K. Clarkson. 1989. Shrimp-bearing sedimentary successions in the Lower Carboniferous (Dinantian) Cementstone and Oil Shale Groups of northern Britain. Transactions of the Royal Society of Edinburgh: Earth Sciences 80:5–15.

Chen, D., Y. Alavi, M. D. Brazeau, H. Blom, D. Millward, and P. E. Ahlberg. 2018. A partial lower jaw of a tetrapod from “Romer’s Gap.” Earth and Environmental Science Transactions of the Royal Society of Edinburgh 108:55–65.

Chen, J., and J. Liu. 2020. The youngest occurrence of embolomeres (Tetrapoda: Anthracosauria) from the Sunjiagou Formation (Lopingian, Permian) of North China. Fossil Record 23:205–213.

Chevrinais, M., C. Jacquet, and R. Cloutier. 2017. Early establishment of vertebrate trophic interactions: Food web structure in Middle to Late Devonian fish assemblages with exceptional fossilization. Bulletin of Geosciences 491–510.

Clack, J. A. 1987a. Pholiderpeton scutigerum Huxley, an Amphibian from the Yorkshire Coal Measures. Philosophical Transactions of the Royal Society B: Biological Sciences 318:1–107.

Clack, J. A. 1987b. Two new specimens of Anthracosaurus (Amphibia: Anthracosauria) from the Northumberland Coal Measures. Palaeontology 30:15–26.

Clack, J. A. 1997. The Scottish Carboniferous tetrapod Crassigyrinus scoticus (Lydekker)—cranial anatomy and relationships. Transactions of the Royal Society of Edinburgh: Earth Sciences 88:127–142.

Clack, J. A. 1998. The neurocranium of Acanthostega gunnari Jarvik and the evolution of the otic region in tetrapods. Zoological Journal of the Linnean Society 122:61–97.

Clack, J. A. 2002a. A revised reconstruction of the dermal skull roof of *Acanthostega gunnari* , an early tetrapod from the Late Devonian. Transactions of the Royal Society of Edinburgh: Earth Sciences 93:163–165.

Clack, J. A. 2002b. The dermal skull roof of Acanthostega gunnari, an early tetrapod from the Late Devonian. Transactions of the Royal Society of Edinburgh: Earth Sciences 93:17–33.

Clack, J. A. 2002c. An early tetrapod from 'Romer's Gap.' Nature 418:72–76.

Clack, J. A. 2009. The Fin to Limb Transition: New Data, Interpretations, and Hypotheses from Paleontology and Developmental Biology. Annual Review of Earth and Planetary Sciences 37:163–179.

Clack, J. A. 2011. A Carboniferous embolomere tail with supraneural radials. Journal of Vertebrate Paleontology 31:1150–1153.

Clack, J. A. 2012. Gaining Ground: The Origin and Evolution of Tetrapods, 2nd ed. Indiana University Press, Bloomington, 523 pp.

Clack, J. A., and R. Holmes. 1988. The braincase of the anthracosaur Archeria crassidisca with comments on the interrelationships of primitive tetrapods. Palaeontology 31:85–107.

Clack, J. A., and P. E. Ahlberg. 2004. A new stem tetrapod from the Early Carboniferous of Northern Ireland; pp. 309–320 in G. Arratia, M. V. H. Wilson, and R. Cloutier (eds.), Recent Advances in the Origin and Early Radiation of Vertebrates. Verlag Dr. Friedrich Pfeil, Munich, Germany.

Clack, J. A., and S. M. Finney. 2005. *Pederpes finneyae* , an articulated tetrapod from the tournaisian of Western Scotland. Journal of Systematic Palaeontology 2:311–346.

Clack, J. A., and A. R. Milner. 2015. Handbook of Paleoherpetology, Part 3A1: Basal Tetrapoda (H.-D. Sues (ed.)). Verlag Dr. Friedrich Pfeil, Munich, Germany, 93 pp.

Clack, J. A., and T. R. Smithson. 2020. A new large embolomere from East Kirkton. Scottish Journal of Geology 56:153–158.

Clack, J. A., L. B. Porro, and C. E. Bennett. 2018. A *Crassigyrinus* -like jaw from the Tournaisian (Early Mississippian) of Scotland. Earth and Environmental Science Transactions of the Royal Society of Edinburgh 108:37–46.

Clack, J. A., P. E. Ahlberg, H. Blom, and S. M. Finney. 2012a. A new genus of Devonian tetrapod from North-East Greenland, with new information on the lower jaw of Ichthyostega. Palaeontology 55:73–86.

Clack, J. A., F. Witzmann, J. Müller, and D. Snyder. 2012b. A Colosteid-Like Early Tetrapod from the St. Louis Limestone (Early Carboniferous, Meramecian), St. Louis, Missouri, USA. Fieldiana Life and Earth Sciences 5:17–39.

Clack, J. A., C. E. Bennett, S. J. Davies, A. C. Scott, J. E. Sherwin, and T. R. Smithson. 2019a. A Tournaisian (earliest Carboniferous) conglomerate-preserved non-marine faunal assemblage and its environmental and sedimentological context. PeerJ 6:e5972.

Clack, J. A., M. Ruta, A. R. Milner, J. E. A. Marshall, T. R. Smithson, and K. Z. Smithson. 2019b. *Acherontiscus caledoniae* : the earliest heterodont and durophagous tetrapod. Royal Society Open Science 6:182087.

Clack, J. A., C. E. Bennett, D. K. Carpenter, S. J. Davies, N. C. Fraser, T. I. Kearsey, J. E. A. Marshall, D. Millward, B. K. A. Otoo, E. J. Reeves, A. J. Ross, M. Ruta, K. Z. Smithson, T. R. Smithson, and S. A. Walsh. 2016. Phylogenetic and environmental context of a Tournaisian tetrapod fauna. Nature Ecology & Evolution 1:0002.

Clark, N. D. L. 1989. A study of a Namurian crustacean-bearing shale from the western Midland Valley of Scotland. PhD, University of Glasgow, 313 pp.

Clark, N. D. L. 1990. *Minicaris brandi* Schram 1979, a syncarid crustacean from the Namurian (Carboniferous). Scottish Journal of Geology 26:125–130.

Clark, N. D. L. 2013. Tealliocaris: a decapod crustacean from the Carboniferous. Palaeodiversity 6.

Clarkson, E. N. K. 1985. Palaeoecology of the Dinantian of Foulden, Berwickshire, Scotland. Transactions of the Royal Society of Edinburgh: Earth Sciences 76:97–100.

Clarkson, E. N. K., A. R. Milner, and M. I. Coates. 1993. Palaeoecology of the Viséan of East Kirkton, West Lothian, Scotland. Transactions of the Royal Society of Edinburgh: Earth Sciences 84:417–425.

Clément, G., and O. Lebedev. 2014. Revision of the early tetrapod Obruchevichthys Vorobyeva, 1977 from the Frasnian (Upper Devonian) of the North-western East European Platform. Paleontological Journal 48:1082–1091.

Clement, G., P. E. Ahlberg, A. Blieck, H. Blom, J. A. Clack, E. Poty, J. Thorez, and P. Janvier. 2004. Devonian tetrapod from Western Europe. Nature 427:412–413.

Cloutier, R., and P. E. Ahlberg. 1996. Morphology, Characters, and the Interrelationships of Basal Sarcopterygians; pp. 445–479 in M. Stiassny, L. Parenti, and G. Johnson (eds.), Interrelationships of Fishes. Elsevier.

Coates, M. I. 1988. A new fauna of Namurian (Upper Carboniferous) fish from Bearsden, Glasgow. PhD, University of Newcastle upon Tyne, Newcastle Upon Tyne, 442 pp.

Coates, M. I. 1993. New actinopterygian fish from the Namurian Manse Burn Formation of Bearsden, Scotland. Palaeontology 36:123–146.

Coates, M. I. 1996. The Devonian tetrapod Acanthostega gunnari Jarvik: postcranial anatomy, basal tetrapod interrelationships and patterns of skeletal evolution. Transactions of the Royal Society of Edinburgh: Earth Sciences 87:363–421.

Coates, M. I., and J. A. Clack. 1990. Polydactyly in the earliest known tetrapod limbs. Nature 347:66–69.

Coates, M. I., and J. A. Clack. 1991. Fish-like gills and breathing in the earliest known tetrapod. Nature 352:234–236.

Coates, M. I., and J. A. Clack. 1995. Romer's gap- tetrapod origins and terrestriality. Bulletin - Museum National d'Histoire Naturelle Section C: Sciences de La Terre 17:373–388.

Coates, M. I., and S. E. K. Sequeira. 2001. A new stethacanthid chondrichthyan from the lower Carboniferous of Bearsden, Scotland. Journal of Vertebrate Paleontology 21:438–459.

Coates, M. I., M. Ruta, and A. R. Milner. 2000. Early tetrapod evolution. Trends in Ecology & Evolution 15:1.

Coates, M. I., J. E. Jeffery, and M. Ruta. 2002. Fins to limbs: what the fossils say. Evolution and Development 4:390–401.

Coates, M. I., M. Ruta, and M. Friedman. 2008. Ever Since Owen: Changing Perspectives on the Early Evolution of Tetrapods. Annual Review of Ecology, Evolution, and Systematics 39:571–592.

Coates, M. I., K. Tietjen, A. M. Olsen, and J. A. Finarelli. 2019. High-performance suction feeding in an early elasmobranch. Science Advances 5:eaax2742.

Connolly, S. R., T. P. Hughes, D. R. Bellwood, and R. H. Karlson. 2005. Community Structure of Corals and Reef Fishes at Multiple Scales. Science 309:1363–1365.

Cowman, P. F., and D. R. Bellwood. 2013. The historical biogeography of coral reef fishes: global patterns of origination and dispersal. Journal of Biogeography 40:209–224.

Cózar, P., and I. D. Somerville. 2021. Paleotethyan faunal/floral evidence in the Mississippian Maritimes Basin of Canada: An overview. Journal of Paleontology 1–20.

Cressler, W. L., E. B. Daeschler, R. Slingerland, and D. A. Peterson. 2010. Terrestrialization in the Late Devonian: a palaeoecological overview of the Red Hill site, Pennsylvania, USA. Geological Society, London, Special Publications 339:111–128.

Cueille, M., E. Green, C. J. Duffin, C. Hildebrandt, and M. J. Benton. 2020. Fish and crab coprolites from the latest Triassic of the UK: From Buckland to the Mesozoic Marine Revolution. Proceedings of the Geologists' Association 131:699–721.

Currie, E. D. 1954. XIV—Scottish Carboniferous Goniatites. Transactions of the Royal Society of Edinburgh 62:527–602.

Daeschler, E. B. 2000. Early tetrapod jaws from the Late Devonian of Pennsylvania, USA. Journal of Paleontology 74:301–308.

Daeschler, E. B., N. H. Shubin, and F. A. Jenkins. 2006. A Devonian tetrapod-like fish and the evolution of the tetrapod body plan. Nature 440:757–763.

Daeschler, E. B., J. A. Clack, and N. H. Shubin. 2009. Late Devonian tetrapod remains from Red Hill, Pennsylvania, USA: how much diversity? Acta Zoologica 90:306–317.

Daeschler, E. B., N. H. Shubin, K. S. Thomson, and W. W. Amaral. 1994. A Devonian Tetrapod from North America. Science 265:639–642.

Dahl, T. W., and S. K. M. Arens. 2020. The impacts of land plant evolution on Earth's climate and oxygenation state – An interdisciplinary review. Chemical Geology 547:119665.

Danto, M., F. Witzmann, and N. B. Fröbisch. 2016. Vertebral Development in Paleozoic and Mesozoic Tetrapods Revealed by Paleohistological Data. PLOS ONE 11:e0152586.

Danto, M., F. Witzmann, S. E. Pierce, and N. B. Fröbisch. 2017. Intercentrum versus pleurocentrum growth in early tetrapods: A paleohistological approach. Journal of Morphology 278:1262–1283.

Denayer, J., C. Prestianni, P. Gueriau, S. Olive, and G. Clément. 2016. Stratigraphy and depositional environments of the Late Famennian (Late Devonian) of Southern Belgium and characterization of the Strud locality. Geological Magazine 153:112–127.

Dickson, B. V., J. A. Clack, T. R. Smithson, and S. E. Pierce. 2020. Functional adaptive landscapes predict terrestrial capacity at the origin of limbs. Nature.

Dineen, A. A., M. L. Fraiser, and P. M. Sheehan. 2014. Quantifying functional diversity in pre- and post-extinction paleocommunities: A test of ecological restructuring after the end-Permian mass extinction. Earth-Science Reviews 136:339–349.

Downs, J. P., E. B. Daeschler, F. A. Jenkins, and N. H. Shubin. 2008. The cranial endoskeleton of Tiktaalik roseae. Nature 455:925–929.

Droser, M. L., D. J. Bottjer, and P. M. Sheehan. 1997. Evaluating the ecological architecture of major events in the Phanerozoic history of marine invertebrate life. Geology 25:167.

Droser, M. L., D. J. Bottjer, P. M. Sheehan, and G. R. M. Jr. 2000. Decoupling of taxonomic and ecologic severity of Phanerozoic marine mass extinctions. Geology 4.

Dunhill, A. M., W. J. Foster, J. Sciberras, and R. J. Twitchett. 2018. Impact of the Late Triassic mass extinction on functional diversity and composition of marine ecosystems. Palaeontology 61:133–148.

Dunn, M. T., G. W. Rothwell, and G. Mapes. 2006. The Fayetteville Flora of Arkansas (USA): A snapshot of terrestrial vegetation patterns within a clastic swamp at Late Mississippian time; pp. in Wetlands through Time. Geological Society of America.

Dunne, J. A., R. J. Williams, N. D. Martinez, R. A. Wood, and D. H. Erwin. 2008. Compilation and Network Analyses of Cambrian Food Webs. PLoS Biology 6:e102.

Dynowski, J. F., J. H. Nebelsick, A. Klein, and A. Roth-Nebelsick. 2016. Computational Fluid Dynamics Analysis of the Fossil Crinoid Encrinus liliiformis (Echinodermata: Crinoidea). PLOS ONE 11:e0156408.

Eberle, J. J. 2008. Localities, Distribution and Stratigraphical Context of the Late Devonian Tetrapods of East Greenland, by Henning Blom, Jennifer A. Clack, and Per E. Ahlberg Henning Blom, Jennifer A. Clack, Per E. Ahlberg . Localities, Distribution and Stratigraphical Context of the Late Devonian Tetrapods of East Greenland. Meddelelser om Grønland, Geoscience. 2005. Vol. 43, 50 pp. DKK 195. (http://www.dpc.dk/graphics/Design/Danish/Videnscenter/DPC_publikationer/MoGpdf/MoG%20Geo/Geo43.pdf). Arctic, Antarctic, and Alpine Research 40:446–446.

Edie, S. M., D. Jablonski, and J. W. Valentine. 2018. Contrasting responses of functional diversity to major losses in taxonomic diversity. Proceedings of the National Academy of Sciences 115:732–737.

Erwin, D. H., J. W. Valentine, and J. J. Sepkoski. 1987. A comparative study of diversification events: the early Paleozoic versus the Mesozoic. Evolution 41:1177–1186.

Estefa, J., J. Klembara, P. Tafforeau, and S. Sanchez. 2020. Limb-Bone Development of Seymouriamorphs: Implications for the Evolution of Growth Strategy in Stem Amniotes. Frontiers in Earth Science 8:97.

Falcon-Lang, H. J., M. J. Benton, S. J. Braddy, and S. J. Davies. 2006. The Pennsylvanian tropical biome reconstructed from the Joggins Formation of Nova Scotia, Canada. Journal of the Geological Society 163:561–576.

Farris, J. S. 1989. The retention index and the rescaled consistency index. Cladistics 5:417–419.

Foster, W. J., and R. J. Twitchett. 2014. Functional diversity of marine ecosystems after the Late Permian mass extinction event. Nature Geoscience 7:233–238.

Foster, W. J., G. Ayzel, J. Münchmeyer, T. Rettelbach, N. H. Kitzmann, T. T. Isson, M. Mutti, and M. Aberhan. 2022. Machine learning identifies ecological selectivity patterns across the end-Permian mass extinction. Paleobiology 1–15.

Fracasso, M. A. 1994. Amphibia: Disparity and Diversification of Early Tetrapods. Short Courses in Paleontology 7:108–128.

Frey, L., M. Rücklin, D. Korn, and C. Klug. 2018. Late Devonian and Early Carboniferous alpha diversity, ecospace occupation, vertebrate assemblages and bio-events of southeastern Morocco. Palaeogeography, Palaeoclimatology, Palaeoecology 496:1–17.

Friedman, M., S. E. Pierce, M. Coates, and S. Giles. 2018. Feeding structures in the ray-finned fish Eurynotus crenatus (Actinopterygii: Eurynotiformes): implications for trophic diversification among Carboniferous actinopterygians. Earth and Environmental Science Transactions of the Royal Society of Edinburgh 1–15.

Garcia, W. J., G. W. Storrs, and S. F. Greb. 2006. The Hancock County tetrapod locality: A new Mississippian (Chesterian) wetlands fauna from western Kentucky (USA); pp. in Wetlands through Time., . Special Papers vol. 399. Geological Society of America.

Garwood, R. J., H. Oliver, and A. R. T. Spencer. 2020. An introduction to the Rhynie chert. Geological Magazine 157:47–64.

Gensel, P. G., I. Glasspool, R. A. Gastaldo, M. Libertin, and J. Kvaček. 2020. Back to the Beginnings: The Silurian-Devonian as a Time of Major Innovation in Plants and Their Communities; pp. 367–398 in E. Martinetto, E. Tschopp, and R. A. Gastaldo (eds.), Nature through Time., . Springer Textbooks in Earth Sciences, Geography and Environment Springer International Publishing, Cham.

Gereke, M., and E. Schindler. 2012. "Time-Specific Facies" and biological crises — The Kellwasser Event interval near the Frasnian/Famennian boundary (Late Devonian). Palaeogeography, Palaeoclimatology, Palaeoecology 367–368:19–29.

Gess, R., and P. E. Ahlberg. 2018. A tetrapod fauna from within the Devonian Antarctic Circle. Science 360:1120–1124.

Gess, R. W., and A. K. Whitfield. 2020. Estuarine fish and tetrapod evolution: insights from a Late Devonian (Famennian) Gondwanan estuarine lake and a southern African Holocene equivalent. Biological Reviews brv.12590.

Godfrey, S. J. 1989. The postcranial skeletal anatomy of the Carboniferous tetrapod Greererpeton burkemorani Romer, 1969. Philosophical Transactions of the Royal Society B: Biological Sciences 323:75–133.

Goedert, J., C. Lécuyer, R. Amiot, F. Arnaud-Godet, X. Wang, L. Cui, G. Cuny, G. Douay, F. Fourel, G. Panczer, L. Simon, J.-S. Steyer, and M. Zhu. 2018. Euryhaline ecology of early tetrapods revealed by stable isotopes. Nature 558:68–72.

Goloboff, P. A., and P. C. Sereno. 2021. Comparative cladistics: identifying the sources for differing phylogenetic results between competing morphology-based datasets. Journal of Systematic Palaeontology 19:761–786.

Goloboff, P. A., A. Torres Galvis, and J. S. Arias. 2018a. Parsimony and model-based phylogenetic methods for morphological data: comments on O'Reilly *et al* . Palaeontology 61:625–630.

Goloboff, P. A., A. Torres, and J. S. Arias. 2018b. Weighted parsimony outperforms other methods of phylogenetic inference under models appropriate for morphology. Cladistics 34:407–437.

Gray, J. 1988. Evolution of the freshwater ecosystem: The fossil record. Palaeogeography, Palaeoclimatology, Palaeoecology 62:1–214.

Greb, S. F., G. W. Storrs, W. J. Garcia, and C. F. Eble. 2016. Late Mississippian vertebrate palaeoecology and taphonomy, Buffalo Wallow Formation, western Kentucky, USA. Lethaia 49:199–218.

Henderson, C. M., S. Z. Shen, F. M. Gradstein, and F. P. Agterberg. 2020. The Permian Period; pp. 875–902 in Geologic Time Scale 2020. Elsevier.

Henderson, S., E. M. Dunne, S. A. Fasey, and S. Giles. 2022. The early diversification of ray-finned fishes (Actinopterygii): hypotheses, challenges and future prospects. Biological Reviews 95.

Herbst, E. C., and J. R. Hutchinson. 2018. New insights into the morphology of the Carboniferous tetrapod *Crassigyrinus scoticus* from computed tomography. Earth and Environmental Science Transactions of the Royal Society of Edinburgh 109:157–175.

Hill, J. J., M. N. Puttick, T. L. Stubbs, E. J. Rayfield, and P. C. J. Donoghue. 2018. Evolution of jaw disparity in fishes. Palaeontology 61:847–854.

Hodge, J. R., L. van Herwerden, and D. R. Bellwood. 2014. Temporal evolution of coral reef fishes: global patterns and disparity in isolated locations. Journal of Biogeography 41:2115–2127.

Holder, M., and P. O. Lewis. 2003. Phylogeny estimation: traditional and Bayesian approaches. Nature Reviews Genetics 4:275–284.

Holmes, R. 1984. The Carboniferous amphibian Proterogyrinus scheeli Romer and the early evolution of tetrapods. Philosophical Transactions of the Royal Society B: Biological Sciences 306:431–524.

Holmes, R. 1989a. The skull and axial skeleton of the Lower Permian anthracosauroid amphibian Archeria crassidisca Cope. Palaeontographica Abt. A. 207:161–206.

Holmes, R., and D. Baird. 2011. The Smaller Embolomerous Amphibians (Anthracosauria) from the Middle Pennsylvanian (Desmoinesian) Localities at Linton and Five Points Coal Mines, Ohio. Breviora 523:1–13.

Holmes, R. B. 1989b. The skull and axial skeleton of the Lower Permian anthracosauroid amphibian Archeria crassidisca Cope. Palaeontographica Abteilung A (Palaeozoologie-Stratigraphie) 207:161–206.

Holmes, R. B., and R. L. Carroll. 1977. A temnospondyl amphibian from the Mississippian of Scotland. Bulletin of the Museum of Comparative Zoology 147:489–511.

Holmes, R. B., and R. L. Carroll. 2010. An articulated embolomere skeleton (Amphibia: Anthracosauria) from the Lower Pennsylvanian (Bashkirian) of Nova Scotia. Canadian Journal of Earth Sciences 47:209–219.

Hook, R. W. 1983. Colosteus scutellatus (Newberry), a Primitive Temnospondyl Amphibian from the Middle Pennsylvanian of Linton, Ohio. American Museum Novitates 44.

Huang, Y., Z.-Q. Chen, P. D. Roopnarine, M. J. Benton, W. Yang, J. Liu, L. Zhao, Z. Li, and Z. Guo. 2021. Ecological dynamics of terrestrial and freshwater ecosystems across three mid-Phanerozoic mass extinctions from northwest China. Proceedings of the Royal Society B: Biological Sciences 288:rspb.2021.0148, 20210148.

Huelsenbeck, J. P., and F. Ronquist. 2001. MRBAYES: Bayesian inference of phylogenetic trees. Bioinformatics 17:754–755.

Huttenlocker, A. K., J. D. Pardo, B. J. Small, and J. S. Anderson. 2013. Cranial morphology of recumbirostrans (Lepospondyli) from the Permian of Kansas and Nebraska, and early morphological evolution inferred by micro-computed tomography. Journal of Vertebrate Paleontology 33:540–552.

Iannuzzi, R., and C. C. Labandeira. 2008. The Oldest Record of External Foliage Feeding and the Expansion of Insect Folivory on Land. Annals of the Entomological Society of America 101:79–94.

Jaekel, O. 1909. Über die Klassen der Tetrapoden. Zoologischer Anzeiger 34:193–212.

Jakubowicz, M., J. Król, M. K. Zapalski, T. Wrzołek, P. Wolniewicz, and B. Berkowski. 2019. At the southern limits of the Devonian reef zone: Palaeoecology of the Aferdou el Mrakib reef (Givetian, eastern Anti-Atlas, Morocco). Geological Journal 54:10–38.

Jarvik, E. 1996. The Devonian tetrapod Ichthyostega. Fossils and Strata 40:1–213.

Jeram, A. J. 1993. Scorpions from the Viséan of East Kirkton, West Lothian, Scotland, with a revision of the infraorder Mesoscorpionina. Transactions of the Royal Society of Edinburgh: Earth Sciences 84:283–299.

Kaiser, S. I., M. Aretz, and R. T. Becker. 2016. The global Hangenberg Crisis (Devonian–Carboniferous transition): review of a first-order mass extinction. Geological Society, London, Special Publications 423:387–437.

Kamska, V., E. B. Daeschler, J. P. Downs, P. E. Ahlberg, P. Tafforeau, and S. Sanchez. 2018. Long-bone development and life-history traits of the Devonian tristichopterid Hyneria lindae. Earth and Environmental Science Transactions of the Royal Society of Edinburgh 1–12.

Kassambara, A., and F. Mundt. 2020. factoextra: Extract and Visualize the Results of Multivariate Data Analyses. .

Kearsey, T. I., C. E. Bennett, D. Millward, S. J. Davies, C. J. B. Gowing, S. J. Kemp, M. J. Leng, J. E. A. Marshall, and M. A. E. Browne. 2016. The terrestrial landscapes of tetrapod evolution in

earliest Carboniferous seasonal wetlands of SE Scotland. Palaeogeography, Palaeoclimatology, Palaeoecology 457:52–69.

Kempf, H. L., I. O. Castro, A. A. Dineen, C. L. Tyler, and P. D. Roopnarine. 2020. Comparisons of Late Ordovician ecosystem dynamics before and after the Richmondian invasion reveal consequences of invasive species in benthic marine paleocommunities. Paleobiology 1–17.

Kimmel, C. B., B. Sidlauskas, and J. A. Clack. 2009. Linked morphological changes during palate evolution in early tetrapods. Journal of Anatomy 215:91–109.

King, B., and M. Rücklin. 2020. A Bayesian approach to dynamic homology of morphological characters and the ancestral phenotype of jawed vertebrates. ELife 9:e62374.

King, B., T. Qiao, M. S. Y. Lee, M. Zhu, and J. A. Long. 2016. Bayesian Morphological Clock Methods Resurrect Placoderm Monophyly and Reveal Rapid Early Evolution in Jawed Vertebrates. Systematic Biology syw107.

King, H. M., N. H. Shubin, M. I. Coates, and M. E. Hale. 2011. Behavioral evidence for the evolution of walking and bounding before terrestriality in sarcopterygian fishes. Proceedings of the National Academy of Sciences 108:21146–21151.

Klasson, W. 2008. The early diversification of ray-finned fishes (Actinopterygii); an ecomorphological approach. Undergraduate, University of Uppsala, Uppsala, Sweden, 69 pp.

Klembara, J. 1985. A new embolomerous amphibian (Anthracosauria) from the Upper Carboniferous of Florence, Nova Scotia. Journal of Vertebrate Paleontology 5:293–302.

Klembara, J., and I. Bartík. 1999. The postcranial skeleton of Discosauriscus Kuhn, a seymouriamorph tetrapod from the Lower Permian of the Boskovice Furrow (Czech Republic). Transactions of the Royal Society of Edinburgh: Earth Sciences 90:287–316.

Klembara, J., J. A. Clack, A. R. Milner, and M. Ruta. 2014. Cranial anatomy, ontogeny, and relationships of the Late Carboniferous tetrapod *Gephyrostegus bohemicus* Jaekel, 1902. Journal of Vertebrate Paleontology 34:774–792.

Kuznetsov, V. G., and L. M. Zhuravleva. 2018. Reef Formation during Mass Extinction Events: Frasnian—Famennian and Devonian—Carboniferous Boundaries. Doklady Earth Sciences 481:984–987.

Lagebro, L., P. Gueriau, T. A. Hegna, N. Rabet, A. D. Butler, and G. E. Budd. 2015. The oldest notostracan (Upper Devonian Strud locality, Belgium). Palaeontology 58:497–509.

Laurin, M. 1998. A reevaluation of the origin of pentadactyly. Evolution 52:1476–1482.

Laurin, M., and R. R. Reesz. 1995. A reevaluation of early amniote phylogeny. Zoological Journal of the Linnean Society 113:165–223.

Laurin, M., and R. R. Reisz. 1997. A new perspective on tetrapod phylogeny; pp. 9–59 in Amniote Origins. Elsevier.

Laurin, M., and R. Soler-Gijón. 2001. The oldest stegocephalian from the Iberian Peninsula: evidence that temnospondyls were euryhaline. Comptes Rendus de l'Académie Des Sciences - Series III - Sciences de La Vie 324:495–501.

Laurin, M., M. Girondot, and A. de Ricqlès. 2000. Early tetrapod evolution. Trends in Ecology & Evolution 15:118–123.

Lautenschlager, S., F. Witzmann, and I. Werneburg. 2016. Palate anatomy and morphofunctional aspects of interpterygoid vacuities in temnospondyl cranial evolution. The Science of Nature 103.

Lawver, L. A., I. W. D. Dalziel, I. O. Norton, L. M. Gahagan, and J. K. Davis. 2015. The PLATES 2014 Atlas of Plate Reconstructions (550 Ma to Present Day). 220 pp.

Lebedev, O. A. 2004. A new tetrapod Jakubsonia livnensis from the Early Famennian (Devonian) of Russia and palaeoecological remarks on the Late Devonian tetrapod habitats. Acta Unversitatis Latviensis 679:79–98.

Lebedev, O. A., and J. A. Clack. 1993. Upper Devonian tetrapods from Andreyevka, Tula Region, Russia. Palaeontology 36:721–734.

Lebedev, O. A., and M. I. Coates. 1995. The postcranial skeleton of the Devonian tetrapod Tulerpeton curtum Lebedev. Zoological Journal of the Linnean Society 114:307–348.

Lebedev, O. A., and G. Clément. 2019. New tetrapodomorph vertebrates from the Yam-Tesovo locality (Amata Regional Stage, Middle–Upper Devonian) of Leningrad Region, northwestern Russia. Earth and Environmental Science Transactions of the Royal Society of Edinburgh 109:61–73.

Lennie, K. I., C. F. Mansky, and J. S. Anderson. 2020. New *Crassigyrinus* -like fibula from the Tournaisian (earliest Carboniferous) of Nova Scotia. Canadian Journal of Earth Sciences 57:1365–1369.

Lennie, K. I., S. L. Manske, C. F. Mansky, and J. S. Anderson. 2021. Locomotory behaviour of early tetrapods from Blue Beach, Nova Scotia, revealed by novel microanatomical analysis. Royal Society Open Science 8:210281.

Lloyd, G. T., S. C. Wang, and S. L. Brusatte. 2012. Identifying heterogeneity in rates of morphological evolution: discrete character change in the evolution of lungfish (Sarcopterygii; Dipnoi). Evolution 66:330–348.

Lombard, E. R., and S. S. Sumida. 1992. Recent progress in understanding early tetrapods. American Zoologist 32:609–622.

Lombard, R. E., and J. R. Bolt. 1979. Evolution of the tetrapod ear: an analysis and reinterpretation. Biological Journal of the Linnean Society 11:19–76.

Lombard, R. E., and J. R. Bolt. 1995. A new primitive tetrapod, Whatcheeria deltae, from the Lower Carboniferous of Iowa. Palaeontology 38:471–494.

Lombard, R. E., and J. R. Bolt. 2006. The mandible of Whatcheeria deltae, and early tetrapod from the Late Mississippian of Iowa; pp. 21–52 in M. T. Carrano, R. W. Blob, T. J. Gaudin, and J. R. Wible (eds.), Amniote Paleobiology: Perspectives on the Evolution of Mammals, Birds, and Reptiles. University of Chicago Press.

Long, J. A., and K. M. Trinajstic. 2018. A review of recent discoveries of exceptionally preserved fossil fishes from the Gogo sites (Late Devonian, Western Australia). Earth and Environmental Science Transactions of the Royal Society of Edinburgh 108:111–117.

Long, J. A., M. E. Anderson, R. Gess, and N. Hiller. 1997. New placoderm fishes from the Late Devonian of South Africa. Journal of Vertebrate Paleontology 17:253–268.

Lund, R., E. Greenfest-Allen, and E. D. Grogan. 2012. Habitat and diversity of the Bear Gulch fish: Life in a 318 million year old marine Mississippian bay. Palaeogeography, Palaeoclimatology, Palaeoecology 342–343:1–16.

Lund, R., E. Greenfest-Allen, and E. D. Grogan. 2015. Ecomorphology of the Mississippian fishes of the Bear Gulch Limestone (Heath formation, Montana, USA). Environmental Biology of Fishes 98:739–754.

MacIver, M. A., L. Schmitz, U. Mugan, T. D. Murphey, and C. D. Mobley. 2017. Massive increase in visual range preceded the origin of terrestrial vertebrates. Proceedings of the National Academy of Sciences 114:E2375–E2384.

Maddin, H. C., F. A. Jenkins, and J. S. Anderson. 2012. The Braincase of Eocaecilia micropodia (Lissamphibia, Gymnophiona) and the Origin of Caecilians. PLoS ONE 7:e50743.

Maddison, W. P., and D. R. Maddison. 2021. Mesquite: a modular system for evolutionary analysis. .

Mann, A., B. M. Gee, J. D. Pardo, D. Marjanović, G. R. Adams, A. S. Calthorpe, H. C. Maddin, and J. S. Anderson. 2020. Reassessment of historic ‘microsaurs’ from Joggins, Nova Scotia, reveals hidden diversity in the earliest amniote ecosystem. Papers in Palaeontology spp2.1316.

Marjanović, D., and M. Laurin. 2007. Fossils, Molecules, Divergence Times, and the Origin of Lissamphibians. Systematic Biology 56:369–388.

Marjanović, D., and M. Laurin. 2008. A reevaluation of the evidence supporting an unorthodox hypothesis on the origin of extant amphibians. Contributions to Zoology 77:149–199.

Marjanović, D., and M. Laurin. 2009. The Origin(s) of Modern Amphibians: A Commentary. Evolutionary Biology 36:336–338.

Marjanović, D., and M. Laurin. 2013. The origin(s) of extant amphibians: a review with emphasis on the “lepospondyl hypothesis.” Geodiversitas 35:207.

Marjanović, D., and M. Laurin. 2019. Phylogeny of Paleozoic limbed vertebrates reassessed through revision and expansion of the largest published relevant data matrix. PeerJ 6:e5565.

Marshall, J. E. A., D. A. Rogers, and M. J. Whiteley. 1996. Devonian marine incursions into the Orcadian Basin, Scotland. Journal of the Geological Society 153:451–466.

McGhee, G. R., P. M. Sheehan, D. J. Bottjer, and M. L. Droser. 2004. Ecological ranking of Phanerozoic biodiversity crises: ecological and taxonomic severities are decoupled. Palaeogeography, Palaeoclimatology, Palaeoecology 211:289–297.

McGhee, G. R., P. M. Sheehan, D. J. Bottjer, and M. L. Droser. 2012. Ecological ranking of Phanerozoic biodiversity crises: The Serpukhovian (early Carboniferous) crisis had a greater ecological impact than the end-Ordovician. Geology 40:147–150.

McGhee, G. R., M. E. Clapham, P. M. Sheehan, D. J. Bottjer, and M. L. Droser. 2013. A new ecological-severity ranking of major Phanerozoic biodiversity crises. Palaeogeography, Palaeoclimatology, Palaeoecology 370:260–270.

Meyer, D., M. Veitch, C. G. Messing, and A. Stevenson. 2021. Crinoid Feeding Strategies: New Insights From Subsea Video And Time-Lapse, 1st ed. Cambridge University Press, pp.

Millward, D., S. J. Davies, F. Williamson, R. Curtis, T. I. Kearsey, C. E. Bennett, J. E. A. Marshall, and M. A. E. Browne. 2018a. Early Mississippian evaporites of coastal tropical wetlands. Sedimentology 65:2278–2311.

Millward, D., S. J. Davies, P. J. Brand, M. A. E. Browne, C. E. Bennett, T. I. Kearsey, J. E. Sherwin, and J. E. A. Marshall. 2018b. Palaeogeography of tropical seasonal coastal wetlands in northern Britain during the early Mississippian Romer's Gap. Earth and Environmental Science Transactions of the Royal Society of Edinburgh 1–22.

Milner, A. C., and W. Lindsay. 1998. Postcranial remains of Baphetes and their bearing on the relationships of the Baphetidae (= Loxommatidae). Zoological Journal of the Linnean Society 122:211–235.

Milner, A. R. 1980a. The temnospondyl amphibian Dendrerpeton from the Upper Carboniferous of Ireland. Palaeontology 23:125–141.

Milner, A. R. 1980b. The tetrapod assemblage from Nýřany Czechoslovakia; pp. in A. L. Panchen (ed.), The Terrestrial Environment and the Origin of Land Vertebrates., . Systematics Association Special Volume Academic Press, London, England, UK.

Milner, A. R. 1982. Small temnospondyl amphibians from the Middle Pennsylvanian of Illinois. Palaeontology 25:635–664.

Milner, A. R. 1987. The Westphalian tetrapod fauna; some aspects of its geography and ecology. Journal of the Geological Society 144:495–506.

Milner, A. R., and S. E. K. Sequeira. 1993. The temnospondyl amphibians from the Viséan of East Kirkton, West Lothian, Scotland. Transactions of the Royal Society of Edinburgh: Earth Sciences 84:331–361.

Milner, A. R., and R. R. Schoch. 2013. Trimerorhachis (Amphibia: Temnospondyli) from the Lower Permian of Texas and New Mexico: cranial osteology, taxonomy and biostratigraphy. Neues Jahrbuch Für Geologie Und Paläontologie - Abhandlungen 270:91–128.

Milner, A. R., T. R. Smithson, A. C. Milner, M. I. Coates, and W. D. I. Rolfe. 1986. The search for early tetrapods. Modern Geology 10:1–28.

Mitchell, J. S., P. D. Roopnarine, and K. D. Angielczyk. 2012. Late Cretaceous restructuring of terrestrial communities facilitated the end-Cretaceous mass extinction in North America. Proceedings of the National Academy of Sciences 109:18857–18861.

Monaghan, A. A., M. A. E. Browne, and D. N. Barfod. 2014. An improved chronology for the Arthur's Seat volcano and Carboniferous magmatism of the Midland Valley of Scotland. Scottish Journal of Geology 50:165–172.

Moulton, J. M. 1974. A description of the vertebral column of Eryops based on the notes and drawings of A.S. Romer. Breviora 44.

Narkiewicz, M., J. Grabowski, K. Narkiewicz, G. Niedźwiedzki, G. J. Retallack, P. Szrek, and D. De Vleeschouwer. 2015. Palaeoenvironments of the Eifelian dolomites with earliest tetrapod trackways (Holy Cross Mountains, Poland). Palaeogeography, Palaeoclimatology, Palaeoecology 420:173–192.

Near, T. J., A. Dornburg, M. Tokita, D. Suzuki, M. C. Brandley, and M. Friedman. 2014. Boom and bust: ancient and Recent diversification in bichirs (Polypteridae: Actinopterygii), relictual lineage of ray-finned fishes. Evolution 68:1014–1026.

Neenan, J. M., M. Ruta, J. A. Clack, and E. J. Rayfield. 2014. Feeding biomechanics in Acanthostega and across the fish-tetrapod transition. Proceedings of the Royal Society B: Biological Sciences 281:20132689–20132689.

Niedźwiedzki, G., P. Szrek, K. Narkiewicz, M. Narkiewicz, and P. E. Ahlberg. 2010. Tetrapod trackways from the early Middle Devonian period of Poland. Nature 463:43–48.

Norton, R. A., P. M. Bonamo, J. D. Grierson, and W. A. Shear. 1988. Oribatid mite fossils from a terrestrial Devonian deposit near Gilboa, New York. Journal of Paleontology 62:259–269.

Ó Gogáin, A., H. J. Falcon-Lang, D. K. Carpenter, R. F. Miller, M. J. Benton, P. K. Pufahl, M. Ruta, T. G. Davies, S. J. Hinds, and M. R. Stimson. 2016. Fish and tetrapod communities across a marine to brackish salinity gradient in the Pennsylvanian (early Moscovian) Minto Formation of New Brunswick, Canada, and their palaeoecological and palaeogeographical implications. Palaeontology 59:689–724.

Olive, S., P. E. Ahlberg, V. N. Pernègre, É. Poty, É. Steurbaut, and G. Clément. 2016. New discoveries of tetrapods (ichthyostegid-like and whatcheeriid-like) in the Famennian (Late Devonian) localities of Strud and Becco (Belgium). Palaeontology 59:827–840.

Olive, S., G. Clement, J. Denayer, V. Dupret, P. Gerrienne, P. Gueriau, J.-M. Marion, B. Mottequin, and C. Prestianni. 2015. Flora and fauna from a new Famennian (Upper Devonian) locality at Becco, eastern Belgium. Geologica Belgica 18:92–101.

Olson, E. C. 1952. The evolution of a Permian vertebrate chronofauna. Evolution 6:181–196.

Olson, E. C. 1966. Community Evolution and the Origin of Mammals. Ecology 47:291–302.

Olson, E. C. 1975. Permo—Carboniferous Paleoecology and Morphotypic Series. American Zoologist 15:371–389.

Olson, E. C. 1977. Permian lake faunas: a sutdy in community evolution. Journal of the Palaeontological Society of India 20:146–163.

Opluštil, S., M. Schmitz, C. J. Cleal, and K. Martínek. 2016. A review of the Middle–Late Pennsylvanian west European regional substages and floral biozones, and their correlation to the Geological Time Scale based on new U–Pb ages. Earth-Science Reviews 154:301–335.

O'Reilly, J. E., M. N. Puttick, L. Parry, A. R. Tanner, J. E. Tarver, J. Fleming, D. Pisani, and P. C. J. Donoghue. 2016. Bayesian methods outperform parsimony but at the expense of precision in the estimation of phylogeny from discrete morphological data. Biology Letters 12:20160081.

Otoo, B. K. A. 2015. A taxonomic and palaeoecological investigation of an earliest Carboniferous fauna from Burnmouth, Scotland, UK. MPhil, University of Cambridge, Cambridge, Cambridgeshire, England, UK, 157 pp.

Otoo, B. K. A., J. R. Bolt, R. E. Lombard, K. D. Angielczyk, and M. I. Coates. 2021. The postcranial anatomy of Whatcheeria deltae and its implications for the family Whatcheeriidae. Zoological Journal of the Linnean Society 193:700–745.

Otoo, B. K. A., J. A. Clack, T. R. Smithson, C. E. Bennett, T. I. Kearsey, and M. I. Coates. 2018. A fish and tetrapod fauna from Romer's Gap preserved in Scottish Tournaisian floodplain deposits. Palaeontology 62:225–253.

Panchen, A. L. 1964. The cranial anatomy of two Coal Measure anthracosaurs. Philosophical Transactions of the Royal Society B: Biological Sciences 742:593–637.

Panchen, A. L. 1966. The axial skeleton of the labyrinthodont Eogyrinus attheyi. Journal of Zoology 150:199–222.

Panchen, A. L. 1972. The Skull and Skeleton of Eogyrinus attheyi Watson (Amphibia: Labyrinthodontia). Philosophical Transactions of the Royal Society B: Biological Sciences 263:279–326.

Panchen, A. L. 1975. A new genus of anthracosaur amphibian from the Lower Carboniferous of Scotland and the status of Pholidogaster pisciformis Huxley. Philosophical Transactions of the Royal Society B: Biological Sciences 269:582–637.

Panchen, A. L. 1977. On Anthracosaurus russelli Huxley (Amphibia: Labyrinthodontia) and the Family Anthracosauridae. Philosophical Transactions of the Royal Society B: Biological Sciences 279:447–512.

Panchen, A. L. 1981. A jaw ramus of the Coal Measure Amphibian Anthracosaurus from Northumberland. Palaeontology 24:85–92.

Panchen, A. L. 1985. On the amphibian Crassigyrinus scoticus Watson from the Carboniferous of Scotland. Philosophical Transactions of the Royal Society B: Biological Sciences.

Panchen, A. L., and T. R. Smithson. 1987. Character diagnosis, fossils, and the origin of tetrapods. Biological Reviews 62:341–436.

Panchen, A. L., and T. R. Smithson. 1988. The relationships of the earliest tetrapods; pp. 1–32 in M. J. Benton (ed.), The Phylogeny and Classification of the Tetrapods. vol. 1: Amphibians, Reptiles, and Birds. Oxford University Press, New York City, New York, USA.

Panchen, A. L., and T. R. Smithson. 1990. The pelvic girdle and hind limb of Crassigyrinus scoticus (Lydekker) from the Scottish Carboniferous and the origin of the tetrapod pelvic skeleton. Transactions of the Royal Society of Edinburgh: Earth Sciences 81:31–44.

Paradis, E., and K. Schliep. 2019. ape 5.0: an environment for modern phylogenetics and evolutionary analyses in R. Bioinformatics 35:526–528.

Pardo, J. D., and A. Mann. 2018. A basal aïstopod from the earliest Pennsylvanian of Canada, and the antiquity of the first limbless tetrapod lineage. Royal Society Open Science 5:181056.

Pardo, J. D., B. J. Small, and A. K. Huttenlocker. 2017a. Stem caecilian from the Triassic of Colorado sheds light on the origins of Lissamphibia. Proceedings of the National Academy of Sciences 114:E5389–E5395.

Pardo, J. D., R. Holmes, and J. S. Anderson. 2019a. An enigmatic braincase from Five Points, Ohio (Westphalian D) further supports a stem tetrapod position for aïstopods. Earth and Environmental Science Transactions of the Royal Society of Edinburgh 255–264.

Pardo, J. D., K. Lennie, and J. S. Anderson. 2020. Can We Reliably Calibrate Deep Nodes in the Tetrapod Tree? Case Studies in Deep Tetrapod Divergences. Frontiers in Genetics 11:506749.

Pardo, J. D., M. Szostakiwskyj, P. E. Ahlberg, and J. S. Anderson. 2017b. Hidden morphological diversity among early tetrapods. Nature 546:642–645.

Pardo, J. D., B. J. Small, A. R. Milner, and A. K. Huttenlocker. 2019b. Carboniferous–Permian climate change constrained early land vertebrate radiations. Nature Ecology & Evolution 3:200–206.

Parravicini, V., M. Kulbicki, D. R. Bellwood, A. M. Friedlander, J. E. Arias-Gonzalez, P. Chabanet, S. R. Floeter, R. Myers, L. Vigliola, S. D'Agata, and D. Mouillot. 2013. Global patterns and predictors of tropical reef fish species richness. Ecography 36:1254–1262.

Paton, R. L., T. R. Smithson, and J. A. Clack. 1999. An amniote-like skeleton from the Early Carboniferous of Scotland. Nature 398:508–513.

Pawley, K. 2007. The postcranial skeleton of Trimerorhachis insignis (Temnospondyli: Trimerorhachidae): a plesiomorphic temnospondyl from the Lower Permian of North America. Journal of Paleontology 81:873–894.

Pawley, K., and A. Warren. 2006. The appendicular skeleton of Eryops megalocephalus Cope 1877 (Temnospondyli: Eryopoidea) from the Lower Permian of North America. Journal of Paleontology 80:561–580.

Pierce, S. E., J. A. Clack, and J. R. Hutchinson. 2012. Three-dimensional limb joint mobility in the early tetrapod Ichthyostega. Nature 486:523–526.

Pierce, S. E., J. R. Hutchinson, and J. A. Clack. 2013a. Historical Perspectives on the Evolution of Tetrapodomorph Movement. Integrative and Comparative Biology 53:209–223.

Pierce, S. E., P. E. Ahlberg, J. R. Hutchinson, J. L. Molnar, S. Sanchez, P. Tafforeau, and J. A. Clack. 2013b. Vertebral architecture in the earliest stem tetrapods. Nature 494:226–229.

Porro, L. B., E. J. Rayfield, and J. A. Clack. 2015. Descriptive Anatomy and Three-Dimensional Reconstruction of the Skull of the Early Tetrapod Acanthostega gunnari Jarvik, 1952. PLOS ONE 10:e0118882.

Puttick, M. N., J. E. O'Reilly, A. R. Tanner, J. F. Fleming, J. Clark, L. Holloway, J. Lozano-Fernandez, L. A. Parry, J. E. Tarver, D. Pisani, and P. C. J. Donoghue. 2017. Uncertain-tree: discriminating among competing approaches to the phylogenetic analysis of phenotype data. Proceedings of the Royal Society B: Biological Sciences 284:20162290.

Quicke, D. L. J., J. Taylor, and A. Purvis. 2001. Changing the Landscape: A New Strategy for Estimating Large Phylogenies. S YSTEMATIC BIOLOGY 50:7.

R Core Team. 2019. R: A Language and Environment for Statistical Computing). .

Rabosky, D. L., F. Santini, J. Eastman, S. A. Smith, B. Sidlauskas, J. Chang, and M. E. Alfaro. 2013. Rates of speciation and morphological evolution are correlated across the largest vertebrate radiation. Nature Communications 4:1958.

Rambaut, A. 2010. FigTree. .

Raup, D. M., and J. J. Sepkoski. 1982. Mass Extinctions in the Marine Fossil Record. Science 215:1501–1503.

Rawson, J. R. G., L. B. Porro, E. Martin-Silverstone, and E. J. Rayfield. 2021. Osteology and digital reconstruction of the skull of the early tetrapod *Whatcheeria deltae*. Journal of Vertebrate Paleontology e1927749.

Reisz, R. R. 1997. The origin and early evolutionary history of amniotes. Trends in Ecology & Evolution 12:218–222.

Richards, K. R., J. E. Sherwin, T. R. Smithson, R. F. Bennion, S. J. Davies, J. E. A. Marshall, and J. A. Clack. 2018. Diverse and durophagous: Early Carboniferous chondrichthyans from the Scottish Borders. Earth and Environmental Science Transactions of the Royal Society of Edinburgh 108:67–87.

Rogers, D. A. 1990. Probable tetrapod tracks rediscovered in the Devonian of N Scotland. Journal of the Geological Society 147:746–748.

Rolfe, W. D. I. 1980. Early Invertebrate Terrestrial Faunas. The Terrestrial Origin of Land Vertebrates 15:117–157.

Rolfe, W. D. I., G. P. Durant, W. J. Baird, C. Chaplin, R. L. Paton, and R. J. Reekie. 1993. The East Kirkton Limestone, Viséan, of West Lothian, Scotland: introduction and stratigraphy. Earth and Environmental Science Transactions of the Royal Society of Edinburgh 84:177–188.

Romer, A. S. 1956. The Early Evolution of Land Vertebrates. Proceedings of the American Philosophical Society 100:157–167.

Romer, A. S. 1957. The appendicular skeleton of the Permian embolomerous amphibian Archeria. University of Michicagn Contributions from the Museum of Paleontology 13:103–159.

Romer, A. S. 1958. Tetrapod limbs and early tetrapod life. Evolution 12:365–369.

Romer, A. S. 1963. The larger embolomerous amphibians of the American Carboniferous. Bullet of the Museum of Comparative Zoology 128:415–454.

Romer, A. S. 1966. Vertebrate Paleontology, 3rd ed. University of Chicago Press, Chicago, IL, pp.

Romer, A. S., and R. V. Witter. 1942. Edops, a Primitive Rhachitomous Amphibian from the Texas Red Beds. The Journal of Geology 50:925–960.

Roopnarine, P. D. 2006. Extinction cascades and catastrophe in ancient food webs. Paleobiology 32:1–19.

Roopnarine, P. D. 2009. Ecological modeling of paleocommunity food webs; pp. 195–220 in G. P. Dietl and K. W. Flessa (eds.), Conservation Paleobiology: Using the Past to Manage for the Future., . Paleontological Society Papers vol. 15. The Paleontological Society.

Roopnarine, P. D., and K. D. Angielczyk. 2012. The evolutionary palaeoecology of species and the tragedy of the commons. Biology Letters 8:147–150.

Roopnarine, P. D., and K. D. Angielczyk. 2015. Community stability and selective extinction during the Permian-Triassic mass extinction. Science 350:90–93.

Roopnarine, P. D., and K. D. Angielczyk. 2016. The Stability of Ecological Communities as an Agent of Evolutionary Selection; pp. 28 in N. Eldredge, T. Pievani, E. Serrilli, and I. Temkin (eds.), Evolutionary Theory: A Hierarchical Perspective. University of Chicago Press.

Roopnarine, P. D., K. D. Angielczyk, S. C. Wang, and R. Hertog. 2007. Trophic network models explain instability of Early Triassic terrestrial communities. Proceedings of the Royal Society B: Biological Sciences 274:2077–2086.

Roopnarine, P. D., K. D. Angielczyk, A. Weik, and A. Dineen. 2019. Ecological persistence, incumbency and reorganization in the Karoo Basin during the Permian-Triassic transition. Earth-Science Reviews 189:244–263.

Roopnarine, P. D., K. D. Angielczyk, S. L. Olroyd, S. J. Nesbitt, J. Botha-brink, B. R. Peecook, M. O. Day, and R. M. H. Smith. 2018. Comparative ecological dynamics of Permian-Triassic

communities from the Karoo, Luangwa, and Ruhuhu Basins of southern Africa. Journal of Vertebrate Paleontology 37:254–272.

Ross, A. J., G. D. Edgecombe, N. D. L. Clark, C. E. Bennett, V. Carrió, R. Contreras-Izquierdo, and B. Crighton. 2018. A new terrestrial millipede fauna of earliest Carboniferous (Tournaisian) age from southeastern Scotland helps fill 'Romer's Gap'. Earth and Environmental Science Transactions of the Royal Society of Edinburgh 108:99–110.

RStudio Team. 2019. RStudio. .

Ruta, M. 2011. Phylogenetic signal and character compatibility in the appendicular skeleton of early tetrapods. Special Papers in Palaeontology 86:31–43.

Ruta, M., and J. A. Clack. 2006. A review of Silvanerpeton miripedes, a stem amniote from the Lower Carboniferous of East Kirkton, West Lothian, Scotland. Transactions of the Royal Society of Edinburgh: Earth Sciences 46:115.

Ruta, M., and M. I. Coates. 2007. Dates, nodes and character conflict: Addressing the Lissamphibian origin problem. Journal of Systematic Palaeontology 5:69–122.

Ruta, M., and M. A. Wills. 2016. Comparable disparity in the appendicular skeleton across the fish-tetrapod transition, and the morphological gap between fish and tetrapod postcrania. Palaeontology 59:249–267.

Ruta, M., A. R. Milner, and M. I. Coates. 2002. The tetrapod Caerorhachis bairdi Holmes and Carroll from the Lower Carboniferous of Scotland. Transactions of the Royal Society of Edinburgh: Earth Sciences 92:229–261.

Ruta, M., M. I. Coates, and D. L. J. Quicke. 2003a. Early tetrapod relationships revisited. Biological Reviews of the Cambridge Philosophical Society 78:251–345.

Ruta, M., J. E. Jeffery, and M. I. Coates. 2003b. A supertree of early tetrapods. Proceedings of the Royal Society of London. Series B: Biological Sciences 270:2507–2516.

Ruta, M., P. J. Wagner, and M. I. Coates. 2006. Evolutionary patterns in early tetrapods. I. Rapid initial diversification followed by decrease in rates of character change. Proceedings of the Royal Society B: Biological Sciences 273:2107–2111.

Ruta, M., J. A. Clack, and T. R. Smithson. 2020. A review of the stem amniote *Eldeceeon rolfei* from the Viséan of East Kirkton, Scotland. Earth and Environmental Science Transactions of the Royal Society of Edinburgh 1–20.

Ruta, M., D. Pisani, G. T. Lloyd, and M. J. Benton. 2007. A supertree of Temnospondyli: cladogenetic patterns in the most species-rich group of early tetrapods. Proceedings of the Royal Society B: Biological Sciences 274:3087–3095.

Ruta, M., J. Krieger, K. D. Angielczyk, and M. A. Wills. 2018. The evolution of the tetrapod humerus: morphometrics, disparity, and evolutionary rates. Earth and Environmental Science Transactions of the Royal Society of Edinburgh 109:351–369.

Sahney, S., M. J. Benton, and P. A. Ferry. 2010. Links between global taxonomic diversity, ecological diversity and the expansion of vertebrates on land. Biology Letters 6:544–547.

Salamon, M. A., P. Gerrienne, P. Steemans, P. Gorzelak, P. Filipiak, A. Le Hérissé, F. Paris, B. Cascales-Miñana, T. Brachaniec, M. Misz-Kennan, R. Niedźwiedzki, and W. Trela. 2018. Putative Late Ordovician land plants. New Phytologist 218:1305–1309.

Sallan, L., and A. K. Galimberti. 2015. Body-size reduction in vertebrates following the end-Devonian mass extinction. Science 350:812–815.

Sallan, L. C. 2014. Major issues in the origins of ray-finned fish (Actinopterygii) biodiversity: Ray-finned fish (Actinopterygii) origins. Biological Reviews 89:950–971.

Sallan, L. C., and M. I. Coates. 2010. End-Devonian extinction and a bottleneck in the early evolution of modern jawed vertebrates. Proceedings of the National Academy of Sciences 107:10131–10135.

Sallan, L. C., T. W. Kammer, W. I. Ausich, and L. A. Cook. 2011. Persistent predator-prey dynamics revealed by mass extinction. Proceedings of the National Academy of Sciences 108:8335–8338.

Sanchez, S., P. Tafforeau, and P. E. Ahlberg. 2014. The humerus of Eusthenopteron: a puzzling organization presaging the establishment of tetrapod limb bone marrow. Proceedings of the Royal Society B: Biological Sciences 281:20140299–20140299.

Sanchez, S., P. Tafforeau, J. A. Clack, and P. E. Ahlberg. 2016. Life history of the stem tetrapod Acanthostega revealed by synchrotron microtomography. Nature 537:408–411.

Sansom, R. S., P. G. Choate, J. N. Keating, and E. Randle. 2018. Parsimony, not Bayesian analysis, recovers more stratigraphically congruent phylogenetic trees. Biology Letters 14:20180263.

Schoch, R. R. 1999. Comparative osteology of Mastodonsaurus giganteus (Jaeger, 1828) from the Middle Triassic (Lettenkeuper: Longobardian) of Germany (Baden-Württemberg, Bayern, Thüringen). Stuttgarter Beiträge Zur Naturkunde B 1–173.

Schoch, R. R. 2002. The Early Formation of the Skull in Extant and Paleozoic Amphibians. Paleobiology 28:278–296.

Schoch, R. R. 2012. Amphibian Evolution: The Life of Early Land Vertebrates (M. J. Benton (ed.)). Wiley-Blackwell, Chichester, West Sussex ; Hoboken, NJ, 322 pp.

Schoch, R. R. 2013. The evolution of major temnospondyl clades: an inclusive phylogenetic analysis. Journal of Systematic Palaeontology 11:673–705.

Schoch, R. R. 2018. Osteology of the temnospondyl *Neldasaurus* and the evolution of basal dvinosaurians. Neues Jahrbuch Für Geologie Und Paläontologie - Abhandlungen 287:1–16.

Schoch, R. R. 2019. The putative lissamphibian stem-group: phylogeny and evolution of the dissorophoid temnospondyls. Journal of Paleontology 93:137–156.

Schoch, R. R., and B. S. Rubidge. 2005. The amphibamid *Micropholis* from the Lystrosaurus Assemblage Zone of South Africa. Journal of Vertebrate Paleontology 25:502–522.

Schram, F. R. 1983. Lower Carboniferous biota of Glencartholm, Eskdale, Dumfriesshire. Scottish Journal of Geology 19:1–15.

Schultze, H.-P., and M. Arsenault. 1985. The panderichthyid fish Elpistostege: a close relative of tetrapods? Palaeontology 28:293–309.

Schultze, H.-P., and J. R. Bolt. 1996. The lungfish Tranodis and the tetrapod fauna from the Upper Mississippian of North America. Special Papers in Palaeontology 52:31–54.

Scotese, C. R. 2021. An Atlas of Phanerozoic Paleogeographic Maps: The Seas Come In and the Seas Go Out. Annual Review of Earth and Planetary Sciences 49:annurev-earth-081320-064052.

Sepkoski, J. J. 1981. A factor analytic description of the Phanerozoic marine fossil record. Paleobiology 7:36–53.

Servais, T., B. Cascales-Miñana, C. J. Cleal, P. Gerrienne, D. A. T. Harper, and M. Neumann. 2019. Revisiting the Great Ordovician Diversification of land plants: Recent data and perspectives. Palaeogeography, Palaeoclimatology, Palaeoecology 534:109280.

Shear, W. A. 1993. Myriapodous arthropods from the Viséan of East Kirkton, West Lothian, Scotland. Earth and Environmental Science Transactions of the Royal Society of Edinburgh 84:309–316.

Shear, W. A., and P. M. Bonamo. 1988. Devonobiomorpha, A New Order of Centipeds (Chilopoda) from the Middle Devonian of Gilboa, New York State, USA, and the Phylogeny of Centiped Orders. American Museum Novitates 32.

Shear, W. A., P. A. Selden, W. D. I. Rolfe, P. M. Bonamo, and J. D. Grierson. 1987. New Terrestrial Arachnids from the Devonian of Gilboa, New York (Arachnida, Trigonotarbida). American Museum Novitates 77.

Shear, W. A., P. M. Bonamo, J. D. Grierson, W. D. I. Rolfe, E. L. Smith, and R. A. Norton. 1984. Early Land Animals in North America: Evidence from Devonian Age Arthropods from Gilboa, New York. Science 224:492–494.

Shubin, N. H., E. B. Daeschler, and M. I. Coates. 2004. The Early Evolution of the Tetrapod Humerus. Science 304:90–93.

Shubin, N. H., E. B. Daeschler, and F. A. Jenkins. 2006. The pectoral fin of Tiktaalik roseae and the origin of the tetrapod limb. Nature 440:764–771.

Shubin, N. H., E. B. Daeschler, and F. A. Jenkins. 2014. Pelvic girdle and fin of Tiktaalik roseae. Proceedings of the National Academy of Sciences 111:893–899.

Sidor, C. A., D. A. Vilhena, K. D. Angielczyk, A. K. Huttenlocker, S. J. Nesbitt, B. R. Peecook, J. S. Steyer, R. M. H. Smith, and L. A. Tsuji. 2013. Provincialization of terrestrial faunas

following the end-Permian mass extinction. Proceedings of the National Academy of Sciences 110:8129–8133.

Sigurdsen, T., and J. R. Bolt. 2010. The Lower Permian amphibamid *Doleserpeton* (Temnospondyli: Dissorophoidea), the interrelationships of amphibamids, and the origin of modern amphibians. Journal of Vertebrate Paleontology 30:1360–1377.

Simões, T. R., and S. E. Pierce. 2021. Sustained high rates of morphological evolution during the rise of tetrapods. Nature Ecology & Evolution.

Slowikowski, K. 2020. ggrepel: Automatically Position Non-Overlapping Text Labels with ggplot2. .

Smith, R. A., D. Stephenson, and S. K. Monro. 1994. The geological setting of the southern Bathgate Hills, West Lothian, Scotland. Transactions of the Royal Society of Edinburgh: Earth Sciences 84:189–196.

Smithson, T. R. 1980. An early tetrapod fauna from the Namurian of Scotland; pp. in A. L. Panchen (ed.), The Terrestrial Environment and the Origin of Land Vertebrates., . Systematics Association Special Volume Academic Press, London, England, UK.

Smithson, T. R. 1982. The cranial morphology of Greererpeton burkemorani Romer (Amphibia: Temnospondyli). Zoological Journal of the Linnean Society 76:29–90.

Smithson, T. R. 1985a. Scottish Carboniferous amphibian localities. Scottish Journal of Geology 21:123–142.

Smithson, T. R. 1985b. The morphology and relationships of the Carboniferous amphibian Eoherpeton watsoni Panchen. Zoological Journal of the Linnean Society 85:317–410.

Smithson, T. R., and J. A. Clack. 2018. A new tetrapod from Romer's Gap reveals an early adaptation for walking. Earth and Environmental Science Transactions of the Royal Society of Edinburgh 108:89–97.

Smithson, T. R., R. L. Carroll, A. L. Panchen, and S. M. Andrews. 1993. Westlothiana lizziae from the Viséan of East Kirkton, West Lothian, Scotland, and the amniote stem. Transactions of the Royal Society of Edinburgh: Earth Sciences 84:383–412.

Smithson, T. R., S. P. Wood, J. E. A. Marshall, and J. A. Clack. 2012. Earliest Carboniferous tetrapod and arthropod faunas from Scotland populate Romer's Gap. Proceedings of the National Academy of Sciences 109:4532–4537.

Snyder, D. 2006. A study of the fossil vertebrate fauna from the Jasper Hiemstra Quarry, Delta, Iowa and its environment. MS, University of Iowa pp.

Song, H., P. B. Wignall, and A. M. Dunhill. 2018. Decoupled taxonomic and ecological recoveries from the Permo-Triassic extinction. Science Advances 4:7.

Stanley, S. M. 2008. Predation defeats competition on the seafloor. Paleobiology 34:1–21.

Stein, W. E., C. M. Berry, L. V. Hernick, and F. Mannolini. 2012. Surprisingly complex community discovered in the mid-Devonian fossil forest at Gilboa. Nature 483:78–81.

Stein, W. E., C. M. Berry, J. L. Morris, L. V. Hernick, F. Mannolini, C. Ver Straeten, E. Landing, J. E. A. Marshall, C. H. Wellman, D. J. Beerling, and J. R. Leake. 2019. Mid-Devonian Archaeopteris Roots Signal Revolutionary Change in Earliest Fossil Forests. Current Biology S0960982219315696.

Stewart, T. A., J. B. Lemberg, A. Daly, E. B. Daeschler, and N. H. Shubin. 2022. A new elpistostegalian from the Late Devonian of the Canadian Arctic. Nature 608:563–568.

Stewart, T. A., J. B. Lemberg, N. K. Taft, I. Yoo, E. B. Daeschler, and N. H. Shubin. 2019. Fin ray patterns at the fin-to-limb transition. Proceedings of the National Academy of Sciences 201915983.

Stössel, I. 1995. The discovery of a new Devonian tetrapod trackway in SW Ireland. Journal of the Geological Society 152:407–413.

Stössel, I., E. A. Williams, and K. T. Higgs. 2016. Ichnology and depositional environment of the Middle Devonian Valentia Island tetrapod trackways, south-west Ireland. Palaeogeography, Palaeoclimatology, Palaeoecology 462:16–40.

Strotz, L. C., and B. S. Lieberman. 2020. The names don’t matter but the numbers do: searching for stability in Carboniferous brachiopod paleocommunities from the North American Midcontinent. Paleobiology 1–18.

Strullu-Derrien, C., C. J. Cleal, C. Ducassou, A. R. T. Spencer, E. Stolle, and V. O. Leshyk. 2021. A rare late Mississipian flora from Northwestern Europe (Maine-et-Loire Coalfield, Pays de la Loire, France). Review of Palaeobotany and Palynology 285:104359.

Swofford, D. 2003. PAUP*. phylogenetic analysis using parsimony (*and other methods). .

Trewin, N. H. 1992. Depositional environment and preservation of biota in the Lower Devonian hot-springs of Rhynie, Aberdeenshire, Scotland. Transactions of the Royal Society of Edinburgh: Earth Sciences 84:433–442.

Trinajstic, K., and J. A. Long. 2009. A new genus and species of Ptyctodont (Placodermi) from the Late Devonian Gneudna Formation, Western Australia, and an analysis of Ptyctodont phylogeny. Geological Magazine 146:743–760.

Trinajstic, K., D. E. G. Briggs, and J. A. Long. 2022. The Gogo Formation Lagerstätte: a view of Australia’s first great barrier reef. Journal of the Geological Society 179:jgs2021-105.

Vermeij, G. J. 1977. The Mesozoic marine revolution: evidence from snails, predators and grazers. Paleobiology 3:245–258.

Vorobyeva, E. I. 1995. Shoulder girdle of Panderichthys rhombolepis (Gross) (Crossopterygii), Upper Devonian, Latvia. Geobios 19:285–288.

Wagner, P. J., M. Ruta, and M. I. Coates. 2006. Evolutionary patterns in early tetrapods. II. Differing constraints on available character space among clades. Proceedings of the Royal Society B: Biological Sciences 273:2113–2118.

Wang, D., M. Qin, L. Liu, L. Liu, Y. Zhou, Y. Zhang, P. Huang, J. Xue, S. Zhang, and M. Meng. 2019. The Most Extensive Devonian Fossil Forest with Small Lycopsid Trees Bearing the Earliest Stigmarian Roots. Current Biology S0960982219307808.

Ward, P., C. Labandeira, M. Laurin, and R. A. Berner. 2006. Confirmation of Romer's Gap as a low oxygen interval constraining the timing of initial arthropod and vertebrate terrestrialization. Proceedings of the National Academy of Sciences 103:16818–16822.

Warren, A. 2007. New data on *Ossinodus pueri* , a stem tetrapod from the Early Carboniferous of Australia. Journal of Vertebrate Paleontology 27:850–862.

Warren, A., and S. Turner. 2004. The First Stem Tetrapod from the Lower Carboniferous of Gondwana. Palaeontology 47:151–184.

Warren, J. W., and N. A. Wakefield. 1972. Trackways of Tetrapod Vertebrates from the Upper Devonian of Victoria, Australia. Nature 238:469–470.

Wellstead, C. F. 1982. A Lower Carboniferous aïstopod amphibian from Scotland. Palaeontology 25:193–208.

Werneburg, R., F. Witzmann, and J. W. Schneider. 2019. The oldest known tetrapod (Temnospondyli) from Germany (Early Carboniferous, Viséan). PalZ.

White, T. E. 1939. Osteology of Seymouria baylorensis Broil. Bulletin of the Museum of Comparative Zoology 85:325–409.

Whitney, M. R., and S. E. Pierce. 2021. Osteohistology of *Greererpeton* provides insight into the life history of an early Carboniferous tetrapod. Journal of Anatomy joa.13520.

Whitney, M. R., B. K. A. Otoo, K. D. Angielczyk, and S. E. Pierce. 2022. Fossil bone histology reveals ancient origins for rapid juvenile growth in tetrapods. Communications Biology 5:1280.

Wickham, H. 2016. ggplot2: Elegant Graphics for Data Analysis. .

Wills, M. A. 1999. Congruence Between Phylogeny and Stratigraphy: Randomization Tests and the Gap Excess Ratio. Systematic Biology 48:559–580.

Wilson, R. B. 1989. A study of the Dinantian marine macrofossils of central Scotland. Transactions of the Royal Society of Edinburgh 89:91–126.

Witzmann, F. 2005. Cranial morphology and ontogeny of the Permo-Carboniferous temnospondyl Archegosaurus decheni Goldfuss, 1847 from the Saar–Nahe Basin, Germany. Transactions of the Royal Society of Edinburgh: Earth Sciences 96:131–162.

Witzmann, F., and I. Werneburg. 2017. The Palatal Interpterygoid Vacuities of Temnospondyls and the Implications for the Associated Eye- and Jaw Musculature. The Anatomical Record 300:1240–1269.

Wood, M. 2018. Glencartholm revisited: describing for the first time Stan Wood's discovery and excavation of Mumbie Quarry, adjacent to the important Palaeozoic fossil site of Glencartholm. Earth and Environmental Science Transactions of the Royal Society of Edinburgh 108:47–54.

Wood, S. P., A. L. Panchen, and T. R. Smithson. 1985. A terrestrial fauna from the Scottish Lower Carboniferous. Nature 314:355–356.

Wright, A. M., and D. M. Hillis. 2014. Bayesian Analysis Using a Simple Likelihood Model Outperforms Parsimony for Estimation of Phylogeny from Discrete Morphological Data. PLoS ONE 9:e109210.

Wright, J. J., S. R. David, and T. J. Near. 2012. Gene trees, species trees, and morphology converge on a similar phylogeny of living gars (Actinopterygii: Holostei: Lepisosteidae), an ancient clade of ray-finned fishes. Molecular Phylogenetics and Evolution 63:848–856.

Yao, L., W. Qie, G. Luo, J. Liu, T. J. Algeo, X. Bai, B. Yang, and X. Wang. 2015. The TICE event: Perturbation of carbon–nitrogen cycles during the mid-Tournaisian (Early Carboniferous) greenhouse–icehouse transition. Chemical Geology 401:1–14.

Yao, L., M. Aretz, P. B. Wignall, J. Chen, D. Vachard, Y. Qi, S. Shen, and X. Wang. 2020. The longest delay: Re-emergence of coral reef ecosystems after the Late Devonian extinctions. Earth-Science Reviews 203:103060.

Young, G. C., and J. A. Long. 2014. New arthrodires (placoderm fishes) from the Aztec Siltstone (late Middle Devonian) of southern Victoria Land, Antarctica. Australian Journal of Zoology 62:44.

Zapalski, M. K., and E. N. K. Clarkson. 2015. Enigmatic Fossils from the Lower Carboniferous Shrimp Bed, Granton, Scotland. PLOS ONE 10:e0144220.

Zhang, F., T. W. Dahl, T. M. Lenton, G. Luo, S. Shen, T. J. Algeo, N. Planavsky, J. Liu, Y. Cui, W. Qie, S. J. Romaniello, and A. D. Anbar. 2020. Extensive marine anoxia associated with the Late Devonian Hangenberg Crisis. Earth and Planetary Science Letters 533:115976.

Zhu, M., and P. E. Ahlberg. 2004. The origin of the internal nostril of tetrapods. Nature 432:94–97.

Zhu, M., P. E. Ahlberg, W. Zhao, and L. Jia. 2002. First Devonian tetrapod from Asia. Nature 420:760–761.

1990. Palaeobiology- A Synthesis (D. E. G. Briggs and P. R. Crowther (eds.)). Blackwell Scientific Publications, 598 pp.

APPENDIX A: SUPPORTING INFORMATION FOR CHAPTER 2

RECONSTRUCTION PROCEDURE

The reconstructions of *Whatcheeria* were produced via synthesis of multiple specimens, which are listed in Table A.1. Specimens used in production of full-body reconstruction.. Figure A.1 shows portions of the full-body reconstruction that were restored and 'repaired'. Figure A.2 shows primary contributions of specimens to the reconstruction.

INITIAL SETUP AND AXIAL SKELETON

Line drawings of FMNH PR 1700 and FMNH PR 1875 were scaled to the size of FMNH PR 1816. These specimens all preserve significant portions of the axial skeleton, that of FMNH PR 1816 being the most complete. Correlation between the FMNH PR 1700 and FMNH PR 1816 was done on the basis of the presence of cervical and pectoral ribs in both specimens; FMNH PR 1875 was correlated with FMNH PR 1816 using the presence of the sacral rib in both specimens. FMNH PR 4998 was scaled to FMNH PR 1816 and its caudal material added to that of FMNH PR 1816 at the beginning of the hemal spines. The tail is thus a minimum estimate of tail length. FMNH PR 1875 preserves hemal spines 2-~9 and thus overlaps with FMNH PR 1816. It is suggestive of the size transition produced by the composite FMNH PR 1816 + FMNH PR 4998 hemal spine series.

The reconstruction of the atlas/axis is described in the main text, and derives primarily from PR 1634, with guidance from *Acanthostega* (Coates, 1996) and *Pederpes* (Clack & Finney, 2005).

The composite axial column is complete for its entire presacral extent, except for the atlas/axis complex (see main text). When vertebrae were poorly exposed or preserved in one specimen they were restored following their counterpart in another. If this was not possible, their morphology was restored based on their neighbors, considering their position in the column. When a vertebral component could not be positively identified but its presence could reasonably be inferred- and its absence would be deeply unusual- it was restored based on its counterpart(s) elsewhere in the reconstruction and in other early tetrapods. It was on this basis that the caudal pleurocentra were restored posterior to the caudal ribs. The region is present in FMNH PR 4998 (see above) but preservation is poor and the pleurocentra cannot be positively identified. However, pleurocentra are present in this region in other tetrapods (Holmes, 1989; Coates, 1996). On a similar basis, in the reconstruction, pleurocentra are absent in posteriormost seven tail segments and the tail terminates in a single conical segment as in *Acanthostega* and *Ichthyostega* (Coates, 1996; Ahlberg, Clack, & Blom, 2005; Pierce, Clack, & Hutchinson, 2012).

RIBS

The cervical ribs are derived from FMNH PR 1700 with minimal modification, though cervical rib 3 has been restored as the specimen is damaged. It was restored was a slight distal expansion to provide a transition between the preceding and succeeding ribs. The second pectoral rib is poorly exposed and was mainly restored based on the preceding rib and its counterparts in *Proterogyrinus* and *Archeria* (Holmes, 1984, 1989). The anterior trunk ribs are derived from the holotype (FMNH FMNH PR 1700), with broken ribs being restored by joining segments in Photoshop to produce the complete rib. Most of anterior trunk rib 2 is not preserved/exposed,

and it has been restored based on its neighbors and isolated anterior trunk ribs. The posterior trunk ribs are derived from FMNH PR 1700, PR 1816, and FMNH PR 1875 with minimal restoration. Posterior trunk rib 8 is not preserved and has been restored.

The sacral rib is based on FMNH PR 1816 and FMNH PR 4997, informed by comparison with *Acanthostega* (Coates, 1996); while it is present in FMNH PR 1875, it is not very informative morphologically. The caudal ribs and the anterior eight hemal spines are derived from FMNH PR 1816, with the rest of the tail derived from FMNH PR 4998 with some restoration (see above).

PECTORAL GIRDLE AND LIMB

The scapulocoracoid and cleithrum are based on SUI 52077, FMNH PR 5004, FMNH PR 1789, FMNH PR 1703, and PR 1635 (Fig.15). SUI 52077, PR 1635, and FMNH PR 5004 were the principal sources. SUI 52077 was overlaid onto FMNH PR 5004, with those two specimens mapped onto PR 1635 to produce a complete scapulocoracoid and cleithrum. FMNH PR 5002 and FMNH PR 5003 provided information

on the dorsal tip of the cleithrum. Further detail, including the lateral overlap with the scapulocoracoid, was provided by UN-A12. The other specimens guided the synthesis. The reconstruction was then scaled to the axial skeleton via PR 1635 and FMNH PR 1816.

The interclavicle is based on PR 1740 and PR 1743, with additional detail of the plate provided by SUI 5208. The clavicle is based on UN-A11 and FMNH PR 5001.

The humerus is based on FMNH PR 1669, a complete but slightly damaged, three-dimensionally preserved specimen. It was scaled based on the relative sizes of the FMNH PR 1816 axial

skeleton and accompanying pectoral girdle and forelimb material (in particular the size of the glenoid), as well as qualitative observations of larger (=? more mature) specimens such as PR 1635. The radius and ulna are based on FMNH PR 1993 and FMNH PR 1998, respectively. FMNH PR 2006 was used to better establish the morphology of the olecranon process. The radius and ulna were scaled each other and then to the humerus based on FMNH PR 1816 and PR 1635.

MANUS

The restoration of the manus is visually represented in Figure 2.22, and the derivation of the phalangeal formula is discussed in the main text. The only modification between FMNH PR 1816 and the reconstruction is the restoration of a proximalmost phalanx in digit V, as we were unable to find an example of a three-segment digit V in the literature and judge it to be a reasonable restoration.

PELVIC GIRDLE AND LIMB

The pelvis is mostly based on PR 1740. FMNH PR 4998, FMNH PR 1733, and SUI 52087 provided the posterior portion of the girdle and additional detail. The pelvis was scaled to the axial skeleton via FMNH PR 4998.

The hindlimb was restored after FMNH PR 1958 (femur) and FMNH PR 5011 (tibia and fibula) (Figure 2.24, Figure 2.25). The three bones were scaled to each other based on FMNH PR 5011, and the result was scaled to the same length as the forelimb. We acknowledge implicitly

assumes that the similarity in lengths between the forelimb and hindlimb remains the same across size classes.

PES

The restoration of the pes is visually represented in Figure 2.27, and the derivation of the phalangeal formula is discussed in the main text. The pes is entirely based on FMNH PR 1700. As with the manus, bones were assigned to digits by minimizing the amount of movement. After the establishment of five digits, several segments were present that had not been assigned, mostly below the layer of phalanges. Based on their size and position, as well as the pattern of disruption illustrated by the phalanges, these segments were identified as distal tarsals and assigned to the ankle.

SKULL

The skull is based on FMNH PR 1634 and was scaled to the axial skeleton via FMNH PR 1700, which originally had the skull and postcrania in articulation before they were separated for study (Lombard & Bolt, 1995, Plate 1). The posterior portion of the left cheek in FMNH PR 1634 was moved ventrally and anteriorly to close the crack in the specimen. The snout was bent posteriorly and ventrally in order to close the crack between the maxilla and premaxilla. The morphology of the prefrontal and frontals (via FMNH PR 1651, a skull table) suggested a bend in the snout similar to *Pederpes*, which is also suggested in other, more damaged skulls (FMNH PR 1700, FMNH PR 1813). The jaw is based on FMNH PR 1634 and the reconstruction in

Lombard & Bolt, 2006 and was scaled to the skull via the jaw in FMNH PR 1634. These specimens are figured in Figure A.3.

The dorsal view was generated by projecting the lateral view reconstruction into dorsal aspect and scaled to the palatal reconstruction published recently by Bolt and Lombard (2018). Specifically, we used the reconstruction wherein the palatal bones are flat in the same plane (Bolt & Lombard, 2018, Fig.1). The authors also present a reconstruction with vaulted pterygoids and a correspondingly narrower skull (Bolt & Lombard, 2018, Fig.8). We chose the former reconstruction as a conservative hypothesis and because it is the reconstruction on which the description is based, as a detailed investigation of skull anatomy is beyond the scope of this study. The skull reconstruction presented in Chapter 2 and detailed here is superseded by the cranial reconstruction by Rawson and colleagues (Rawson et al., 2021). This skull is the one used in Figure 2.33, Figure 2.34, and the updated *Whatcheeria* reconstruction presented in CHAPTER 3 (see also APPENDIX B).

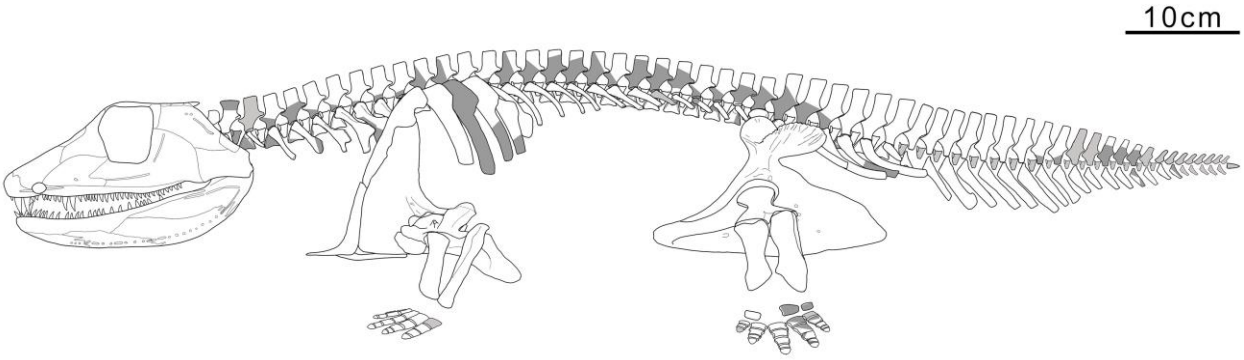

Figure A-1. Full body reconstruction of *Whatcheeria* in standing posture, with restored areas in grey. Lighter grey bones are those which are either not preserved or are preserved but the morphology of which could not be discerned in specimens and had to be restored based on other taxa. Darker grey bones are preserved and discernible but poorly exposed, and were restored after isolated specimens.

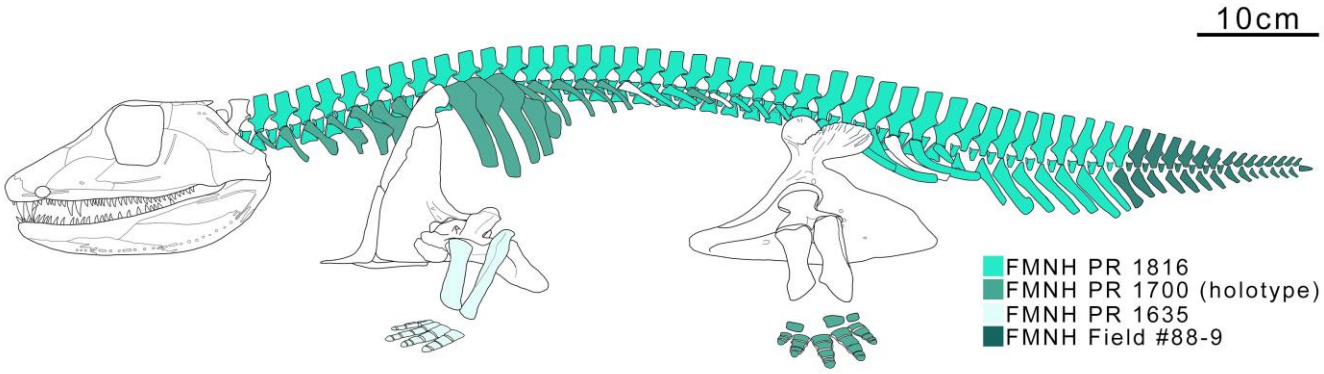

Figure A.2. Full body reconstruction of *Whatcheeria* showing contributions of major specimens to the reconstruction. The girdles and limbs are not colored because of the large number of specimens (mostly isolated) that were consulted.

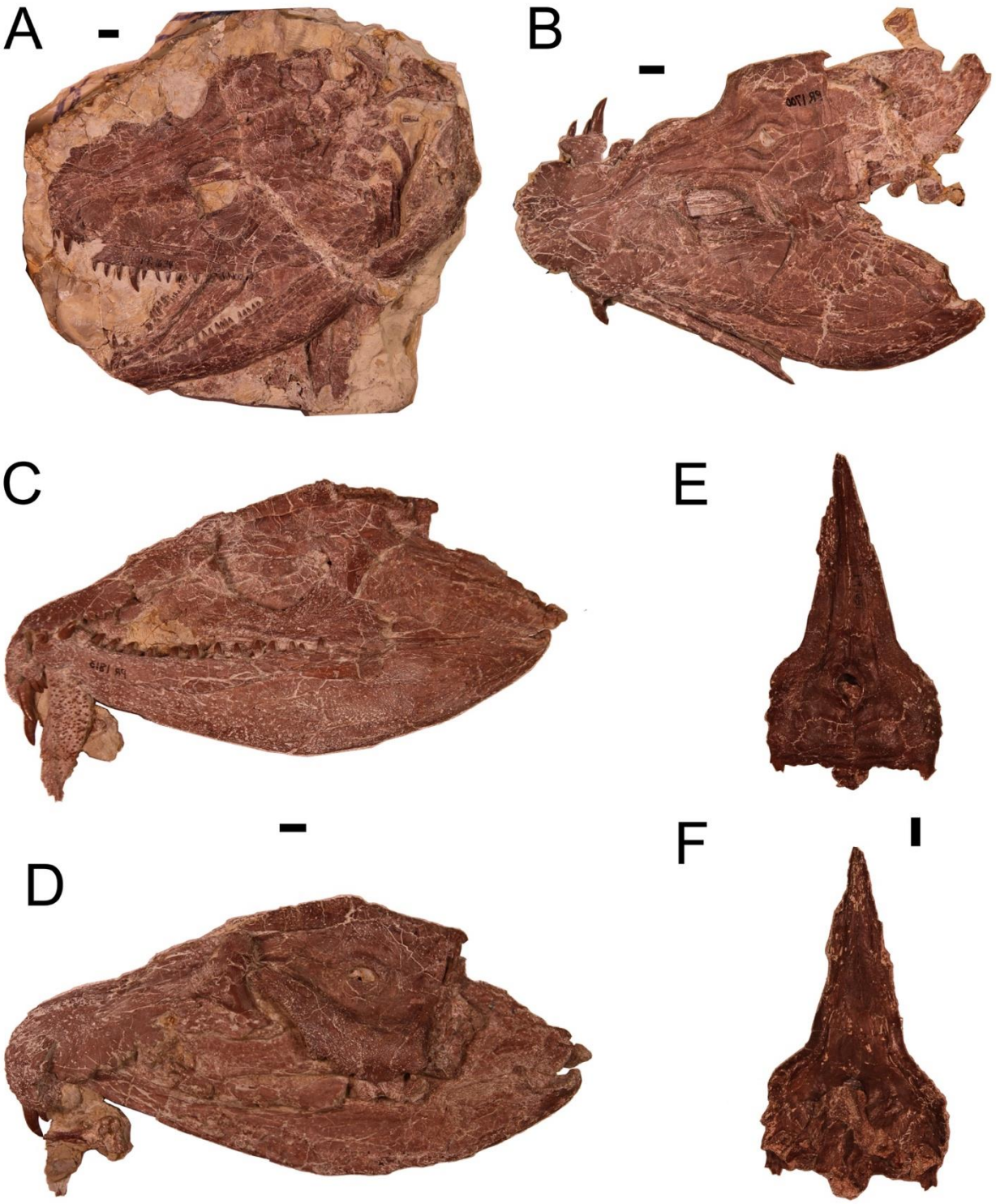

Figure A.3. Cranial material of *Whatcheeria* used in reconstruction. A) FMNH PR 1634; B) FMNH PR 1700; C) FMNH PR 1813, right lateral view (mirrored); D) FMNH PR 1813, left lateral view; E) FMNH PR 1651, external view; F) FMNH PR 1651, interal view. In A-D, anterior is to the left and dorsal is up. In E) and F), anterior is up.

PROJECTION AND POSTURE

Reconstructions of early tetrapods are not always restored with bones in life orientation and foreshortened relative to the viewer. We feel that the extra work involved is justified by the improved anatomical data and provides an explicit and reproducible hypothesis of how the skeleton fits together, allowing for improved functional and ecological inferences. Generally, after the orientation and posture of a bone was established, it was modeled in clay and its proportional change in length due to projection was measured; line art of that bone was foreshortened accordingly and redrawn.

The orientations of the ribs were established based on comparisons with three-dimensional early tetrapod material, especially the CT reconstruction of *Ichthyostega* in (Pierce *et al.*, 2012) and mounted specimens of *Eryops* at the Smithsonian and Field Museum.

The lateral view of the clavicles is based on three-dimensional material. *Ichthyostega* (Jarvik, 1996; Pierce *et al.*, 2012) was used to inform the reconstruction. The ventral portion of the scapulocoracoid was dorsoventrally shortened based on *Acanthostega* (Coates, 1996). View of the humerus was obtained by orienting a cast of FMNH PR 1669 and drawing from a photograph. The other bones of the forelimb and hindlimb, as well as those of the manus and pes, were modeled in clay and projected using the same procedure as for the ribs.

The standing posture (Figure 2.2A) was based on that of the *Proterogyrinus* reconstruction by Holmes (Holmes, 1984), with the aim to portray a plausible posture while maintaining visibility in lateral view. The axial column was made convex upwards along the trunk, and the cervical and caudal regions were made convex down. This slightly shortened the axial column overall

and brought the head closer to the shoulder girdle. Figure A.4 shows an alternative standing reconstruction with a straight axial column. The floating posture (Figure 2.2B) was based on that adopted by crocodilians and was produced by projecting the manus and pes more or less straight downwards as much as possible. The pes was slightly foreshortened in accordance with the change in orientation.

RECONSTRUCTION SPECIMENS

Table A.1. Specimens used in production of full-body reconstruction.

Specimen number	Identity
FMNH PR 1700	Articulated cervical, trunk vertebrae with ribs, partial shoulder girdle, left hindlimb with pes
FMNH PR 1816	Articulated presacral and partial sacral axial column, ribs, mandibles, pectoral girdle, ?right forelimb
FMNH PR 1875	Articulated posterior trunk and anterior caudal vertebrae, ribs, hemal spines
FMNH PR 4998	Partial right pelvis, disrupted caudal series
FMNH PR 4997	?left sacral rib
SUI 52077	Partial left scapulocoracoid
FMNH PR 5004	Left scapulocoracoid and cleithrum
FMNH PR 1789	Left scapulocoracoid
FMNH PR 1703	Left scapulocoracoid and cleithrum
FMNH PR 5006	Right scapulocoracoid and cleithrum
FMNH PR 5003	Left cleithrum dorsal tip
FMNH PR 5002	Left cleithrum dorsal tip
FMNH PR 5007	Right cleithrum and unknown bone (fibula?)
FMNH PR 1635	Partial articulated axial column, shoulder girdles, right forelimb and partial manus, assorted ribs, tibia, fibula
FMNH PR 1740	Interclavicle, right pelvis
FMNH PR 1743	Interclavicle
SUI 52088	Interclavicle plate
FMNH PR 5001	Left clavicle stem
FMNH PR 5018	Right clavicle ventral plate
FMNH PR 1669	Left humerus
FMH PR 1993	Radius
FMNH PR 1998	Ulna
FMNH PR 2006	Olecranon process

FMNH PR 1733	Partial pelvis
SUI 52087	Partial pelvis
FMNH PR 5011	Associated left femur, tibia, and fubla
FMNH PR 1634	Skull jaws, cervicle vertebrae, clavicles
FMNH PR 1651	Skull table, frontals

ALTERNATE POSITION OF PECTORAL GIRDLE

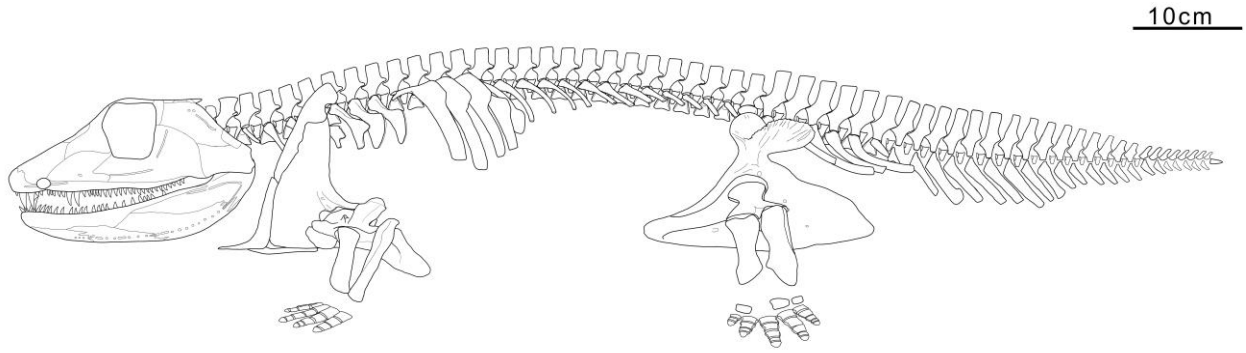

Figure A.4. Alternate version of full-body reconstruction, with the pectoral girdle moved anteriorly to a ‘tetrapod normal’ position immediately behind the skull. This anterior shift exposes the discontinuity in the rib series at the transition from the pectoral ribs to the much longer anterior trunk ribs. See main text for further discussion of trunk rib morphology and pectoral girdle placement, Figure 2.2 in the main text for the full-body reconstruction, and Reconstruction procedure (see above) for a detailed discussion of how the reconstructions were produced.

ADDITIONAL RESULTS FROM PRINCIPAL COMPONENTS ANALYSIS

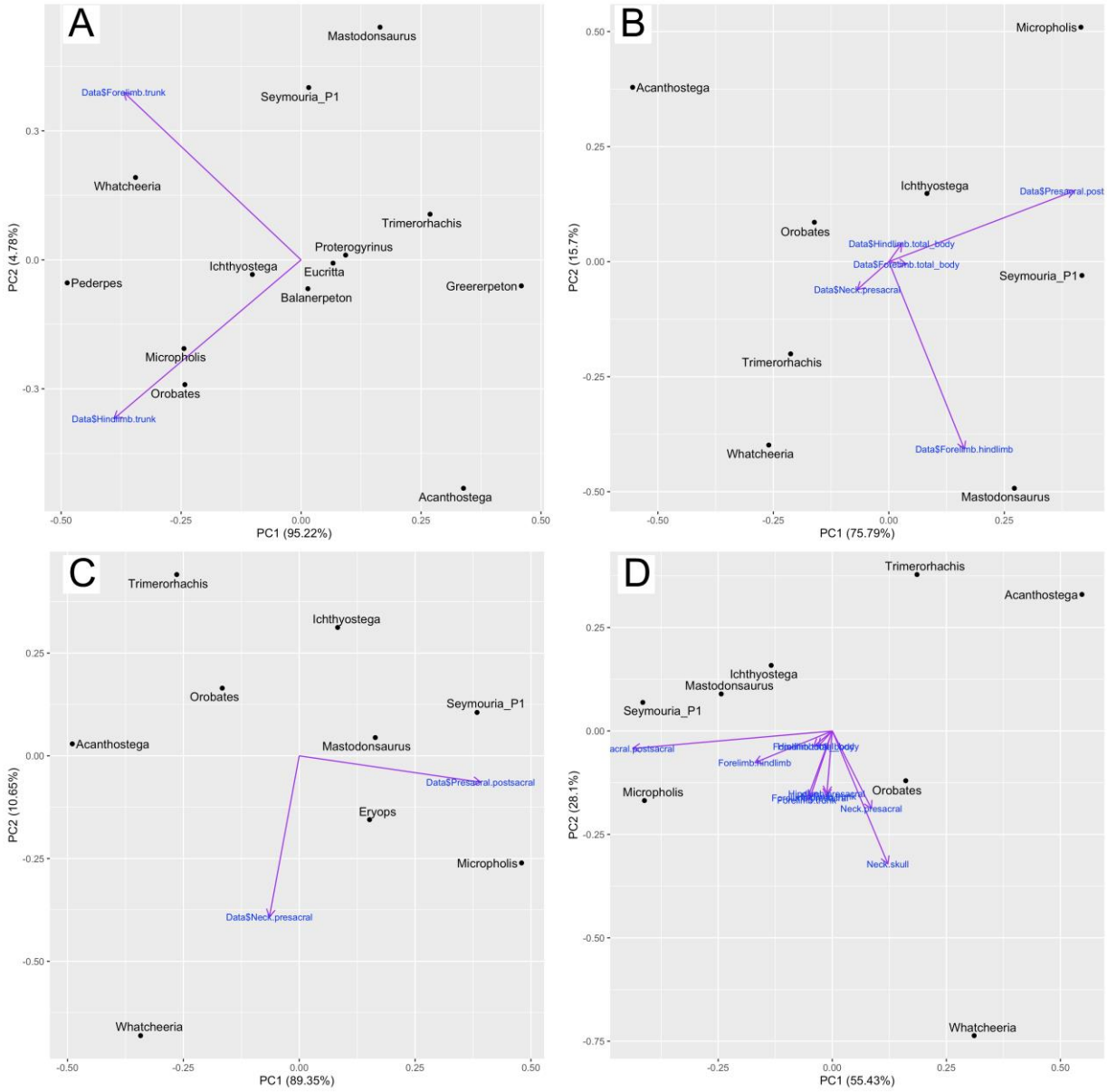

Figure A.5. Results from additional permutations of the Principal Components Analysis. A) Forelimb/trunk length, hindlimb/trunk length; B) presacral/postsacral length, forelimb/total body length, hindlimb/total body length, neck/presacral length, forelimb/hindlimb length; C) neck/presacral length, presacral/postsacral length; D) all variables. In particular, note the effect of Whatcheeria's uniquely long neck (and correspondingly high neck/presacral length ratio) in placing it far away from other taxa in morphospace.

ADDITIONAL RECONSTRUCTIONS OF PECTORAL AND PELVIC GIRDLES

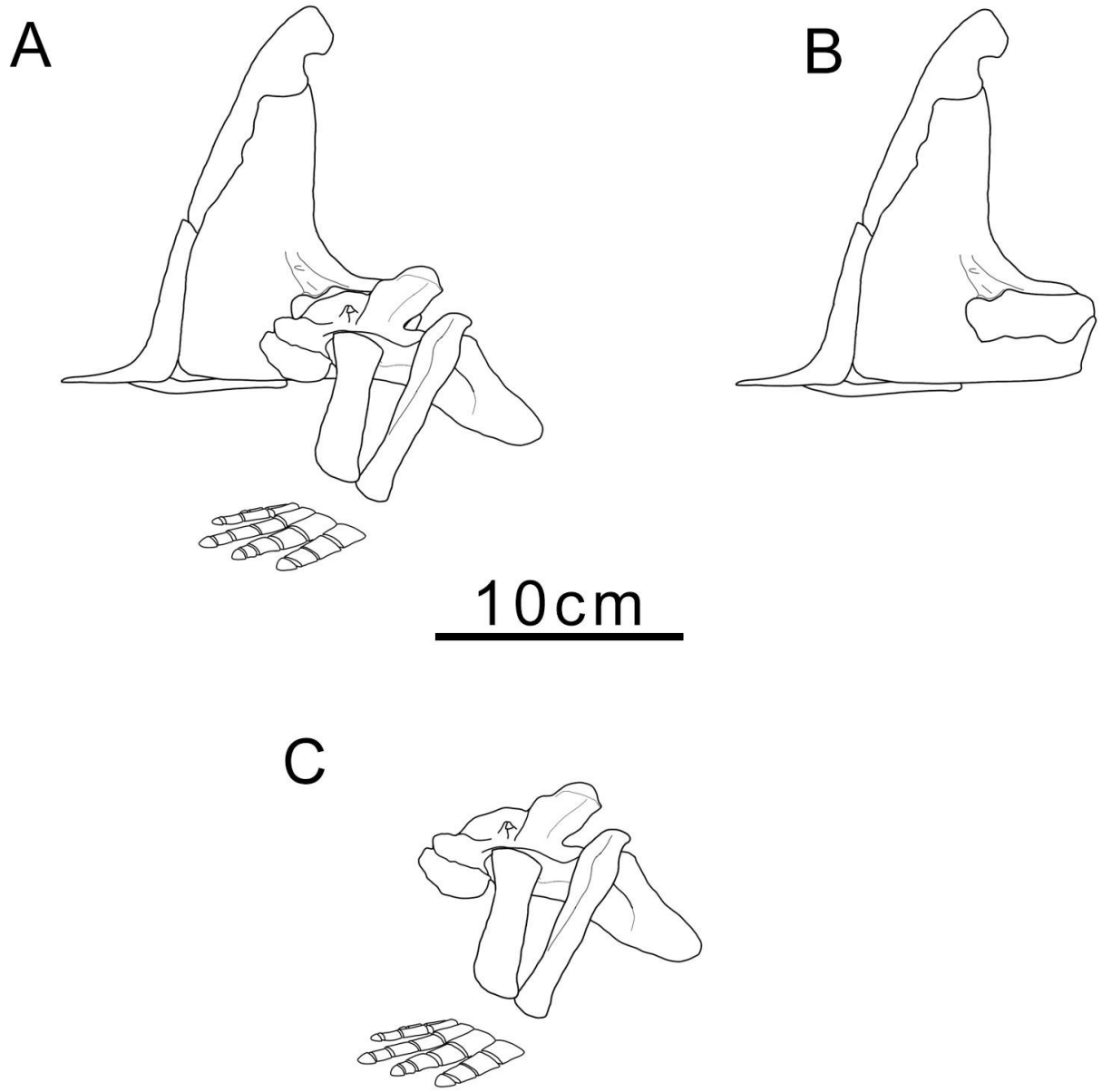

Figure A.6. Additional reconstructions of the pectoral girdle and forelimb. A) Articulated forelimb and shoulder girdle in left lateral view; B) pectoral girdle in left lateral view; C) left forelimb in articulation.

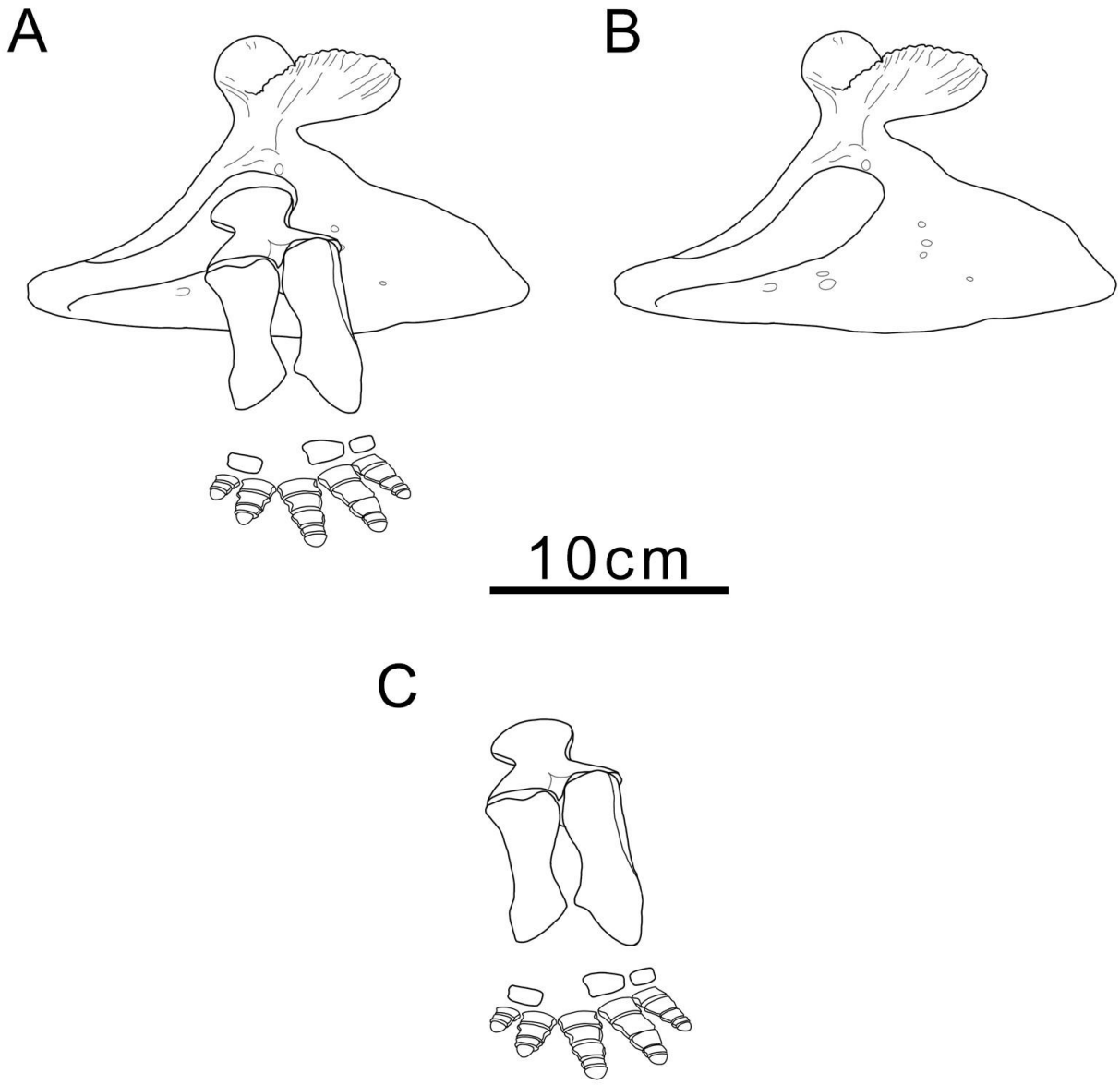

Figure A.7. Additional reconstructions of the pectoral girdle and forelimb. A) Articulated forelimb and shoulder girdle in left lateral view; B) pectoral girdle in left lateral view; C) left forelimb in articulation.

ILLUSTRATION OF HUMERAL TORSION MEASUREMENTS IN *WHATCHEERIA*

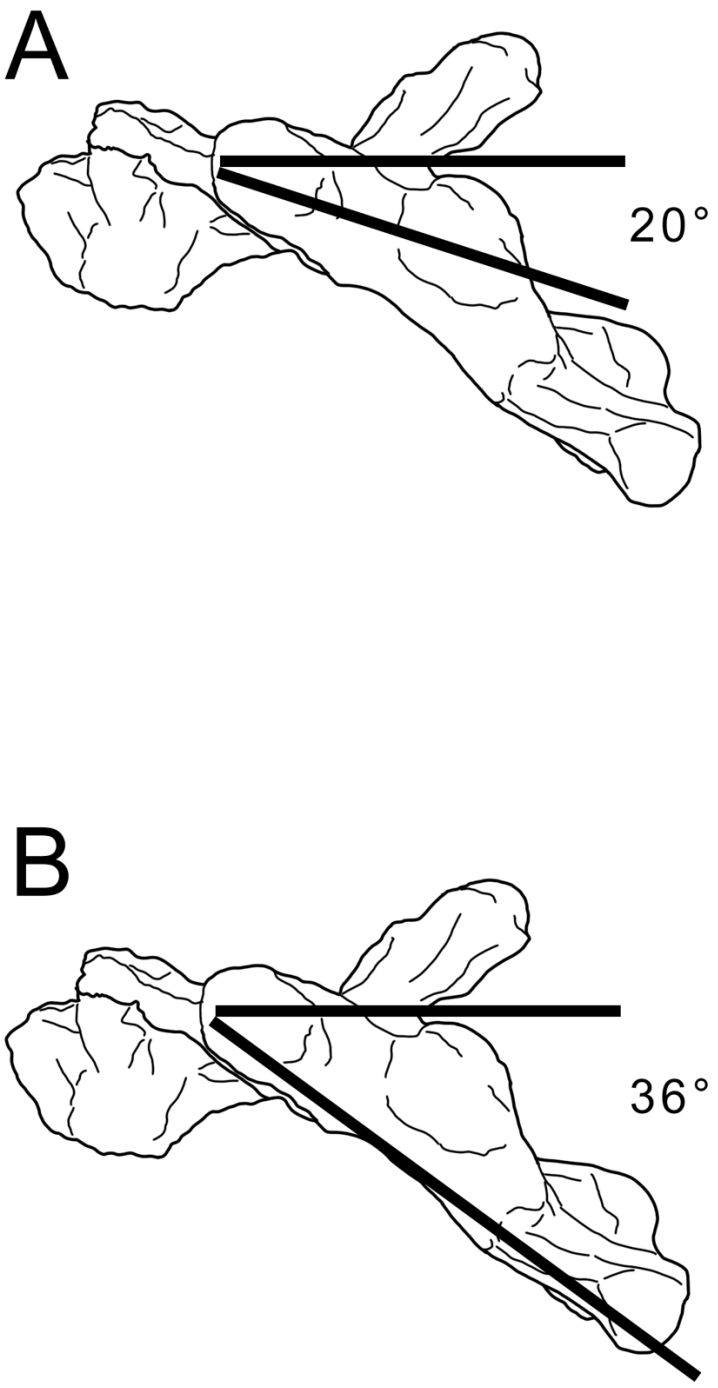

Figure A.8. Humeral torsion measurements in *Whatcheeria*. A) measurement of torsion when projected through the radial and ulnar condyles; B) measurement of torsion when projected through the radial condyle and laterodistal corner of the entepicondyle. Both A) and B) are oriented such that the longest axis of the proximal end of the humerus is at horizontal.

APPENDIX B: SUPPORTING INFORMATION FOR CHAPTER 3

B.1 *WHATCHEERIA* RECONSTRUCTION PROCEDURE

The reconstruction of *Whatcheeria* presented herein is identical to that of (Otoo et al., 2021) in the postcranial skeleton. The dorsal view of the skull and lateral view of the skull and mandible are based on those of (Rawson et al., 2021).

B.2 *GREERERPETON* RECONSTRUCTION PROCEDURE

The fully-body reconstruction of *Greererpeton burkemorani* presented by Godfrey (Godfrey, 1989a) formed the basis for our updated reconstruction, and was not changed beyond minor adjustments detailed below.

The Godfrey reconstruction uses the skull reconstruction of Smithson (Smithson, 1982). While the anatomy is well-described and well-figured, the specimens available were dorsoventrally compressed (pers. obsv. BKAO and MIC), resulting in a very flat, shallow skull. Three-dimensional skulls of *Greererpeton* frome Goreville, Illinois, show a more domed skull and an interpremaxillary fenestra (Schultze and Bolt, 1996). Therefore, we used the Goreville skull in our reconstruction. The lateral view was traced directly from the specimen drawing,; the dorsal view was generated by tracing the less-disturbed right side, mirroring it, and adjusting sutures to fit as guided by the full dorsal view being traced. The jaw was based on the revised reconstructions by Bolt and Lombard (Bolt and Lombard, 2001) of the mandible of *Greererpeton*, which also incorporate information from the Goreville specimens. The angle and

depth of the pectoral girdle in lateral view were adjusted slightly to fit with the new skull and jaws.

The Goreville specimens were assigned to '*Greererpeton sp.*' pending a full description (Schultze and Bolt, 1996). Without an a priori reason to taxonomically separate the Illinois and West Virginia *Greererpeton*, we feel that our reconstruction does not represent a chimera and is sufficient for purposes here.

This revised cranial reconstruction of *Greererpeton* contrasts with the flattened, shallow skull of *Colosteus* as reconstructed by Hook (Hook, 1983), but is much more similar to that of *Pholidogaster* by Panchen (Panchen, 1975), and both the holotype specimen (Clack et al., 2016) and new revised reconstruction (this study) of *Aytonerpeton*. As the described and figured specimens of *Colosteus* and *Deltaherpeton* (Bolt and Lombard, 2010) are flattened, it is likely that they in fact has similarly vaulted skulls, and that this skull shape may be general to colosteids.

The Godfrey reconstruction has a four-fingered manus (Godfrey, 1989a). This is particularly significant as a four-digit manus is currently considered a defining temnospondyl (a thus often lissamphibian total group) character (with the caveat that the four-digit manus is found in non-temnospondyl tetrapods (Carroll and Gaskill, 1978)). Evidence for manual pentadactyly in *Greererpeton* was described and figured by MIC (Coates, 1996), which has been incorporated into our reconstruction. The fifth digit is incomplete, so the phalangeal formula was restored

based on comparisons with the other manual and pedal digits of *Greererpeton* (Godfrey, 1989a), *Proterogyrinus* (Holmes, 1984), *Trimerorhachis* (Case, 1935), and *Eryops* (Dilkes, 2015).

B.3 *ACANTHOSTEGA* RECONSTRUCTION PROCEDURE

The basis of the reconstruction was the postcranial skeleton as described by MIC (Coates, 1996), using a drawing in lateral view that was figured in (Ahlberg et al., 2005). The skull in dorsal and ventral view was traced from the renders Porro and colleagues, guided by the line drawings in that same study (Porro et al., 2015a). The pectoral girdle in lateral view was then slightly adjusted to accommodate the new skull. The dorsal views of the limbs were traced from figures in (Coates, 1996).

B.4 *AYTONERPETON* RECONSTRUCTION PROCEDURE

The well-preserved portion of the holotype skull (Otoo, 2015; Clack et al., 2016) was taken as the base. The exterior dermal bones were assumed to be preserved in-place, the palatal bones having been flattened against the internal surface of the skull. The external dermal bones were traced from the CT scan renders. The missing postorbital portion of the skull was restored using the referred skull table (Otoo et al., 2018) and data from *Pholidogaster* (Panchen, 1975) and the Goreville *Greererpeton* specimens (Schultze and Bolt, 1996). The overall shape of the skull was also guided by reconstructions of other small tetrapods, such as *Lethiscus* (Pardo et al., 2017b), *Westlothiana* (Smithson et al., 1993), *Microbrachis* (Carroll and Gaskill, 1978; Vallin and Laurin, 2004), *Adelogyrinus* and *Adelospondylus* (Andrews and Carroll, 1991), and *Silvanerpeton* (Ruta and Clack, 2006).

The palatal view was based on the holotype skull renders (tracing the right side and mirroring it), with additional data from *Greererpeton* (Smithson, 1982) and guidance from *Acanthostega* (Porro et al., 2015a) and *Proterogyrinus* (Holmes, 1984). To have the two halves of the skull articulate, we vaulted the palate, though this is may not be visible within the limited detail of our reconstruction drawing. The parasphenoid is the referred parasphenoid described by Otoo and colleagues (Otoo et al., 2018).

Most of the jaw of the holotype is well-preserved, and was traced from figures and renders (Otoo, 2015; Clack et al., 2016). The missing posterior portion was restored after *Greererpeton* (Bolt and Lombard, 2001).

B.5 *ICHTHYOSTEGA* RECONSTRUCTION PROCEDURE

With this reconstruction, we have attempted to combine outstanding information on *Ichthyostega* into a single reconstruction, alongside our own observations and interpretations. The foundation for this reconstruction were the 3D renders of CT scan data presented in (Pierce et al., 2012). This was not an anatomical investigation, so some portions (ex. the skull) have not been retrodeformed, and others are incomplete (eg. the hindlimb). Additionally, those renders represent a combining of specimens representing multiple individuals (see discussion therein). However, this is the only extant full-body 3D reconstruction of *Ichthyostega*, and thus even with caveats it is an extremely valuable resource for reconstruction.

The Pierce et al. (2012) skull is still partially flattened. In lateral view, the render was cross-referenced with other line drawings by Ahlberg et al. (2005) and Clack and Milner (2015). Relative to the render, the snout was made more convex and the skull deepened slightly. (Ahlberg et al., 2005) and (Blom, 2005) provided guidance on the sutures. The dorsal view of the skull is from (Blom, 2005), after (Jarvik, 1996).

The resulting skull is very similar to that of (Ahlberg et al., 2005), though the snout is not 'flexed' ventrally and the skull is marginally shallower overall in lateral view. Of particular note are the 'orbital ridges' formed by the prefrontal, postfrontal, and postorbital, common to our reconstruction, the (Jarvik, 1996) and (Ahlberg et al., 2005) drawings, and the (Pierce et al., 2012) render. Similar features are present in *Acanthostega* (Porro et al., 2015a), *Ventastega* (Ahlberg et al., 2008), *Tiktaalik* (Daeschler et al., 2006; Lemberg et al., 2021), *Parmastega* (Beznosov et al., 2019), and, possibly, *Elpistostege* (Schultze and Arsenault, 1985; Cloutier et al., 2020). Of these taxa, the feature is least developed in *Ichthyostega* and *Acanthostega*. It may be a feature general to panderichthyids that was reduced and eventually lost in tetrapods, possibly in conjunction with increasing visual actuity in air as per the evolutionary scenario outlined by (MacIver et al., 2017).

The initial profile of the jaw from the render was straightened and made shallower posteriorly after (Ahlberg and Clack, 1998; Ahlberg et al., 2005; Clack et al., 2012a). This was to reflect the ventral deflection of the splenial, postsplenial, angular, and surangular. The lateral lines on the skull and jaw were drawn from (Jarvik, 1996).

Neural spines of the render are often incomplete, and these were completed based on (Jarvik, 1996; Coates, 2001; Pierce et al., 2013b). The morphology and structure of the centra was based on (Pierce et al., 2013b) but with modifications as with the *Pederpes* reconstruction (see above). Trunk ribs were filled in after (Coates, 2001; Ahlberg et al., 2005), with guidance from the (Otoo et al., 2021), which has similar trunk rib morphology. The tail, including caudal ribs, was drawn from (Coates, 2001) with some guidance from (Jarvik, 1996; Ahlberg et al., 2005).

The pectoral girdle was drawn from the (Pierce et al., 2012) render with additional perspective from (Pierce et al., 2013a), as were the lateral views of the humerus, radius, and ulna. Dorsal views of the forelimb bones were drawn after (Callier et al., 2009) (humerus) and (Pierce et al., 2013a) (radius and ulna).

The manus of *Ichthyostega* is unknown; the manus presented here is purely conjectural and is not at all meant to represent a source of data. Seven digits were posited based on the agreement in manus/pes digit count fellow polydactylous Devonian tetrapods *Acanthostega* (Coates, 1996) and *Tulerpeton* (Lebedev and Coates, 1995). The digit formula was estimated after *Acanthostega*, *Tulerpeton*, *Whatcheeria* (Otoo et al., 2021), and *Greererpeton* (Godfrey, 1989a).

The pelvic girdle was drawn after (Ahlberg, 2018). The lateral view of the hindlimb was drawn from (Coates, 2001). The dorsal view was drawn from (Jarvik, 1996).

B.6 ADDITIONS TO TAXON LIST

Additional taxa were added to groups present in the dataset already:

‘Anthracosauria’:

- *Anthracosaurus russelli*
- “*Eogyrinus*” (=*Pholiderpeton*) *attheyi*
- *Palaeoherpeton decorus*
- *Eldeceeon rolfei*
- Unnamed Joggins embolomere NSM 994 GF 1.1 (Holmes and Carroll, 2010)

Colosteidae:

- *Deltaherpeton hiemstrae*
- *Pholidogaster pisciformis*
- St. Louis tetrapod
- *Aytonerpeton microps*

The Frasnian taxon *Parmastega aelidae* (Beznosov et al., 2019) was added in order to help polarize characters near the base of limbed tetrapods.

Further additions were made for the reasons stated below:

Adelospondyli- testing aistopod stem tetrapod hypothesis (Pardo et al., 2017b; Clack et al., 2019a) and single stem tetrapod origin of limblessness hypothesis (Clack et al., 2019a). These taxa were absent from (Clack et al., 2016) and were included in this matrix prior to the publication of (Clack et al., 2019a) in which they were present:

- *Adelospondylus watsoni*
- *Adelogyrinus simorhynchus*

Temnospondyli- increase number of temnospondyl (=stem lissamphibian) taxa to create a more balanced crown group sample and test whether a terrestrial tetrapod bodyplan arose once near/at the crown node or independently:

- Edopoids- increase in basal/plesiomorphic temnospondyls similar to *Edops* (Schoch, 2013). The edopoids have been proposed as the earliest-diverging temnospondyls (Ruta and Coates, 2007; Ruta et al., 2007; Schoch, 2013). Their inclusion may break up the

Edops/*Eryops* clade recovered by Clack et al. (2016, 2019). This clade has not been recovered in analyses with more comprehensive sampling of temnospondyls (Ruta et al., 2007; Schoch, 2013; Pardo et al., 2017a) and may be the result of insufficient character data to more fully separate *Eryops* and *Edops*:

    - *Capetus palustris*
    - *Adamanterpeton ohioensis*

- Dvinosauria- test the crown tetrapod colosteid hypothesis of Clack et al. (2016) and relationship of dvinosaurs to basal temnospondyls. The colosteids were previously considered temnospondyls affiliated with the dvinosaurs (Smithson, 1982; Hook, 1983; Godfrey, 1989a, 1989b; Milner and Sequeira, 2011). The dvinosaurs are considered early-diverging temnospondyls (Ruta et al., 2007; Schoch, 2013; Marjanović and Laurin, 2019) and have recently been proposed to be the first- diverging temnospondyls (Pardo et al., 2017a). The inclusion of dvinosaurs may help clarify the relationship of the colosteids to the crown group:

    - *Trimerorhachis insignis*
    - *Erpetosaurus radiatus*
    - *Neldasaurus wrightae*

- Other temnospondyls- additional representation of strongly aquatic and terrestrial Permo-Carboniferous temnospondyls with recent, thorough descriptions:

    - *Archegosaurus decheni* (aquatic)
    - *Platyrhinops lyelli* (terrestrial)

B.7 EXCLUSIONS FROM TAXON LIST

The following taxa were removed as they are very incomplete and thus are highly unstable. They were also deemed unnecessary for the purposes of timetree calibration, as OTUs of comparable ages and phylogenetic position are available elsewhere in the dataset.

- *Metaxygnathus denticulus* (Late Devonian, ?Frasnian-Famennian)
- *Ossirarus kierani* (Mississippian, Tournaisian) [undergoing redescription by M Ruta and TR Smithson, pers. comm. May 2022]
- *Perittodus apsconditus* (Mississippian, Tournaisian)
- *Diploradus austiumensis* (Mississippian, Tournaisian)

The following taxa were removed because they are generally agreed to be derived total group amniotes with stable phylogenetic positions, and they are morphologically and phylogenetic far from the areas of interest:

- *Paleothyris* (Eureptilia)
- *Discosauriscus* (Seymouriamorpha; less complete than *Seymouria*, which was retained in the dataset due to its completeness and character combination contribution)

The following taxa were removed because they are considered ‘microsaurs’. The phylogeny of the ‘microsaurs’ is currently a topic of active research (Reisz and Modesto, 1996; Huttenlocker et al., 2013; Pardo et al., 2015; Mann and Maddin, 2019; Mann et al., 2020, 2021) and is beyond the scope of this study. These ‘microsaur’ taxa group together in (Clack et al., 2016, 2019a) and are less complete than *Microbrachis.* Therefore, they were deemed redundant for the current study, as they would not present meaningfully new character combinations and their incompleteness could have destructive effects on node stability:

- *Asaphestra* [recently reidentified as the oldest synapsid (Mann et al., 2020)]
- *Hyloplesion*

These urocordylid ‘lepospondyls’ were removed from the initial (Clack et al., 2019a) taxon set, as their relationships are beyond the scope of the present study, and should likely be reserved for an analysis more focused on ‘lepospondyls’:

- *Ptyonius*
- *Sauropleura*

The following limbless taxa were removed from the initial (Clack et al., 2019a) taxon set because they could be scored for fewer characters than the other taxa used to represent their respective clades, the internal relationships of which are outside the scope of this study :

- *Dolichopareias* (Adelospondyli)
- *Acherontiscus* (Adelospondyli)
- *Oestocephalus* (Aistopoda)

B.8 AGES OF OTUs IN PHYLOGENETIC ANALYSIS (CHAPTER 3)

Table B.1. Relative ages for OTUs.

OTU	First_stage	Last_stage
Acanthostega	Famennian	Famennian
Adamanterpeton	Moscovian	Moscovian
Adelogyrinus	Visean	Visean
Adelospondylus	Serpukhovian	Serpukhovian
Anthracosaurus	Moscovian	Moscovian
AnthracosaurusPlus	Moscovian	Moscovian
Archegosaurus	Asselian	Asselian
Archeria	Asselian	Asselian
Aytonerpeton	Tournaisian	Tournaisian
*Aytonerpeton*Plus	Tournaisian	Tournaisian
Balanerpeton	Visean	Visean
Baphetes	Moscovian	Moscovian
Brittagnathus	Famennian	Famennian
Caerorhachis	Serpukhovian	Serpukhovian
Capetus	Moscovian	Moscovian
Casineria	Visean	Visean
Coloraderpeton	Kasimovian	Kasimovian
Colosteus	Moscovian	Kasimovian
Crassigyrinus	Visean	Serpukhovian
Deltaherpeton	Serpukhovian	Serpukhovian
Dendrerpeton	Bashkirian	Moscovian
Doragnathus	Serpukhovian	Serpukhovian
Edops	Asselian	Asselian
Eldeceeon	Visean	Visean
Elpistostege	Frasian	Frasnian
Eogyrinus_attheyi	Serpukhovian	Serpukhovian
*Eogyrinus*Plus	Serpukhovian	Serpukhovian
Eoherpeton	Visean	Visean
Erpetosaurus	Moscovian	Moscovian
Eryops	Kasimovian	Asselian
Eucritta	Visean	Visean
Eusthenopteron	Frasian	Frasnian
Gephyrostegus	Moscovian	Moscovian
Greererpeton	Serpukhovian	Bashkirian
Ichthyostega	Famennian	Famennian

Koilops	Tournaisian	Tournaisian
Lethiscus	Visean	Visean
Loxomma	Serpukhovian	Serpukhovian
Megalocephalus	Moscovian	Moscovian
Microbrachis	Moscovian	Moscovian
Neldasaurus	Asselian	Asselian
Neopteroplax	Moscovian	Kasimovian
NSM_994_GF_1.1	Bashkirian	Moscovian
Occidens	Tournaisian	Visean
Ossinodus	Visean	Visean
Palaeoherpeton	Bashkirian	Bashkirian
Panderichthys	Givetian	Givetian
Parmastega	Frasian	Frasnian
Pederpes	Tournaisian	Tournaisian
Pholiderpeton_scutigerum	Bashkirian	Bashkirian
Pholidogaster	Visean	Visean
Platyrhinops	Moscovian	Kasimovian
Proterogyrinus	Serpukhovian	Serpukhovian
Seymouria	Artinskian	Artinskian
Sigournea	Serpukhovian	Serpukhovian
Silvanerpeton	Visean	Visean
St_Louis_tetrapod	Visean	Visean
Tiktaalik	Frasian	Frasnian
Trimerorhachis	Asselian	Artinskian
Tulerpeton	Famennian	Famennian
Tulerpeton_Plus	Famennian	Famennian
Ventastega	Famennian	Famennian
Westlothiana	Visean	Visean
Whatcheeria	Serpukhovian	Serpukhovian
Ymeria	Famennian	Famennian

B.9 NUMERICAL INFORMATION FROM BAYESIAN SEARCH

Credible sets of trees (15002 trees sampled):
50 % credible set contains 7501 trees
90 % credible set contains 13502 trees
95 % credible set contains 14252 trees
99 % credible set contains 14852 trees

Summarizing parameters in files NX43_Bayes.nex.run1.p and NX43_Bayes.nex.run2.p
Writing summary statistics to file NX43_Bayes.nex.pstat
Using relative burnin ('relburnin=yes'), discarding the first 25 % of samples

Below are rough plots of the generation (x-axis) versus the log probability of observing the data (y-axis). You can use these graphs to determine what the burn in for your analysis should be. When the log probability starts to plateau you may be at stationarity. Sample trees and parameters after the log probability plateaus. Of course, this is not a guarantee that you are at stationarity. Also examine the convergence diagnostics provided by the 'sump' and 'sumt' commands for all the parameters in your model. Remember that the burn in is the number of samples to discard. There are a total of ngen / samplefreq samples taken during a MCMC analysis.

Overlay plot for both runs:
(1 = Run number 1; 2 = Run number 2; * = Both runs)

```
+-------------------------------------------------------------+ -6864.08
|                                1              |
|                                              |
|                                              |
|          2            1                      |
|      1  1    11    2                 *   1    2    |
|2  2    2     1    2    1   2           * 2      2     1|
| 1  2  2 1      2   1 11 1 1   2     2    1         1  11  |
|  1       2 *    111  2 2 221 11       221      2  1    2 1 |
|  2  2        2               211     2    2  2 * 1  22 |
| 2    1  2    2       2 21      2 221      *    *         |
|    12    2 1   22         2  21    1                2|
|         1       21         1            1     1    |
|1      1                        1 2        2       |
|   1                   2      2       1     2     |
|  1                       1         1           |
+------+-----+-----+-----+-----+-----+-----+-----+-----+-----+ -6872.28
```

```
^                                   ^
2500000                             10000000


Estimated marginal likelihoods for runs sampled in files
  "NX43_Bayes.nex.run1.p" and "NX43_Bayes.nex.run2.p":
  (Use the harmonic mean for Bayes factor comparisons of models)

  (Values are saved to the file NX43_Bayes.nex.lstat)

Run   Arithmetic mean   Harmonic mean
------------------------------------
 1     -6843.19         -6901.65
 2     -6840.65         -6901.63
------------------------------------
TOTAL  -6841.27         -6901.64
------------------------------------


Model parameter summaries over the runs sampled in files
  "NX43_Bayes.nex.run1.p" and "NX43_Bayes.nex.run2.p":
  Summaries are based on a total of 15002 samples from 2 runs.
  Each run produced 10001 samples of which 7501 samples were included.
  Parameter summaries saved to file "NX43_Bayes.nex.pstat".

                              95% HPD Interval
                             -------------------
  Parameter      Mean      Variance     Lower       Upper       Median    min ESS*  avg ESS
PSRF+
  ---------------------------------------------------------------------------------------------
  TL        15.248849    0.817089   13.516420   17.041520   15.210630   5300.10   5589.47
1.000
  alpha      1.397750    0.022985    1.107554    1.700922    1.391366   6164.64   6480.05
1.000
  ---------------------------------------------------------------------------------------------
  * Convergence diagnostic (ESS = Estimated Sample Size); min and avg values
    correspond to minimal and average ESS among runs.
    ESS value below 100 may indicate that the parameter is undersampled.
  + Convergence diagnostic (PSRF = Potential Scale Reduction Factor; Gelman
    and Rubin, 1992) should approach 1.0 as runs converge.
```

B.10 BRANCH LISTS FOR REWEIGHTED TREE (STRICT CONSENSUS) FROM STANDARD DATASET SEARCH (ALL CHARACTERS) GENERATED WITH MACCLADE

Reconstructed changes along branches (from node below to node at top of branch)
(Unambiguous)

==========
Adelospondylus (branch number 1):
Total changes along branch: 4

Character: Change
34. Jugal V-shaped indentation of posterodorsal margin: absent = 0, present = 1 C23: 0->1
State at this node convergent with a state outside this clade
62. Prefrontal less than three times longer than wide: present = 0, more than, = 1 ? C53: 0->1
State at this node found in an ancestor, thus representing a reversal,
OR convergent with a state outside this clade
64. Prefrontal contributes to half or more than half anteromesial orbit margin = 0, less than half = 1 C55: 1->0
State at this node found in an ancestor, thus representing a reversal
179. Mandibular canal exposure: entirely enclosed apart from pores = 0, mostly enclosed = 1, mostly or entirely open = 2 C135: 2->0
State at this node found in an ancestor, thus representing a reversal

==========
Adelogyrinus (branch number 2):
Total changes along branch: 5

Character: Change
10. Pineal foramen position along interparietal suture: behind midpoint = 0, at the midpoint = 1, anterior to midpoint = 2 C166: 1->0
State at this node found in an ancestor, thus representing a reversal
22. Frontal anterior margin wedged between nasals: absent = 0, present = 1 C11: 0->1
State at this node convergent with a state outside this clade
41. Maxilla sutures to prefrontal: absent = 0, present = 1 C30: 0->1
State at this node convergent with a state outside this clade
199. Splenial, rearmost extension of mesial lamina closer to anterior margin of adductor fossa than to the anterior end of the jaw: absent = 0, present = 1 C152: 1->0
State at this node found in an ancestor, thus representing a reversal
326. Scale distribution: gastralia present = 0, gastralia and dorsal scales/osteoderms/other dermal ossifications present = 1, no scales = 2 N71: 0->1
State at this node convergent with a state outside this clade

==========

Coloraderpeton (branch number 3):
Total changes along branch: 21

Character: Change
2. Preorbital region of skull less than twice as wide as long = 0, or at least twice as wide as long = 1 C155: 1->0
State at this node found in an ancestor, thus representing a reversal
11. Suspensorium proportions: quadrate to anterior margin of temporal embayment about equal to maximum orbit width (discounting any anterior extensions) = 0, quadrate to anterior margin of temporal embayment < maximum orbit width = 1, quadrate to anterio:
State at this node found in an ancestor, thus representing a reversal
31. Jugal length of postorbital region relative to one-third of the length of the postorbital cheek region: greater = 0 or less =1 0 C20: 0->1
State at this node found in an ancestor, thus representing a reversal,
OR convergent with a state outside this clade
33. Jugal excluded from lower jaw margin by maxilla and quadratojugal: yes = 0, or no = 1 C22: 1->0
State at this node found in an ancestor, thus representing a reversal
62. Prefrontal less than three times longer than wide: present = 0, more than, = 1 ? C53: 0->1
State at this node found in an ancestor, thus representing a reversal,
OR convergent with a state outside this clade
63. Prefrontal enters naris: absent = 0, present = 1 ? C54: 0->1
State at this node convergent with a state outside this clade
64. Prefrontal contributes to half or more than half anteromesial orbit margin = 0, less than half = 1 C55: 1->0
State at this node found in an ancestor, thus representing a reversal
77. Tabular shape in dorsal view (aside from horn, if present): rectangle or square = 0, irregular rectangular/quadrangle = 1, elongate oval or teardrop = 2, triangular = 3 N1: 1->2
State at this node found in an ancestor, thus representing a reversal
133. Ectopterygoid row (3+) of smaller teeth: present = 0, absent = 1 C93: 1->0
State at this node found in an ancestor, thus representing a reversal
140. Palatine row of smaller teeth: present = 0, absent = 1 C99: 1->0
State at this node found in an ancestor, thus representing a reversal
156. Marginal tooth shape: conical and straight/slightly recurved = 0, small and more or less straight and 'needle-like' = 1, right-trapezoid 'chisel' shape = 2, spearhead shape = 3, thin and greatly recurved = 4 N22: 0->4
Uniquely derived state, unchanged above
Two or more other states found outside this clade
158. Adductor fossa faces dorsally = 0, mesially = 1 C114: 1->0
State at this node found in an ancestor, thus representing a reversal
159. Angular mesial lamina suture with prearticular: absent = 0, present = 1 $C115: 1->0
State at this node found in an ancestor, thus representing a reversal
161. Coronoid (anterior) contacts splenial (or presplenial if present): absent = 0, present = 1 C117: 1->0
State at this node found in an ancestor, thus representing a reversal
181. Meckelian bone visible between prearticular and infradentary series: present = 0, absent = 1 C137: 1->0
State at this node found in an ancestor, thus representing a reversal
185. Meckelian bone or space exposure in middle part of jaw, depth much less than prearticular = 0, depth similar to prearticular or greater = 1 C138: 0->1
State at this node convergent with a state outside this clade
194. Postsplenial pit line present: present = 0, absent = 1 ? C146: 1->0
State at this node found in an ancestor, thus representing a reversal,

OR convergent with a state outside this clade
198. Prearticular with longitudinal ridge below coronoids: absent = 0, present = 1 C150: 0->1
State at this node found in an ancestor, thus representing a reversal
199. Splenial, rearmost extension of mesial lamina closer to anterior margin of adductor fossa than to the anterior end of the jaw: absent = 0, present = 1 C152: 1->0
State at this node found in an ancestor, thus representing a reversal
211. Neural arches with distinct convex lateral surfaces (?swollen?): absent = 0, present = 1 C200: 0->1
Uniquely derived state, unchanged above
Character is uniform outside this clade
326. Scale distribution: gastralia present = 0, gastralia and dorsal scales/osteoderms/other dermal ossifications present = 1, no scales = 2 N71: 0->1
State at this node convergent with a state outside this clade

==========
Lethiscus (branch number 4):
Total changes along branch: 10

Character: Change
3. Internarial/ interpremaxillary fenestra (independent of presence of median rostrals) on dorsal surface of skull: absent = 0, present = 1 C157: 0->1
State at this node found in an ancestor, thus representing a reversal,
OR convergent with a state outside this clade
4. Interorbital distance compared with maximum orbit diameter: greater = 0, smaller = 1, subequal = 2 C158: 2->1
State at this node found in an ancestor, thus representing a reversal
50. Parietal shape of anteriormost third: not wider than frontals = 0, at least marginally wider = 1 C41: 1->0
State at this node found in an ancestor, thus representing a reversal
60. Postparietal occipital flange (="postparietal lappet) exposure: absent = 0, present = 1 C51: 1->0
State at this node found in an ancestor, thus representing a reversal
78. Tabular horn: absent, tabular does not form horn = 0, tabular forms notable horn = 1 N2: 0->1
State at this node found in an ancestor, thus representing a reversal,
OR convergent with a state outside this clade
86. Postparietals: paired = 0 or fused = 1 N6: 0->1
State at this node convergent with a state outside this clade
100. Parasphenoid cultriform process shape: biconvex = 0, narrowly triangular =1, parallel-sided = 2, or with proximal constriction followed by swelling = 3 C76: 1->2
State at this node found in an ancestor, thus representing a reversal
115. Ectopterygoid/ palatine exposure: more or less confined to tooth row = 0, broad mesial exposure (additional to tooth row if present) = 1 C73: 1->0
State at this node found in an ancestor, thus representing a reversal
178. Mandibular sensory canal: present = 0, absent = 1 C134: 0->1
State at this node found in an ancestor, thus representing a reversal
204. Centra strongly notochordal such that notochordal space more than 2/3 diameter of entire centrum: present = 0, absent = 1 C172: 1->0
State at this node found in an ancestor, thus representing a reversal

==========
Microbrachis (branch number 5):
Total changes along branch: 17

Character: Change
10. Pineal foramen position along interparietal suture: behind midpoint = 0, at the midpoint = 1, anterior to midpoint = 2 C166: 1->2
State at this node convergent with a state outside this clade
13. Skull table shape: longer than broad = 0, approximately square = 1, shorter than broad = 2 C169: 0->2
State at this node found in an ancestor, thus representing a reversal
14. Dermal ornament character: Pit-and-ridge with visible center of ossification = 0, pit-and-ridge with no obvious center of ossification = 1, irregular pit-and-ridge with no obvious center of ossification =2, short radiating grooves = 3, pitted = 4, ir:
State at this node convergent with a state outside this clade
40. Maxilla extends behind level of posterior margin of orbit: present = 0, absent = 1 C29: 0->1
State at this node convergent with a state outside this clade
45. Nasal ? parietal length ratio less than 1.45 = 0 or greater than 1.45 = 1 C34: 0->1
State at this node convergent with a state outside this clade
52. Postfrontal ? prefrontal contact: broad = 0; or point-like = 1 C43: 1->0
State at this node found in an ancestor, thus representing a reversal
57. Postorbital longer than anteroposterior width of orbit: absent = 0, present = 1 C48: 0->1
State at this node found in an ancestor, thus representing a reversal
69. Squamosal contact with tabular: smooth = 0, interdigitating = 1, absent = 2 C60: 2->1
State at this node convergent with a state outside this clade
73. Squamosal contacts tabular: absent = 0, present = 1 C64: 0->1
State at this node convergent with a state outside this clade
77. Tabular shape in dorsal view (aside from horn, if present): rectangle or square = 0, irregular rectangular/quadrangle = 1, elongate oval or teardrop = 2, triangular = 3 N1: 1->3
State at this node found in an ancestor, thus representing a reversal
82. (Infraorbital) lateral line relationship to naris: continuous ventral to naris within lateral rostral = 0, discontinuous across ventral naris = 1, discontinuous ventral to naris across maxilla to premaxilla = 2, continuous ventral to naris in maxilla:
State at this node found in an ancestor, thus representing a reversal
97. Exoccipitals enlarged to form double horizontally orientated occipital condyle, (may exclude basioccipital from articular surface): absent = 0, present = 1 C9: 0->1
State at this node convergent with a state outside this clade
103. Parasphenoid depression in body: absent = 0, single median = 1, multiple = 2 C77: 1->0
State at this node found in an ancestor, thus representing a reversal
116. Pterygoids flank parasphenoid for most of length of cultriform process = 0, not so = 1 C84: 0->1
State at this node found in an ancestor, thus representing a reversal,
OR convergent with a state outside this clade
131. Palatal ramus of pterygoid (lateral to palatal vacuities if present): narrow/'strap-like' about only as wide as a tooth/tooth row if present] = 0, or broad = 1 N18: 1->0
State at this node convergent with a state outside this clade
142. Parasphenoid shagreen field: present = 0, absent = 1 ? C101: 1->0
State at this node found in an ancestor, thus representing a reversal
197. Prearticular sutures with surangular (check rear of jaw): absent = 0, present = 1 C149: 1->0
State at this node found in an ancestor, thus representing a reversal

==========
Westlothiana (branch number 6):
Total changes along branch: 12

Character: Change

53. Postfrontal ? prefrontal suture: anterior half of orbit = 0, middle or posterior half of ?orbit = 1, absent = 2 C44: 1->0

State at this node found in an ancestor, thus representing a reversal

75. Supratemporal forms part of skull margin posteriorly, including temporal ebayment: absent = 0, present = 1 C66: 1->0

State at this node found in an ancestor, thus representing a reversal

77. Tabular shape in dorsal view (aside from horn, if present): rectangle or square = 0, irregular rectangular/quadrangle = 1, elongate oval or teardrop = 2, triangular = 3 N1: 1->0

State at this node found in an ancestor, thus representing a reversal

101. Basal plate of parasphenoid, measured posteriorly from basipterygoid processes/basal articulation: about as long as wide = 0, wider than long = 1, longer than wide = 2 N8: 0->2

State at this node convergent with a state outside this clade

128. Median meeting of ptergyoids (measured anteriorly from basal articulation): approximately 1/3 or less of pterygoid length = 0, about 1/2 of pteryoid length = 1, approximately 2/3-3/4 of pterygoid length = 2, almost all or all of pterygoid length = 3:

State at this node convergent with a state outside this clade

145. Premaxillary tooth number: > 15 = 0, 10 - 14 = 1, < 10 = 2 ? C105: 2->1

State at this node found in an ancestor, thus representing a reversal

201. Dentary teeth size: same size as maxillary teeth (0), larger than maxillary teeth = 1, smaller than maxillary teeth = 2 C250: 0->1

State at this node convergent with a state outside this clade

249. Percentage of humerus posterior margin proximal to entepicondyle, measured from proximal base of entepicondyle: about a third or less = 0, about half = 1, about two thirds = 2, more than two thirds = 3 N33: 1->2

State at this node found in an ancestor, thus representing a reversal

274. Illium, ischium, pubis separate ossifications: no not separate= 0, yes separate (including one or more of these unossified)= 1 C212: 1->0

State at this node found in an ancestor, thus representing a reversal

295. Anteroposterior maximum distance between femur distal condyles i(=tibia and fibula condyles) in extensor view 55 pecent or more of femur length = 0, between 55 and 40 percent of femur length = 1, 40 percent or less than femur length = 2 R117: 1->

State at this node found in an ancestor, thus representing a reversal

301. Tibia without = 0, or with = 1 flange along its posterior edge R121: 0->1

State at this node found in an ancestor, thus representing a reversal,
OR convergent with a state outside this clade

326. Scale distribution: gastralia present = 0, gastralia and dorsal scales/osteoderms/other dermal ossifications present = 1, no scales = 2 N71: 0->1

State at this node convergent with a state outside this clade

==========

Casineria (branch number 7):
Total changes along branch: 2

Character: Change

220. Ribs (trunk) differ strongly in length and morphology along ?thoracic? region: absent = 0, present = 1 C207: 0->1

State at this node convergent with a state outside this clade

297. Distal condyle alignment in extensor view: condyles about level = 0, one condyle extends farther distally = 1 N48: 1->0

State at this node found in an ancestor, thus representing a reversal,
OR convergent with a state outside this clade

==========
Gephyrostegus (branch number 8):
Total changes along branch: 19

Character: Change
4. Interorbital distance compared with maximum orbit diameter: greater = 0, smaller = 1, subequal = 2 C158: 0->2
State at this node found in an ancestor, thus representing a reversal
8. Orbit position re snout/postparietal length: centre closer to front than rear = 0, centre near middle = 1, centre closer to rear than front = 2 C164: 1->2
State at this node found in an ancestor, thus representing a reversal
10. Pineal foramen position along interparietal suture: behind midpoint = 0, at the midpoint = 1, anterior to midpoint = 2 C166: 1->2
State at this node convergent with a state outside this clade
22. Frontal anterior margin wedged between nasals: absent = 0, present = 1 C11: 0->1
State at this node convergent with a state outside this clade
23. Frontal/ nasal length ratio: frontals approximately equal to or less than one-third as long as nasals = 0, more than one-third as long = 1 C12: 1->0
State at this node found in an ancestor, thus representing a reversal
39. Maxilla highest point in posterior half = 0, anterior third of its length = 1, or at its midlength = 2, or same height all along length =3 C28: 1->2
State at this node found in an ancestor, thus representing a reversal,
OR convergent with a state outside this clade
54. Postorbital suture to skull table (usually intertemporal or supratemporal when present) interdigitating vs smooth: smooth = 0, interdigitating = 1 C45: 1->0
State at this node found in an ancestor, thus representing a reversal
64. Prefrontal contributes to half or more than half anteromesial orbit margin = 0, less than half = 1 C55: 1->0
State at this node found in an ancestor, thus representing a reversal
78. Tabular horn: absent, tabular does not form horn = 0, tabular forms notable horn = 1 N2: 0->1
State at this node found in an ancestor, thus representing a reversal,
OR convergent with a state outside this clade
80. Tabular prolonged posterolateral ornamented surface absent = 0, present = 1 C68: 0->1
State at this node convergent with a state outside this clade
106. Parasphenoid contacts or sutures to vomers: present = 0, absent = 1 ? C80: 1->0
State at this node found in an ancestor, thus representing a reversal
121. Vomers separated by pterygoids: for > half length = 0, < half length = 1, not separated by pterygoids = 2 C89: 0/1->2
State at this node found in an ancestor, thus representing a reversal
163. Coronoid (middle) contacts postsplenial: absent = 0, present = 1 C119: 0->1
State at this node convergent with a state outside this clade
167. Coronoid: at least one has fang pair recognisable because at least twice the height of coronoid teeth: present = 0, absent = 1 C123: 1->0
State at this node found in an ancestor, thus representing a reversal
174. Dentary tooth number: more than 70 = 0, 56-70 = 1, 46-55 = 2, 36-45 = 3, less than 35 = 4 C130: 2/4->3
State at this node found in an ancestor, thus representing a reversal,
OR convergent with a state outside this clade
182. Number of Meckelian openings: more than three = 0, three = 1, two = 2, one = 3 N73: 3->2
State at this node convergent with a state outside this clade

234. Interclavicle parasternal process shape: absent = 0, parallel sided = 1, or tapering = 2 C197: 2->1
State at this node found in an ancestor, thus representing a reversal,
OR convergent with a state outside this clade
326. Scale distribution: gastralia present = 0, gastralia and dorsal scales/osteoderms/other dermal ossifications present = 1, no scales = 2 N71: 0->1
State at this node convergent with a state outside this clade
327. Gastralia: tapered and elongate, four times longer than broad or longer = 0, ovoid = 1, around three times longer than broad one end tapering = 2 C211: 1->0
State at this node found in an ancestor, thus representing a reversal

==========
NSM 994 GF 1.1 (branch number 9):
Total changes along branch: 13

Character: Change
48. Parietal ? postorbital suture: absent = 0, present = 1 C39: 0->1
State at this node found in an ancestor, thus representing a reversal
59. Postparietal: longer than wide = 0, approximately square or pentagonal = 1, wider than long = 2, triangular and about as long as wide = 3 C50: 2->0
State at this node found in an ancestor, thus representing a reversal
75. Supratemporal forms part of skull margin posteriorly, including temporal ebayment: absent = 0, present = 1 C66: 0->1
State at this node found in an ancestor, thus representing a reversal
119. Pterygoid junction with squamosal: present = 0; absent =1 C87: 0->1
State at this node convergent with a state outside this clade
156. Marginal tooth shape: conical and straight/slightly recurved = 0, small and more or less straight and 'needle-like' = 1, right-trapezoid 'chisel' shape = 2, spearhead shape = 3, thin and greatly recurved = 4 N22: 0->1
State at this node found in an ancestor, thus representing a reversal
217. Ribs (trunk) tapered distally =0, parallel-sided = 1, flared at distal tip= 2 C205: 1->0
State at this node found in an ancestor, thus representing a reversal
221. Ribs (cervical): flared distally = 0, tapered distally = 1 C208: 0->1
State at this node found in an ancestor, thus representing a reversal,
OR convergent with a state outside this clade
261. Ectepicondyle foramen: present = 0, absent = 1 R43: 1->0
State at this node found in an ancestor, thus representing a reversal
265. Length of posterior margin of entepicondyle smaller than = 0, subequal to = 1, or larger than = 2, humerus anteroposterior length at the level of proximal insertion of entepicondyle onto humerus shaft R66: 2->1
State at this node found in an ancestor, thus representing a reversal
267. Radius: longer than ulna = 0, same length as ulna = 1, shorter than ulna (including olecranon process if present) = 2 C202: 2->1
State at this node convergent with a state outside this clade
268. Radius longer than = 0, as long as = 1, or shorter than = 2, humerus. R78: 2->1
State at this node convergent with a state outside this clade
269. Radius without = 0, or with = 1, distinctly expanded proximal extremity R82: 1->0
State at this node found in an ancestor, thus representing a reversal
326. Scale distribution: gastralia present = 0, gastralia and dorsal scales/osteoderms/other dermal ossifications present = 1, no scales = 2 N71: 0->1
State at this node convergent with a state outside this clade

==========
Archeria (branch number 10):
Total changes along branch: 24

Character: Change
12. Otic notch/temporal ebayment approaching orbit: more than 1/2 postorbital skull length = 0, 1/4-1/2 postorbital skull length = 1, less than 1/4 postorbital skull length = 2 P35: 1->0
State at this node found in an ancestor, thus representing a reversal
22. Frontal anterior margin wedged between nasals: absent = 0, present = 1 C11: 0->1
State at this node convergent with a state outside this clade
26. Intertemporal lateral edge: not interdigitating with cheek = 0, interdigitates = 1 C15: 1->0
State at this node found in an ancestor, thus representing a reversal,
OR convergent with a state outside this clade
31. Jugal length of postorbital region relative to one-third of the length of the postorbital cheek region: greater = 0 or less =1 0 C20: 0->1
State at this node found in an ancestor, thus representing a reversal,
OR convergent with a state outside this clade
39. Maxilla highest point in posterior half = 0, anterior third of its length = 1, or at its midlength = 2, or same height all along length =3 C28: 1->0
State at this node found in an ancestor, thus representing a reversal,
OR convergent with a state outside this clade
40. Maxilla extends behind level of posterior margin of orbit: present = 0, absent = 1 C29: 0->1
State at this node convergent with a state outside this clade
54. Postorbital suture to skull table (usually intertemporal or supratemporal when present) interdigitating vs smooth: smooth = 0, interdigitating = 1 C45: 1->0
State at this node found in an ancestor, thus representing a reversal
56. Postorbital shape: irregularly polygonal = 0, broadly cresentic and narrowing to a posterior point = 1 C47: 0->1
State at this node found in an ancestor, thus representing a reversal
75. Supratemporal forms part of skull margin posteriorly, including temporal ebayment: absent = 0, present = 1 C66: 0->1
State at this node found in an ancestor, thus representing a reversal
79. Tabular horn shape: short projection = 0, single elongate projection = 1, double prong (either incipient or two distinct points) = 2 N3: 2->1
State at this node found in an ancestor, thus representing a reversal,
OR convergent with a state outside this clade
92. Basioccipital: ventrally exposed portion longer than wide = 0, shorter than wide = 1 C4: 1->0
State at this node found in an ancestor, thus representing a reversal
100. Parasphenoid cultriform process shape: biconvex = 0, narrowly triangular =1, parallel-sided = 2, or with proximal constriction followed by swelling = 3 C76: 1->3
State at this node found in an ancestor, thus representing a reversal
102. Parasphenoid basal plate: square/rectangular = 0, or triangular/distinctly tapering at one end = 1 N9: 1->0
State at this node found in an ancestor, thus representing a reversal
121. Vomers separated by pterygoids: for > half length = 0, < half length = 1, not separated by pterygoids = 2 C89: 1->2
State at this node found in an ancestor, thus representing a reversal
130. Median margin of pterygoid palatal ramus where separate: straight = 0, slightly concave medially = 1, convex medially = 2, greatly concave medially = 3 N17: 1->0
State at this node found in an ancestor, thus representing a reversal
132. Ectopterygoid fang pairs: present = 0, absent = 1 C92: 0->1

State at this node found in an ancestor, thus representing a reversal
153. Upper marginal teeth number: greater than lower = 0, same = 1, smaller than lower = 2 C113: 1->0
State at this node found in an ancestor, thus representing a reversal,
OR convergent with a state outside this clade
178. Mandibular sensory canal: present = 0, absent = 1 C134: 0->1
State at this node found in an ancestor, thus representing a reversal
190. Adsymphysial plate dentition: shagreen, denticles or irregular tooth field = 0, organised dentition aligned parallel to jaw margin = 1, no dentition = 2 C142: 2->1
State at this node found in an ancestor, thus representing a reversal
193. Postsplenial with mesial lamina: absent = 0, present = 1 C145: 1->0
State at this node found in an ancestor, thus representing a reversal
194. Postsplenial pit line present: present = 0, absent = 1 ? C146: 1->0
State at this node found in an ancestor, thus representing a reversal,
OR convergent with a state outside this clade
195. Postsplenial mesial suture with prearticular: absent = 0, present but interrupted by Meckelian foramina or fenestrae = 1, uninterrupted suture = 2 C147: 1->0
State at this node found in an ancestor, thus representing a reversal
234. Interclavicle parasternal process shape: absent = 0, parallel sided = 1, or tapering = 2 C197: 2->1
State at this node found in an ancestor, thus representing a reversal,
OR convergent with a state outside this clade
263. Humerus length up to and no more than twice its width = 0, or more than twice its width = 1 R49: 0->1
State at this node convergent with a state outside this clade

==========
Pholiderpeton scutigerum (branch number 11):
Total changes along branch: 11

Character: Change
10. Pineal foramen position along interparietal suture: behind midpoint = 0, at the midpoint = 1, anterior to midpoint = 2 C166: 2->1
State at this node found in an ancestor, thus representing a reversal
14. Dermal ornament character: Pit-and-ridge with visible center of ossification = 0, pit-and-ridge with no obvious center of ossification = 1, irregular pit-and-ridge with no obvious center of ossification =2, short radiating grooves = 3, pitted = 4, ir:
State at this node found in an ancestor, thus representing a reversal
23. Frontal/ nasal length ratio: frontals approximately equal to or less than one-third as long as nasals = 0, more than one-third as long = 1 C12: 1->0
State at this node found in an ancestor, thus representing a reversal
33. Jugal excluded from lower jaw margin by maxilla and quadratojugal: yes = 0, or no = 1 C22: 1->0
State at this node found in an ancestor, thus representing a reversal
68. Squamosal posterodorsal margin shape: convex = 0, sigmoid or approximately straight = 1, entirely concave = 2 C59: 1->0
State at this node found in an ancestor, thus representing a reversal,
OR convergent with a state outside this clade
101. Basal plate of parasphenoid, measured posteriorly from basipterygoid processes/basal articulation: about as long as wide = 0, wider than long = 1, longer than wide = 2 N8: 2->0
State at this node convergent with a state outside this clade
118. Pterygoids not visible in lateral aspect below ventral margin of jugal and quadratojugal = 0, or visible = 1 C86: 1->0
State at this node found in an ancestor, thus representing a reversal

119. Pterygoid junction with squamosal: present = 0; absent =1 C87: 0->1
State at this node convergent with a state outside this clade
150. Vomerine shagreen field: absent = 0, present = 1 ? C110: 1->0
State at this node found in an ancestor, thus representing a reversal
233. Interclavicle anterior tip: squared = 0, broadly rounded = 1, pointed = 2. N85: 2->0
State at this node found in an ancestor, thus representing a reversal
258. Humerus ectepicondylar ridge distal end aligned with ulnar condyle = 0, between radial and ulnar condyles = 1, aligned with radial condyle = 2 C193: 2->1
State at this node found in an ancestor, thus representing a reversal,
OR convergent with a state outside this clade

==========
St Louis tetrapod (branch number 12):
Total changes along branch: 7

Character: Change
9. Orbit position re snout /quadrate length: centre closer to front than rear = 0, centre near middle = 1, centre closer to rear than front = 2 C165: 2->0
State at this node found in an ancestor, thus representing a reversal
14. Dermal ornament character: Pit-and-ridge with visible center of ossification = 0, pit-and-ridge with no obvious center of ossification = 1, irregular pit-and-ridge with no obvious center of ossification =2, short radiating grooves = 3, pitted = 4, ir:
Uniquely derived state, unchanged above
Two or more other states found outside this clade
19. Septomaxilla (= ?anterior tectal?) present = 0, absent = 1 C1: 1->0
State at this node found in an ancestor, thus representing a reversal
39. Maxilla highest point in posterior half = 0, anterior third of its length = 1, or at its midlength = 2, or same height all along length =3 C28: 1->3
State at this node found in an ancestor, thus representing a reversal,
OR convergent with a state outside this clade
114. Ectopterygoid reaches subtemporal fossa: absent = 0, present = 1 C72: 0->1
State at this node found in an ancestor, thus representing a reversal
133. Ectopterygoid row (3+) of smaller teeth: present = 0, absent = 1 C93: 0->1
State at this node found in an ancestor, thus representing a reversal
177. Dentary notch: absent = 0, present = 1 C214: 0->1
State at this node convergent with a state outside this clade

==========
Eogyrinus attheyi (branch number 13):
Total changes along branch: 6

Character: Change
5. Naris position: ventral rim closer to jaw margin than height of naris = 0, distance to jaw margin similar to or greater than height of naris = 1 C160: 0->1
State at this node found in an ancestor, thus representing a reversal,
OR convergent with a state outside this clade
7. Orbit shape: round, circle or oval = 0; square or rectangular = 1, triangular = 2, anterior projection giving orbit 'keyhole' shape = 3 C163: 0->2
State at this node convergent with a state outside this clade
70. Squamosal-supratemporal suture position: at apex of temporal embayment = 0, dorsal to apex = 1, ventral to apex = 2 C61: 0->1

State at this node convergent with a state outside this clade
101. Basal plate of parasphenoid, measured posteriorly from basipterygoid processes/basal articulation: about as long as wide = 0, wider than long = 1, longer than wide = 2 N8: 2->0
State at this node convergent with a state outside this clade
150. Vomerine shagreen field: absent = 0, present = 1 ? C110: 1->0
State at this node found in an ancestor, thus representing a reversal
165. Coronoid (posterior) posterodorsal process: absent = 0, present = 1 C121: 1->0
State at this node found in an ancestor, thus representing a reversal

==========
Neopteroplax (branch number 14):
Total changes along branch: 16

Character: Change
10. Pineal foramen position along interparietal suture: behind midpoint = 0, at the midpoint = 1, anterior to midpoint = 2 C166: 2->1
State at this node found in an ancestor, thus representing a reversal
12. Otic notch/temporal ebayment approaching orbit: more than 1/2 postorbital skull length = 0, 1/4-1/2 postorbital skull length = 1, less than 1/4 postorbital skull length = 2 P35: 1->0
State at this node found in an ancestor, thus representing a reversal
13. Skull table shape: longer than broad = 0, approximately square = 1, shorter than broad = 2 C169: 0->1
State at this node found in an ancestor, thus representing a reversal
27. Intertemporal contacts squamosal: absent = 0, present = 1 C16: 0->1
State at this node found in an ancestor, thus representing a reversal,
OR convergent with a state outside this clade
30. Jugal alary process ("insula jugalis") on palate: absent = 0, present = 1 C19: 1->0
State at this node found in an ancestor, thus representing a reversal
40. Maxilla extends behind level of posterior margin of orbit: present = 0, absent = 1 C29: 0->1
State at this node convergent with a state outside this clade
42. Maxilla ? premaxilla contact shelf-like mesial to tooth row on palate: absent = 0, present = 1 C31: 0->1
State at this node found in an ancestor, thus representing a reversal,
OR convergent with a state outside this clade
55. Postorbital without distinct dorsomedial ramus for postfrontal = 0, with incipient ramus = 1, ?with elongate ramus = 2 C46: 0->1
State at this node convergent with a state outside this clade
59. Postparietal: longer than wide = 0, approximately square or pentagonal = 1, wider than long = 2, triangular and about as long as wide = 3 C50: 2->0
State at this node found in an ancestor, thus representing a reversal
68. Squamosal posterodorsal margin shape: convex = 0, sigmoid or approximately straight = 1, entirely concave = 2 C59: 1->0
State at this node found in an ancestor, thus representing a reversal,
OR convergent with a state outside this clade
102. Parasphenoid basal plate: square/rectangular = 0, or triangular/distinctly tapering at one end = 1 N9: 1->0
State at this node found in an ancestor, thus representing a reversal
114. Ectopterygoid reaches subtemporal fossa: absent = 0, present = 1 C72: 0->1
State at this node found in an ancestor, thus representing a reversal
117. Pterygoid quadrate ramus margin in adductor fossa: concave = 0, with some convex component = 1 C85: 1->0

State at this node found in an ancestor, thus representing a reversal
121. Vomers separated by pterygoids: for > half length = 0, < half length = 1, not separated by pterygoids = 2 C89: 1->2
State at this node found in an ancestor, thus representing a reversal
135. Ectopterygoid / palatine shagreen field: absent = 0, present = 1 ? C95: 0->1
State at this node found in an ancestor, thus representing a reversal
200. Surangular crest: absent = 0, present = 1 C153: 1->0
State at this node found in an ancestor, thus representing a reversal

==========
Palaeoherpeton (branch number 15):
Total changes along branch: 5

Character: Change
9. Orbit position re snout /quadrate length: centre closer to front than rear = 0, centre near middle = 1, centre closer to rear than front = 2 C165: 1->0
State at this node found in an ancestor, thus representing a reversal
14. Dermal ornament character: Pit-and-ridge with visible center of ossification = 0, pit-and-ridge with no obvious center of ossification = 1, irregular pit-and-ridge with no obvious center of ossification =2, short radiating grooves = 3, pitted = 4, ir:
State at this node found in an ancestor, thus representing a reversal
22. Frontal anterior margin wedged between nasals: absent = 0, present = 1 C11: 0->1
State at this node convergent with a state outside this clade
34. Jugal V-shaped indentation of posterodorsal margin: absent = 0, present = 1 C23: 0->1
State at this node convergent with a state outside this clade
150. Vomerine shagreen field: absent = 0, present = 1 ? C110: 1->0
State at this node found in an ancestor, thus representing a reversal

==========
Anthracosaurus (branch number 16):
Total changes along branch: 25

Character: Change
5. Naris position: ventral rim closer to jaw margin than height of naris = 0, distance to jaw margin similar to or greater than height of naris = 1 C160: 0->1
State at this node found in an ancestor, thus representing a reversal,
OR convergent with a state outside this clade
7. Orbit shape: round, circle or oval = 0; square or rectangular = 1, triangular = 2, anterior projection giving orbit 'keyhole' shape = 3 C163: 0->2
State at this node convergent with a state outside this clade
10. Pineal foramen position along interparietal suture: behind midpoint = 0, at the midpoint = 1, anterior to midpoint = 2 C166: 2->1
State at this node found in an ancestor, thus representing a reversal
11. Suspensorium proportions: quadrate to anterior margin of temporal embayment about equal to maximum orbit width (discounting any anterior extensions) = 0, quadrate to anterior margin of temporal embayment < maximum orbit width = 1, quadrate to anterio:
State at this node found in an ancestor, thus representing a reversal
13. Skull table shape: longer than broad = 0, approximately square = 1, shorter than broad = 2 C169: 0->1
State at this node found in an ancestor, thus representing a reversal

14. Dermal ornament character: Pit-and-ridge with visible center of ossification = 0, pit-and-ridge with no obvious center of ossification = 1, irregular pit-and-ridge with no obvious center of ossification =2, short radiating grooves = 3, pitted = 4, ir:
State at this node found in an ancestor, thus representing a reversal,
OR convergent with a state outside this clade
22. Frontal anterior margin wedged between nasals: absent = 0, present = 1 C11: 0->1
State at this node convergent with a state outside this clade
45. Nasal ? parietal length ratio less than 1.45 = 0 or greater than 1.45 = 1 C34: 0->1
State at this node convergent with a state outside this clade
48. Parietal ? postorbital suture: absent = 0, present = 1 C39: 0->1
State at this node found in an ancestor, thus representing a reversal
55. Postorbital without distinct dorsomedial ramus for postfrontal = 0, with incipient ramus = 1, ?with elongate ramus = 2 C46: 0->1
State at this node convergent with a state outside this clade
65. Premaxilla posterodorsal alary process onto snout: absent = 0, present = 1 C56: 0->1
State at this node convergent with a state outside this clade
77. Tabular shape in dorsal view (aside from horn, if present): rectangle or square = 0, irregular rectangular/quadrangle = 1, elongate oval or teardrop = 2, triangular = 3 N1: 1->0
State at this node found in an ancestor, thus representing a reversal
82. (Infraorbital) lateral line relationship to naris: continuous ventral to naris within lateral rostral = 0, discontinuous across ventral naris = 1, discontinuous ventral to naris across maxilla to premaxilla = 2, continuous ventral to naris in maxilla:
State at this node found in an ancestor, thus representing a reversal
88. Temporal fenestra: absent = 0, present = 1 C238: 0->1
State at this node convergent with a state outside this clade
110. Posterior extent of parasphenoid beneath braincase: floors sphenoid region only (0); floors sphenoid and otic regions = 1; floors sphenoid, otic, and occipital regions = 2 P205: 1->0
State at this node found in an ancestor, thus representing a reversal
117. Pterygoid quadrate ramus margin in adductor fossa: concave = 0, with some convex component = 1 C85: 1->0
State at this node found in an ancestor, thus representing a reversal
118. Pterygoids not visible in lateral aspect below ventral margin of jugal and quadratojugal = 0, or visible = 1 C86: 1->0
State at this node found in an ancestor, thus representing a reversal
128. Median meeting of ptergyoids (measured anteriorly from basal articulation): approximately 1/3 or less of pterygoid length = 0, about 1/2 of pteryoid length = 1, approximately 2/3-3/4 of pterygoid length = 2, almost all or all of pterygoid length = 3:
State at this node convergent with a state outside this clade
137. Maxillary caniniform teeth (about twice the size of neighbouring teeth): absent = 0, present = 1 C97: 0->1
State at this node found in an ancestor, thus representing a reversal
153. Upper marginal teeth number: greater than lower = 0, same = 1, smaller than lower = 2 C113: 1->0
State at this node found in an ancestor, thus representing a reversal,
OR convergent with a state outside this clade
159. Angular mesial lamina suture with prearticular: absent = 0, present = 1 $C115: 1->0
State at this node found in an ancestor, thus representing a reversal
193. Postsplenial with mesial lamina: absent = 0, present = 1 C145: 1->0
State at this node found in an ancestor, thus representing a reversal
195. Postsplenial mesial suture with prearticular: absent = 0, present but interrupted by Meckelian foramina or fenestrae = 1, uninterrupted suture = 2 C147: 1->0
State at this node found in an ancestor, thus representing a reversal

199. Splenial, rearmost extension of mesial lamina closer to anterior margin of adductor fossa than to the anterior end of the jaw: absent = 0, present = 1 C152: 1->0
        State at this node found in an ancestor, thus representing a reversal
201. Dentary teeth size: same size as maxillary teeth (0), larger than maxillary teeth = 1, smaller than maxillary teeth = 2 C250: 0->2
        State at this node convergent with a state outside this clade

==========
Eoherpeton (branch number 17):
Total changes along branch: 1

Character: Change
182. Number of Meckelian openings: more than three = 0, three = 1, two = 2, one = 3 N73: 2->1
        State at this node convergent with a state outside this clade

==========
Doragnathus (branch number 18):
Total changes along branch: 4

Character: Change
1. Skull longer than broad = 0, as broad as long =1, or broader than long = 2 C154: 0->1
        State at this node convergent with a state outside this clade
156. Marginal tooth shape: conical and straight/slightly recurved = 0, small and more or less straight and 'needle-like' = 1, right-trapezoid 'chisel' shape = 2, spearhead shape = 3, thin and greatly recurved = 4 N22: 0->1
        State at this node found in an ancestor, thus representing a reversal
170. Coronoid: at least one carries shagreen: absent = 0, present = 1 C126: 1->0
        State at this node found in an ancestor, thus representing a reversal
200. Surangular crest: absent = 0, present = 1 C153: 1->0
        State at this node found in an ancestor, thus representing a reversal

==========
Proterogyrinus (branch number 19):
Total changes along branch: 19

Character: Change
25. Intertemporal smaller than supratemporal = 0, or larger than/comparable in size with supratemporal = 1 C14: 0->1
        State at this node found in an ancestor, thus representing a reversal
34. Jugal V-shaped indentation of posterodorsal margin: absent = 0, present = 1 C23: 0->1
        State at this node convergent with a state outside this clade
44. Nasals contribute to narial margin: absent = 0, present = 1 C33: 1->0
        State at this node found in an ancestor, thus representing a reversal
75. Supratemporal forms part of skull margin posteriorly, including temporal ebayment: absent = 0, present = 1 C66: 0->1
        State at this node found in an ancestor, thus representing a reversal
80. Tabular prolonged posterolateral ornamented surface absent = 0, present = 1 C68: 0->1
        State at this node convergent with a state outside this clade
83. Maximum parietal-parietal width is shorter than distance between posterior skull table margin (discounting tabular horn if present) and posterior orbit margin as projected along skull midline: present = 0, absent = 1 C231: 1->0

State at this node found in an ancestor, thus representing a reversal
101. Basal plate of parasphenoid, measured posteriorly from basipterygoid processes/basal articulation: about as long as wide = 0, wider than long = 1, longer than wide = 2 N8: 1->0
State at this node convergent with a state outside this clade
119. Pterygoid junction with squamosal: present = 0; absent =1 C87: 0->1
State at this node convergent with a state outside this clade
136. Maxilla tooth number: > 40 = 0, 30-40 = 1, < 30 = 2 ? C96: 2->0
State at this node found in an ancestor, thus representing a reversal
156. Marginal tooth shape: conical and straight/slightly recurved = 0, small and more or less straight and 'needle-like' = 1, right-trapezoid 'chisel' shape = 2, spearhead shape = 3, thin and greatly recurved = 4 N22: 0->2
State at this node convergent with a state outside this clade
167. Coronoid: at least one has fang pair recognisable because at least twice the height of coronoid teeth: present = 0, absent = 1 C123: 1->0
State at this node found in an ancestor, thus representing a reversal
173. Dentary with parasymphysial fangs internal to marginal tooth row: present = 0, absent = 1 C129: 1->0
State at this node found in an ancestor, thus representing a reversal
198. Prearticular with longitudinal ridge below coronoids: absent = 0, present = 1 C150: 0->1
State at this node found in an ancestor, thus representing a reversal
249. Percentage of humerus posterior margin proximal to entepicondyle, measured from proximal base of entepicondyle: about a third or less = 0, about half = 1, about two thirds = 2, more than two thirds = 3 N33: 1->0
State at this node found in an ancestor, thus representing a reversal,
OR convergent with a state outside this clade
255. Humerus radial/ulnar facets: confluent = 0, separated by perichondral strip of bone = 1 C189: 0->1
State at this node found in an ancestor, thus representing a reversal
258. Humerus ectepicondylar ridge distal end aligned with ulnar condyle = 0, between radial and ulnar condyles = 1, aligned with radial condyle = 2 C193: 2->0
State at this node found in an ancestor, thus representing a reversal
259. Humerus entepicondyle width relative to humeral head width: smaller = 0, greater = 1 C195: 1->0
State at this node found in an ancestor, thus representing a reversal,
OR convergent with a state outside this clade
281. Number of pubic obturator foramina: multiple = 0, single = 1, absent = 2 R105: 1->0
State at this node found in an ancestor, thus representing a reversal
307. Posterior (lateral) surface of fibula concave = 0, straight = 1, convex = 2, in its proximal half R132: 1->0
State at this node found in an ancestor, thus representing a reversal

==========
Eldeceeon (branch number 20):
Total changes along branch: 9

Character: Change
58. Postorbital at least one quarter of the width of the skull table at the same transverse level: absent = 0, present = 1 ? C49: 0->1
State at this node found in an ancestor, thus representing a reversal
87. Parietals: more than 2.5 times as long as wide = 0 or less than 2.5 times as long as wide = 1 C224: 1->0
State at this node found in an ancestor, thus representing a reversal

117. Pterygoid quadrate ramus margin in adductor fossa: concave = 0, with some convex component = 1 C85: 1->0
State at this node found in an ancestor, thus representing a reversal
144. Pterygoid shagreen: dense = 0, a few discontinuous patches or absent = 1 C103: 0->1
State at this node convergent with a state outside this clade
154. Premaxilla caniniform teeth: absent = 0, present = 1 N20: 0->1
State at this node convergent with a state outside this clade
204. Centra strongly notochordal such that notochordal space more than 2/3 diameter of entire centrum: present = 0, absent = 1 C172: 1->0
State at this node found in an ancestor, thus representing a reversal
234. Interclavicle parasternal process shape: absent = 0, parallel sided = 1, or tapering = 2 C197: 2->1
State at this node found in an ancestor, thus representing a reversal,
OR convergent with a state outside this clade
274. Illium, ischium, pubis separate ossifications: no not separate= 0, yes separate (including one or more of these unossified)= 1 C212: 1->0
State at this node found in an ancestor, thus representing a reversal
283. Internal trochanter in adult: present = 0, or absent = 1 R108: 0->1
State at this node found in an ancestor, thus representing a reversal,
OR convergent with a state outside this clade

==========
Silvanerpeton (branch number 21):
Total changes along branch: 13

Character: Change
21. Frontal/ parietal length ratio: frontals shorter = 0; longer = 1, subequal = 2 C10: 1->2
State at this node found in an ancestor, thus representing a reversal
23. Frontal/ nasal length ratio: frontals approximately equal to or less than one-third as long as nasals = 0, more than one-third as long = 1 C12: 1->0
State at this node found in an ancestor, thus representing a reversal
59. Postparietal: longer than wide = 0, approximately square or pentagonal = 1, wider than long = 2, triangular and about as long as wide = 3 C50: 2->1
State at this node found in an ancestor, thus representing a reversal,
OR convergent with a state outside this clade
69. Squamosal contact with tabular: smooth = 0, interdigitating = 1, absent = 2 C60: 2->0
State at this node convergent with a state outside this clade
72. Squamosal suture with supratemporal: absent = 0, present = 1 C63: 1->0
State at this node found in an ancestor, thus representing a reversal
73. Squamosal contacts tabular: absent = 0, present = 1 C64: 0->1
State at this node convergent with a state outside this clade
233. Interclavicle anterior tip: squared = 0, broadly rounded = 1, pointed = 2. N85: 1->2
State at this node found in an ancestor, thus representing a reversal
239. Shape of ventral clavicle plate: elongate triangle = 0, sub-equilateral triangle = 1, spoon-shaped/spatulate/ovoid = 2 N30: 0/1->2
State at this node found in an ancestor, thus representing a reversal,
OR convergent with a state outside this clade
270. Ossified olecranon process: absent = 0, present = 1 R83: 1->0
State at this node found in an ancestor, thus representing a reversal
276. Ilium dorsalmost process (one that articulates with sacral rib) orientation: straight dorsal = 0, canted posteriorly = 1, canted anteriorly = 2 N39: 0->1
State at this node found in an ancestor, thus representing a reversal

280. Acetabulum finished = 0, or unfinished, including unossified pubis = 1 R99: 0->1
State at this node found in an ancestor, thus representing a reversal
282. Pubis ossified = 0, or unossified = 1 N72: 0->1
State at this node convergent with a state outside this clade
297. Distal condyle alignment in extensor view: condyles about level = 0, one condyle extends farther distally = 1 N48: 1->0
State at this node found in an ancestor, thus representing a reversal,
OR convergent with a state outside this clade

==========
Seymouria (branch number 22):
Total changes along branch: 31

Character: Change
7. Orbit shape: round, circle or oval = 0; square or rectangular = 1, triangular = 2, anterior projection giving orbit 'keyhole' shape = 3 C163: 0->1
State at this node found in an ancestor, thus representing a reversal,
OR convergent with a state outside this clade
11. Suspensorium proportions: quadrate to anterior margin of temporal embayment about equal to maximum orbit width (discounting any anterior extensions) = 0, quadrate to anterior margin of temporal embayment < maximum orbit width = 1, quadrate to anterio:
State at this node found in an ancestor, thus representing a reversal
12. Otic notch/temporal ebayment approaching orbit: more than 1/2 postorbital skull length = 0, 1/4-1/2 postorbital skull length = 1, less than 1/4 postorbital skull length = 2 P35: 1->0
State at this node found in an ancestor, thus representing a reversal
13. Skull table shape: longer than broad = 0, approximately square = 1, shorter than broad = 2 C169: 0->2
State at this node found in an ancestor, thus representing a reversal
19. Septomaxilla (= ?anterior tectal?) present = 0, absent = 1 C1: 1->0
State at this node found in an ancestor, thus representing a reversal
32. Jugal extends anterior to anterior orbit margin: absent = 0, present = 1 C21: 0->1
State at this node found in an ancestor, thus representing a reversal,
OR convergent with a state outside this clade
38. Maxilla external contact with premaxilla: narrow contact point not interdigitated = 0, interdigitating suture = 1 C27: 0->1
State at this node convergent with a state outside this clade
40. Maxilla extends behind level of posterior margin of orbit: present = 0, absent = 1 C29: 0->1
State at this node convergent with a state outside this clade
48. Parietal ? postorbital suture: absent = 0, present = 1 C39: 0->1
State at this node found in an ancestor, thus representing a reversal
52. Postfrontal ? prefrontal contact: broad = 0; or point-like = 1 C43: 1->0
State at this node found in an ancestor, thus representing a reversal
58. Postorbital at least one quarter of the width of the skull table at the same transverse level: absent = 0, present = 1 ? C49: 0->1
State at this node found in an ancestor, thus representing a reversal
70. Squamosal-supratemporal suture position: at apex of temporal embayment = 0, dorsal to apex = 1, ventral to apex = 2 C61: 0->1
State at this node convergent with a state outside this clade
97. Exoccipitals enlarged to form double horizontally orientated occipital condyle, (may exclude basioccipital from articular surface): absent = 0, present = 1 C9: 0->1
State at this node convergent with a state outside this clade

137. Maxillary caniniform teeth (about twice the size of neighbouring teeth): absent = 0, present = 1 C97: 0->1
State at this node found in an ancestor, thus representing a reversal
138. Number of maxilla caniniform teeth: single = 0, multiple = 1 N19: 1->0
State at this node convergent with a state outside this clade
153. Upper marginal teeth number: greater than lower = 0, same = 1, smaller than lower = 2 C113: 1->2
State at this node found in an ancestor, thus representing a reversal,
OR convergent with a state outside this clade
154. Premaxilla caniniform teeth: absent = 0, present = 1 N20: 0->1
State at this node convergent with a state outside this clade
201. Dentary teeth size: same size as maxillary teeth (0), larger than maxillary teeth = 1, smaller than maxillary teeth = 2 C250: 0->1
State at this node convergent with a state outside this clade
206. Centra (trunk) pleurocentra fused middorsally: absent = 0, present = 1 C174: 0->1
State at this node convergent with a state outside this clade
212. Neural arches of trunk vertebrae: not fused to centra = 0; fused to pleurocentrum or combined centrum = 1 N83: 0->1
State at this node convergent with a state outside this clade
215. Ribs (trunk): straight or weakly curved = 0, strongly ventrally curved = 1 C203: 1->0
State at this node found in an ancestor, thus representing a reversal
226. Clavicles meet anteriorly: present = 0, absent = 1 C176: 1->0
State at this node found in an ancestor, thus representing a reversal,
OR convergent with a state outside this clade
234. Interclavicle parasternal process shape: absent = 0, parallel sided = 1, or tapering = 2 C197: 2->1
State at this node found in an ancestor, thus representing a reversal,
OR convergent with a state outside this clade
242. Glenoid subterminal, i.e. the scapulocoracoid does not extend ventral and slightly posterior to its posteroventral margin, and does not form a distinct 'wall' of bone, visible in lateral aspect: yes = 0, no = 1 R25: 0->1
State at this node found in an ancestor, thus representing a reversal
249. Percentage of humerus posterior margin proximal to entepicondyle, measured from proximal base of entepicondyle: about a third or less = 0, about half = 1, about two thirds = 2, more than two thirds = 3 N33: 1->2
State at this node found in an ancestor, thus representing a reversal
259. Humerus entepicondyle width relative to humeral head width: smaller = 0, greater = 1 C195: 1->0
State at this node found in an ancestor, thus representing a reversal,
OR convergent with a state outside this clade
281. Number of pubic obturator foramina: multiple = 0, single = 1, absent = 2 R105: 1->2
State at this node found in an ancestor, thus representing a reversal,
OR convergent with a state outside this clade
296. Tibia and fibula condyles greatest width in distal view: equal = 0, tibia condyle broader = 1, fibula condyle broader = 2 N47: 1->2
Uniquely derived state, unchanged above
Two or more other states found outside this clade
304. Tibia proximal extremity wider = 0, as wide as = 1, or narrow than = 2 its distal extremity R126: 0->1
State at this node found in an ancestor, thus representing a reversal
320. Wrist ossifications in adult: fully ossified = 0, or fully unossified = 1, or partially ossified = 2 N65: 1->0
State at this node found in an ancestor, thus representing a reversal,
OR convergent with a state outside this clade

326. Scale distribution: gastralia present = 0, gastralia and dorsal scales/osteoderms/other dermal ossifications present = 1, no scales = 2 N71: 0->2
State at this node convergent with a state outside this clade

==========
Caerorhachis (branch number 23):
Total changes along branch: 13

Character: Change
37. Maxilla sutures to vomer: absent = 0, present = 1 C26: 0->1
State at this node convergent with a state outside this clade
52. Postfrontal ? prefrontal contact: broad = 0; or point-like = 1 C43: 1->0
State at this node found in an ancestor, thus representing a reversal
55. Postorbital without distinct dorsomedial ramus for postfrontal = 0, with incipient ramus = 1, ?with elongate ramus = 2 C46: 0->1
State at this node convergent with a state outside this clade
77. Tabular shape in dorsal view (aside from horn, if present): rectangle or square = 0, irregular rectangular/quadrangle = 1, elongate oval or teardrop = 2, triangular = 3 N1: 1->3
State at this node found in an ancestor, thus representing a reversal
114. Ectopterygoid reaches subtemporal fossa: absent = 0, present = 1 C72: 1->0
State at this node convergent with a state outside this clade
166. Coronoid (posterior) posterodorsal process visible in lateral view: absent = 0, present = 1 C122: 1->0
State at this node found in an ancestor, thus representing a reversal
182. Number of Meckelian openings: more than three = 0, three = 1, two = 2, one = 3 N73: 3->1
State at this node convergent with a state outside this clade
189. Adsymphysial plate fang-pair (distinct from other teeth): absent = 0, present = 1 C141: 0->1
State at this node found in an ancestor, thus representing a reversal
196. Prearticular shagreen field, distribution: gradually decreasing from dorsal to ventral = 0, well defined dorsal longitudinal band = 1, scattered patches or absent = 2 C148: 2->0
State at this node found in an ancestor, thus representing a reversal,
OR convergent with a state outside this clade
276. Ilium dorsalmost process (one that articulates with sacral rib) orientation: straight dorsal = 0, canted posteriorly = 1, canted anteriorly = 2 N39: 0->2
State at this node found in an ancestor, thus representing a reversal
293. Femur without = 0, or with = 1 distinctly expanded proximal head R115: 1->0
State at this node found in an ancestor, thus representing a reversal
308. Relative lengths of hindlimb epipodials and femur: epipodials less than 50% of femur length = 0, about 50% femur length = 1, or >50% of femur length = 2 N52: 2->0
State at this node convergent with a state outside this clade
327. Gastralia: tapered and elongate, four times longer than broad or longer = 0, ovoid = 1, around three times longer than broad one end tapering = 2 C211: 1->0
State at this node found in an ancestor, thus representing a reversal

==========
Adamanterpeton (branch number 24):
Total changes along branch: 12

Character: Change
13. Skull table shape: longer than broad = 0, approximately square = 1, shorter than broad = 2 C169: 1->0

State at this node found in an ancestor, thus representing a reversal
19. Septomaxilla (= ?anterior tectal?) present = 0, absent = 1 C1: 1->0
State at this node found in an ancestor, thus representing a reversal
30. Jugal alary process ("insula jugalis") on palate: absent = 0, present = 1 C19: 0->1
State at this node convergent with a state outside this clade
35. Lacrimal contributes to narial margin: absent, excluded by anterior tectal = 0: present = 1, absent, excluded by nasal/maxillary or prefrontal/maxillary suture = 2 C24: 1->0
State at this node found in an ancestor, thus representing a reversal
36. Lacrimal reaches orbit margin (= prefrontal/ jugal suture): present = 0, absent = 1 C25: 0->1
State at this node convergent with a state outside this clade
53. Postfrontal ? prefrontal suture: anterior half of orbit = 0, middle or posterior half of ?orbit = 1, absent = 2 C44: 0->1
State at this node found in an ancestor, thus representing a reversal,
OR convergent with a state outside this clade
54. Postorbital suture to skull table (usually intertemporal or supratemporal when present) interdigitating vs smooth: smooth = 0, interdigitating = 1 C45: 1->0
State at this node found in an ancestor, thus representing a reversal
66. Premaxilla forms part of choanal margin: broadly = 0, point = 1, not, excluded by ?vomer = 2 C57: 2->0
State at this node found in an ancestor, thus representing a reversal
77. Tabular shape in dorsal view (aside from horn, if present): rectangle or square = 0, irregular rectangular/quadrangle = 1, elongate oval or teardrop = 2, triangular = 3 N1: 1->0
State at this node found in an ancestor, thus representing a reversal
103. Parasphenoid depression in body: absent = 0, single median = 1, multiple = 2 C77: 0->2
State at this node convergent with a state outside this clade
114. Ectopterygoid reaches subtemporal fossa: absent = 0, present = 1 C72: 1->0
State at this node convergent with a state outside this clade
154. Premaxilla caniniform teeth: absent = 0, present = 1 N20: 0->1
State at this node convergent with a state outside this clade

==========
Capetus (branch number 25):
Total changes along branch: 9

Character: Change
10. Pineal foramen position along interparietal suture: behind midpoint = 0, at the midpoint = 1, anterior to midpoint = 2 C166: 1->0
State at this node found in an ancestor, thus representing a reversal
15. Center of ornament on squamosal: no center of ornamentation= 0, center closer to dorsal apex of temporal embayment (or midline of skull if no temporal ebayment) = 1, center closer to posteroventral margin of squamosal = 2 N77: 0->1
State at this node found in an ancestor, thus representing a reversal
28. Jugal deep below orbit (vs narrow process): > 50% orbit diam = 0, <50% = 1 C17: 1->0
State at this node found in an ancestor, thus representing a reversal
50. Parietal shape of anteriormost third: not wider than frontals = 0, at least marginally wider = 1 C41: 0->1
State at this node found in an ancestor, thus representing a reversal
57. Postorbital longer than anteroposterior width of orbit: absent = 0, present = 1 C48: 0->1
State at this node found in an ancestor, thus representing a reversal
73. Squamosal contacts tabular: absent = 0, present = 1 C64: 0->1
State at this node convergent with a state outside this clade

117. Pterygoid quadrate ramus margin in adductor fossa: concave = 0, with some convex component = 1 C85: 1->0
State at this node found in an ancestor, thus representing a reversal
135. Ectopterygoid / palatine shagreen field: absent = 0, present = 1 ? C95: 1->0
State at this node found in an ancestor, thus representing a reversal
200. Surangular crest: absent = 0, present = 1 C153: 0->1
State at this node convergent with a state outside this clade

==========
Balanerpeton (branch number 26):
Total changes along branch: 18

Character: Change
2. Preorbital region of skull less than twice as wide as long = 0, or at least twice as wide as long = 1 C155: 0->1
State at this node convergent with a state outside this clade
4. Interorbital distance compared with maximum orbit diameter: greater = 0, smaller = 1, subequal = 2 C158: 0->1
State at this node found in an ancestor, thus representing a reversal
8. Orbit position re snout/postparietal length: centre closer to front than rear = 0, centre near middle = 1, centre closer to rear than front = 2 C164: 1/2->0
State at this node found in an ancestor, thus representing a reversal
9. Orbit position re snout /quadrate length: centre closer to front than rear = 0, centre near middle = 1, centre closer to rear than front = 2 C165: 1->0
State at this node found in an ancestor, thus representing a reversal
10. Pineal foramen position along interparietal suture: behind midpoint = 0, at the midpoint = 1, anterior to midpoint = 2 C166: 1->2
State at this node convergent with a state outside this clade
13. Skull table shape: longer than broad = 0, approximately square = 1, shorter than broad = 2 C169: 1->2
State at this node found in an ancestor, thus representing a reversal
15. Center of ornament on squamosal: no center of ornamentation= 0, center closer to dorsal apex of temporal embayment (or midline of skull if no temporal ebayment) = 1, center closer to posteroventral margin of squamosal = 2 N77: 0->1
State at this node found in an ancestor, thus representing a reversal
31. Jugal length of postorbital region relative to one-third of the length of the postorbital cheek region: greater = 0 or less =1 0 C20: 0->1
State at this node found in an ancestor, thus representing a reversal,
OR convergent with a state outside this clade
39. Maxilla highest point in posterior half = 0, anterior third of its length = 1, or at its midlength = 2, or same height all along length =3 C28: 1->2
State at this node found in an ancestor, thus representing a reversal,
OR convergent with a state outside this clade
53. Postfrontal ? prefrontal suture: anterior half of orbit = 0, middle or posterior half of ?orbit = 1, absent = 2 C44: 0->1
State at this node found in an ancestor, thus representing a reversal,
OR convergent with a state outside this clade
60. Postparietal occipital flange (="postparietal lappet) exposure: absent = 0, present = 1 C51: 1->0
State at this node found in an ancestor, thus representing a reversal
144. Pterygoid shagreen: dense = 0, a few discontinuous patches or absent = 1 C103: 0->1
State at this node convergent with a state outside this clade

174. Dentary tooth number: more than 70 = 0, 56-70 = 1, 46-55 = 2, 36-45 = 3, less than 35 = 4 C130: 3->4
State at this node found in an ancestor, thus representing a reversal
186. Meckelian foramina/ fenestrae, dorsal margins formed by; mostly meckelian bone = 0, mostly prearticular = 1, mostly infradentary (postsplenial) = 2 C139: 1->2
State at this node convergent with a state outside this clade
201. Dentary teeth size: same size as maxillary teeth (0), larger than maxillary teeth = 1, smaller than maxillary teeth = 2 C250: 0->1
State at this node convergent with a state outside this clade
233. Interclavicle anterior tip: squared = 0, broadly rounded = 1, pointed = 2. N85: 1->2
State at this node found in an ancestor, thus representing a reversal
267. Radius: longer than ulna = 0, same length as ulna = 1, shorter than ulna (including olecranon process if present) = 2 C202: 2->1
State at this node convergent with a state outside this clade
308. Relative lengths of hindlimb epipodials and femur: epipodials less than 50% of femur length = 0, about 50% femur length = 1, or >50% of femur length = 2 N52: 2->0
State at this node convergent with a state outside this clade

==========
Dendrerpeton (branch number 27):
Total changes along branch: 13

Character: Change
3. Internarial/ interpremaxillary fenestra (independent of presence of median rostrals) on dorsal surface of skull: absent = 0, present = 1 C157: 0->1
State at this node found in an ancestor, thus representing a reversal,
OR convergent with a state outside this clade
21. Frontal/ parietal length ratio: frontals shorter = 0; longer = 1, subequal = 2 C10: 1->0
State at this node found in an ancestor, thus representing a reversal,
OR convergent with a state outside this clade
29. Jugal contribution to orbit margin: less than one-third = 0, equal to or more than one-third = 1 C18: 0->1
State at this node convergent with a state outside this clade
37. Maxilla sutures to vomer: absent = 0, present = 1 C26: 0->1
State at this node convergent with a state outside this clade
50. Parietal shape of anteriormost third: not wider than frontals = 0, at least marginally wider = 1 C41: 0->1
State at this node found in an ancestor, thus representing a reversal
71. Squamosal anterior part lying behind mid-parietal length: present = 0, absent = 1 C62: 1->0
State at this node found in an ancestor, thus representing a reversal
122. Vomers as broad as long or broader = 0, about twice as long as broad or longer = 1 C91: 0->1
State at this node convergent with a state outside this clade
136. Maxilla tooth number: > 40 = 0, 30-40 = 1, < 30 = 2 ? C96: 1->0
State at this node found in an ancestor, thus representing a reversal
164. Coronoid (middle) separated from splenial (or presplenial if present): present, by prearticular = 0, absent = 1, present, by postsplenial = 2 C120: 2->1
State at this node convergent with a state outside this clade
217. Ribs (trunk) tapered distally =0, parallel-sided = 1, flared at distal tip= 2 C205: 1->0
State at this node found in an ancestor, thus representing a reversal

235. Interclavicle body shape (excluding parasternal process of present): small scute = 0, triangle longest anteriorly = 1, triangle longest laterally = 2, spatulate or fan-shaped = 3, equilateral triangle = 4 N78: 2->3

State at this node found in an ancestor, thus representing a reversal,
OR convergent with a state outside this clade

302. Tibia distal articular surface absent = 0, present and with L-shaped outline = 1, present and with subelliptical outline = 2 R122: 2->1

State at this node found in an ancestor, thus representing a reversal

327. Gastralia: tapered and elongate, four times longer than broad or longer = 0, ovoid = 1, around three times longer than broad one end tapering = 2 C211: 1->0

State at this node found in an ancestor, thus representing a reversal

==========

Edops (branch number 28):
Total changes along branch: 11

Character: Change

57. Postorbital longer than anteroposterior width of orbit: absent = 0, present = 1 C48: 0->1

State at this node found in an ancestor, thus representing a reversal

58. Postorbital at least one quarter of the width of the skull table at the same transverse level: absent = 0, present = 1 ? C49: 0->1

State at this node found in an ancestor, thus representing a reversal

126. Interpterygoid vacuities that intersect with orbit: absent = 0, or present = 1 N14: 1->0

State at this node found in an ancestor, thus representing a reversal

127. Pterygoids meet along midline: yes = 0, or no = 1 N15: 1->0

State at this node found in an ancestor, thus representing a reversal

129. Vomer contributes to interpterygoid vacuity: absent = 0, present = 1 C90: 1->0

State at this node found in an ancestor, thus representing a reversal

130. Median margin of pterygoid palatal ramus where separate: straight = 0, slightly concave medially = 1, convex medially = 2, greatly concave medially = 3 N17: 3->1

State at this node found in an ancestor, thus representing a reversal,
OR convergent with a state outside this clade

136. Maxilla tooth number: > 40 = 0, 30-40 = 1, < 30 = 2 ? C96: 1->2

State at this node found in an ancestor, thus representing a reversal,
OR convergent with a state outside this clade

145. Premaxillary tooth number: > 15 = 0, 10 - 14 = 1, < 10 = 2 ? C105: 1->2

State at this node found in an ancestor, thus representing a reversal

257. Humerus ectepicondyle distinct: present = 0, absent = 1 C192: 0->1

State at this node convergent with a state outside this clade

265. Length of posterior margin of entepicondyle smaller than = 0, subequal to = 1, or larger than = 2, humerus anteroposterior length at the level of proximal insertion of entepicondyle onto humerus shaft R66: 2->1

State at this node found in an ancestor, thus representing a reversal

307. Posterior (lateral) surface of fibula concave = 0, straight = 1, convex = 2, in its proximal half R132: 1->0

State at this node found in an ancestor, thus representing a reversal

==========

Eryops (branch number 29):
Total changes along branch: 18

Character: Change

12. Otic notch/temporal ebayment approaching orbit: more than 1/2 postorbital skull length = 0, 1/4-1/2 postorbital skull length = 1, less than 1/4 postorbital skull length = 2 P35: 1->0

State at this node found in an ancestor, thus representing a reversal

13. Skull table shape: longer than broad = 0, approximately square = 1, shorter than broad = 2 C169: 1->2

State at this node found in an ancestor, thus representing a reversal

24. Intertemporal present: present = 0, absent = 1 C13: 0->1

State at this node found in an ancestor, thus representing a reversal

31. Jugal length of postorbital region relative to one-third of the length of the postorbital cheek region: greater = 0 or less =1 0 C20: 0->1

State at this node found in an ancestor, thus representing a reversal,
OR convergent with a state outside this clade

45. Nasal ? parietal length ratio less than 1.45 = 0 or greater than 1.45 = 1 C34: 0->1

State at this node convergent with a state outside this clade

49. Parietal anterior portion extent relative to orbit midlength: in front of = 0, level with ?= 1, posterior to = 2 C40: 2->1

State at this node found in an ancestor, thus representing a reversal

56. Postorbital shape: irregularly polygonal = 0, broadly cresentic and narrowing to a posterior point = 1 C47: 1->0

State at this node found in an ancestor, thus representing a reversal

78. Tabular horn: absent, tabular does not form horn = 0, tabular forms notable horn = 1 N2: 0->1

State at this node found in an ancestor, thus representing a reversal,
OR convergent with a state outside this clade

80. Tabular prolonged posterolateral ornamented surface absent = 0, present = 1 C68: 0->1

State at this node convergent with a state outside this clade

97. Exoccipitals enlarged to form double horizontally orientated occipital condyle, (may exclude basioccipital from articular surface): absent = 0, present = 1 C9: 0->1

State at this node convergent with a state outside this clade

100. Parasphenoid cultriform process shape: biconvex = 0, narrowly triangular =1, parallel-sided = 2, or with proximal constriction followed by swelling = 3 C76: 2->3

State at this node convergent with a state outside this clade

137. Maxillary caniniform teeth (about twice the size of neighbouring teeth): absent = 0, present = 1 C97: 0->1

State at this node found in an ancestor, thus representing a reversal

142. Parasphenoid shagreen field: present = 0, absent = 1 ? C101: 0->1

State at this node found in an ancestor, thus representing a reversal,
OR convergent with a state outside this clade

174. Dentary tooth number: more than 70 = 0, 56-70 = 1, 46-55 = 2, 36-45 = 3, less than 35 = 4 C130: 3->2

State at this node convergent with a state outside this clade

204. Centra strongly notochordal such that notochordal space more than 2/3 diameter of entire centrum: present = 0, absent = 1 C172: 0->1

State at this node convergent with a state outside this clade

259. Humerus entepicondyle width relative to humeral head width: smaller = 0, greater = 1 C195: 1->0

State at this node found in an ancestor, thus representing a reversal,
OR convergent with a state outside this clade

266. Deltopectoral crest present = 0, separate deltoid and pectoral processes = 1, only pectoral process = 2, none of these = 3 N35: 0->1

State at this node convergent with a state outside this clade

294. Femur intercondylar groove: absent = 0, present and not longer than distal end of femur = 1, present and longer than distal end of femur = 2 R116: 1->2
State at this node found in an ancestor, thus representing a reversal

==========
Platyrhinops (branch number 30):
Total changes along branch: 21

Character: Change
1. Skull longer than broad = 0, as broad as long =1, or broader than long = 2 C154: 0->1
State at this node convergent with a state outside this clade
2. Preorbital region of skull less than twice as wide as long = 0, or at least twice as wide as long = 1 C155: 0->1
State at this node convergent with a state outside this clade
9. Orbit position re snout /quadrate length: centre closer to front than rear = 0, centre near middle = 1, centre closer to rear than front = 2 C165: 1->0
State at this node found in an ancestor, thus representing a reversal
10. Pineal foramen position along interparietal suture: behind midpoint = 0, at the midpoint = 1, anterior to midpoint = 2 C166: 1->2
State at this node convergent with a state outside this clade
12. Otic notch/temporal ebayment approaching orbit: more than 1/2 postorbital skull length = 0, 1/4-1/2 postorbital skull length = 1, less than 1/4 postorbital skull length = 2 P35: 1->0
State at this node found in an ancestor, thus representing a reversal
13. Skull table shape: longer than broad = 0, approximately square = 1, shorter than broad = 2 C169: 1->2
State at this node found in an ancestor, thus representing a reversal
24. Intertemporal present: present = 0, absent = 1 C13: 0->1
State at this node found in an ancestor, thus representing a reversal
83. Maximum parietal-parietal width is shorter than distance between posterior skull table margin (discounting tabular horn if present) and posterior orbit margin as projected along skull midline: present = 0, absent = 1 C231: 0->1
State at this node convergent with a state outside this clade
84. Maxilla contribution to orbit margin: absent = 0, or present = 1 C239: 0->1
State at this node convergent with a state outside this clade
97. Exoccipitals enlarged to form double horizontally orientated occipital condyle, (may exclude basioccipital from articular surface): absent = 0, present = 1 C9: 0->1
State at this node convergent with a state outside this clade
156. Marginal tooth shape: conical and straight/slightly recurved = 0, small and more or less straight and 'needle-like' = 1, right-trapezoid 'chisel' shape = 2, spearhead shape = 3, thin and greatly recurved = 4 N22: 0->1
State at this node found in an ancestor, thus representing a reversal
201. Dentary teeth size: same size as maxillary teeth (0), larger than maxillary teeth = 1, smaller than maxillary teeth = 2 C250: 0->1
State at this node convergent with a state outside this clade
206. Centra (trunk) pleurocentra fused middorsally: absent = 0, present = 1 C174: 0->1
State at this node convergent with a state outside this clade
244. Scapulocoracoid without = 0, or with = 1 supraglenoid excavation/supraglenoid fossa R34: 1->0
State at this node found in an ancestor, thus representing a reversal
249. Percentage of humerus posterior margin proximal to entepicondyle, measured from proximal base of entepicondyle: about a third or less = 0, about half = 1, about two thirds = 2, more than two thirds = 3 N33: 1->0

State at this node found in an ancestor, thus representing a reversal,
OR convergent with a state outside this clade
255. Humerus radial/ulnar facets: confluent = 0, separated by perichondral strip of bone = 1 C189: 0->1
State at this node found in an ancestor, thus representing a reversal
263. Humerus length up to and no more than twice its width = 0, or more than twice its width = 1 R49: 0->1
State at this node convergent with a state outside this clade
265. Length of posterior margin of entepicondyle smaller than = 0, subequal to = 1, or larger than = 2, humerus anteroposterior length at the level of proximal insertion of entepicondyle onto humerus shaft R66: 2->0
State at this node found in an ancestor, thus representing a reversal
269. Radius without = 0, or with = 1, distinctly expanded proximal extremity R82: 1->0
State at this node found in an ancestor, thus representing a reversal
274. Illium, ischium, pubis separate ossifications: no not separate= 0, yes separate (including one or more of these unossified)= 1 C212: 1->0
State at this node found in an ancestor, thus representing a reversal
277. Dorsal iliac process oblique and flared = 0, fan-shaped = 1, subrectangular and truncated = 2, blunt and digitiform = 3, low elongate = 4 R93: 3->2
State at this node convergent with a state outside this clade

==========
Erpetosaurus (branch number 31):
Total changes along branch: 18

Character: Change
13. Skull table shape: longer than broad = 0, approximately square = 1, shorter than broad = 2 C169: 1->2
State at this node found in an ancestor, thus representing a reversal
14. Dermal ornament character: Pit-and-ridge with visible center of ossification = 0, pit-and-ridge with no obvious center of ossification = 1, irregular pit-and-ridge with no obvious center of ossification =2, short radiating grooves = 3, pitted = 4, ir:
State at this node convergent with a state outside this clade
24. Intertemporal present: present = 0, absent = 1 C13: 0->1
State at this node found in an ancestor, thus representing a reversal
30. Jugal alary process ("insula jugalis") on palate: absent = 0, present = 1 C19: 0->1
State at this node convergent with a state outside this clade
42. Maxilla ? premaxilla contact shelf-like mesial to tooth row on palate: absent = 0, present = 1 C31: 0->1
State at this node found in an ancestor, thus representing a reversal,
OR convergent with a state outside this clade
48. Parietal ? postorbital suture: absent = 0, present = 1 C39: 0->1
State at this node found in an ancestor, thus representing a reversal
92. Basioccipital: ventrally exposed portion longer than wide = 0, shorter than wide = 1 C4: 1->0
State at this node found in an ancestor, thus representing a reversal
130. Median margin of pterygoid palatal ramus where separate: straight = 0, slightly concave medially = 1, convex medially = 2, greatly concave medially = 3 N17: 3->1
State at this node found in an ancestor, thus representing a reversal,
OR convergent with a state outside this clade
133. Ectopterygoid row (3+) of smaller teeth: present = 0, absent = 1 C93: 0->1
State at this node found in an ancestor, thus representing a reversal,
OR convergent with a state outside this clade

140. Palatine row of smaller teeth: present = 0, absent = 1 C99: 0->1
State at this node found in an ancestor, thus representing a reversal,
OR convergent with a state outside this clade
147. Vomerine fang pairs noticeably smaller than other palatal fang pairs: absent = 0, present = 1 C107: 0->1
State at this node found in an ancestor, thus representing a reversal,
OR convergent with a state outside this clade
151. Vomerine denticle row lateral to tooth row: present = 0, absent = 1 C111: 1->0
State at this node found in an ancestor, thus representing a reversal,
OR convergent with a state outside this clade
177. Dentary notch: absent = 0, present = 1 C214: 0->1
State at this node convergent with a state outside this clade
178. Mandibular sensory canal: present = 0, absent = 1 C134: 0->1
State at this node found in an ancestor, thus representing a reversal,
OR convergent with a state outside this clade
218. Ribs (trunk) bear uncinate processes: absent = 0, present = 1 C206: 0->1
State at this node found in an ancestor, thus representing a reversal
248. Angle between proximal and distal ends of humerus: 30 degrees or less = 0, 31-60 degrees = 1, more than 60 degrees = 2 N84: 1->0
State at this node found in an ancestor, thus representing a reversal
276. Ilium dorsalmost process (one that articulates with sacral rib) orientation: straight dorsal = 0, canted posteriorly = 1, canted anteriorly = 2 N39: 0->1
State at this node found in an ancestor, thus representing a reversal
327. Gastralia: tapered and elongate, four times longer than broad or longer = 0, ovoid = 1, around three times longer than broad one end tapering = 2 C211: 1->0
State at this node found in an ancestor, thus representing a reversal

==========
Trimerorhachis (branch number 32):
Total changes along branch: 25

Character: Change
5. Naris position: ventral rim closer to jaw margin than height of naris = 0, distance to jaw margin similar to or greater than height of naris = 1 C160: 1->0
State at this node found in an ancestor, thus representing a reversal
46. Nasal smaller in area than postparietal: absent = 0, present = 1 C35: 0->1
State at this node found in an ancestor, thus representing a reversal,
OR convergent with a state outside this clade
55. Postorbital without distinct dorsomedial ramus for postfrontal = 0, with incipient ramus = 1, ?with elongate ramus = 2 C46: 0->1
State at this node convergent with a state outside this clade
65. Premaxilla posterodorsal alary process onto snout: absent = 0, present = 1 C56: 1->0
State at this node found in an ancestor, thus representing a reversal
70. Squamosal-supratemporal suture position: at apex of temporal embayment = 0, dorsal to apex = 1, ventral to apex = 2 C61: 0->1
State at this node convergent with a state outside this clade
71. Squamosal anterior part lying behind mid-parietal length: present = 0, absent = 1 C62: 1->0
State at this node found in an ancestor, thus representing a reversal
72. Squamosal suture with supratemporal: absent = 0, present = 1 C63: 1->0
State at this node found in an ancestor, thus representing a reversal

75. Supratemporal forms part of skull margin posteriorly, including temporal ebayment: absent = 0, present = 1 C66: 1->0

State at this node found in an ancestor, thus representing a reversal

82. (Infraorbital) lateral line relationship to naris: continuous ventral to naris within lateral rostral = 0, discontinuous across ventral naris = 1, discontinuous ventral to naris across maxilla to premaxilla = 2, continuous ventral to naris in maxilla:

Uniquely derived state, unchanged above

Two or more other states found outside this clade

103. Parasphenoid depression in body: absent = 0, single median = 1, multiple = 2 C77: 1->2

State at this node convergent with a state outside this clade

116. Pterygoids flank parasphenoid for most of length of cultriform process = 0, not so = 1 C84: 0->1

State at this node found in an ancestor, thus representing a reversal,
OR convergent with a state outside this clade

120. Vomers separated by parasphenoid > half vomer mesial length: present = 0, absent = 1 C88: 1->0

State at this node found in an ancestor, thus representing a reversal

132. Ectopterygoid fang pairs: present = 0, absent = 1 C92: 0->1

State at this node found in an ancestor, thus representing a reversal

136. Maxilla tooth number: > 40 = 0, 30-40 = 1, < 30 = 2 ? C96: 0->2

State at this node found in an ancestor, thus representing a reversal,
OR convergent with a state outside this clade

144. Pterygoid shagreen: dense = 0, a few discontinuous patches or absent = 1 C103: 0->1

State at this node convergent with a state outside this clade

148. Vomer anterior wall forming posterior margin of palatal fossa bears tooth row meeting in midline: present = 0, absent = 1 C108: 1->0

State at this node found in an ancestor, thus representing a reversal

149. Vomerine row of small teeth : present = 0, absent = 1 ? C109: 1->0

State at this node found in an ancestor, thus representing a reversal

150. Vomerine shagreen field: absent = 0, present = 1 ? C110: 1->0

State at this node found in an ancestor, thus representing a reversal

176. Dentary ventral edge: smooth continuous line = 0, abruptly tapering or ?stepped? margin = 1 C133: 0->1

State at this node found in an ancestor, thus representing a reversal

217. Ribs (trunk) tapered distally =0, parallel-sided = 1, flared at distal tip= 2 C205: 1->0/2

Derived state unclear

State at this node found in an ancestor, thus representing a reversal

230. Scapulocoracoid dorsal blade: absent = 0, present = 1 $C209: 1->0

State at this node found in an ancestor, thus representing a reversal

244. Scapulocoracoid without = 0, or with = 1 supraglenoid excavation/supraglenoid fossa R34: 1->0

State at this node found in an ancestor, thus representing a reversal

266. Deltopectoral crest present = 0, separate deltoid and pectoral processes = 1, only pectoral process = 2, none of these = 3 N35: 0->1

State at this node convergent with a state outside this clade

267. Radius: longer than ulna = 0, same length as ulna = 1, shorter than ulna (including olecranon process if present) = 2 C202: 2->0

State at this node found in an ancestor, thus representing a reversal

277. Dorsal iliac process oblique and flared = 0, fan-shaped = 1, subrectangular and truncated = 2, blunt and digitiform = 3, low elongate = 4 R93: 3->1

State at this node found in an ancestor, thus representing a reversal,
OR convergent with a state outside this clade

==========

Neldasaurus (branch number 33):
Total changes along branch: 23

Character: Change
10. Pineal foramen position along interparietal suture: behind midpoint = 0, at the midpoint = 1, anterior to midpoint = 2 C166: 1->2
State at this node convergent with a state outside this clade
13. Skull table shape: longer than broad = 0, approximately square = 1, shorter than broad = 2 C169: 1->0
State at this node found in an ancestor, thus representing a reversal
25. Intertemporal smaller than supratemporal = 0, or larger than/comparable in size with supratemporal = 1 C14: 0->1
State at this node found in an ancestor, thus representing a reversal,
OR convergent with a state outside this clade
27. Intertemporal contacts squamosal: absent = 0, present = 1 C16: 0->1
State at this node convergent with a state outside this clade
37. Maxilla sutures to vomer: absent = 0, present = 1 C26: 0->1
State at this node convergent with a state outside this clade
53. Postfrontal ? prefrontal suture: anterior half of orbit = 0, middle or posterior half of ?orbit = 1, absent = 2 C44: 0->1
State at this node found in an ancestor, thus representing a reversal,
OR convergent with a state outside this clade
56. Postorbital shape: irregularly polygonal = 0, broadly cresentic and narrowing to a posterior point = 1 C47: 0->1
State at this node convergent with a state outside this clade
58. Postorbital at least one quarter of the width of the skull table at the same transverse level: absent = 0, present = 1 ? C49: 1->0
State at this node found in an ancestor, thus representing a reversal
70. Squamosal-supratemporal suture position: at apex of temporal embayment = 0, dorsal to apex = 1, ventral to apex = 2 C61: 0->2
State at this node found in an ancestor, thus representing a reversal,
OR convergent with a state outside this clade
82. (Infraorbital) lateral line relationship to naris: continuous ventral to naris within lateral rostral = 0, discontinuous across ventral naris = 1, discontinuous ventral to naris across maxilla to premaxilla = 2, continuous ventral to naris in maxilla:
State at this node found in an ancestor, thus representing a reversal
91. Basioccipital: indistinguishable from exoccipitals = 0, separated by suture = 1 C3: 1->0
State at this node found in an ancestor, thus representing a reversal
103. Parasphenoid depression in body: absent = 0, single median = 1, multiple = 2 C77: 1->0
State at this node found in an ancestor, thus representing a reversal
136. Maxilla tooth number: > 40 = 0, 30-40 = 1, < 30 = 2 ? C96: 0->1
State at this node found in an ancestor, thus representing a reversal
160. Angular reaches posteriormost point of lower jaw: absent = 0, present = 1 C116: 0->1
State at this node convergent with a state outside this clade
186. Meckelian foramina/ fenestrae, dorsal margins formed by; mostly meckelian bone = 0, mostly prearticular = 1, mostly infradentary (postsplenial) = 2 C139: 1->2
State at this node convergent with a state outside this clade
199. Splenial, rearmost extension of mesial lamina closer to anterior margin of adductor fossa than to the anterior end of the jaw: absent = 0, present = 1 C152: 0->1
State at this node found in an ancestor, thus representing a reversal
225. Ossified pectoral girdle: present = 0, absent = 1 N28: 0->1

State at this node convergent with a state outside this clade
233. Interclavicle anterior tip: squared = 0, broadly rounded = 1, pointed = 2. N85: 1->2
State at this node found in an ancestor, thus representing a reversal
249. Percentage of humerus posterior margin proximal to entepicondyle, measured from proximal base of entepicondyle: about a third or less = 0, about half = 1, about two thirds = 2, more than two thirds = 3 N33: 1->0
State at this node found in an ancestor, thus representing a reversal,
OR convergent with a state outside this clade
257. Humerus ectepicondyle distinct: present = 0, absent = 1 C192: 0->1
State at this node convergent with a state outside this clade
265. Length of posterior margin of entepicondyle smaller than = 0, subequal to = 1, or larger than = 2, humerus anteroposterior length at the level of proximal insertion of entepicondyle onto humerus shaft R66: 2->0
State at this node found in an ancestor, thus representing a reversal
271. Ulna wider at its distal extremity = 0, of about the same width at proximal and distal extremities = 1, wider at its proximal extremity = 2 R84: 2->1
State at this node found in an ancestor, thus representing a reversal
318. Phalanges cross-section shape (manual): circular = 0, square-shaped or elongate oval-shaped = 1, convex upwards = 2 N63: 2->1
State at this node found in an ancestor, thus representing a reversal

==========
Archegosaurus (branch number 34):
Total changes along branch: 35

Character: Change
8. Orbit position re snout/postparietal length: centre closer to front than rear = 0, centre near middle = 1, centre closer to rear than front = 2 C164: 1->2
State at this node found in an ancestor, thus representing a reversal
9. Orbit position re snout /quadrate length: centre closer to front than rear = 0, centre near middle = 1, centre closer to rear than front = 2 C165: 1->2
State at this node convergent with a state outside this clade
24. Intertemporal present: present = 0, absent = 1 C13: 0->1
State at this node found in an ancestor, thus representing a reversal
29. Jugal contribution to orbit margin: less than one-third = 0, equal to or more than one-third = 1 C18: 0->1
State at this node convergent with a state outside this clade
31. Jugal length of postorbital region relative to one-third of the length of the postorbital cheek region: greater = 0 or less =1 0 C20: 0->1
State at this node found in an ancestor, thus representing a reversal,
OR convergent with a state outside this clade
32. Jugal extends anterior to anterior orbit margin: absent = 0, present = 1 C21: 0->1
State at this node found in an ancestor, thus representing a reversal,
OR convergent with a state outside this clade
36. Lacrimal reaches orbit margin (= prefrontal/ jugal suture): present = 0, absent = 1 C25: 0->1
State at this node convergent with a state outside this clade
45. Nasal ? parietal length ratio less than 1.45 = 0 or greater than 1.45 = 1 C34: 0->1
State at this node convergent with a state outside this clade
49. Parietal anterior portion extent relative to orbit midlength: in front of = 0, level with ?= 1, posterior to = 2 C40: 2->1
State at this node found in an ancestor, thus representing a reversal

71. Squamosal anterior part lying behind mid-parietal length: present = 0, absent = 1 C62: 1->0
State at this node found in an ancestor, thus representing a reversal
78. Tabular horn: absent, tabular does not form horn = 0, tabular forms notable horn = 1 N2: 0->1
State at this node found in an ancestor, thus representing a reversal,
OR convergent with a state outside this clade
79. Tabular horn shape: short projection = 0, single elongate projection = 1, double prong (either incipient or two distinct points) = 2 N3: 0->1
State at this node found in an ancestor, thus representing a reversal,
OR convergent with a state outside this clade
87. Parietals: more than 2.5 times as long as wide = 0 or less than 2.5 times as long as wide = 1 C224: 1->0
State at this node found in an ancestor, thus representing a reversal
97. Exoccipitals enlarged to form double horizontally orientated occipital condyle, (may exclude basioccipital from articular surface): absent = 0, present = 1 C9: 0->1
State at this node convergent with a state outside this clade
132. Ectopterygoid fang pairs: present = 0, absent = 1 C92: 0->1
State at this node found in an ancestor, thus representing a reversal
180. Mandibular oral sulcus/ surangular pit line: present = 0, absent = 1 ? C136: 1->0
State at this node found in an ancestor, thus representing a reversal
185. Meckelian bone or space exposure in middle part of jaw, depth much less than prearticular = 0, depth similar to prearticular or greater = 1 C138: 0->1
State at this node convergent with a state outside this clade
200. Surangular crest: absent = 0, present = 1 C153: 0->1
State at this node convergent with a state outside this clade
213. Presacral count: 25-35 = 0, 20-24 = 1, >35 = 2, <20 = 3 P107: 0->1
State at this node convergent with a state outside this clade
214. Presacral (trunk) ribs: length of longest ribs: short = 0, long = 1 P140: 0->1
State at this node convergent with a state outside this clade
218. Ribs (trunk) bear uncinate processes: absent = 0, present = 1 C206: 0->1
State at this node found in an ancestor, thus representing a reversal
220. Ribs (trunk) differ strongly in length and morphology along ?thoracic? region: absent = 0, present = 1 C207: 0->1
State at this node convergent with a state outside this clade
264. Entepicondyle shape: three-dimmensional spike = 0, dorsoventrally flattened rectangle or trapezoid = 1, dorsoventrally flattened triangle = 2 N34: 1->2
State at this node found in an ancestor, thus representing a reversal
265. Length of posterior margin of entepicondyle smaller than = 0, subequal to = 1, or larger than = 2, humerus anteroposterior length at the level of proximal insertion of entepicondyle onto humerus shaft R66: 2->1
State at this node found in an ancestor, thus representing a reversal
266. Deltopectoral crest present = 0, separate deltoid and pectoral processes = 1, only pectoral process = 2, none of these = 3 N35: 0->3
State at this node found in an ancestor, thus representing a reversal
269. Radius without = 0, or with = 1, distinctly expanded proximal extremity R82: 1->0
State at this node found in an ancestor, thus representing a reversal
270. Ossified olecranon process: absent = 0, present = 1 R83: 1->0
State at this node found in an ancestor, thus representing a reversal
283. Internal trochanter in adult: present = 0, or absent = 1 R108: 0->1
State at this node found in an ancestor, thus representing a reversal,
OR convergent with a state outside this clade

284. Internal torchanter/proximal end of adductor blade relationship to proximal head of femur in adult: separated by deep and clear notch of finished bone = 0, separated by broad open space = 1, on ridge continuous with proximal head of femur = 2 N40:
State at this node convergent with a state outside this clade
286. Fourth trochanter shape: short and narrow = 0, short and broad with flat top = 1, long rugose region = 2, short rugose region = 3, nub or bump = 4 N41: 3->0
Uniquely derived state, unchanged above
Two or more other states found outside this clade
291. Adductor blade shape in adult: broad rectangular blade = 0, narrow blade = 1, broad ridge = 2, narrow parallelogram = 3, spike or prong = 4 N44: 4->2
State at this node found in an ancestor, thus representing a reversal,
OR convergent with a state outside this clade
292. Adductor crest length: shorter than adductor blade = 0, similar length to adductor blade = 1, longer than adductor blade = 2 N46: 2->1
State at this node convergent with a state outside this clade
301. Tibia without = 0, or with = 1 flange along its posterior edge R121: 0->1
State at this node found in an ancestor, thus representing a reversal,
OR convergent with a state outside this clade
310. Interepipodial space shape: elongate tapering oval/'spindle shaped' = 0, broad, elongate oval/subrectangle = 1, small circle that does not reach ends of epipodials = 2 N54: 0->1
State at this node found in an ancestor, thus representing a reversal,
OR convergent with a state outside this clade
320. Wrist ossifications in adult: fully ossified = 0, or fully unossified = 1, or partially ossified = 2 N65: 1->2
State at this node found in an ancestor, thus representing a reversal,
OR convergent with a state outside this clade

==========
Aytonerpeton (branch number 35):
Total changes along branch: 8

Character: Change
2. Preorbital region of skull less than twice as wide as long = 0, or at least twice as wide as long = 1 C155: 0->1
State at this node convergent with a state outside this clade
14. Dermal ornament character: Pit-and-ridge with visible center of ossification = 0, pit-and-ridge with no obvious center of ossification = 1, irregular pit-and-ridge with no obvious center of ossification =2, short radiating grooves = 3, pitted = 4, ir:
State at this node found in an ancestor, thus representing a reversal
20. Septomaxilla: narial opening ventral to it = 0: narial opening anterior to it = 1 C2: 1->0
State at this node found in an ancestor, thus representing a reversal
155. Number of premaxilla caniniform teeth: single = 0, multiple = 1 N21: 0->1
State at this node convergent with a state outside this clade
156. Marginal tooth shape: conical and straight/slightly recurved = 0, small and more or less straight and 'needle-like' = 1, right-trapezoid 'chisel' shape = 2, spearhead shape = 3, thin and greatly recurved = 4 N22: 1->0
State at this node found in an ancestor, thus representing a reversal
177. Dentary notch: absent = 0, present = 1 C214: 1->0
State at this node found in an ancestor, thus representing a reversal
180. Mandibular oral sulcus/ surangular pit line: present = 0, absent = 1 ? C136: 1->0
State at this node found in an ancestor, thus representing a reversal

239. Shape of ventral clavicle plate: elongate triangle = 0, sub-equilateral triangle = 1, spoon-shaped/spatulate/ovoid = 2 N30: 0->1
State at this node found in an ancestor, thus representing a reversal,
OR convergent with a state outside this clade

==========
Pholidogaster (branch number 36):
Total changes along branch: 6

Character: Change
5. Naris position: ventral rim closer to jaw margin than height of naris = 0, distance to jaw margin similar to or greater than height of naris = 1 C160: 0->1
State at this node found in an ancestor, thus representing a reversal,
OR convergent with a state outside this clade
33. Jugal excluded from lower jaw margin by maxilla and quadratojugal: yes = 0, or no = 1 C22: 0->1
State at this node convergent with a state outside this clade
38. Maxilla external contact with premaxilla: narrow contact point not interdigitated = 0, interdigitating suture = 1 C27: 0->1
State at this node convergent with a state outside this clade
40. Maxilla extends behind level of posterior margin of orbit: present = 0, absent = 1 C29: 0->1
State at this node convergent with a state outside this clade
178. Mandibular sensory canal: present = 0, absent = 1 C134: 0->1
State at this node convergent with a state outside this clade
304. Tibia proximal extremity wider = 0, as wide as = 1, or narrow than = 2 its distal extremity R126: 0->2
Uniquely derived state, unchanged above
Two or more other states found outside this clade

==========
Colosteus (branch number 37):
Total changes along branch: 15

Character: Change
8. Orbit position re snout/postparietal length: centre closer to front than rear = 0, centre near middle = 1, centre closer to rear than front = 2 C164: 1->0
State at this node found in an ancestor, thus representing a reversal
9. Orbit position re snout /quadrate length: centre closer to front than rear = 0, centre near middle = 1, centre closer to rear than front = 2 C165: 1->0
State at this node found in an ancestor, thus representing a reversal
28. Jugal deep below orbit (vs narrow process): > 50% orbit diam = 0, <50% = 1 C17: 0->1
State at this node found in an ancestor, thus representing a reversal
45. Nasal ? parietal length ratio less than 1.45 = 0 or greater than 1.45 = 1 C34: 0->1
State at this node convergent with a state outside this clade
69. Squamosal contact with tabular: smooth = 0, interdigitating = 1, absent = 2 C60: 1->0
State at this node convergent with a state outside this clade
109. Anterior extent of cultriform process along palate: ends nearer choana posterior margin = 0, or ends nearer orbit posterior margin = 1 P201: 0->1
State at this node found in an ancestor, thus representing a reversal,
OR convergent with a state outside this clade
136. Maxilla tooth number: > 40 = 0, 30-40 = 1, < 30 = 2 ? C96: 0->1
State at this node found in an ancestor, thus representing a reversal

146. Vomer fang pairs: present = 0, absent = 1 ? C106: 0->1
State at this node convergent with a state outside this clade
149. Vomerine row of small teeth : present = 0, absent = 1 ? C109: 1->0
State at this node found in an ancestor, thus representing a reversal
165. Coronoid (posterior) posterodorsal process: absent = 0, present = 1 C121: 1->0
State at this node found in an ancestor, thus representing a reversal
169. Coronoid: at least one has organized tooth row: present = 0, absent =1 C125: 1->0
State at this node found in an ancestor, thus representing a reversal
173. Dentary with parasymphysial fangs internal to marginal tooth row: present = 0, absent = 1 C129: 1->0
State at this node found in an ancestor, thus representing a reversal
176. Dentary ventral edge: smooth continuous line = 0, abruptly tapering or ?stepped? margin = 1 C133: 1->0
State at this node found in an ancestor, thus representing a reversal
193. Postsplenial with mesial lamina: absent = 0, present = 1 C145: 0->1
State at this node convergent with a state outside this clade
267. Radius: longer than ulna = 0, same length as ulna = 1, shorter than ulna (including olecranon process if present) = 2 C202: 2->1
State at this node convergent with a state outside this clade

==========
Greererpeton (branch number 38):
Total changes along branch: 7

Character: Change
3. Internarial/ interpremaxillary fenestra (independent of presence of median rostrals) on dorsal surface of skull: absent = 0, present = 1 C157: 0->1
State at this node found in an ancestor, thus representing a reversal,
OR convergent with a state outside this clade
4. Interorbital distance compared with maximum orbit diameter: greater = 0, smaller = 1, subequal = 2 C158: 0->2
State at this node found in an ancestor, thus representing a reversal
102. Parasphenoid basal plate: square/rectangular = 0, or triangular/distinctly tapering at one end = 1 N9: 0->1
State at this node convergent with a state outside this clade
106. Parasphenoid contacts or sutures to vomers: present = 0, absent = 1 ? C80: 1->0
State at this node found in an ancestor, thus representing a reversal
119. Pterygoid junction with squamosal: present = 0; absent =1 C87: 0->1
State at this node convergent with a state outside this clade
197. Prearticular sutures with surangular (check rear of jaw): absent = 0, present = 1 C149: 1->0
State at this node found in an ancestor, thus representing a reversal
200. Surangular crest: absent = 0, present = 1 C153: 0->1
State at this node convergent with a state outside this clade

==========
Deltaherpeton (branch number 39):
Total changes along branch: 6

Character: Change
3. Internarial/ interpremaxillary fenestra (independent of presence of median rostrals) on dorsal surface of skull: absent = 0, present = 1 C157: 0->1

State at this node found in an ancestor, thus representing a reversal,
OR convergent with a state outside this clade
15. Center of ornament on squamosal: no center of ornamentation= 0, center closer to dorsal apex of temporal embayment (or midline of skull if no temporal ebayment) = 1, center closer to posteroventral margin of squamosal = 2 N77: 0->1
State at this node found in an ancestor, thus representing a reversal
33. Jugal excluded from lower jaw margin by maxilla and quadratojugal: yes = 0, or no = 1 C22: 0->1
State at this node convergent with a state outside this clade
34. Jugal V-shaped indentation of posterodorsal margin: absent = 0, present = 1 C23: 0->1
State at this node convergent with a state outside this clade
43. Median rostral (=internasal): mosaic = 0, paired = 1, single = 2, absent = 3 C32: 3->2
State at this node found in an ancestor, thus representing a reversal,
OR convergent with a state outside this clade
86. Postparietals: paired = 0 or fused = 1 N6: 0->1
State at this node convergent with a state outside this clade

==========
Crassigyrinus (branch number 40):
Total changes along branch: 35

Character: Change
3. Internarial/ interpremaxillary fenestra (independent of presence of median rostrals) on dorsal surface of skull: absent = 0, present = 1 C157: 0->1
State at this node found in an ancestor, thus representing a reversal,
OR convergent with a state outside this clade
5. Naris position: ventral rim closer to jaw margin than height of naris = 0, distance to jaw margin similar to or greater than height of naris = 1 C160: 0->1
State at this node found in an ancestor, thus representing a reversal,
OR convergent with a state outside this clade
9. Orbit position re snout /quadrate length: centre closer to front than rear = 0, centre near middle = 1, centre closer to rear than front = 2 C165: 1->0
State at this node found in an ancestor, thus representing a reversal
11. Suspensorium proportions: quadrate to anterior margin of temporal embayment about equal to maximum orbit width (discounting any anterior extensions) = 0, quadrate to anterior margin of temporal embayment < maximum orbit width = 1, quadrate to anterio:
State at this node found in an ancestor, thus representing a reversal
14. Dermal ornament character: Pit-and-ridge with visible center of ossification = 0, pit-and-ridge with no obvious center of ossification = 1, irregular pit-and-ridge with no obvious center of ossification =2, short radiating grooves = 3, pitted = 4, ir:
State at this node found in an ancestor, thus representing a reversal
37. Maxilla sutures to vomer: absent = 0, present = 1 C26: 0->1
State at this node convergent with a state outside this clade
38. Maxilla external contact with premaxilla: narrow contact point not interdigitated = 0, interdigitating suture = 1 C27: 0->1
State at this node convergent with a state outside this clade
42. Maxilla ? premaxilla contact shelf-like mesial to tooth row on palate: absent = 0, present = 1 C31: 0->1
State at this node found in an ancestor, thus representing a reversal,
OR convergent with a state outside this clade
54. Postorbital suture to skull table (usually intertemporal or supratemporal when present) interdigitating vs smooth: smooth = 0, interdigitating = 1 C45: 1->0

State at this node found in an ancestor, thus representing a reversal
63. Prefrontal enters naris: absent = 0, present = 1 ? C54: 0->1
State at this node convergent with a state outside this clade
66. Premaxilla forms part of choanal margin: broadly = 0, point = 1, not, excluded by ?vomer = 2 C57: 1->2
State at this node found in an ancestor, thus representing a reversal,
OR convergent with a state outside this clade
72. Squamosal suture with supratemporal: absent = 0, present = 1 C63: 1->0
State at this node found in an ancestor, thus representing a reversal
77. Tabular shape in dorsal view (aside from horn, if present): rectangle or square = 0, irregular rectangular/quadrangle = 1, elongate oval or teardrop = 2, triangular = 3 N1: 0->3
State at this node found in an ancestor, thus representing a reversal
80. Tabular prolonged posterolateral ornamented surface absent = 0, present = 1 C68: 0->1
State at this node convergent with a state outside this clade
101. Basal plate of parasphenoid, measured posteriorly from basipterygoid processes/basal articulation: about as long as wide = 0, wider than long = 1, longer than wide = 2 N8: 1->2
State at this node convergent with a state outside this clade
114. Ectopterygoid reaches subtemporal fossa: absent = 0, present = 1 C72: 1->0
State at this node convergent with a state outside this clade
121. Vomers separated by pterygoids: for > half length = 0, < half length = 1, not separated by pterygoids = 2 C89: 1->0
State at this node convergent with a state outside this clade
123. Anterior palatal fenestra: present = 0, absent = 1 N11: 1->0
State at this node found in an ancestor, thus representing a reversal
125. Anterior palatal fenestra(e) open(s) on dorsal surface of skull: no = 0, yes = 1 N13: 0->1
State at this node convergent with a state outside this clade
148. Vomer anterior wall forming posterior margin of palatal fossa bears tooth row meeting in midline: present = 0, absent = 1 C108: 1->0
State at this node found in an ancestor, thus representing a reversal
152. Vomer with toothed anterolateral crest: present = 0, absent = 1 ? C112: 1->0
State at this node found in an ancestor, thus representing a reversal
158. Adductor fossa faces dorsally = 0, mesially = 1 C114: 1->0
State at this node found in an ancestor, thus representing a reversal
161. Coronoid (anterior) contacts splenial (or presplenial if present): absent = 0, present = 1 C117: 1->0
State at this node found in an ancestor, thus representing a reversal
184. Meckelian opening(s) without ventromesial bony margin = 0, or with ventromesial bony margin = 1 N75: 1->0
State at this node found in an ancestor, thus representing a reversal
210. Neural arch ossification: paired in adult = 0, single in adult = 1 C198: 1->0
State at this node found in an ancestor, thus representing a reversal,
OR convergent with a state outside this clade
215. Ribs (trunk): straight or weakly curved = 0, strongly ventrally curved = 1 C203: 0->1
State at this node convergent with a state outside this clade
235. Interclavicle body shape (excluding parasternal process of present): small scute = 0, triangle longest anteriorly = 1, triangle longest laterally = 2, spatulate or fan-shaped = 3, equilateral triangle = 4 N78: 2->4
State at this node found in an ancestor, thus representing a reversal,
OR convergent with a state outside this clade
261. Ectepicondyle foramen: present = 0, absent = 1 R43: 1->0
State at this node found in an ancestor, thus representing a reversal

267. Radius: longer than ulna = 0, same length as ulna = 1, shorter than ulna (including olecranon process if present) = 2 C202: 2->1
State at this node convergent with a state outside this clade
270. Ossified olecranon process: absent = 0, present = 1 R83: 1->0
State at this node found in an ancestor, thus representing a reversal
271. Ulna wider at its distal extremity = 0, of about the same width at proximal and distal extremities = 1, wider at its proximal extremity = 2 R84: 2->1
State at this node found in an ancestor, thus representing a reversal
297. Distal condyle alignment in extensor view: condyles about level = 0, one condyle extends farther distally = 1 N48: 1->0
State at this node found in an ancestor, thus representing a reversal,
OR convergent with a state outside this clade
298. Tibia and fibula condyles differentiated from each other, including being joined by unfinished bone = 0, or not = 1 N51: 0->1
State at this node convergent with a state outside this clade
301. Tibia without = 0, or with = 1 flange along its posterior edge R121: 0->1
State at this node found in an ancestor, thus representing a reversal,
OR convergent with a state outside this clade
308. Relative lengths of hindlimb epipodials and femur: epipodials less than 50% of femur length = 0, about 50% femur length = 1, or >50% of femur length = 2 N52: 2->0
State at this node convergent with a state outside this clade

==========
Baphetes (branch number 41):
Total changes along branch: 8

Character: Change
22. Frontal anterior margin wedged between nasals: absent = 0, present = 1 C11: 0->1
State at this node convergent with a state outside this clade
33. Jugal excluded from lower jaw margin by maxilla and quadratojugal: yes = 0, or no = 1 C22: 0->1
State at this node convergent with a state outside this clade
102. Parasphenoid basal plate: square/rectangular = 0, or triangular/distinctly tapering at one end = 1 N9: 0->1
State at this node convergent with a state outside this clade
118. Pterygoids not visible in lateral aspect below ventral margin of jugal and quadratojugal = 0, or visible = 1 C86: 0->1
State at this node convergent with a state outside this clade
122. Vomers as broad as long or broader = 0, about twice as long as broad or longer = 1 C91: 0->1
State at this node convergent with a state outside this clade
142. Parasphenoid shagreen field: present = 0, absent = 1 ? C101: 0->1
State at this node found in an ancestor, thus representing a reversal,
OR convergent with a state outside this clade
145. Premaxillary tooth number: > 15 = 0, 10 - 14 = 1, < 10 = 2 ? C105: 2->1
State at this node found in an ancestor, thus representing a reversal
156. Marginal tooth shape: conical and straight/slightly recurved = 0, small and more or less straight and 'needle-like' = 1, right-trapezoid 'chisel' shape = 2, spearhead shape = 3, thin and greatly recurved = 4 N22: 0->3
Uniquely derived state, unchanged above
Two or more other states found outside this clade

==========

Megalocephalus (branch number 42):
Total changes along branch: 5

Character: Change
24. Intertemporal present: present = 0, absent = 1 C13: 0->1
State at this node found in an ancestor, thus representing a reversal
30. Jugal alary process ("insula jugalis") on palate: absent = 0, present = 1 C19: 0->1
State at this node convergent with a state outside this clade
35. Lacrimal contributes to narial margin: absent, excluded by anterior tectal = 0: present = 1, absent, excluded by nasal/maxillary or prefrontal/maxillary suture = 2 C24: 0->2
State at this node convergent with a state outside this clade
58. Postorbital at least one quarter of the width of the skull table at the same transverse level: absent = 0, present = 1 ? C49: 0->1
State at this node found in an ancestor, thus representing a reversal
123. Anterior palatal fenestra: present = 0, absent = 1 N11: 1->0
State at this node found in an ancestor, thus representing a reversal

==========
Loxomma (branch number 43):
Total changes along branch: 1

Character: Change
136. Maxilla tooth number: > 40 = 0, 30-40 = 1, < 30 = 2 ? C96: 1->2
State at this node found in an ancestor, thus representing a reversal,
OR convergent with a state outside this clade

==========
Brittagnathus (branch number 44):
Total changes along branch: 3

Character: Change
167. Coronoid: at least one has fang pair recognisable because at least twice the height of coronoid teeth: present = 0, absent = 1 C123: 1->0
State at this node found in an ancestor, thus representing a reversal
180. Mandibular oral sulcus/ surangular pit line: present = 0, absent = 1 ? C136: 1->0
State at this node found in an ancestor, thus representing a reversal
190. Adsymphysial plate dentition: shagreen, denticles or irregular tooth field = 0, organised dentition aligned parallel to jaw margin = 1, no dentition = 2 C142: 1->2
State at this node convergent with a state outside this clade

==========
Eucritta (branch number 45):
Total changes along branch: 13

Character: Change
10. Pineal foramen position along interparietal suture: behind midpoint = 0, at the midpoint = 1, anterior to midpoint = 2 C166: 0->1
State at this node found in an ancestor, thus representing a reversal
70. Squamosal-supratemporal suture position: at apex of temporal embayment = 0, dorsal to apex = 1, ventral to apex = 2 C61: 0/2->1
State at this node convergent with a state outside this clade

101. Basal plate of parasphenoid, measured posteriorly from basipterygoid processes/basal articulation: about as long as wide = 0, wider than long = 1, longer than wide = 2 N8: 1->2
State at this node convergent with a state outside this clade
107. Parasphenoid carotid grooves: curve round basipterygoid process = 0, lie posteromedial to basipterygoid process (or enter via foramina there) = 1, absent = 2 C81: 2->1
State at this node convergent with a state outside this clade
117. Pterygoid quadrate ramus margin in adductor fossa: concave = 0, with some convex component = 1 C85: 0->1
State at this node convergent with a state outside this clade
130. Median margin of pterygoid palatal ramus where separate: straight = 0, slightly concave medially = 1, convex medially = 2, greatly concave medially = 3 N17: 0->1
State at this node convergent with a state outside this clade
178. Mandibular sensory canal: present = 0, absent = 1 C134: 0->1
State at this node convergent with a state outside this clade
232. Interclavicle anterior edge fimbricated: absent = 0, present = 1 N24: 0->1
State at this node convergent with a state outside this clade
233. Interclavicle anterior tip: squared = 0, broadly rounded = 1, pointed = 2. N85: 2->1
State at this node convergent with a state outside this clade
236. Interclavicle parasternal process length: equal to rest of interclavicle = 0 or longer than rest of interclavicle = 1, shorter than rest of interclavicle = 2 N79: 0->1
State at this node convergent with a state outside this clade
282. Pubis ossified = 0, or unossified = 1 N72: 0->1
State at this node convergent with a state outside this clade
303. Tibia width at mid-length of bone less than = 0, comparable to = 1, or greater than = 2, width of fibula at mid- length of bone R123: 2->1
State at this node convergent with a state outside this clade
306. Fibula without = 0, or with = 1 oblique distal extremity R128: 1->0
State at this node found in an ancestor, thus representing a reversal

==========
Sigournea (branch number 46):
Total changes along branch: 4

Character: Change
14. Dermal ornament character: Pit-and-ridge with visible center of ossification = 0, pit-and-ridge with no obvious center of ossification = 1, irregular pit-and-ridge with no obvious center of ossification =2, short radiating grooves = 3, pitted = 4, ir:
State at this node found in an ancestor, thus representing a reversal
156. Marginal tooth shape: conical and straight/slightly recurved = 0, small and more or less straight and 'needle-like' = 1, right-trapezoid 'chisel' shape = 2, spearhead shape = 3, thin and greatly recurved = 4 N22: 0->1
State at this node found in an ancestor, thus representing a reversal
174. Dentary tooth number: more than 70 = 0, 56-70 = 1, 46-55 = 2, 36-45 = 3, less than 35 = 4 C130: 3/4->0
State at this node found in an ancestor, thus representing a reversal
176. Dentary ventral edge: smooth continuous line = 0, abruptly tapering or ?stepped? margin = 1 C133: 1->0
State at this node found in an ancestor, thus representing a reversal

==========
Pederpes (branch number 47):

Total changes along branch: 20

Character: Change
11. Suspensorium proportions: quadrate to anterior margin of temporal embayment about equal to maximum orbit width (discounting any anterior extensions) = 0, quadrate to anterior margin of temporal embayment < maximum orbit width = 1, quadrate to anterio:
State at this node found in an ancestor, thus representing a reversal
39. Maxilla highest point in posterior half = 0, anterior third of its length = 1, or at its midlength = 2, or same height all along length =3 C28: 1->0
State at this node found in an ancestor, thus representing a reversal,
OR convergent with a state outside this clade
55. Postorbital without distinct dorsomedial ramus for postfrontal = 0, with incipient ramus = 1, ?with elongate ramus = 2 C46: 0->1
State at this node convergent with a state outside this clade
64. Prefrontal contributes to half or more than half anteromesial orbit margin = 0, less than half = 1 C55: 0->1
State at this node found in an ancestor, thus representing a reversal,
OR convergent with a state outside this clade
100. Parasphenoid cultriform process shape: biconvex = 0, narrowly triangular =1, parallel-sided = 2, or with proximal constriction followed by swelling = 3 C76: 1->3
State at this node convergent with a state outside this clade
104. Parasphenoid posterolateral wings (ridged): absent = 0, present = 1 ? C78: 0->1
State at this node convergent with a state outside this clade
111. Basal tubera (='basal tuberosities', swellings, bumps, or eminences on underside of braincase/parasphenoid): present = 0, or absent = 1 N10: 1->0
State at this node convergent with a state outside this clade
123. Anterior palatal fenestra: present = 0, absent = 1 N11: 1->0
State at this node found in an ancestor, thus representing a reversal
135. Ectopterygoid / palatine shagreen field: absent = 0, present = 1 ? C95: 0->1
State at this node convergent with a state outside this clade
150. Vomerine shagreen field: absent = 0, present = 1 ? C110: 0->1
State at this node convergent with a state outside this clade
160. Angular reaches posteriormost point of lower jaw: absent = 0, present = 1 C116: 0->1
State at this node convergent with a state outside this clade
210. Neural arch ossification: paired in adult = 0, single in adult = 1 C198: 1->0
State at this node found in an ancestor, thus representing a reversal,
OR convergent with a state outside this clade
248. Angle between proximal and distal ends of humerus: 30 degrees or less = 0, 31-60 degrees = 1, more than 60 degrees = 2 N84: 0->1
State at this node convergent with a state outside this clade
259. Humerus entepicondyle width relative to humeral head width: smaller = 0, greater = 1 C195: 1->0
State at this node found in an ancestor, thus representing a reversal,
OR convergent with a state outside this clade
267. Radius: longer than ulna = 0, same length as ulna = 1, shorter than ulna (including olecranon process if present) = 2 C202: 2->1
State at this node convergent with a state outside this clade
270. Ossified olecranon process: absent = 0, present = 1 R83: 1->0
State at this node found in an ancestor, thus representing a reversal
282. Pubis ossified = 0, or unossified = 1 N72: 0->1
State at this node convergent with a state outside this clade

292. Adductor crest length: shorter than adductor blade = 0, similar length to adductor blade = 1, longer than adductor blade = 2 N46: 2->1
State at this node convergent with a state outside this clade
298. Tibia and fibula condyles differentiated from each other, including being joined by unfinished bone = 0, or not = 1 N51: 0->1
State at this node convergent with a state outside this clade
307. Posterior (lateral) surface of fibula concave = 0, straight = 1, convex = 2, in its proximal half R132: 1->0
State at this node found in an ancestor, thus representing a reversal

==========
Whatcheeria (branch number 48):
Total changes along branch: 32

Character: Change
12. Otic notch/temporal ebayment approaching orbit: more than 1/2 postorbital skull length = 0, 1/4-1/2 postorbital skull length = 1, less than 1/4 postorbital skull length = 2 P35: 0->1
State at this node found in an ancestor, thus representing a reversal
13. Skull table shape: longer than broad = 0, approximately square = 1, shorter than broad = 2 C169: 2->0
State at this node found in an ancestor, thus representing a reversal
14. Dermal ornament character: Pit-and-ridge with visible center of ossification = 0, pit-and-ridge with no obvious center of ossification = 1, irregular pit-and-ridge with no obvious center of ossification =2, short radiating grooves = 3, pitted = 4, ir:
State at this node convergent with a state outside this clade
31. Jugal length of postorbital region relative to one-third of the length of the postorbital cheek region: greater = 0 or less =1 0 C20: 0->1
State at this node found in an ancestor, thus representing a reversal,
OR convergent with a state outside this clade
32. Jugal extends anterior to anterior orbit margin: absent = 0, present = 1 C21: 0->1
State at this node found in an ancestor, thus representing a reversal,
OR convergent with a state outside this clade
33. Jugal excluded from lower jaw margin by maxilla and quadratojugal: yes = 0, or no = 1 C22: 0->1
State at this node convergent with a state outside this clade
36. Lacrimal reaches orbit margin (= prefrontal/ jugal suture): present = 0, absent = 1 C25: 0->1
State at this node convergent with a state outside this clade
68. Squamosal posterodorsal margin shape: convex = 0, sigmoid or approximately straight = 1, entirely concave = 2 C59: 1->2
State at this node convergent with a state outside this clade
109. Anterior extent of cultriform process along palate: ends nearer choana posterior margin = 0, or ends nearer orbit posterior margin = 1 P201: 0->1
State at this node found in an ancestor, thus representing a reversal,
OR convergent with a state outside this clade
112. Buccohypophyseal foramen in parasphenoid: open = 0, absent = 1. P208: 1->0
State at this node found in an ancestor, thus representing a reversal
113. Ectopterygoid as long or longer than palatines: present = 0, absent = 1 ? C71: 0->1
State at this node convergent with a state outside this clade
115. Ectopterygoid/ palatine exposure: more or less confined to tooth row = 0, broad mesial exposure (additional to tooth row if present) = 1 C73: 1->0
State at this node found in an ancestor, thus representing a reversal

121. Vomers separated by pterygoids: for > half length = 0, < half length = 1, not separated by pterygoids = 2 C89: 1->0

State at this node convergent with a state outside this clade

128. Median meeting of ptergyoids (measured anteriorly from basal articulation): approximately 1/3 or less of pterygoid length = 0, about 1/2 of pteryoid length = 1, approximately 2/3-3/4 of pterygoid length = 2, almost all or all of pterygoid length = 3:

State at this node convergent with a state outside this clade

147. Vomerine fang pairs noticeably smaller than other palatal fang pairs: absent = 0, present = 1 C107: 0->1

State at this node convergent with a state outside this clade

148. Vomer anterior wall forming posterior margin of palatal fossa bears tooth row meeting in midline: present = 0, absent = 1 C108: 1->0

State at this node found in an ancestor, thus representing a reversal

151. Vomerine denticle row lateral to tooth row: present = 0, absent = 1 C111: 1->0

State at this node found in an ancestor, thus representing a reversal,
OR convergent with a state outside this clade

179. Mandibular canal exposure: entirely enclosed apart from pores = 0, mostly enclosed = 1, mostly or entirely open = 2 C135: 2->1

State at this node found in an ancestor, thus representing a reversal,
OR convergent with a state outside this clade

206. Centra (trunk) pleurocentra fused middorsally: absent = 0, present = 1 C174: 0->1

State at this node convergent with a state outside this clade

207. Centra (trunk) intercentra fused middorsally: absent = 0, present = 1 N81: 0->1

State at this node convergent with a state outside this clade

214. Presacral (trunk) ribs: length of longest ribs: short = 0, long = 1 P140: 0->1

State at this node convergent with a state outside this clade

215. Ribs (trunk): straight or weakly curved = 0, strongly ventrally curved = 1 C203: 0->1

State at this node convergent with a state outside this clade

226. Clavicles meet anteriorly: present = 0, absent = 1 C176: 1->0

State at this node found in an ancestor, thus representing a reversal,
OR convergent with a state outside this clade

233. Interclavicle anterior tip: squared = 0, broadly rounded = 1, pointed = 2. N85: 2->1

State at this node convergent with a state outside this clade

235. Interclavicle body shape (excluding parasternal process of present): small scute = 0, triangle longest anteriorly = 1, triangle longest laterally = 2, spatulate or fan-shaped = 3, equilateral triangle = 4 N78: 2->3

State at this node found in an ancestor, thus representing a reversal,
OR convergent with a state outside this clade

239. Shape of ventral clavicle plate: elongate triangle = 0, sub-equilateral triangle = 1, spoon-shaped/spatulate/ovoid = 2 N30: 0->2

State at this node found in an ancestor, thus representing a reversal,
OR convergent with a state outside this clade

260. Entepicondyle foramen: present subcircular or round elliptical = 0, present slit-like or elongate elliptical = 1, absent = 2 R42: 0->1

State at this node convergent with a state outside this clade

265. Length of posterior margin of entepicondyle smaller than = 0, subequal to = 1, or larger than = 2, humerus anteroposterior length at the level of proximal insertion of entepicondyle onto humerus shaft R66: 0->2

State at this node found in an ancestor, thus representing a reversal,
OR convergent with a state outside this clade

303. Tibia width at mid-length of bone less than = 0, comparable to = 1, or greater than = 2, width of fibula at mid- length of bone R123: 2->1
State at this node convergent with a state outside this clade
317. Phalanges shape (pedal, non-terminal): longer than wide = 0, about as wide as long = 1, wider than long = 2 N62: 0->1/2
Derived state unclear
Character is uniform outside this clade
319. Phalanges cross-section shape (pedal): dumbell-shaped, thin medially and thicker laterally = 0, square-shaped or elongate oval-shaped = 1, convex upwards = 2, circular = 3 N64: 1->0
State at this node convergent with a state outside this clade
326. Scale distribution: gastralia present = 0, gastralia and dorsal scales/osteoderms/other dermal ossifications present = 1, no scales = 2 N71: 0->2
State at this node convergent with a state outside this clade

==========
Occidens (branch number 49):
Total changes along branch: 2

Character: Change
156. Marginal tooth shape: conical and straight/slightly recurved = 0, small and more or less straight and 'needle-like' = 1, right-trapezoid 'chisel' shape = 2, spearhead shape = 3, thin and greatly recurved = 4 N22: 0->1
State at this node found in an ancestor, thus representing a reversal
185. Meckelian bone or space exposure in middle part of jaw, depth much less than prearticular = 0, depth similar to prearticular or greater = 1 C138: 0->1
State at this node convergent with a state outside this clade

==========
Ymeria (branch number 50):
Total changes along branch: 3

Character: Change
114. Ectopterygoid reaches subtemporal fossa: absent = 0, present = 1 C72: 1->0
State at this node convergent with a state outside this clade
172. Coronoid: size of teeth (excluding fangs) on anterior and middle coronoids relative to dentary tooth size: about the same = 0, half height or less = 1 C128: 1->0
State at this node found in an ancestor, thus representing a reversal
187. Ventral border of Meckelian fenestra/large posterior Meckelian opening: formed by postsplenial mostly = 0, or angular mostly = 1 P95: 0->1
State at this node found in an ancestor, thus representing a reversal,
OR convergent with a state outside this clade

==========
Ossinodus (branch number 51):
Total changes along branch: 15

Character: Change
9. Orbit position re snout /quadrate length: centre closer to front than rear = 0, centre near middle = 1, centre closer to rear than front = 2 C165: 1->0
State at this node found in an ancestor, thus representing a reversal

12. Otic notch/temporal ebayment approaching orbit: more than 1/2 postorbital skull length = 0, 1/4-1/2 postorbital skull length = 1, less than 1/4 postorbital skull length = 2 P35: 0->1
State at this node found in an ancestor, thus representing a reversal
30. Jugal alary process ("insula jugalis") on palate: absent = 0, present = 1 C19: 0->1
State at this node convergent with a state outside this clade
48. Parietal ? postorbital suture: absent = 0, present = 1 C39: 0->1
State at this node found in an ancestor, thus representing a reversal
53. Postfrontal ? prefrontal suture: anterior half of orbit = 0, middle or posterior half of ?orbit = 1, absent = 2 C44: 0->1
State at this node convergent with a state outside this clade
58. Postorbital at least one quarter of the width of the skull table at the same transverse level: absent = 0, present = 1 ? C49: 0->1
State at this node found in an ancestor, thus representing a reversal
87. Parietals: more than 2.5 times as long as wide = 0 or less than 2.5 times as long as wide = 1 C224: 1->0
State at this node found in an ancestor, thus representing a reversal
115. Ectopterygoid/ palatine exposure: more or less confined to tooth row = 0, broad mesial exposure (additional to tooth row if present) = 1 C73: 1->0
State at this node found in an ancestor, thus representing a reversal
128. Median meeting of ptergyoids (measured anteriorly from basal articulation): approximately 1/3 or less of pterygoid length = 0, about 1/2 of pteryoid length = 1, approximately 2/3-3/4 of pterygoid length = 2, almost all or all of pterygoid length = 3:
State at this node convergent with a state outside this clade
146. Vomer fang pairs: present = 0, absent = 1 ? C106: 0->1
State at this node convergent with a state outside this clade
148. Vomer anterior wall forming posterior margin of palatal fossa bears tooth row meeting in midline: present = 0, absent = 1 C108: 1->0
State at this node found in an ancestor, thus representing a reversal
151. Vomerine denticle row lateral to tooth row: present = 0, absent = 1 C111: 1->0
State at this node found in an ancestor, thus representing a reversal,
OR convergent with a state outside this clade
182. Number of Meckelian openings: more than three = 0, three = 1, two = 2, one = 3 N73: 0->2
State at this node convergent with a state outside this clade
239. Shape of ventral clavicle plate: elongate triangle = 0, sub-equilateral triangle = 1, spoon-shaped/spatulate/ovoid = 2 N30: 0->1
State at this node found in an ancestor, thus representing a reversal,
OR convergent with a state outside this clade
260. Entepicondyle foramen: present subcircular or round elliptical = 0, present slit-like or elongate elliptical = 1, absent = 2 R42: 0->1
State at this node convergent with a state outside this clade

==========
Koilops (branch number 52):
Total changes along branch: 4

Character: Change
2. Preorbital region of skull less than twice as wide as long = 0, or at least twice as wide as long = 1 C155: 0->1
State at this node convergent with a state outside this clade
31. Jugal length of postorbital region relative to one-third of the length of the postorbital cheek region: greater = 0 or less =1 0 C20: 0->1

State at this node found in an ancestor, thus representing a reversal,
OR convergent with a state outside this clade
41. Maxilla sutures to prefrontal: absent = 0, present = 1 C30: 0->1
State at this node convergent with a state outside this clade
104. Parasphenoid posterolateral wings (ridged): absent = 0, present = 1 ? C78: 0->1
State at this node convergent with a state outside this clade

==========
Tulerpeton (branch number 53):
Total changes along branch: 11

Character: Change
150. Vomerine shagreen field: absent = 0, present = 1 ? C110: 0->1
State at this node convergent with a state outside this clade
203. Trunk pleurocentrum height relative to intercentrum height: pleurocentrum less than intercentrum = 0, same as intercentrum = 1, greater than intercentrum = 2,, intercentrum and pleurocentrum fused into single bone (holospondylous) = 3 N80: 0->1
State at this node convergent with a state outside this clade
226. Clavicles meet anteriorly: present = 0, absent = 1 C176: 1->0
State at this node found in an ancestor, thus representing a reversal,
OR convergent with a state outside this clade
248. Angle between proximal and distal ends of humerus: 30 degrees or less = 0, 31-60 degrees = 1, more than 60 degrees = 2 N84: 0->1
State at this node convergent with a state outside this clade
252. Humerus latissimus dorsi process position relative to ectepicondyle: offset anteriorly = 0, in line = 1 C185: 0->1
State at this node convergent with a state outside this clade
266. Deltopectoral crest present = 0, separate deltoid and pectoral processes = 1, only pectoral process = 2, none of these = 3 N35: 0->1
State at this node convergent with a state outside this clade
279. Dorsal and posterodorsal iliac processes overlapping in lateral view = 0, or separated by distinct space = 1 R96: 0->1
State at this node convergent with a state outside this clade
304. Tibia proximal extremity wider = 0, as wide as = 1, or narrow than = 2 its distal extremity R126: 1->0
State at this node found in an ancestor, thus representing a reversal
308. Relative lengths of hindlimb epipodials and femur: epipodials less than 50% of femur length = 0, about 50% femur length = 1, or >50% of femur length = 2 N52: 2->1
State at this node convergent with a state outside this clade
326. Scale distribution: gastralia present = 0, gastralia and dorsal scales/osteoderms/other dermal ossifications present = 1, no scales = 2 N71: 0->1
State at this node convergent with a state outside this clade
327. Gastralia: tapered and elongate, four times longer than broad or longer = 0, ovoid = 1, around three times longer than broad one end tapering = 2 C211: 0->1
State at this node convergent with a state outside this clade

==========
Ichthyostega (branch number 54):
Total changes along branch: 29

Character: Change

4. Interorbital distance compared with maximum orbit diameter: greater = 0, smaller = 1, subequal = 2 C158: 2->0

State at this node found in an ancestor, thus representing a reversal,
OR convergent with a state outside this clade

11. Suspensorium proportions: quadrate to anterior margin of temporal embayment about equal to maximum orbit width (discounting any anterior extensions) = 0, quadrate to anterior margin of temporal embayment < maximum orbit width = 1, quadrate to anterio:

State at this node convergent with a state outside this clade

12. Otic notch/temporal ebayment approaching orbit: more than 1/2 postorbital skull length = 0, 1/4-1/2 postorbital skull length = 1, less than 1/4 postorbital skull length = 2 P35: 0->2

State at this node convergent with a state outside this clade

14. Dermal ornament character: Pit-and-ridge with visible center of ossification = 0, pit-and-ridge with no obvious center of ossification = 1, irregular pit-and-ridge with no obvious center of ossification =2, short radiating grooves = 3, pitted = 4, ir:

State at this node convergent with a state outside this clade

37. Maxilla sutures to vomer: absent = 0, present = 1 C26: 0->1

State at this node convergent with a state outside this clade

49. Parietal anterior portion extent relative to orbit midlength: in front of = 0, level with ?= 1, posterior to = 2 C40: 1->0

State at this node found in an ancestor, thus representing a reversal

68. Squamosal posterodorsal margin shape: convex = 0, sigmoid or approximately straight = 1, entirely concave = 2 C59: 1->0

State at this node found in an ancestor, thus representing a reversal,
OR convergent with a state outside this clade

69. Squamosal contact with tabular: smooth = 0, interdigitating = 1, absent = 2 C60: 2->1

State at this node convergent with a state outside this clade

77. Tabular shape in dorsal view (aside from horn, if present): rectangle or square = 0, irregular rectangular/quadrangle = 1, elongate oval or teardrop = 2, triangular = 3 N1: 2->1

State at this node found in an ancestor, thus representing a reversal

82. (Infraorbital) lateral line relationship to naris: continuous ventral to naris within lateral rostral = 0, discontinuous across ventral naris = 1, discontinuous ventral to naris across maxilla to premaxilla = 2, continuous ventral to naris in maxilla:

State at this node found in an ancestor, thus representing a reversal

86. Postparietals: paired = 0 or fused = 1 N6: 0->1

State at this node convergent with a state outside this clade

112. Buccohypophyseal foramen in parasphenoid: open = 0, absent = 1. P208: 1->0

State at this node found in an ancestor, thus representing a reversal

113. Ectopterygoid as long or longer than palatines: present = 0, absent = 1 ? C71: 0->1

State at this node convergent with a state outside this clade

130. Median margin of pterygoid palatal ramus where separate: straight = 0, slightly concave medially = 1, convex medially = 2, greatly concave medially = 3 N17: 0->1

State at this node convergent with a state outside this clade

139. Palatine fang pairs: present = 0, absent = 1 ? C98: 0->1

State at this node convergent with a state outside this clade

144. Pterygoid shagreen: dense = 0, a few discontinuous patches or absent = 1 C103: 0->1

State at this node convergent with a state outside this clade

146. Vomer fang pairs: present = 0, absent = 1 ? C106: 0->1

State at this node convergent with a state outside this clade

196. Prearticular shagreen field, distribution: gradually decreasing from dorsal to ventral = 0, well defined dorsal longitudinal band = 1, scattered patches or absent = 2 C148: 1->2

State at this node found in an ancestor, thus representing a reversal,

OR convergent with a state outside this clade
214. Presacral (trunk) ribs: length of longest ribs: short = 0, long = 1 P140: 0->1
State at this node convergent with a state outside this clade
216. Trunk ribs overlapping: absent = 0, or present = 1 N25: 0->1
State at this node convergent with a state outside this clade
220. Ribs (trunk) differ strongly in length and morphology along ?thoracic? region: absent = 0, present = 1 C207: 0->1
State at this node convergent with a state outside this clade
233. Interclavicle anterior tip: squared = 0, broadly rounded = 1, pointed = 2. N85: 2->1
State at this node convergent with a state outside this clade
236. Interclavicle parasternal process length: equal to rest of interclavicle = 0 or longer than rest of interclavicle = 1, shorter than rest of interclavicle = 2 N79: 0->1
State at this node convergent with a state outside this clade
239. Shape of ventral clavicle plate: elongate triangle = 0, sub-equilateral triangle = 1, spoon-shaped/spatulate/ovoid = 2 N30: 0->2
State at this node found in an ancestor, thus representing a reversal,
OR convergent with a state outside this clade
254. Humerus radial facet position: distal and terminal = 0, anteroventral = 1, ventral = 2 C188: 0->1
State at this node convergent with a state outside this clade
259. Humerus entepicondyle width relative to humeral head width: smaller = 0, greater = 1 C195: 1->0
State at this node found in an ancestor, thus representing a reversal,
OR convergent with a state outside this clade
277. Dorsal iliac process oblique and flared = 0, fan-shaped = 1, subrectangular and truncated = 2, blunt and digitiform = 3, low elongate = 4 R93: 0->2
State at this node convergent with a state outside this clade
294. Femur intercondylar groove: absent = 0, present and not longer than distal end of femur = 1, present and longer than distal end of femur = 2 R116: 2->1
State at this node convergent with a state outside this clade
315. Relative length of foot and rear epopodials: foot equal to or less than length of epipodials = 0, foot longer than epipodials = 1 N60: 1->0
State at this node convergent with a state outside this clade

==========
Ventastega (branch number 55):
Total changes along branch: 14

Character: Change
11. Suspensorium proportions: quadrate to anterior margin of temporal embayment about equal to maximum orbit width (discounting any anterior extensions) = 0, quadrate to anterior margin of temporal embayment < maximum orbit width = 1, quadrate to anterio:
State at this node found in an ancestor, thus representing a reversal
13. Skull table shape: longer than broad = 0, approximately square = 1, shorter than broad = 2 C169: 1->0
State at this node found in an ancestor, thus representing a reversal
24. Intertemporal present: present = 0, absent = 1 C13: 1->0
State at this node found in an ancestor, thus representing a reversal,
OR convergent with a state outside this clade
30. Jugal alary process ("insula jugalis") on palate: absent = 0, present = 1 C19: 0->1
State at this node convergent with a state outside this clade
36. Lacrimal reaches orbit margin (= prefrontal/ jugal suture): present = 0, absent = 1 C25: 0->1
State at this node convergent with a state outside this clade

64. Prefrontal contributes to half or more than half anteromesial orbit margin = 0, less than half = 1 C55: 0->1
State at this node found in an ancestor, thus representing a reversal,
OR convergent with a state outside this clade
100. Parasphenoid cultriform process shape: biconvex = 0, narrowly triangular =1, parallel-sided = 2, or with proximal constriction followed by swelling = 3 C76: 1->2
State at this node convergent with a state outside this clade
107. Parasphenoid carotid grooves: curve round basipterygoid process = 0, lie posteromedial to basipterygoid process (or enter via foramina there) = 1, absent = 2 C81: 2->0
State at this node convergent with a state outside this clade
168. Coronoid: at least one has fangs recognisable because noticeably mesial to vertical lamina of bone and to all other teeth: present = 0, absent = 1 C124: 1->0
State at this node found in an ancestor, thus representing a reversal
187. Ventral border of Meckelian fenestra/large posterior Meckelian opening: formed by postsplenial mostly = 0, or angular mostly = 1 P95: 0->1
State at this node found in an ancestor, thus representing a reversal,
OR convergent with a state outside this clade
189. Adsymphysial plate fang-pair (distinct from other teeth): absent = 0, present = 1 C141: 1->0
State at this node found in an ancestor, thus representing a reversal
191. Adsymphysial lateral foramen present: absent = 0, present = 1 C143: 0->1
Uniquely derived state, unchanged above
Character is uniform outside this clade
226. Clavicles meet anteriorly: present = 0, absent = 1 C176: 1->0
State at this node found in an ancestor, thus representing a reversal,
OR convergent with a state outside this clade
279. Dorsal and posterodorsal iliac processes overlapping in lateral view = 0, or separated by distinct space = 1 R96: 0->1
State at this node convergent with a state outside this clade

==========
Acanthostega (branch number 56):
Total changes along branch: 13

Character: Change
8. Orbit position re snout/postparietal length: centre closer to front than rear = 0, centre near middle = 1, centre closer to rear than front = 2 C164: 2->0
State at this node found in an ancestor, thus representing a reversal
34. Jugal V-shaped indentation of posterodorsal margin: absent = 0, present = 1 C23: 0->1
State at this node convergent with a state outside this clade
68. Squamosal posterodorsal margin shape: convex = 0, sigmoid or approximately straight = 1, entirely concave = 2 C59: 1->0
State at this node found in an ancestor, thus representing a reversal,
OR convergent with a state outside this clade
69. Squamosal contact with tabular: smooth = 0, interdigitating = 1, absent = 2 C60: 2->0
State at this node convergent with a state outside this clade
80. Tabular prolonged posterolateral ornamented surface absent = 0, present = 1 C68: 0->1
State at this node convergent with a state outside this clade
100. Parasphenoid cultriform process shape: biconvex = 0, narrowly triangular =1, parallel-sided = 2, or with proximal constriction followed by swelling = 3 C76: 1->0
Uniquely derived state, unchanged above
Two or more other states found outside this clade

124. Anterior palatal fenestra: paired (0); unpaired (1) N12: 1->0
State at this node convergent with a state outside this clade
167. Coronoid: at least one has fang pair recognisable because at least twice the height of coronoid teeth: present = 0, absent = 1 C123: 0->1
State at this node convergent with a state outside this clade
174. Dentary tooth number: more than 70 = 0, 56-70 = 1, 46-55 = 2, 36-45 = 3, less than 35 = 4 C130: 0->1
State at this node convergent with a state outside this clade
179. Mandibular canal exposure: entirely enclosed apart from pores = 0, mostly enclosed = 1, mostly or entirely open = 2 C135: 0->1
State at this node convergent with a state outside this clade
217. Ribs (trunk) tapered distally =0, parallel-sided = 1, flared at distal tip= 2 C205: 0->1/2
Derived state unclear
State at this node convergent with a state outside this clade
260. Entepicondyle foramen: present subcircular or round elliptical = 0, present slit-like or elongate elliptical = 1, absent = 2 R42: 0->1
State at this node convergent with a state outside this clade
308. Relative lengths of hindlimb epipodials and femur: epipodials less than 50% of femur length = 0, about 50% femur length = 1, or >50% of femur length = 2 N52: 2->0
State at this node convergent with a state outside this clade

==========
Parmastega (branch number 57):
Total changes along branch: 20

Character: Change
4. Interorbital distance compared with maximum orbit diameter: greater = 0, smaller = 1, subequal = 2 C158: 2->1
State at this node convergent with a state outside this clade
9. Orbit position re snout /quadrate length: centre closer to front than rear = 0, centre near middle = 1, centre closer to rear than front = 2 C165: 1->2
State at this node convergent with a state outside this clade
13. Skull table shape: longer than broad = 0, approximately square = 1, shorter than broad = 2 C169: 1->2
State at this node convergent with a state outside this clade
17. Jaw articulation position: posterior to occiput = 0, level with occiput = 1, anterior to occiput = 2 C222: 0->1
State at this node convergent with a state outside this clade
22. Frontal anterior margin wedged between nasals: absent = 0, present = 1 C11: 0->1
State at this node convergent with a state outside this clade
36. Lacrimal reaches orbit margin (= prefrontal/ jugal suture): present = 0, absent = 1 C25: 0->1
State at this node convergent with a state outside this clade
45. Nasal ? parietal length ratio less than 1.45 = 0 or greater than 1.45 = 1 C34: 0->1
State at this node convergent with a state outside this clade
53. Postfrontal ? prefrontal suture: anterior half of orbit = 0, middle or posterior half of ?orbit = 1, absent = 2 C44: 0->1
State at this node convergent with a state outside this clade
55. Postorbital without distinct dorsomedial ramus for postfrontal = 0, with incipient ramus = 1, ?with elongate ramus = 2 C46: 0->1
State at this node convergent with a state outside this clade

83. Maximum parietal-parietal width is shorter than distance between posterior skull table margin (discounting tabular horn if present) and posterior orbit margin as projected along skull midline: present = 0, absent = 1 C231: 0->1
State at this node convergent with a state outside this clade
99. Basicranial fissure (=ventral cranial fissure): present = 0, absent = 1. P210: 0->1
State at this node convergent with a state outside this clade
110. Posterior extent of parasphenoid beneath braincase: floors sphenoid region only (0); floors sphenoid and otic regions = 1; floors sphenoid, otic, and occipital regions = 2 P205: 0->1
State at this node convergent with a state outside this clade
122. Vomers as broad as long or broader = 0, about twice as long as broad or longer = 1 C91: 0->1
State at this node convergent with a state outside this clade
137. Maxillary caniniform teeth (about twice the size of neighbouring teeth): absent = 0, present = 1 C97: 0->1
State at this node convergent with a state outside this clade
145. Premaxillary tooth number: > 15 = 0, 10 - 14 = 1, < 10 = 2 ? C105: 1->2
State at this node convergent with a state outside this clade
152. Vomer with toothed anterolateral crest: present = 0, absent = 1 ? C112: 0->1
State at this node convergent with a state outside this clade
173. Dentary with parasymphysial fangs internal to marginal tooth row: present = 0, absent = 1 C129: 0->1
State at this node convergent with a state outside this clade
179. Mandibular canal exposure: entirely enclosed apart from pores = 0, mostly enclosed = 1, mostly or entirely open = 2 C135: 0->2
State at this node convergent with a state outside this clade
197. Prearticular sutures with surangular (check rear of jaw): absent = 0, present = 1 C149: 0->1
State at this node convergent with a state outside this clade
237. Postbranchial lamina on cleithrum present = 0, or absent = 1 R1: 0->1
State at this node convergent with a state outside this clade

==========
Tiktaalik (branch number 58):
Total changes along branch: 9

Character: Change
10. Pineal foramen position along interparietal suture: behind midpoint = 0, at the midpoint = 1, anterior to midpoint = 2 C166: 1->0
State at this node convergent with a state outside this clade
14. Dermal ornament character: Pit-and-ridge with visible center of ossification = 0, pit-and-ridge with no obvious center of ossification = 1, irregular pit-and-ridge with no obvious center of ossification =2, short radiating grooves = 3, pitted = 4, ir:
State at this node convergent with a state outside this clade
62. Prefrontal less than three times longer than wide: present = 0, more than, = 1 ? C53: 0->1
State at this node found in an ancestor, thus representing a reversal,
OR convergent with a state outside this clade
71. Squamosal anterior part lying behind mid-parietal length: present = 0, absent = 1 C62: 0->1
State at this node convergent with a state outside this clade
111. Basal tubera (='basal tuberosities', swellings, bumps, or eminences on underside of braincase/parasphenoid): present = 0, or absent = 1 N10: 1->0
State at this node convergent with a state outside this clade
124. Anterior palatal fenestra: paired (0); unpaired (1) N12: 1->0
State at this node convergent with a state outside this clade

176. Dentary ventral edge: smooth continuous line = 0, abruptly tapering or ?stepped? margin = 1 C133: 0->1
State at this node found in an ancestor, thus representing a reversal,
OR convergent with a state outside this clade
216. Trunk ribs overlapping: absent = 0, or present = 1 N25: 0->1
State at this node convergent with a state outside this clade
258. Humerus ectepicondylar ridge distal end aligned with ulnar condyle = 0, between radial and ulnar condyles = 1, aligned with radial condyle = 2 C193: 0->1
State at this node convergent with a state outside this clade

==========
Panderichthys (branch number 59):
Total changes along branch: 8

Character: Change
54. Postorbital suture to skull table (usually intertemporal or supratemporal when present) interdigitating vs smooth: smooth = 0, interdigitating = 1 C45: 0->1
State at this node convergent with a state outside this clade
100. Parasphenoid cultriform process shape: biconvex = 0, narrowly triangular =1, parallel-sided = 2, or with proximal constriction followed by swelling = 3 C76: 1->2
State at this node convergent with a state outside this clade
182. Number of Meckelian openings: more than three = 0, three = 1, two = 2, one = 3 N73: 3->2
State at this node convergent with a state outside this clade
184. Meckelian opening(s) without ventromesial bony margin = 0, or with ventromesial bony margin = 1 N75: 0->1
State at this node convergent with a state outside this clade
193. Postsplenial with mesial lamina: absent = 0, present = 1 C145: 0->1
State at this node convergent with a state outside this clade
230. Scapulocoracoid dorsal blade: absent = 0, present = 1 $C209: 0->1
State at this node convergent with a state outside this clade
268. Radius longer than = 0, as long as = 1, or shorter than = 2, humerus. R78: 0->1
State at this node convergent with a state outside this clade
307. Posterior (lateral) surface of fibula concave = 0, straight = 1, convex = 2, in its proximal half R132: 0->2
Uniquely derived state, unchanged above
Two or more other states found outside this clade

==========
Elpistostege (branch number 60): Not Available

==========
Eusthenopteron (branch number 61): Not Available

==========
below Adelospondylus - Eusthenopteron (branch number 62):
Total changes along branch:

no unambiguous changes

==========
below Adelospondylus - Panderichthys (branch number 63): Not Available

==========
below Adelospondylus - Tiktaalik (branch number 64):
Total changes along branch: 10

Character: Change
8. Orbit position re snout/postparietal length: centre closer to front than rear = 0, centre near middle = 1, centre closer to rear than front = 2 C164: 0->2
Reversed above to a state found in an ancestor
9. Orbit position re snout /quadrate length: centre closer to front than rear = 0, centre near middle = 1, centre closer to rear than front = 2 C165: 0->1
Reversed above to a state found in an ancestor
12. Otic notch/temporal ebayment approaching orbit: more than 1/2 postorbital skull length = 0, 1/4-1/2 postorbital skull length = 1, less than 1/4 postorbital skull length = 2 P35: 1->0
Reversed above to a state found in an ancestor
13. Skull table shape: longer than broad = 0, approximately square = 1, shorter than broad = 2 C169: 0->1
Reversed above to a state found in an ancestor
16. Operculum (=opercular) present = 0, or absent = 1 C245: 0->1
Uniquely derived state, unchanged above
Character is uniform outside this clade
77. Tabular shape in dorsal view (aside from horn, if present): rectangle or square = 0, irregular rectangular/quadrangle = 1, elongate oval or teardrop = 2, triangular = 3 N1: 1->3
Reversed above to a state found in an ancestor
161. Coronoid (anterior) contacts splenial (or presplenial if present): absent = 0, present = 1 C117: 0->1
Reversed above to a state found in an ancestor
168. Coronoid: at least one has fangs recognisable because noticeably mesial to vertical lamina of bone and to all other teeth: present = 0, absent = 1 C124: 0->1
Reversed above to a state found in an ancestor
175. Dentary with a row of very small teeth or denticles lateral to tooth row: present = 0, absent = 1 C131: 0->1
Uniquely derived state, unchanged above
Character is uniform outside this clade
255. Humerus radial/ulnar facets: confluent = 0, separated by perichondral strip of bone = 1 C189: 0->1
Reversed above to a state found in an ancestor

==========
below Adelospondylus - Parmastega (branch number 65):
Total changes along branch: 10

Character: Change
11. Suspensorium proportions: quadrate to anterior margin of temporal embayment about equal to maximum orbit width (discounting any anterior extensions) = 0, quadrate to anterior margin of temporal embayment < maximum orbit width = 1, quadrate to anterio:
Reversed above to a state found in an ancestor
43. Median rostral (=internasal): mosaic = 0, paired = 1, single = 2, absent = 3 C32: 0->1
Uniquely derived state, but changed above to a state not found outside this clade
48. Parietal ? postorbital suture: absent = 0, present = 1 C39: 0->1
Reversed above to a state found in an ancestor
57. Postorbital longer than anteroposterior width of orbit: absent = 0, present = 1 C48: 1->0
Reversed above to a state found in an ancestor

State at this node found in an ancestor, thus representing a reversal,
OR convergent with a state outside this clade
112. Buccohypophyseal foramen in parasphenoid: open = 0, absent = 1. P208: 0->1
Reversed above to a state found in an ancestor
156. Marginal tooth shape: conical and straight/slightly recurved = 0, small and more or less straight and 'needle-like' = 1, right-trapezoid 'chisel' shape = 2, spearhead shape = 3, thin and greatly recurved = 4 N22: 1->0
Reversed above to a state found in an ancestor
State at this node found in an ancestor, thus representing a reversal,
OR convergent with a state outside this clade
181. Meckelian bone visible between prearticular and infradentary series: present = 0, absent = 1 C137: 0->1
Reversed above to a state found in an ancestor
186. Meckelian foramina/ fenestrae, dorsal margins formed by; mostly meckelian bone = 0, mostly prearticular = 1, mostly infradentary (postsplenial) = 2 C139: 0->1
Reversed above to a state found in an ancestor
227. Cleithrum co-ossified with scapulocoracoid = 0, separate = 1 C177: 1->0
Reversed above to a state found in an ancestor
240. Clavicles without = 0, or with = 1 a distinct ascending process. R16: 0->1
State at this node found in an ancestor, thus representing a reversal,
OR convergent with a state outside this clade

==========
below Adelospondylus - Acanthostega (branch number 66):
Total changes along branch: 10

Character: Change
23. Frontal/ nasal length ratio: frontals approximately equal to or less than one-third as long as nasals = 0, more than one-third as long = 1 C12: 1->0
Reversed above to a state found in an ancestor
State at this node found in an ancestor, thus representing a reversal,
OR convergent with a state outside this clade
77. Tabular shape in dorsal view (aside from horn, if present): rectangle or square = 0, irregular rectangular/quadrangle = 1, elongate oval or teardrop = 2, triangular = 3 N1: 3->2
Reversed above to a state found in an ancestor
106. Parasphenoid contacts or sutures to vomers: present = 0, absent = 1 ? C80: 0->1
Reversed above to a state found in an ancestor
115. Ectopterygoid/ palatine exposure: more or less confined to tooth row = 0, broad mesial exposure (additional to tooth row if present) = 1 C73: 0->1
Reversed above to a state found in an ancestor
120. Vomers separated by parasphenoid > half vomer mesial length: present = 0, absent = 1 C88: 0->1
Reversed above to a state found in an ancestor
121. Vomers separated by pterygoids: for > half length = 0, < half length = 1, not separated by pterygoids = 2 C89: 2->1
Reversed above to a state found in an ancestor
127. Pterygoids meet along midline: yes = 0, or no = 1 N15: 1->0
Reversed above to a state found in an ancestor
132. Ectopterygoid fang pairs: present = 0, absent = 1 C92: 0->1
Reversed above to a state found in an ancestor
172. Coronoid: size of teeth (excluding fangs) on anterior and middle coronoids relative to dentary tooth size: about the same = 0, half height or less = 1 C128: 0->1

Reversed above to a state found in an ancestor
State at this node found in an ancestor, thus representing a reversal,
OR convergent with a state outside this clade
229. Dermal ornamanet on cleithrum: present = 0, or absent = 1 N29: 0->1
Uniquely derived state, unchanged above
Character is uniform outside this clade

==========
below Adelospondylus - Ventastega (branch number 67):
Total changes along branch: 7

Character: Change
54. Postorbital suture to skull table (usually intertemporal or supratemporal when present) interdigitating vs smooth: smooth = 0, interdigitating = 1 C45: 0->1
Reversed above to a state found in an ancestor
State at this node convergent with a state outside this clade
58. Postorbital at least one quarter of the width of the skull table at the same transverse level: absent = 0, present = 1 ? C49: 1->0
Reversed above to a state found in an ancestor
State at this node found in an ancestor, thus representing a reversal,
OR convergent with a state outside this clade
143. Parasphenoid shagreen field anterior and posterior to basal articulation = 0, posterior to basal articulation only = 1, anterior to basal articulation only = 2 C102: 2->0
Reversed above to a state found in an ancestor
182. Number of Meckelian openings: more than three = 0, three = 1, two = 2, one = 3 N73: 3->0
Reversed above to a state found in an ancestor
184. Meckelian opening(s) without ventromesial bony margin = 0, or with ventromesial bony margin = 1 N75: 0->1
Reversed above to a state found in an ancestor
State at this node convergent with a state outside this clade
190. Adsymphysial plate dentition: shagreen, denticles or irregular tooth field = 0, organised dentition aligned parallel to jaw margin = 1, no dentition = 2 C142: 0->1
Reversed above to a state found in an ancestor
233. Interclavicle anterior tip: squared = 0, broadly rounded = 1, pointed = 2. N85: 0->2
Reversed above to a state found in an ancestor

==========
below Adelospondylus - Ichthyostega (branch number 68):
Total changes along branch: 5

Character: Change
8. Orbit position re snout/postparietal length: centre closer to front than rear = 0, centre near middle = 1, centre closer to rear than front = 2 C164: 2->1
Reversed above to a state found in an ancestor
State at this node found in an ancestor, thus representing a reversal,
OR convergent with a state outside this clade
48. Parietal ? postorbital suture: absent = 0, present = 1 C39: 1->0
Reversed above to a state found in an ancestor
State at this node found in an ancestor, thus representing a reversal
148. Vomer anterior wall forming posterior margin of palatal fossa bears tooth row meeting in midline: present = 0, absent = 1 C108: 0->1

Reversed above to a state found in an ancestor
174. Dentary tooth number: more than 70 = 0, 56-70 = 1, 46-55 = 2, 36-45 = 3, less than 35 = 4 C130: 0->4
Reversed above to a state found in an ancestor
276. Ilium dorsalmost process (one that articulates with sacral rib) orientation: straight dorsal = 0, canted posteriorly = 1, canted anteriorly = 2 N39: 2->0
Reversed above to a state found in an ancestor

==========
below Adelospondylus - Tulerpeton (branch number 69):
Total changes along branch: 10

Character: Change
123. Anterior palatal fenestra: present = 0, absent = 1 N11: 0->1
Reversed above to a state found in an ancestor
227. Cleithrum co-ossified with scapulocoracoid = 0, separate = 1 C177: 0->1
State at this node found in an ancestor, thus representing a reversal
230. Scapulocoracoid dorsal blade: absent = 0, present = 1 $C209: 0->1
Reversed above to a state found in an ancestor
State at this node convergent with a state outside this clade
237. Postbranchial lamina on cleithrum present = 0, or absent = 1 R1: 0->1
Reversed above to a state found in an ancestor
State at this node convergent with a state outside this clade
238. Cleithrum without = 0, or with = 1 a distinct shaft R11: 0->1
Uniquely derived state, unchanged above
Character is uniform outside this clade
261. Ectepicondyle foramen: present = 0, absent = 1 R43: 0->1
Reversed above to a state found in an ancestor
299. Tibia waisted: no = 0, yes = 1 R118: 0->1
State at this node found in an ancestor, thus representing a reversal,
OR convergent with a state outside this clade
305. Fibula waisted: no = 0, yes = 1 R127: 0->1
State at this node found in an ancestor, thus representing a reversal,
OR convergent with a state outside this clade
306. Fibula without = 0, or with = 1 oblique distal extremity R128: 0->1
Reversed above to a state found in an ancestor
309. Interepipodial space: present = 0, or absent = 1 N53: 1->0
State at this node found in an ancestor, thus representing a reversal,
OR convergent with a state outside this clade

==========
below Adelospondylus - Koilops (branch number 70):
Total changes along branch: 1

Character: Change
14. Dermal ornament character: Pit-and-ridge with visible center of ossification = 0, pit-and-ridge with no obvious center of ossification = 1, irregular pit-and-ridge with no obvious center of ossification =2, short radiating grooves = 3, pitted = 4, ir:
Reversed above to a state found in an ancestor

==========

below Adelospondylus - Ossinodus (branch number 71):
Total changes along branch: 1

Character: Change
49. Parietal anterior portion extent relative to orbit midlength: in front of = 0, level with ?= 1, posterior to = 2 C40: 1->2
Reversed above to a state found in an ancestor
State at this node found in an ancestor, thus representing a reversal,
OR convergent with a state outside this clade

==========
below Adelospondylus - Ymeria (branch number 72):
Total changes along branch: 2

Character: Change
14. Dermal ornament character: Pit-and-ridge with visible center of ossification = 0, pit-and-ridge with no obvious center of ossification = 1, irregular pit-and-ridge with no obvious center of ossification =2, short radiating grooves = 3, pitted = 4, ir:
Reversed above to a state found in an ancestor
132. Ectopterygoid fang pairs: present = 0, absent = 1 C92: 1->0
Reversed above to a state found in an ancestor
State at this node found in an ancestor, thus representing a reversal

==========
below Adelospondylus - Occidens (branch number 73):
Total changes along branch: 2

Character: Change
176. Dentary ventral edge: smooth continuous line = 0, abruptly tapering or ?stepped? margin = 1 C133: 0->1
Reversed above to a state found in an ancestor
State at this node found in an ancestor, thus representing a reversal,
OR convergent with a state outside this clade
186. Meckelian foramina/ fenestrae, dorsal margins formed by; mostly meckelian bone = 0, mostly prearticular = 1, mostly infradentary (postsplenial) = 2 C139: 1->0
Reversed above to a state found in an ancestor
State at this node found in an ancestor, thus representing a reversal

==========
below Adelospondylus - Whatcheeria (branch number 74):
Total changes along branch: 1

Character: Change
167. Coronoid: at least one has fang pair recognisable because at least twice the height of coronoid teeth: present = 0, absent = 1 C123: 0->1
Reversed above to a state found in an ancestor
State at this node convergent with a state outside this clade

==========
below Adelospondylus - Sigournea (branch number 75):
Total changes along branch: 4

Character: Change
158. Adductor fossa faces dorsally = 0, mesially = 1 C114: 0->1
Reversed above to a state found in an ancestor
159. Angular mesial lamina suture with prearticular: absent = 0, present = 1 $C115: 0->1
Reversed above to a state found in an ancestor
165. Coronoid (posterior) posterodorsal process: absent = 0, present = 1 C121: 0->1
Reversed above to a state found in an ancestor
196. Prearticular shagreen field, distribution: gradually decreasing from dorsal to ventral = 0, well defined dorsal longitudinal band = 1, scattered patches or absent = 2 C148: 1->2
Reversed above to a state found in an ancestor
OR changed above to a state convergent with a state outside this clade
State at this node found in an ancestor, thus representing a reversal,
OR convergent with a state outside this clade

==========
below Adelospondylus - Eucritta (branch number 76):
Total changes along branch:

no unambiguous changes

==========
below Adelospondylus - Brittagnathus (branch number 77):
Total changes along branch:

no unambiguous changes

==========
below Adelospondylus - Loxomma (branch number 78):
Total changes along branch: 2

Character: Change
169. Coronoid: at least one has organized tooth row: present = 0, absent =1 C125: 0->1
Reversed above to a state found in an ancestor
186. Meckelian foramina/ fenestrae, dorsal margins formed by; mostly meckelian bone = 0, mostly prearticular = 1, mostly infradentary (postsplenial) = 2 C139: 0->1
State at this node found in an ancestor, thus representing a reversal

==========
below Adelospondylus - Crassigyrinus (branch number 79):
Total changes along branch: 8

Character: Change
8. Orbit position re snout/postparietal length: centre closer to front than rear = 0, centre near middle = 1, centre closer to rear than front = 2 C164: 2->1
Reversed above to a state found in an ancestor
State at this node found in an ancestor, thus representing a reversal
15. Center of ornament on squamosal: no center of ornamentation= 0, center closer to dorsal apex of temporal embayment (or midline of skull if no temporal ebayment) = 1, center closer to posteroventral margin of squamosal = 2 N77: 1->0
Reversed above to a state found in an ancestor

State at this node found in an ancestor, thus representing a reversal,
OR convergent with a state outside this clade
124. Anterior palatal fenestra: paired (0); unpaired (1) N12: 1->0
State at this node convergent with a state outside this clade
182. Number of Meckelian openings: more than three = 0, three = 1, two = 2, one = 3 N73: 0->3
Reversed above to a state found in an ancestor
State at this node found in an ancestor, thus representing a reversal
189. Adsymphysial plate fang-pair (distinct from other teeth): absent = 0, present = 1 C141: 1->0
Reversed above to a state found in an ancestor
State at this node found in an ancestor, thus representing a reversal
252. Humerus latissimus dorsi process position relative to ectepicondyle: offset anteriorly = 0, in line = 1 C185: 0->1
State at this node convergent with a state outside this clade
265. Length of posterior margin of entepicondyle smaller than = 0, subequal to = 1, or larger than = 2, humerus anteroposterior length at the level of proximal insertion of entepicondyle onto humerus shaft R66: 0->1
Reversed above to a state found in an ancestor
State at this node convergent with a state outside this clade
327. Gastralia: tapered and elongate, four times longer than broad or longer = 0, ovoid = 1, around three times longer than broad one end tapering = 2 C211: 0->1
Reversed above to a state found in an ancestor
State at this node convergent with a state outside this clade

==========
below Adelospondylus - Deltaherpeton (branch number 80):
Total changes along branch: 11

Character: Change
21. Frontal/ parietal length ratio: frontals shorter = 0; longer = 1, subequal = 2 C10: 2->1
Reversed above to a state found in an ancestor
State at this node found in an ancestor, thus representing a reversal
23. Frontal/ nasal length ratio: frontals approximately equal to or less than one-third as long as nasals = 0, more than one-third as long = 1 C12: 0->1
Reversed above to a state found in an ancestor
State at this node found in an ancestor, thus representing a reversal
35. Lacrimal contributes to narial margin: absent, excluded by anterior tectal = 0: present = 1, absent, excluded by nasal/maxillary or prefrontal/maxillary suture = 2 C24: 1->2
Reversed above to a state found in an ancestor
State at this node convergent with a state outside this clade
60. Postparietal occipital flange (="postparietal lappet) exposure: absent = 0, present = 1 C51: 0->1
Reversed above to a state found in an ancestor
State at this node convergent with a state outside this clade
61. Postparietal ? exoccipital suture: absent = 0, present = 1 C52: 0->1
Reversed above to a state found in an ancestor
64. Prefrontal contributes to half or more than half anteromesial orbit margin = 0, less than half = 1 C55: 0->1
Reversed above to a state found in an ancestor
State at this node found in an ancestor, thus representing a reversal,
OR convergent with a state outside this clade
100. Parasphenoid cultriform process shape: biconvex = 0, narrowly triangular =1, parallel-sided = 2, or with proximal constriction followed by swelling = 3 C76: 1->2

Reversed above to a state found in an ancestor
State at this node convergent with a state outside this clade
136. Maxilla tooth number: > 40 = 0, 30-40 = 1, < 30 = 2 ? C96: 1->0
Reversed above to a state found in an ancestor
State at this node found in an ancestor, thus representing a reversal
250. Humerus latissimus dorsi process part of ridge = 0, distinct but low process = 1, spike = 2 C183: 2->1
Reversed above to a state found in an ancestor
251. Humerus latissimus dorsi process position compared with deltopectoral crest: more proximal to head = 0, equidistant from head = 1 C184: 1->0
Reversed above to a state found in an ancestor
State at this node found in an ancestor, thus representing a reversal
264. Entepicondyle shape: three-dimmensional spike = 0, dorsoventrally flattened rectangle or trapezoid = 1, dorsoventrally flattened triangle = 2 N34: 2->1
Reversed above to a state found in an ancestor
State at this node found in an ancestor, thus representing a reversal

==========
below Adelospondylus - Archegosaurus (branch number 81):
Total changes along branch: 8

Character: Change
10. Pineal foramen position along interparietal suture: behind midpoint = 0, at the midpoint = 1, anterior to midpoint = 2 C166: 0->1
Reversed above to a state found in an ancestor
State at this node found in an ancestor, thus representing a reversal
77. Tabular shape in dorsal view (aside from horn, if present): rectangle or square = 0, irregular rectangular/quadrangle = 1, elongate oval or teardrop = 2, triangular = 3 N1: 0->1
Reversed above to a state found in an ancestor
State at this node found in an ancestor, thus representing a reversal
150. Vomerine shagreen field: absent = 0, present = 1 ? C110: 0->1
Reversed above to a state found in an ancestor
State at this node convergent with a state outside this clade
176. Dentary ventral edge: smooth continuous line = 0, abruptly tapering or ?stepped? margin = 1 C133: 1->0
Reversed above to a state found in an ancestor
State at this node found in an ancestor, thus representing a reversal
193. Postsplenial with mesial lamina: absent = 0, present = 1 C145: 0->1
Reversed above to a state found in an ancestor
State at this node convergent with a state outside this clade
233. Interclavicle anterior tip: squared = 0, broadly rounded = 1, pointed = 2. N85: 2->1
Reversed above to a state found in an ancestor
State at this node convergent with a state outside this clade
265. Length of posterior margin of entepicondyle smaller than = 0, subequal to = 1, or larger than = 2, humerus anteroposterior length at the level of proximal insertion of entepicondyle onto humerus shaft R66: 1->2
Reversed above to a state found in an ancestor
State at this node found in an ancestor, thus representing a reversal,
OR convergent with a state outside this clade
318. Phalanges cross-section shape (manual): circular = 0, square-shaped or elongate oval-shaped = 1, convex upwards = 2 N63: 1->2

Reversed above to a state found in an ancestor

==========
below Adelospondylus - Caerorhachis (branch number 82):
Total changes along branch: 4

Character: Change
56. Postorbital shape: irregularly polygonal = 0, broadly cresentic and narrowing to a posterior point = 1 C47: 0->1
Reversed above to a state found in an ancestor
State at this node convergent with a state outside this clade
205. Centra (trunk) pleurocentra fused midventrally: absent = 0, present = 1 C173: 0->1
Uniquely derived state, unchanged above
Character is uniform outside this clade
215. Ribs (trunk): straight or weakly curved = 0, strongly ventrally curved = 1 C203: 0->1
Reversed above to a state found in an ancestor
State at this node convergent with a state outside this clade
277. Dorsal iliac process oblique and flared = 0, fan-shaped = 1, subrectangular and truncated = 2, blunt and digitiform = 3, low elongate = 4 R93: 3->4
Reversed above to a state found in an ancestor

==========
below Adelospondylus - Seymouria (branch number 83):
Total changes along branch: 9

Character: Change
25. Intertemporal smaller than supratemporal = 0, or larger than/comparable in size with supratemporal = 1 C14: 0->1
Reversed above to a state found in an ancestor
State at this node found in an ancestor, thus representing a reversal,
OR convergent with a state outside this clade
33. Jugal excluded from lower jaw margin by maxilla and quadratojugal: yes = 0, or no = 1 C22: 0->1
Reversed above to a state found in an ancestor
State at this node convergent with a state outside this clade
47. Parietal meets tabular: absent = 0, present = 1 ? C38: 0->1
State at this node convergent with a state outside this clade
100. Parasphenoid cultriform process shape: biconvex = 0, narrowly triangular =1, parallel-sided = 2, or with proximal constriction followed by swelling = 3 C76: 2->1
Reversed above to a state found in an ancestor
State at this node found in an ancestor, thus representing a reversal
102. Parasphenoid basal plate: square/rectangular = 0, or triangular/distinctly tapering at one end = 1 N9: 0->1
Reversed above to a state found in an ancestor
State at this node convergent with a state outside this clade
122. Vomers as broad as long or broader = 0, about twice as long as broad or longer = 1 C91: 0->1
State at this node convergent with a state outside this clade
136. Maxilla tooth number: > 40 = 0, 30-40 = 1, < 30 = 2 ? C96: 0->1/2
Derived state unclear
State at this node found in an ancestor, thus representing a reversal
289. Adductor blade: present = 0, absent =1 N42: 0->1
State at this node found in an ancestor, thus representing a reversal,

OR convergent with a state outside this clade
295. Anteroposterior maximum distance between femur distal condyles i(=tibia and fibula condyles) in extensor view 55 pecent or more of femur length = 0, between 55 and 40 percent of femur length = 1, 40 percent or less than femur length = 2 R117: 2->
Reversed above to a state found in an ancestor
State at this node found in an ancestor, thus representing a reversal,
OR convergent with a state outside this clade

==========
below Adelospondylus - Gephyrostegus (branch number 84):
Total changes along branch: 6

Character: Change
72. Squamosal suture with supratemporal: absent = 0, present = 1 C63: 1->0
State at this node found in an ancestor, thus representing a reversal
101. Basal plate of parasphenoid, measured posteriorly from basipterygoid processes/basal articulation: about as long as wide = 0, wider than long = 1, longer than wide = 2 N8: 1->0
Changed above to a state convergent with a state outside this clade
State at this node convergent with a state outside this clade
142. Parasphenoid shagreen field: present = 0, absent = 1 ? C101: 0->1
Reversed above to a state found in an ancestor
State at this node found in an ancestor, thus representing a reversal,
OR convergent with a state outside this clade
157. Labyrinthine infolding on teeth: present = 0, or absent = 1 N23: 0->1
Uniquely derived state, unchanged above
Character is uniform outside this clade
176. Dentary ventral edge: smooth continuous line = 0, abruptly tapering or ?stepped? margin = 1 C133: 0->1
Reversed above to a state found in an ancestor
State at this node found in an ancestor, thus representing a reversal
200. Surangular crest: absent = 0, present = 1 C153: 0->1
Reversed above to a state found in an ancestor
State at this node convergent with a state outside this clade

==========
below Adelospondylus - Casineria (branch number 85):
Total changes along branch: 2

Character: Change
221. Ribs (cervical): flared distally = 0, tapered distally = 1 C208: 0->1
State at this node found in an ancestor, thus representing a reversal,
OR convergent with a state outside this clade
239. Shape of ventral clavicle plate: elongate triangle = 0, sub-equilateral triangle = 1, spoon-shaped/spatulate/ovoid = 2 N30: 0->2
State at this node found in an ancestor, thus representing a reversal,
OR convergent with a state outside this clade

==========
below Adelospondylus - Westlothiana (branch number 86):
Total changes along branch: 4

Character: Change
206. Centra (trunk) pleurocentra fused middorsally: absent = 0, present = 1 C174: 0->1
State at this node convergent with a state outside this clade
213. Presacral count: 25-35 = 0, 20-24 = 1, >35 = 2, <20 = 3 P107: 1->2
State at this node convergent with a state outside this clade
257. Humerus ectepicondyle distinct: present = 0, absent = 1 C192: 0->1
State at this node convergent with a state outside this clade
263. Humerus length up to and no more than twice its width = 0, or more than twice its width = 1 R49: 0->1
State at this node convergent with a state outside this clade

==========
below Adelospondylus - Microbrachis (branch number 87):
Total changes along branch: 8

Character: Change
2. Preorbital region of skull less than twice as wide as long = 0, or at least twice as wide as long = 1 C155: 0->1
Reversed above to a state found in an ancestor
State at this node convergent with a state outside this clade
8. Orbit position re snout/postparietal length: centre closer to front than rear = 0, centre near middle = 1, centre closer to rear than front = 2 C164: 1->0
State at this node found in an ancestor, thus representing a reversal
9. Orbit position re snout /quadrate length: centre closer to front than rear = 0, centre near middle = 1, centre closer to rear than front = 2 C165: 1->0
State at this node found in an ancestor, thus representing a reversal
56. Postorbital shape: irregularly polygonal = 0, broadly cresentic and narrowing to a posterior point = 1 C47: 1->0
State at this node found in an ancestor, thus representing a reversal
71. Squamosal anterior part lying behind mid-parietal length: present = 0, absent = 1 C62: 1->0
State at this node found in an ancestor, thus representing a reversal
120. Vomers separated by parasphenoid > half vomer mesial length: present = 0, absent = 1 C88: 1->0
State at this node found in an ancestor, thus representing a reversal
178. Mandibular sensory canal: present = 0, absent = 1 C134: 1->0
Reversed above to a state found in an ancestor
State at this node found in an ancestor, thus representing a reversal
203. Trunk pleurocentrum height relative to intercentrum height: pleurocentrum less than intercentrum = 0, same as intercentrum = 1, greater than intercentrum = 2,, intercentrum and pleurocentrum fused into single bone (holospondylous) = 3 N80: 2->3
Uniquely derived state, unchanged above
Two or more other states found outside this clade

==========
below Adelospondylus - Lethiscus (branch number 88):
Total changes along branch: 14

Character: Change
4. Interorbital distance compared with maximum orbit diameter: greater = 0, smaller = 1, subequal = 2 C158: 0->2
Reversed above to a state found in an ancestor
State at this node found in an ancestor, thus representing a reversal

58. Postorbital at least one quarter of the width of the skull table at the same transverse level: absent = 0, present = 1 ? C49: 0->1
State at this node found in an ancestor, thus representing a reversal
65. Premaxilla posterodorsal alary process onto snout: absent = 0, present = 1 C56: 0->1
State at this node convergent with a state outside this clade
83. Maximum parietal-parietal width is shorter than distance between posterior skull table margin (discounting tabular horn if present) and posterior orbit margin as projected along skull midline: present = 0, absent = 1 C231: 1->0
State at this node found in an ancestor, thus representing a reversal
84. Maxilla contribution to orbit margin: absent = 0, or present = 1 C239: 0->1
State at this node convergent with a state outside this clade
149. Vomerine row of small teeth : present = 0, absent = 1 ? C109: 1->0
State at this node found in an ancestor, thus representing a reversal
160. Angular reaches posteriormost point of lower jaw: absent = 0, present = 1 C116: 1->0
State at this node found in an ancestor, thus representing a reversal
200. Surangular crest: absent = 0, present = 1 C153: 1->0
State at this node found in an ancestor, thus representing a reversal
214. Presacral (trunk) ribs: length of longest ribs: short = 0, long = 1 P140: 1->0
State at this node found in an ancestor, thus representing a reversal
215. Ribs (trunk): straight or weakly curved = 0, strongly ventrally curved = 1 C203: 1->0
State at this node found in an ancestor, thus representing a reversal
217. Ribs (trunk) tapered distally =0, parallel-sided = 1, flared at distal tip= 2 C205: 1->0
State at this node found in an ancestor, thus representing a reversal
224. Forelimbs/paired pectoral appendages: present = 0, absent = 1 N27: 0->1
Uniquely derived state, unchanged above
Character is uniform outside this clade
272. Hindlimbs/paired pelvic appendages: present = 0, absent = 1 N36: 0->1
Uniquely derived state, unchanged above
Character is uniform outside this clade
273. (Ossified) pelvic girdle at least in part: present = 0, absent = 1 N37: 0->1
Uniquely derived state, unchanged above
Character is uniform outside this clade

==========
below Adelospondylus - Adelogyrinus (branch number 89):
Total changes along branch: 7

Character: Change
14. Dermal ornament character: Pit-and-ridge with visible center of ossification = 0, pit-and-ridge with no obvious center of ossification = 1, irregular pit-and-ridge with no obvious center of ossification =2, short radiating grooves = 3, pitted = 4, ir:
State at this node found in an ancestor, thus representing a reversal
18. Ossified branchial arches/gill supports in adult: present = 0, or absent = 1 N72: 1->0
State at this node found in an ancestor, thus representing a reversal
53. Postfrontal ? prefrontal suture: anterior half of orbit = 0, middle or posterior half of ?orbit = 1, absent = 2 C44: 1->0
State at this node found in an ancestor, thus representing a reversal
156. Marginal tooth shape: conical and straight/slightly recurved = 0, small and more or less straight and 'needle-like' = 1, right-trapezoid 'chisel' shape = 2, spearhead shape = 3, thin and greatly recurved = 4 N22: 0->2
State at this node convergent with a state outside this clade

176. Dentary ventral edge: smooth continuous line = 0, abruptly tapering or ?stepped? margin = 1 C133: 1->0
State at this node found in an ancestor, thus representing a reversal
202. Dentary chin: absent = 0, or present = 1 C215: 0->1
Uniquely derived state, unchanged above
Character is uniform outside this clade
218. Ribs (trunk) bear uncinate processes: absent = 0, present = 1 C206: 0->1
State at this node found in an ancestor, thus representing a reversal

==========
below Coloraderpeton - Lethiscus (branch number 90):
Total changes along branch: 11

Character: Change
17. Jaw articulation position: posterior to occiput = 0, level with occiput = 1, anterior to occiput = 2 C222: 1->0
State at this node found in an ancestor, thus representing a reversal
35. Lacrimal contributes to narial margin: absent, excluded by anterior tectal = 0: present = 1, absent, excluded by nasal/maxillary or prefrontal/maxillary suture = 2 C24: 2->1
State at this node found in an ancestor, thus representing a reversal
88. Temporal fenestra: absent = 0, present = 1 C238: 0->1
State at this node convergent with a state outside this clade
93. Basioccipital condyle (= contribution to occipital condyle) : absent, notochordal = 0 present = 1 C5: 1->0
State at this node found in an ancestor, thus representing a reversal
114. Ectopterygoid reaches subtemporal fossa: absent = 0, present = 1 C72: 1->0
State at this node convergent with a state outside this clade
118. Pterygoids not visible in lateral aspect below ventral margin of jugal and quadratojugal = 0, or visible = 1 C86: 0->1
State at this node found in an ancestor, thus representing a reversal,
OR convergent with a state outside this clade
135. Ectopterygoid / palatine shagreen field: absent = 0, present = 1 ? C95: 1->0
State at this node found in an ancestor, thus representing a reversal
144. Pterygoid shagreen: dense = 0, a few discontinuous patches or absent = 1 C103: 0->1
State at this node convergent with a state outside this clade
165. Coronoid (posterior) posterodorsal process: absent = 0, present = 1 C121: 1->0
State at this node found in an ancestor, thus representing a reversal
188. Adsymphysial tooth plate: present = 0, absent = 1 C140: 1->0
State at this node found in an ancestor, thus representing a reversal
225. Ossified pectoral girdle: present = 0, absent = 1 N28: 0->1
State at this node convergent with a state outside this clade

==========
below NSM 994 GF 1.1 - Seymouria (branch number 91):
Total changes along branch: 6

Character: Change
35. Lacrimal contributes to narial margin: absent, excluded by anterior tectal = 0: present = 1, absent, excluded by nasal/maxillary or prefrontal/maxillary suture = 2 C24: 2->1
Reversed above to a state found in an ancestor
State at this node found in an ancestor, thus representing a reversal

61. Postparietal ? exoccipital suture: absent = 0, present = 1 C52: 1->0
State at this node found in an ancestor, thus representing a reversal
98. Opisthotic forms substantial plate (with supraoccipital if present) beneath skull table, separating it from the exoccipitals: present = 0, absent = 1 C37: 1->0
State at this node found in an ancestor, thus representing a reversal
277. Dorsal iliac process oblique and flared = 0, fan-shaped = 1, subrectangular and truncated = 2, blunt and digitiform = 3, low elongate = 4 R93: 4->2
State at this node convergent with a state outside this clade
310. Interepipodial space shape: elongate tapering oval/'spindle shaped' = 0, broad, elongate oval/subrectangle = 1, small circle that does not reach ends of epipodials = 2 N54: 0->1
Reversed above to a state found in an ancestor
OR changed above to a state convergent with a state outside this clade
State at this node found in an ancestor, thus representing a reversal,
OR convergent with a state outside this clade
324. Intermedium (hindlimb) contribution to interepipodial space: forms most/all of distal margin as a trough = 0, in line with distal end of fibula = 1 N69: 0->1
Reversed above to a state found in an ancestor
State at this node convergent with a state outside this clade

==========
below NSM 994 GF 1.1 - Silvanerpeton (branch number 92):
Total changes along branch: 5

Character: Change
4. Interorbital distance compared with maximum orbit diameter: greater = 0, smaller = 1, subequal = 2 C158: 0->1
Reversed above to a state found in an ancestor
State at this node found in an ancestor, thus representing a reversal
10. Pineal foramen position along interparietal suture: behind midpoint = 0, at the midpoint = 1, anterior to midpoint = 2 C166: 1->2
Reversed above to a state found in an ancestor
State at this node convergent with a state outside this clade
75. Supratemporal forms part of skull margin posteriorly, including temporal ebayment: absent = 0, present = 1 C66: 1->0
Reversed above to a state found in an ancestor
State at this node found in an ancestor, thus representing a reversal
78. Tabular horn: absent, tabular does not form horn = 0, tabular forms notable horn = 1 N2: 0->1
State at this node found in an ancestor, thus representing a reversal,
OR convergent with a state outside this clade
128. Median meeting of ptergyoids (measured anteriorly from basal articulation): approximately 1/3 or less of pterygoid length = 0, about 1/2 of pteryoid length = 1, approximately 2/3-3/4 of pterygoid length = 2, almost all or all of pterygoid length = 3:
Reversed above to a state found in an ancestor
State at this node convergent with a state outside this clade

==========
below NSM 994 GF 1.1 - Eldeceeon (branch number 93):
Total changes along branch: 6

Character: Change

15. Center of ornament on squamosal: no center of ornamentation= 0, center closer to dorsal apex of temporal embayment (or midline of skull if no temporal ebayment) = 1, center closer to posteroventral margin of squamosal = 2 N77: 0->1
Reversed above to a state found in an ancestor
State at this node found in an ancestor, thus representing a reversal
25. Intertemporal smaller than supratemporal = 0, or larger than/comparable in size with supratemporal = 1 C14: 1->0
Reversed above to a state found in an ancestor
State at this node found in an ancestor, thus representing a reversal
100. Parasphenoid cultriform process shape: biconvex = 0, narrowly triangular =1, parallel-sided = 2, or with proximal constriction followed by swelling = 3 C76: 1->3
Reversed above to a state found in an ancestor
State at this node convergent with a state outside this clade
109. Anterior extent of cultriform process along palate: ends nearer choana posterior margin = 0, or ends nearer orbit posterior margin = 1 P201: 0->1
Reversed above to a state found in an ancestor
State at this node found in an ancestor, thus representing a reversal,
OR convergent with a state outside this clade
176. Dentary ventral edge: smooth continuous line = 0, abruptly tapering or ?stepped? margin = 1 C133: 0->1
Reversed above to a state found in an ancestor
State at this node found in an ancestor, thus representing a reversal
203. Trunk pleurocentrum height relative to intercentrum height: pleurocentrum less than intercentrum = 0, same as intercentrum = 1, greater than intercentrum = 2,, intercentrum and pleurocentrum fused into single bone (holospondylous) = 3 N80: 2->1
State at this node found in an ancestor, thus representing a reversal,
OR convergent with a state outside this clade

==========
below NSM 994 GF 1.1 - Proterogyrinus (branch number 94):
Total changes along branch: 5

Character: Change
32. Jugal extends anterior to anterior orbit margin: absent = 0, present = 1 C21: 0->1
State at this node found in an ancestor, thus representing a reversal,
OR convergent with a state outside this clade
56. Postorbital shape: irregularly polygonal = 0, broadly cresentic and narrowing to a posterior point = 1 C47: 1->0
Reversed above to a state found in an ancestor
State at this node found in an ancestor, thus representing a reversal
113. Ectopterygoid as long or longer than palatines: present = 0, absent = 1 ? C71: 1->0
State at this node found in an ancestor, thus representing a reversal
114. Ectopterygoid reaches subtemporal fossa: absent = 0, present = 1 C72: 1->0
Reversed above to a state found in an ancestor
State at this node convergent with a state outside this clade
324. Intermedium (hindlimb) contribution to interepipodial space: forms most/all of distal margin as a trough = 0, in line with distal end of fibula = 1 N69: 1->0
State at this node found in an ancestor, thus representing a reversal

==========
below NSM 994 GF 1.1 - Palaeoherpeton (branch number 95):

Total changes along branch: 4

Character: Change
30. Jugal alary process ("insula jugalis") on palate: absent = 0, present = 1 C19: 0->1
Reversed above to a state found in an ancestor
State at this node convergent with a state outside this clade
36. Lacrimal reaches orbit margin (= prefrontal/ jugal suture): present = 0, absent = 1 C25: 0->1
State at this node convergent with a state outside this clade
101. Basal plate of parasphenoid, measured posteriorly from basipterygoid processes/basal articulation: about as long as wide = 0, wider than long = 1, longer than wide = 2 N8: 1->2
Changed above to a state convergent with a state outside this clade
State at this node convergent with a state outside this clade
142. Parasphenoid shagreen field: present = 0, absent = 1 ? C101: 0->1
State at this node found in an ancestor, thus representing a reversal,
OR convergent with a state outside this clade

==========
below NSM 994 GF 1.1 - Neopteroplax (branch number 96):
Total changes along branch: 2

Character: Change
100. Parasphenoid cultriform process shape: biconvex = 0, narrowly triangular =1, parallel-sided = 2, or with proximal constriction followed by swelling = 3 C76: 3->1
Reversed above to a state found in an ancestor
State at this node found in an ancestor, thus representing a reversal
132. Ectopterygoid fang pairs: present = 0, absent = 1 C92: 1->0
Reversed above to a state found in an ancestor
State at this node found in an ancestor, thus representing a reversal

==========
below Archeria - Neopteroplax (branch number 97):
Total changes along branch: 3

Character: Change
9. Orbit position re snout /quadrate length: centre closer to front than rear = 0, centre near middle = 1, centre closer to rear than front = 2 C165: 1->2
Reversed above to a state found in an ancestor
State at this node convergent with a state outside this clade
25. Intertemporal smaller than supratemporal = 0, or larger than/comparable in size with supratemporal = 1 C14: 0->1
State at this node found in an ancestor, thus representing a reversal
207. Centra (trunk) intercentra fused middorsally: absent = 0, present = 1 N81: 0->1
State at this node convergent with a state outside this clade

==========
below Archeria - St Louis tetrapod (branch number 98):
Total changes along branch: 1

Character: Change
188. Adsymphysial tooth plate: present = 0, absent = 1 C140: 1->0
State at this node found in an ancestor, thus representing a reversal

==========
below Archeria - Pholiderpeton scutigerum (branch number 99):
Total changes along branch: 2

Character: Change
156. Marginal tooth shape: conical and straight/slightly recurved = 0, small and more or less straight and 'needle-like' = 1, right-trapezoid 'chisel' shape = 2, spearhead shape = 3, thin and greatly recurved = 4 N22: 0->2
State at this node convergent with a state outside this clade
180. Mandibular oral sulcus/ surangular pit line: present = 0, absent = 1 ? C136: 1->0
State at this node found in an ancestor, thus representing a reversal

==========
below Eogyrinus attheyi - Neopteroplax (branch number 100):
Total changes along branch: 8

Character: Change
14. Dermal ornament character: Pit-and-ridge with visible center of ossification = 0, pit-and-ridge with no obvious center of ossification = 1, irregular pit-and-ridge with no obvious center of ossification =2, short radiating grooves = 3, pitted = 4, ir:
Uniquely derived state, unchanged above
Two or more other states found outside this clade
15. Center of ornament on squamosal: no center of ornamentation= 0, center closer to dorsal apex of temporal embayment (or midline of skull if no temporal ebayment) = 1, center closer to posteroventral margin of squamosal = 2 N77: 1->0
State at this node found in an ancestor, thus representing a reversal
69. Squamosal contact with tabular: smooth = 0, interdigitating = 1, absent = 2 C60: 2->0
State at this node convergent with a state outside this clade
109. Anterior extent of cultriform process along palate: ends nearer choana posterior margin = 0, or ends nearer orbit posterior margin = 1 P201: 1->0
State at this node found in an ancestor, thus representing a reversal
128. Median meeting of ptergyoids (measured anteriorly from basal articulation): approximately 1/3 or less of pterygoid length = 0, about 1/2 of pteryoid length = 1, approximately 2/3-3/4 of pterygoid length = 2, almost all or all of pterygoid length = 3:
State at this node found in an ancestor, thus representing a reversal
130. Median margin of pterygoid palatal ramus where separate: straight = 0, slightly concave medially = 1, convex medially = 2, greatly concave medially = 3 N17: 1->0
State at this node found in an ancestor, thus representing a reversal
137. Maxillary caniniform teeth (about twice the size of neighbouring teeth): absent = 0, present = 1 C97: 0->1
State at this node found in an ancestor, thus representing a reversal
160. Angular reaches posteriormost point of lower jaw: absent = 0, present = 1 C116: 1->0
State at this node found in an ancestor, thus representing a reversal

==========
below Anthracosaurus - Proterogyrinus (branch number 101):
Total changes along branch: 6

Character: Change

12. Otic notch/temporal ebayment approaching orbit: more than 1/2 postorbital skull length = 0, 1/4-1/2 postorbital skull length = 1, less than 1/4 postorbital skull length = 2 P35: 1->0
Changed above to a state convergent with a state outside this clade
State at this node found in an ancestor, thus representing a reversal
33. Jugal excluded from lower jaw margin by maxilla and quadratojugal: yes = 0, or no = 1 C22: 1->0
State at this node found in an ancestor, thus representing a reversal
136. Maxilla tooth number: > 40 = 0, 30-40 = 1, < 30 = 2 ? C96: 1->2
Reversed above to a state found in an ancestor
State at this node found in an ancestor, thus representing a reversal,
OR convergent with a state outside this clade
165. Coronoid (posterior) posterodorsal process: absent = 0, present = 1 C121: 1->0
State at this node found in an ancestor, thus representing a reversal
166. Coronoid (posterior) posterodorsal process visible in lateral view: absent = 0, present = 1 C122: 1->0
State at this node found in an ancestor, thus representing a reversal
169. Coronoid: at least one has organized tooth row: present = 0, absent =1 C125: 1->0
State at this node found in an ancestor, thus representing a reversal

==========
below Eoherpeton - Proterogyrinus (branch number 102):
Total changes along branch: 4

Character: Change
23. Frontal/ nasal length ratio: frontals approximately equal to or less than one-third as long as nasals = 0, more than one-third as long = 1 C12: 1->0
State at this node found in an ancestor, thus representing a reversal
72. Squamosal suture with supratemporal: absent = 0, present = 1 C63: 1->0
State at this node found in an ancestor, thus representing a reversal
102. Parasphenoid basal plate: square/rectangular = 0, or triangular/distinctly tapering at one end = 1 N9: 1->0
State at this node found in an ancestor, thus representing a reversal
160. Angular reaches posteriormost point of lower jaw: absent = 0, present = 1 C116: 1->0
State at this node found in an ancestor, thus representing a reversal

==========
below Eoherpeton - Doragnathus (branch number 103):
Total changes along branch: 1

Character: Change
185. Meckelian bone or space exposure in middle part of jaw, depth much less than prearticular = 0, depth similar to prearticular or greater = 1 C138: 1->0
State at this node found in an ancestor, thus representing a reversal

==========
below Adamanterpeton - Archegosaurus (branch number 104):
Total changes along branch: 9

Character: Change
65. Premaxilla posterodorsal alary process onto snout: absent = 0, present = 1 C56: 0->1
Reversed above to a state found in an ancestor
State at this node convergent with a state outside this clade

66. Premaxilla forms part of choanal margin: broadly = 0, point = 1, not, excluded by ?vomer = 2 C57: 1->2
Reversed above to a state found in an ancestor
State at this node found in an ancestor, thus representing a reversal,
OR convergent with a state outside this clade
106. Parasphenoid contacts or sutures to vomers: present = 0, absent = 1 ? C80: 1->0
Reversed above to a state found in an ancestor
State at this node found in an ancestor, thus representing a reversal
121. Vomers separated by pterygoids: for > half length = 0, < half length = 1, not separated by pterygoids = 2 C89: 1->2
State at this node found in an ancestor, thus representing a reversal
126. Interpterygoid vacuities that intersect with orbit: absent = 0, or present = 1 N14: 0->1
Reversed above to a state found in an ancestor
127. Pterygoids meet along midline: yes = 0, or no = 1 N15: 0->1
Reversed above to a state found in an ancestor
State at this node found in an ancestor, thus representing a reversal
129. Vomer contributes to interpterygoid vacuity: absent = 0, present = 1 C90: 0->1
Reversed above to a state found in an ancestor
199. Splenial, rearmost extension of mesial lamina closer to anterior margin of adductor fossa than to the anterior end of the jaw: absent = 0, present = 1 C152: 1->0
Reversed above to a state found in an ancestor
State at this node found in an ancestor, thus representing a reversal
312. Manus digit number: eight = 0, six = 1, five = 2, four = 3, three = 4 N56: 2->3
State at this node convergent with a state outside this clade

==========
below Adamanterpeton - Platyrhinops (branch number 105):
Total changes along branch: 9

Character: Change
55. Postorbital without distinct dorsomedial ramus for postfrontal = 0, with incipient ramus = 1, ?with elongate ramus = 2 C46: 0->1
Reversed above to a state found in an ancestor
State at this node convergent with a state outside this clade
70. Squamosal-supratemporal suture position: at apex of temporal embayment = 0, dorsal to apex = 1, ventral to apex = 2 C61: 0->1
Reversed above to a state found in an ancestor
State at this node convergent with a state outside this clade
94. Basipterygoid junction: basipterygoid process fits into socket recessed into epipterygoid/pterygoid = 0, pterygoid/epipterygoid forms narrow bar and clasps basipterygoid process fore and aft = 1, pterygoid/epipterygoid and parasphenoid sutured = 2:
Changed above to a state convergent with a state outside this clade
117. Pterygoid quadrate ramus margin in adductor fossa: concave = 0, with some convex component = 1 C85: 0->1
Reversed above to a state found in an ancestor
State at this node convergent with a state outside this clade
162. Coronoid (anterior) contacts postsplenial: absent = 0, present = 1 C118: 0->1
Uniquely derived state, unchanged above
Character is uniform outside this clade
163. Coronoid (middle) contacts postsplenial: absent = 0, present = 1 C119: 0->1
Reversed above to a state found in an ancestor

State at this node convergent with a state outside this clade
164. Coronoid (middle) separated from splenial (or presplenial if present): present, by prearticular = 0, absent = 1, present, by postsplenial = 2 C120: 0->2
Changed above to a state convergent with a state outside this clade
239. Shape of ventral clavicle plate: elongate triangle = 0, sub-equilateral triangle = 1, spoon-shaped/spatulate/ovoid = 2 N30: 0->1
State at this node found in an ancestor, thus representing a reversal,
OR convergent with a state outside this clade
300. Tibia without cnemial crest = 0, crest present and running distally = 1, present and running mesiolaterally while subsiding distally = 2 R119: 2->0
Reversed above to a state found in an ancestor
State at this node found in an ancestor, thus representing a reversal,
OR convergent with a state outside this clade

==========
below Adamanterpeton - Eryops (branch number 106):
Total changes along branch: 6

Character: Change
35. Lacrimal contributes to narial margin: absent, excluded by anterior tectal = 0: present = 1, absent, excluded by nasal/maxillary or prefrontal/maxillary suture = 2 C24: 2->1
Reversed above to a state found in an ancestor
State at this node found in an ancestor, thus representing a reversal
56. Postorbital shape: irregularly polygonal = 0, broadly cresentic and narrowing to a posterior point = 1 C47: 0->1
Reversed above to a state found in an ancestor
State at this node convergent with a state outside this clade
103. Parasphenoid depression in body: absent = 0, single median = 1, multiple = 2 C77: 1->0
Changed above to a state convergent with a state outside this clade
State at this node found in an ancestor, thus representing a reversal
136. Maxilla tooth number: > 40 = 0, 30-40 = 1, < 30 = 2 ? C96: 0->1
Reversed above to a state found in an ancestor
State at this node found in an ancestor, thus representing a reversal
174. Dentary tooth number: more than 70 = 0, 56-70 = 1, 46-55 = 2, 36-45 = 3, less than 35 = 4 C130: 1->3
Reversed above to a state found in an ancestor
State at this node found in an ancestor, thus representing a reversal,
OR convergent with a state outside this clade
176. Dentary ventral edge: smooth continuous line = 0, abruptly tapering or ?stepped? margin = 1 C133: 0->1
State at this node found in an ancestor, thus representing a reversal

==========
below Adamanterpeton - Capetus (branch number 107):
Total changes along branch: 4

Character: Change
21. Frontal/ parietal length ratio: frontals shorter = 0; longer = 1, subequal = 2 C10: 1->2
State at this node found in an ancestor, thus representing a reversal
29. Jugal contribution to orbit margin: less than one-third = 0, equal to or more than one-third = 1 C18: 0->1

State at this node convergent with a state outside this clade
122. Vomers as broad as long or broader = 0, about twice as long as broad or longer = 1 C91: 0->1
State at this node convergent with a state outside this clade
129. Vomer contributes to interpterygoid vacuity: absent = 0, present = 1 C90: 1->0
State at this node found in an ancestor, thus representing a reversal

==========
below Balanerpeton - Eryops (branch number 108):
Total changes along branch: 3

Character: Change
58. Postorbital at least one quarter of the width of the skull table at the same transverse level: absent = 0, present = 1 ? C49: 1->0
Reversed above to a state found in an ancestor
State at this node found in an ancestor, thus representing a reversal
66. Premaxilla forms part of choanal margin: broadly = 0, point = 1, not, excluded by ?vomer = 2 C57: 2->1
State at this node found in an ancestor, thus representing a reversal
94. Basipterygoid junction: basipterygoid process fits into socket recessed into epipterygoid/pterygoid = 0, pterygoid/epipterygoid forms narrow bar and clasps basipterygoid process fore and aft = 1, pterygoid/epipterygoid and parasphenoid sutured = 2:
State at this node convergent with a state outside this clade

==========
below Dendrerpeton - Eryops (branch number 109):
Total changes along branch: 6

Character: Change
23. Frontal/ nasal length ratio: frontals approximately equal to or less than one-third as long as nasals = 0, more than one-third as long = 1 C12: 1->0
State at this node found in an ancestor, thus representing a reversal
52. Postfrontal ? prefrontal contact: broad = 0; or point-like = 1 C43: 1->0
State at this node found in an ancestor, thus representing a reversal
55. Postorbital without distinct dorsomedial ramus for postfrontal = 0, with incipient ramus = 1, ?with elongate ramus = 2 C46: 1->0
State at this node found in an ancestor, thus representing a reversal
200. Surangular crest: absent = 0, present = 1 C153: 0->1
State at this node convergent with a state outside this clade
228. Cleithrum smoothly broadening to spatulate dorsal end = 0, distal expansion marked from narrow stem by notch or process or decrease in thickness = 1, end simply tapering = 2 C178: 2->1
State at this node found in an ancestor, thus representing a reversal,
OR convergent with a state outside this clade
290. Adductor blade length: occupying most or all of the femur length = 0, restricted to midshaft = 1, restricted to proximal part of femur = 2 N43: 2->1
State at this node found in an ancestor, thus representing a reversal

==========
below Edops - Eryops (branch number 110):
Total changes along branch: 8

Character: Change

9. Orbit position re snout /quadrate length: centre closer to front than rear = 0, centre near middle = 1, centre closer to rear than front = 2 C165: 1->2
State at this node convergent with a state outside this clade
10. Pineal foramen position along interparietal suture: behind midpoint = 0, at the midpoint = 1, anterior to midpoint = 2 C166: 1->0
State at this node found in an ancestor, thus representing a reversal
19. Septomaxilla (= ?anterior tectal?) present = 0, absent = 1 C1: 1->0
State at this node found in an ancestor, thus representing a reversal
28. Jugal deep below orbit (vs narrow process): > 50% orbit diam = 0, <50% = 1 C17: 1->0
State at this node found in an ancestor, thus representing a reversal
35. Lacrimal contributes to narial margin: absent, excluded by anterior tectal = 0: present = 1, absent, excluded by nasal/maxillary or prefrontal/maxillary suture = 2 C24: 1->0
State at this node found in an ancestor, thus representing a reversal
36. Lacrimal reaches orbit margin (= prefrontal/ jugal suture): present = 0, absent = 1 C25: 0->1
State at this node convergent with a state outside this clade
248. Angle between proximal and distal ends of humerus: 30 degrees or less = 0, 31-60 degrees = 1, more than 60 degrees = 2 N84: 1->2
State at this node convergent with a state outside this clade
326. Scale distribution: gastralia present = 0, gastralia and dorsal scales/osteoderms/other dermal ossifications present = 1, no scales = 2 N71: 0->1
State at this node convergent with a state outside this clade

==========
below Erpetosaurus - Archegosaurus (branch number 111):
Total changes along branch: 8

Character: Change
15. Center of ornament on squamosal: no center of ornamentation= 0, center closer to dorsal apex of temporal embayment (or midline of skull if no temporal ebayment) = 1, center closer to posteroventral margin of squamosal = 2 N77: 0->1
State at this node found in an ancestor, thus representing a reversal
19. Septomaxilla (= ?anterior tectal?) present = 0, absent = 1 C1: 1->0
State at this node found in an ancestor, thus representing a reversal
122. Vomers as broad as long or broader = 0, about twice as long as broad or longer = 1 C91: 0->1
State at this node convergent with a state outside this clade
131. Palatal ramus of pterygoid (lateral to palatal vacuities if present): narrow/'strap-like' about only as wide as a tooth/tooth row if present] = 0, or broad = 1 N18: 1->0
State at this node convergent with a state outside this clade
235. Interclavicle body shape (excluding parasternal process of present): small scute = 0, triangle longest anteriorly = 1, triangle longest laterally = 2, spatulate or fan-shaped = 3, equilateral triangle = 4 N78: 2->1
State at this node found in an ancestor, thus representing a reversal,
OR convergent with a state outside this clade
282. Pubis ossified = 0, or unossified = 1 N72: 0->1
State at this node convergent with a state outside this clade
297. Distal condyle alignment in extensor view: condyles about level = 0, one condyle extends farther distally = 1 N48: 1->0
State at this node found in an ancestor, thus representing a reversal,
OR convergent with a state outside this clade
298. Tibia and fibula condyles differentiated from each other, including being joined by unfinished bone = 0, or not = 1 N51: 0->1

State at this node convergent with a state outside this clade

==========
below Erpetosaurus - Neldasaurus (branch number 112):
Total changes along branch: 8

Character: Change
57. Postorbital longer than anteroposterior width of orbit: absent = 0, present = 1 C48: 0->1
State at this node found in an ancestor, thus representing a reversal
69. Squamosal contact with tabular: smooth = 0, interdigitating = 1, absent = 2 C60: 2->0
State at this node convergent with a state outside this clade
73. Squamosal contacts tabular: absent = 0, present = 1 C64: 0->1
State at this node convergent with a state outside this clade
77. Tabular shape in dorsal view (aside from horn, if present): rectangle or square = 0, irregular rectangular/quadrangle = 1, elongate oval or teardrop = 2, triangular = 3 N1: 1->3
State at this node found in an ancestor, thus representing a reversal
123. Anterior palatal fenestra: present = 0, absent = 1 N11: 1->0
State at this node found in an ancestor, thus representing a reversal
182. Number of Meckelian openings: more than three = 0, three = 1, two = 2, one = 3 N73: 3->2
State at this node convergent with a state outside this clade
243. Scapulocoracoid without = 0, or with = 1 expanded coracoid plate extending ventromedially R33: 1->0
State at this node found in an ancestor, thus representing a reversal,
OR convergent with a state outside this clade
326. Scale distribution: gastralia present = 0, gastralia and dorsal scales/osteoderms/other dermal ossifications present = 1, no scales = 2 N71: 0->1
State at this node convergent with a state outside this clade

==========
below Erpetosaurus - Trimerorhachis (branch number 113):
Total changes along branch: 12

Character: Change
2. Preorbital region of skull less than twice as wide as long = 0, or at least twice as wide as long = 1 C155: 0->1
State at this node convergent with a state outside this clade
8. Orbit position re snout/postparietal length: centre closer to front than rear = 0, centre near middle = 1, centre closer to rear than front = 2 C164: 1->0
State at this node found in an ancestor, thus representing a reversal
9. Orbit position re snout /quadrate length: centre closer to front than rear = 0, centre near middle = 1, centre closer to rear than front = 2 C165: 1->0
State at this node found in an ancestor, thus representing a reversal
12. Otic notch/temporal ebayment approaching orbit: more than 1/2 postorbital skull length = 0, 1/4-1/2 postorbital skull length = 1, less than 1/4 postorbital skull length = 2 P35: 1->2
State at this node convergent with a state outside this clade
35. Lacrimal contributes to narial margin: absent, excluded by anterior tectal = 0: present = 1, absent, excluded by nasal/maxillary or prefrontal/maxillary suture = 2 C24: 2->1
State at this node found in an ancestor, thus representing a reversal
66. Premaxilla forms part of choanal margin: broadly = 0, point = 1, not, excluded by ?vomer = 2 C57: 2->0
State at this node found in an ancestor, thus representing a reversal

94. Basipterygoid junction: basipterygoid process fits into socket recessed into epipterygoid/pterygoid = 0, pterygoid/epipterygoid forms narrow bar and clasps basipterygoid process fore and aft = 1, pterygoid/epipterygoid and parasphenoid sutured = 2:
State at this node convergent with a state outside this clade
114. Ectopterygoid reaches subtemporal fossa: absent = 0, present = 1 C72: 1->0
State at this node convergent with a state outside this clade
125. Anterior palatal fenestra(e) open(s) on dorsal surface of skull: no = 0, yes = 1 N13: 0->1
State at this node convergent with a state outside this clade
232. Interclavicle anterior edge fimbricated: absent = 0, present = 1 N24: 0->1
State at this node convergent with a state outside this clade
234. Interclavicle parasternal process shape: absent = 0, parallel sided = 1, or tapering = 2 C197: 2->0
State at this node found in an ancestor, thus representing a reversal,
OR convergent with a state outside this clade
263. Humerus length up to and no more than twice its width = 0, or more than twice its width = 1 R49: 0->1
State at this node convergent with a state outside this clade

==========
below Aytonerpeton - Deltaherpeton (branch number 114):
Total changes along branch: 8

Character: Change
22. Frontal anterior margin wedged between nasals: absent = 0, present = 1 C11: 0->1
State at this node convergent with a state outside this clade
24. Intertemporal present: present = 0, absent = 1 C13: 0->1
State at this node found in an ancestor, thus representing a reversal
48. Parietal ? postorbital suture: absent = 0, present = 1 C39: 0->1
State at this node found in an ancestor, thus representing a reversal
57. Postorbital longer than anteroposterior width of orbit: absent = 0, present = 1 C48: 0->1
State at this node found in an ancestor, thus representing a reversal
154. Premaxilla caniniform teeth: absent = 0, present = 1 N20: 0->1
State at this node convergent with a state outside this clade
156. Marginal tooth shape: conical and straight/slightly recurved = 0, small and more or less straight and 'needle-like' = 1, right-trapezoid 'chisel' shape = 2, spearhead shape = 3, thin and greatly recurved = 4 N22: 0->1
Reversed above to a state found in an ancestor
State at this node found in an ancestor, thus representing a reversal
177. Dentary notch: absent = 0, present = 1 C214: 0->1
Reversed above to a state found in an ancestor
State at this node convergent with a state outside this clade
201. Dentary teeth size: same size as maxillary teeth (0), larger than maxillary teeth = 1, smaller than maxillary teeth = 2 C250: 0->1
State at this node convergent with a state outside this clade

==========
below Aytonerpeton - Greererpeton (branch number 115):
Total changes along branch: 6

Character: Change
52. Postfrontal ? prefrontal contact: broad = 0; or point-like = 1 C43: 1->0
State at this node found in an ancestor, thus representing a reversal

69. Squamosal contact with tabular: smooth = 0, interdigitating = 1, absent = 2 C60: 2->1
Changed above to a state convergent with a state outside this clade
State at this node convergent with a state outside this clade
71. Squamosal anterior part lying behind mid-parietal length: present = 0, absent = 1 C62: 1->0
State at this node found in an ancestor, thus representing a reversal
73. Squamosal contacts tabular: absent = 0, present = 1 C64: 0->1
State at this node convergent with a state outside this clade
75. Supratemporal forms part of skull margin posteriorly, including temporal ebayment: absent = 0, present = 1 C66: 1->0
State at this node found in an ancestor, thus representing a reversal
189. Adsymphysial plate fang-pair (distinct from other teeth): absent = 0, present = 1 C141: 0->1
State at this node found in an ancestor, thus representing a reversal

==========
below Aytonerpeton - Pholidogaster (branch number 116):
Total changes along branch: 3

Character: Change
19. Septomaxilla (= ?anterior tectal?) present = 0, absent = 1 C1: 1->0
State at this node found in an ancestor, thus representing a reversal
35. Lacrimal contributes to narial margin: absent, excluded by anterior tectal = 0: present = 1, absent, excluded by nasal/maxillary or prefrontal/maxillary suture = 2 C24: 2->0
State at this node found in an ancestor, thus representing a reversal
136. Maxilla tooth number: > 40 = 0, 30-40 = 1, < 30 = 2 ? C96: 0->2
State at this node found in an ancestor, thus representing a reversal,
OR convergent with a state outside this clade

==========
below Colosteus - Greererpeton (branch number 117):
Total changes along branch: 9

Character: Change
41. Maxilla sutures to prefrontal: absent = 0, present = 1 C30: 0->1
State at this node convergent with a state outside this clade
44. Nasals contribute to narial margin: absent = 0, present = 1 C33: 1->0
State at this node found in an ancestor, thus representing a reversal
63. Prefrontal enters naris: absent = 0, present = 1 ? C54: 0->1
State at this node convergent with a state outside this clade
87. Parietals: more than 2.5 times as long as wide = 0 or less than 2.5 times as long as wide = 1 C224: 1->0
State at this node found in an ancestor, thus representing a reversal
123. Anterior palatal fenestra: present = 0, absent = 1 N11: 1->0
State at this node found in an ancestor, thus representing a reversal
226. Clavicles meet anteriorly: present = 0, absent = 1 C176: 1->0
State at this node found in an ancestor, thus representing a reversal,
OR convergent with a state outside this clade
233. Interclavicle anterior tip: squared = 0, broadly rounded = 1, pointed = 2. N85: 2->0
State at this node found in an ancestor, thus representing a reversal
235. Interclavicle body shape (excluding parasternal process of present): small scute = 0, triangle longest anteriorly = 1, triangle longest laterally = 2, spatulate or fan-shaped = 3, equilateral triangle = 4 N78: 2->1

State at this node found in an ancestor, thus representing a reversal,
OR convergent with a state outside this clade
327. Gastralia: tapered and elongate, four times longer than broad or longer = 0, ovoid = 1, around three times longer than broad one end tapering = 2 C211: 1->0
State at this node found in an ancestor, thus representing a reversal

==========
below Baphetes - Loxomma (branch number 118):
Total changes along branch: 7

Character: Change
19. Septomaxilla (= ?anterior tectal?) present = 0, absent = 1 C1: 1->0
State at this node found in an ancestor, thus representing a reversal
35. Lacrimal contributes to narial margin: absent, excluded by anterior tectal = 0: present = 1, absent, excluded by nasal/maxillary or prefrontal/maxillary suture = 2 C24: 1->0
Changed above to a state convergent with a state outside this clade
State at this node found in an ancestor, thus representing a reversal
43. Median rostral (=internasal): mosaic = 0, paired = 1, single = 2, absent = 3 C32: 3->1
State at this node found in an ancestor, thus representing a reversal
68. Squamosal posterodorsal margin shape: convex = 0, sigmoid or approximately straight = 1, entirely concave = 2 C59: 1->0
State at this node found in an ancestor, thus representing a reversal,
OR convergent with a state outside this clade
103. Parasphenoid depression in body: absent = 0, single median = 1, multiple = 2 C77: 1->2
State at this node convergent with a state outside this clade
107. Parasphenoid carotid grooves: curve round basipterygoid process = 0, lie posteromedial to basipterygoid process (or enter via foramina there) = 1, absent = 2 C81: 2->0
State at this node convergent with a state outside this clade
133. Ectopterygoid row (3+) of smaller teeth: present = 0, absent = 1 C93: 0->1
State at this node found in an ancestor, thus representing a reversal,
OR convergent with a state outside this clade

==========
below Baphetes - Megalocephalus (branch number 119):
Total changes along branch: 6

Character: Change
11. Suspensorium proportions: quadrate to anterior margin of temporal embayment about equal to maximum orbit width (discounting any anterior extensions) = 0, quadrate to anterior margin of temporal embayment < maximum orbit width = 1, quadrate to anterio:
State at this node found in an ancestor, thus representing a reversal
21. Frontal/ parietal length ratio: frontals shorter = 0; longer = 1, subequal = 2 C10: 2->1
State at this node found in an ancestor, thus representing a reversal
45. Nasal ? parietal length ratio less than 1.45 = 0 or greater than 1.45 = 1 C34: 0->1
State at this node convergent with a state outside this clade
50. Parietal shape of anteriormost third: not wider than frontals = 0, at least marginally wider = 1 C41: 1->0
State at this node found in an ancestor, thus representing a reversal
135. Ectopterygoid / palatine shagreen field: absent = 0, present = 1 ? C95: 0->1
State at this node convergent with a state outside this clade
150. Vomerine shagreen field: absent = 0, present = 1 ? C110: 0->1

State at this node convergent with a state outside this clade

==========
below Pederpes - Whatcheeria (branch number 120):
Total changes along branch: 15

Character: Change
27. Intertemporal contacts squamosal: absent = 0, present = 1 C16: 0->1
State at this node convergent with a state outside this clade
29. Jugal contribution to orbit margin: less than one-third = 0, equal to or more than one-third = 1 C18: 0->1
State at this node convergent with a state outside this clade
60. Postparietal occipital flange (="postparietal lappet) exposure: absent = 0, present = 1 C51: 0->1
State at this node convergent with a state outside this clade
78. Tabular horn: absent, tabular does not form horn = 0, tabular forms notable horn = 1 N2: 0->1
State at this node found in an ancestor, thus representing a reversal,
OR convergent with a state outside this clade
81. Tabular occipital flange exposure: absent = 0, extends as far ventrally as does postparietal = 1, extends further ventrally than does postparietal = 2, extends less far than does postparietal= 3 C70: 0->2
State at this node convergent with a state outside this clade
83. Maximum parietal-parietal width is shorter than distance between posterior skull table margin (discounting tabular horn if present) and posterior orbit margin as projected along skull midline: present = 0, absent = 1 C231: 0->1
State at this node convergent with a state outside this clade
119. Pterygoid junction with squamosal: present = 0; absent =1 C87: 0->1
State at this node convergent with a state outside this clade
122. Vomers as broad as long or broader = 0, about twice as long as broad or longer = 1 C91: 0->1
State at this node convergent with a state outside this clade
138. Number of maxilla caniniform teeth: single = 0, multiple = 1 N19: 1->0
State at this node convergent with a state outside this clade
216. Trunk ribs overlapping: absent = 0, or present = 1 N25: 0->1
State at this node convergent with a state outside this clade
220. Ribs (trunk) differ strongly in length and morphology along ?thoracic? region: absent = 0, present = 1 C207: 0->1
State at this node convergent with a state outside this clade
283. Internal trochanter in adult: present = 0, or absent = 1 R108: 0->1
State at this node found in an ancestor, thus representing a reversal,
OR convergent with a state outside this clade
288. Femur shorter than = 0, as long as = 1, or longer than humerus = 2 R112: 2->1
Uniquely derived state, unchanged above
Two or more other states found outside this clade
315. Relative length of foot and rear epopodials: foot equal to or less than length of epipodials = 0, foot longer than epipodials = 1 N60: 1->0
State at this node convergent with a state outside this clade
316. Phalanges shape (manual, non-terminal): longer than wide = 0, about as wide as long = 1, wider than long = 2 N61: 0->1/2
Derived state unclear
Character is uniform outside this clade

B.11 TAXON LIST

Adelospondylus and *Adelogyrinus*
- Sources: (Andrews and Carroll, 1991)

Adamanterpeton
- Sources: (Milner and Sequeira, 1998)

Erpetosaurus
- Sources: (Milner and Sequeira, 2011)

Platyrhinops lyelli
- Sources: (Carroll, 1964; Hook and Baird, 1984, 1986; Clack and Milner, 2009)
- Synonyms: "*Amphibamus lyelli*" (Carroll, 1964) and "*Ichthyacanthus leylli*" (Hook and Baird, 1984)

Archegosaurus
- Sources: (Witzmann, 2005; Witzmann and Schoch, 2006)

Neldasaurus
- Sources: (Chase, 1965; Schoch, 2018)

Capetus
- Sources: (Sequeira and Milner, 1993)

NSM 994GF1.1
- Sources: (Holmes and Carroll, 2010)
- Synonyms: may be referrable to *Callignethelon* (Adams, 2020)
- Notes:
    - For convenience and consistency, we follow the original publication (Holmes and Carroll, 2010) we refer to this OTU by its specimen number NSM 994GF1.1, due to the taxonomic uncertainty expressed therein

Acanthostega
- Sources: (Coates, 1996; Ahlberg and Clack, 1998; Clack, 1998a, 2002a, 2002b; Porro et al., 2015a)

Anthracosaurus
- Sources: (Panchen, 1977, 1981; Clack, 1987a)
- Notes:
    - Insofar as (Clack, 1987a) supersedes (Panchen, 1977) have followed the former

*Anthracosaurus*Plus

- Sources: (Panchen, 1977, 1981; Clack, 1987a)
- Notes:
    - Includes postcranial material attributed to *Anthracosaurus* in (Panchen, 1977) but discounted in (Clack, 1987a)

Archeria

- Sources: (Romer, 1957; Clack and Holmes, 1988; Holmes, 1989), in addition to personal (BKAO) observations
- Specimens studied: MCZ "2049" [unnumbered specimen], "17" [unnumbered specimen], MCZ 201, MCZ 1172, MCZ 1173/1148, MCZ 1238, MCZ 1363, MCZ 2006, MCZ 2045, MCZ 2047, MCZ 2061, MCZ 2063, MCZ 2066, MCZ 2068, MCZ 2072, MCZ 2472, MCZ 2473, MCZ 2495, MCZ 2496, MCZ 2498, MCZ 5655, MCZ 5957, MCZ 6295, MCZ 6555, MCZ 6556, MCZ 6586, MCZ 6811

Eoherpeton

- Sources: (Panchen, 1975; Smithson, 1985)

Palaeoherpeton

- Sources: (Panchen, 1964)
- Taxonomy: formerly *Palaeogyrinus* (Panchen, 1964), renamed in (Panchen, 1970)

Neopteroplax

- Sources: (Romer, 1963), in addition to personal (BKAO) observations
- Specimens studied: USNM 20636

Pholiderpeton scutigerum

- Sources: (Clack, 1987b)

"Eogyrinus" attheyi

- Sources: (Panchen, 1964, 1966, 1972; Clack, 1987b)
- Taxonomy: generically synonymized with *Pholiderpeton* (Clack, 1987b), however see below
- Notes:
    - Despite taxonomic conclusions of (Clack, 1987b), *P. attheyi* and *P. scutigerum* have not been recovered as an exclusive clade in analyses including both (Ruta et al., 2003; Marjanović and Laurin, 2019). In order to distinguish between the two in our dataset, we have used *Eogyrinus* for the '*P. attheyi*' species

EogyrinusPlus

- Sources: (Panchen, 1964, 1966, 1972; Clack, 1987b)
- Taxonomy: see above
- Notes:
    - Differs from *Eogyrinus attheyi* OTU in inclusion of ilium attributed to *Eogyrinus* by (Panchen, 1972)

Proterogyrinus

- Sources: (Romer, 1970; Holmes, 1984) in addition to personal (BKAO) observations
- Specimens studied: CMNH 1111, CMNH 10938, CMNH 10950, CMNH 11035, CMNH 11067, CMNH 11078, CMNH 11091, CMNH 11112, CMNH 11228, CMNH 11241, CMNH 10933, MCZ 2577, MCZ 4537
- Taxonomy: includes *Mauchchunkia bassa* (Hotton, 1970) following (Holmes, 1984) but not *Proterogyrinus pancheni* (Smithson, 1986). *P. pancheni* differs from *P. scheeli* in details of the dentition and vertebrae, but the remains of the latter are highly fragmentary, and we did not feel that either the incorporation of *P. pancheni* into a '*Proterogyrinus* sp.' OTU or the creation of a separate *P. pancheni* OTU would be useful within the context of this analysis

Balanerpeton

- Sources: (Milner and Sequeira, 1993)

Baphetes kirkbyi

- Sources: (Beaumont, 1977; Milner and Lindsay, 1998)
- Notes:
    - Multiple species of *Baphetes* are recognized; we specifically chose *B. kirkbyi* because it is the only one for which postcranial specimens are known (Milner and Lindsay, 1998)

Caerorhachis

- Sources: (Ruta et al., 2002)

Casineria

- Sources: (Paton et al., 1999; Marjanović and Laurin, 2019)

Lethiscus and *Coloraderpeton*

- Sources: (Wellstead, 1982; Anderson, 2003; Anderson et al., 2003; Pardo et al., 2017b)

Dendrepeton

- Sources: (Carroll, 1967; Godfrey et al., 1987; Holmes et al., 1998; Robinson et al., 2005)
- Synonyms: there is some confusion about the specific taxonomy of *Denderpeton* generally and at Joggins in particular. While a more detailed review is pending (T Arbez, H Maddin unpublished data and in prep), it seems likely that the material used here and elsewhere (Ruta et al., 2003; Ruta and Coates, 2007) as *Denderpeton* should probably be referred to *Dendrysekos helogenes* (Marjanović and Laurin, 2019); this convention has recently been adopted by the analysis of (Ruta et al., 2020). (Marjanović and Laurin, 2019) do note that *Denderpeton* and *Dendreysekos* differ in character scores in their dataset, they are generally regarded as sister groups (see discussion in that publication), and they themselves collapse both to a 'Dendrerpetidae OTU'. For the time being we retain usage of *Denderpeton* to provide consistency with previous analyses for purposes of comparison with previous analyses

Doragnathus

- Sources: (Smithson, 1980)
- Notes:
    - Postcranial material has been suggested to belong to *Doragnathus* (Smithson and Clack, 2013). However, this hypothesis is merely suggested, and the authors explicitly advise again referring the material to *Doragnathus*.

Edops

- Sources: (Romer and Witter, 1942)

Eryops

- Sources: (Olson, 1936; Romer and Witter, 1941; Sawin, 1941; Moulton, 1974; Pawley and Warren, 2006) in addition to personal (BKAO) observations
- Specimens studied: MCZ 1931, MCZ 2564

Eucritta

- Sources: (Clack, 2001)

Eusthenopteron

- Sources: (Andrews and Westoll, 1970; Sanchez et al., 2014; Porro et al., 2015a)

Gephyrostegus

- Sources: (Brough and Brough, 1967a; Carroll, 1970; Ahlberg and Clack, 1998; Klembara et al., 2014)

Ichthyostega

- Sources: (Jarvik, 1996; Coates, 2001; Ahlberg et al., 2005; Callier et al., 2009; Clack et al., 2012a; Pierce et al., 2012, 2013a, 2013b)
- Notes:
    - While multiple species of *Ichthyostega* are recognized (Blom, 2005), we have not elected to create separate OTUs, following other analyses (Clack et al., 2016; Pardo et al., 2017b; Clack et al., 2019a) in using what is in effect *Ichthyostega* sp.

Loxomma

- Sources: (Beaumont, 1977; Ahlberg and Clack, 1998)

Megalocephalus

- Sources: (Beaumont, 1977; Ahlberg and Clack, 1998)

Ossinodus

- Sources: (Warren and Turner, 2004; Warren, 2007; Bishop, 2014; Bishop et al., 2015), in addition to personal (BKAO) observations
- Specimens studied: QMF 34280, QMF 34284, QMF 34601, QMF 34610, QMF 34621, QMF 34622, QMF 36907, QMF 36955, QMF 37404, QMF 37405, QMF 37406, QMF 37414, QMF 37415, QMF 37417, QMF 37418, QMF 37426, QMF 37427, QMF 37430, QMF 37432, QMF 37433, QMF 37434, QMF 37436, QMF 37437, QMF 37439, QMF 37440, QMF 37441, QMF 37444, QMF 37449, QMF 37451, QMF 37452, QMF 37453,

QMF 37456, QMF 37483, QMF 37509, QMF 37510, QMF 37512, QMF 37513, QMF 37514

Panderichthys
- Sources: (Vorobyeva, 1995; Ahlberg et al., 1996; Boisvert, 2005, 2009; Boisvert et al., 2008)

Pederpes
- Sources: (Clack, 2002c; Ahlberg et al., 2005; Pierce et al., 2013b; Otoo et al., 2021)

Sigournea
- Sources: (Bolt and Lombard, 2006)

Elpistostege
- Sources: (Schultze and Arsenault, 1985; Cloutier et al., 2020)

Trimerorhachis
- Sources: (Case, 1935; Colbert, 1955; Olson, 1979; Berman and Reisz, 1980; Pawley, 2007; Milner and Schoch, 2013), in addition to personal (BKAO) observations
- Specimens studied: MCZ 2321, MCZ 8245, MCZ 8347, MCZ 8494
- Notes:
    - While multiple species of *Trimerorhachis* have been identified, *T. insignis* was chosen as it is the best-studied and best-known

Ventastega
- Sources: (Ahlberg et al., 1994, 2008)

Westlothiana
- Sources: (Smithson et al., 1993)

Ymeria
- Sources: (Clack et al., 2012a)

Microbrachis
- Sources: (Brough and Brough, 1967b; Carroll and Gaskill, 1978; Vallin and Laurin, 2004; Milner, 2008; Olori, 2015)

Silvanerpeton
- Sources: (Clack, 1993; Ruta and Clack, 2006)

Eldeceeon
- Sources: (Smithson, 1993; Ruta et al., 2020)
- Notes:
    - Insofar as (Smithson, 1993) is superseded by (Ruta et al., 2020), we have followed the latter

Parmastega
- Sources: (Beznosov et al., 2019)

Crassigyrinus

- Sources: (Panchen, 1985; Panchen and Smithson, 1990; Clack, 1997; Herbst and Hutchinson, 2018)
- Notes:
    - Additional comparative data: (Clack et al., 2018; Lennie et al., 2020)

Seymouria

- Sources: (White, 1939; Berman et al., 2000; Klembara et al., 2006; Bazzana et al., 2020a, 2020b)
- Notes:
    - In scoring characters for our *Seymouria* OTU we have, in common with other studies focusing on 'lower' early tetrapods (Clack et al., 2016, 2019a) not distinguished between *Seymouria baylorensis* and *Seymouria sanjuanensis*, creating a '*Seymouria* spp.' OTU. This allowed for greater incorporation of character data, and the interspecific differences were not judged great enough to warrant separate OTUs in this analysis

St Louis Tetrapod

- Sources: (Clack et al., 2012b), pers. obsv. (BKAO)
- Specimens studied: MB.Am.1441 (cast)
- Notes:
    - For convenience and consistency, we follow previous studies (Clack et al., 2012b, 2019a; Marjanović and Laurin, 2019) by referring to this OTU as the 'St Louis tetrapod' rather than its specimen number MB.Am.1441

Aytonerpeton

- Sources: (Otoo, 2015; Clack et al., 2016; Otoo et al., 2018; Ahlberg and Clack, 2020), pers. obsv. (BKAO)
- Specimens studied: UMZC 2015.46b (holotype)

*Aytonerpeton*Plus

- Sources: (Otoo, 2015; Clack et al., 2016; Otoo et al., 2018; Ahlberg and Clack, 2020), pers. obsv. (BKAO)
- Specimens studied: as for *Aytonerpeton* (see above) with additions mentioned below
- Notes:
    - This OTU includes the material attributed to *Aytonerpeton* by Otoo et al. (2018): UMZAC 2016.7 partial skull table, and UMZC 2016.6b parasphenoid. Because the attribution therein is qualified by the observation that both specimens are too large to belong to the *Aytonerpeton* holotype or an individual of similar size, and the phylogenetic placement of *Aytonerpeton* may have significant implicates for node age estimations, we decided it would be worthwhile to create a 'strict' and a 'loose' OTU to test the impact of the referred material

Koilops

- Sources: (Clack et al., 2016)

Colosteus

- Sources: (Hook, 1983), in addition to personal (BKAO) observations of specimens
- Specimens studied: MCZ 2136, MCZ 2158, MCZ 2159

Tiktaalik

- Sources: (Daeschler et al., 2006, 2006; Downs et al., 2008; Shubin et al., 2014; Stewart et al., 2019; Lemberg et al., 2021)

Tulerpeton

- Sources: (Lebedev and Clack, 1993; Lebedev and Coates, 1995)
- Notes:
    - Includes the premaxilla + vomer (PIN 2921/8, 9) and jugal (PIN 2921/36, 37) referred to *Tulerpeton* by Lebedev and Clack (Lebedev and Clack, 1993)

*Tulerpeton*Plus

- Sources: (Lebedev and Clack, 1993; Lebedev and Coates, 1995)
- Notes:
    - Differs from *Tulerpeton* OTU in incorporation of "undertermined tetrapod" material from Andreyevka described by Lebedev and Clack (Lebedev and Clack, 1993): PIN 2921/457 left postborbital and parietal, PIN 2121/41 right postfrontal, PIN 2921/38 left parietal, PIN 2921/458 right tabular, PIN 2921/42 right tabular, PIN 2921/39 right supratemporal, PIN 2921/40 left supratemporal, PIN 2921/3002 right postorbital, PIN 2921/3003 left intertemporal, PIN 2921/447 right tabular, PIN 2921/32 right dentary, PIN 2921/33 left coronoid, 2921/31 right angular

Brittagnathus

- Sources: (Ahlberg and Clack, 2020)

Occidens

- Sources: (Clack and Ahlberg, 2004)

Whatcheeria

- Sources: (Lombard and Bolt, 1995, 2006; Bolt and Lombard, 2000, 2018; Otoo et al., 2021; Rawson et al., 2021)

Greererpeton

- Sources: (Smithson, 1982; Godfrey, 1989a; Bolt and Lombard, 2001, 2010), in addition to personal (BKAO) observations
- Specimens studied: CMNH 9006, CMNH 9008, CMNH 10931, CMNH 11036, CMNH 11040, CMNH 11073, CMNH 11219, CMH 11220, CMNH 11232, CMNH 11233, CMNH 11236, CMNH 11238, CMNH 11319
- Taxonomy: includes '*Greererpeton* sp.' from Goreville (Schultze and Bolt, 1996; Bolt and Lombard, 2001), excepting that material which later classified as *Deltaherpeton* (Bolt and Lombard, 2001, 2010)

Pholidogaster

- Sources: (Romer, 1964; Panchen, 1975)

Deltaherpeton

- Sources: (Bolt and Lombard, 2010)

B.12 CHARACTER LIST

Each character has a unique identifier that represents its source publication, followed by its number in the matrix therein:

- C: (Clack et al., 2019a)
- $C: (Clack et al., 2016)
- P: (Pardo et al., 2017b)
- R: (Ruta, 2011)
- N: this study (these are numbered by their addition)

The new characters are listed below.

1. Tabular shape in dorsal view (aside from horn, if present): U-shaped = 0, small rectangle or square = 1, irregular rectangular/quadrangle = 2, elongate oval or teardrop = 3, triangular = 4 N1
2. Tabular horn: absent, tabular does not form horn = 0, tabular forms notable horn = 1 N2
3. Tabular horn shape: short projection = 0, single elongate projection = 1, double prong (either incipient or two distinct points) = 2 N3
4. (Infraorbital) lateral line relationship to naris: continuous ventral to naris within lateral rostral = 0, discontinuous across ventral naris = 1, discontinuous ventral to naris across maxilla to premaxilla = 2, continuous ventral to naris in maxilla and premaxilla = 3, deflected ventrally and opening to ventral skull margin anterior and posterior to naris = 4, lateral line not present on premaxilla/maxilla = 5 N4
5. Postparietals: present = 0, or absent = 1 N5
6. Postparietals: paired = 0 or fused = 1 N6
7. Frontals: paired = 0 or single = 1 N7
8. Basal plate of parasphenoid, measured posteriorly from basipterygoid processes/basal articulation: about as long as wide = 0, wider than long = 1, longer than wide = 2 N8
9. Parasphenoid basal plate: square/rectangular = 0, or triangular/distinctly tapering at one end = 1 N9
10. Anterior palatal fenestra: present = 0, absent = 1 N11
11. Anterior palatal fenestra: paired = 0, unpaired = 1 N12
12. Anterior palatal fenestra(e) open(s) on dorsal surface of skull: no = 0, yes = 1 N13
13. Interpterygoid vacuities that intersect with orbit: absent = 0, or present = 1 N14
14. Pterygoids meet along midline: yes = 0, or no = 1 N15
15. Median meeting of ptergyoids (measured anteriorly from basal articulation): approximately 1/3 or less of pterygoid length = 0, about 1/2 of pteryoid length = 1, approximately 2/3-3/4 of pterygoid length = 2, almost all or all of pterygoid length = 3 N16
16. Median margin of pterygoid palatal ramus where separate: straight = 0, slightly concave medially = 1, convex medially = 2, greatly concave medially = 3 N17
17. Palatal ramus of pterygoid (lateral to palatal vacuities if present): narrow/'strap-like' about only as wide as a tooth/tooth row if present] = 0, or broad = 1 N18
18. Number of maxilla caniniform teeth: single = 0, multiple = 1 N19
19. Premaxilla caniniform teeth: absent = 0, present = 1 N20
20. Number of premaxilla caniniform teeth: single = 0, multiple = 1 N21

21. Marginal tooth shape: conical and straight/slightly recurved = 0, small and more or less straight and 'needle-like' = 1, right-trapezoid 'chisel' shape = 2, spearhead shape = 3, thin and greatly recurved = 4 N22
22. Labyrinthine infolding on teeth: present = 0, or absent = 1 N23
23. Interclavicle anterior edge fimbriated: absent = 0, present = 1 N24
24. Trunk ribs overlapping: absent = 0, or present = 1 N25
25. Uncinate processes shape: pointed and triangular = 0, or broad and either rounded or rectangular = 1 N26
26. Forelimbs/paired pectoral appendages: present = 0, absent = 1 N27
27. Ossified pectoral girdle: present = 0, absent = 1 N28
28. Dermal ornament on cleithrum: present = 0, or absent = 1 N29
29. Shape of ventral clavicle plate: elongate triangle = 0, sub-equilateral triangle = 1, spoon-shaped/spatulate/ovoid = 2 N30
30. Interclavicle: present = 0, or absent = 1 N31
31. Scapulocoracoid: present, including only scapular or coracoid portion = 0, or absent = 1 N32
32. Scapulocoracoid: present, including only scapular or coracoid portion = 0, or absent = 1 N32
33. Percentage of humerus posterior margin proximal to entepicondyle, measured from proximal base of entepicondyle: about a third or less = 0, about half = 1, about two thirds = 2, more than two thirds = 3 N33
34. Entepicondyle shape: three-dimmensional spike = 0, dorsoventrally flattened rectangle or trapezoid = 1, dorsoventrally flattened triangle = 2 N34
35. Deltopectoral crest present = 0, separate deltoid and pectoral processes = 1, only pectoral process = 2, none of these = 3 N35
36. (Ossified) pelvic girdle at least in part: present = 0, absent = 1 N37
37. Number of ilium dorsal processes: one = 0, two = 1 N38
38. Ilium dorsalmost process (one that articulates with sacral rib) orientation: straight dorsal = 0, canted posteriorly = 1, canted anteriorly = 2 N39
39. Internal torchanter/proximal end of adductor blade relationship to proximal head of femur in adult: separated by deep and clear notch of finished bone = 0, separated by broad open space = 1, on ridge continuous with proximal head of femur = 2 N40
40. Fourth trochanter of femur absent = 0, or present = 1 R110
41. Fourth trochanter shape: short and narrow = 0, short and broad with flat top = 1, long rugose region = 2, short rugose region = 3, nub or bump = 4 N41
42. Adductor blade: present = 0, absent =1 N42
43. Adductor blade length: occupying most or all of the femur length = 0, restricted to midshaft = 1, restricted to proximal part of femur = 2 N43
44. Adductor blade shape in adult: broad rectangular blade = 0, narrow blade = 1, broad ridge = 2, narrow parallelogram = 3, spike or prong = 4 N44
45. Adductor crest length: shorter than adductor blade = 0, similar length to adductor blade = 1, longer than adductor blade = 2 N46
46. Tibia and fibula condyles greatest width in distal view: equal = 0, tibia condyle broader = 1, fibula condyle broader = 2 N47
47. Distal condyle alignment in extensor view: condyles about level = 0, one condyle extends farther distally = 1 N48

48. Tibia and fibula condyles differentiated from each other, including being joined by unfinished bone = 0, or not = 1 N51
49. Relative lengths of hindlimb epipodials and femur: epipodials less than 50% of femur length = 0, about 50% femur length = 1, or >50% of femur length = 2 N52
50. Interepipodial space: present = 0, or absent = 1 N53
51. Interepipodial space shape: elongate tapering oval/'spindle shaped' = 0, broad, elongate oval/subrectangle = 1, small circle that does not reach ends of epipodials = 2 N54
52. Manus digits: absent = 0, or present = 1 N55
53. Manus digit number: eight = 0, six = 1, five = 2, four = 3, three = 4 N56
54. Pes digits: absent = 0, or present = 1 N57
55. Pes digit number: eight = 0, seven = 1, six = 2, five = 3 N58
56. Relative length of foot and rear epopodials: foot equal to or less than length of epipodials = 0, foot longer than epipodials = 1 N60
57. Phalanges shape (manual, non-terminal): longer than wide = 0, about as wide as long = 1, wider than long = 2 N61
58. Phalanges shape (pedal, non-terminal): longer than wide = 0, about as wide as long = 1, wider than long = 2 N62
59. Phalanges cross-section shape (manual): circular = 0, square-shaped or elongate oval-shaped = 1, convex upwards = 2 N63
60. Phalanges cross-section shape (pedal): square or elongate oval =0, convex upwards = 1, circular = 2 N64
61. Wrist ossifications in adult: fully ossified = 0, or fully unossified = 1, or partially ossified = 2 N65
62. Ankle ossifications: fully ossified = 0, or fully unossified = 1, or partially ossified = 2 N66
63. Intermedium contacts interepipodial space in forelimb: yes = 0, or no = 1 N67
64. Intermedium contacts interepipodial space in hindlimb: yes = 0, or no = 1 N68
65. Intermedium (hindlimb) contribution to interepipodial space: forms most/all of distal margin as a trough = 0, in line with distal end of fibula = 1 N69
66. Full-body scale covering: present = 0, absent = 1 N70
67. Scale distribution: gastralia present = 0, gastralia and dorsal scales/osteoderms/other dermal ossifications present = 0, no scales = 2 N71
68. Ossified branchial arches/gill supports in adult: present = 0, or absent = 1 N72
69. Number of Meckelian openings: more than three = 0, three = 1, two = 2, one = 3 N73
70. Meckelian opening(s): face ventrally = 0, or mesially = 1 N74
71. Meckelian opening(s) without ventromesial bony margin = 0, or with ventromesial bony margin = 1 N75
72. Dermal ornament character: Pit-and-ridge with visible center of ossification = 0, pit-and-ridge with no obvious center of ossification = 1, irregular pit-and-ridge with no obvious center of ossification =2, short radiating grooves = 3, pitted = 4, irregular pitting with prominent pits on dorsal surface of snout = 5, ornament very faint or absent = 6, irregular pores = 7 N76
73. Center of ornament on squamosal: no center of ornamentation= 0, center closer to dorsal apex of temporal embayment = 1, center closer to posteroventral margin of squamosal = 2 N77

74. Interclavicle body shape (excluding parasternal process of present): small scute = 0, triangle longest anteriorly = 1, triangle longest laterally = 2, spatulate or fan-shaped = 3, equilateral triangle = 4 N78
75. Interclavicle parasternal process length: equal to rest of interclavicle = 0 or longer than rest of interclavicle = 1 N79
76. Trunk pleurocentrum height relative to intercentrum height: pleurocentrum less than intercentrum = 0, same as intercentrum = 1, greater than intercentrum = 2, intercentrum and pleurocentrum fused into single bone (holospondylous) = 3 N80
77. Centra (trunk) intercentra fused middorsally: absent = 0, present = 1 N81
78. Centra (trunk) intercentra fused midventrally: absent = 0, present = 1 N82
79. Neural arches of trunk vertebrae: not fused to centra = 0; fused to pleurocentrum or combined centrum = 1 N83
80. Angle between proximal and distal ends of humerus: 30 degrees or less = 0, 31-60 degrees = 1, more than 60 degrees = 2 N84
81. Interclavicle anterior tip: squared = 0, broadly rounded = 1, pointed = 2. N85

The full character list is presented below, with comments on characters and taxa as deemed useful. References for all citations in this document are included at the end. The character list is also presented in a separate spreadsheet file, which contains additional numerical information, as well as character partition assignments.

1. Skull longer than broad = 0, as broad as long =1, or broader than long = 2 C154
2. Preorbital region of skull less than twice as wide as long = 0, or at least twice as wide as long = 1 C155
3. Internarial/ interpremaxillary fenestra (independent of presence of median rostrals) on dorsal surface of skull: absent = 0, present = 1 C157
    a. *Erpetosaurus* (Milner and Sequeira, 2011) and *Trimerorhachis* (Milner and Schoch, 2013) have small holes in the premaxilla which open to the dorsal surface of the skull; the presumably accommodated the dentary fangs in life. We regard these as fundamentally different from internarial/interpremaxillary fenestrae
    b. The dorsal snout surface of *Greererpeton* in the reconstruction of Smithson (Smithson, 1982) is imperforate. However, attributed specimens from Goreville, Illinois (Schultze and Bolt, 1996) show a single fenestra. We have therefore scored as present, following the attribution of the specimens therein to '*Greererpeton sp.*' (for practical purposes synonymous with *Greererpeton burkemorani*) until the specimens are fully described and any necessary taxonomic adjustments are made
4. Interorbital distance compared with maximum orbit diameter: greater = 0, smaller = 1, subequal = 2 C158
5. Naris position: ventral rim closer to jaw margin than height of naris = 0, distance to jaw margin similar to or greater than height of naris = 1 C160
6. Naris shape: ventrally facing = 0, dorsolaterally facing = 1 C162
7. Orbit shape: round, circle or oval = 0; square or rectangular = 1, triangular = 2, anterior projection giving orbit 'keyhole' shape = 3 C163
    a. Modified from the original with the inclusion of state three to represent *Anthracosaurus* (Panchen, 1977; Clack, 1987a)
8. Orbit position re: snout/postparietal length: centre closer to front than rear = 0, centre near middle = 1, centre closer to rear than front = 2 C164
9. Orbit position re: snout /quadrate length: centre closer to front than rear = 0, centre near middle = 1, centre closer to rear than front = 2 C165
10. Pineal foramen position along interparietal suture: behind midpoint = 0, at the midpoint = 1, anterior to midpoint = 2 C166
11. Suspensorium proportions: quadrate to anterior margin of temporal embayment about equal to maximum orbit width (discounting any anterior extensions) = 0, quadrate to anterior margin of temporal embayment < maximum orbit width = 1, quadrate to anterior margin of temporal embayment > maximum orbit width = 2 C167
12. Temporal embayment (="otic notch") approaching orbit: more than 1/2 postorbital skull length = 0, 1/4-1/2 postorbital skull length = 1, less than 1/4 postorbital skull length = 2 P35
13. Skull table shape: longer than broad = 0, approximately square = 1, shorter than broad = 2 C169

    a. Here we define the skull table as consisting of the following bones: postorbitals, parietals, surpatemporals, intertemporals, postparietals, and tabulars. Not all these bones are present in all taxa. This definition follows the one used (both implicitly and explicitly) by workers such as Panchen, Clack, Ahlberg, and Ruta (Panchen, 1972; Smithson, 1982, 1985, 1985; Clack, 1987a, 1987b; Ruta and Clack, 2006; Clack and Milner, 2009; Ruta et al., 2020). In particular we here specify the exclusion of the frontals, as their exclusion would cause very nearly all taxa to be scored as 'longer than broad'

14. Dermal ornament character: Pit-and-ridge with visible center of ossification = 0, pit-and-ridge with no obvious center of ossification = 1, irregular pit-and-ridge with no obvious center of ossification =2, short radiating grooves = 3, pitted = 4, irregular pitting with prominent pits on dorsal surface of snout = 5, ornament very faint or absent = 6, irregular pores = 7 N76
    a. Dermal ornament in early tetrapods is highly variable both between taxa and across the ornamented surfaces of the dermal skeleton (the skull in particular). A regular 'pit and ridge' pattern, consisting of hexagonal or polygonal pits separated by ridges that together produce a honeycomb-like appearance, seems to be plesiomorphic for early tetrapod and possibly tetrapodomorphs generally (Jeffery, 2012). A reduction and eventual in dermal ornament have long been considered a characteristic of the amniote total group (Carroll, 1970). For this character the objective was to capture more variation in dermal ornament pattern to reveal possible synapomorphies and character state trends. Given variation in ornament (see above), each state represents a generalization of the cranial ornament
    b. Replaces C170
    c. State one is present in *Ichthyostega* (Jarvik, 1996); state two is present in *Acanthostega* (Coates, 1996; Clack, 2002a; Porro et al., 2015a); state three is present in *Adelospondylus* (Andrews and Carroll, 1991) and *Pholiderpeton scutigerum* (Clack, 1987b); state four is present in *Proterogyrinus* (Holmes, 1984); state five is present in *Caerorhachis* (Ruta et al., 2002); state six is present in "*Eogyrinus*" *attheyi* (Panchen, 1964, 1972); state seven is present in *Anthracosaurus* (Panchen, 1977, 1981; Clack, 1987a) and *Whatcheeria* (Lombard and Bolt, 1995, 2006); state seven is present in the St Louis tetrapod (Clack et al., 2012b)
15. Center of ornament on squamosal: no center of ornamentation= 0, center closer to dorsal apex of temporal embayment = 1, center closer to posteroventral margin of squamosal = 2 N77
    a. State one is present in *Dendrerpeton* (Godfrey et al., 1987; Holmes et al., 1998)*;* state two is present in *Balanerpeton* (Milner and Sequeira, 1993); state three is present in *Ichthyostega* (Jarvik, 1996)
16. Operculum (=opercular) present = 0, or absent = 1 C245
17. Jaw articulation position: posterior to occiput = 0, level with occiput = 1, anterior to occiput = 2 C222
18. Ossified branchial arches/gill supports in adult: present = 0, or absent = 1 N72
19. Septomaxilla (= "anterior tectal") present = 0, absent = 1 C1
    a. Here the septomaxilla is defined as: "accessory dermal bone associated with naris having surface ornament and absent lateral line canal" (Clack et al., 2016, 2019a)

    b. The above definition of septomaxilla has been moved from within the character itself (its original state) to the gloss here, to improve clarity and simplicity
20. Septomaxilla: narial opening ventral to it = 0: narial opening anterior to it = 1 C2
    a. Modified as C1 (see above)
21. Frontal/parietal length ratio: frontals shorter = 0; longer = 1, subequal = 2 C10
22. Frontal anterior margin wedged between nasals: absent = 0, present = 1 C11
23. Frontal/nasal length ratio: frontals approximately equal to or less than one-third as long as nasals = 0, more than one-third as long = 1 C12
24. Intertemporal present: present = 0, absent = 1 C13
25. Intertemporal smaller than supratemporal = 0, or larger than/comparable in size with supratemporal = 1 C14
26. Intertemporal lateral edge: not interdigitating with cheek = 0, interdigitates = 1 C15
    a. This character is about the contact between the bones- observable from the surface- as opposed to the actual 3D architecture of the suture
27. Intertemporal contacts squamosal: absent = 0, present = 1 C16
28. Jugal deep below orbit (vs narrow process): > 50% orbit diam = 0, <50% = 1 C17
29. Jugal contribution to orbit margin: less than one-third = 0, equal to or more than one-third = 1 C18
30. Jugal alary process ("insula jugalis") on palate: absent = 0, present = 1 C19
31. Jugal length of postorbital region relative to one-third of the length of the postorbital cheek region: greater = 0 or less =1 0 C20
32. Jugal extends anterior to anterior orbit margin: absent = 0, present = 1 C21
33. Jugal excluded from lower jaw margin by maxilla and quadratojugal: yes = 0, or no = 1 C22
34. Jugal V-shaped indentation of posterodorsal margin: absent = 0, present = 1 C23
35. Lacrimal contributes to narial margin: absent, excluded by anterior tectal = 0: present = 1, absent, excluded by nasal/maxillary or prefrontal/maxillary suture = 2 C24
36. Lacrimal reaches orbit margin (= prefrontal/ jugal suture): present = 0, absent = 1 C25
37. Maxilla sutures to vomer: absent = 0, present = 1 C26
38. Maxilla external contact with premaxilla: narrow contact point not interdigitated = 0, interdigitating suture = 1 C27
39. Maxilla highest point in posterior half = 0, anterior third of its length = 1, or at its midlength = 2, or same height all along length =3 C28
40. Maxilla extends behind level of posterior margin of orbit: present = 0, absent = 1 C29
41. Maxilla sutures to prefrontal: absent = 0, present = 1 C30
42. Maxilla/premaxilla contact shelf-like mesial to tooth row on palate: absent = 0, present = 1 C31
43. Median rostral (=internasal): mosaic = 0, paired = 1, single = 2, absent = 3 C32
44. Nasals contribute to narial margin: absent = 0, present = 1 C33
45. Nasal/ parietal length ratio less than 1.45 = 0 or greater than 1.45 = 1 C34
46. Nasal smaller in area than postparietal: absent = 0, present = 1 C35
47. Parietal meets tabular: absent = 0, present = 1 C38
48. Parietal/postorbital suture: absent = 0, present = 1 C39
49. Parietal anterior portion extent relative to orbit midlength: in front of = 0, level with = 1, posterior to = 2 C40

50. Parietal shape of anteriormost third: not wider than frontals = 0, at least marginally wider = 1 C41
51. Parietal/postparietal suture strongly interdigitated: absent = 0, present = 1 C42
52. Postfrontal/prefrontal contact: broad = 0; or point-like = 1 C43
53. Postfrontal/prefrontal suture: anterior half of orbit = 0, middle or posterior half of orbit = 1, absent = 2 C44
54. Postorbital suture to skull table (usually intertemporal or supratemporal when present) interdigitating vs smooth: smooth = 0, interdigitating = 1 C45
55. Postorbital without distinct dorsomedial ramus for postfrontal = 0, with incipient ramus = 1, with elongate ramus = 2 C46
56. Postorbital shape: irregularly polygonal = 0, broadly cresentic and narrowing to a posterior point = 1 C47
57. Postorbital longer than anteroposterior width of orbit: absent = 0, present = 1 C48
58. Postorbital at least one quarter of the width of the skull table at the same transverse level: absent = 0, present = 1 C49
59. Postparietal: longer than wide = 0, approximately square or pentagonal = 1, wider than long = 2, triangular and about as long as wide = 3 C50
60. Postparietal occipital flange (="postparietal lappet) exposure: absent = 0, present = 1 C51
61. Postparietal/exoccipital suture: absent = 0, present = 1 C52
62. Prefrontal less than three times longer than wide: present = 0, more than, = 1 C53
63. Prefrontal enters naris: absent = 0, present = 1 C54
64. Prefrontal contributes to half or more than half anteromesial orbit margin = 0, less than half = 1 C55
65. Premaxilla posterodorsal alary process onto snout: absent = 0, present = 1 C56
66. Premaxilla forms part of choanal margin: broadly = 0, point = 1, not, excluded by vomer = 2 C57
67. Preopercular present = 0, absent = 1 C58
68. Squamosal posterodorsal margin shape: convex = 0, sigmoid or approximately straight = 1, entirely concave = 2 C59
69. Squamosal contact with tabular: smooth = 0, interdigitating = 1, absent = 2 C60
70. Squamosal-supratemporal suture position: at apex of temporal embayment = 0, dorsal to apex = 1, ventral to apex = 2 C61
71. Squamosal anterior part lying behind mid-parietal length: present = 0, absent = 1 C62
72. Squamosal suture with supratemporal: absent = 0, present = 1 C63
73. Squamosal contacts tabular: absent = 0, present = 1 C64
74. Supratemporal present as a separate ossification: present = 0, absent = 1 C65
75. Supratemporal forms part of skull margin posteriorly, including temporal ebayment: absent = 0, present = 1 C66
76. Supratemporal descending flange on occiput: absent = 0; present = 1. P4
77. Tabular shape in dorsal view (aside from horn, if present): U-shaped = 0, small rectangle or square = 1, irregular rectangular/quadrangle = 2, elongate oval or teardrop = 3, triangular = 4 N1
    a. This is one of a set of characters (N1, N2, N3) designed to better capture variation in the tabular horn. This character specifically is designed to assess the shape of the tabular separately from the horn (if present). That way tabular morphology

can be captured regardless of whether or not a horn is present. Tabular horns are widely distributed, and may be diagnostic of some groups; biramous tabular horns have been suggested an a synapomorphy of Embolomeri (Smithson, 1985); while not all embolomeres have biramous tabular horns, to date biramous tabular horns are only found in embolomeres, and may be the primitive state for the group

   b. State one is present in *Whatcheeria* (Lombard and Bolt, 1995; Otoo et al., 2021); state two is present in *Ichthyostega* (Jarvik, 1996); state three is present in *Greererpeton* (Smithson, 1982; Schultze and Bolt, 1996); state four is present in *Crassigyrinus* (Clack, 1997)

78. Tabular horn: absent, tabular does not form horn = 0, tabular forms notable horn = 1 N2
   a. This is a contingent character with N1 and N3
79. Tabular horn shape: short projection = 0, single elongate projection = 1, double prong (either incipient or two distinct points) = 2 N3
   a. State one is present in *Whatcheeria* (Lombard and Bolt, 1995; Otoo et al., 2021) and *Pederpes* (Clack and Finney, 2005); state two is present in *Acanthostega* (Clack, 2002a; Porro et al., 2015a) and *Archeria* (Holmes, 1989); state three is present in *Proterogyrinus* (Holmes, 1984) and *Anthracosaurus* (Panchen, 1977; Clack, 1987a)
80. Tabular prolonged posterolateral ornamented surface absent = 0, present = 1 C68
81. Tabular occipital flange exposure: absent = 0, extends as far ventrally as does postparietal = 1, extends further ventrally than does postparietal = 2, extends less far than does postparietal= 3 C70
82. (Infraorbital) lateral line relationship to naris: continuous ventral to naris within lateral rostral = 0, discontinuous across ventral naris = 1, discontinuous ventral to naris across maxilla to premaxilla = 2, continuous ventral to naris in maxilla and premaxilla = 3, deflected ventrally and opening to ventral skull margin anterior and posterior to naris = 4, lateral line not present on premaxilla/maxilla = 5 N4
   a. This character is based on the description of *Deltaherpeton* (Bolt and Lombard, 2010), wherein the authors survey the conditions of the infraorbital lateral line in the context of reevaluating colosteid synapomorphies
   b. State one is present in *Ichthyostega* (Jarvik, 1996); state two is present in "*Eogyrinus*" *attheyi* (Panchen, 1972); state three is present in *Acanthostega* (Clack, 2002a; Porro et al., 2015a); state four is present in *Trimerorhachis* (Milner and Schoch, 2013); state five is present in *Aytonerpeton* (Otoo, 2015; Clack et al., 2016), *Colosteus* (Hook, 1983), *Greererpeton* (Smithson, 1982; Schultze and Bolt, 1996), and *Deltaherpeton* (Bolt and Lombard, 2010)- its state in *Pholidogaster* is currently unknown; state six is present in *Eryops* (Sawin, 1941)
83. Maximum parietal-parietal width is shorter than distance between posterior skull table margin (discounting tabular horn if present) and posterior orbit margin as projected along skull midline: present = 0, absent = 1 C231
84. Maxilla contribution to orbit margin: absent = 0, or present = 1 C239
85. Postparietals: present = 0, or absent = 1 N5
86. Postparietals: paired = 0 or fused = 1 N6
87. Parietals: more than 2.5 times as long as wide = 0 or less than 2.5 times as long as wide = 1 C224

88. Temporal fenestra: absent = 0, present = 1 C238
89. Frontal: absent = 0, present = 1 C244
90. Frontals: paired = 0 or single = 1 N7
91. Basioccipital: indistinguishable from exoccipitals = 0, separated by suture = 1 C3
92. Basioccipital: ventrally exposed portion longer than wide = 0, shorter than wide = 1 C4
93. Basioccipital condyle (= contribution to occipital condyle) : absent, notochordal = 0 present = 1 C5
94. Basipterygoid junction: basipterygoid process fits into socket recessed into epipterygoid/pterygoid = 0, pterygoid/epipterygoid forms narrow bar and clasps basipterygoid process fore and aft = 1, pterygoid/epipterygoid and parasphenoid sutured = 2 C6
95. Exoccipitals contact skull table bone(s) (usually postparietal) on occiput: absent = 0, present =1 C7
96. Exoccipital contributes to condyle: absent = 0, present = 1 C8
97. Exoccipitals enlarged to form double horizontally orientated occipital condyle, (may exclude basioccipital from articular surface): absent = 0, present = 1 C9
98. Opisthotic forms substantial plate (with supraoccipital if present) beneath skull table, separating it from the exoccipitals: present = 0, absent = 1 C37
99. Basicranial fissure (=ventral cranial fissure): present = 0, absent = 1. P210
100. Parasphenoid cultriform process shape: biconvex = 0, narrowly triangular =1, parallel-sided = 2, or with proximal constriction followed by swelling = 3 C76
    a. Biconvex here basically means teardrop-like (convex laterally on each side)
101. Basal plate of parasphenoid, measured posteriorly from basipterygoid processes/basal articulation: about as long as wide = 0, wider than long = 1, longer than wide = 2 N8
102. Parasphenoid basal plate: square/rectangular = 0, or triangular/distinctly tapering at one end = 1 N9
103. Parasphenoid depression in body: absent = 0, single median = 1, multiple = 2 C77
104. Parasphenoid posterolateral wings (ridged): absent = 0, present = 1 C78
105. Parasphenoid wings: separate = 0, joined by web of bone = 1 C79
106. Parasphenoid contacts or sutures to vomers: present = 0, absent = 1 C80
107. Parasphenoid carotid grooves: curve round basipterygoid process = 0, lie posteromedial to basipterygoid process (or enter via foramina there) = 1, absent = 2 C81
108. Parasphenoid/basisphenoid ventral cranial fissure: not sutured = 0, sutured but traceable = 1, eliminated = 2 C82
109. Anterior extent of cultriform process along palate: ends nearer choana posterior margin = 0, or ends nearer orbit posterior margin = 1 P201
110. Posterior extent of parasphenoid beneath braincase: floors sphenoid region only (0); floors sphenoid and otic regions = 1; floors sphenoid, otic, and occipital regions = 2 P205
111. Basal tubera (='basal tuberosities', swellings, bumps, or eminences on underside of braincase/parasphenoid): present = 0, or absent = 1 N10
    a. These features have recently been discussed as possible evidence of bony gill attachments and cited as support for the hypothesis that both aistopods and embolomeres are stem tetrapods (Pardo et al., 2017b, 2019). This character was

added to assess their presence among taxa in the dataset, and in anticipation its use in a potentially more endocranially-focused analysis

b. State one is present in *Pederpes* (Clack and Finney, 2005) and *Archeria* (Clack and Holmes, 1988; Holmes, 1989); state two is present in *Proterogyrinus* (Holmes, 1984)

112. Buccohypophyseal foramen in parasphenoid: open = 0, absent = 1. P208

113. Ectopterygoid as long or longer than palatines: present = 0, absent = 1 C71

114. Ectopterygoid reaches subtemporal fossa: absent = 0, present = 1 C72

115. Ectopterygoid/ palatine exposure: more or less confined to tooth row = 0, broad mesial exposure (additional to tooth row if present) = 1 C73

116. Pterygoids flank parasphenoid for most of length of cultriform process = 0, not so = 1 C84

117. Pterygoid quadrate ramus margin in adductor fossa: concave = 0, with some convex component = 1 C85

118. Pterygoids not visible in lateral aspect below ventral margin of jugal and quadratojugal = 0, or visible = 1 C86

119. Pterygoid junction with squamosal: present = 0; absent =1 C87

120. Vomers separated by parasphenoid > half vomer mesial length: present = 0, absent = 1 C88

121. Vomers separated by pterygoids: for > half length = 0, < half length = 1, not separated by pterygoids = 2 C89

122. Vomers as broad as long or broader = 0, about twice as long as broad or longer = 1 C91

123. Anterior palatal fenestra: present = 0, absent = 1 N11

a. This character is part of a set of contingent characters (N11, N12, N13, N14) designed to capture the conditions of the anterior palatal fenestra(e). Together they serve as a replacement for C56

b. State one is present in *Erpetosaurus* (Milner and Sequeira, 2011); state two is present in *Platyrhinops* (Clack and Milner, 2009)

124. Anterior palatal fenestra: paired = 0, unpaired = 1 N12

a. This character is part of a contingent set (see N11)

b. State one is present in *Neldasaurus* (Schoch, 2018); state two is present in *Ichthyostega* (Jarvik, 1996)

125. Anterior palatal fenestra(e) open(s) on dorsal surface of skull: no = 0, yes = 1 N13

a. This character is part of a contingent set (see N11)

b. State one is present in *Neldasaurus* (Schoch, 2018); state two is present in *Trimerorhachis* (Milner and Schoch, 2013)

126. Interpterygoid vacuities that intersect with orbit: absent = 0, or present = 1 N14

a. This character is part of a contingent set (N14, N15, N16, N17, N18) designed to better capture the morphology of the interpterygoid vacuities. Interpterygoid vacuities are current regarded as a synapomorphy of temnospondyls (Schoch, 2013) and one of the characters placing lissamphibians within temnospondyls (Ruta and Coates, 2007; Schoch, 2019). However, interpterygoid vacuities of various sizes are widely distributed across early tetrapods (see Further Character Discussion)

127. Pterygoids meet along midline: yes = 0, or no = 1 N15
    a. See gloss for N14
    b. State one is present in *Acanthostega* (Porro et al., 2015a); state two is present in *Eryops* (Sawin, 1941)
128. Median meeting of ptergyoids (measured anteriorly from basal articulation): approximately 1/3 or less of pterygoid length = 0, about 1/2 of pteryoid length = 1, approximately 2/3-3/4 of pterygoid length = 2, almost all or all of pterygoid length = 3 N16
    a. See gloss for N14
    b. State one is present in *Acanthostega* (Porro et al., 2015a); state two is present in *Proterogyrinus* (Holmes, 1984); state three is present in *Ossinodus* (Warren, 2007); state four is present in *Megalocephalus* (Beaumont, 1977)
129. Vomer contributes to interpterygoid vacuity: absent = 0, present = 1 C90
130. Median margin of pterygoid palatal ramus where separate: straight = 0, slightly concave medially = 1, convex medially = 2, greatly concave medially = 3 N17
    a. See gloss for N14
    b. State one is present in *Whatcheeria* (Bolt and Lombard, 2018); state two is present in *Proterogyrinus* (Holmes, 1984); state three is present in (Ruta et al., 2020); state four is present in *Balanerpeton* (Milner and Sequeira, 1993)
131. Palatal ramus of pterygoid (lateral to palatal vacuities if present): narrow/'strap-like' about only as wide as a tooth/tooth row if present] = 0, or broad = 1 N18
    a. See gloss for N14
    b. State one is present in *Trimerorhachis* (Milner and Schoch, 2013); state two is present in *Whatcheeria* (Bolt and Lombard, 2018)
132. Ectopterygoid fang pairs: present = 0, absent = 1 C92
133. Ectopterygoid row (3+) of smaller teeth: present = 0, absent = 1 C93
134. Ectopterygoid denticle row lateral to tooth row: present = 0, absent = 1 C94
135. Ectopterygoid / palatine shagreen field: absent = 0, present = 1 C95
136. Maxilla tooth number: > 40 = 0, 30-40 = 1, < 30 = 2 C96
137. Maxillary caniniform teeth (about twice the size of neighbouring teeth): absent = 0, present = 1 C97
138. Number of maxilla caniniform teeth: single = 0, multiple = 1 N19
    a. Maxillary caniniform (markedly larger than nearby teeth, usually approximately twice the size) teeth have been proposed (Warren and Turner, 2004; Warren, 2007) as a synapomorphies of whatcheeriids (inclusive of *Ossinodus*), and were discussed in (Otoo et al., 2021)
    b. State one is present in *Whatcheeria* (Lombard and Bolt, 1995; Bolt and Lombard, 2018; Otoo et al., 2021); state two is present in *Ossinodus* (Warren and Turner, 2004; Warren, 2007)
139. Palatine fang pairs: present = 0, absent = 1 C98
140. Palatine row of smaller teeth: present = 0, absent = 1 C99
141. Palatine denticle row lateral to tooth row: present = 0, absent = 1 C100
142. Parasphenoid shagreen field: present = 0, absent = 1 C101
143. Parasphenoid shagreen field anterior and posterior to basal articulation = 0, posterior to basal articulation only = 1, anterior to basal articulation only = 2 C102

144. Pterygoid shagreen: dense = 0, a few discontinuous patches or absent = 1 C103
145. Premaxillary tooth number: > 15 = 0, 10 - 14 = 1, < 10 = 2 C105
146. Vomer fang pairs: present = 0, absent = 1 C106
147. Vomerine fang pairs noticeably smaller than other palatal fang pairs: absent = 0, present = 1 C107
148. Vomer anterior wall forming posterior margin of palatal fossa bears tooth row meeting in midline: present = 0, absent = 1 C108
149. Vomerine row of small teeth : present = 0, absent = 1 C109
150. Vomerine shagreen field: absent = 0, present = 1 C110
151. Vomerine denticle row lateral to tooth row: present = 0, absent = 1 C111
152. Vomer with toothed anterolateral crest: present = 0, absent = 1 C112
153. Upper marginal teeth number: greater than lower = 0, same = 1, smaller than lower = 2 C113
154. Premaxilla caniniform teeth: absent = 0, present = 1 N20
    a. This character is part of a contingent set with N21 to capture the number and morphology of the premaxillary caniniform teeth. Premaxillary caniniform teeth (also referred to as premaxillary fangs) with an accompanying dentary notch is a colosteid synapomorphy (Hook, 1983; Godfrey, 1989a; Bolt and Lombard, 2010); its presence in the dvinosaur *Erpetosaurus* has been the source of previous taxonomic confusion (Milner and Sequeira, 2011). The St Louis tetrapod (Clack et al., 2012b) and *Aytonerpeton* (Otoo, 2015; Clack et al., 2016) have one and two premaxillary caniniform teeth, respectively and have been proposed to have colosteid affinities. These two characters allow for assessment of the presence and number of premaxillary fangs across the taxa in the dataset
    b. State on is present in *Megalocephalus* (Beaumont, 1977); state two is present in *Whatcheeria* (Lombard and Bolt, 1995; Bolt and Lombard, 2018)
155. Number of premaxilla caniniform teeth: single = 0, multiple = 1 N21
    a. See gloss for N22
    b. State one is *Eryops* (Sawin, 1941); state two is present in *Aytonerpeton* (Otoo, 2015; Clack et al., 2016)
156. Marginal tooth shape: conical and straight/slightly recurved = 0, small and more or less straight and 'needle-like' = 1, right-trapezoid 'chisel' shape = 2, spearhead shape = 3, thin and greatly recurved = 4 N22
    a. State one is present in *Trimerorhachis* (Milner and Schoch, 2013); state two is present in *Greererpeton* (Smithson, 1982; Schultze and Bolt, 1996; Bolt and Lombard, 2001); state three is present in *Pholiderpeton* (Clack, 1987b); state four is present in *Baphetes* (Beaumont, 1977; Milner and Lindsay, 1998); state five is present in *Coloraderpeton* (Anderson, 2003; Pardo et al., 2017b)
157. Labyrinthine infolding on teeth: present = 0, or absent = 1 N23
    a. State one is present in *Archeria* (Holmes, 1984) and nearly all taxa; state two is present in *Westlothiana* (Smithson et al., 1993), *Adelospondylus* and *Adelogyrinus* (Andrews and Carroll, 1991), *Lethiscus* (Anderson et al., 2003; Pardo et al., 2017b), and *Coloraderpeton* (Anderson, 2003; Pardo et al., 2017b)
158. Adductor fossa faces dorsally = 0, mesially = 1 C114
    a. The main difference between the first and second states is dorsolateral extent of the surangular, and, to a lesser extent, the dorsomedial extent of the prearticular.

When the dorsal extents of the surangular and prearticular are similar, the adductor fossa faces dorsally; the dorsolateral extent of the surangular is greater than dorsomedial extent of the prearticular, the adductor fossa faces mesially.

b. State one is present in *Whatcheeria* (Lombard and Bolt, 2006); state two is present in *Brittagnathus* (Ruta et al., 2020)

159. Angular mesial lamina suture with prearticular: absent = 0, present = 1 $C115
160. Angular reaches posteriormost point of lower jaw: absent = 0, present = 1 C116
161. Coronoid (anterior) contacts splenial (or presplenial if present): absent = 0, present = 1 C117
162. Coronoid (anterior) contacts postsplenial: absent = 0, present = 1 C118
163. Coronoid (middle) contacts postsplenial: absent = 0, present = 1 C119
164. Coronoid (middle) separated from splenial (or presplenial if present): present, by prearticular = 0, absent = 1, present, by postsplenial = 2 C120
165. Coronoid (posterior) posterodorsal process: absent = 0, present = 1 C121
166. Coronoid (posterior) posterodorsal process visible in lateral view: absent = 0, present = 1 C122
167. Coronoid: at least one has fang pair recognizable because at least twice the height of coronoid teeth: present = 0, absent = 1 C123
168. Coronoid: at least one has fangs recognisable because noticeably mesial to vertical lamina of bone and to all other teeth: present = 0, absent = 1 C124
169. Coronoid: at least one has organized tooth row: present = 0, absent =1 C125
170. Coronoid: at least one carries shagreen: absent = 0, present = 1 C126
171. Coronoid with a row of very small teeth or denticles lateral to tooth row: present = 0, absent = 1 C127
172. Coronoid: size of teeth (excluding fangs) on anterior and middle coronoids relative to dentary tooth size: about the same = 0, half height or less = 1 C128
173. Dentary with parasymphysial fangs internal to marginal tooth row: present = 0, absent = 1 C129
174. Dentary tooth number: more than 70 = 0, 56-70 = 1, 46-55 = 2, 36-45 = 3, less than 35 = 4 C130
175. Dentary with a row of very small teeth or denticles lateral to tooth row: present = 0, absent = 1 C131
176. Dentary ventral edge: smooth continuous line = 0, abruptly tapering or stepped margin = 1 C133
177. Dentary notch: absent = 0, present = 1 C214
178. Mandibular sensory canal: present = 0, absent = 1 C134
179. Mandibular canal exposure: entirely enclosed apart from pores = 0, mostly enclosed = 1, mostly or entirely open = 2 C135
180. Mandibular oral sulcus/ surangular pit line: present = 0, absent = 1 C136
181. Meckelian bone visible between prearticular and infradentary series: present = 0, absent = 1 C137
182. Number of Meckelian openings: more than three = 0, three = 1, two = 2, one = 3 N73

a. This character is part of a contingent set (N73, N74, N75) about the Meckelian openings (foramina and fenestrae) in the mandible. For more information, see Further Character Discussion

b. Replaces P94
c. State one is present in *Megalocephalus* (Ahlberg and Clack, 1998); state two is present in *Caerorhachis* (Ruta et al., 2002); state three is present in *Pholiderpeton scutigerum* (Clack, 1987b); state four is present in *Greererpeton* (Smithson, 1982; Bolt and Lombard, 2001)

183. Meckelian opening(s): face ventrally = 0, or mesially = 1 N74
a. See gloss for N73
b. State one is present in *Eusthenopteron* (Porro et al., 2015b); state two is present in all other taxa- for examples see (Ahlberg and Clack, 1998, 2020; Bolt and Lombard, 2001; Lombard and Bolt, 2006)

184. Meckelian opening(s) without ventromesial bony margin = 0, or with ventromesial bony margin = 1 N75
a. See gloss for N73
b. Replaces P94
c. State one is present in *Acanthostega* (Ahlberg and Clack, 1998; Porro et al., 2015a); state two is present in *Megalocephalus* (Ahlberg and Clack, 1998)
d. Parmastega-Acanthostega-Crassigyrinus/most everybody else

185. Meckelian bone or space exposure in middle part of jaw, depth much less than prearticular = 0, depth similar to prearticular or greater = 1 C138

186. Meckelian foramina/ fenestrae, dorsal margins formed by; mostly meckelian bone = 0, mostly prearticular = 1, mostly infradentary (postsplenial) = 2 C139

187. Ventral border of Meckelian fenestra/large posterior Meckelian opening: formed by postsplenial mostly = 0, or angular mostly = 1 P95

188. Adsymphysial tooth plate: present = 0, absent = 1 C140

189. Adsymphysial plate fang-pair (distinct from other teeth): absent = 0, present = 1 C141

190. Adsymphysial plate dentition: shagreen, denticles or irregular tooth field = 0, organised dentition aligned parallel to jaw margin = 1, no dentition = 2 C142

191. Adsymphysial lateral foramen present: absent = 0, present = 1 C143

192. Adsymphysial mesial foramen present: absent = 0, present = 1 C144

193. Postsplenial with mesial lamina: absent = 0, present = 1 C145

194. Postsplenial pit line present: present = 0, absent = 1 C146

195. Postsplenial mesial suture with prearticular: absent = 0, present but interrupted by Meckelian foramina or fenestrae = 1, uninterrupted suture = 2 C147

196. Prearticular shagreen field, distribution: gradually decreasing from dorsal to ventral = 0, well defined dorsal longitudinal band = 1, scattered patches or absent = 2 C148

197. Prearticular sutures with surangular (check rear of jaw): absent = 0, present = 1 C149

198. Prearticular with longitudinal ridge below coronoids: absent = 0, present = 1 C150

199. Splenial, rearmost extension of mesial lamina closer to anterior margin of adductor fossa than to the anterior end of the jaw: absent = 0, present = 1 C152

200. Surangular crest: absent = 0, present = 1 C153

201. Dentary teeth size: same size as maxillary teeth (0), larger than maxillary teeth = 1, smaller than maxillary teeth = 2 C250

202. Dentary chin: absent = 0, or present = 1 C215
203. Trunk pleurocentrum height relative to intercentrum height: pleurocentrum less than intercentrum = 0, same as intercentrum = 1, greater than intercentrum = 2, intercentrum and pleurocentrum fused into single bone (holospondylous) = 3 N80
    a. This character is part of a contingent set (N80, C173, C174, N81, N82, N83) about the structure of the vertebral centra. For more information see Further Character Discussion
    b. Replaces C171
    c. State one is present in *Acanthostega* (Coates, 1996); state two is present in *Eoherpeton* (Smithson, 1985); state three is present in *Gephyrostegus* (Carroll, 1970); state four is present in *Adelospondylus* (Andrews and Carroll, 1991)
204. Centra strongly notochordal such that notochordal space more than 2/3 diameter of entire centrum: present = 0, absent = 1 C172
    a. See gloss for N80
    b. State one is present in *Caerorhachis* (Ruta et al., 2002); state two is present in *Eryops* (Moulton, 1974);
205. Centra (trunk) pleurocentra fused midventrally: absent = 0, present = 1 C173
206. Centra (trunk) pleurocentra fused middorsally: absent = 0, present = 1 C174
207. Centra (trunk) intercentra fused middorsally: absent = 0, present = 1 N81
    a. See gloss for N203
    b. State one is present in *Caerorhachis* (Ruta et al., 2002); state two is present in *Whatcheeria* (Lombard and Bolt, 1995; Otoo et al., 2021)
208. Centra (trunk) intercentra fused midventrally: absent = 0, present = 1 N82
    a. See gloss for N80
    b. State one is present in *Whatcheeria* (Lombard and Bolt, 1995; Otoo et al., 2021); state two is present in *Eryops* (Moulton, 1974)
209. Centrum (sacral) not distinguishable by size or shape from pre- and postsacrals = 0, distinguishable = 1 C175
210. Neural arch ossification: paired in adult = 0, single in adult = 1 C198
211. Neural arches with distinct convex lateral surfaces (swollen): absent = 0, present = 1 C200
212. Neural arches of trunk vertebrae: not fused to centra = 0; fused to pleurocentrum or combined centrum = 1 N83
    a. See gloss for N80
    b. State one is present in *Acanthostega* (Coates, 1996); state two is present in *Adelospondylus* (Andrews and Carroll, 1991)
    c. Replaces C201
213. Presacral count: 25-35 = 0, 20-24 = 1, >35 = 2, <20 = 3 P107
214. Presacral (trunk) ribs: length of longest ribs: short = 0, long = 1 P140
215. Ribs (trunk): straight or weakly curved = 0, strongly ventrally curved = 1 C203
216. Trunk ribs overlapping: absent = 0, or present = 1 N25
    a. State one is present in *Whatcheeria* (Lombard and Bolt, 1995; Otoo et al., 2021), *Pederpes* (Clack and Finney, 2005), and *Eryops* (Moulton, 1974); state two is present in most other taxa, ex. *Acanthostega* (Coates, 1996)
217. Ribs (trunk) tapered distally =0, parallel-sided = 1, flared at distal tip= 2 C205
218. Ribs (trunk) bear uncinate processes: absent = 0, present = 1 C206

219. Uncinate processes shape: pointed and triangular = 0, or broad and either rounded or rectangular = 1 N26
    a. State one is present in *Erpetosaurus* (Milner and Sequeira, 2011); state two is present in *Whatcheeria* (Lombard and Bolt, 1995; Otoo et al., 2021)
220. Ribs (trunk) differ strongly in length and morphology along thoracic region: absent = 0, present = 1 C207
221. Ribs (cervical): flared distally = 0, tapered distally = 1 C208
222. Sacral rib distinguishable by size: same length as presacrals = 0, shorter than trunk ribs and longer than immediate presacrals = 1 R106
223. Sacral rib distinguishable by shape: broader than immediate presacrals but not broader than mid-trunk proximal shafts = 0, broader than mid-trunk proximal shafts = 1 R107
224. Forelimbs/paired pectoral appendages: present = 0, absent = 1 N27
    a. State one is present in all taxa except for the following: *Lethiscus* (Wellstead, 1982), *Coloraderpeton* (Anderson, 2003; Pardo et al., 2017b), *Adelospondylus* and *Adelogyrinus* (Andrews and Carroll, 1991)
225. Ossified pectoral girdle: present = 0, absent = 1 N28
    a. State one is present in all taxa except the following: *Lethiscus* (Wellstead, 1982), *Coloraderpeton* (Anderson, 2003; Pardo et al., 2017b), *Adelospondylus* and *Adelogyrinus* (Andrews and Carroll, 1991)
226. Clavicles meet anteriorly: present = 0, absent = 1 C176
227. Cleithrum co-ossified with scapulocoracoid = 0, separate = 1 C177
228. Cleithrum smoothly broadening to spatulate dorsal end = 0, distal expansion marked from narrow stem by notch or process or decrease in thickness = 1, end simply tapering = 2 C178
229. Dermal ornament on cleithrum: present = 0, or absent = 1 N29
    a. State one is present in *Tiktaalik* (Daeschler et al., 2006; Shubin et al., 2006), *Elpistostege* (Cloutier et al., 2020), *Panderichthys* (Vorobyeva, 1995; Boisvert et al., 2008), and *Eusthenopteron* (Andrews and Westoll, 1970); state two is present in all other taxa
230. Scapulocoracoid dorsal blade: absent = 0, present = 1 $C209
231. Scapular ossification separate from coracoid or coracoid unossified: absent = 0, present = 1
    C210
232. Interclavicle anterior edge fimbriated: absent = 0, present = 1 N24
    a. State one is present in *Acanthostega* (Coates, 1996); state two is present in *Eryops* (Pawley and Warren, 2006)
233. Interclavicle anterior tip: squared = 0, broadly rounded = 1, pointed = 2. N85
    a. State one is present in *Greererpeton* (Godfrey, 1989a); state two is present in *Whatcheeria* (Lombard and Bolt, 1995; Otoo et al., 2021); state three is present in *Pederpes* (Clack and Finney, 2005)
234. Interclavicle parasternal process shape: absent = 0, parallel sided = 1, or tapering = 2 C197

State one is present in *Eryops* (Pawley and Warren, 2006); state two is present in *Whatcheeria* (Lombard and Bolt, 1995; Otoo et al., 2021); state three is present in *Greererpeton* (Godfrey, 1989a)

235. Interclavicle body shape (excluding parasternal process of present): small scute = 0, triangle longest anteriorly = 1, triangle longest laterally = 2, spatulate or fan-shaped = 3, equilateral triangle = 4 N78
    a. State one is present in *Eusthenopteron* (Andrews and Westoll, 1970); state two is present in *Greererpeton* (Godfrey, 1989a); state three is present in *Ossinodus* (Warren and Turner, 2004); state four is present in *Whatcheeria* (Lombard and Bolt, 1995; Otoo et al., 2021); state five is present in *Crassigyrinus* (Panchen, 1985)
    b. Replaces C196
236. Interclavicle parasternal process length: equal to rest of interclavicle = 0 or longer than rest of interclavicle = 1 N79
    a. State one is present in *Acanthostega* (Coates, 1996); state two is present in *Ichthyostega* (Jarvik, 1996)
237. Postbranchial lamina on cleithrum present = 0, or absent = 1 R1
    a. We define the postbranchial lamina as a an anteriorly projecting flange of bone originating near the ventral tip of the cleithrum; see (Coates, 1996) for discussion. In this definition we differ from that in (Pawley, 2006). (Marjanović and Laurin, 2019) review this character in detail, particularly relating to *Casineria*, where they claim to identify a postbranchial lamina. Examining their figures (in particular main text Fig.7 therein), we do not agree that the feature they identify is a postbranchial lamina. We do agree that a three-dimensional morphological investigation of *Casineria* (either the holotype or additional specimens) would be extremely valuable
238. Cleithrum without = 0, or with = 1 a distinct shaft R11
239. Shape of ventral clavicle plate: elongate triangle = 0, sub-equilateral triangle = 1, spoon-shaped/spatulate/ovoid = 2 N30
    a. State one is present in *Greererpeton* (Godfrey, 1989a); state two is present in *Eryops* (Pawley and Warren, 2006); state three is present in *Whatcheeria* (Otoo et al., 2021)
240. Clavicles without = 0, or with = 1 a distinct ascending process. R16
241. Interclavicle small and scute-like = 0, enlarged = 1 R23
242. Glenoid subterminal, i.e. the scapulocoracoid does not extend ventral and slightly posterior to its posteroventral margin, and does not form a distinct 'wall' of bone, visible in lateral aspect: yes = 0, no = 1 R25
243. Scapulocoracoid without = 0, or with = 1 expanded coracoid plate extending ventromedially R33
244. Scapulocoracoid without = 0, or with = 1 supraglenoid excavation/supraglenoid fossa R34
245. Glenoid greater axis oriented mostly horizontally = 0, or obliquely = 1 R35
246. Interclavicle: present = 0, or absent = 1 N31
    a. State one is present in all taxa except the following, for which the character is inapplicable: *Lethiscus* (Wellstead, 1982198) and *Coloraderpeton* (Anderson, 2003; Pardo et al., 2017b)
247. Scapulocoracoid: present, including only scapular or coracoid portion = 0, or absent = 1 N32

a. State one is present in all taxa except the following: it is in applicable for *Lethiscus* (Wellstead, 1982198) and *Coloraderpeton* (Anderson, 2003; Pardo et al., 2017b); state two is present in *Adelospondylus* and *Adelogyrinus* (Andrews and Carroll, 1991)

248. Angle between proximal and distal ends of humerus: 30 degrees or less = 0, 31-60 degrees = 1, more than 60 degrees = 2 N84
   a. Replaces C180
   b. State one is present in *Whatcheeria* (Otoo et al., 2021); state two is present in *Pederpes* (Clack and Finney, 2005; Smithson and Clack, 2018); state three is present in *Casineria* (Paton et al., 1999199)

249. Percentage of humerus posterior margin proximal to entepicondyle, measured from proximal base of entepicondyle: about a third or less = 0, about half = 1, about two thirds = 2, more than two thirds = 3 N33
   a. State one is present in *Pederpes* (Clack and Finney, 2005); state two is present in *Greererpeton* (Godfrey, 1989a); state three is present in *Eucritta* (Clack, 2001)

250. Humerus latissimus dorsi process part of ridge = 0, distinct but low process = 1, spike = 2 C183

251. Humerus latissimus dorsi process position compared with deltopectoral crest: more proximal to head = 0, equidistant from head = 1 C184

252. Humerus latissimus dorsi process position relative to ectepicondyle: offset anteriorly = 0, in line = 1 C185

253. Humerus latissimus dorsi process confluent with deltopectoral crest: present = 0, distinct from = 1 C186

254. Humerus radial facet position: distal and terminal = 0, anteroventral = 1, ventral = 2 C188

255. Humerus radial/ulnar facets: confluent = 0, separated by perichondral strip of bone = 1 C189

256. Humerus with distinct supinator process: absent = 0, present = 1 C190

257. Humerus ectepicondyle distinct: present = 0, absent = 1 C192

258. Humerus ectepicondylar ridge distal end aligned with ulnar condyle = 0, between radial and ulnar condyles = 1, aligned with radial condyle = 2 C193

259. Humerus entepicondyle width relative to humeral head width: smaller = 0, greater = 1 C195

260. Entepicondyle foramen: present subcircular or round elliptical = 0, present slit-like or elongate elliptical = 1, absent = 2 R42

261. Ectepicondyle foramen: present = 0, absent = 1 R43

262. Ectepicondyle ridge reaching distal humeral end: no = 0, yes = 1 R45

263. Humerus length up to and no more than twice its width = 0, or more than twice its width = 1 R49

264. Entepicondyle shape: three-dimmensional spike = 0, dorsoventrally flattened rectangle or trapezoid = 1, dorsoventrally flattened triangle = 2 N34
   a. State one is present in *Tiktaalik* (Shubin et al., 2006; Stewart et al., 2019); state two is present in *Whatcheeria* (Lombard and Bolt, 1995; Otoo et al., 2021); state three is present in *Ossinodus* (Bishop, 2014)

265. Length of posterior margin of entepicondyle smaller than = 0, subequal to = 1, or larger than = 2, humerus anteroposterior length at the level of proximal insertion of entepicondyle onto humerus shaft R66
266. Deltopectoral crest present = 0, separate deltoid and pectoral processes = 1, only pectoral process = 2, none of these = 3 N35
    a. State one is present in *Whatcheeria* (Otoo et al., 2021); state two is *Tulerpeton* (Lebedev and Coates, 1995); state three is present in *Eusthenopteron* (Andrews and Westoll, 1970; Stewart et al., 2019); state four is present in *Archegosaurus* (Witzmann and Schoch, 2006)
267. Radius: longer than ulna = 0, same length as ulna = 1, shorter than ulna (including olecranon process if present) = 2 C202
268. Radius longer than = 0, as long as = 1, or shorter than = 2, humerus. R78
269. Radius without = 0, or with = 1, distinctly expanded proximal extremity R82
270. Ossified olecranon process: absent = 0, present = 1 R83
271. Ulna wider at its distal extremity = 0, of about the same width at proximal and distal extremities = 1, wider at its proximal extremity = 2 R84
272. Hindlimbs/paired pelvic appendages: present = 0, absent = 1 N36
    a. This character and N37 are the posterior counterparts of N27 and N28
    b. State one is present in all taxa except the following: *Adelospondylus* and *Adelogyrinus* (Andrews and Carroll, 1991), Lethiscus (Wellstead, 1982198) and *Coloraderpeton* (Anderson, 2003; Pardo et al., 2017b). All pelvic limb characters are thus inapplicable for these taxa listed
273. (Ossified) pelvic girdle at least in part: present = 0, absent = 1 N37
    a. See gloss for N36
    b. State one is present in all taxa except for the following: *Lethiscus* (Wellstead, 1982198) and *Coloraderpeton* (Anderson, 2003; Pardo et al., 2017b). All pelvic girdle characters are thus inapplicable for these taxa listed
274. Ilium, ischium, pubis separate ossifications: no not separate= 0, yes separate (including one or more of these unossified)= 1 C212
275. Number of ilium dorsal processes: one = 0, two = 1 N38
    a. There has historically been some confusion with the terms ‘iliac process’, ‘dorsal iliac process’, and ‘posterior iliac process’. Whereas the latter two can be clearly assigned in taxa with two processes, such as *Acanthostega* (Coates, 1996), in taxa with a single process such as *Greererpeton*, *Eryops*, *Westlothiana*, and *Tiktaalik* (Godfrey, 1989a; Smithson et al., 1993; Pawley and Warren, 2006; Shubin et al., 2014), it has variously been referred to as the iliac process or the dorsal iliac process, with some uncertainty as to whether it is homologous with the dorsal or posterior process in taxa that have two. This character, in conjunction with N39 and R93, is meant to circumvent this confusion by identifying the ‘dorsal iliac process’ as the one which articulates with the sacral rib, regardless of number, and assess its morphology
    b. State one is present in *Acanthostega* (Coates, 1996); state two is present in *Greererpeton* (Godfrey, 1989a)
276. Ilium dorsalmost process (one that articulates with sacral rib) orientation: straight dorsal = 0, canted posteriorly = 1, canted anteriorly = 2 N39
    a. See gloss for N38

b. State one is present in *Whatcheeria* (Lombard and Bolt, 1995; Otoo et al., 2021); state two is present in *Greererpeton* (Godfrey, 1989a)

277. Dorsal iliac process oblique and flared = 0, fan-shaped = 1, subrectangular and truncated = 2, blunt and digitiform = 3, low elongate = 4 R93

278. Supraacetabular iliac buttress less = 0, or more = 1, prominent than postacetabular buttress on ischium R94

279. Dorsal and posterodorsal iliac processes overlapping in lateral view = 0, or separated by distinct space = 1 R96

280. Acetabulum finished = 0, or unfinished, including unossified pubis = 1 R99

281. Number of pubic obturator foramina: multiple = 0, single = 1, absent = 2 R105

282. Pubis ossified = 0, or unossified = 1 N72

283. Internal trochanter in adult: present = 0, or absent = 1 R108

284. Internal torchanter/proximal end of adductor blade relationship to proximal head of femur in adult: separated by deep and clear notch of finished bone = 0, separated by broad open space = 1, on ridge continuous with proximal head of femur = 2 N40

a. For more on this and other important femoral characters in this dataset, see Further Character Discussion

b. State one is present in *Greererpeton* (Godfrey, 1989a); state two is present in *Whatcheeria* (Lombard and Bolt, 1995; Otoo et al., 2021); state three is present in *Proterogyrinus* (Holmes, 1984)

285. Fourth trochanter of femur absent = 0, or present = 1 R110

286. Fourth trochanter shape: short and narrow = 0, short and broad with flat top = 1, long rugose region = 2, short rugose region = 3, nub or bump = 4 N41

a. See gloss for N40

b. State one is present in *Archegosaurus* (Witzmann and Schoch, 2006); state two is present in *Whatcheeria* (Otoo et al., 2021) and *Pederpes* (Clack and Finney, 2005; Otoo et al., 2021); state three is present in *Proterogyrinus* (Holmes, 1984); state four is present in *Greererpeton* (Godfrey, 1989a)*;* state five is present in *Acanthostega* (Coates, 1996)

287. Proximal end of femur adductor crest reaching midshaft length: no = 0, yes = 1 R111

288. Femur shorter than = 0, as long as = 1, or longer than humerus = 2 R112

289. Adductor blade: present = 0, absent =1 N42

a. The adductor blade is distinguished from the adductor crest by its more proximal position on the femur, and its bearing the fourth trochanter (as well as the internal trochanter in some taxa). They are occasionally conflated or confused for each other (Otoo et al., 2021). See character 11 in (Coates, 1996) for further discussion

b. State one is present in *Acanthostega* (Coates, 1996); state two is present in *Proterogyrinus* (Holmes, 1984)

290. Adductor blade length: occupying most or all of the femur length = 0, restricted to midshaft = 1, restricted to proximal part of femur = 2 N43

a. State one is present in *Acanthostega* (Coates, 1996); state two is present in *Whatcheeria* (Otoo et al., 2021); state three is present in *Greererpeton* (Godfrey, 1989a)

291. Adductor blade shape in adult: broad rectangular blade = 0, narrow blade = 1, broad ridge = 2, narrow parallelogram = 3, spike or prong = 4 N44

a. For discussion see Further Character Discussion
b. State one is present in *Acanthostega* (Coates, 1996); state two is present in *Balanerpeton* (Milner and Sequeira, 1993); state three is present in *Whatcheeria* (Otoo et al., 2021); state four is present in *Ossinodus* (Warren and Turner, 2004); state five is present in *Greererpeton* (Godfrey, 1989a)

292. Adductor crest length: shorter than adductor blade = 0, similar length to adductor blade = 1, longer than adductor blade = 2 N46
a. For discussion see Further Character Discussion
b. State one is present in *Acanthostega* (Coates, 1996); state two is present in *Pederpes* (Clack and Finney, 2005); state three is present in *Whatcheeria* (Otoo et al., 2021); state

293. Femur without = 0, or with = 1 distinctly expanded proximal head R115

294. Femur intercondylar groove: absent = 0, present and not longer than distal end of femur = 1, present and longer than distal end of femur = 2 R116

295. Anteroposterior maximum distance between femur distal condyles i(=tibia and fibula condyles) in extensor view 55 pecent or more of femur length = 0, between 55 and 40 percent of femur length = 1, 40 percent or less than femur length = 2 R117

296. Tibia and fibula condyles greatest width in distal view: equal = 0, tibia condyle broader = 1, fibula condyle broader = 2 N47
a. State one is present in *Eusthenopteron* (Andrews and Westoll, 1970); state two is present in *Whatcheeria* (Lombard and Bolt, 1995; Otoo et al., 2021); state three is present in *Seymouria* (White, 1939; Berman et al., 2000; Bazzana et al., 2020b)

297. Distal condyle alignment in extensor view: condyles about level = 0, one condyle extends farther distally = 1 N48
a. State one is present in *Trimerorhachis* (Pawley, 2007); state two is present in *Whatcheeria* (Lombard and Bolt, 1995; Otoo et al., 2021)

298. Tibia and fibula condyles differentiated from each other, including being joined by unfinished bone = 0, or not = 1 N51
a. State one is present in *Whatcheeria* (Lombard and Bolt, 1995; Otoo et al., 2021); state two is present in *Pederpes* (Clack and Finney, 2005)

299. Tibia waisted: no = 0, yes = 1 R118

300. Tibia without cnemial crest = 0, crest present and running distally = 1, present and running mesiolaterally while subsiding distally = 2 R119

301. Tibia without = 0, or with = 1 flange along its posterior edge R121

302. Tibia distal articular surface absent = 0, present and with L-shaped outline = 1, present and with subelliptical outline = 2 R122

303. Tibia width at mid-length of bone less than = 0, comparable to = 1, or greater than = 2, width of fibula at mid- length of bone R123

304. Tibia proximal extremity wider = 0, as wide as = 1, or narrow than = 2 its distal extremity R126

305. Fibula waisted: no = 0, yes = 1 R127

306. Fibula without = 0, or with = 1 oblique distal extremity R128

307. Posterior (lateral) surface of fibula concave = 0, straight = 1, convex = 2, in its proximal half R132

308. Relative lengths of hindlimb epipodials and femur: epipodials less than 50% of femur length = 0, about 50% femur length = 1, or >50% of femur length = 2 N52

a. State one is present in *Acanthostega* (Coates, 1996); state two is present in *Proterogyrinus* (Holmes, 1984); state three is present in *Whatcheeria* (Otoo et al., 2021)

309. Interepipodial space: present = 0, or absent = 1 N53

a. State one is present in *Whatcheeria* (Otoo et al., 2021); state two is present in *Acanthostega* (Coates, 1996)

310. Interepipodial space shape: elongate tapering oval/'spindle shaped' = 0, broad, elongate oval/subrectangle = 1, small circle that does not reach ends of epipodials = 2 N54

a. *Whatcheeria* has been coded as polymorphic for this character, with both states one (spindle-shaped) and two (broad elongate oval) present. Aside from ontogenetic variation in the hindlimb epipodials and shape of the interepipodial space (Otoo et al., 2021), there is much variation in the quality of preservation of the tibia and fibula. Due to similar variation in *Seymouria* (White, 1939; Berman et al., 2000), it has also been coded as polymorphic

b. State one is present in *Tulerpeton* (Lebedev and Coates, 1995); state two is present in *Eryops* (Pawley and Warren, 2006; Dilkes, 2015); state three is present in *Pederpes* (Clack and Finney, 2005)

311. Manus digits: absent = 0, or present = 1 N55

a. This character is part of a contingent set with N56, and collectively they replace R139

b. We have coded digits as being absent in *Elpistostege*, contra (Cloutier et al., 2020). We disagree with the identification therein of some of the radials as digits. The non-branching end-to-end articulation cited are not clear in the specimen photos or the figured CT renderings (Fig.3 therein). Moreover, the radials are not terminal, and are contained within a fin web of lepidotrichia. We feel that, among other things, being terminal on the autopod is an important part of defining digits. However, we agree with those and other authors (Shubin et al., 2006; Boisvert et al., 2008; Boisvert, 2009; Stewart et al., 2019; Cloutier et al., 2020) that panderichthyids/elpistostegalians appear to possess increased adaptations of the pectoral fin for weight-bearing and/or interaction with the substrate, and feel that both the macroevolutionary and evolutionary ecological implications are highly interesting

c. State one is present in *Elpistostege* (Cloutier et al., 2020); state two is present in *Whatcheeria* (Otoo et al., 2021)

312. Manus digit number: eight = 0, six = 1, five = 2, four = 3, three = 4 N56

a. While a manual digit count of six was proposed in the full description of *Pederpes* (Clack and Finney, 2005), due to the uncertainty caused by a lack of a complete manus, we have scored *Pederpes* as uncertain

b. See gloss for N55

c. State one is present in *Acanthostega* (Coates, 1996); state two is present in *Tulerpeton* (Coates, 1996); state three is present in *Greererpeton* (Coates, 1996); state four is present in *Eryops* (Dilkes, 2015)

313. Pes digits: absent = 0, or present = 1 N57

a. This character and N58 are the pedal analogues of N55 and N56. Collectively they replace R144

b. State one is present *Tiktaalik* (Shubin et al., 2014); state two is present in *Acanthostega* (Coates, 1996)

314. Pes digit number: eight = 0, seven = 1, six = 2, five = 3 N58
   a. See gloss for N57
   b. State one is present in *Acanthostega* (Coates, 1996); state two is present in *Ichthyostega* (Jarvik, 1996); state three is present in *Tulerpeton* (Coates, 1996); state four is present in *Whatcheeria* (Otoo et al., 2021)

315. Relative length of foot and rear epopodials: foot equal to or less than length of epipodials = 0, foot longer than epipodials = 1 N60
   a. State one is present in *Whatcheeria* (Otoo et al., 2021); state two is present in *Acanthostega*
   b. *Whatcheeria* when compared with other early tetrapods (Otoo et al., 2021)

316. Phalanges shape (manual, non-terminal): longer than wide = 0, about as wide as long = 1, wider than long = 2 N61
   a. This character, along with N61, was added in order to capture the unusual breadth of the phalanges of *Whatcheeria* (Otoo et al., 2021). Digit morphology and functional implications were discussed with the full description of *Pederpes* (Clack and Finney, 2005)
   b. It may be important to note that here we define 'phalanges' as all those bones which are distal to the wrist/ankle, following (Otoo et al., 2021). This would include bones usually classified as metacarpals and metatarsals. We feel that this decreases ambiguity when attempting to discern digit formulae, particularly in disrupted or incomplete fossils (which is to say, most early tetrapod fossils)
   c. This character is uniform (state one) for all ingroup taxa for which there is data, with the exception of *Whatcheeria* and *Pederpes* (Clack and Finney, 2005; Otoo et al., 2021), which are polymorphic for states two and three, as the manual phalanges vary in shape between square (state two) and rectangular (state three)

317. Phalanges shape (pedal, non-terminal): longer than wide = 0, about as wide as long = 1, wider than long = 2 N62
   a. This character is uniform (state one) for ingroup taxa except for *Whatcheeria* (Otoo et al., 2021), which is polymorphic for states one and two
   b. The morphologies of the manual and pedal phalanges in *Whatcheeria* is near-identical (Otoo et al., 2021). This is one of the key ways in which *Whatcheeria* differs from *Pederpes*, which has pedal phalanges that, like those of most other early tetrapods, are longer than broad, possibly suggesting a degree of ecological difference between the two (Otoo et al., 2021)

318. Phalanges cross-section shape (manual): circular = 0, square-shaped or elongate oval-shaped = 1, convex upwards = 2 N63
   a. See (Clack and Finney, 2005) for further discussion
   b. State one is present in *Acanthostega* (Coates, 1996); state two is present in *Whatcheeria* (Otoo et al., 2021); state three is present in *Proterogyrinus* (Holmes, 1984; Clack and Finney, 2005)

319. Phalanges cross-section shape (pedal): square or elongate oval =0, convex upwards = 1, circular = 2 N64
   a. State one is present in *Whatcheera* (Otoo et al., 2021); state two is present in *Pederpes* (Clack and Finney, 2005)

320. Wrist ossifications in adult: fully ossified = 0, or fully unossified = 1, or partially ossified = 2 N65
    a. State one is present in *Eryops* (Dilkes, 2015); state two is present in *Whatcheeria* (Otoo et al., 2021); state three is present in *Proterogyrinus* (Holmes, 1984)
321. Ankle ossifications: fully ossified = 0, or fully unossified = 1, or partially ossified = 2 N66
    a. State one is present in *Eryops* (Dilkes, 2015); state two is present in *Eucritta* (Clack, 2001); state three is present in *Whatcheeria* (Otoo et al., 2021)
322. Intermedium contacts interepipodial space in forelimb: yes = 0, or no = 1 N67
    a. State one is present in *Tulerpeton* (Lebedev and Coates, 1995); state two is present in *Eryops* (Dilkes, 2015)
323. Intermedium contacts interepipodial space in hindlimb: yes = 0, or no = 1 N68
    a. State one is present in *Tulerpeton* (Lebedev and Coates, 1995); state two is present in *Eryops* (Dilkes, 2015)
324. Intermedium (hindlimb) contribution to interepipodial space: forms most/all of distal margin as a trough = 0, in line with distal end of fibula = 1 N69
    a. State one is present in *Tulerpeton* (Lebedev and Coates, 1995); state two is present in *Eryops* (Dilkes, 2015)
325. Full-body scale covering: present = 0, absent = 1 N70
    a. State one is present in *Eusthenopteron* (Andrews and Westoll, 1970); state two is present in *Pederpes* (Clack and Finney, 2005)
326. Scale distribution: gastralia present = 0, gastralia and dorsal scales/osteoderms/other dermal ossifications present = 0, no scales = 2 N71
    a. State one is present in *Pederpes* (Clack and Finney, 2005); state two is present in *Greererpeton* (Godfrey, 1989a); state three is present in *Whatcheeria* (Otoo et al., 2021)
327. Gastralia: tapered and elongate, four times longer than broad or longer = 0, ovoid = 1, around three times longer than broad one end tapering = 2 C211
    a. State one is present in *Greererpeton* (Godfrey, 1989a); state two is present in *Tulerpeton* (Lebedev and Coates, 1995); state three is present in *Pederpes* (Clack and Finney, 2005)

B.13 FURTHER CHARACTER INFORMATION

PTERYGOID VACUITIES

Relevant characters:

- N14
- N15
- N16
- C90
- N17
- N18

Interpterygoid vacuities- a separation of the pterygoids at the midline, creating an opening in the palate- are widespread among early tetrapods, and have a history of use in classification (Smithson, 1982; Ruta et al., 2002; Kimmel et al., 2009) and morphometric studies (Lautenschlager et al., 2016; Witzmann and Werneburg, 2017). In particular, they are considered an important synapomorphy supporting a temnospondyl origin of lissamphibians (Ruta and Coates, 2007; Schoch, 2019). Previous datasets have used rather simple presence/absence or small/large characters to capture the nature of the interpterygoid vacuities (Clack et al., 2016, 2019a); their broad distribution across diverse taxa and diverse morphologies, in our view, requires a greater number of characters to be both precise and useful. Instead of grouping very different kinds of interpterygoid vacuities together, we used separate characters to capture the anteroposterior extent of the vacuity, the breadth of the lateral palatal bones, and the shape of the mesial margins of the pterygoids. In this way, we hope to more accurately determine, among other things, the relationships of the colosteids and *Caerorhachis* to the temnospondyls. Both taxa have previously (Smithson, 1982; Hook, 1983; Ruta et al., 2002) been suggested to have temnospondyl affinities on the basis of their interpterygoid vacuities. In the case of *Caerorhachis,* it has been suggested that such a hypothesis is countered by the greater weight of anatomical features supporting a closer relationship with the amniote total group (Ruta et al.,

2002). The colosteids, previously placed within Temnospondyli (Smithson, 1982; Hook, 1983) have been recovered on the tetrapod stem in most analyses over the last 20 years (Ruta et al., 2003; Ruta and Coates, 2007; Ruta, 2011; Clack et al., 2019a; Marjanović and Laurin, 2019); however, the prospect of a temnospondyl affinity has recently been mooted at least once (Clack et al., 2016). An important distinction we make is whether or not the interpterygoid vacuities intersect the orbit; with the exception of *Edops* (Romer and Witter, 1942), this condition seems to be both unique to temnospondyls and at least symplesiomorphic of the group.

VERTEBRAE

Relevant characters:

- N80
- C172
- C173
- C174
- N81
- N82
- C175
- C198
- C200
- N83
- P107

Early tetrapod vertebrae are primitively multipart structures, composed of a pleurocentrum and intercentrum (which enclose the notochord dorsally and ventrally, respectively), and a neural spine which contains the neural arch through which the spinal cord passes. The pleurocentra, intercentrum, and neural spine may each be paired or fused along the midline, with or without a suture. This arrangement is modified in various lineages, with terms applied to various conditions hypothesized to be diagnostic. Here we have added and modified characters to

individually categorize the morphologies of the pleurocentruma and intercentrum. This allows for greater precision in characterizing vertebral morphology within our dataset.

In *Acanthostega*, the whatcheeriids, and the colosteids, the vertebrae are tripartite as described above; the pleurocentra open ventrally and the intercentra open dorsally (Godfrey, 1989a; Coates, 1996; Pierce et al., 2013b; Otoo et al., 2021). The intercentrum is genrally larger than the pleurocentrum. This also the case in the temnospondyls *Balanerpeton*, *Dendrerpeton*, and *Eryops* (Moulton, 1974; Milner and Sequeira, 1993; Holmes et al., 1998), where the pleurocentrum and intercentrum and more equal in size. This is the 'rhachitomous' condition, and appears to be plesiomrophic for limbed tetrapods. In the 'gastrocentrous' condition, both the pleurocentra and intercentra are fused ventrally and open dorsally. This condition is present in *Caerorhachis*, *Silvanerpeton*, *Eldeceeon*, *Gephyrostegus*, and *Proterogyrinus* (Carroll, 1970; Holmes, 1984; Ruta et al., 2002, 2020; Ruta and Clack, 2006). This condition has been hypothesized (Holmes, 1984; Ruta et al., 2002) to be ancestral to the embolomerous condition (see below), evidence of the basal position of *Proterogyrinus* among anthracosaurs (=embolomeres) and the close relationship of the rest of these taxa to anthracosaurs (including their inclusion within the group under various definitions) and their membership within the amniote total group more generally. The progressive consolidation of vertebral components into a single fused unit has been hypothesized to be a characteristic of the amniote stem group (Danto et al., 2017), often linked to terrestrial locomotion (Carroll, 1970; Bazzana et al., 2020b).

Holmes (1984) posited that gastrocentrous intercentra and pleurocentra in *Proterogyrinus* were completed dorsally, and that they were simply less-ossified versions of embolomerous vertebrae.

Embolomerous vertebrae are defined by having both pleurocentra and intercentra which are fused dorsally and ventrally, forming complete disks. Additionally, the opening for the notochord is greatly reduced, and the pleurocentrum and intercentrum are of similar size. Embolomerous vertebrae are diagnostic for Embolomeri, though they are present in the tail of *Gephyrostegus* (Smithson, 1985) and absent in *Proterogyrinus* as noted above.

A variation of the 'schizomerous' condition is present in *Seymouria*, where the intercentra are open dorsally and greatly reduced, the pleurocentra are enlarged and fused dorsally and ventrally, and the neural spines are fused to the pleurocentra (White, 1939). The relationships of lepospondyls are debated (Ruta and Coates, 2007; Pardo et al., 2017b, 2020; Marjanović and Laurin, 2019), but they are united by holospondylous vertebrae, where the neural spines (which have distinctive lateral swellings) are fused to a single-part centrum (Carroll and Gaskill, 1978; Andrews and Carroll, 1991; Ruta and Coates, 2007; Pardo et al., 2017b). Holospondylous vertebrae are also present in *Westlothiana* (Smithson et al., 1993). *Westlothiana* and lepospondyls (either whole or in part) have long been considered total group amniotes and possibly close relatives in large part due to their vertebrae, though this is not universally agreed-upon (Marjanović and Laurin, 2019; Pardo et al., 2020).

FEMORA

Relevant characters:

- R108
- N40
- R110
- N41
- R111
- R112
- N42
- N43
- N44
- N46
- R115
- R116
- R117
- N47
- N48
- N51

The humerus of early tetrapods has received considerable attention, given the substantial anatomical and functional changes associated with the fin-limb and water-land transitions (Coates, 1996; Shubin et al., 2006; Boisvert et al., 2008; Ahlberg, 2011; Ruta, 2011; Bishop, 2014; Dickson and Pierce, 2018; Smithson and Clack, 2018; Cloutier et al., 2020; Dickson et al., 2020; Otoo et al., 2021). However, the femur has received less attention. Personal observations and recent work (Pawley and Warren, 2006, 2006; Pierce et al., 2013a; Otoo et al., 2021) have, in combination with previous descriptions (Romer, 1957; Godfrey, 1989a; Coates, 1996), revealed new morphological patterns within early tetrapods. Arguably the most significant of these is the unqiue combination of femoral characters that unites *Whatcheeria* and *Pederpes* and contributes to a revised diagnosis of Whatcheeriidae (Otoo et al., 2021). Additionally, previous work has suggested that the anterior and posterior skeletons in early tetrapods changed characters at different rates (Coates et al., 2002). A phylogenetic analysis of postcranial characters

recovered a phylogeny similar to full-body analyses (Ruta, 2011). For all these reasons, we were interested to increase the number of femoral characters within our dataset.

The femora of *Acanthostega*, *Ichthyostega*, and *Tulerpeton* are united by the possession of a large rectangular adductor blade that occupies almost the entirety of the femur, which connects to a short, narrow adductor crest distally, and small internal and fourth trochanters proximally4. The ends of the femur are also minimally expanded relative to the shaft, in contrast to post-Devonian tetrapods. The femora of *Whatcheeria* and *Pederpes* have a broad, rugose-topped fourth trochanter on a thick adductor blade restricted to the midshaft, and no internal trochanter (Clack and Finney, 2005; Otoo et al., 2021).

The femora of colosteids (as represented by *Greererpeton*) have a spike-like adductor blade and adductor crest that are close to the proximal end of the femur; the fourth trochanter is a rugose patch on the adductor blade mesially and the internal trochanter is a nub on top of the dorsal/proximal end of the adductor blade that is separated from the proximal end by a deep notch of finished bone (Godfrey, 1989a). This adult morphology is in contrast with that of juveniles, where the adductor blade is contiguous with the proximal end of the femur. Over ontogeny, the adductor blade, with its trochanters, gradually differentiates and 'pinches out' mesially until the separating notch is fully developed in the adult. This is also the case in *Trimerorhachis* (Pawley, 2007). This contrasts with whatcheeriids and embolomeres (see below), the femora of which exhibit minimal changes over ontogeny aside from increases in size. The same adult femoral morphology is present in *Crassigyrinus* (Panchen and Smithson, 1990), *Caerorhachis* (Ruta et al., 2002), and (possibly) extant *Pleurodeles* (Karakasiliotis et al., 2013),

though the adductor crest is absent in the former. At least some stereospondyls may have pedomorphic femora relative to the condition in *Trimerorhachis*, where the differentiation of the adductor blade and proximal end of the femur is incomplete in the adult (pers. obsv., see Taxon List).

The femora of at least most embolomeres (Romer, 1957; Holmes, 1984; Smithson, 1985) lacks an adductor blade but retains a distal adductor crest. The fourth trochanter is a rugose strip near the proximal end of the femur, and the internal trochanter is contiguous with the proximal end of the femur. This morphology also seems to be present in *Seymouria* (White, 1939; Bazzana et al., 2020b), though the position of the fourth trochanter may be more distal. In contrast to *Greererpeton* and *Trimerorhachis*, these femora, as well as those of whatcheeriids, though the latter with some caveats (Otoo et al., 2021), more or less 'direct develop' (pers. obsv., see Taxon List); the position of the muscle attachments is consistent between small and large femora, and the latter are only distinguished by being larger and relatively longer.

Functional interpretations are difficult and generally beyond the scope of this study, though see (Otoo et al., 2021) for some comments on *Whatcheeria*. It seems plausible, however, that the whatcheeriid and embolomere-*Seymouria* patterns reflect an emphasis on appendicular locomotion, i.e. walking, whether subaerially or subaqueously (Otoo et al., 2021); by contrast, the colosteid-*Trimerorhachis*-*Crassigyrinus* arrangement is likely an adaptation for use of the limb as a paddle or rudder (Panchen and Smithson, 1990), with primary thrust generated by axial movement. Both are likely separate derivations of an *Acanthostega*-like condition. Broader phylogenetic interpretation of these patterns depends greatly on the phylogenetic position of the

colosteids and embolomeres. If both are stem tetrapods (Marjanović and Laurin, 2019), then these patterns are plesiomorphies which were sampled independently by the lissamphibian and amniote total groups, probably in accordance with lifestyle. If embolomeres are stem amniotes (Ruta and Coates, 2007; Ruta et al., 2020), that would suggest that increasing emphasis on appendicular locomotion was present at the origin of the amniote total group (and that amniotes may have been primitively aquatic). If colosteids are stem lissamphibians (Clack et al., 2016), then lissamphibians were primitively aquatic, and their plesiomorphic femur pattern may be deeply concerned. In addition to phylogenetic uncertainty, fossil record gaps and issues of ecological context complicate the issue, which is one of many surrounding the origin and earliest history of the tetrapod crown group (see CHAPTER 3 main text for discussion).

MECKELIAN OPENINGS

Relevant characters:

- N73
- N74
- N75
- C138
- C139
- P95

The lower jaws of early tetrapods have long been of anatomical, phylogenetic, and functional interest (Ahlberg and Clack, 1998, 2020; Bolt and Lombard, 2001; Neenan et al., 2014). Mandibles and parts thereof are one of the portions of the skeleton which are disproportionately represented in the highly fragmentary early tetrapod record; a number of taxa are known solely from mandibular material (Campbell and Bell, 1977; Daeschler, 2000a; Zhu et al., 2002; Bolt and Lombard, 2006; Clément and Lebedev, 2014; Ahlberg and Clack, 2020). One of the key features is the nature of the Meckelian ossification and the accompanying Meckelian openings. Here we modified existing characters and added new ones to better capture the conditions of the Meckelian ossification and accompanying Meckelian openings. Previous workers have distinguished between the larger Meckelian fenestrae and smaller Meckelian foramina (Ahlberg and Clack, 1998; Pardo et al., 2017b). For simplicity's sake we refer to all Meckelian openings as 'Meckelian openings' or 'Meckelian fenestrae'.

Primitively the Meckelian cartilage appears to have been a single unossified cartilage, accommodated by a single slot opening ventrally- this is the condition in *Eusthenopteron* (Porro et al., 2015b). The subsequent sequence of character transformations is unclear, and different lineages probably took different paths. In *Panderichthys*, the Meckelian cartilage is ossified as the Meckelian bone, and is perforated by more than three foramina (Ahlberg and Clack, 1998),

which open mesially and the margins of which are entirely formed by bone. This is the condition in *Ichthyostega*, *Ymeria*, *Ventastega*, *Whatcheeria*, *Brittagnathus*, and *Megalocephalus* (Ahlberg and Clack, 1998, 2020; Bolt and Lombard, 2006; Lombard and Bolt, 2006; Ahlberg et al., 2008; Clack et al., 2012a). By contrast, in *Acanthostega* the Meckelian cartilage was apparently unossified and accommodated by a single extensive slot opening mesially (Ahlberg and Clack, 1998). This is also the condition in *Parmastega* (Beznosov et al., 2019) and *Crassigyrinus* (Ahlberg and Clack, 1998), though in the latter taxon the Meckelian fenestra is considerably smaller. The condition in *Tiktaalik* is presently unknown.

Thus it is not clear whether *Acanthostega* and *Parmastega* represent the primitive state for limbed tetrapods or a derived condition. Recent phylogenetic analyses agree that *Parmastega* is more derived than the panderichthyids and sister to all more derived taxa (Beznosov et al., 2019; Ahlberg and Clack, 2020); the uncertainty as to whether *Parmastega* was digited or not adds to the uncertainty. The condition in *Crassigyrinus* appears to be a convergence, likely associated with its aquatic lifestyle. It is of course possible that this may also be the case for *Acanthostega* and/or *Parmastega*.

With the exception of *Whatcheeria*, *Crassigyrinus*, *Sigournea*, *Balanerpeton* (Milner and Sequeira, 1993), and the baphetids (as represented by *Megalocephalus*), the overall trend in post-Devonian tetrapods appears to be a reduction of the number of bony-margin Meckelian openings; some of these patterns are diagnostic of clades or other groups. The colosteids have a single elongate opening (Smithson, 1982; Bolt and Lombard, 2001, 2010), as does *Aytonerpeton* (Otoo, 2015; Clack et al., 2016). The St Louis tetrapod has a single larger opening and another

small opening anterior to it; in the context of its proposed colosteid affinities, this may be a primitive antecedent to the colosteid/*Aytonerpeton* single opening or an autapomorphic state (Clack et al., 2012a). Anthracosaurs (=Embolomeri) have two large openings (Romer, 1963; Holmes, 1984, 1989), with the exception of *Anthracosaurus* (Panchen, 1981), which has one. *Eoherpeton* has three small fenestrae,which may support its basal position within the anthracosaurs, as suggested by previous phylogenetic analyses (Ruta and Coates, 2007; Ruta et al., 2020). *Dendrerpeton* has three small fenestrae (Godfrey et al., 1987); *Eryops* has two (Sawin, 1941); a single moderately-sized fenstra is present in *Adamanterpeton* and *Archegosaurus* (Milner and Sequeira, 1998; Witzmann, 2005). A single fenestra is present in *Microbrachis*, *Lethiscus*, *Coloaraderpeton*, and *Seymouria* (Carroll and Gaskill, 1978; Laurin, 1996; Vallin and Laurin, 2004; Pardo et al., 2017b); in *Lethiscus* and *Coloraderpeton*, this appears to be a primitive condition relative to other aistopods (Carroll, 1998).

B.14 A DISCUSSION OF MANUAL DIGIT COUNTS IN THE WHATCHEERIIDAE AND IMPLICATIONS FOR THE ORIGINS TETRAPOD PENTADACTYLY

Even with the exclusion from the Whatcheeriidae of fragmentary Frasnian and Famennian specimens (Otoo et al., 2021), a soft Devonian origin for the clade is supported by the results of this study. The whatcheeriids and several other Mississippian lineages are bracketed by two Devonian taxa: *Ymeria* (stemward) and *Brittagnathus* (crownward). *Brittagnathus* is part of an unstable region between the whatcheeriids (stemward) and baphetids (crownward), alongside the Mississippian taxa *Occidens*, *Sigournea*, and *Eucritta*. With the exception of *Eucritta*, all these taxa are based on single jaw rami (*Occidens* is a partial chunk). While the jaw of *Eucritta* remains unknown and *Occidens* is too incomplete to assess, *Whatcheeria* (the condition is unknown in *Pederpes*), *Brittagnathus*, and *Ymeria* share- not uniquely- a Meckelian bone with more than three openings that open mesially, the margins of which are entirely bony. *Brittagnathus* also shares with the whatcheeriids a stepped posteroventral margin to the dentary. This may indicate a character distinction between *Parmastega*, *Acanthostega*, and the more (ostensibly) more derived taxa listed above but could be due to adaptations for aquatic function (see below).

Another character that does blur the distinction between Devonian tetrapods and the whatcheeriids is polydactyly (presence of more than five digits). Manual/pedal digit numbers known for Devonian tetrapods are: 8/8 (*Acanthostega*), ?/7 (*Ichthyostega*), and 6/6 (*Tulerpeton*). A pentadactyl manus and pes have been confirmed for *Whatcheeria*. The pes of *Pederpes* has five digits, but the manus is only represented by two digits in the holotype. Based on the

morphology of these manual phalanges, Clack and Finney (2005) proposed that these were digits V and VI. This would create a manual/pedal digit formula of 6/5. Pentadactyly in the manus and pes may then not be directly linked. Whatcheeriids, then, may have diverged during the Devonian prior to the stabilization to five digits at a crownward node. Where/when this stabilization took place is unclear. Manual and pedal pentadactyly are present in *Greererpeton* (Godfrey, 1989a; Coates, 1996), the only colosteids for which the manus and pes are known in detail. No crownward tetrapods are known to be polydactylous. 'Full' pentadactyly (manual and pedal) can be considered a synapomorphy of at least colosteids + crown group tetrapods. Both *Eucritta* (Clack, 2001) and *Crassigyrinus* (Panchen, 1985; Panchen and Smithson, 1990) have a five-digit pes but unknown manual counts. If manual and pedal digit counts independently reduced to five, then pedal pentadactyly is a synapomorphy of whatcheeriids + all crownward tetrapods, with the caveat that pedal counts are unknown in the baphetids, and the postcrania of *Sigournea* and *Brittagnathus* are entirely known.

However, these trees and others (Ruta and Coates, 2007; Clack et al., 2016, 2019a; Marjanović and Laurin, 2019) require multiple reductions to pentadactyly. If *Pederpes* is (manually) polydactylous, then pentadactyly evolved a minimum of two times: once on the *Whatcheeria* branch and once at or before the colosteids + crown tetrapods node. The lack of baphetid data allows for further instances of reduction. The initial phase of labile digit counts may then have extended across nearly the entire tetrapod stem group- or even its entirety, if colosteids are crown tetrapods.

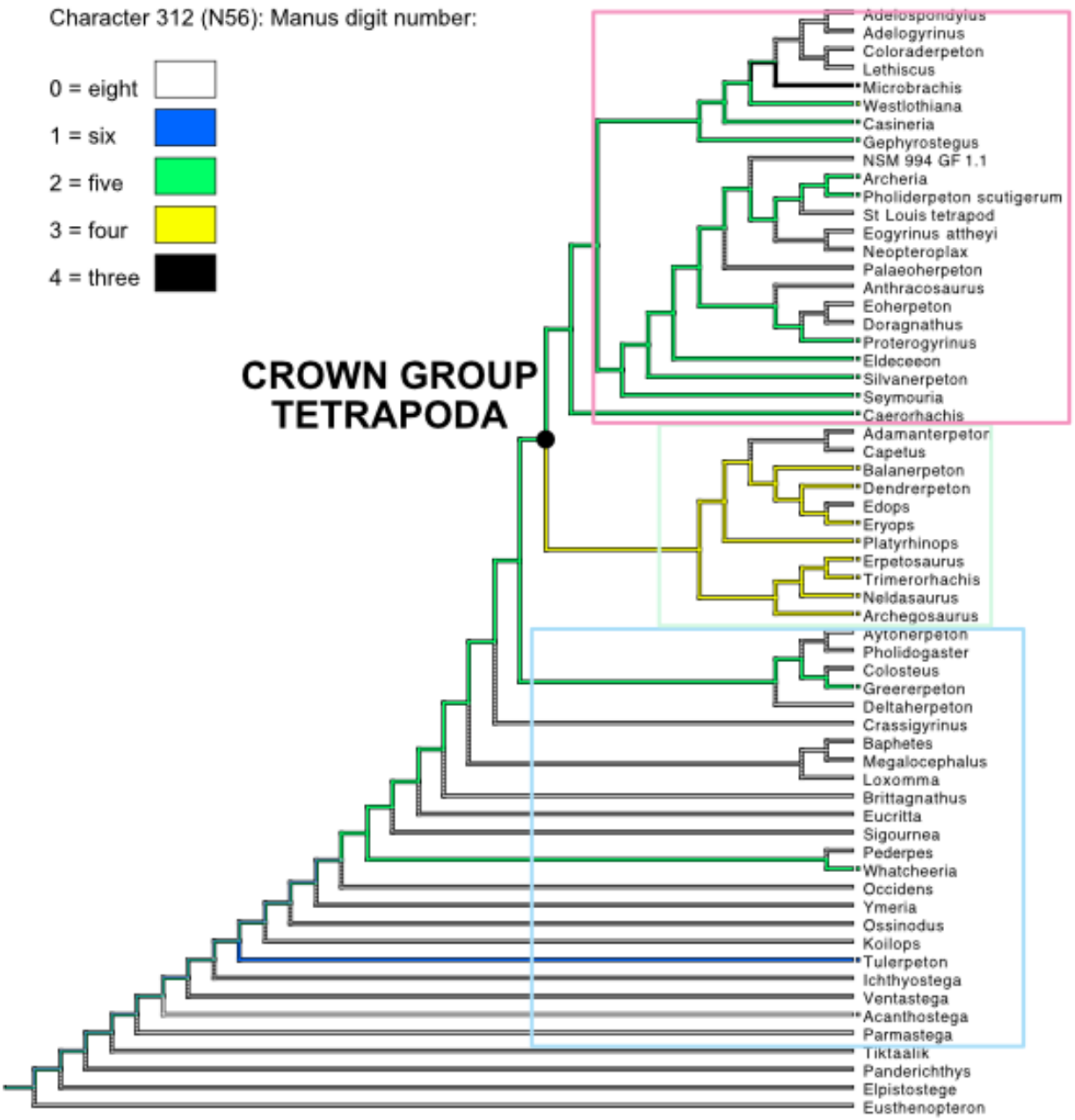

Figure B.1. Tree showing reconstructed character distribution of digit number across tree topology from primary hypothesis.

B.15 A DISCUSSION OF THE DISTRIBUTION OF THE SUBORBITAL, INFRAORBITAL, AND JUGAL BRANCHES OF THE LATERAL LINE EARLY TETRAPODS

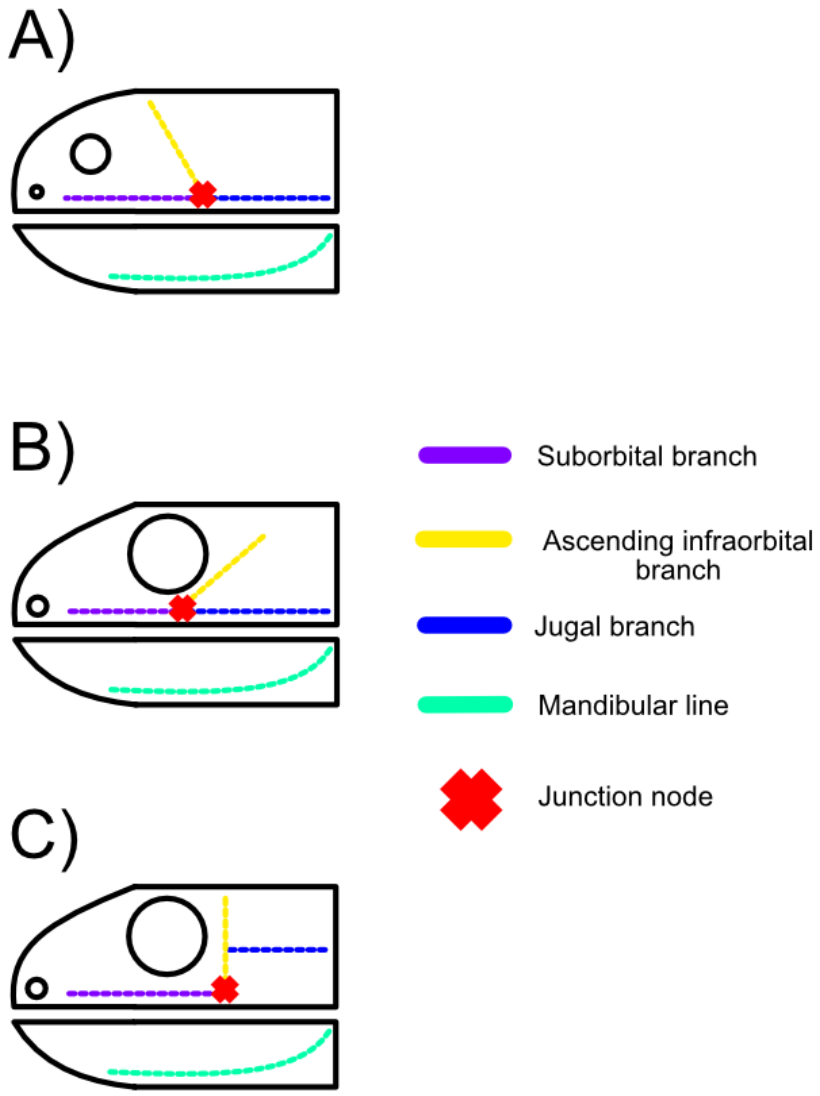

Figure B.2. Schematic representation of suborbital (= suborbital branch of infraorbital), ascending infraorbital, and jugal lateral lines on the skull of tetrapodomorphs and tetrapods. A: tetrapodomorph condition present in *Eusthenopteron*; B: 'lower' tetrapod condition found in Devonian and some Carboniferous tetrapods; C: 'higher' tetrapod condition found in Carboniferous and Permian tetrapods.

One source of characters uniting colosteids with crown tetrapods may be the patterns of the suborbital portion of the infraorbital canal, ascending portion of the infraorbital canal, and jugal canal of the lateral line system (Figure B.2). Developmental studies of extant animals indicate that the fundamental structure of these sensory canals is laid down early in ontogeny and may be deeply conserved. Three patterns of organization (taxa with substantial modifications within a given pattern-set are marked with an asterisk) are discernable within the taxon sample. These are described below.

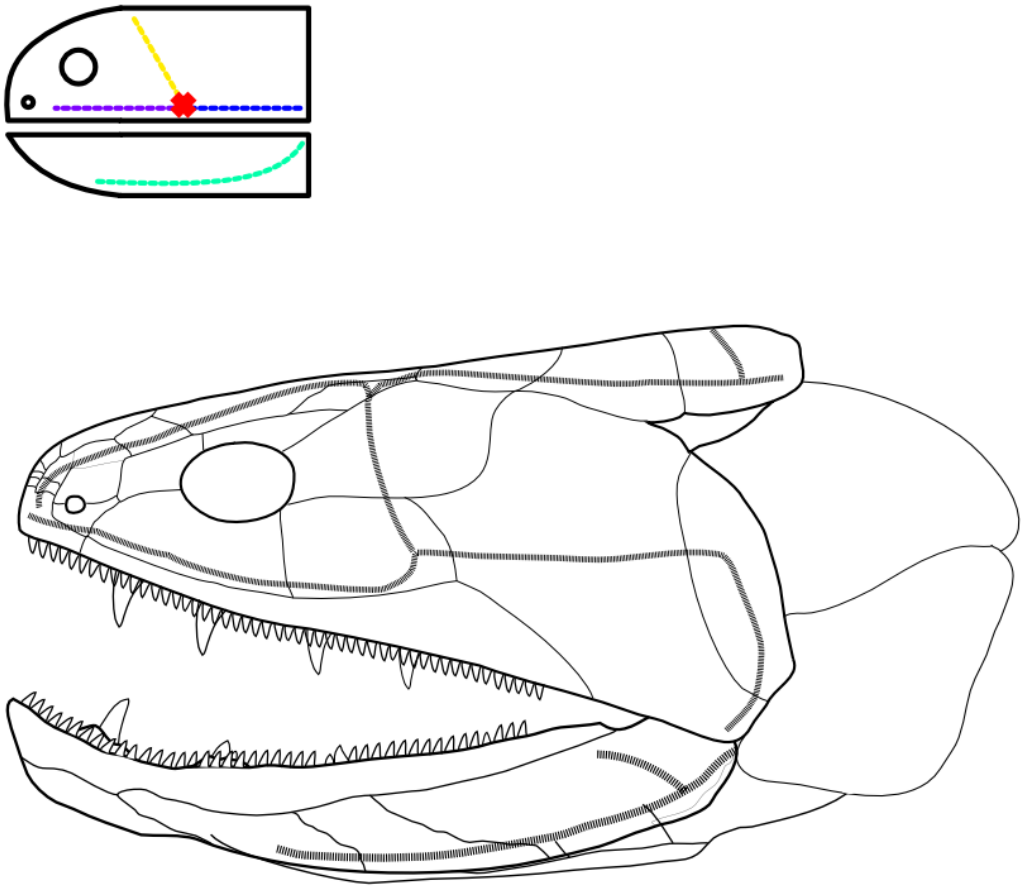

Figure B.3. Reconstruction of *Eusthenopteron* in left lateral view showing course of lateral line.

Outgroup condition (Figure 3.21): acute angle between the suborbital and ascending infraorbital; oblique angle between the ascending infraorbital and jugal; three-way junction between suborbital, ascending infraorbital, and jugal; junction posterior to orbit. Present in *Eusthenopteron*.

'Lower' tetrapod condition (Figure 3.22. Figure 3.23): oblique angle between suborbital and ascending infraorbital; acute angle between ascending infraorbital and jugal; three-way junction; junction suborbital. Present in *Parmastega*, *Acanthostega*, *Ventastega**, *Ichthyostega*, *Ossinodus**, *Pederpes**, *Whatcheeria*, "*Baphetes*" *lintonensis*, *Baphetes orientalis.* Also present in *Eogyrinus*, *Pholiderpeton*, *Palaeoherpeton*, and *Archeria*.

A variety of conditions are present in the baphetids (Figure 3.24). Some of this variation may support a separation of "*Baphetes*" *lintonensis* and *Baphetes orientalis* into a separate genus from *Baphetes kirkbyi*. Lateral lines are unknown in *Loxomma* (Beaumont, 1977), and absent in *Spathicephalus mirus* (Beaumont and Smithson, 1998). Lateral line canals are "clearly visible in the natural mould" (p.548) of *Spathicephalus marsdeni* (Smithson et al., 2017) but could not be reconstructed from published figures. The lateral line in *Crassigyrinus* is difficult to trace. In current reconstructions (Clack, 1997), the ascending infraorbital and jugal canals are absent, frustrating classification in the present scheme. However, an in-review manuscript by L Porro and colleagues (August 2022) presents a new reconstruction of the skull of *Crassigyrinus* with different proportions and may also contain new information on the lateral line system.

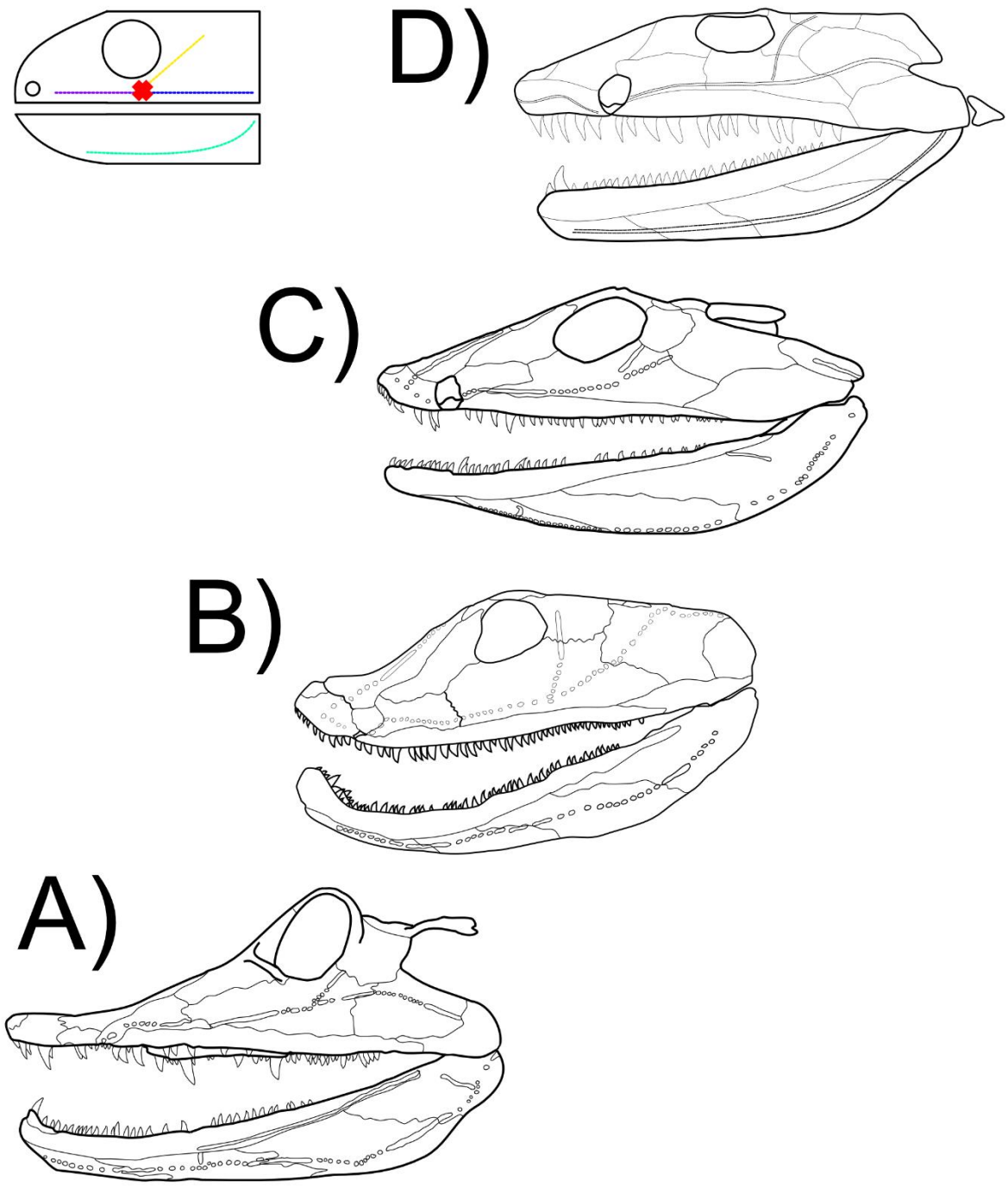

Figure B.4. Reconstructions of Parmastega and Devonian tetrapods showing ‘lower’ tetrapod condition. A) *Parmastega*; B) *Acanthostega*; C) *Ventastega*; D: *Ichthyostega*.

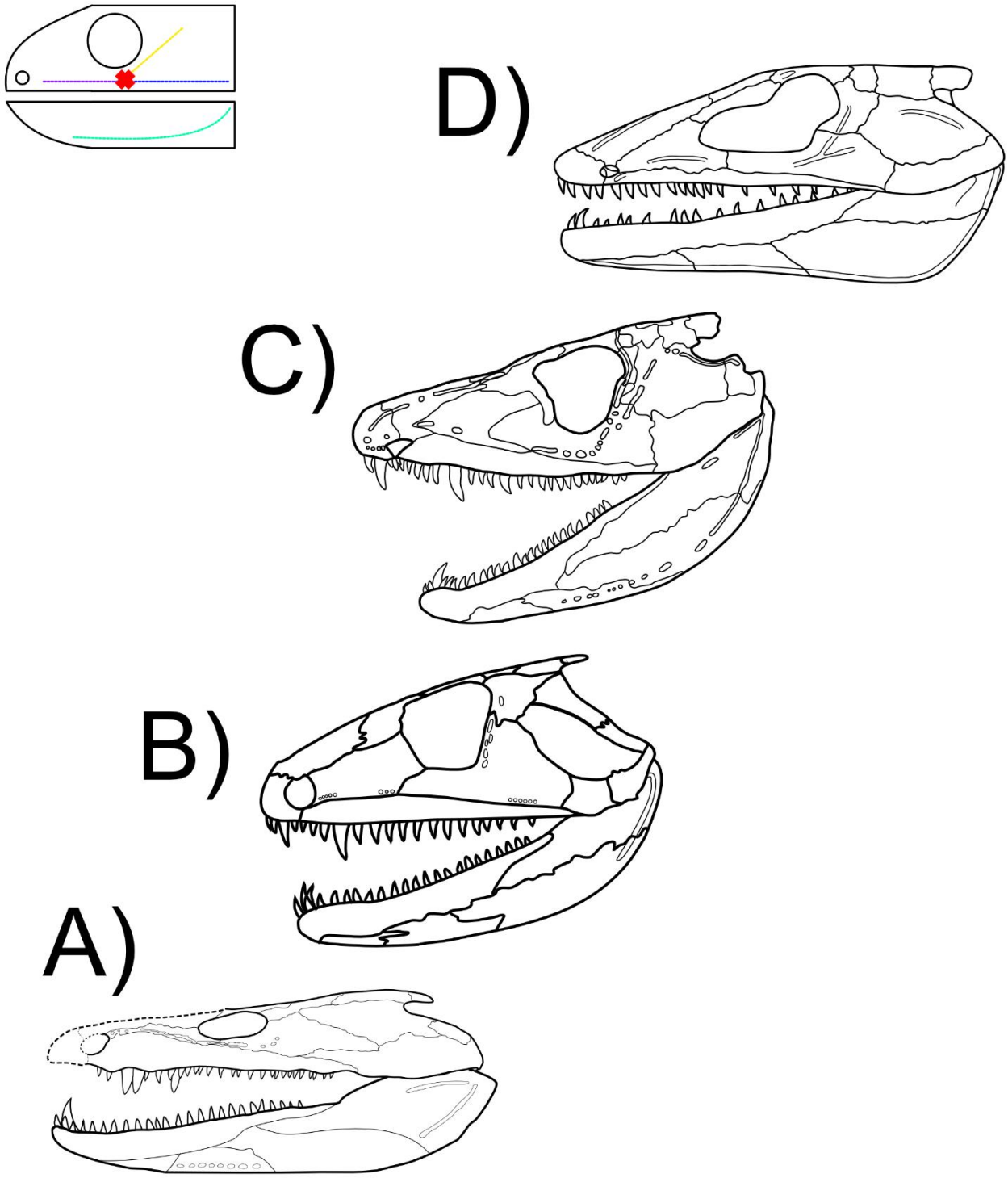

Figure B.5. Reconstructions of Carboniferous tetrapods showing 'lower' tetrapod condition. A) *Ossinodus*; B: *Pederpes*; C: *Whatcheeria*; D: "*Baphetes*" *lintonensis*.

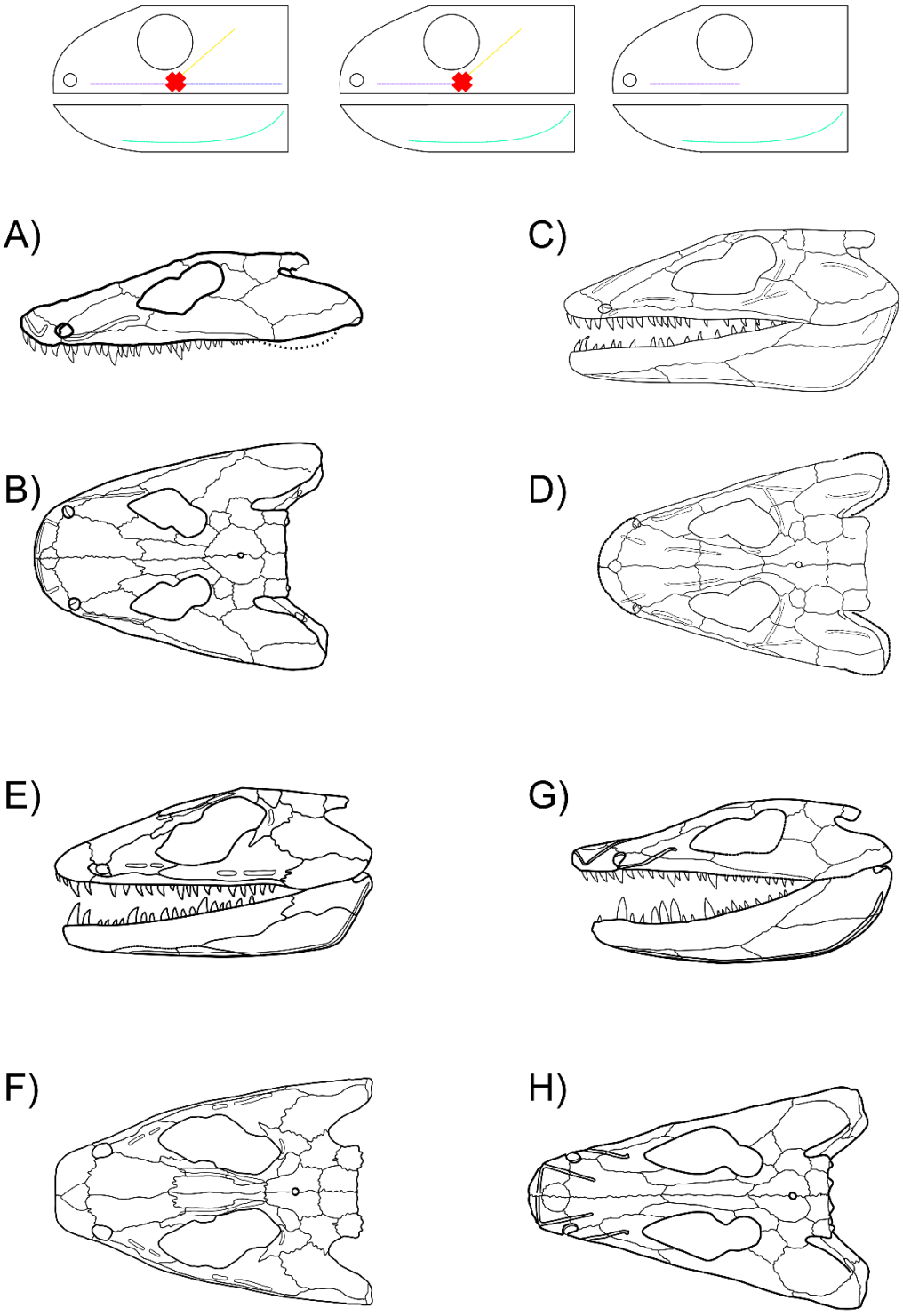

Figure B.6. Reconstructions of baphetids showing variations of lateral line expression in Baphetidae. *Baphetes kirkbyi* in lateral (A) and dorsal (B) view; "*Baphetes*" *lintonensis* in lateral (C) and dorsal (D) view; *Baphetes orientalis* in lateral (E) and dorsal (F) view; *Megalocephalus pachycephalus* in lateral (G) and dorsal (H) view.

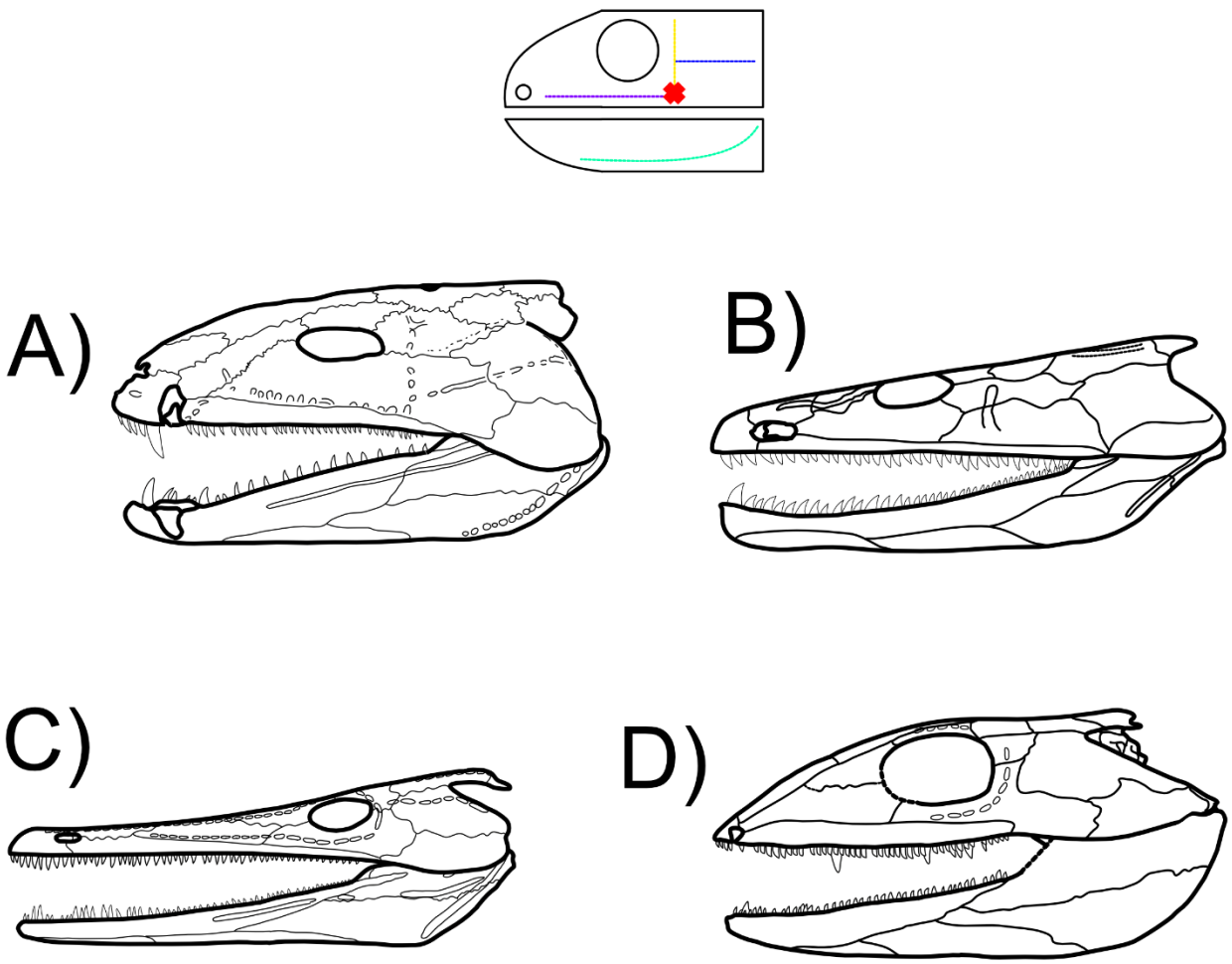

Figure B.7. Reconstructions of Carboniferous and Permian tetrapods showing ‘higher’ tetrapod condition. A: *Greererpeton*; B: *Trimerorhachis*; C: *Archegosaurus*; D: *Proterogyrinus*.

‘Higher’ tetrapod condition (Figure 3.25): angle between suborbital and ascending infraorbital approximately 90 degrees; dorsal displacement of jugal canal such that it does not participate in junction with suborbital and ascending infraorbital; suborbital/ascending infraorbital junction postorbital. Present in *Greererpeton*, *Colosteus*, *Pholidogaster*, *Deltaherpeton*, *Proterogyrinus*, *Archegosaurus*, and *Trimerorhachis**. The *Aytonerpeton* holotype is incomplete postorbitally and the course of the lateral line is extremely difficult to

reconstruct. A modified version of the 'higher' tetrapod condition has been depicted here. It can be compared and contrasted with the pattern in *Greererpeton*, *Archegosaurus*, *Trimerorhachis*, and the total loss in *Eryops* (Figure 3.26).

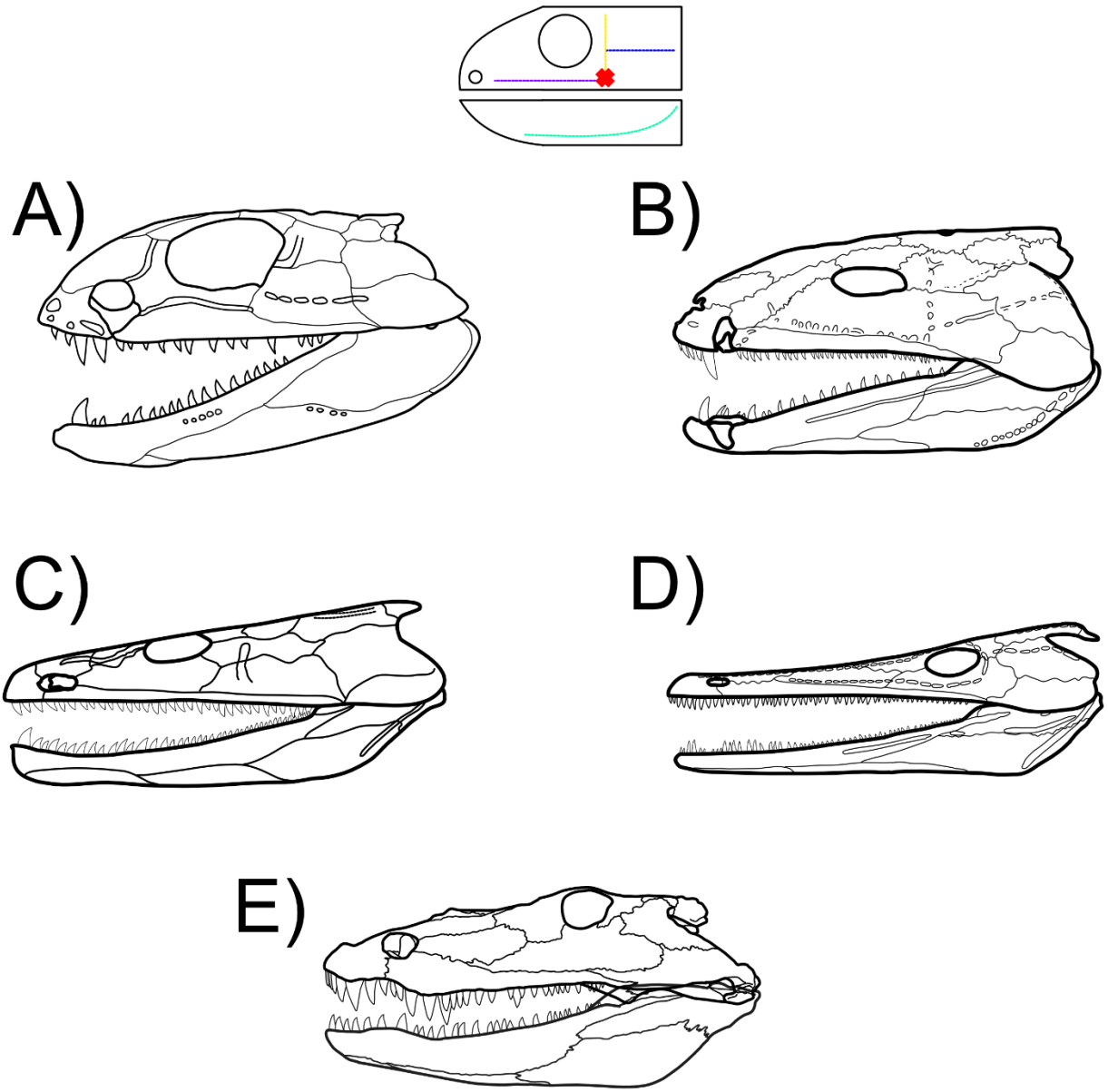

Figure B.8. Reconstructions of colosteids and temnospondyls showing variations in lateral line expression. A) *Aytonerpeton*; B) *Greererpeton*; C) *Trimerorhachis*; D) *Archegosaurus*; E) *Eryops*.

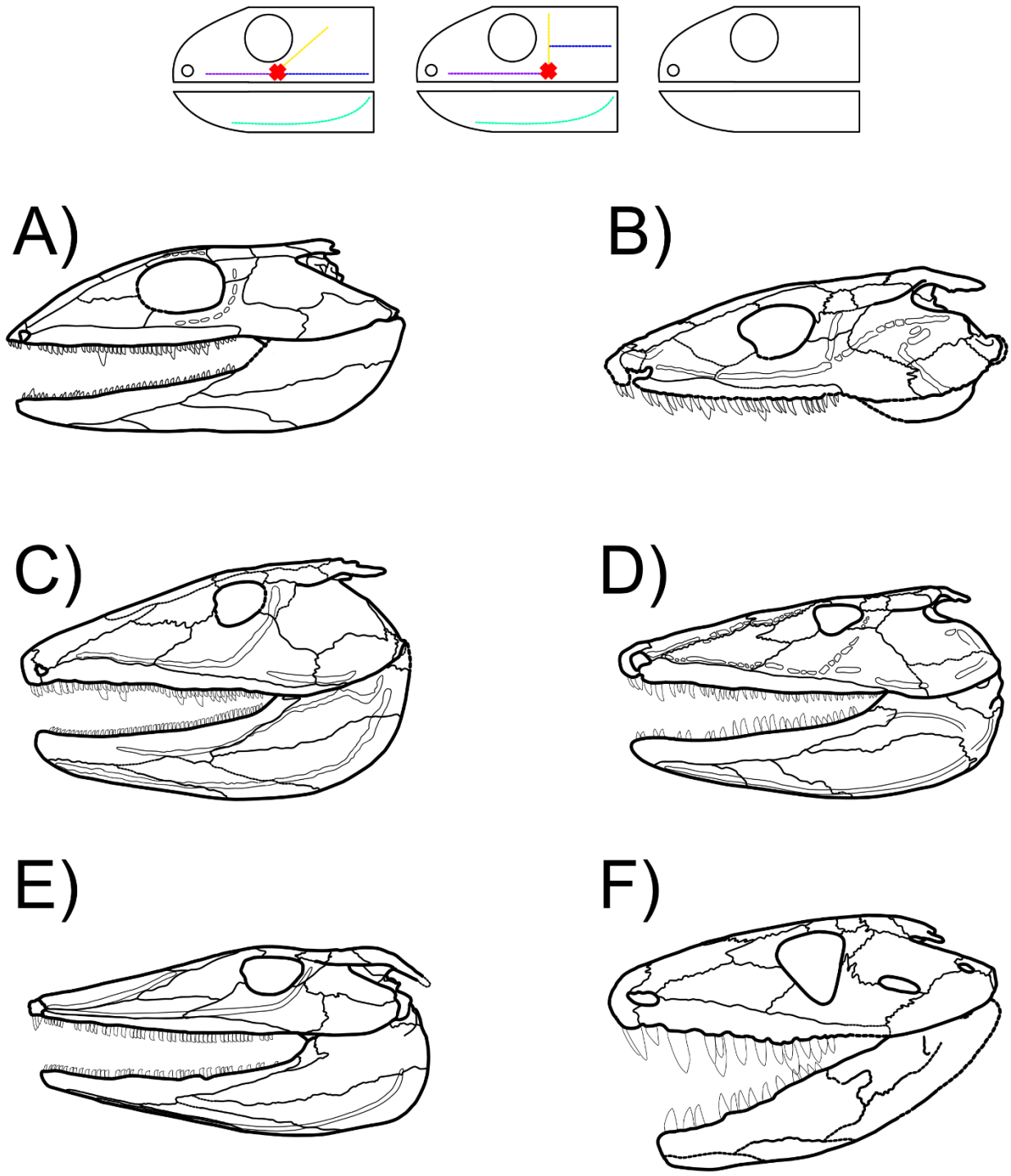

Figure B.9. Reconstructions of embolomeres showing variations of lateral line expression in Embolomeri. A) *Proterogyrinus*; B) *Palaeoherpeton*; C) *Pholiderpeton scutigerum*; D) *Eogyrinus attheyi*; E) *Archeria*; F) *Anthracosaurus*.

A necessary caveat is that among the embolomeres in this dataset, both the ‘lower’ and ‘higher’ tetrapod conditions are present (Figure 3.27). Three initial hypotheses can be proposed to explain this observation: 1) this reflects a phylogenetic division between two embolomere clades; 2) this supports a stem tetrapod position for embolomeres; 3) or this reflects transitions between the ‘lower’ and ‘higher’ conditions across short stretches of the phylogeny, suggestive of high evolutionary rates for the lateral line system in at least some cases. Investigating these will require a future analysis integrating these lateral line data.

Reductions of the lateral line are present from the Devonian, as indicated by *Ventastega* (Figure 3.22). The jugal canal appears to be reduced or lost most frequently, but distribution of reductions and losses does not indicate directional adaptation, such as would be expected if terrestrial adaptations were being collected (or aquatic adaptations being lost) moving up the stem toward the crown (Figure 3.28). Inferring from modern taxa, the distribution of lateral line geometries suggests that the lateral line system lags behind alterations of the dermal skull elements. As a result, the canals are ’dragged’ around the skull as proportions change during the fish-tetrapod transition. The emergence of the ‘higher’ tetrapod condition may then represent a change in the development of the skull. If so, the ‘higher’ tetrapod condition would be a good character supporting a close relationship between the colosteids and tetrapod crown group.

TAXONOMIC NOTE

The lack of a (consistent) sister group relationship between “*Eogyrinus*” (=*Pholiderpeton*) *attheyi* and *Pholiderpeton scutigerum* (Figure 3.8-3.11, Figure 3.15, Figure 3.16), is contra the taxonomic judgement by (Clack, 1987b) but has repeatedly been recovered in

other analyses (Ruta et al., 2003, 2020; Ruta and Coates, 2007; Marjanović and Laurin, 2019). Although both share the same ‘lower’ tetrapod lateral line pattern, there are differences between them Figure 3.27. A more conclusive assessment of their relationship will likely require a revision of the anatomy of both taxa and focused phylogenetic analysis. In the meantime, I recommend that *Eogyrinus* be reinstated for “*Pholiderpeton*” *attheyi*.

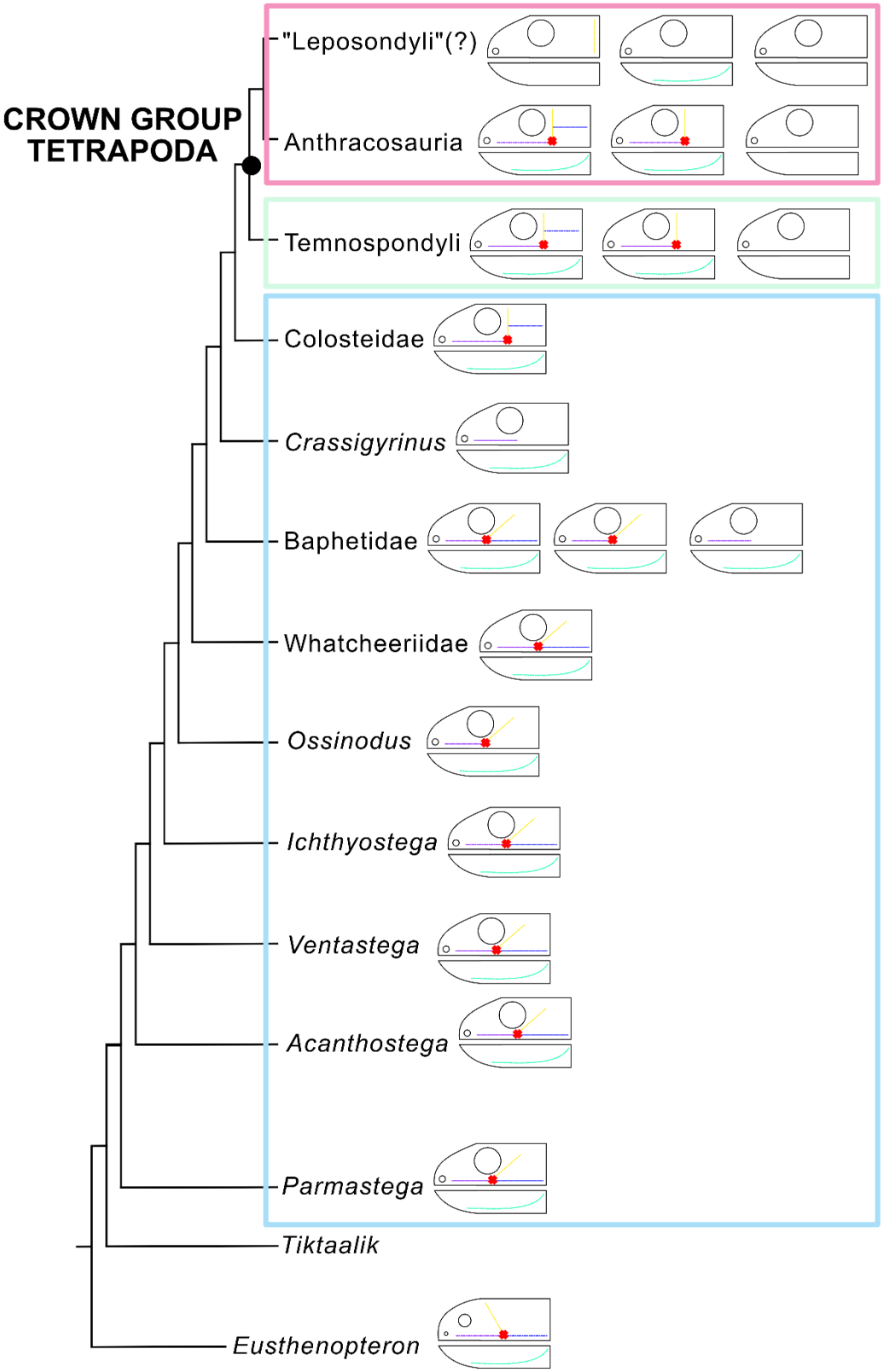

Figure B.10. Schematics representing distribution of lateral line conditions mapped onto a simplified representation of the topology from the primary hypothesis.

APPENDIX C: SUPPORTING INFORMATION FOR CHAPTER 4

C.1 REFERENCES FOR DEVONIAN PALEOCOMMUNITIES

AZTEC

(Young, 1989; Turner and Young, 1992; Young et al., 1992; McLoughlin and Long, 1994; Long, 1995; Long and Young, 1995; Donoghue and Smith, 2001; Johanson and Ahlberg, 2001; Young and Burrow, 2004; Young and Long, 2005; Klasson, 2008; Long et al., 2008a; Burrow et al., 2009; Choo et al., 2009; Sallan and Coates, 2010; Young et al., 2010; Bradshaw, 2013; Young and Long, 2014; Sallan and Galimberti, 2015; Young and Lu, 2020).

GILBOA

(Shear et al., 1984, 1989; Norton et al., 1988; Shear and Bonamo, 1988; Schawaller and Bonamo, 1991; Selden et al., 1991, 2008; Shear and Selden, 1995; Dunlop et al., 2002; Stein et al., 2007, 2012; Tetlie, 2007; Garwood and Edgecombe, 2011; Judson, 2012).

GLADBACH

(Ørvig, 1960, 1961; Miles, 1971; Ahlberg and Trewin, 1994; Forey et al., 2000; Burrow, 2004; Hartkopf-Fröder et al., 2004; Friedman and Coates, 2006; Klasson, 2008; Moloshnikov, 2008; Sallan and Coates, 2010; Choo, 2015; Sallan and Galimberti, 2015; Hairapetian and Burrow, 2016; Burrow et al., 2020).

KERMAN

(Schultze, 1973; Janvier, 1974, 1977, 1979; Janvier and Martin, 1978, 1979; Lelièvre et al., 1981; Wendt et al., 2002, 2005; Klasson, 2008; Hairapetian and Ginter, 2009, 2010; Sallan and Coates, 2010; Shen et al., 2019; Zamani et al., 2020).

GOGO

(Glenister, 1958; Klapper, 1966; Seddon, 1970; Miles, 1971, 1977; Dennis and Miles, 1979, 1980, 1981, 1982; Dennis-Bryan, 19871; Long, 1987a, 1987b, 1992, 1994, 1997, 1998; Gardiner and Miles, 1990; Becker et al., 1993; George et al., 1997; Won, 1997a, 1997b; Wood, 1998, 2000; Trinajstic, 1999; Trinajstic and McNamara, 1999; Kemp, 2001; Dunlop et al., 2002; Tetlie et al., 2004; Andrews et al., 2005; Long et al., 2006, 2008b, 2009, 2015b, 2015a, 2018; Trinajstic and Hazelton, 2007; Trinajstic et al., 2007, 2012, 2013, 2014; Choo, 2009, 2011, 2015; Copper and Edinger, 2009; Holland and Long, 2009; Trinajstic and George, 2009; Trinajstic and Long, 2009; Clement and Long, 2010; Long and Trinajstic, 2010, 2018; Lu and Zhu, 2010; Briggs et al., 2011; Burrow et al., 2012; Clement, 2012; Holland, 2013, 2014; Sanchez et al., 2013; Johanson and Trinajstic, 2014; Challands, 2015; Roelofs et al., 2015; Henderson and Challands, 2018; Choo et al., 2019; Bicknell et al., 2020).

MIGUASHA

(Schultze, 1984; Jeram, 1993; Cloutier et al., 1996; Janvier et al., 2006; Janvier, 2007; Cloutier et al., 2011; Cloutier, 2013; Béchard et al., 2014; Chevrinais et al., 2015a, 2015b; Olive et al., 2015a; Porro et al., 2015b; Olive et al., 2016b; Chevrinais et al., 2017; Charest et al., 2018; Downs, et al., 2018; Cloutier et al., 2020; Klug et al., 2021; Mondéjar-Fernández et al., 2021).

RED HILL

(Thomson, 1968; Daeschler, 2000b, 2000a, 2019; Frumes, 2003; Davis et al., 2004; Lane, 2005; Cressler, 2006; Friedman and Daeschler, 2006; Daeschler et al., 2009; Daeschler and Cressler, 2011; Downs et al., 2011; Bishop, 2013; Long and Daeschler, 2013; Young et al., 2013; Broussard et al., 2018, 2020; Daeschler and Downs, 2018; Kamska et al., 2018; Downs and Daeschler, 2020).

CLEVELAND SHALE

(Newberry, 1889; Claypole, 1893; Harris, 1938a, 1938b, 1951; Dunkle and Bungart, 1939, 1940, 1942a, 1942b, 1943, 1945; Dunkle, 1947; Halvin and Boreske Jr., 1973; Hlavin, 1976; Boylan and Murphy, 1978; Barron and Ettensohn, 1981; Carr, 1994, 1996, 2005, 2018, n.d.; Carr and Hlavin, 1995, 2010; Williams, 1998; Chitaley and Cai, 2001; Carr and Jackson, 2008; Tomita, 2015; Boyle and Ryan, 2017; Ferrón et al., 2017; Johanson et al., 2019; Martinez et al., 2019; Coatham et al., 2020).

EVIEUX FORMATION

(Cloutier and Cloutier, Anne-Marie, 1995; Derycke et al., 1995, 2014; Clement, 2002; Clement et al., 2004, 2009; Janvier and Clément, 2005; Garrouste et al., 2012; Hörnschemeyer et al., 2013; Olive, 2013; Young et al., 2013; Gueriau et al., 2014, 2016, 2020; Kumpan et al., 2014; Lagebro et al., 2015; Olive et al., 2015b, 2016a, 2016b, 2020; Denayer et al., 2016; Mottequin and Poty, 2016; Lamsdell et al., 2019; Wilk et al., 2021).

WATERLOO FARM

(Anderson et al., 1995, 1999; Gess and Hiller, 1995; Long et al., 1997; Gess, 2001, 2011, 2013; Amler, 2004; Gess et al., 2006; Coates and Gess, 2007; Young et al., 2013; Gess and Coates, 2015; Coates et al., 2017; Gess and Trinajstic, 2017; Scholze and Gess, 2017, 2021; Gess and Ahlberg, 2018; Gess and Clement, 2019; Gess and Whitfield, 2020; Miyashita et al., 2021).

C.2 REFERENCES FOR MISSISSIPPIAN PALEOCOMMUNITIES

UPPER BALLAGAN FORMATION

(Almond, 1985; Anderton, 1985; Andrews, 1985; Briggs and Clarkson, 1985; Clarkson, 1985; Clayton, 1985; Forey and Young, 1985; Gardiner, 1985; Pollard, 1985; Scott and Meyer-Berthaud, 1985; Waterston, 1985; Waterston et al., 1985; Clack, 2002c; Clack and Finney, 2005; Jeffery, 2006, 2012; Smithson et al., 2012, 2016; Otoo, 2015; Bennett et al., 2016, 2017; Clack et al., 2016, 2018, 2019b; Kearsey et al., 2016; Chen et al., 2018; Millward et al., 2018a, 2018b; Otoo et al., 2018; Ross et al., 2018; Smithson and Clack, 2018; Challands et al., 2019; Marshall et al., 2019).

EAST KIRKTON

(Brown et al., 1993; Clack, 1993; Clarkson et al., 1993; Coates, 1993a; Durant, 1993; Jeram, 1993; Jeram and Selden, 1993; McGill et al., 1993; Milner and Sequeira, 1993; Paton, 1993; Rolfe et al., 1993; Scott et al., 1993; Shear, 1993; Smithson, 1993; Smithson et al., 1993; Sumner, 1993; Walkden et al., 1993; Clack, 1998b, 2001; Dunlop and Anderson, 2005; Ruta and

Clack, 2006; Lamsdell et al., 2010; Clack, 2011; Hughes, 2019; Lamsdell et al., 2020; Ruta et al., 2020; Hughes and Lamsdell, 2021; Clack et al., 2022).

GLENCARTHOLM

(Moy-Thomas, 1936; Moy-Thomas and Bradley Dyne, 1938; Wood, 1982, 2018; Schram, 1983; Cater, 1987; Coates and Gess, 2007; Ginter, 2009; Sallan, 2012; Finarelli and Coates, 2014).

BEARSDEN

(Traquair, 1884; Jefferies and Minton, 1965; Wood, 1982; Briggs and Clarkson, 1985, 1989; Zhang and Pojeta, 1986; Coates, 1988, 1993b, 1998; Cater et al., 1989; Clark, 1989, 1990, 1991, 2013; Coates and Sequeira, 2001; Mergil et al., 2001; Sallan, 2012; Bitner and Cohen, 2013; Finarelli and Coates, 2014; Hyžný et al., 2014; Elliott, 2016; Torres-Martínez and Sour-Tovar, 2016; Coates et al., 2019).

BEAR GULCH

(Traquair, 1886; Zangerl and Case, 1973; Lund and Zangerl, 1974; Schram and Horner, 1978; Lowney, 1980; Lund, 1980, 1982, 1983, 1984, 1985a, 1985b, 1986, 1988, 1989, 1990, 2000; Ann, 1981; Lund and Melton, 1982; Janvier and Lund, 1983; Williams, 1983; Lund and Lund, 1984, 1985; Lund and Mapes, 1984; Welch, 1984; Cox, 1986; Lund and Janvier, 1986;

McRoberts and Stanley, 1989; Briggs and Gall, 1990; Feldman et al., 1994; Grogan and Lund, 1995, 1997, 2000, 2008, 2009, 2011, 2015; Lund and Grogan, 1997; Lund and Poplin, 1997, 1999, 2002; Jenner et al., 1998; Rosenberg, 1998; Poplin and Lund, 2000, 2002; Janvier et al., 2004; Thomas, 2004; Mutter and Neuman, 2006; Mapes et al., 2007, 2010; Moore et al., 2007; Mickle et al., 2009a, 2009b; Lund et al., 2012, 2014, 2015; Grogan et al., 2014; Martill et al., 2014; Bronson et al., 2018; Klug et al., 2019; Ginter, 2022; Whalen and Landman, 2022).

LOANHEAD

(Eastman, 1899; Wellburn, 1901, 1903; Gardiner and Mason, 1974; Beaumont, 1977; Smithson, 1980; Dick, 1981; Andrews, 1985; Smith et al., 1987; Andrews and Carroll, 1991; Beaumont and Smithson, 1998; Heidtke, 1998; Milner and Lindsay, 1998; Johanson et al., 2000; Warren et al., 2000; Hampe, 2002; Ruta et al., 2002; Parker et al., 2005; Turner et al., 2005; Jeffery, 2006, 2012; Sharp and Clack, 2011, 2013; Snyder, 2011; Smithson et al., 2019).

C.3 REFERENCES FOR PHYLOPIC SILHOUETTES USED

Table C.1. Key to PhyloPic images used in Figure 4.3. Images are meant as approximations and do not necessarily represent organisms present within the Cleveland Shale food web.

Taxon	PhyloPic creator
Cheirolepis trailli	T. Michael Keesey
Ciliophora	Emily Jane McTavish
Cladoselache fyleri	Lankester Edwin Ray (vectorized by T. Michael Keesey)
Coccosteus decipiens	*Nobu Tamura (vectorized by T. Michael Keesey)*
Cooperoceras texanum	David Tana
Daphina galeata	Mathilde Cordellier
Dunkleosteus terrelli	T. Michael Keesey
Dunkleosteus terrelli	Jagged Fang Designs
Dunkleosteus terrelli	Jagged Fang Designs
Edestus [sp.]	Tyler Greenfield
Lingula [sp.]	T. Michael Keesey
Pomatoceros lamarckii	Reka Szabo
Protobranchia	Scott Hartman

Table C.2. Key to PhyloPic images used in Figure 4.29. Images are meant as approximations and do not necessarily represent specific organisms present in specific communities.

Taxon	PhyloPic creator
Westlothiana lizzae	Scott Hartman
Tiktaalik roseae	Obsidian Soul (vectorized by T. Michael Keesey)
Squalus acanthias	Ignacia Contreras
Scutigeridae	Yan Wong
Scaumenacia curta	Steven Coombs
Sauripteridae	Chase Brownstein
Protoischnurus axelrodor	Dean Schnabel
Megarachne servinei	Gareth Monger
Marattia	Mason McNair
Hynerpeton bassetti	Nobu Tamura (vectorized by T. Michael Keesey)

Gephyrostegus bohemicus	Dmitry Bogdanov (vectorized by T. Michael Keesey)
Eusthenopteron foordi	Steven Coombs (vectorized by T. Michael Keesey)
Eucritta melanolimnetes	Dmitry Bogdanov (vectorized by T. Michael Keesey)
Eoherpeton watsoni	Nobu Tamura, modified by Andrew A. Farke
Cheirolepis trailli	Anonymous
Callorhinchus milii	Ingo Braasch
Bothriolepis [sp.]	Ghedoghedo
Balanerpeton woodi	Scott Hartman
Arthropleura	Tim Bertelink (modified by T. Michael Keesey)
Archaeopteris	Falconaumanni and T. Michael Keesey
Acanthodes bronni	Nobu Tamura
Iberospondylus schultzei	Dmitry Bogdanov (vectorized by T. Michael Keesey)
Ptomacanthus anglicus	T. Michael Keesey
Shielia taiti	Verisimilus

APPENDIX D: REFERENCES FOR APPENDICES

Adams, G. R. 2020. Description of Calligenethlon watsoni based on computed tomography and resulting implications for the phylogenetic placement of embolomeres. MS, Carleton University, Ottawa, Ontario, Canada, 155 pp.

Ahlberg, P. E. 2011. Humeral homology and the origin of the tetrapod elbow: a reinterpretation of the enigmatic specimens ANSP 21350 and GSM 104536. Special Papers in Palaeontology 86:17–29.

Ahlberg, P. E. 2018. Follow the footprints and mind the gaps: a new look at the origin of tetrapods. Earth and Environmental Science Transactions of the Royal Society of Edinburgh 109:115–137.

Ahlberg, P. E., and N. H. Trewin. 1994. The postcranial skeleton of the Middle Devonian lungfish Dipterus valenciennesi. Transactions of the Royal Society of Edinburgh: Earth Sciences 85:159–175.

Ahlberg, P. E., and J. A. Clack. 1998. Lower jaws, lower tetrapods-a review based on the Devonian genus Acanthostega. Transactions of the Royal Society of Edinburgh: Earth Sciences 89:11–46.

Ahlberg, P. E., and J. A. Clack. 2020. The smallest known Devonian tetrapod shows unexpectedly derived features. Royal Society Open Science 7:192117.

Ahlberg, P. E., E. Lukševičs, and O. Lebedev. 1994. The first tetrapod finds from the Devonian (Upper Famennian) of Latvia. Philosophical Transactions of the Royal Society B: Biological Sciences 343:303–328.

Ahlberg, P. E., J. A. Clack, and E. Luksevics. 1996. Rapid braincase evolution between Panderichthys and the earliest tetrapods. Nature 381:61–64.

Ahlberg, P. E., J. A. Clack, and H. Blom. 2005. The axial skeleton of the Devonian tetrapod Ichthyostega. Nature 437:137–140.

Ahlberg, P. E., J. A. Clack, E. Lukševičs, H. Blom, and I. Zupiņš. 2008. Ventastega curonica and the origin of tetrapod morphology. Nature 453:1199–1204.

Almond, J. E. 1985. A vermiform problematicum from the Dinantian of Foulden, Berwickshire, Scotland. Transactions of the Royal Society of Edinburgh: Earth Sciences 76:41–47.

Amler, M. R. W. 2004. Bivalve biostratigraphy of the Kulm Facies (Early Carboniferous, Mississippian) in central Europe. Newsletters on Stratigraphy 40:183–207.

Anderson, H. M., N. Hiller, and R. W. Gess. 1995. Archaeopteris (Progymnospermopsida) from the Devonian of southern Africa. Botanical Journal of the Linnean Society 117:305–320.

Anderson, J. S. 2003. Cranial Anatomy of Coloraderpeton brilli, Postcranial Anatomy of Oestocephalus amphiuminus, and Reconsideration of Ophiderpetontidae (Tetrapoda: Lepospondyli: Aistopoda). Journal of Vertebrate Paleontology 23:532–543.

Anderson, J. S., R. L. Carroll, and T. B. Rowe. 2003. New information on *Lethiscus stocki* (Tetrapoda: Lepospondyli: Aistopoda) from high-resolution computed tomography and a phylogenetic analysis of Aistopoda. Canadian Journal of Earth Sciences 40:1071–1083.

Anderson, M. E., J. A. Long, R. W. Gess, and N. Hiller'. 1999. An unusual new fossil shark (Pisces: Chondrichthyes> from the Late Devonian of South Africa. Records of the Australian Museum, Supplement 151–156.

Anderton, R. 1985. Sedimentology of the Dinantian of Foulden, Berwickshire, Scotland. Transactions of the Royal Society of Edinburgh: Earth Sciences 76:7–12.

Andrews, M., J. Long, P. Ahlberg, R. Barwick, and K. Campbell. 2005. The structure of the sarcopterygian Onychodus jandemarrai n. sp. from Gogo, Western Australia: with a functional interpretation of the skeleton. Transactions of the Royal Society of Edinburgh: Earth Sciences 96:197–307.

Andrews, S. M. 1985. Rhizodont crossopterygian fish from the Dinantian of Foulden, Berwickshire, Scotland, with a re-evaluation of this group. Transactions of the Royal Society of Edinburgh: Earth Sciences 76:67–85.

Andrews, S. M., and T. S. Westoll. 1970. Postcranial skeleton of Eusthenopteron foordi Whiteaves. Transactions of the Royal Society of Edinburgh 68:30–328.

Andrews, S. M., and R. L. Carroll. 1991. The Order Adelospondyli: Carboniferous lepospondyl amphibians. Transactions of the Royal Society of Edinburgh: Earth Sciences 82:239–275.

Ann, L. 1981. The sedimentational history of the Bear Gulch Limestone (Middle Carboniferous central Montana): an explanation of "How them fish swam between them rocks." PhD, Princeton University, Princeton, New Jersey, USA, 251 pp.

Barron, L. S., and F. R. Ettensohn. 1981. Paleoecology of the Devonian-Mississippian Black-Shale Sequence in Eastern Kentucky with an Atlas of Some Common Fossils. pp.

Bazzana, K. D., B. M. Gee, J. J. Bevitt, and R. R. Reisz. 2020a. Neurocranial anatomy of *Seymouria* from Richards Spur, Oklahoma. Journal of Vertebrate Paleontology e1694535.

Bazzana, K. D., B. M. Gee, J. J. Bevitt, and R. R. Reisz. 2020b. Postcranial anatomy and histology of Seymouria, and the terrestriality of seymouriamorphs. PeerJ 8:e8698.

Beaumont, E. H. 1977. Cranial morphology of the Loxommatidae (Amphibia: Labyrinthodontia). Philosophical Transactions of the Royal Society B: Biological Sciences 280:29–101.

Beaumont, E. H., and T. R. Smithson. 1998. The cranial morphology and relationships of the aberrant Carboniferous amphibian Spathicephalus mirus Watson. Zoological Journal of the Linnean Society 122:187–209.

Béchard, I., F. Arsenault, R. Cloutier, and J. Kerr. 2014. The Devonian placoderm fish Bothriolepis canadensis revisited with three-dimensional digital imagery. Palaeontologia Electronica.

Becker, R. T., M. R. House, and W. T. Kirchgasser. 1993. Devonian goniatite biostratigraphy and timing of facies movements in the Frasnian of the Canning Basin, Western Australia. Geological Society, London, Special Publications 70:293–321.

Bennett, C. E., T. I. Kearsey, S. J. Davies, D. Millward, J. A. Clack, T. R. Smithson, and J. E. A. Marshall. 2016. Early Mississippian sandy siltstones preserve rare vertebrate fossils in seasonal flooding episodes. Sedimentology 63:1677–1700.

Bennett, C. E., A. S. Howard, S. J. Davies, T. I. Kearsey, D. Millward, P. J. Brand, M. A. E. Browne, E. J. Reeves, and J. E. A. Marshall. 2017. Ichnofauna record cryptic marine incursions

onto a coastal floodplain at a key Lower Mississippian tetrapod site. Palaeogeography, Palaeoclimatology, Palaeoecology 468:287–300.

Berman, D. S., and R. Reisz. 1980. A new species of Trimerorhachis (Amphibia, Temnospondyli) from the Lower Permian Abo Formation of New Mexico, with discussion of Permian faunal distributions in that state. Annals of Carnegie Museum 49:455–485.

Berman, D. S., A. C. Henrici, S. S. Sumida, and T. Martens. 2000. Redescription of *Seymouria sanjuanensis* (Seymouriamorpha) from the Lower Permian of Germany based on complete, mature specimens with a discussion of paleoecology of the Bromacker locality assemblage. Journal of Vertebrate Paleontology 20:253–268.

Beznosov, P. A., J. A. Clack, E. Lukševičs, M. Ruta, and P. E. Ahlberg. 2019. Morphology of the earliest reconstructable tetrapod Parmastega aelidae. Nature 574:527–533.

Bicknell, R. D. C., P. M. Smith, and M. Poschmann. 2020. Re-evaluating evidence of Australian eurypterids. Gondwana Research 86:164–181.

Bishop, P. J. 2013. Fang histology of the Late Devonian tristichopterid Hyneria lindae Thomson, 1968. Memoirs of the Queensland Museum- Nature 56:311–312.

Bishop, P. J. 2014. The humerus of *Ossinodus pueri*, a stem tetrapod from the Carboniferous of Gondwana, and the early evolution of the tetrapod forelimb. Alcheringa: An Australasian Journal of Palaeontology 38:209–238.

Bishop, P. J., C. W. Walmsley, M. J. Phillips, M. R. Quayle, C. A. Boisvert, and C. R. McHenry. 2015. Oldest Pathology in a Tetrapod Bone Illuminates the Origin of Terrestrial Vertebrates. PLOS ONE 10:1–18.

Bitner, M. A., and B. L. Cohen. 2013. Brachiopoda; pp. in John Wiley & Sons, Ltd (ed.), eLS, 1st ed. Wiley, Chichester, England, UK.

Blom, H. 2005. Taxonomic revision of the Late Devonian tetrapod Ichthyostega from East Greenland. Palaeontology 48:111–134.

Boisvert, C. A. 2005. The pelvic fin and girdle of Panderichthys and the origin of tetrapod locomotion. Nature 438:1145–1147.

Boisvert, C. A. 2009. The humerus of *Panderichthys* in three dimensions and its significance in the context of the fish-tetrapod transition. Acta Zoologica 90:297–305.

Boisvert, C. A., E. Mark-Kurik, and P. E. Ahlberg. 2008. The pectoral fin of Panderichthys and the origin of digits. Nature 456:636–638.

Bolt, J. R., and R. E. Lombard. 2000. Palaeobiology of Whatcheeria deltae; pp. 1044–1052 in H. Heatwole and R. L. Carroll (eds.), Amphibian Biology. Surrey Beatty & Sons, Chipping Norton, New South Wales, Australia.

Bolt, J. R., and R. E. Lombard. 2001. The Mandible of the Primitive Tetrapod Greererpeton, and the Early Evolution of the Tetrapod Lower Jaw. Journal of Paleontology 75:1016–1042.

Bolt, J. R., and R. E. Lombard. 2006. Sigournea multidentata, a new stem tetrapod from the Upper Mississippian of Iowa, USA. Journal of Paleontology 80:717–725.

Bolt, J. R., and R. E. Lombard. 2010. Deltaherpeton hiemstrae, a new colosteid tetrapod from the Mississippian of Iowa. Journal of Paleontology 84:1135–1151.

Bolt, J. R., and R. E. Lombard. 2018. Palate and braincase of *Whatcheeria deltae* Lombard & Bolt, 1995. Earth and Environmental Science Transactions of the Royal Society of Edinburgh 1–24.

Boylan, J. C., and P. A. Murphy. 1978. The Ventral Armor and Feeding Biomechanics of Glyptaspis verrucosa Newberry, a Placoderm From the Fammenian Cleveland Shale. American Museum Novitates 1–12.

Boyle, J., and M. J. Ryan. 2017. New information on *Titanichthys* (Placodermi, Arthrodira) from the Cleveland Shale (Upper Devonian) of Ohio, USA. Journal of Paleontology 91:318–336.

Bradshaw, M. A. 2013. The Taylor Group (Beacon Supergroup): the Devonian sediments of Antarctica. Geological Society, London, Special Publications 381:67–97.

Briggs, D. E. G., and E. N. K. Clarkson. 1985. Malacostracan Crustacea from the Dinantian of Foulden, Berwickshire, Scotland. Transactions of the Royal Society of Edinburgh: Earth Sciences 76:35–40.

Briggs, D. E. G., and E. N. K. Clarkson. 1989. Environmental controls on the taphonomy and distribution of Carboniferous malacostracan crustaceans. Transactions of the Royal Society of Edinburgh: Earth Sciences 80:9.

Briggs, D. E. G., and J.-C. Gall. 1990. The continuum in soft-bodied biotas from transitional environments: a quantitative comparison of Triassic and Carboniferous Konservat-Lagerstätten. Paleobiology 16:204–218.

Briggs, D. E. G., W. D. I. Rolfe, P. D. Butler, J. J. Liston, and J. K. Ingham. 2011. Phyllocarid crustaceans from the Upper Devonian Gogo Formation, Western Australia. Journal of Systematic Palaeontology 9:399–424.

Bronson, A. W., R. H. Mapes, and J. G. Maisey. 2018. Chondrocranial morphology of *Carcharopsis wortheni* (Chondrichthyes, Euselachii *incertae sedis*) based on new material from the Fayetteville Shale (upper Mississippian, middle Chesterian). Papers in Palaeontology 4:349–362.

Brough, M. C., and J. Brough. 1967a. III. The Genus Gephyrostegus. Philosophical Transactions of the Royal Society B: Biological Sciences 252:21.

Brough, M. C., and J. Brough. 1967b. II. *Microbrachis* , the type microsaur. Philosophical Transactions of the Royal Society B: Biological Sciences 252:131–146.

Broussard, D. R., J. M. Trop, J. A. Benowitz, E. B. Daeschler, J. A. Chamberlain, and R. B. Chamberlain. 2018. Depositional setting, taphonomy and geochronology of new fossil sites in the Catskill Formation (Upper Devonian) of north-central Pennsylvania, USA, including a new early tetrapod fossil. Palaeogeography, Palaeoclimatology, Palaeoecology 511:168–187.

Broussard, D. R., C. J. Treaster, J. M. Trop, E. B. Daeschler, P. A. Zippi, M. B. Vrazo, and M. C. Rygel. 2020. VERTEBRATE TAPHONOMY, PALEONTOLOGY, SEDIMENTOLOGY, AND PALYNOLOGY OF A FOSSILIFEROUS LATE DEVONIAN FLUVIAL SUCCESSION, CATSKILL FORMATION, NORTH-CENTRAL PENNSYLVANIA, USA. PALAIOS 35:470–494.

Brown, R. E., A. C. Scott, and T. P. Jones. 1993. Taphonomy of plant fossils from the Viséan of East Kirkton, West Lothian, Scotland. Transactions of the Royal Society of Edinburgh: Earth Sciences 84:267–274.

Burrow, C., J. den Blaauwen, and M. Newman. 2020. A redescription of the three longest-known species of the acanthodian Cheiracanthus from the Middle Devonian of Scotland. Palaeontologia Electronica.

Burrow, C. J. 2004. A redescription of *Atopacanthus dentatus* Hussakof and Bryant, 1918 (Acanthodii, Ischnacanthidae). Journal of Vertebrate Paleontology 24:257–267.

Burrow, C. J., J. A. Long, and K. Trinajstic. 2009. Disarticulated acanthodian and chondrichthyan remains from the upper Middle Devonian Aztec Siltstone, southern Victoria Land, Antarctica. Antarctic Science 21:71–88.

Burrow, C. J., K. Trinajstic, and J. Long. 2012. First acanthodian from the Upper Devonian (Frasnian) Gogo Formation, Western Australia. Historical Biology 24:349–357.

Callier, V., J. A. Clack, and P. E. Ahlberg. 2009. Contrasting Developmental Trajectories in the Earliest Known Tetrapod Forelimbs. Science 324:364–367.

Campbell, K. S. W., and M. W. Bell. 1977. A primitive amphibian from the Late Devonian of New South Wales. Alcheringa: An Australasian Journal of Palaeontology 1:369–381.

Carr, R. 2005. Diplognathus lafargei sp. nov . from the Antrim Shale (Upper Devonian) of the Michigan Basin, Michigan, U.S.A. Revista Brasileira de Paleontologia 8:109–116.

Carr, R. K. 1994. A redescription of Gymnotrachelus (Placodermi: Arthrodira) from the Cleveland Shale (Famennian) of northern Ohio, U.S.A. Kirtlandia 3–21.

Carr, R. K. 1996. Stenosteus angustopectus sp. nov. from the Cleveland Shale (Famennian) of northern ohio with a review of selenosteid (Placodermi) systematics. Kirtlandia 19–43.

Carr, R. K. 2018. A new aspinothoracid arthrodire from the Late Devonian of Ohio, U.S.A. Acta Geologica Polonica 68:363–379.

Carr, R. K. Opportunity knocked and no one was home: aspinothoracid arthrodires (Placodermi) from the Ohio Shale Formation (Upper Devonian, North America). Geobios 19:81–83.

Carr, R. K., and W. J. Hlavin. 1995. Dinichthyidae (Placodermi):A paleontological fiction? Geobios 28:85–87.

Carr, R. K., and G. L. Jackson. 2008. The Vertebrate Fauna of the Cleveland Member (Famennian) of the Ohio Shale. 20.

Carr, R. K., and W. J. Hlavin. 2010. Two new species of Dunkleosteus Lehman, 1956, from the Ohio Shale Formation (USA, Famennian) and the Kettle Point Formation (Canada, Upper Devonian), and a cladistic analysis of the Eubrachythoraci (Placodermi, Arthrodira): DUNKLEOSTEIDAE AND DINICHTHYIDAE ARTHRODIRES. Zoological Journal of the Linnean Society 159:195–222.

Carroll, R. L. 1964. Early evolution of the dissorophid amphibians. Bullet of the Museum of Comparative Zoology 131:161–250.

Carroll, R. L. 1967. Labyrinthodonts from the Joggins Formation. Journal of Paleontology 41:111–142.

Carroll, R. L. 1970. The Ancestry of Reptiles. Philosophical Transactions of the Royal Society B: Biological Sciences 257:267–308.

Carroll, R. L. 1998. Cranial anatomy of ophiderpetontid aïstopods: Palaeozoic limbless amphibians. Zoological Journal of the Linnean Society 122:143–166.

Carroll, R. L., and P. Gaskill. 1978. The Order Microsauria. The American Philosophical Society, Independence Square, Philadelphia, USA, 214 pp.

Case, E. C. 1935. Description of a collection of associated skeletons of Trimerorhachis. University of Michicagn Contributions from the Museum of Paleontology 4:227–274.

Cater, J. M. L. 1987. Sedimentology of part of the Lower Oil-Shale Group (Dinantian) sequence at Granton, Edinburgh, including the Granton "shrimp-bed." Transactions of the Royal Society of Edinburgh: Earth Sciences 78:29–40.

Cater, J. M. L., D. E. G. Briggs, and E. N. K. Clarkson. 1989. Shrimp-bearing sedimentary successions in the Lower Carboniferous (Dinantian) Cementstone and Oil Shale Groups of northern Britain. Transactions of the Royal Society of Edinburgh: Earth Sciences 80:5–15.

Challands, T. J. 2015. The cranial endocast of the Middle Devonian dipnoan *Dipterus valenciennesi* and a fossilized dipnoan otoconial mass. Papers in Palaeontology 1:289–317.

Challands, T. J., T. R. Smithson, J. A. Clack, C. E. Bennett, J. E. A. Marshall, S. M. Wallace-Johnson, and H. Hill. 2019. A lungfish survivor of the end-Devonian extinction and an Early Carboniferous dipnoan radiation. Journal of Systematic Palaeontology 1–22.

Charest, F., Z. Johanson, and R. Cloutier. 2018. Loss in the making: absence of pelvic fins and presence of paedomorphic pelvic girdles in a Late Devonian antiarch placoderm (jawed stem-gnathostome). Biology Letters 14:20180199.

Chase, J. N. 1965. Neldasaurus wrightae, a new rhachitomous labyrinthodont from the Texas Lower Permian. Bulletin of the Museum of Comparative Zoology 133:153–225.

Chen, D., Y. Alavi, M. D. Brazeau, H. Blom, D. Millward, and P. E. Ahlberg. 2018. A partial lower jaw of a tetrapod from “Romer’s Gap.” Earth and Environmental Science Transactions of the Royal Society of Edinburgh 108:55–65.

Chevrinais, M., R. Cloutier, and J.-Y. Sire. 2015a. The revival of a so-called rotten fish: the ontogeny of the Devonian acanthodian *Triazeugacanthus*. Biology Letters 11:20140950.

Chevrinais, M., E. Balan, and R. Cloutier. 2015b. New Insights in the Ontogeny and Taphonomy of the Devonian Acanthodian Triazeugacanthus affinis From the Miguasha Fossil-Lagerstätte, Eastern Canada. Minerals 6:1.

Chevrinais, M., C. Jacquet, and R. Cloutier. 2017. Early establishment of vertebrate trophic interactions: Food web structure in Middle to Late Devonian fish assemblages with exceptional fossilization. Bulletin of Geosciences 491–510.

Chitaley, S., and C. Cai. 2001. Permineralized Callixylon woods from the Late Devonian Cleveland Shale of Ohio, U.S.A. and that of Kettle Point, Ontario, Canada. Review of Palaeobotany and Palynology 114:127–144.

Choo, B. 2009. A Basal Actinopterygian Fish from the Middle Devonian Bunga Beds of New South Wales, Australia. Proc. Linn. Soc. N.S.W. 11.

Choo, B. 2011. Revision of the actinopterygian genus Mimipiscis (=Mimia) from the Upper Devonian Gogo Formation of Western Australia and the interrelationships of the early

Actinopterygii. Earth and Environmental Science Transactions of the Royal Society of Edinburgh 102:77–104.

Choo, B. 2015. A new species of the Devonian actinopterygian *Moythomasia* from Bergisch Gladbach, Germany, and fresh observations on *M. durgaringa* from the Gogo Formation of Western Australia. Journal of Vertebrate Paleontology 35:e952817.

Choo, B., J. A. Long, and K. Trinajstic. 2009. A new genus and species of basal actinopterygian fish from the Upper Devonian Gogo Formation of Western Australia. Acta Zoologica 90:194–210.

Choo, B., J. Lu, S. Giles, K. Trinajstic, and J. A. Long. 2019. A new actinopterygian from the Late Devonian Gogo Formation, Western Australia. Papers in Palaeontology 5:343–363.

Clack, J. A. 1987a. Two new specimens of Anthracosaurus (Amphibia: Anthracosauria) from the Northumberland Coal Measures. Palaeontology 30:15–26.

Clack, J. A. 1987b. Pholiderpeton scutigerum Huxley, an Amphibian from the Yorkshire Coal Measures. Philosophical Transactions of the Royal Society B: Biological Sciences 318:1–107.

Clack, J. A. 1993. Silvanerpeton miripedes, a new anthracosauroid from the Viséan of East Kirkton, West Lothian, Scotland. Transactions of the Royal Society of Edinburgh: Earth Sciences 84:369–376.

Clack, J. A. 1997. The Scottish Carboniferous tetrapod Crassigyrinus scoticus (Lydekker)—cranial anatomy and relationships. Transactions of the Royal Society of Edinburgh: Earth Sciences 88:127–142.

Clack, J. A. 1998a. The neurocranium of Acanthostega gunnari Jarvik and the evolution of the otic region in tetrapods. Zoological Journal of the Linnean Society 122:61–97.

Clack, J. A. 1998b. A new Early Carboniferous tetrapod with a mélange of crown-group characters. Nature 394:66–69.

Clack, J. A. 2001. Eucritta melanolimnetes from the Early Carboniferous of Scotland, a stem tetrapod showing a mosaic of characteristics. Geochimica et Cosmochimica Acta 92:75–95.

Clack, J. A. 2002a. A revised reconstruction of the dermal skull roof of *Acanthostega gunnari* , an early tetrapod from the Late Devonian. Transactions of the Royal Society of Edinburgh: Earth Sciences 93:163–165.

Clack, J. A. 2002b. The dermal skull roof of Acanthostega gunnari, an early tetrapod from the Late Devonian. Transactions of the Royal Society of Edinburgh: Earth Sciences 93:17–33.

Clack, J. A. 2002c. An early tetrapod from 'Romer's Gap.' Nature 418:72–76.

Clack, J. A. 2011. A new microsaur from the early carboniferous (Viséan) of East Kirkton, Scotland, showing soft tissue evidence. Palaeontology 26:45–55.

Clack, J. A., and R. Holmes. 1988. The braincase of the anthracosaur Archeria crassidisca with comments on the interrelationships of primitive tetrapods. Palaeontology 31:85–107.

Clack, J. A., and P. E. Ahlberg. 2004. A new stem tetrapod from the Early Carboniferous of Northern Ireland; pp. 309–320 in G. Arratia, M. V. H. Wilson, and R. Cloutier (eds.), Recent Advances in the Origin and Early Radiation of Vertebrates. Verlag Dr. Friedrich Pfeil, Munich, Germany.

Clack, J. A., and S. M. Finney. 2005. *Pederpes finneyae* , an articulated tetrapod from the tournaisian of Western Scotland. Journal of Systematic Palaeontology 2:311–346.

Clack, J. A., and A. R. Milner. 2009. Morphology and systematics of the Pennsylvanian amphibian Platyrhinops lyelli (Amphibia: Temnospondyli). Earth and Environmental Science Transactions of the Royal Society of Edinburgh 100:275–295.

Clack, J. A., L. B. Porro, and C. E. Bennett. 2018. A *Crassigyrinus* -like jaw from the Tournaisian (Early Mississippian) of Scotland. Earth and Environmental Science Transactions of the Royal Society of Edinburgh 108:37–46.

Clack, J. A., T. R. Smithson, and M. Ruta. 2022. A Mississippian (early Carboniferous) tetrapod showing early diversification of the hindlimbs. Communications Biology 5:283.

Clack, J. A., P. E. Ahlberg, H. Blom, and S. M. Finney. 2012a. A new genus of Devonian tetrapod from North-East Greenland, with new information on the lower jaw of Ichthyostega. Palaeontology 55:73–86.

Clack, J. A., F. Witzmann, J. Müller, and D. Snyder. 2012b. A Colosteid-Like Early Tetrapod from the St. Louis Limestone (Early Carboniferous, Meramecian), St. Louis, Missouri, USA. Fieldiana Life and Earth Sciences 5:17–39.

Clack, J. A., M. Ruta, A. R. Milner, J. E. A. Marshall, T. R. Smithson, and K. Z. Smithson. 2019a. *Acherontiscus caledoniae* : the earliest heterodont and durophagous tetrapod. Royal Society Open Science 6:182087.

Clack, J. A., C. E. Bennett, S. J. Davies, A. C. Scott, J. E. Sherwin, and T. R. Smithson. 2019b. A Tournaisian (earliest Carboniferous) conglomerate-preserved non-marine faunal assemblage and its environmental and sedimentological context. PeerJ 6:e5972.

Clack, J. A., C. E. Bennett, D. K. Carpenter, S. J. Davies, N. C. Fraser, T. I. Kearsey, J. E. A. Marshall, D. Millward, B. K. A. Otoo, E. J. Reeves, A. J. Ross, M. Ruta, K. Z. Smithson, T. R. Smithson, and S. A. Walsh. 2016. Phylogenetic and environmental context of a Tournaisian tetrapod fauna. Nature Ecology & Evolution 1:0002.

Clark, N. D. L. 1989. A study of a Namurian crustacean-bearing shale from the western Midland Valley of Scotland. PhD, University of Glasgow, 313 pp.

Clark, N. D. L. 1990. *Minicaris brandi* Schram 1979, a syncarid crustacean from the Namurian (Carboniferous). Scottish Journal of Geology 26:125–130.

Clark, N. D. L. 1991. *Palaemysis dunlopi* Peach 1908 (Eocarida, Crustacea) from the Namurian (Carboniferous) of the western Midland Valley. Scottish Journal of Geology 27:1–10.

Clark, N. D. L. 2013. Tealliocaris: a decapod crustacean from the Carboniferous. Palaeodiversity 6.

Clarkson, E. N. K. 1985. Palaeoecology of the Dinantian of Foulden, Berwickshire, Scotland. Transactions of the Royal Society of Edinburgh: Earth Sciences 76:97–100.

Clarkson, E. N. K., A. R. Milner, and M. I. Coates. 1993. Palaeoecology of the Viséan of East Kirkton, West Lothian, Scotland. Transactions of the Royal Society of Edinburgh: Earth Sciences 84:417–425.

Claypole, E. W. 1893. III.—The Upper Devonian Fishes of Ohio. Geological Magazine 10:443–448.

Clayton, G. 1985. Plant miospores from the Dinantian of Foulden, Berwickshire, Scotland. Transactions of the Royal Society of Edinburgh: Earth Sciences 76:21–24.

Clement, A. M. 2012. A new species of long-snouted lungfish from the Late Devonian of Australia, and its functional and biogeographical implications. Palaeontology 55:51–71.

Clement, A. M., and J. A. Long. 2010. *Xeradipterus hatcheri* , a new dipnoan from the Late Devonian (Frasnian) Gogo Formation, Western Australia, and other new holodontid material. Journal of Vertebrate Paleontology 30:681–695.

Clement, G. 2002. Large Tristichopteridae (Sarcopterygii, Tetrapodomorpha) from the Late Famennian Evieux Formation of Belgium. Palaeontology 45:577–593.

Clément, G., and O. Lebedev. 2014. Revision of the early tetrapod Obruchevichthys Vorobyeva, 1977 from the Frasnian (Upper Devonian) of the North-western East European Platform. Paleontological Journal 48:1082–1091.

Clement, G., D. Snitting, and P. E. Ahlberg. 2009. A new tristichopterid (Sarcopterygii, Tetrapodomorpha) from the Upper Famennian Evieux Formation (Upper Devonian) of Belgium. Palaeontology 52:823–836.

Clement, G., P. E. Ahlberg, A. Blieck, H. Blom, J. A. Clack, E. Poty, J. Thorez, and P. Janvier. 2004. Devonian tetrapod from Western Europe. Nature 427:412–413.

Cloutier, R. 2013. Great Canadian Lagerstätten 4. The Devonian Miguasha Biota (Québec): UNESCO World Heritage Site and a Time Capsule in the Early History of Vertebrates. Geoscience Canada 40:149.

Cloutier, R., and Cloutier, Anne-Marie. 1995. Palaeozoic vertebrates of northern France and Belgium: Part III- Sarcopterygii (Devonian to Carboniferous). Geobios 28:335–341.

Cloutier, R., J.-N. Proust, and B. Tessier. 2011. The Miguasha Fossil-Fish-Lagerstätte: a consequence of the Devonian land–sea interactions. Palaeobiodiversity and Palaeoenvironments 91:293–323.

Cloutier, R., S. Loboziak, A.-M. Candilier, and A. Blieck. 1996. Biostratigraphy of the Upper Devonian Escuminac Formation, eastern Québec, Canada: a comparative study based on miospores and fishes. Review of Palaeobotany and Palynology 93:191–215.

Cloutier, R., A. M. Clement, M. S. Y. Lee, R. Noël, I. Béchard, V. Roy, and J. A. Long. 2020. Elpistostege and the origin of the vertebrate hand. Nature 579:549–554.

Coates, M. I. 1988. A new fauna of Namurian (Upper Carboniferous) fish from Bearsden, Glasgow. PhD, University of Newcastle upon Tyne, Newcastle Upon Tyne, 442 pp.

Coates, M. I. 1993a. Actinopterygian and acanthodian fishes from the Viséan of East Kirkton, West Lothian, Scotland. Transactions of the Royal Society of Edinburgh: Earth Sciences 84:317–327.

Coates, M. I. 1993b. New actinopterygian fish from the Namurian Manse Burn Formation of Bearsden, Scotland. Palaeontology 36:123–146.

Coates, M. I. 1996. The Devonian tetrapod Acanthostega gunnari Jarvik: postcranial anatomy, basal tetrapod interrelationships and patterns of skeletal evolution. Transactions of the Royal Society of Edinburgh: Earth Sciences 87:363–421.

Coates, M. I. 1998. Actinopterygians from the Namurian of Bearsden, Scotland, with comments on early actinopterygian neurocrania. Zoological Journal of the Linnean Society 122:27–59.

Coates, M. I. 2001. Origin of Tetrapods; pp. 74–79 in D. E. G. Briggs and P. R. Crowther (eds.), Palaeobiology II. Blackwell Science Ltd, Malden, MA, USA.

Coates, M. I., and S. E. K. Sequeira. 2001. A new stethacanthid chondrichthyan from the lower Carboniferous of Bearsden, Scotland. Journal of Vertebrate Paleontology 21:438–459.

Coates, M. I., and R. W. Gess. 2007. A new reconstruction of Onychoselache traquairi, comments on early chondrichthyan pectoral girdles and hybodontiform phylogeny. Palaeontology 50:1421–1446.

Coates, M. I., J. E. Jeffery, and M. Ruta. 2002. Fins to limbs: what the fossils say. Evolution and Development 4:390–401.

Coates, M. I., K. Tietjen, A. M. Olsen, and J. A. Finarelli. 2019. High-performance suction feeding in an early elasmobranch. Science Advances 5:eaax2742.

Coates, M. I., R. W. Gess, J. A. Finarelli, K. E. Criswell, and K. Tietjen. 2017. A symmoriiform chondrichthyan braincase and the origin of chimaeroid fishes. Nature 541:208–211.

Coatham, S. J., J. Vinther, E. J. Rayfield, and C. Klug. 2020. Was the Devonian placoderm *Titanichthys* a suspension feeder? Royal Society Open Science 7:200272.

Colbert, E. H. 1955. Scales in the Permian Amphibian Trimerorhachis. American Museum Novitates 18.

Copper, P., and E. Edinger. 2009. Distribution, geometry and palaeogeography of the Frasnian (Late Devonian) reef complexes of Banks Island, NWT, western arctic, Canada. Geological Society, London, Special Publications 314:109–124.

Cox, R. S. 1986. Preliminary report on the age and palynology of the Bear Gulch Limestone (Mississippian, Montana). Journal of Paleontology 60:952–956.

Cressler, W. L. 2006. Plant paleoecology of the Late Devonian Red Hill locality, north-central Pennsylvania, an Archaeopteris-dominated wetland plant community and early tetrapod site; pp. in Wetlands through Time. Geological Society of America.

Daeschler, E. B. 2000a. Early tetrapod jaws from the Late Devonian of Pennsylvania, USA. Journal of Paleontology 74:301–308.

Daeschler, E. B. 2000b. An Early Actinopterygian Fish from the Catskill Formation (Late Devonian, Famennian) in Pennsylvania, U.S.A. Proceedings of the Academy of Natural Sciences of Philadelphia 15:181–192.

Daeschler, E. B. 2019. New material supports a description and taxonomic revision of Holoptychius ? radiatus (Sarcopterygii, Tristichopteridae) from the Upper Devonian Catskill Formation in Pennsylvania, USA. Proceedings of the Academy of Natural Sciences of Philadelphia 167:11.

Daeschler, E. B., and W. L. Cressler. 2011. Late Devonian paleontology and paleoenvironments at Red Hill and other fossil sites in the Catskill Formation of north-central Pennsylvania; pp. 1–

16 in From the Shield to the Sea: Geological Field Trips from the 2011 Joint Meeting of the GSA Northeastern and North-Central Sections. Geological Society of America.

Daeschler, E. B., and J. P. Downs. 2018. New description and diagnosis of *Hyneria lindae* (Sarcopterygii, Tristichopteridae) from the Upper Devonian Catskill Formation in Pennsylvania, U.S.A. Journal of Vertebrate Paleontology 38:e1448834.

Daeschler, E. B., N. H. Shubin, and F. A. Jenkins. 2006. A Devonian tetrapod-like fish and the evolution of the tetrapod body plan. Nature 440:757–763.

Daeschler, E. B., J. A. Clack, and N. H. Shubin. 2009. Late Devonian tetrapod remains from Red Hill, Pennsylvania, USA: how much diversity? Acta Zoologica 90:306–317.

Danto, M., F. Witzmann, S. E. Pierce, and N. B. Fröbisch. 2017. Intercentrum versus pleurocentrum growth in early tetrapods: A paleohistological approach. Journal of Morphology 278:1262–1283.

Davis, M. C., N. Shubin, and E. B. Daeschler. 2004. A new specimen of *Sauripterus taylori* (Sarcopterygii, Osteichthyes) from the Famennian Catskill Formation of North America. Journal of Vertebrate Paleontology 24:26–40.

Denayer, J., C. Prestianni, P. Gueriau, S. Olive, and G. Clément. 2016. Stratigraphy and depositional environments of the Late Famennian (Late Devonian) of Southern Belgium and characterization of the Strud locality. Geological Magazine 153:112–127.

Dennis, K., and R. S. Miles. 1979. A second eubrachythoracid arthrodire from Gogo, Western Australia. Zoological Journal of the Linnean Society 67:1–29.

Dennis, K., and R. S. Miles. 1980. New durophagous arthrodires from Gogo, Western Australia. Zoological Journal of the Linnean Society 69:43–85.

Dennis, K., and R. S. Miles. 1981. A pachyosteomorph arthrodire from Gogo, Western Australia. Zoological Journal of the Linnean Society 73:213–258.

Dennis, K., and R. S. Miles. 1982. A eubrachythoracid arthrodire with a snubnose from Gogo, Western Australia. Zoological Journal of the Linnean Society 75:153–166.

Dennis-Bryan, K. 1987. A new species of eastmanosteid arthrodire (Pisces: Placodermi) from Gogo, Western Australia. Zoological Journal of the Linnean Society 90:1–64.

Derycke, C., R. Cloutier, and A.-M. Candilier. 1995. Palaeozoic vertebrates of northern France and Belgium: Part II- Chondrichthyes, Acanthodii, Actinopterygii (uppermist Silurian to Carboniferous). Geobios 28:343–350.

Derycke, C., S. Olive, E. Groessens, and D. Goujet. 2014. Paleogeographical and paleoecological constraints on paleozoic vertebrates (chondrichthyans and placoderms) in the Ardenne Massif. Palaeogeography, Palaeoclimatology, Palaeoecology 414:61–67.

Dick, J. R. F. 1981. Diplodoselache woodi gen. et sp. nov., an early Carboniferous shark from the Midland Valley of Scotland. Transactions of the Royal Society of Edinburgh: Earth Sciences 72:99–113.

Dickson, B. V., and S. E. Pierce. 2018. How (and why) fins turn into limbs: insights from anglerfish. Earth and Environmental Science Transactions of the Royal Society of Edinburgh 1–17.

Dickson, B. V., J. A. Clack, T. R. Smithson, and S. E. Pierce. 2020. Functional adaptive landscapes predict terrestrial capacity at the origin of limbs. Nature.

Dilkes, D. 2015. Carpus and tarsus of Temnospondyli. Vertebrate Anatomy Morphology Palaeontology 1:51.

Donoghue, P. C. J., and M. P. Smith. 2001. The anatomy of Turinia pagei (Powrie), and the phylogenetic status of the Thelodonti. Transactions of the Royal Society of Edinburgh: Earth Sciences 92:15–37.

Downs, J. P., and E. B. Daeschler. 2020. A New Species of Megalichthys (Sarcopterygii, Megalichthyidae) from the Upper Devonian (Famennian) of Pennsylvania, U.S.A., and a Report on the Cosmine-Covered Osteolepiform Fossils of the Catskill Formation. Journal of Vertebrate Paleontology.

Downs, J. P., K. E. Criswell, and E. B. Daeschler. 2011. Mass Mortality of Juvenile Antiarchs (*Bothriolepis* sp.) from the Catskill Formation (Upper Devonian, Famennian Stage), Tioga County, Pennsylvania. Proceedings of the Academy of Natural Sciences of Philadelphia 161:191–203.

Downs, J. P., E. B. Daeschler, F. A. Jenkins, and N. H. Shubin. 2008. The cranial endoskeleton of Tiktaalik roseae. Nature 455:925–929.

Downs, J. P., E. B. Daeschler, A. M. Long, and N. H. Shubin. 2018. *Eusthenopteron jenkinsi* sp. nov. (Sarcopterygii, Tristichopteridae) from the Upper Devonian of Nunavut, Canada, and a Review of *Eusthenopteron* Taxonomy. Breviora 562:1–24.

Dunkle, D. H. 1947. A new genus and species of arthrodiran fish from the Upper Devonian Cleveland Shale. Scientific Publications of the Cleveland Museum of Natural History 8:103–117.

Dunkle, D. H., and P. A. Bungart. 1939. A new arthrodire from the Cleveland Shale Formation. Scientific Publications of the Cleveland Museum of Natural History 8:12–28.

Dunkle, D. H., and P. A. Bungart. 1940. On one of the least known of the Cleveland Shale Arthrodira. Scientific Publications of the Cleveland Museum of Natural History 8:30–49.

Dunkle, D. H., and P. A. Bungart. 1942a. A new genus and species of Arthrodira from the Cleveland Shale. Scientific Publications of the Cleveland Museum of Natural History 8:65–71.

Dunkle, D. H., and P. A. Bungart. 1942b. The infero-gnathal plates of Titanichthys. Scientific Publications of the Cleveland Museum of Natural History 8:49–59.

Dunkle, D. H., and P. A. Bungart. 1943. Comments on Diplognathus mirabilis Newberry. Scientific Publications of the Cleveland Museum of Natural History 8:73–84.

Dunkle, D. H., and P. A. Bungart. 1945. A new arthrodiran fish from the Upper Devonian Ohio Shales. Scientific Publications of the Cleveland Museum of Natural History 8:85–95.

Dunlop, J. A., and L. I. Anderson. 2005. A fossil harvestman (Arachnida, Opiliones) from the Mississippian of East Kirkton, Scotland. Journal of Arachnology 33:482–489.

Dunlop, J. A., S. J. Braddy, and E. Tetlie. 2002. The Early Devonian eurypterid *Grossopterus overathi* (Gross, 1933) from Overath, Germany. Fossil Record 5:93–104.

Durant, G. P. 1993. Volcanogenic sediments of the East Kirkton Limestone (Viséan) of West Lothian, Scotland. Transactions of the Royal Society of Edinburgh: Earth Sciences 84:203–207.

Eastman, C. R. 1899. Descriptions of New Species of Diplodus Teeth from the Devonian of Northeastern Illinois. The Journal of Geology 7:489–493.

Elliott, F. M. 2016. An early actinopterygian ichthyofauna from the Scottish Lower Coal Measures Formation: Westphalian A (Bashkirian). Earth and Environmental Science Transactions of the Royal Society of Edinburgh 107:351–394.

Feldman, H. R., R. Lund, C. G. Maples, and A. W. Archer. 1994. Origin of the Bear Gulch Beds (Namurian, Montana, USA). Geobios 16:283–291.

Ferrón, H. G., C. Martínez-Pérez, and H. Botella. 2017. Ecomorphological inferences in early vertebrates: reconstructing *Dunkleosteus terrelli* (Arthrodira, Placodermi) caudal fin from palaeoecological data. PeerJ 5:e4081.

Finarelli, J. A., and M. I. Coates. 2014. *Chondrenchelys problematica* (Traquair, 1888) redescribed: a Lower Carboniferous, eel-like holocephalan from Scotland. Earth and Environmental Science Transactions of the Royal Society of Edinburgh 105:35–59.

Forey, P. L., and V. T. Young. 1985. Acanthodian and coelacanth fish from the Dinantian of Foulden, Berwickshire, Scotland. Transactions of the Royal Society of Edinburgh: Earth Sciences 76:53–59.

Forey, P. L., P. E. Ahlberg, E. Lukševičs, and I. Zupinš. 2000. A new coelacanth from the Middle Devonian of Latvia. Journal of Vertebrate Paleontology 20:243–252.

Friedman, M., and M. I. Coates. 2006. A newly recognized fossil coelacanth highlights the early morphological diversification of the clade. Proceedings of the Royal Society B: Biological Sciences 273:245–250.

Friedman, M., and E. B. Daeschler. 2006. Late Devonian (Famennian) lungfishes from the Catskill Formation of Pennsylvania, USA. Palaeontology 49:1167–1183.

Frumes, D. 2003. Groenlandaspidid placoderm fishes from the Late Devonian of North America. Records of the Australian Museum 55:45–60.

Gardiner, B. G. 1985. Actinopterygian fish from the Dinantian of Foulden, Berwickshire, Scotland. Transactions of the Royal Society of Edinburgh: Earth Sciences 76:61–66.

Gardiner, B. G., and T. R. Mason. 1974. On the Occurrence of the Palaeoniscid Fish Elonichthys serratus in the Viséan of Fermanagh, with a Note on the Enniskillen and Egerton Collections. Proceedings of the Royal Irish Academy. Section B: Biological, Geological, and Chemical Science 7:31–36.

Gardiner, B. G., and R. S. Miles. 1990. A new genus of eubrachythoracid arthrodire from Gogo, Western Australia. Zoological Journal of the Linnean Society 99:159–204.

Garrouste, R., G. Clément, P. Nel, M. S. Engel, P. Grandcolas, C. D'Haese, L. Lagebro, J. Denayer, P. Gueriau, P. Lafaite, S. Olive, C. Prestianni, and A. Nel. 2012. A complete insect from the Late Devonian period. Nature 488:82–85.

Garwood, R. J., and G. D. Edgecombe. 2011. Early Terrestrial Animals, Evolution, and Uncertainty. Evolution: Education and Outreach 4:489–501.

George, A., P. Playford, C. McA. Powell, and P. M. Tornatora. 1997. Lithofacies and sequence development on an Upper Devonian mixed carbonate-siliciclastic fore-reef slope, Canning Basin, Western Australia. Sedimentology 44:843–867.

Gess, R., and P. E. Ahlberg. 2018. A tetrapod fauna from within the Devonian Antarctic Circle. Science 360:1120–1124.

Gess, R. W. 2001. A new species of Diplacanthus from the Late Devonian (Famennian) of South Africa. Annales de Paléontologie 87:49–60.

Gess, R. W. 2011. High latitude Gondwanan Famennian biodiversity patterns- evidence from the South African Witpoort Formation (Cape Supergroup, Witteberg Group). University of the Witwatersrand, Johannesburg pp.

Gess, R. W. 2013. The Earliest Record of Terrestrial Animals in Gondwana: A Scorpion from the Famennian (Late Devonian) Witpoort Formation of South Africa. African Invertebrates 54:373–379.

Gess, R. W., and N. Hiller. 1995. Late Devonian charophytes from the Witteberg Group, South Africa. Review of Palaeobotany and Palynology 89:417–428.

Gess, R. W., and M. I. Coates. 2015. Fossil juvenile coelacanths from the Devonian of South Africa shed light on the order of character acquisition in actinistians: Fossil Coelacanths from the South African Devonian. Zoological Journal of the Linnean Society 175:360–383.

Gess, R. W., and K. M. Trinajstic. 2017. New morphological information on, and species of placoderm fish Africanaspis (Arthrodira, Placodermi) from the Late Devonian of South Africa. PLOS ONE 12:e0173169.

Gess, R. W., and A. M. Clement. 2019. A high latitude Devonian lungfish, from the Famennian of South Africa. PeerJ 7:e8073.

Gess, R. W., and A. K. Whitfield. 2020. Estuarine fish and tetrapod evolution: insights from a Late Devonian (Famennian) Gondwanan estuarine lake and a southern African Holocene equivalent. Biological Reviews brv.12590.

Gess, R. W., M. I. Coates, and B. S. Rubidge. 2006. A lamprey from the Devonian period of South Africa. Nature 443:981–984.

Ginter, M. 2009. The dentition of *Goodrichthys* , a Carboniferous ctenacanthiform shark from Scotland. Acta Zoologica 90:152–158.

Ginter, M. 2022. The biostratigraphy of Carboniferous chondrichthyans. Geological Society, London, Special Publications 512:769–790.

Glenister, B. F. 1958. Upper Devonian Ammonoids from the Manticoceras Zone, Fitzroy Basin, Western Australia. Journal of Paleontology 32:58–96.

Godfrey, S. J. 1989a. The postcranial skeletal anatomy of the Carboniferous tetrapod Greererpeton burkemorani Romer, 1969. Philosophical Transactions of the Royal Society B: Biological Sciences 323:75–133.

Godfrey, S. J. 1989b. Ontogenetic changes in the skull of the Carboniferous tetrapod Greererpeton burkemorani Romer 1969. Philosophical Transactions of the Royal Society B: Biological Sciences 323.

Godfrey, S. J., A. R. Fiorillo, and R. L. Carroll. 1987. A newly discovered skull of the temnospondyl amphibian Dendrerpeton acadianum Owen. Canadian Journal of Earth Sciences 24:796–805.

Grogan, E. D., and R. Lund. 1995. Pigment patterns; soft anatomy and relationships of Bear Gulch Chondrichthyes (Namurian E2b; Lower Carboniferous; Montana; USA). Geobios 28:145–146.

Grogan, E. D., and R. Lund. 1997. Soft tissue pigments of the Upper Mississippian chondrenchelyid, *Harpagofututor volsellorhinus* (Chondrichthyes, Holocephali) from the Bear Gulch Limestone, Montana, USA. Journal of Paleontology 71:337–342.

Grogan, E. D., and R. Lund. 2000. Debeerius ellefseni (Fam. Nov., Gen. Nov., Spec. Nov.), an autodiastylic chondrichthyan from the Mississippian Bear Gulch Limestone of Montana (USA), the relationships of the chondrichthyes, and comments on gnathostome evolution. Journal of Morphology 243:219–245.

Grogan, E. D., and R. Lund. 2008. A basal elasmobranch, *Thrinacoselache gracia* n. gen and sp., (Thrinacodontidae, new family) from the Bear Gulch Limestone, Serpukhovian of Montana, USA. Journal of Vertebrate Paleontology 28:970–988.

Grogan, E. D., and R. Lund. 2009. Two new iniopterygians (Chondrichthyes) from the Mississippian (Serpukhovian) Bear Gulch Limestone of Montana with evidence of a new form of chondrichthyan neurocranium. Acta Zoologica 90:134–151.

Grogan, E. D., and R. Lund. 2011. Superfoetative viviparity in a Carboniferous chondrichthyan and reproduction in early gnathostomes: PALEOZOIC CHONDRICHTHYAN LIVE BIRTH. Zoological Journal of the Linnean Society 161:587–594.

Grogan, E. D., and R. Lund. 2015. Two new Actinopterygii (Vertebrata, Osteichthyes) with cosmine from the Bear Gulch Limestone (Heath Fm., Serpukhovian, Mississippian) of Montana USA. Proceedings of the Academy of Natural Sciences of Philadelphia 164:111–132.

Grogan, E. D., R. Lund, and M. Fath. 2014. A new petalodont chondrichthyan from the bear gulch limestone of montana, USA, with reassessment of Netsepoye hawesi and comments on the morphology of holomorphic petalodonts. Paleontological Journal 48:1003–1014.

Gueriau, P., S. Charbonnier, and G. Clément. 2014. Angustidontid crustaceans from the Late Devonian of Strud (Namur Province, Belgium): insights into the origin of Decapoda. Neues Jahrbuch Für Geologie Und Paläontologie - Abhandlungen 273:327–337.

Gueriau, P., J. C. Lamsdell, R. A. Wogelius, P. L. Manning, V. M. Egerton, U. Bergmann, L. Bertrand, and J. Denayer. 2020. A new Devonian euthycarcinoid reveals the use of different respiratory strategies during the marine-to-terrestrial transition in the myriapod lineage. Royal Society Open Science 7:201037.

Gueriau, P., N. Rabet, G. Clément, L. Lagebro, J. Vannier, D. E. G. Briggs, S. Charbonnier, S. Olive, and O. Béthoux. 2016. A 365-Million-Year-Old Freshwater Community Reveals Morphological and Ecological Stasis in Branchiopod Crustaceans. Current Biology 26:383–390.

Hairapetian, V., and M. Ginter. 2009. Famennian chondrichthyan remains from the Chahriseh section, central Iran. Acta Geologica Polonica 59:173–200.

Hairapetian, V., and M. Ginter. 2010. Pelagic chondrichthyan microremains from the Upper Devonian of the Kale Sardar section, eastern Iran. Acta Geologica Polonica 60:357–371.

Hairapetian, V., and C. J. Burrow. 2016. A new ischnacanthiform (Acanthodii) from the latest Devonian of Iran and the palaeogeography of Late Devonian ischnacanthiforms. Journal of Asian Earth Sciences 124:227–232.

Halvin, W., J., and J. R. Boreske Jr. 1973. Mylostoma variabile Newberry, an Upper Devonian durophagous brachythoracid arthrodire, with notes on related taxa. Breviora 1–12.

Hampe, O. 2002. Revision of the Xenacanthida (Chondrichthyes: Elasmobranchii) from the Carboniferous of the British Isles. Earth and Environmental Science Transactions of the Royal Society of Edinburgh 93:191–237.

Harris, J. E. 1938a. The neurocranium and jaws of Cladoselache. Scientific Publications of the Cleveland Museum of Natural History 8:7–12.

Harris, J. E. 1938b. The dorsal spine of Cladoselache. Scientific Publications of the Cleveland Museum of Natural History 8:1–6.

Harris, J. E. 1951. *Diademodus hydei* , a new fossil shark from the Cleveland Shale. Proceedings of the Zoological Society of London 120:683–697.

Hartkopf-Fröder, C., U. Jux, G. Knapp, and M. Piecha. 2004. The Late Devonian of the Bergisch Gladbach-Paffrath Syncline (Ardennes-Rhenish Massif, Germany): an overview. CFS Courier Forschungsinstitut Senckenberg 25:7–18.

Heidtke, U. H. J. 1998. Revision der GattungOrthacanthus Agassiz 1843 (Chondrichthyes: Xenacanthida). Paläontologische Zeitschrift 72:135–147.

Henderson, S. A. C., and T. J. Challands. 2018. The cranial endocast of the Upper Devonian dipnoan ‘ Chirodipterus’ australis. PeerJ 6:e5148.

Herbst, E. C., and J. R. Hutchinson. 2018. New insights into the morphology of the Carboniferous tetrapod *Crassigyrinus scoticus* from computed tomography. Earth and Environmental Science Transactions of the Royal Society of Edinburgh 109:157–175.

Hlavin, W. J. 1976. Biostratigraphy of the Late Devonian black shales on the cratonal margin of the Appalachian Geosyncline. PhD, Boston University, Boston, MA, 194 pp.

Holland, T. 2013. Pectoral girdle and fin anatomy of *Gogonasus andrewsae* long, 1985: Implications for tetrapodomorph limb evolution. Journal of Morphology 274:147–164.

Holland, T. 2014. The endocranial anatomy of *Gogonasus andrewsae* Long, 1985 revealed through micro CT-scanning. Earth and Environmental Science Transactions of the Royal Society of Edinburgh 105:9–34.

Holland, T., and J. A. Long. 2009. On the phylogenetic position of *Gogonasus andrewsae* Long 1985, within the Tetrapodomorpha. Acta Zoologica 90:285–296.

Holmes, R. 1984. The Carboniferous amphibian Proterogyrinus scheeli Romer and the early evolution of tetrapods. Philosophical Transactions of the Royal Society B: Biological Sciences 306:431–524.

Holmes, R. B. 1989. The skull and axial skeleton of the Lower Permian anthracosauroid amphibian Archeria crassidisca Cope. Palaeontographica Abteilung A (Palaeozoologie-Stratigraphie) 207:161–206.

Holmes, R. B., and R. L. Carroll. 2010. An articulated embolomere skeleton (Amphibia: Anthracosauria) from the Lower Pennsylvanian (Bashkirian) of Nova Scotia. Canadian Journal of Earth Sciences 47:209–219.

Holmes, R. B., R. L. Carroll, and R. R. Reisz. 1998. The First Articulated Skeleton of Dendrerpeton acadianum (Temnospondyli, Dendrerpetontidae) from the Lower Pennsylvanian Locality of Joggins, Nova Scotia, and a Review of Its Relationships. Journal of Vertebrate Paleontology 18:64–79.

Hook, R. W. 1983. Colosteus scutellatus (Newberry), a Primitive Temnospondyl Amphibian from the Middle Pennsylvanian of Linton, Ohio. American Museum Novitates 44.

Hook, R. W., and D. Baird. 1984. Ichthycanthus platypus Cope, 1877, Reidentified as the Dissorophoid Amphibian Amphibamus lyelli. Journal of Paleontology 58:697–702.

Hook, R. W., and D. Baird. 1986. The Diamond Coal Mine of Linton, Ohio, and Its Pennsylvanian-Age Vertebrates. Journal of Vertebrate Paleontology 6:174–190.

Hörnschemeyer, T., J. T. Haug, O. Bethoux, R. G. Beutel, S. Charbonnier, T. A. Hegna, M. Koch, J. Rust, S. Wedmann, S. Bradler, and R. Willmann. 2013. Is Strudiella a Devonian insect? Nature 494:E3–E4.

Hotton, N. I. 1970. Mauchchunkia bassa, gen. et sp. nov., an anthracosaur (Amphibia, Labyrinthodontia) from the Upper Mississippian. Kirtlandia 2–38.

Hughes, E. S. 2019. Discerning the Diets of Sweep-Feeding Eurypterids Through Analyses of Mesh-Modified Appendage Armature. West Virginia University, Morgantown, West Virginia, USA, 61 pp.

Hughes, E. S., and J. C. Lamsdell. 2021. Discerning the diets of sweep-feeding eurypterids: assessing the importance of prey size to survivorship across the Late Devonian mass extinction in a phylogenetic context. Paleobiology 47:271–283.

Huttenlocker, A. K., J. D. Pardo, B. J. Small, and J. S. Anderson. 2013. Cranial morphology of recumbirostrans (Lepospondyli) from the Permian of Kansas and Nebraska, and early morphological evolution inferred by micro-computed tomography. Journal of Vertebrate Paleontology 33:540–552.

Hyžný, M., I. Hoch, F. R. Schram, and S. Rybár. 2014. Crangopsis Salter, 1863 from the Lower Carboniferous (Mississippian) of the Ostrava Formation - the first record of Aeschronectida (Malacostraca: Hoplocarida) from continental Europe. Bulletin of Geosciences 707–717.

Janvier, P. 1974. Preliminary Report on Late Devonian Fishes from Central and Eastern Iran. Geological Survey of Iran, pp.

Janvier, P. 1977. Les poissons dévoniens de l'Iran central et de l'Afghanistan. Mémoires Hors Série de La Société Géologique de France 8:277–289.

Janvier, P. 1979. Les Vertebrates Devoniens de l'Iran central. III- antiarches. Geobios 12:605–608.

Janvier, P. 2007. The anatomy of Euphanerops longaevus Woodward, 1900, an anaspid-like jawless vertebrate from the Upper Devonian of Miguasha, Quebec, Canada. Geodiversitas 29:143–216.

Janvier, P., and M. Martin. 1978. Les Vertebrates Devoniens de L'Iran Central I- dipneustes. Geobios 11:819–833.

Janvier, P., and M. Martin. 1979. Les Vertebrates Devoniens de L'Iran central II-coelacanthiformes, struniiformes, osteolepiformes. Geobios 12:497–511.

Janvier, P., and R. Lund. 1983. *Hardistiella montanensis* n. gen. et sp. (Petromyzontida) from the Lower Carboniferous of Montana, with remarks on the affinities of the lampreys. Journal of Vertebrate Paleontology 2:407–413.

Janvier, P., and G. Clément. 2005. A new groenlandaspidid arthrodire (Vertebrata: Placodermi) from the Famennian of Belgium. Geologica Belgica 8:51–67.

Janvier, P., R. Lund, and E. D. Grogan. 2004. Further consideration of the earliest known lamprey, *Hardistiella montanensis* Janvier and Lund, 1983, from the Carboniferous of Bear Gulch, Montana, U.S.A. Journal of Vertebrate Paleontology 24:742–743.

Janvier, P., S. Desbiens, J. A. Willett, and M. Arsenault. 2006. Lamprey-like gills in a gnathostome-related Devonian jawless vertebrate. Nature 440:1183–1185.

Jarvik, E. 1996. The Devonian tetrapod Ichthyostega. Fossils and Strata 40:1–213.

Jefferies, R. P. S., and P. Minton. 1965. The mode of life of two Jurassic species of "Posidonia" (Bivalvia). Palaeontology 8:156–185.

Jeffery, J. E. 2006. The Carboniferous fish genera Strepsodus and Archichthys (Sarcopterygii: Rhizodontida): clarifying 150 years of confusion. Palaeontology 49:113–132.

Jeffery, J. E. 2012. Cranial morphology of the Carboniferous rhizodontid *Screbinodus ornatus* (Osteichthyes: Sarcopterygii). Journal of Systematic Palaeontology 10:475–519.

Jenner, R. A., C. H. J. Hof, and F. R. Schram. 1998. Palaeo- and archaeostomatopods (Hoplocarida, Crustacea) from the Bear Gulch Limestone, Mississippian (Namurian), of central Montana. Contributions to Zoology 67:155–185.

Jeram, A. J. 1993. Scorpions from the Viséan of East Kirkton, West Lothian, Scotland, with a revision of the infraorder Mesoscorpionina. Transactions of the Royal Society of Edinburgh: Earth Sciences 84:283–299.

Jeram, A. J., and P. A. Selden. 1993. Eurypterids from the Visean of East Kirkton, West Lothian, Scotland. Transactions of the Royal Society of Edinburgh: Earth Sciences 84:301–308.

Johanson, Z., and P. E. Ahlberg. 2001. Devonian rhizodontids and tristichopterids (Sarcopterygii: Tetrapodomorpha) from East Gondwana. Transactions of the Royal Society of Edinburgh: Earth Sciences 92:115.

Johanson, Z., and K. Trinajstic. 2014. Fossilized ontogenies: the contribution of placoderm ontogeny to our understanding of the evolution of early gnathostomes. Palaeontology 57:505–516.

Johanson, Z., S. Turner, and A. Warren. 2000. First East Gondwanan record of Strepsodus (Sarcopterygii, Rhizodontida) from the Lower Carboniferous Ducabrook Formation, central Queensland, Australia. Geodiversitas 22:161–170.

Johanson, Z., K. Trinajstic, S. Cumbaa, and M. Ryan. 2019. Fusion in the vertebral column of the pachyosteomorph arthrodire Dunkleosteus terrelli (‘Placodermi’). Palaeontologia Electronica.

Judson, M. L. I. 2012. Reinterpretation of Dracochela deprehendor (Arachnida: Pseudoscorpiones) as a stem-group pseudoscorpion. Palaeontology 55:261–283.

Kamska, V., E. B. Daeschler, J. P. Downs, P. E. Ahlberg, P. Tafforeau, and S. Sanchez. 2018. Long-bone development and life-history traits of the Devonian tristichopterid Hyneria lindae. Earth and Environmental Science Transactions of the Royal Society of Edinburgh 1–12.

Karakasiliotis, K., N. Schilling, J.-M. Cabelguen, and A. J. Ijspeert. 2013. Where are we in understanding salamander locomotion: biological and robotic perspectives on kinematics. Biological Cybernetics 107:529–544.

Kearsey, T. I., C. E. Bennett, D. Millward, S. J. Davies, C. J. B. Gowing, S. J. Kemp, M. J. Leng, J. E. A. Marshall, and M. A. E. Browne. 2016. The terrestrial landscapes of tetrapod evolution in earliest Carboniferous seasonal wetlands of SE Scotland. Palaeogeography, Palaeoclimatology, Palaeoecology 457:52–69.

Kemp, A. 2001. *Chirodipterus potteri* , a new Devonian lungfish from New South Wales, Australia: and the ontogeny of chirodipterid tooth plates. Journal of Vertebrate Paleontology 20:665–674.

Kimmel, C. B., B. Sidlauskas, and J. A. Clack. 2009. Linked morphological changes during palate evolution in early tetrapods. Journal of Anatomy 215:91–109.

Klapper, G. 1966. Upper Devonian Conodonts from the Canning Basin, Western Australia. Journal of Paleontology 40:777–842.

Klasson, W. 2008. The early diversification of ray-finned fishes (Actinopterygii); an ecomorphological approach. Undergraduate, University of Uppsala, Uppsala, Sweden, 69 pp.

Klembara, J., J. A. Clack, A. R. Milner, and M. Ruta. 2014. Cranial anatomy, ontogeny, and relationships of the Late Carboniferous tetrapod *Gephyrostegus bohemicus* Jaekel, 1902. Journal of Vertebrate Paleontology 34:774–792.

Klembara, J., D. S. Berman, A. C. Henrici, A. Ĉerňanský, and R. Werneburg. 2006. Comparison of cranial anatomy and proportions of similarly sized Seymouria sanjuanensis and Discosauriscus austriacus. Annals of Carnegie Museum 75:37–49.

Klug, C., J. Kerr, M. S. Y. Lee, and R. Cloutier. 2021. A late-surviving stem-ctenophore from the Late Devonian of Miguasha (Canada). Scientific Reports 11:19039.

Klug, C., N. H. Landman, D. Fuchs, R. H. Mapes, A. Pohle, P. Guériau, S. Reguer, and R. Hoffmann. 2019. Anatomy and evolution of the first Coleoidea in the Carboniferous. Communications Biology 2:280.

Kumpan, T., O. Bábek, J. Kalvoda, T. Matys Grygar, and J. Frýda. 2014. Sea-level and environmental changes around the Devonian–Carboniferous boundary in the Namur–Dinant Basin (S Belgium, NE France): A multi-proxy stratigraphic analysis of carbonate ramp archives and its use in regional and interregional correlations. Sedimentary Geology 311:43–59.

Lagebro, L., P. Gueriau, T. A. Hegna, N. Rabet, A. D. Butler, and G. E. Budd. 2015. The oldest notostracan (Upper Devonian Strud locality, Belgium). Palaeontology 58:497–509.

Lamsdell, J. C., S. J. Braddy, and O. E. Tetlie. 2010. The systematics and phylogeny of the Stylonurina (Arthropoda: Chelicerata: Eurypterida). Journal of Systematic Palaeontology 8:49–61.

Lamsdell, J. C., V. E. McCoy, O. A. Perron-Feller, and M. J. Hopkins. 2020. Air Breathing in an Exceptionally Preserved 340-Million-Year-Old Sea Scorpion. Current Biology 30:4316-4321.e2.

Lamsdell, J. C., L. Lagebro, G. D. Edgecombe, G. E. Budd, and P. Gueriau. 2019. Stylonurine eurypterids from the Strud locality (Upper Devonian, Belgium): new insights into the ecology of freshwater sea scorpions. Geological Magazine 1–7.

Lane, J. 2005. Phyllolepis rossimontina sp. nov. (Placodermi) from the uppermost Devonian at Red Hill, North-Central Pennsylvania. Revista Brasileira de Paleontologia 8:117–126.

Laurin, M. 1996. A redescription of the cranial anatomy of Seymouria baylorensis, the best known seymouriamorph (Vertebrata: Seymouriamorpha). PaleoBios 17:1–16.

Lautenschlager, S., F. Witzmann, and I. Werneburg. 2016. Palate anatomy and morphofunctional aspects of interpterygoid vacuities in temnospondyl cranial evolution. The Science of Nature 103.

Lebedev, O. A., and J. A. Clack. 1993. Upper Devonian tetrapods from Andreyevka, Tula Region, Russia. Palaeontology 36:721–734.

Lebedev, O. A., and M. I. Coates. 1995. The postcranial skeleton of the Devonian tetrapod Tulerpeton curtum Lebedev. Zoological Journal of the Linnean Society 114:307–348.

Lelièvre, H., P. Janvier, and D. Goujet. 1981. Les Vertebrates Devoniens de L'Iran central IV – arthrodires et ptyctodontes. Geobios 14:677–709.

Lemberg, J. B., E. B. Daeschler, and N. H. Shubin. 2021. The feeding system of *Tiktaalik roseae* : an intermediate between suction feeding and biting. Proceedings of the National Academy of Sciences 118:e2016421118.

Lennie, K. I., C. F. Mansky, and J. S. Anderson. 2020. New *Crassigyrinus* -like fibula from the Tournaisian (earliest Carboniferous) of Nova Scotia. Canadian Journal of Earth Sciences 57:1365–1369.

Lombard, R. E., and J. R. Bolt. 1995. A new primitive tetrapod, Whatcheeria deltae, from the Lower Carboniferous of Iowa. Palaeontology 38:471–494.

Lombard, R. E., and J. R. Bolt. 2006. The mandible of Whatcheeria deltae, and early tetrapod from the Late Mississippian of Iowa; pp. 21–52 in M. T. Carrano, R. W. Blob, T. J. Gaudin, and J. R. Wible (eds.), Amniote Paleobiology: Perspectives on the Evolution of Mammals, Birds, and Reptiles. University of Chicago Press.

Long, J. A. 1987a. Upper Devonian conodonts associated with alarge placoderm fish skull from the Canning Basin, Western Australia. Records of the Western Australia Museum 13:501–513.

Long, J. A. 1987b. A new dinichthyid fish (Placodermi: Arthrodira) from the Upper Devonian of Western Australia, with a discussion of dinichthyid interrelationships. Records of the Western Australia Museum 13:515–540.

Long, J. A. 1992. Gogodipterus paddyensis (Miles), gen. nov., a new chirodipterid lungfish from the late Devonian Gogo formation, Western Australia. The Beagle : Records of the Museums and Art Galleries of the Northern Territory 9:11–20.

Long, J. A. 1994. A second incisoscutid arthrodire (Pisces, Placodermi) from the Late Devonian Gogo Formation, Western Australia. Alcheringa: An Australasian Journal of Palaeontology 18:59–69.

Long, J. A. 1995. A new groenlandaspidid arthrodire (Pisces;Placodermi) from the Middle Devonian Aztec Siltstone, southern Victoria Land, Antarctica. Records of the Western Australian Museum 17:35–41.

Long, J. A. 1997. Ptyctodontid fishes (Vertebrata, Placodermi) from the Late Devonian Gogo Formation, Western Australia, with a revision of the European genus Ctenurella Ørvig, 1960. Geodiversitas 19:515–555.

Long, J. A. 1998. Two new arthrodires (placoderm fishes) from the Upper Devonian Gogo Formation, Western Australia. Memoirs of the Queensland Museum 28:51–63.

Long, J. A., and G. C. Young. 1995. Sharks from the Middle-Late Devonian Aztec Siltstone, southern Victoria Land, Antarctica. Records of the Western Australian Museum 17:287–308.

Long, J. A., and K. Trinajstic. 2010. The Late Devonian Gogo Formation Lägerstatte of Western Australia: Exceptional Early Vertebrate Preservation and Diversity. Annual Review of Earth and Planetary Sciences 38:255–279.

Long, J. A., and E. B. Daeschler. 2013. First Articulated Phyllolepid Placoderm from North America, with Comments on Phyllolepid Systematics. Proceedings of the Academy of Natural Sciences of Philadelphia 162:33–46.

Long, J. A., and K. M. Trinajstic. 2018. A review of recent discoveries of exceptionally preserved fossil fishes from the Gogo sites (Late Devonian, Western Australia). Earth and Environmental Science Transactions of the Royal Society of Edinburgh 108:111–117.

Long, J. A., B. Choo, and G. C. Young. 2008a. A new basal actinopterygian fish from the Middle Devonian Aztec Siltstone of Antarctica. Antarctic Science 20:393–412.

Long, J. A., K. Trinajstic, and Z. Johanson. 2009. Devonian arthrodire embryos and the origin of internal fertilization in vertebrates. Nature 457:1124–1127.

Long, J. A., A. M. Clement, and B. Choo. 2018. New insights into the origins and radiation of the mid-Palaeozoic Gondwanan stem tetrapods. Earth and Environmental Science Transactions of the Royal Society of Edinburgh 1–17.

Long, J. A., M. E. Anderson, R. Gess, and N. Hiller. 1997. New placoderm fishes from the Late Devonian of South Africa. Journal of Vertebrate Paleontology 17:253–268.

Long, J. A., K. Trinajstic, G. C. Young, and T. Senden. 2008b. Live birth in the Devonian period. Nature 453:650–652.

Long, J. A., G. C. Young, T. Holland, T. J. Senden, and E. M. G. Fitzgerald. 2006. An exceptional Devonian fish from Australia sheds light on tetrapod origins. Nature 444:199–202.

Long, J. A., C. J. Burrow, M. Ginter, J. G. Maisey, K. M. Trinajstic, M. I. Coates, G. C. Young, and T. J. Senden. 2015a. First Shark from the Late Devonian (Frasnian) Gogo Formation, Western Australia Sheds New Light on the Development of Tessellated Calcified Cartilage. PLOS ONE 10:e0126066.

Long, J. A., E. Mark-Kurik, Z. Johanson, M. S. Y. Lee, G. C. Young, Z. Min, P. E. Ahlberg, M. Newman, R. Jones, J. den Blaauwen, B. Choo, and K. Trinajstic. 2015b. Copulation in antiarch placoderms and the origin of gnathostome internal fertilization. Nature 517:196–199.

Lowney, K. A. 1980. Certain Bear Gulch (Namurian A, Montana) actinopterygii (Osteichthyes) and a reevaluation of the evolution of the Paleozoic actinopterygians. PhD, New York University, New York City, New York, USA, 490 pp.

Lu, J., and M. Zhu. 2010. An onychodont fish (Osteichthyes, Sarcopterygii) from the Early Devonian of China, and the evolution of the Onychodontiformes. Proceedings of the Royal Society B: Biological Sciences 277:293–299.

Lund, R. 1980. Viviparity and Intrauterine Feeding in a New Holocephalan Fish from the Lower Carboniferous of Montana. Science 209:697–699.

Lund, R. 1982. Harpagofututor volsellorhinus New Genus and Species (Chondrichthyes, Chondrenchelyiformes) from the Namurian Bear Gulch Limestone, Chondrenchelys problematica Traquair (Visean), and Their Sexual Dimorphism. Journal of Paleontology 56:938–958.

Lund, R. 1983. On a dentition of *Polyrhizodus* (Chondrichthyes, Petalodontiformes) from the Namurian bear gulch limestone of Montana. Journal of Vertebrate Paleontology 3:1–6.

Lund, R. 1984. On the spines of the Stethacanthidae (Chondrichthyes), with a description of a new genus from the Mississippian Bear Gulch limestone. Geobios 17:281–295.

Lund, R. 1985a. Stethacanthid Elasmobranch Remains from the Bear Gulch Limestone (Namurian E2b) of Montana. AMERICAN MUSEUM NOVITATES 24.

Lund, R. 1985b. The morphology of *Falcatus falcatus* (St. John and Worthen), a Mississippian stethacanthid chondrichthyan from the Bear Gulch Limestone of Montana. Journal of Vertebrate Paleontology 5:1–19.

Lund, R. 1986. On *Damocles serratus* , nov. gen. et sp. (Elasmobranchii: Cladodontida) from the Upper Mississippian Bear Gulch Limestone of Montana. Journal of Vertebrate Paleontology 6:12–19.

Lund, R. 1988. New information on *Squatinactis caudispinatus* (Chondrichthyes, Cladodontida) from the Chesterian Bear Gulch Limestone of Montana. Journal of Vertebrate Paleontology 8:340–342.

Lund, R. 1989. New petalodonts (Chondrichthyes) from the Upper Mississippian Bear Gulch Limestone (Namurian E_2 b) of Montana. Journal of Vertebrate Paleontology 9:350–368.

Lund, R. 1990. Chondrichthyan life history styles as revealed by the 320 million years old Mississippian of Montana. Environmental Biology of Fishes 27:1–19.

Lund, R. 2000. The new Actinopterygian order Guildayichthyiformes from the Lower Carboniferous of Montana (USA). Geodiversitas 22:171–206.

Lund, R., and R. Zangerl. 1974. Squatinactis caudispinatus, a new elasmobranch from the Upper Mississippian of Montana. Annals of Carnegie Museum of Natural History 45:43–55.

Lund, R., and W. G. J. Melton. 1982. A new actinopterygian fish from the Mississippian Bear Gulch Limestone of Montana. Palaeontology 25:485–498.

Lund, R., and W. Lund. 1984. New genera and species of coelacanths from the Bear Gulch Limestone (Lower Carboniferous) of Montana (U.S.A.). Geobios 17:237–244.

Lund, R., and R. H. Mapes. 1984. Carcharopsis wortheni from the Fayetteville Formation (Mississippian) of Arkansas. Journal of Paleontology 58:709–717.

Lund, R., and W. L. Lund. 1985. Coelacanths from the Bear Gulch Limestone (Namurian) of Montana and the evolution of the Coelacanthiformes. Bulletin of Carnegie Museum of Natural History 1–74.

Lund, R., and P. Janvier. 1986. A second lamprey from the Lower Carboniferous (Namurian) of Bear Gulch, Montana (U.S.A.). Geobios 19:647–652.

Lund, R., and E. D. Grogan. 1997. Cochliodonts from the Mississippian Bear Gulch Limestone (Heath Formation; Big Snowy Group; Chesterian) of Montana and the relationships of the Holocephali. Dinofest International Proceedings.

Lund, R., and C. Poplin. 1997. The rhadinichthyids (paleoniscoid actinopterygians) from the Bear Gulch Limestone of Montana (USA, Lower Carboniferous). Journal of Vertebrate Paleontology 17:466–486.

Lund, R., and C. Poplin. 1999. Fish diversity of the Bear Gulch Limestone, Namurian, Lower Carboniferous of Montana, USA. Geobios 32:285–295.

Lund, R., and C. Poplin. 2002. Cladistic analysis of the relationships of the Tarrasiids (Lower Carboniferous Actinopterygians). Journal of Vertebrate Paleontology 22:480–486.

Lund, R., E. Greenfest-Allen, and E. D. Grogan. 2012. Habitat and diversity of the Bear Gulch fish: Life in a 318 million year old marine Mississippian bay. Palaeogeography, Palaeoclimatology, Palaeoecology 342–343:1–16.

Lund, R., E. D. Grogan, and M. Fath. 2014. On the relationships of the Petalodontiformes (Chondrichthyes). Paleontological Journal 48:1015–1029.

Lund, R., E. Greenfest-Allen, and E. D. Grogan. 2015. Ecomorphology of the Mississippian fishes of the Bear Gulch Limestone (Heath formation, Montana, USA). Environmental Biology of Fishes 98:739–754.

MacIver, M. A., L. Schmitz, U. Mugan, T. D. Murphey, and C. D. Mobley. 2017. Massive increase in visual range preceded the origin of terrestrial vertebrates. Proceedings of the National Academy of Sciences 114:E2375–E2384.

Mann, A., and H. C. Maddin. 2019. Diabloroter bolti, a short-bodied recumbirostran 'microsaur' from the Francis Creek Shale, Mazon Creek, Illinois. Zoological Journal of the Linnean Society zlz025.

Mann, A., A. S. Calthorpe, and H. C. Maddin. 2021. *Joermungandr bolti* , an exceptionally preserved 'microsaur' from the Mazon Creek Lagerstätte reveals patterns of integumentary evolution in Recumbirostra. Royal Society Open Science 8:210319.

Mann, A., B. M. Gee, J. D. Pardo, D. Marjanović, G. R. Adams, A. S. Calthorpe, H. C. Maddin, and J. S. Anderson. 2020. Reassessment of historic 'microsaurs' from Joggins, Nova Scotia, reveals hidden diversity in the earliest amniote ecosystem. Papers in Palaeontology spp2.1316.

Mapes, R. H., H. Mutvei, and L. A. Doguzhaeva. 2007. A Late Carboniferous Coleoid Cephalopod from the Mazon Creek Lagerstätte (USA), with a Radula, Arm Hooks, Mantle Tissues, and Ink; pp. 121–143 in N. H. Landman, R. A. Davis, and R. H. Mapes (eds.), Cephalopods Present and Past: New Insights and Fresh Perspectives. Springer Netherlands, Dordrecht.

Mapes, R. H., E. A. Weller, and L. A. Doguzhaeva. 2010. Early Carboniferous (Late Namurian) coleoid cephalopods showing a tentacle with arm hooks and an ink sac from Montana, USA; pp. 155–170 in S. K. Tanabe, T. Sasaki, and H. Hirano (eds.), Cephalopods- Present and Past. Tokai University Press, Tokyo.

Marjanović, D., and M. Laurin. 2019. Phylogeny of Paleozoic limbed vertebrates reassessed through revision and expansion of the largest published relevant data matrix. PeerJ 6:e5565.

Marshall, J. E. A., E. J. Reeves, C. E. Bennett, S. J. Davies, T. I. Kearsey, D. Millward, T. R. Smithson, and M. A. E. Browne. 2019. Reinterpreting the age of the uppermost 'Old Red Sandstone' and Early Carboniferous in Scotland. Earth and Environmental Science Transactions of the Royal Society of Edinburgh 1–14.

Martill, D. M., P. J. A. Del Strother, and F. Gallien. 2014. *Acanthorhachis* , a new genus of shark from the Carboniferous (Westphalian) of Yorkshire, England. Geological Magazine 151:517–533.

Martinez, A. M., D. L. Boyer, M. L. Droser, C. Barrie, and G. D. Love. 2019. A stable and productive marine microbial community was sustained through the end-Devonian Hangenberg Crisis within the Cleveland Shale of the Appalachian Basin, United States. Geobiology 17:27–42.

McGill, R. A. R., A. J. Hall, A. E. Fallick, and A. J. Boyce. 1993. The palaeoenvironment of East Kirkton, West Lothian, Scotland: stable isotope evidence from silicates and sulphides. Transactions of the Royal Society of Edinburgh: Earth Sciences 84:223–237.

McLoughlin, S., and J. A. Long. 1994. New records of Devonian plants from southern Victoria Land, Antarctica. Geological Magazine 131:81–90.

McRoberts, C. A., and G. D. Stanley. 1989. A unique bivalve–algae life assemblage from the Bear Gulch Limestone (Upper Mississippian) of central Montana. Journal of Paleontology 63:578–581.

Mergil, M., D. Massa, and B. Plauchut. 2001. Devonian and Carboniferous brachiopods and bivalces of the Djado sub-basin (North Niger, SW Libya). Journal of the Czech Geological Society 46:169–188.

Mickle, K. E., R. Lund, and E. D. Grogan. 2009a. Three new palaeoniscoid fishes from the Bear Gulch Limestone (Serpukhovian, Mississippian) of Montana (USA) and the relationships of lower actinopterygians. Geodiversitas 31:623–668.

Mickle, K. E., R. Lund, and E. D. Grogan. 2009b. Three new palaeoniscoid fishes from the Bear Gulch Limestone (Serpukhovian, Mississippian) of Montana (USA) and the relationships of lower actinopterygians. Geodiversitas 31:623–668.

Miles, R. S. 1971. The Holonematidae (placoderm fishes), a review based on new specimens of Holonema from the Upper Devonian of Western Australia. Proceedings of the Royal Society of London. Series B: Biological Sciences 263:101–234.

Miles, R. S. 1977. Dipnoan (lungfish) skulls and the relationships of the group: a study based on new species from the Devonian of Australia. Zoological Journal of the Linnean Society 61:1–328.

Millward, D., S. J. Davies, F. Williamson, R. Curtis, T. I. Kearsey, C. E. Bennett, J. E. A. Marshall, and M. A. E. Browne. 2018a. Early Mississippian evaporites of coastal tropical wetlands. Sedimentology 65:2278–2311.

Millward, D., S. J. Davies, P. J. Brand, M. A. E. Browne, C. E. Bennett, T. I. Kearsey, J. E. Sherwin, and J. E. A. Marshall. 2018b. Palaeogeography of tropical seasonal coastal wetlands in

northern Britain during the early Mississippian Romer's Gap. Earth and Environmental Science Transactions of the Royal Society of Edinburgh 1–22.

Milner, A. C., and W. Lindsay. 1998. Postcranial remains of Baphetes and their bearing on the relationships of the Baphetidae (= Loxommatidae). Zoological Journal of the Linnean Society 122:211–235.

Milner, A. R. 2008. The tail of *Microbrachis* (Tetrapoda; Microsauria). Lethaia 41:257–261.

Milner, A. R., and S. E. K. Sequeira. 1993. The temnospondyl amphibians from the Viséan of East Kirkton, West Lothian, Scotland. Transactions of the Royal Society of Edinburgh: Earth Sciences 84:331–361.

Milner, A. R., and S. E. K. Sequeira. 1998. A cochleosaurid temnospondyl amphibian from the Middle Pennsylvanian of Linton, Ohio, U.S.A. Zoological Journal of the Linnean Society 122:261–290.

Milner, A. R., and S. E. K. Sequeira. 2011. The amphibian Erpetosaurus radiatus (Temnospondyli, Dvinosauria) from the Middle Pennsylvanian of Linton, Ohio- morphology and systematic position. Special Papers in Palaeontology 86:57–73.

Milner, A. R., and R. R. Schoch. 2013. Trimerorhachis (Amphibia: Temnospondyli) from the Lower Permian of Texas and New Mexico: cranial osteology, taxonomy and biostratigraphy. Neues Jahrbuch Für Geologie Und Paläontologie - Abhandlungen 270:91–128.

Miyashita, T., R. W. Gess, K. Tietjen, and M. I. Coates. 2021. Non-ammocoete larvae of Palaeozoic stem lampreys. Nature.

Moloshnikov, S. V. 2008. Devonian antiarchs (Pisces, Antiarchi) from central and Southern European Russia. Paleontological Journal 42:691–773.

Mondéjar-Fernández, J., F. J. Meunier, R. Cloutier, G. Clément, and M. Laurin. 2021. A microanatomical and histological study of the scales of the Devonian sarcopterygian *Miguashaia bureaui* and the evolution of the squamation in coelacanths. Journal of Anatomy joa.13428.

Moore, R. A., S. C. McKENZIE, and B. S. Lieberman. 2007. A Carboniferous synziphosurine (Xiphosura) from the Bear Gulch Limestone, Montana, USA. Palaeontology 50:1013–1019.

Mottequin, B., and E. Poty. 2016. Kellwasser horizons, sea-level changes and brachiopod–coral crises during the late Frasnian in the Namur–Dinant Basin (southern Belgium): a synopsis. Geological Society, London, Special Publications 423:235–250.

Moulton, J. M. 1974. A description of the vertebral column of Eryops based on the notes and drawings of A.S. Romer. Breviora 44.

Moy-Thomas, J. A. 1936. The Structure and Affinities of the Fossil Elasmobranch Fishes from the Lower Carboniferous Rocks of Glencartholm, Eskdale. Proceedings of the Zoological Society of London 106:761–788.

Moy-Thomas, J. A., and M. Bradley Dyne. 1938. Actinopterygian fishes from the Lower Carboniferous of Glencartholm, Eskdale, Dumfrieshire. Transactions of the Royal Society of Edinburgh: Earth Sciences 59:437–480.

Mutter, R. J., and A. G. Neuman. 2006. An enigmatic chondrichthyan with Paleozoic affinities from the Lower Triassic of western Canada. ACTA PALAEONTOLOGICA POLONICA 12.

Neenan, J. M., M. Ruta, J. A. Clack, and E. J. Rayfield. 2014. Feeding biomechanics in Acanthostega and across the fish-tetrapod transition. Proceedings of the Royal Society B: Biological Sciences 281:20132689–20132689.

Newberry, J. S. 1889. The Paleozoic Fishes of North America. United States Geological Survey, Washington, DC, USA, pp.

Norton, R. A., P. M. Bonamo, J. D. Grierson, and W. A. Shear. 1988. Oribatid mite fossils from a terrestrial Devonian deposit near Gilboa, New York. Journal of Paleontology 62:259–269.

Olive, S. 2013. Revision and updating of the antiarch (Placodermi, Vertebrata) fauna from the Devonian of Belgium with palaeobiogeographical considerations. Acta Palaeontologica Polonica.

Olive, S., G. Clément, E. B. Daeschler, and V. Dupret. 2015a. Characterization of the placoderm (Gnathostomata) assemblage from the tetrapod-bearing locality of Strud (Belgium, upper Famennian). Palaeontology 58:981–1002.

Olive, S., G. Clément, E. B. Daeschler, and V. Dupret. 2016a. Placoderm Assemblage from the Tetrapod-Bearing Locality of Strud (Belgium, Upper Famennian) Provides Evidence for a Fish Nursery. PLOS ONE 11:e0161540.

Olive, S., P. E. Ahlberg, V. N. Pernègre, É. Poty, É. Steurbaut, and G. Clément. 2016b. New discoveries of tetrapods (ichthyostegid-like and whatcheeriid-like) in the Famennian (Late Devonian) localities of Strud and Becco (Belgium). Palaeontology 59:827–840.

Olive, S., Y. Leroy, E. B. Daeschler, J. P. Downs, S. Ladevèze, and G. Clément. 2020. Tristichopterids (Sarcopterygii, Tetrapodomorpha) from the Upper Devonian tetrapod-bearing

locality of Strud (Belgium, upper Famennian), with phylogenetic and paleobiogeographic considerations. Journal of Vertebrate Paleontology e1768105.

Olive, S., G. Clement, J. Denayer, V. Dupret, P. Gerrienne, P. Gueriau, J.-M. Marion, B. Mottequin, and C. Prestianni. 2015b. Flora and fauna from a new Famennian (Upper Devonian) locality at Becco, eastern Belgium. Geologica Belgica 18:92–101.

Olori, J. C. 2015. Skeletal Morphogenesis of Microbrachis and Hyloplesion (Tetrapoda: Lepospondyli), and Implications for the Developmental Patterns of Extinct, Early Tetrapods. PLOS ONE 10:e0128333.

Olson, E. C. 1936. The Ilio-Sacral Attachment of Eryops. Journal of Paleontology 10:648–651.

Olson, E. C. 1979. Aspects of the Biology of Trimerorhachis (Amphibia: Temnospondyli). Journal of Paleontology 53:1–17.

Ørvig, T. 1960. New Finds of acanthodians, arthrodires, crossopterygians, ganoids and dipnoans in the Upper Middle Devonian Calcareous Flags (Oberer Plattenkalk) of the Bergisch Gladbach-Paffrath Trough. Part 1. Paläontologische Zeitschrift 34:295–335.

Ørvig, T. 1961. New finds of acanthodians, arthrodires, crossopterygians, ganoids and dipnoans in the Upper Middle Devonian Calcareous Flags (Oberer Plattenkalk) of the Bergisch Gladbach-Paffrath Trough. Part 2. Paläontologische Zeitschrift 35:10–27.

Otoo, B. K. A. 2015. A taxonomic and palaeoecological investigation of an earliest Carboniferous fauna from Burnmouth, Scotland, UK. MPhil, University of Cambridge, Cambridge, Cambridgeshire, England, UK, 157 pp.

Otoo, B. K. A., J. R. Bolt, R. E. Lombard, K. D. Angielczyk, and M. I. Coates. 2021. The postcranial anatomy of Whatcheeria deltae and its implications for the family Whatcheeriidae. Zoological Journal of the Linnean Society 193:700–745.

Otoo, B. K. A., J. A. Clack, T. R. Smithson, C. E. Bennett, T. I. Kearsey, and M. I. Coates. 2018. A fish and tetrapod fauna from Romer's Gap preserved in Scottish Tournaisian floodplain deposits. Palaeontology 62:225–253.

Panchen, A. L. 1964. The cranial anatomy of two Coal Measure anthracosaurs. Philosophical Transactions of the Royal Society B: Biological Sciences 742:593–637.

Panchen, A. L. 1966. The axial skeleton of the labyrinthodont Eogyrinus attheyi. Journal of Zoology 150:199–222.

Panchen, A. L. 1970. Handbook of Paleoherpetology, Part 5 Batrachosauria: Part A Anthracosauria. Verlag Dr. Friedrich Pfeil, Munich, Germany, 84 pp.

Panchen, A. L. 1972. The Skull and Skeleton of Eogyrinus attheyi Watson (Amphibia: Labyrinthodontia). Philosophical Transactions of the Royal Society B: Biological Sciences 263:279–326.

Panchen, A. L. 1975. A new genus of anthracosaur amphibian from the Lower Carboniferous of Scotland and the status of Pholidogaster pisciformis Huxley. Philosophical Transactions of the Royal Society B: Biological Sciences 269:582–637.

Panchen, A. L. 1977. On Anthracosaurus russelli Huxley (Amphibia: Labyrinthodontia) and the Family Anthracosauridae. Philosophical Transactions of the Royal Society B: Biological Sciences 279:447–512.

Panchen, A. L. 1981. A jaw ramus of the Coal Measure Amphibian Anthracosaurus from Northumberland. Palaeontology 24:85–92.

Panchen, A. L. 1985. On the amphibian Crassigyrinus scoticus Watson from the Carboniferous of Scotland. Philosophical Transactions of the Royal Society B: Biological Sciences.

Panchen, A. L., and T. R. Smithson. 1990. The pelvic girdle and hind limb of Crassigyrinus scoticus (Lydekker) from the Scottish Carboniferous and the origin of the tetrapod pelvic skeleton. Transactions of the Royal Society of Edinburgh: Earth Sciences 81:31–44.

Pardo, J. D., M. Szostakiwskyj, and J. S. Anderson. 2015. Cranial Morphology of the Brachystelechid 'Microsaur' Quasicaecilia texana Carroll Provides New Insights into the Diversity and Evolution of Braincase Morphology in Recumbirostran 'Microsaurs.' PLOS ONE 10:e0130359.

Pardo, J. D., B. J. Small, and A. K. Huttenlocker. 2017a. Stem caecilian from the Triassic of Colorado sheds light on the origins of Lissamphibia. Proceedings of the National Academy of Sciences 114:E5389–E5395.

Pardo, J. D., R. Holmes, and J. S. Anderson. 2019. An enigmatic braincase from Five Points, Ohio (Westphalian D) further supports a stem tetrapod position for aïstopods. Earth and Environmental Science Transactions of the Royal Society of Edinburgh 255–264.

Pardo, J. D., K. Lennie, and J. S. Anderson. 2020. Can We Reliably Calibrate Deep Nodes in the Tetrapod Tree? Case Studies in Deep Tetrapod Divergences. Frontiers in Genetics 11:506749.

Pardo, J. D., M. Szostakiwskyj, P. E. Ahlberg, and J. S. Anderson. 2017b. Hidden morphological diversity among early tetrapods. Nature 546:642–645.

Parker, K., A. Warren, and Z. Johanson. 2005. *Strepsodus* (Rhizodontida, Sarcopterygii) pectoral elements from the Lower Carboniferous Ducabrook Formation, Queensland, Australia. Journal of Vertebrate Paleontology 25:46–62.

Paton, R. L. 1993. Elasmobranch fishes from the Viséan of East Kirkton, West Lothian, Scotland. Transactions of the Royal Society of Edinburgh: Earth Sciences 84:329–330.

Paton, R. L., T. R. Smithson, and J. A. Clack. 1999. An amniote-like skeleton from the Early Carboniferous of Scotland. Nature 398:508–513.

Pawley, K. 2006. The postcranial skeleton of Temnospondyls (Tetrapoda: Temnospondyli). La Trobe University, Melbourne, Victoria, Australia, 442 pp.

Pawley, K. 2007. The postcranial skeleton of Trimerorhachis insignis (Temnospondyli: Trimerorhachidae): a plesiomorphic temnospondyl from the Lower Permian of North America. Journal of Paleontology 81:873–894.

Pawley, K., and A. Warren. 2006. The appendicular skeleton of Eryops megalocephalus Cope 1877 (Temnospondyli: Eryopoidea) from the Lower Permian of North America. Journal of Paleontology 80:561–580.

Pierce, S. E., J. A. Clack, and J. R. Hutchinson. 2012. Three-dimensional limb joint mobility in the early tetrapod Ichthyostega. Nature 486:523–526.

Pierce, S. E., J. R. Hutchinson, and J. A. Clack. 2013a. Historical Perspectives on the Evolution of Tetrapodomorph Movement. Integrative and Comparative Biology 53:209–223.

Pierce, S. E., P. E. Ahlberg, J. R. Hutchinson, J. L. Molnar, S. Sanchez, P. Tafforeau, and J. A. Clack. 2013b. Vertebral architecture in the earliest stem tetrapods. Nature 494:226–229.

Pollard, J. E. 1985. Coprolites and ostracods from the Dinantian of Foulden, Berwickshire, Scotland. Transactions of the Royal Society of Edinburgh: Earth Sciences 76:49–51.

Poplin, C., and R. Lund. 2000. Two new deep-bodied palaeoniscoid actinopterygians from Bear Gulch (Montana, USA, Lower Carboniferous). Journal of Vertebrate Paleontology 20:428–449.

Poplin, C. M., and R. Lund. 2002. Two Carboniferous fine-eyed palaeoniscoids (Pisces, Actinopterygii) from Bear Gulch (USA). Journal of Paleontology 76:1014–1028.

Porro, L. B., E. J. Rayfield, and J. A. Clack. 2015a. Descriptive Anatomy and Three-Dimensional Reconstruction of the Skull of the Early Tetrapod Acanthostega gunnari Jarvik, 1952. PLOS ONE 10:e0118882.

Porro, L. B., E. J. Rayfield, and J. A. Clack. 2015b. Computed tomography, anatomical description and three-dimensional reconstruction of the lower jaw of *Eusthenopteron foordi* Whiteaves, 1881 from the Upper Devonian of Canada. Palaeontology 58:1031–1047.

Rawson, J. R. G., L. B. Porro, E. Martin-Silverstone, and E. J. Rayfield. 2021. Osteology and digital reconstruction of the skull of the early tetrapod *Whatcheeria deltae*. Journal of Vertebrate Paleontology e1927749.

Reisz, R. R., and S. P. Modesto. 1996. *Archerpeton anthracos* from the Joggins Formation of Nova Scotia: a microsaur, not a reptile. Canadian Journal of Earth Sciences 33:703–709.

Robinson, J., P. E. Ahlberg, and G. Koentges. 2005. The braincase and middle ear region of Dendrerpeton acadianum (Tetrapoda: Temnospondyli). Zoological Journal of the Linnean Society 143:577–597.

Roelofs, B., T. Playton, M. Barham, and K. Trinajstic. 2015. Upper Devonian microvertebrates from the Canning Basin, Western Australia. Acta Geologica Polonica 65:69–101.

Rolfe, W. D. I., G. P. Durant, W. J. Baird, C. Chaplin, R. L. Paton, and R. J. Reekie. 1993. The East Kirkton Limestone, Viséan, of West Lothian, Scotland: introduction and stratigraphy. Transactions of the Royal Society of Edinburgh: Earth Sciences 84:177–188.

Romer, A. S. 1957. The appendicular skeleton of the Permian embolomerous amphibian Archeria. University of Michicagn Contributions from the Museum of Paleontology 13:103–159.

Romer, A. S. 1963. The larger embolomerous amphibians of the American Carboniferous. Bullet of the Museum of Comparative Zoology 128:415–454.

Romer, A. S. 1964. The skeleton of the Lower Carboniferous labyrinthodont Pholidogaster pisciformis. Bulletin of the Museum of Comparative Zoology 131:131–159.

Romer, A. S. 1970. A new anthracosaurian labyrinthodont, Proterogyrinus scheeli, from the Lower Carboniferous. Kirtlandia 1–16.

Romer, A. S., and R. V. Witter. 1941. The skin of the rhachitomous amphibian Eryops. American Journal of Science 239:822–824.

Romer, A. S., and R. V. Witter. 1942. Edops, a Primitive Rhachitomous Amphibian from the Texas Red Beds. The Journal of Geology 50:925–960.

Rosenberg, L. S. 1998. Comparison of the mineralized endoskeletal tissues of several Recent and fossil Chondrichthyans from the Bear Gulch Limestone of Montana. MS, Adelphi University, Garden City, New York, USA, 69 pp.

Ross, A. J., G. D. Edgecombe, N. D. L. Clark, C. E. Bennett, V. Carrió, R. Contreras-Izquierdo, and B. Crighton. 2018. A new terrestrial millipede fauna of earliest Carboniferous (Tournaisian) age from southeastern Scotland helps fill 'Romer's Gap'. Earth and Environmental Science Transactions of the Royal Society of Edinburgh 108:99–110.

Ruta, M. 2011. Phylogenetic signal and character compatibility in the appendicular skeleton of early tetrapods. Special Papers in Palaeontology 86:31–43.

Ruta, M., and J. A. Clack. 2006. A review of Silvanerpeton miripedes, a stem amniote from the Lower Carboniferous of East Kirkton, West Lothian, Scotland. Transactions of the Royal Society of Edinburgh: Earth Sciences 46:115.

Ruta, M., and M. I. Coates. 2007. Dates, nodes and character conflict: Addressing the Lissamphibian origin problem. Journal of Systematic Palaeontology 5:69–122.

Ruta, M., A. R. Milner, and M. I. Coates. 2002. The tetrapod Caerorhachis bairdi Holmes and Carroll from the Lower Carboniferous of Scotland. Transactions of the Royal Society of Edinburgh: Earth Sciences 92:229–261.

Ruta, M., M. I. Coates, and D. L. J. Quicke. 2003. Early tetrapod relationships revisited. Biological Reviews of the Cambridge Philosophical Society 78:251–345.

Ruta, M., J. A. Clack, and T. R. Smithson. 2020. A review of the stem amniote *Eldeceeon rolfei* from the Viséan of East Kirkton, Scotland. Earth and Environmental Science Transactions of the Royal Society of Edinburgh 1–20.

Ruta, M., D. Pisani, G. T. Lloyd, and M. J. Benton. 2007. A supertree of Temnospondyli: cladogenetic patterns in the most species-rich group of early tetrapods. Proceedings of the Royal Society B: Biological Sciences 274:3087–3095.

Sallan, L., and A. K. Galimberti. 2015. Body-size reduction in vertebrates following the end-Devonian mass extinction. Science 350:812–815.

Sallan, L. C. 2012. Tetrapod-like axial regionalization in an early ray-finned fish. Proceedings of the Royal Society B: Biological Sciences 279:3264–3271.

Sallan, L. C., and M. I. Coates. 2010. End-Devonian extinction and a bottleneck in the early evolution of modern jawed vertebrates. Proceedings of the National Academy of Sciences 107:10131–10135.

Sanchez, S., P. Tafforeau, and P. E. Ahlberg. 2014. The humerus of Eusthenopteron: a puzzling organization presaging the establishment of tetrapod limb bone marrow. Proceedings of the Royal Society B: Biological Sciences 281:20140299–20140299.

Sanchez, S., V. Dupret, P. Tafforeau, K. M. Trinajstic, B. Ryll, P.-J. Gouttenoire, L. Wretman, L. Zylberberg, F. Peyrin, and P. E. Ahlberg. 2013. 3D Microstructural Architecture of Muscle Attachments in Extant and Fossil Vertebrates Revealed by Synchrotron Microtomography. PLoS ONE 8:e56992.

Sawin, H. J. 1941. The cranial anatomy of Eryops megacephalus. Bulletin of the Museum of Comparative Zoology 88:405–464.

Schawaller, W., and P. M. Bonamo. 1991. The First Paleozoic Pseudoscorpions (Arachnida, Pseudoscorpionida). American Museum Novitates 20.

Schoch, R. R. 2013. The evolution of major temnospondyl clades: an inclusive phylogenetic analysis. Journal of Systematic Palaeontology 11:673–705.

Schoch, R. R. 2018. Osteology of the temnospondyl *Neldasaurus* and the evolution of basal dvinosaurians. Neues Jahrbuch Für Geologie Und Paläontologie - Abhandlungen 287:1–16.

Schoch, R. R. 2019. The putative lissamphibian stem-group: phylogeny and evolution of the dissorophoid temnospondyls. Journal of Paleontology 93:137–156.

Scholze, F., and R. W. Gess. 2017. Oldest known naiaditid bivalve from the high-latitude Late Devonian (Famennian) of South Africa offers clues to survival strategies following the Hangenberg mass extinction. Palaeogeography, Palaeoclimatology, Palaeoecology 471:31–39.

Scholze, F., and R. W. Gess. 2021. Late Devonian non-marine Naiadites devonicus nov. sp. (Bivalvia: Pteriomorphia) from the Waterloo Farm Lagerstätte in South Africa. Geobios 69:55–67.

Schram, F. R. 1983. Lower Carboniferous biota of Glencartholm, Eskdale, Dumfriesshire. Scottish Journal of Geology 19:1–15.

Schram, F. R., and J. Horner. 1978. Crustacea of the Mississippian Bear Gulch Limestone of Central Montana. Journal of Paleontology 52:394–406.

Schultze, H.-P. 1973. Large Upper Devonian arthrodires from Iran. Fieldiana Geology 23:53–78.

Schultze, H.-P. 1984. Juvenile specimens of *Eusthenopteron foordi* Whiteaves, 1881 (osteolepiform rhipidistian, Pisces) from the Late Devonian of Miguasha, Quebec, Canada. Journal of Vertebrate Paleontology 4:1–16.

Schultze, H.-P., and M. Arsenault. 1985. The panderichthyid fish Elpistostege: a close relative of tetrapods? Palaeontology 28:293–309.

Schultze, H.-P., and J. R. Bolt. 1996. The lungfish Tranodis and the tetrapod fauna from the Upper Mississippian of North America. Special Papers in Palaeontology 52:31–54.

Scott, A. C., and B. Meyer-Berthaud. 1985. Plants from the Dinantian of Foulden, Berwickshire, Scotland. Transactions of the Royal Society of Edinburgh: Earth Sciences 76:13–20.

Scott, A. C., R. Brown, J. Galtier, and B. Meyer-Berthaud. 1993. Fossil plants from the Viséan of East Kirkton, West Lothian, Scotland. Transactions of the Royal Society of Edinburgh: Earth Sciences 84:249–260.

Seddon, G. 1970. Frasnian conodonts from the Sadler ridge-Bugle Gap area, Canning Basin, Western Australia. Journal of the Geological Society of Australia 16:723–753.

Selden, P. A., W. A. Shear, and P. M. Bonamo. 1991. A spider and other arachnids from the Devonian of New York, and reinterpretations of Devonian Araneae. Palaeontology 34:241–281.

Selden, P. A., W. A. Shear, and M. D. Sutton. 2008. Fossil evidence for the origin of spider spinnerets, and a proposed arachnid order. Proceedings of the National Academy of Sciences 105:20781–20785.

Sequeira, S. E. K., and A. R. Milner. 1993. The temnospondyl Capetus from the Upper Carboniferous of the Czech Republic. Palaeontology 36:657–680.

Sharp, E. L., and J. A. Clack. 2011. Redescription of the lungfish Straitonia waterstoni from the Viséan of Lothian, Scotland. Earth and Environmental Science Transactions of the Royal Society of Edinburgh 102:179–190.

Sharp, E. L., and J. A. Clack. 2013. A review of the Carboniferous lungfish genus Ctenodus Agassiz, 1838 from the United Kingdom, with new data from an articulated specimen of Ctenodus interruptus Barkas, 1869. Earth and Environmental Science Transactions of the Royal Society of Edinburgh 104:169–204.

Shear, W., and P. Selden. 1995. Eoarthropleura (Arthropoda, Arthropleurida) from the Silurian of Britain and the Devonian of North America. Neues Jahrbuch Für Geologie Und Paläontologie - Abhandlungen 196:347–375.

Shear, W. A. 1993. Myriapodous arthropods from the Viséan of East Kirkton, West Lothian, Scotland. Earth and Environmental Science Transactions of the Royal Society of Edinburgh 84:309–316.

Shear, W. A., and P. M. Bonamo. 1988. Devonobiomorpha, A New Order of Centipeds (Chilopoda) from the Middle Devonian of Gilboa, New York State, USA, and the Phylogeny of Centiped Orders. American Museum Novitates 32.

Shear, W. A., J. M. Palmer, J. A. Coddington, and P. M. Bonamo. 1989. A Devonian Spinneret: Early Evidence of Spiders and Silk Use. Science 246:479–481.

Shear, W. A., P. M. Bonamo, J. D. Grierson, W. D. I. Rolfe, E. L. Smith, and R. A. Norton. 1984. Early Land Animals in North America: Evidence from Devonian Age Arthropods from Gilboa, New York. Science 224:492–494.

Shen, Z., J. Song, T. Servais, and Y. Gong. 2019. Late Devonian palaeobiogeography of marine organic-walled phytoplankton. Palaeogeography, Palaeoclimatology, Palaeoecology 531:108706.

Shubin, N. H., E. B. Daeschler, and F. A. Jenkins. 2006. The pectoral fin of Tiktaalik roseae and the origin of the tetrapod limb. Nature 440:764–771.

Shubin, N. H., E. B. Daeschler, and F. A. Jenkins. 2014. Pelvic girdle and fin of Tiktaalik roseae. Proceedings of the National Academy of Sciences 111:893–899.

Smith, M. M., T. R. Smithson, and K. S. W. Campbell. 1987. The Relationships of Uronemus: A Carboniferous Dipnoan with Highly Modified Tooth Plates. Philosophical Transactions of the Royal Society of London. Series B, Biological Sciences 317:299–327.

Smithson, T. R. 1980. A new labyrinthodont amphibian from the Carboniferous of Scotland. Palaeontology 23:915–923.

Smithson, T. R. 1982. The cranial morphology of Greererpeton burkemorani Romer (Amphibia: Temnospondyli). Zoological Journal of the Linnean Society 76:29–90.

Smithson, T. R. 1985. The morphology and relationships of the Carboniferous amphibian Eoherpeton watsoni Panchen. Zoological Journal of the Linnean Society 85:317–410.

Smithson, T. R. 1986. A new anthracosaur amphibian from the Carboniferous of Scotland. Palaeontology 29:603–628.

Smithson, T. R. 1993. Eldeceeon rolfei, a new reptiliomorph from the Viséan of East Kirkton, West Lothian, Scotland. Transactions of the Royal Society of Edinburgh: Earth Sciences 84:377–382.

Smithson, T. R., and J. A. Clack. 2013. Tetrapod appendicular skeletal elements from the Early Carboniferous of Scotland. Comptes Rendus Palevol 12:405–417.

Smithson, T. R., and J. A. Clack. 2018. A new tetrapod from Romer's Gap reveals an early adaptation for walking. Earth and Environmental Science Transactions of the Royal Society of Edinburgh 108:89–97.

Smithson, T. R., K. R. Richards, and J. A. Clack. 2016. Lungfish diversity in Romer's Gap: reaction to the end-Devonian extinction. Palaeontology 59:29–44.

Smithson, T. R., T. J. Challands, and K. Z. Smithson. 2019. Traquair's lungfish from Loanhead: dipnoan diversity and tooth plate growth in the late Mississippian. Earth and Environmental Science Transactions of the Royal Society of Edinburgh 1–11.

Smithson, T. R., R. L. Carroll, A. L. Panchen, and S. M. Andrews. 1993. Westlothiana lizziae from the Viséan of East Kirkton, West Lothian, Scotland, and the amniote stem. Transactions of the Royal Society of Edinburgh: Earth Sciences 84:383–412.

Smithson, T. R., S. P. Wood, J. E. A. Marshall, and J. A. Clack. 2012. Earliest Carboniferous tetrapod and arthropod faunas from Scotland populate Romer's Gap. Proceedings of the National Academy of Sciences 109:4532–4537.

Smithson, T. R., M. A. E. Browne, S. J. Davies, J. E. A. Marshall, D. Millward, S. A. Walsh, and J. A. Clack. 2017. A new Mississippian tetrapod from Fife, Scotland, and its environmental context. Papers in Palaeontology 3:547–557.

Snyder, D. 2011. Gyracanthid gnathostome remains from the Carboniferous of Illinois. Journal of Vertebrate Paleontology 31:902–906.

Stein, W. E., C. M. Berry, L. V. Hernick, and F. Mannolini. 2012. Surprisingly complex community discovered in the mid-Devonian fossil forest at Gilboa. Nature 483:78–81.

Stein, W. E., F. Mannolini, L. V. Hernick, E. Landing, and C. M. Berry. 2007. Giant cladoxylopsid trees resolve the enigma of the Earth's earliest forest stumps at Gilboa. Nature 446:904–907.

Stewart, T. A., J. B. Lemberg, N. K. Taft, I. Yoo, E. B. Daeschler, and N. H. Shubin. 2019. Fin ray patterns at the fin-to-limb transition. Proceedings of the National Academy of Sciences 201915983.

Sumner, D. 1993. Coprolites from the Viséan of East Kirkton, West Lothian, Scotland. Transactions of the Royal Society of Edinburgh: Earth Sciences 84:413–416.

Tetlie, O. E. 2007. Distribution and dispersal history of Eurypterida (Chelicerata). Palaeogeography, Palaeoclimatology, Palaeoecology 252:557–574.

Tetlie, O. E., S. J. Braddy, P. D. Butler, and D. E. G. Briggs. 2004. A New Eurypterid (Chelicerata: Eurypterida) from the Upper Devonian Gogo Formation of Western Australia, With A Review of the Rhenopteridae. Palaeontology 47:801–809.

Thomas, N. 2004. The Taphonomy of a Carboniferous Lagerstatte: the Invertebrates of the Bear Gulch Limestone Member. MSc, University of Leicester, Leicester, England, UK, 94 pp.

Thomson, K. S. 1968. A new Devonian fish (Crossopterygii: Rhipidistia) considered in relation to the origin of the Amphibia. Postilla 1–13.

Tomita, T. 2015. Pectoral fin of the Paleozoic shark, *Cladoselache* : new reconstruction based on a near-complete specimen. Journal of Vertebrate Paleontology 35:e973029.

Torres-Martínez, M. A., and F. Sour-Tovar. 2016. New productide brachiopods (Productoidea) from the Carboniferous of Ixtaltepec Formation, Oaxaca, Mexico. Journal of Paleontology 90:418–432.

Traquair, R. H. 1884. IV.—Remarks on the Genus Megalichthys, Agassiz, with Description of a New Species. Geological Magazine 1:115.

Traquair, R. H. 1886. XLV.— *On* Harpacanthus, *a new genus of Carboniferous Selachian Spines*. Annals and Magazine of Natural History 18:493–496.

Trinajstic, K. 1999. New anatomical information on Holonema (Placodermi) based on material from the Frasnian Gogo Formation and the Givetian- Frasnian Gneudna Formation, Western Australia. Geodiversitas 21:69–84.

Trinajstic, K., and M. Hazelton. 2007. Ontogeny, phenotypic variation and phylogenetic implications of arthrodires from the Gogo Formation, Western Australia. Journal of Vertebrate Paleontology 27:571–583.

Trinajstic, K., and A. D. George. 2009. MICROVERTEBRATE BIOSTRATIGRAPHY OF UPPER DEVONIAN (FRASNIAN) CARBONATE ROCKS IN THE CANNING AND CARNARVON BASINS OF WESTERN AUSTRALIA. Palaeontology 52:641–659.

Trinajstic, K., and J. A. Long. 2009. A new genus and species of Ptyctodont (Placodermi) from the Late Devonian Gneudna Formation, Western Australia, and an analysis of Ptyctodont phylogeny. Geological Magazine 146:743–760.

Trinajstic, K., C. Marshall, J. Long, and K. Bifield. 2007. Exceptional preservation of nerve and muscle tissues in Late Devonian placoderm fish and their evolutionary implications. Biology Letters 3:197–200.

Trinajstic, K., J. A. Long, Z. Johanson, G. Young, and T. Senden. 2012. New morphological information on the ptyctodontid fishes (Placodermi, Ptyctodontida) from Western Australia. Journal of Vertebrate Paleontology 32:757–780.

Trinajstic, K., B. Roelofs, C. J. Burrow, J. A. Long, and S. Turner. 2014. Devonian vertebrates from the Canning and Carnarvon Basins with an overview of Paleozoic vertebrates of Western Australia. Journal of the Royal Society of Western Australia 20.

Trinajstic, K., S. Sanchez, V. Dupret, P. Tafforeau, J. Long, G. Young, T. Senden, C. Boisvert, N. Power, and P. E. Ahlberg. 2013. Fossil Musculature of the Most Primitive Jawed Vertebrates. Science 341:160–164.

Trinajstic, K. M., and K. J. McNamara. 1999. Heterochrony in the Late Devonian arthrodiran fishes Compagopiscis and Incisoscutum. Records of the Western Australian Museum 57:77–91.

Turner, S., and G. C. Young. 1992. Thelodont scales from the Middle-Late Devonian Aztec Siltstone, southern Victoria Land, Antarctica. Antarctic Science 4:89–105.

Turner, S., C. J. Burrow, and A. Warren. 2005. Gyracanthides hawkinsi sp. nov. (Acanthodii, Gyracanthidae) from the Lower Carboniferous of Queensland, Australia, with a review of gyracanthid taxa. Palaeontology 48:963–1006.

Vallin, G., and M. Laurin. 2004. Cranial morphology and affinities of *Microbrachis* , and a reappraisal of the phylogeny and lifestyle of the first amphibians. Journal of Vertebrate Paleontology 24:56–72.

Vorobyeva, E. I. 1995. Shoulder girdle of Panderichthys rhombolepis (Gross) (Crossopterygii), Upper Devonian, Latvia. Geobios 19:285–288.

Walkden, G. M., J. R. Irwin, and A. E. Fallick. 1993. Carbonate spherules and botryoids as lake floor cements in the East Kirkton Limestone of West Lothian, Scotland. Transactions of the Royal Society of Edinburgh: Earth Sciences 84:213–221.

Warren, A. 2007. New data on *Ossinodus pueri* , a stem tetrapod from the Early Carboniferous of Australia. Journal of Vertebrate Paleontology 27:850–862.

Warren, A., and S. Turner. 2004. The First Stem Tetrapod from the Lower Carboniferous of Gondwana. Palaeontology 47:151–184.

Warren, A., B. P. Currie, C. Burrow, and S. Turner. 2000. A redescription and reinterpretation of *Gyracanthides murrayi* Woodward 1906 (Acanthodii, Gyracanthidae) from the Lower Carboniferous of the Mansfield Basin, Victoria, Australia. Journal of Vertebrate Paleontology 20:225–242.

Waterston, C. D. 1985. Chelicerata from the Dinantian of Foulden, Berwickshire, Scotland. Transactions of the Royal Society of Edinburgh: Earth Sciences 76:25–33.

Waterston, C. D., B. W. Oelofsen, and R. D. F. Oosthuizen. 1985. *Cyrtoctenus wittebergensis* sp. nov. (Chelicerata: Eurypterida), a large sweep-feeder from the Carboniferous of South Africa. Earth and Environmental Science Transactions of the Royal Society of Edinburgh 76:339–358.

Welch, J. R. 1984. The Asteroid, Lepidasterella montanensis n. sp., from the Upper Mississippian Bear Gulch Limestone of Montana. Journal of Paleontology 58:843–851.

Wellburn, E. D. 1901. The fish fauna of the Millstone Grits of Great Britain. Geological Magazine 8:216–222.

Wellburn, E. D. 1903. On some new species of fossil fish from the Millstone Grit rocks, with an amended list of genera and species. Geological Magazine 18:216–222.

Wellstead, C. F. 1982. A Lower Carboniferous aïstopod amphibian from Scotland. Palaeontology 25:193–208.

Wendt, J., B. Kaufmann, Z. Belka, N. Farsan, and A. K. Bavandpur. 2002. Devonian/Lower Carboniferous stratigraphy, facies patterns and palaeogeography of Iran. Part I. Southeastern Iran. Acta Geologica Polonica 52:129–168.

Wendt, J., B. Kaufmann, Z. Belka, N. Farsan, and A. K. Bavandpur. 2005. Devonian/Lower Carboniferous stratigraphy, facies patterns and palaeogeography of Iran Part II. Northern and central Iran). Acta Geologica Polonica 55:31–97.

Whalen, C. D., and N. H. Landman. 2022. Fossil coleoid cephalopod from the Mississippian Bear Gulch Lagerstätte sheds light on early vampyropod evolution. Nature Communications 13:1107.

White, T. E. 1939. Osteology of Seymouria baylorensis Broil. Bulletin of the Museum of Comparative Zoology 85:325–409.

Wilk, O., S. Olive, A. Pradel, J. L. den Blaauwen, and P. Szrek. 2021. The first lower jaw of a ctenacanthid shark from the Late Devonian (Famennian) of Belgium. Journal of Vertebrate Paleontology e1960537.

Williams, L. A. 1983. Deposition of the Bear Gulch Limestone: a Carboniferous Plattenkalk from central Montana. Sedimentology 30:843–860.

Williams, M. E. 1998. A new specimen of *Tamiobatis vetustus* (Chondrichthyes, Ctenacanthoidea) from the Late Devonian Cleveland Shale of Ohio. Journal of Vertebrate Paleontology 18:251–260.

Witzmann, F. 2005. Cranial morphology and ontogeny of the Permo-Carboniferous temnospondyl Archegosaurus decheni Goldfuss, 1847 from the Saar–Nahe Basin, Germany. Transactions of the Royal Society of Edinburgh: Earth Sciences 96:131–162.

Witzmann, F., and R. R. Schoch. 2006. The postcranium of Archegosaurus decheni, and a phylogenetic analysis of temnospondyl postcrania. Palaeontology 49:1211–1235.

Witzmann, F., and I. Werneburg. 2017. The Palatal Interpterygoid Vacuities of Temnospondyls and the Implications for the Associated Eye- and Jaw Musculature. The Anatomical Record 300:1240–1269.

Won, M.-Z. 1997a. Review of Family Entactiniidae (Radiolaria), and Taxonomy and Morphology of Entactiniidae in the Late Devonian (Frasnian) Gogo Formation, Australia. Micropaleontology 43:333–369.

Won, M.-Z. 1997b. The Proposed New Radiolarian Subfamily Retentactiniinae (Entactiniidae) from the Late Devonian (Frasnian) Gogo Formation, Australia. Micropaleontology 43:371–418.

Wood, M. 2018. Glencartholm revisited: describing for the first time Stan Wood's discovery and excavation of Mumbie Quarry, adjacent to the important Palaeozoic fossil site of Glencartholm. Earth and Environmental Science Transactions of the Royal Society of Edinburgh 108:47–54.

Wood, R. 1998. Novel reef fabrics from the Devonian Canning Basin, Western Australia. Sedimentary Geology 121:149–156.

Wood, R. 2000. Palaeoecology Of A Late Devonian Back Reef: Canning Basin, Western Australia. Palaeontology 43:671–703.

Wood, S. P. 1982. New basal Namurian (Upper Carboniferous) fishes and crustaceans found near Glasgow. Nature 297:574–577.

Young, B., R. L. Dunstone, T. J. Senden, and G. C. Young. 2013. A Gigantic Sarcopterygian (Tetrapodomorph Lobe-Finned Fish) from the Upper Devonian of Gondwana (Eden, New South Wales, Australia). PLoS ONE 8:e53871.

Young, G. C. 1989. The Aztec fish fauna (Devonian) of Southern Victoria Land: Evolutionary and biogeographic significance. Geological Society, London, Special Publications 47:43–62.

Young, G. C., and C. J. Burrow. 2004. Diplacanthid acanthodians from the Aztec Siltstone (late Middle Devonian) of southern Victoria Land, Antarctica. Fossils and Strata 50:23–43.

Young, G. C., and J. A. Long. 2005. Phyllolepid placoderm fish remains from the Devonian Aztec Siltstone, southern Victoria Land, Antarctica. Antarctic Science 17:387–408.

Young, G. C., and J. A. Long. 2014. New arthrodires (placoderm fishes) from the Aztec Siltstone (late Middle Devonian) of southern Victoria Land, Antarctica. Australian Journal of Zoology 62:44.

Young, G. C., and J. Lu. 2020. Asia–Gondwana connections indicated by Devonian fishes from Australia: palaeogeographic considerations. Journal of Palaeogeography 9:8.

Young, G. C., J. A. Long, and A. Ritchie. 1992. Crossopterygian fishes from the Devonian of Antarctica: systematics, relationships, and biogeographic significance. Records of the Australian Museum, Supplement 14:1–77.

Young, G. C., C. J. Burrow, J. A. Long, S. Turner, and B. Choo. 2010. Devonian macrovertebrate assemblages and biogeography of East Gondwana (Australasia, Antarctica). Palaeoworld 19:55–74.

Zamani, F., M. Yazdi, A. Bahrami, C. Girard, C. Spalletta, and H. Ameri. 2020. Middle Givetian to late Famennian (Middle to Late Devonian) conodonts from the northern margin of Gondwana (Kerman region, Central Iran). Historical Biology 1–19.

Zangerl, R., and G. R. Case. 1973. Iniopterygia : a new order of Chondrichthyan fishes from the Pennsylvanian of North America. Fieldiana Geology Memoirs 6:1–67.

Zhang, R., and J. Pojeta. 1986. New bivalves from the Datang Stage, Lower Carboniferous, Guangdong Province, China. Journal of Paleontology 60:669–679.

Zhu, M., P. E. Ahlberg, W. Zhao, and L. Jia. 2002. First Devonian tetrapod from Asia. Nature 420:760–761.